

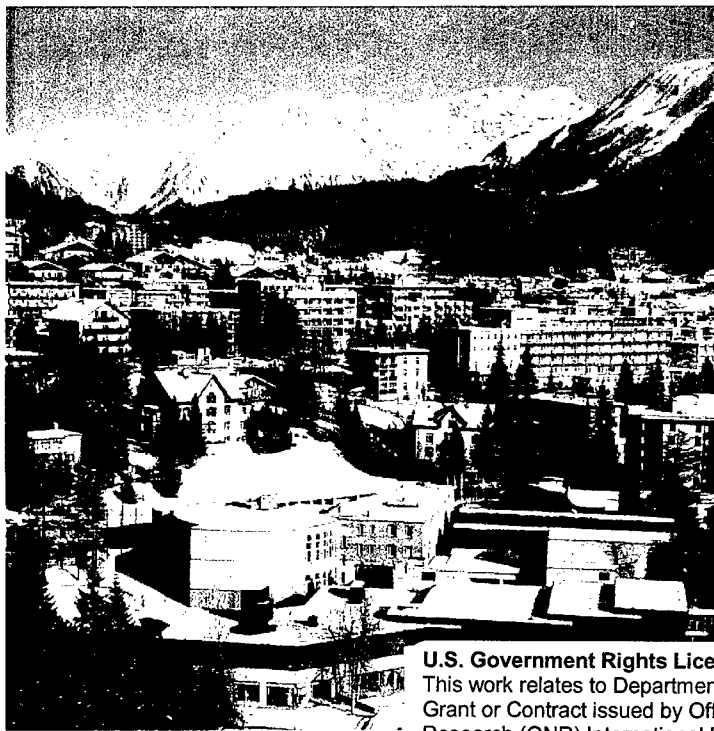
DISTRIBUTION STATEMENT
Approved for Public Release
Distribution Unlimited

 **ICONO'5**
2000

**5th International Conference on
Organic Nonlinear Optics**

Davos, Switzerland, March 12 – 16, 2000

Final Program



U.S. Government Rights License

This work relates to Department of the Navy Grant or Contract issued by Office of Naval Research (ONR) International Field Office-Europe. The United States Government has a royalty-free license throughout the world in all copyrightable material contained herein.

AQ F02-02-0286

Committees

■ Conference Chair

Peter Günter (ETH Zürich, Switzerland)

■ Co-Chairs

François Kajzar, European Chair

Mark Kuzyk, American Chair

Hiroyuki Sasabe, Pacific Chair

(LETI, CEA, France)

(Washington State U., USA)

(CIST, Japan)

■ International Advisory Committee

Fernando Agullo-Lopez	(Spain)	André Persoons	(Belgium)
Werner Blau	(Ireland)	Nasser Peyghambarian	(USA)
Donald C. Bradley	(UK)	Paras Prasad	(USA)
Christoph Bräuchle	(Germany)	Takatomo Sasaki	(Japan)
Jean-Luc Brédas	(USA)	Ron Shen	(USA)
Vittorio Degiorgio	(Italy)	Ken Singer	(USA)
Christos Flytzanis	(France)	George I. Stegeman	(USA)
Toshikuni Kaino	(Japan)	Carlo Taliani	(Italy)
Nakjoong Kim	(Korea)	Sukant Tripathy	(USA)
Takayoshi Kobayashi	(Japan)	Robert Twieg	(USA)
Charles Lee	(USA)	Shinsuke Umegaki	(Japan)
Seth Marder	(USA)	Kenneth Wynne	(USA)
Seizo Miyata	(Japan)	Joseph Zyss	(France)
Hachiro Nakanishi	(Japan)		

■ Conference Secretariat

Christian Bosshard
Nonlinear Optics Laboratory
Institute of Quantum Electronics
ETH Hönggerberg, HPF E14
CH-8093 Zürich, Switzerland

Tel: +41-1-633-2329
Fax: +41-1-633-1056
E-mail: icono5@wntweb.ethz.ch
Web: <http://www.icono5.ethz.ch>

■ Local Organizing Committee

Ivan Biaggio (ETH)
Christian Bosshard (ETH)
François Diederich (ETH)
Peter Günter (ETH)
Carolina Medrano (ETH)
Germano Montemezzani (ETH)
Ulrich Suter (ETH)

Conference Program and Information
Secretary General

Conference Chair
Treasurer
Local Arrangements

20011203 224

Contents

Preface	4
Conference Location Information _____	5
Contact Information	5
Congress Center _____	5
Congress Center House B _____	6
General Information _____	7
Oral Talks	7
Poster Sessions	7
Proceedings	8
Internet Access	8
Insurance	8
Train Schedule	8
Program Overview _____	9
Program and Invited Talks _____	10-14
Poster Session I _____	15-18
Poster Session II _____	19-22
Poster Session III _____	23-27
Extended Abstracts	
Invited Talks	INV 1 - INV 33
Poster Session I	A 1 - C 17
Poster Session II	D 1 - F 10
Poster Session III	G 1 - I 15
Authors Index	i - Vi
Sponsors and Exhibitors	
Program Overview	

■ Preface

Optical wave manipulation is one of the future technologies for optical processing and communication. Organic nonlinear optical materials are thought to have a key role in those technologies, and a lot of effort to develop new molecules/materials as well as fundamental understanding is under way throughout the world.

ICONO'5 is the fifth International Conference on Organic Nonlinear Optics, a conference series that was started in Val Thorens, France, in January 1994. The conference aims at achieving international exchange of information and cooperation among researchers in academia, government laboratories, and industries, and to stimulate growth in the field of organic nonlinear optics. It will provide a forum for discussion of all aspects of nonlinear optics, e.g. new phenomena, novel optoelectronic devices, and advanced organic materials.

It is already a tradition, that ICONO conferences in winter usually take place in a skiing resort. We have chosen Davos as the conference location because of the excellent infrastructure and the relatively easy connection from Zurich airport and from most of the European cities. In addition we think that the spectacular alpine atmosphere of the surroundings will stimulate interactions between participants.

During this conference there will be 33 invited talks and 143 posters presented. In addition a round-table discussion on "The Future of Electro-optic Polymers" will take place. A total of 180 participants have registered up to now. We are convinced, that the quality of the invited as well as the contributed papers will find your interest as in the earlier conferences of this conference series.

I would like to acknowledge support from several government agencies, industrial companies as well as research laboratories (see inside back cover). Without their generous support this conference could not have been organized.

Finally I also gratefully acknowledge the help and support of the members of the International Advisory Committee and the Local Organizing Committee. Their advice and support made it easy for me to put this program together.

I wish all the participants a successful, interesting and pleasant conference.

Zurich, March 1st, 2000

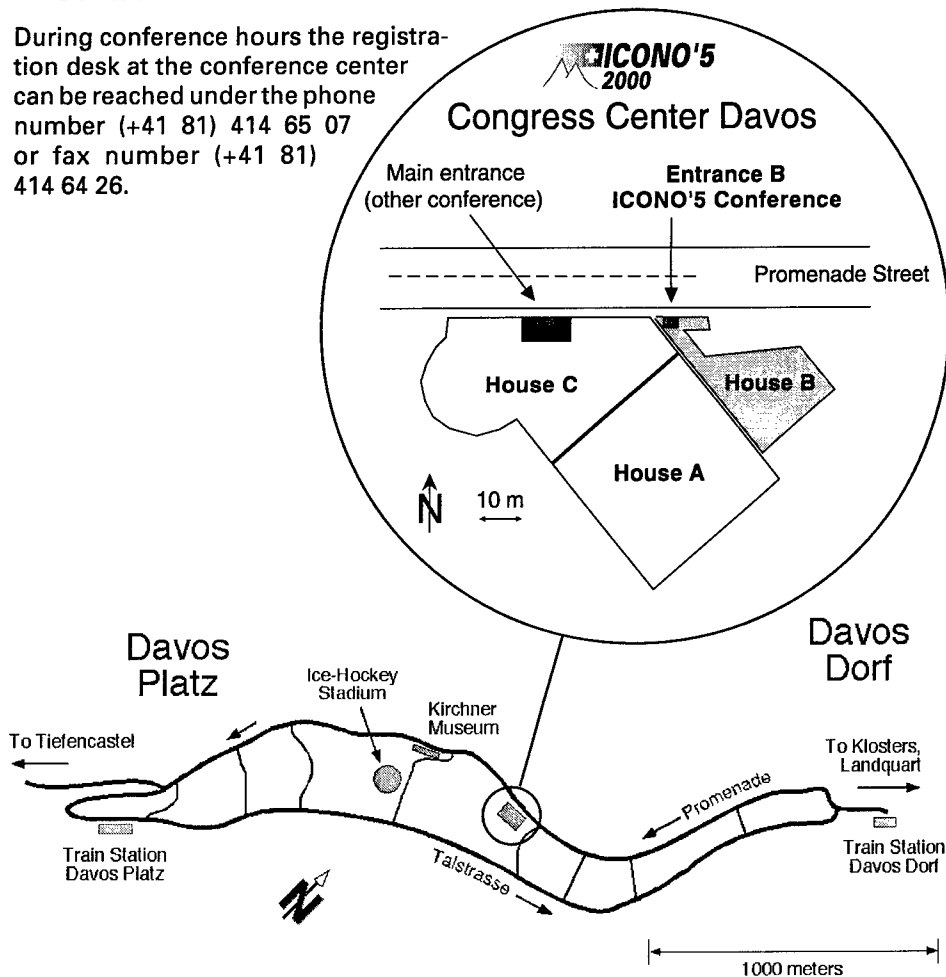
Peter Günter

Conference Location Information

The DAVOS CONGRESS CENTER (Promenade 92), situated approximately half-way between the town quarters DAVOS DORF and DAVOS PLATZ (see map), is divided into three independent sections. The ICONO'5 conference will be held in section (House) B, which is accessed from the Davos main street (Promenade) through the entrance marked B. Several bus lines of the Davos public transport system run along the Promenade street and all of them stop in front of the Congress Center (stop called Hallenbad/Kongresszentrum).

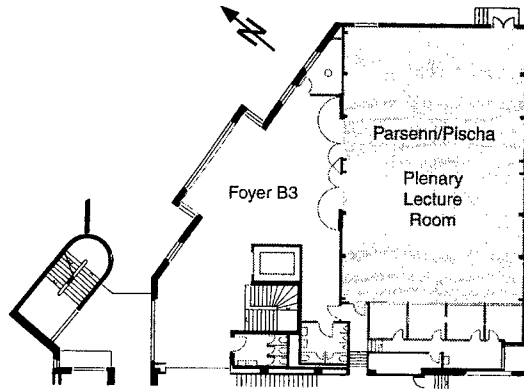
Contact Information

During conference hours the registration desk at the conference center can be reached under the phone number (+41 81) 414 65 07 or fax number (+41 81) 414 64 26.

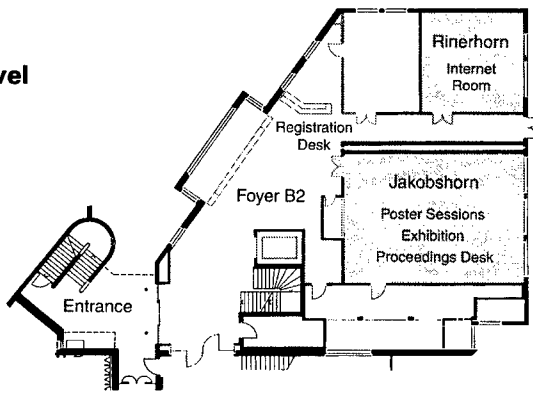


Congress Center: House B

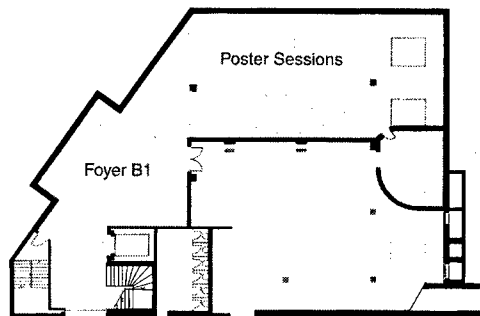
Upper Level



Entrance Level



Lower Level



■ General Information

The invited oral contributions will be presented at plenary sessions during the morning and in the afternoon. All contributed and postdeadline papers are in the form of posters. Three two-and-a-half-hour long poster sessions are scheduled in the late afternoons. In addition, a round table panel discussion will take place on Tuesday evening. Tuesday afternoon will be free of lectures. You may want to experience some of the impressive and wide ski slopes of the Davos area. The social program includes three main events. After the welcome reception on Sunday evening at the conference center, you are invited to attend the conference reception at the Kirchner Museum (see map page 5) on Monday evening and the conference dinner at the Hotel «Belvedere/Steigenberger» on Wednesday evening. The Hotel «Belvedere» is situated in front of the Kirchner Museum.

■ Oral Talks

The oral talks will be held in the room «Parsenn/Pischa» on the upper level. The length of each invited oral talk is 25 minutes plus 5 minutes for discussions. Speakers are requested to check-in with the session chairperson at least five minutes prior to the start of the session. Speakers requiring special equipment are asked to contact the organizers well in advance of their talk.

■ Poster Sessions

All contributed papers as well as the postdeadline papers are scheduled to be presented during the three afternoon poster sessions. Contributed posters will be on display a full day. They must be mounted at the latest during the morning coffee break and must be removed in the evening, after the end of each poster session.

The posters will be divided between the room «Jakobshorn» (entrance level) and the Foyer B1 on the lower level according to following list.

		Jakobshorn	Foyer B1
Monday	March 13	B 2 — B 13	A 1 — A 18 C 1 — C 17
Tuesday	March 14	F 1 — F 10	D 1 — D 9 E 1 — E 29
Wednesday	March 15	I 2 — I 15	G 1 — G 7 H 1 — H 30

■ Proceedings

Proceedings of ICONO'5 will be published in a special issue of the journal *Nonlinear Optics* by Gordon and Breach. They will be published from Camera-Ready Copy (CRC) to be provided by the authors. The manuscripts (one original and three copies) have to be submitted when registering on-site for the conference, but by 10 am on Monday, March 13, at the latest. They will be refereed during the conference by the participants, and given back by the reviewers by 10.30 am on Wednesday at the proceedings desk. The authors can inform themselves about the acceptance of their contribution at the proceedings desk starting at 16.30 on Wednesday afternoon.

■ Internet Access

A limited number of internet stations will be made available in the room «Rinerhorn» (middle level).

■ Insurance

Insurance has to be arranged individually by each participant.

■ Train Schedule

The following table gives the most important train connections between Davos and Zürich Airport.

Thursday, March 16

Davos Platz (Departure)	Davos Dorf (Departure)	Landquart (Departure)	Zürich Main Station (Departure)	Zürich Airport (Arrival)	Travelling time (hours)
12.09 (D 44)	12.13	13.26 (EC 96)	15.04 (IR 1974)	15.13	3.04
13.07 (D 50)	13.11	14.26 (IR 782)	16.04 (IR 1976)	16.13	3.06
14.09 (D 54)	13.13	15.26 (IR 1784)	17.04 (IR 1976)	17.13	3.04
15.07 (D 60)	15.11	16.22 (IC 786)	17.40 (IC 729)	17.51	2.44
16.09 (D 64)	16.13	17.26 (IR 1788)	19.04 (IR 1984)	19.13	3.04
17.09 (D 70)	17.13	18.22 (IC 792)	19.40 (IC 737)	19.51	2.42
18.09 (D 74)	18.13	19.26 (IR 1792)	21.07 (IC 941)	21.16	3.07

Sunday, March 12	Monday, March 13	Tuesday, March 14	Wednesday, March 15	Thursday, March 16
	8.30-9.00 Opening Future Photonic Appl. 9.00-10.30 Melchior Schadt Shen 10.30-11.00 Coffee/Tee EO Polymers 11.00-12.30 Dalton Lee Kaino 12.30-14.30 Lunch Optical Memories 14.30-16.30 Haarer Wilson Peyghamb. Meerholz 16.30-19.00 Poster I 19.30-21.30 Kirchner Museum (Conference Reception)	High NL Org. Crystals 8.30-10.30 Kobayashi Karl Nakanishi Mori 10.30-11.00 Coffee/Tee NLO Polymers 11.00-12.30 Stegeman Kim Nunzi 12.30-16.30 Free time 16.30-19.00 Poster II 19.00-20.00 Round Table Discussion	Third-order NLO 8.30-10.30 Marder Brédas Bubeck Wada 10.30-11.00 Coffee/Tee OLED's 11.00-12.00 Schwöerer Batlogg 12.00-14.30 Lunch Novel Molecules 14.30-16.30 Zyss Persoons Kajzar Twieg 16.30-19.00 Poster III 20.00 Conference Dinner (Hotel Belvedere)	Fund. Investigations 8.30-10.30 Flytzanis Banfi Kuzyk Singer 10.30-11.00 Coffee/Tee New Phenomena 11.00-12.00 Zhang Ito 12.00-12.30 Closing
16.00-18.00 Registration (House B, Congress Center)				
18.00-20.00 Welcome Reception (House B, Congress Center)				

Monday, March 13

Program and
Invited Talks**8.30-9.00 Opening****9:00-10:30 Future Photonic Applications** Chair: P. Günter

9:00-9:30 **Advanced telecommunication components and materials research in Europe**
INV 1
Hans Melchior

9:30-10:00 **Optics and applications of photo-aligned liquid crystalline surfaces**
INV 2
Martin Schadt

10:00-10:30 **Nonlinear optical spectroscopic studies of polymer surfaces and interfaces**
INV 3
Yuen-Ron Shen

10:30-11:00 Coffee/Tee

11:00-12:30 Electro-optical Polymers Chair: G. Stegeman

11:00-11:30 **Production of high bandwidth polymeric electro-optic modulators with V_{π} voltages of less than 1 Volt**
INV 4
Larry Dalton

11:30-12:00 **Organic-inorganic hybrid NLO materials with different chromophore bonding directions**
INV 5
Kwang-Sup Lee, Tae-Dong Kim, Yu Hong Min, and Choon Sup Yoon

12:00-12:30 **Refractive index volume grating fabrication by photo-bleaching of azo-dye functionalized polymer waveguides**
INV 6
Toshikuni Kaino, Tomoaki Shibata, and Toshiaki Hattori

12:30-14.30 Lunch

14:30-16:30 Optical Memories Chair: R. Twieg

14:30-15:00 **Memory applications of novel organic materials**
INV 7
D. Haarer

15:00-15:30 **High density, high performance optical data storage via volume holography: Viability at last?**
INV 8
William L. Wilson

15:30-16:00 **Recent advances in fast photorefractive polymers and bright OLEDs**
INV 9
Nasser Peyghambarian

16:00-16:30 **Organic photorefractive materials with sub-millisecond response and large dynamic range**
INV 10
K. Meerholz, E. Mecher, R. Bittner, F. Gallego, and H.H. Hoerhold

16.30-19.00 Poster Session I (page 15)**19.30-21.30 Conference Reception (Kirchner Museum)**

**Program and
Invited Talks**

11

Tuesday, March 14

8:30-10:30 High Nonlinearity Organic Crystals Chair: T. Kaino

8:30-9:00 **Sub-5fs nonlinear optical processes in polydiacetylenes**
INV 11 *Takayoshi Kobayashi*

9:00-9:30 **Organic crystal growth and epitaxy**
INV 12 *Norbert Karl*

9:30-10:00 **Growth of high quality DAST crystals by using slope
nucleation method**
INV 13 *Yusuke Mori*

10:00-10:30 **Molecular engineering of the DAST family**
INV 14 *Hachiro Nakanishi*

10:30-11:00 Coffee/Tee

11:00-12:30 Nonlinear Optical Polymers Chair: L. Dalton

11:00-11:30 **Photodegradation of various electro-optic polymer
families**
INV 15 *George I. Stegeman, A. Galvan-Gonzales, M. Canva,
R. Twieg, T. C. Kowalczyk, X. Q. Zhang, H. S. Lackritz,
S. Marder, S. Thayumanavan, K. P. Chan, A. K.-Y. Jen,
and X. Wu*

11:30-12:00 **Nonlinear optics and photorefractivity of polymer
composites**
INV 16 *N. Kim, W. S. Jahng, S. Song, D.-H. Shin, H. Chun, and M. Joo*

12:00-12:30 **Periodically structured polymer films and applications**
INV 17 *J.-M. Nunzi, L. Rocha, V. Dumarcher, C. Denis, P. Raimond,
C. Fiorini, F. Sobel, B. Sahraoui, and D. Gindre*

12:30-16.30 Free time

16.30-19.00 Poster Session II (page 19)

19.00-20.00 Round Table Discussion

Chair: C. Lee

"The Future of Electro-Optical Polymers"

8:30-10:30 Third Order Nonlinear Optics Chair: M.G. Kuzyk**8:30-9:00 Applications of molecules with large two-photon
INV 18 absorption cross sections***V. Alain, S. Ananthavel, J. K. Cammack, M. Halik, S. Kuebler,
S. Marder, J. W. Perry, M. Rumi, S. Thayumanavan,
W. Wenselers, B. Cumpston, M. Dickinson, S. E. Fraser,
A. Heikal, and M. Lipson***9:00-9:30 Dimensionality aspects for two-photon absorption in
INV 19 conjugated chromophores***Jean-Luc Brédas, H. Vogel, J. W. Perry, S. R. Marder, and D. Beljonne***9:30-10:00 Waveguides of PPV-derivatives with large cubic
INV 20 nonlinearities***Christoph Bubeck***10:00-10:30 Multifunctional macrocycles and polymers with
INV 21 carbazole oligomeric units***Tatsuo Wada, Atsushi Gunji, Yoshihiro Imase, Tetsuya Aoyama
Hiromi Kimura-Suda, and Hiroyuki Sasabe***10:30-11:00 Coffee/Tee****11:00-12:00 Organic Semiconductors and Light Emitting Diodes**

Chair: N. Peyghambarian

**11:00-11:30 The current in organic light-emitting diodes
INV 22** *M. Schworer***11:30-12:00 Charge transport in oligothiophene single crystals
INV 23** *B. Batlogg, J. H. Schön, and Ch. Kloc***12:00-14.30 Lunch**

**Program and
Invited Talks**

13

Wednesday, March 15

14:30-16:30 Novel Molecules Chair: K. Singer

14:30-15:00 **Hypercubic octupolar molecular crystals for quadratic
INV 24 nonlinear optics**

Joseph Zyss

15:00-15:30 **Molecular chirality as a tool for second-order
INV 25 nonlinear optics**

*André Persoons, M. Kauranen, N. Bussin, S. Van Elshocht,
T. Verbiest, T. J. Katz, K. E. S. Phillips, and C. Nuckolls*

15:30-16:00 **Spectroscopy of excited states in organic molecules
INV 26 studied by optical limiting**

*P-A. Chollet, B. Paci, V. Hully, A. Sornin, J-M. Nunzi, F. Kajzar, P. Baldeck,
Y. Morel, M. Maggini, G. Scorra, A. Bianco, M. Prato, and T. Da Ros*

16:00-16:30 **Synthesis and photonic properties of some novel
INV 27 heterocyclic molecules**

*R. J. Twieg, S. Gu, M. He, F. You, A. Semyonov,
L. Sukhomlinova, G. G. Malliaras R. Fan; D. Culjkovic,
W. E. Moerner, D. Wright, K. D. Singer, R. G. Petschek,
V. Ostroverkhov, and O. Ostroverkhova*

16.30-19.00 Poster Session III (page 23)

20.00 Conference Dinner

Hotel Belvedere/Steigenberger

Thursday, March 16**Program and
Invited Talks**

8:30-10:30 Fundamental Investigations Chair: F. Kajzar8:30-9:00 **Polarization state sensitive processes in chiral molecular
INV 28 systems and gyrotropic materials**

F. Jonsson, M. Haddad, R. Frey, and C. Flytzanis

8:30-9:00 **Frequency conversion through parametric interaction
INV 29 and cascaded processes in a NPP crystal***Gian Piero Banfi, P. K. Datta, V. Degiorgio, D. Fortusini,
E. E. A. Shepherd, and J. N. Sherwood*9:30-10:00 **Quantum mechanical limits of the nonlinear optical
INV 30 susceptibility***Mark G. Kuzyk*10:00-10:30 **Molecular considerations for optimizing the second-order
INV 31 nonlinear optical response in chiral media***V. Ostroverkhov, O. Ostroverkhova, R.G. Petschek,
K.D. Singer, L. Sukhomlinova, R.J. Twieg, X.-Y. Wang,
and L.C. Chien*

10:30-11:00 Coffee/Tee

11:00-12:00 New Phenomena Chair: C. Flytzanis11:00-11:30 **THz wave sensors and their applications
INV 32***P. Y. Han, M. Tani, F. Pan, and X.-C. Zhang*11:30-12:00 **Growth and processing of DAST crystals and its
INV 33 application toward Tera-Hertz***Hiromasa Ito*

12:00-12:30 Closing

Monday, March 13

Poster Session I

Poster Session I, Monday 16:30-19:00

A

Novel Nonlinear Optical Phenomena and Applications

Foyer B1

- A 1 Spatial solitons in dye-doped nematic liquid crystals**
G. Abbate, J.F. Henninot, F. Derrien, and M. Warenghem
- A 2 Molecular engineering for optical limiting in the visible**
C. Andraud, R. Anémian, A. Collet, J.-F. Nicoud, B. Paci, P. A. Chollet, J.-M. Nunzi, N. Sanz, A. Ibanez, Y. Morel, and P. L. Baldeck
- A 3 Nonlinear optical properties of octupoles**
C. Andraud, T. Zabulon, R. Anémian, X. L. Lang, A. Collet, S. Brasselet, I. Ledoux-Rak, and J. Zyss
- A 4 Biphenyl derivatives for optical limiting in the visible**
R. Anémian, C. Andraud, A. Collet, B. Paci, J.M. Nunzi, Y. Morel, and P.L. Baldeck
- A 5 Theoretical investigation of the nonlinear circular dichroism in a liquid of chiral molecules**
F. Hache, M.C. Schanne-Klein, and H. Mesnil
- A 6 New properties of COANP-polyimide compound: optical limiting effect**
Natalie V. Kamanina, Lev N. Kaporskii, Alex Leyderman, and Alfonso Barrientos
- A 7 Optical limiting effect in polymer organic systems**
Natalie V. Kamanina and Lev N. Kaporskii
- A 8 In-situ observation of thermochromic behavior in merocyanine J-aggregate monolayer using the multipurpose nonlinear optical microscope**
Noritaka Kato, Kentaro Saito, and Yoshiaki Uesu
- A 9 Time-domain transmission spectroscopy with ultrashort THz pulses**
P. Kuzel, A. V. Pashkin, and J. Kroupa
- A 10 Nonlinear optical phenomena in turbid media of living tissue**
Asatur Lalayan
- A 11 Optically controlled reversible structuring of doped polymer thin film waveguides**
S. Lecomte, U. Gubler, M. Jäger, Ch. Bosshard, P. Günter, L. Gobbi, and F. Diederich
- A 12 Quantum and semi-classical modeling of NLO properties in organic systems**
Y. Luo, P. Norman, P. Macak, and H. Ågren

- A 13 Membrane imaging by simultaneous second-harmonic generation and two-photon microscopy**
L. Moreaux, O. Sandre, M. Blanchard-Desce, and J. Mertz
- A 14 Narrow-line laser emission from dendrimer doped polymer waveguides**
Akira Otomo, Shiyoshi Yokoyama, and Shinro Mashiko
- A 15 Nonlinear optical properties of push-pull stilbenes based on a strong carbocation acceptor moiety**
B. Paci, C. Schmidt, C. Fiorini, J.M. Nunzi, C. Arbez-Gindre, and C. G. Screttas
- A 16 All-optically poled polymer microcavities: enhancement of nonlinear optical effects**
R. Piron, E. Toussaere, D. Josse, S. Brasselet, and J. Zyss
- A 17 Characterization of two-photon absorption in symmetric conjugated systems with carbazol end groups**
J. Segal, Z. Kotler, M. Sigalov, A. Ben-Asuly, and V. Khodorkovsky
- A 18* Absolute values of third-order susceptibilities: Third-harmonic generation in the gas phase**
U. Gubler and Ch. Bosshard

B**Photorefractive Effects**

- B 2 High speed PVK-based photorefractive polymer composites**
M. A. Díaz-García, D. Wright, J. D. Casperson, B. Smith, E. Glazer, W. E. Moerner, L. I. Sukhomlinova, and R. J. Twieg
- B 3 Modelization and experimental characterization of angular redistribution in optical ordering processes in dye containing polymers**
Michel Dumont
- B 4 Photorefractive effects in DAST and other organic crystals**
S. Follonier, Ch. Bosshard, I. Biaggio, and P. Günter
- B 5 Formation of an anti-guide structure in a photorefractive polymer by a pump-light beam**
Takashi Fujihara, Kazutoshi Ozawa, Takafumi Sassa, Shinsuke Umegaki, Masaaki Yokoyama, Tatsuo Wada, and Hiroyuki Sasabe
- B 6 LC SLM based on fullerene doped polyimide**
Natalie V. Kamanina and Natalie A. Vasilenko
- B 7 Application of the phase-modulated beam technique for Bacteriorhodopsin Langmuir-Blodgett thin films characterization**
A. Kir'yanov, Yu. Barmenkov, A. N. Starodumov, N. Kozhevnikov, and H. Lemmetyinen
- B 8 Influence of rheological properties on photorefractive polymer electrooptic response**
L. Mager, J.-C. Ribierre, A. Fort, S. Méry, and J.-F. Nicoud,

Monday, March 13

Poster Session I

- B 9 Optical image correlators based on nematic liquid crystals**
A. Miniewicz, P. Sikorski, A. Januszko, S. Bartkiewicz, J. Parka, and F. Kajzar
- B 10 Influence of the chromophore ionization potential on the magnitude of photorefractive effects in PVK-based polymer composites**
David Van Steenwinckel, Eric Hendrickx, Andre Persoons, Kurt Van Den Broeck, and Celest Samyn
- B 11 Photorefractive effects in nematic liquid crystals under rigid boundary conditions**
G. Zhang, D. Haertle, G. Montemezzani, and P. Günter
- B 12 Surface mediated photorefractive mechanisms in liquid crystals**
J. Zhang, V. Ostroverkhov, K.D. Singer, V. Reshetnyak, and Yu. Reznikov
- B 13 Theory for self-enhancement of second-harmonic generation in a photorefractive polymer based on formation of an anti-guide structure**
Takafumi Sassa, Takashi Fujihara, Kazutoshi Ozawa, Shinsuke Umegaki, Masaaki Yokoyama, Tatsuo Wada, and Hiroyuki Sasabe

C Poled Polymers for SHG and Electro-Optic Devices

- C 1 3D- $\chi^{(2)}$ -analysis of high field poled polymers**
R. Blum, K. Pfeifer, G. Schoer, and M. Eich
- C 2 Polymer based electro-optic inline fiber modulator with 1 GHz bandwidth**
M. Bösch, M. Jäger, Ch. Bosshard, and P. Günter
- C 3 Photostability of highly nonlinear chromophores for electro-optic applications**
M. Bösch, C. Fischer, C. Cai, I. Liakatas, Ch. Bosshard, and P. Günter
- C 4 Towards stable hybrid materials for electro-optic modulation and photorefractive applications**
F. Chaput, K. Lahlil, J.-P. Boilot, M. Mladenova, L. Ventelon, M. Blanchard-Desce, B. Darracq, J. Reyes, and Y. Levy
- C 5 Polarization-insensitive polymer amplitude modulator**
A. Donval, E. Toussaere, R. Hierle, and J. Zyss
- C 6 Doped planar and channel sol-gel waveguides for nonlinear devices operating at telecommunications wavelengths**
Anne-Claire Le Duff, Michael Canva, Yves Lévy, Alain Brun, Frédéric Chaput, Jean-Pierre Boilot, Tomas Pliska, and George I. Stegeman
- C 7 Second harmonic generation in photo-bleached PU1-C4B film channel waveguides**
Suguru Horinouchi, Kwang-Sup Lee, Je-Hyun Lee, Primož Kerkoc, Junichi Yoshida, and Keisuke Sasaki

- C 8 New SCLCPs based on 3,3'-bipyridine chromophores for applications in NLO**
N. Lemaître, A.-J. Attias, I. Ledoux, and J. Zyss
- C 9 Photobleaching mechanism studies in side-chain polyimides**
I. Liakatas, M. Jäger, Ch. Bosshard, P. Günter, and T. Kaino
- C 10 Measurement of relative electrical resistivities for optimized poling of nonlinear optical polymeric waveguides**
Tomas Pliska, Vincent Ricci, Joachim Meier, Arne Eckau, Anne-Claire Le Duff, Michael Canva, George I. Stegeman, Paul Raymond, François Kajzar, and Kwok Pong Chan
- C 11 Second-harmonic generation at telecommunication wavelengths in polymeric waveguides**
Tomas Pliska, Wook-Rae Cho, Vincent Ricci, Joachim Meier, Anne-Claire Le Duff, Michael Canva, George I. Stegeman, Paul Raymond, and François Kajzar
- C 12 Relaxation behavior of the second-order nonlinear response of spin-coated polyphosphazenes films**
G. Rojo, G. Martín, F. Agulló-López, G. A. Carriedo, F. J. García-Alonso, and J. I. Fidalgo
- C 13 Synthesis and nonlinear optical properties of high glass transition polyimides and poly(maleimide-styrene)s**
Celest Samyn, Kurt Van den Broeck, Thierry Verbiest, and André Persoons
- C 14 Second harmonic generation in molecular-doped poly(ethylene oxide)/ *atactic*-poly(methyl methacrylate) blends**
A.V. Vannikov, A.D. Grishina, L.Ya. Pereshivko, and T.V. Krivenko
- C 15 Organized organic multilayer structures for frequency doubling and electro-optics**
V. Zauls, S. Schrader, B. Dietzel, B. Schultz, C. Fluerau, H. Motschmann, and G. Decher
- C 16* Ultra-efficient electro-optic polymer modulators for short-distance high-speed optical interconnects**
N.S. Lagali, D.J.W. Klunder, G.J. Gerritsma, and A. Driessen
- C 17 Second harmonic generation at near resonance of a functionalized pDR1A thin film oriented by corona poling**
V. Rodriguez and C. Sourisseau

Tuesday, March 14

Poster Session II

Poster Session II, Tuesday 16:30-19:00

D Nonlinear Optical Organic Crystals

Foyer B1

- D 1 Rationalising the SHG response in DCNP through anomalous atomic thermal motion and hydrogen-bonding**
J. M. Cole, C. C. Wilson, and J. A. K. Howard
- D 2 Preparing polydiacetylene single crystal thin films**
A. Feldner, T. Fehn, T. Vogtmann, and M. Schwoerer
- D 3 Linear optical properties of p-toluene sulfonate PTS**
Lars Friedrich, Tomás Pliska, Mingguo Liu, George I. Stegeman, Seung-Han Park, Andreas Feldner, Thomas Vogtmann, and Markus Schwoerer
- D 4 Molecular recognition concept in the growth of organic nonlinear optical crystals**
Hyung-ki Hong, Jaewoo Park, and Choon Sup Yoon
- D 5 SHG-active p-nitroaniline thin films grown by dip-coating**
Hiroyuki Kobayashi, Hiroyuki Okuyama, and Masahiro Kotani
- D 6 DAST thin film growth: seven exploratory methods**
S. Manetta, M. Ehrensperger, Ch. Bosshard, and P. Günter
- D 7 Observations of 180° polar domains in molecular crystals using phase-sensitive second harmonic microscopy**
P. Rechsteiner and J. Hulliger
- D 8 Organic nanocrystals in sol-gel glasses: a new type of nonlinear organic material**
I. Wang, P. L. Baldeck, N. Sanz, and A. Ibanez
- D 9* Phase-matching properties of (S)-3-methyl-5nitro-N-(1-phenylethyl)-2-pyridinamine**
M. Rini, G.P. Banfi, V. Degiorgio, and J.N. Sherwood

E Fundamental Studies

Foyer B1

- E 1 Anharmonicity effects in spectra of alcohols**
N.A. Atamas, A.M. Yaremko, L. A. Bulavin, V. E. Pogorelev, S. Berski, Zd. Latajka, H. Ratajczak, and J. Leszczynski
- E 2 Photosensitive media on the base of bacteriorhodopsin**
I. K. Bandrovskaya, Z. I. Batori-Tartzi, A. A. Grabar, O. I. Korposh, N. P. Frolova, and J. P. Sharkany
- E 3 Investigation of the third-order optical susceptibility of chromophores through electrooptic spectroscopy**
Brian K. Canfield, Robert J. Kruhlak, and Mark G. Kuzyk

- E 4 Second-harmonic generation in chiral smectic liquid crystals**
M. Copic, I. Drevensek Olenik, and M. Zgonik
- E 5 Modelling and characterisation of nonlinear materials for optical limiting. Mononuclear and binuclear platinum ethynyls**
Anders Eriksson, Cesar Lopes, Mikael Lindgren, Soren Svensson, Tim McKay, and Julianne Davy
- E 6 Electronic defects and conjugation length in a mesoscopic π system**
Luca Del Freato, Anna Painelli, Alberto Girlando, and Z.G. Soos
- E 7 Improved photogeneration efficiency of C_{60} sensitized arylamines**
E. Hendrickx, B. Kippelen, S. R. Marder, A. Persoons, and N. Peyghambarian
- E 8 Control of the first hyperpolarizability of functionalized mesostructures through cation binding**
Stephan Houbrechts, Tatsuo Wada, Hiroyuki Sasabe, and Yuji Kubo
- E 9 Ellipsometric polarization contour measurement for anisotropy in organic materials**
Minsoo Joo and Nakjoong Kim
- E 10 Determining the nature of excited states using an inhomogeneous-broadening analysis of third-order processes**
Robert J. Kruhlak, and Mark G. Kuzyk
- E 11 Application of the optical and positron spectroscopy to the study of structural transformations in milk fat and its simple purified fractions**
V. Y. Kudryavtsev, S. M. Yablochkov, S. P. Likhtorovich, M. M. Nishchenko, T. A. Rashevskaya, and I. S. Gulyi
- E 12 Strong field poling of multipolar structures: fundamentals and device implications**
Isabelle Ledoux, Irène Cazenobe, Sophie Brasselet, Eric Toussaere, and Joseph Zyss
- E 13 Second-order nonlinear optical response at the two-photon resonance in a two dimensional NLO molecule**
G. Meshulam, G. Berkovic, Z. Kotler, A. Ben-Asuly, R. Mazor, L. Shapiro, and V. Khodorkovsky
- E 14 Enhanced two-photon absorption in phenyl and fluorene oligomers**
Y. Morel, O. Stephan, P.L. Baldeck, and C. Andraud
- E 15 Response theory calculations of optical limiting processes**
P. Norman, Y. Luo, P. Cronstrand, P. Macak, and H. Ågren
- E 16 Theoretical study on the third-order nonlinear optical properties of thiophene derivatives**
Koji Ohta, Ryo Shikata, Kenji Kiyohara, Keiko Tawa, and Kenji Kamada

Tuesday, March 14**Poster Session II**

- E 17 Polarization recording and reconstruction in a photoinduced anisotropic medium**
Yoshiko Okada-Shudo
- E 18 Optical properties of composite materials**
Anatoliy O. Pinchuk
- E 19 Femtosecond spectroscopy of polymethine dyes in liquid and polymeric media**
Olga V. Przhonska, Mikhail V. Bondar, Yuriy L. Slominskyà, Raluca Negres, JinHong Lim, David J. Hagan, and Eric W. Van Stryland
- E 20 Microscopic and macroscopic third-order nonlinear optical properties of organobimetallic compounds**
Gema Rojo, José A. Campo, José V. Heras, Mercedes Cano, and Fernando Agulló-López
- E 21 Quantum chemical ab initio search for novel molecular technologies**
A. Tamulis, J. Tamuliene, M. L. Balevicius, J.-M. Nunzi, R. Abdreimova, M. Peruzzini, and A. Graja
- E 22 Understanding non-linearity: a toy model for push-pull chromophores**
Francesca Terenziani, Luca Del Freato, and Anna Painelli
- E 23 Establishing the optical parameters of thin films in the case of bacteriorhodopsin molecules**
Radu Todoran, Daniela Todoran, and J. Sharkany
- E 24 Second harmonic spectroscopy and SHG microscopic observation of J-aggregate domains in merocyanine at air-water interface**
Y. Uesu, N. Kato, and K. Saito
- E 25 Longitudinal and transverse dynamics of soliton excitations on a multileg ladder lattice**
Oleksiy O. Vakhnenko
- E 26 Orientation and non linear optical properties of DAN crystals on PTFE substrates**
R. Vallée, P. Damman, M. Dosière, E. Toussaere, and J. Zyss
- E 27 Holographic time of flight for the sub-nanosecond investigation of charge transport**
Marc Wintermantel, Ivan Biaggio, and P. Günter
- E 28 Influence of conjugation length on first hyperpolarizability of fluorescent hemicyanine (DAST) derivatives**
Kurt Wostyn, Geels Olbrechts, Koen Clays, André Persoons, Akira Watanabe, Kyoki Nogi, Xuan-Ming Duan, Shuji Okada, Hidetoshi Oikawa, H. Nakanishi, Henryk Vogel, David Beljonne, and Jean-Luc Brédas
- E 29* Preparation of the anisotropic thin films on an substrate for application to opto-electronic device**
T. Tano, T. Kodzasa, H. Ushijima, and T. Kamata

F Ultrafast Nonlinear Optics In Organics

Jakobshorn

- F 1 Influence of the molecular orientation on the stimulated emission and gain dynamics of phenylene vinylene oligomers**
T. Barisien, T.-A. Pham, L. Guidoni, M. Albrecht, and J.-Y. Bigot
- F 2 Femtosecond Z-scan measurement of the third order nonlinear optical coefficient of CuPc thin films**
H.J. Chang, S.H. Han, and J.W. Wu
- F 3 Measurement of relations between molecular structure and two-photon absorption spectra in fluorene dye compounds**
David J. Hagan, Kevin D. Belfield, Katherine J. Schafer, Raluca Negres, Wael Mourad, and Eric W. Van Stryland
- F 4 Influence of molecular orientation and arrangement to two-dimensionality of metallophthalocyanines**
Takashi Isoshima, Tatsuo Wada, and Hiroyuki Sasabe
- F 5 Optical and nonlinear optical properties of low-dimensional aggregates of the amphiphilic cyanine dyes**
R.V. Markov, P.A. Chubakov, A.I. Plekhanov, Z.M. Ivanova, N.A. Orlova, T.N. Gerasimova, V.V. Shelkovnikov, and J. Knoester
- F 6 Picosecond optical limiting action through a thin MMA-octupole copolymer layer near the total reflection state**
R. Mountasser, H. Maillotte, M. Ayadi, and F. Chérioux
- F 7 Resonant nonlinearities in an organic material: irradiance dependence**
R. Rangel-Rojo, H. Matsuda, H. Kasai, and H. Nakanishi
- F 8 Studies of third-order nonlinearity, nonlinear absorption, and excited state dynamics in tetra tolyl porphyrins using degenerate four-wave mixing and Z-scan**
S. Venugopal Rao, N.K.M. Naga Srinivas, Reji Philip, G. Ravindra Kumar, L. Giribabu, Bhaskar G. Maiya, and D. Narayana Rao
- F 9 Nonlinear optical properties of model polyenes studied with femtosecond Z-scan at 800 nm**
Anna Samoc, Marek Samoc, Barry Luther-Davies, Chantal Andraud, Thierry Brotin, and André Collet
- F 10 Thin films of a novel polydiacetylene for applications to all-optical signal processing**
S. Sottini, G. Margheri, E. Giorgetti, F. Gelli, A. Cravino, D. Comoretto, C. Cuniberti, C. Dell'Erba, I. Moggio, and G. Dellepiane

Wednesday, March 15

Poster Session III

Poster Session III, Wednesday 16:30-19:00

G

Fibers and Waveguides

Foyer B1

- G 1 Drift correction in organic intensity modulators**
P. Labbé, A. Clouqueur, R. Hierle, E. Toussaere, and J. Zyss
- G 2 Gaussian profile Bragg gratings in polydiacetylene waveguides: characterization and application in integrated optics**
G. Marowsky and M. A. Bader
- G 3 Compression of soliton-like pulses in Kerr-type planar waveguides**
Monika E. Pietrzyk
- G 4 Functionalized polymers for photonic applications**
Claire Pitois, Anders Hult, Dorothea Wiesmann, Åsa Claesson, and Mikael Lindgren
- G 6 Three dimensional optical fiber simulation**
D. M. Sullivan
- G 7 Channel waveguide fabrication of the organic nonlinear optical crystal DAST by using oxygen RIE**
K. Takayama, M. Yoshida, H. -H. Deng, K. Komatsu, and T. Kaino

H

Novel Molecular Designs and Synthesis

Foyer B1

- H 1 New disubstituted organic compounds with enhanced non-resonant nonlinear refraction in the picosecond range**
André-Jean Attias, Frédéric Chérioux, and Hervé Maillotte
- H 2 Tuning of the mesogenic, electronic, and optical properties of new conjugated 3,3'-bipyridine derivatives**
A.-J. Attias, B. Bloch, and C. Cavalli
- H 3 Synthesis of a new nonlinear optical chromophore based on a novel N-aryl carbazole derivative**
Amos Ben-Asuly, Lev Shapiro, Arkady Ellern, and Vladimir Khodorkovsky
- H 4 Molecular engineering of push-pull chromophores for nonlinear optics**
M. Blanchard-Desce, V. Alain, S. Rédoglia, M. Barzoukas, R. Wortmann, S. Lebus, K. Lukaszuk, P. Günter, C. Bosshard, and U. Gubler
- H 5 Tetra(4-methoxyphenyl)phosphonium iodide : a new NLO crystal built-up with tetrahedral-like octupolar chromophores**
Cyril Bourgoigne, Patrick Masson, Jean-François Nicoud, Yvette Le Fur, Patrick Juen, and René Masse

- H 6 Nonlinear optical thin films based on strong head-to-tail hydrogen bonding grown by oblique incidence organic molecular beam epitaxy**
C. Cai, M. Kiy, A. Taponnier, R. Ono, I. Biaggio, Ch. Bosshard and P. Günter
- H 7 New octupolar star-shaped molecules with non-resonant quadratic optical nonlinearities**
Frédéric Chérioux, Pierre Audebert, Sophie Brasselet, and Joseph Zyss
- H 8 Synthesis and characterisation of an octupolar polymer and new molecular octupoles with off-resonant refractive index**
Frédéric Chérioux, Hervé Maillotte, Joseph Zyss, and Pierre Audebert
- H 9 Structure-property relations in nonlinear optical molecular wires and planar sheets**
U. Gubler, Ch. Bosshard, R. Martin, R. Tykwinski, F. Diederich, and P. Günter
- H 10 Second-order nonlinear optical and photorefractive properties of amorphous calix[4]arene containing carbazole derivatives**
Atsushi Gunji, Hiromi Kimura-Suda, Takafumi Sassa, Tatsuo Wada, and Hiroyuki Sasabe
- H 11 Linear and nonlinear optical properties of hypervalent iodine derivatives**
K. Kamada, K. Ohta, R. R. Tykwinski, and D. Bykowski
- H 12 Nonlinear optical properties of the Langmuir-Blodgett films of an intermolecular charge transfer complex**
J. Kawamata, T. Akutagawa, T. Hasegawa, K. Inoue, and T. Nakamura
- H 13 Structural analyses of clay-metal complex hybrid films by observing optical second harmonic generation**
Jun Kawamata, Kuon Inoue, Yuichirou Ogata, and Akihiko Yamagishi
- H 14 Dithienothiophene-based organic molecules with large two-photon absorption cross sections**
Kwang-Sup Lee, Jong Hyoup Lee, Oh-Kil Kim, Han Young Woo, and Kie-Soo Kim
- H 16 New photoisomerizable organometallic chromophores as precursors of optically poled materials**
Olivier Maury, Hubert Le Bozec, Isabelle Ledoux, Michel Dumont, and Joseph Zyss
- H 17 Synthesis and characterization of a series of NLO chromophores based on 1,3-indandione derivatives**
Royi Mazor, Lev Shapiro, Arkady Ellern, Vladimir Khodorkovsky, Zvi Kotler, Garry Berkovic, and Guilía Meshulam

- H 18 Nonlinear optical properties of cyanines and oligoenes: influence of bond-length alternation, substituents, chain length**
D. Scherer, A. Feldner, R. Dörfler, M. Welscher, T. Vogtmann, M. Schwoerer, U. Lawrentz, H.-H. Johannes, and W. Grahn
- H 19 MO calculations of dyes for the solid state absorption spectra**
Hisayoshi Shiozaki, Yoshiaki Sakurai, Satoru Nakao, and Masaki Kimoto
- H 20 Novel aminopyrazine fluorescent dyes for NLO materials; their solid state spectra and crystal structures**
Kazuko Shirai and Masaru Matsuoka
- H 21 Novel carbazole derivatives for two-photon absorption applications**
Mark Sigalov, Amos Ben-Asuly, Lev Shapiro, and Vladimir Khodorkovsky
- H 22 Multifunctional TCNQ adducts**
Marek Szablewski, Mosurkal Ravi, Nancy-Ann Hackman, Graham H Cross, and David Bloor
- H 23 Organic / inorganic quantum confinement structures based on lead halide perovskites**
Yuko Tabuchi, Keisuke Asai, Masahiro Rikukawa, Kohei Sanui, and Kenkichi Ishigure
- H 24 Novel organic-inorganic quantum confinement structure (VII) Structural characterization and optical properties for low dimensional compounds with PbX_6 octahedra**
Kenjiro Teshima, Satoshi Kano, Mitsuyasu Kawahara, Masahiro Rikukawa, and Kohei Sanui
- H 25 Novel organic-inorganic quantum confinement structure (VIII) Structural characterization for self-organized compounds with quaterary ammonium salt**
Kenjiro Teshima, Satoshi Kano, Masahiro Rikukawa, and Kohei Sanui
- H 26 New quadrupolar fluorophores with high two-photon excited fluorescence**
L. Ventelon, L. Moreaux, J. Mertz, and M. Blanchard-Desce
- H 27 Intermolecular coupling enhancement of the molecular hyperpolarizability in multichromophoric dipolar dendrimers**
Shiyoshi Yokoyama, Tatsuo Nakahama, Akira Otomo, and Shinro Mashiko
- H 28 Octupolar engineering for nonlinear optics**
J. Zyss and I. Ledoux
- H 29 Nonlinear third-order optical susceptibilities of some metallo-complexes compounds**
B. Sahraoui, J.A. Weinstein, M. Ya. Mel'nikov, N.N. Zheligovskaya, and X. Nguyen Phu

H 30* New quinoline-based thermally stable polymers

S. Concilio, N. Tirelli, P. Pfister, and U.W. Suter

Organic Light Emitting Materials

- I 2 Performance of organic light emitting devices based 8-hydroxyquinolato boron emitters**
Marie D'lorio, Yeh Tao, Suning Wang, Qing-guo Wu, and James Lavigne
- I 3 Hetero-layer light-emitting devices based on PPQ/PPV/TPQ films**
P. Imperia, S. Schrader, M.B. Casu, M. Jandke, and P. Strohrriegl
- I 4 Ultra high vacuum reveals interface-dependent charge-injection properties of organic light emitting diodes, and the effects of exposure to impurity gases**
M. Kiy, I. Gamboni, I. Biaggio, and P. Günter
- I 5 Blue organic light-emitting diode based on dipyrvole3**
WeiLing Guo, E.H. Li Chi-Ming Che, Yi-Zhao, and S.Y.Liu
- I 6 Organic DFB-lasers with mode emission tuneability by dynamic and permanent photoinduced gratings**
G. Kranzelbinder, E. Toussaere, R. Mathevet, D. Josse, and J. Zyss
- I 7 Influence of hole transport materials on the properties of organic LED**
Zugang Liu, Jorge Soares, and Estela Peireira
- I 8 Probing space charge distributions in polymer LEDs by means of an electro-optic technique**
F. Michelotti, S. Bussi, M. Bertolotti, and Z. Bao
- I 9 Impedance spectroscopy of Alq₃ based- organic light emitting diodes measured in ultra high vacuum and air**
Rudi Ono, Paolo Losio, Michael Kiy, Axelle Tapponnier, Iris Gamboni, Ivan Biaggio, and Peter Günter
- I 10 A comparative study of photoluminescence spectra of chromophores and semiconducting polymer films**
J. Shin, H. Choi, J. Ro, H. Kim, J. Noh, S. Lee, H. Suh, C. Ha, K. Lee, and M. Cha
- I 11 Amplification of raman scattering in an oriented poly(p-phenylenevinylene) film**
Seungwoo Shin, Jeongmi Shin, Hongki Kim, Jung Hoon Ro, Heayoung Choi, Kwanghee Lee, and Myoungsik Cha
- I 12 Blue-green light-emitting electrochemical cells based on a copolymer derived from fluorene**
O. Stéphan, V. Collomb, and J.-C. Vial

- I 13 Luminescent and electronic properties of end-substituted oligo(phenylene vinylene)s**
Y. Tao, M. D'lorio, A. Donat-Bouillud, J. Lam, M.S. Wong, and Z.H. Li
- I 14 Transient photocurrent investigation of charge transport in electroluminescent organic thin films**
A. Tapponnier, I. Biaggio, and P. Günter
- I 15* Injection and charge transport phenomena in polymer multilayer systems for electronic applications**
A. Wedel and S. Janietz

Invited Talks

Advanced Telecommunication Components and Materials Research in Europe

Hans Melchior

**Swiss Federal Institute of Technology Zurich
CH-8093 Zürich, Switzerland**

Phone: +41 1 633 2101, Fax: +41 1 633 1109, E-mail: h.melchior@iqe.phys.ethz.ch

High-capacity telecommunications expands at a rapid pace, driven by insatiable market demands and enabled by revolutionary materials- and component technology advances. Ongoing materials and components developments include glass and plastic for low-loss, wide-band-widths fibers, planar and fiber based optical filters, gratings and passive optical components optical amplifiers. Inorganic and organic materials for optical modulators and switches. Three-five compound semiconductor lasers, light-emission diodes, photodetectors, modulators, switches, filters and entire opto-electronic integrated circuits. Challenges ahead include materials for optical amplifiers throughout the 0.8 to 1.8 micrometer wavelengths range, wavelength-division multiplex filters, switches and dispersion control components, all-optical, high-speed signal processing components, large, low-loss, low-crosstalk space switches as well as affordable, mass manufacturable opto-electronics components.

Invited Talks

Optics and Applications of Photo-Aligned Liquid Crystalline Surfaces

Martin Schadt

ROLIC Research Ltd, 4123 Allschwil, Switzerland

Photo-alignment and photo-patterning of monomeric and polymeric liquid crystals renders a plethora of new birefringent optical elements and improved LCDs possible. Linearly photo-polymerization (LPP) is shown to render photo-alignment of multi-domain VAN-LCDs with very broad field of view feasible. Moreover, novel LPP-aligned thin-film stacks of polymeric liquid crystals with controllable spatial uniaxiality, non-absorbing, bright interference R, G, B color filters, photo-structured polarizers, positive and negative optical retarders and wide-view films are presented.

Without external aligning forces the long axes of liquid crystal (LC)-molecules align spontaneously only over microscopic domains. Since LC-alignment is a prerequisite for rendering any liquid crystal display (LCD) operable, functional display boundaries are essential. Conventionally, display alignment is achieved by sandwiching a liquid crystal layer between two brushed polyimide coated display substrates. LC-molecules align parallel at the discrete, uniaxial brushing traces, whereas the aligning information between traces is communicated via the long range elastic coupling forces of liquid crystals. With increasing distance between traces and/or decreasing aligning strength, thermal LC-director fluctuations reduce display contrast and in the extreme –under thermal or optical stress – lead to display failure.

Uniaxiality of LC-alignment at the boundaries of field-effect LCDs – such as in twisted nematic (TN)-, supertwisted nematic (STN)-, or vertically aligned nematic (VAN)-LCDs – is only one of two essential prerequisites for proper display operation. The other is the generation of display-specific bias tilt angles $0^\circ < \Theta < 90^\circ$ between substrate(s) and LC-director(s) $\hat{n}(\Theta, \varphi)$ at the LCD boundaries; φ = azimuthal angle. Without defined bias tilt, director dislocations occur and display appearance deteriorates [1]. LC-alignment must be thermally and optically stable.

There are a number of drawbacks associated with brushing LCD substrates, such as: the generation of dust and electrostatic charges, reduced contrast of weakly brushed micro-displays due to thermal LC-director fluctuations between brushing traces, or defects which become visible when projected. Moreover, multi-domain LC-alignment to improve the field of view of displays requires alignment patterning within individual pixels which cannot be achieved by brushing.

In the 1980's first attempts were made to induce molecular reorientation in guest host materials by exposing LC-polymers, comprising mainly azo guest molecules, to linearly polarized light [2-4]. In the early 1990's two research groups showed that it is possible to align monomeric liquid crystals at surfaces not by mechanical means but optically [5,6]. Two fundamentally different aligning strategies were pursued, namely (i) *single-molecular* processes such as photo-alignment in azo-type guest host systems [5] which reorients LCs through optically induced cis-trans isomerization by linear polarized light, or by directional bleaching of polyimide layers by linear polarized light [7] versus (ii) *bi-molecular* photo-alignment by linear photo-polymerization (LPP) which generates alignment *and simultaneously* cross-links

Invited Talks

pairs of pre-polymer molecules by linear polarized UV-light, thus fixing the alignment in-situ [6,8]. The LPP-process is inherently photo-stable [8] and capable to simultaneously align *and* induce tilt angles in monomeric as well as in polymeric liquid crystals [9,10]. The following photo-aligned devices and novel optical thin-film elements are based on the LPP technology developed in our labs.

Discussed are the broadening effect of LPP photo-patterned alignment on the field of view of multi-domain LCDs, such as twisted nematic (TN)- and vertically aligned nematic (VAN)-LCDs [8,10]. Moreover, LPP photo-aligned thin-film stacks of liquid crystal polymers (LCPs) with controllable spatial uniaxiality on *single* substrates are shown to render virtually any optical retarder configuration feasible, namely planar, tilted or homeotropic retarders with positive as well as negative birefringence. This enables the realization of such diverse optical thin-film devices as wide-view films, optical compensation films or interference color filters on plastic substrates for any type of LCD by a single technology [11-15].

References

- [1] D. W. Berreman, Phys. Rev. Lett. **28**, 1683 (1972)
- [2] M. Eich and J. H. Wendorff, Macromol. Chem. Rapid Commun. **8**, 467 (1987)
- [3] T. Todorov, L. Nikolova and N. Tomova, Appl. Optics **23**, 4309 (1984)
- [4] K. Ichimura, Y. Suzuki, T. Seki et al, Langmuir **4**, 1214 (1988)
- [5] W. M. Gibbons, P. J. Shannon, S. T. Sun et al, Nature **351**, 49 (1991)
- [6] M. Schadt, K. Schmitt, V. Kozenkov et al, Jpn. J. Appl. Phys. **31**, 2155 (1992)
- [7] J. Chen, D. L. Johnson, P. J. Bos et al, Phys. Rev. **54E**, 54 (1996)
- [8] M. Schadt and H. Seiberle, Digest **SID97**, 367 (1997)
- [9] M. Schadt, H. Seiberle and A. Schuster, Nature **381**, 212 (1996)
- [10] M. Schadt, H. Seiberle, A. Schuster et al, Jpn. J. Appl. Phys. **34**, 3240 (1995)
- [11] J. Chen, K. C. Chang, J. DelPico et al, Digest **SID99**, 98 (1999)
- [12] C. Chiulli, J. DelPico, W. Vetterling et al, Digest **SID99**, 1054 (1999)
- [13] H. Seiberle and M. Schadt, SID Digest **ASIA Display98**, 193 (1998)
- [14] H. Seiberle, K. Schmitt and M. Schadt, SID Digest **Eurodisplay'99**, 121 (1999)
- [15] K. Schmitt, J. Fünfschilling, Z. Cherkaoui and M. Schadt, SID Digest **Eurodisplay'99**, 437 (1999)

Nonlinear Optical Spectroscopic Studies of Polymer Surfaces and Interfaces

Y.R. Shen

Physics Department, University of California, Berkeley CA 94720-USA
shenyr@socrates.berkeley.edu

Sum-frequency vibrational spectroscopy has been developed into a powerful and highly versatile probe for surface and interface studies. Its possible application to study surface properties of bulk materials in real environment is particularly attractive because few other techniques can provide similar information. Polymeric material is an important example. Although the success or failure of polymeric materials in many applications often depends on their surface properties, the latter have not yet been well studied.

We have demonstrated that sum-frequency vibrational spectroscopy can indeed be used to probe surface composition and structure of a polymer surface. We show that the vibrational spectra obtained have little contribution from the bulk. We have applied the spectroscopic technique to a number of different polymers, but we discuss here only a few selected examples that are of more general interest. (1) We find that surface and bulk compositions can be very different for polymer mixtures. Small amounts of additive in a polymer can precipitate onto the surface and dominate the surface properties. (2) We observe that surface structure of a polymer can change in response to change of the environment. This happens by rearrangement of various atomic groups at the surface. (3) We show that rubbing of a polymer surface can effectively align polymer chains at the surface. By measuring the surface vibrational spectrum versus the sample azimuth position, orientational distributions of selected atomic groups on the surface polymer chains, and hence that of the polymer chains themselves can be deduced.

This work was supported by the U.S. Department of Energy and the U.S. National Science Foundation.

Invited Talks

Production of High Bandwidth Polymeric Electro-optic Modulators with V_{π} Voltages of less than 1 Volt

Larry R. Dalton

*Department of Chemistry, University of Washington
Seattle, Washington 98195-1700 U.S.A.*

The roles played by spatially anisotropic intermolecular electrostatic interactions, chromophore shape, host dielectric constant, and poling field strength in defining maximum achievable electro-optic activity for electrically poled chromophore/polymer materials are investigated by equilibrium and Monte-Carlo quantum statistical mechanical calculations. Even simple Hamiltonians reproduce critical qualitative features, such as the existence of a maximum in plots of electro-optic activity versus chromophore number density in a polymer matrix. Comparison of theoretical results for various methods provides a useful check on the validity of approximations employed with individual methods. The most significant conclusion to derive from a comparison of experimental and theoretical results is the dependence of maximum achievable electro-optic activity upon chromophore shape. Theoretical calculations suggest a new paradigm for the design of optimum electro-optic chromophores; realization of the desired shapes may be facilitated by dendritic synthetic approaches. In the presence of intermolecular electrostatic interactions, the dependence of electro-optic activity upon material dielectric permittivity and electric poling field strength is more complex than in the absence of such interactions. Of particular interest are conditions that lead to second order phase transitions to lattices containing centrally (antiferroelectrically) ordered chromophore domains. Such phase transitions can lead to further complications in the attempted preparation of device quality materials but can be effectively avoided by utilization of theoretically derived phase diagrams.

Putative advantages of electro-optic devices fabricated from second-order nonlinear optical chromophores-incorporated polymeric materials include low drive voltage (V_{π}) requirements, large (GHz) bandwidths, and ease of integration with semiconductor electronics, diode lasers, and silica transmission fibers. Because of the low and relatively frequency-independent dielectric constants and refractive indices of organic materials, large devices bandwidths have been easily realized. Devices with bandwidths in excess of 100 GHz are now routinely fabricated. In like manner, dramatic progress has been made in the 3-D integration of active and passive optical circuitry and in the integration of electro-optic circuitry with very large scale integration (VLSI) semiconductor electronics. A number of novel new devices, such as voltage controlled radiofrequency phase shifters, exploit the ability to achieve sophisticated integration. Very low crosstalk is observed for densely packaged modulators. Robust modulator circuits can be fabricated particularly when attention is given to the details of materials processing (spin casting, poling, and lattice hardening). In short, the ease of processing of polymeric materials into sophisticated 3-D circuits has been proven to be a significant advantage for the use of such materials.

Although a number of chromophores have been synthesized with large molecular hyperpolarizabilities, beta, and dipole moments, μ , long anticipated large macroscopic electro-optic coefficients have only recently been realized for poled polymer materials. Fortunately, the advent of modified CLD-type chromophores has permitted realization of devices with digital level drive voltage requirements. Typical results for CLD-1 covalently incorporated into 3-D crosslinked polyurethane materials is shown in table I. Even

Invited Talks

lower drive voltages have recently been observed by researcher at TACAN Corporation employing CLD-1 in PMMA or amorphous poly(carbonate), APC, and a push-pull Mach Zehnder modulator configuration. They observed an average drive voltage of 0.8 volts for six 3-cm interaction length modulators tested and an average drive voltage of 1.08 volts for six 2-cm interaction length modulators. A poling voltage of 500 volts was used to prepare the 3-cm modulators and a poling voltage of 750 volts was used in the preparation of the 2-cm modulators. The preceding results, achieved for the CLD-1 chromophore incorporated in various polymer lattices, suggest that the putative high electro-optic activity of organic materials can indeed be realized. It is important for us to understand the process by which these improved electro-optic materials were produced and to understand what can be expected in the future. To do this, we must understand the detailed dependence of electro-optic activity upon chromophore concentration (number density) in the polymer lattice, upon chromophore shape, upon chromophore dipole moment (electrostatic interactions), upon polymer dielectric permittivity, upon poling field strength, etc. Here, we attempt to elucidate structure/function relationships that define maximum achievable electro-optic activity by considering both equilibrium and Monte Carlo (molecular dynamics) statistical mechanical calculations.

Table I. Performance Characteristics of CLD-PU Modulators

$V_{\pi} = 2.5 \text{ V @ } 1300 \text{ nm ; } 3.7 \text{ V @ } 1550 \text{ nm}$

Frequency to $\sim 60 \text{ GHz}$; Temperature Maximum $\sim 90^{\circ}\text{C}$

Insertion Loss 5 - 6 dB; Extinction ratio 25-30 dB

Organic-Inorganic Hybrid NLO Materials with Different Chromophore Bonding Directions

Kwang-Sup Lee, Tae-Dong Kim

Department of Polymer Science & Engineering, Hannam University, Taejon 306-791, Korea

Yu Hong Min, Choon Sup Yoon

Department of Physics, KAIST, Taejon 305-701, Korea

Organic-inorganic hybrid materials, which possess large second-order nonlinear optical (NLO) effect, were prepared and their linear and nonlinear optical properties, thermal stabilities, and poling efficiency were investigated. The measured values of NLO coefficient strongly depend on poling conditions such as a poling temperature, a poling time and a heating rate. The resulting films heated at 200°C exhibited $d_{33} = 50\text{--}58 \text{ pm V}^{-1}$ in maker-fringe measurement. It was found that the thermal stabilities of the films were greatly enhanced as a poling time increased and a poling temperature became higher.

Second-order NLO materials are currently of interest to a large number of research groups as they can be used for a number of photonic applications, for example, doubled-frequency laser sources, electro-optic modulation, optical signal processing, optical interconnects, etc [1].

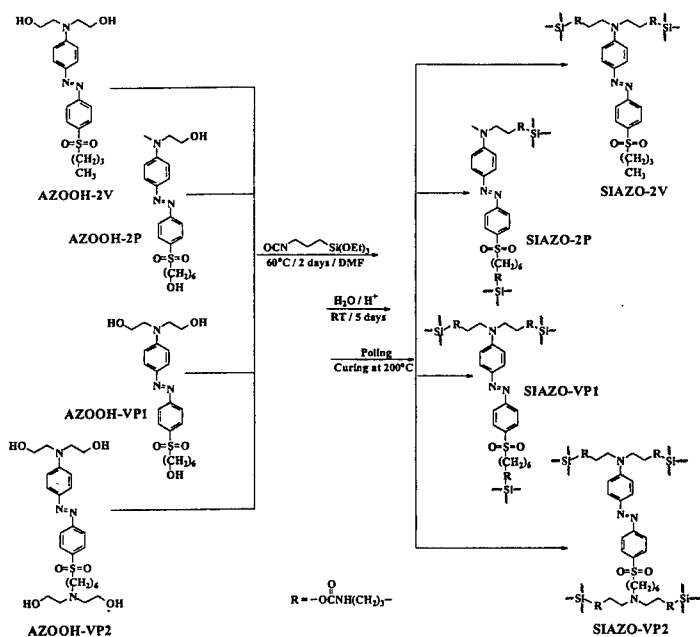
Most NLO chromophores have generally not been found to be good photonic media due to thermal relaxation, large absorption and high optical losses. Inorganic glasses, however, are excellent photonic media because of their high optical quality and extremely low optical losses. Therefore, combining inorganic glass and organic photo-functional molecules is one of the best ways to develop optical materials with large optical nonlinearity and low losses. In addition to this, the use of highly cross-linked silica matrix can be remarkably reduced the thermal relaxation of the molecular dipoles [2-3].

Taking advantages of these, we have recently developed three different azosulfone dye/silica glass hybrid materials. They are characterized as vertical (V), parallel (P), and vertical-parallel (VP) systems, depending on bonding direction between the chromophores and the silica matrix (Scheme 1).

The thermal properties of the organic-inorganic hybrid materials were examined by differential scanning calorimeter (DSC) and thermogravimetric analysis (TGA). We could not observe clearly the glass transition temperature of SIAZO-2V, SIAZO-2P, and SIAZO-VP1. The TGA data under a nitrogen atmosphere exhibits the initial decomposition temperature at 223, 235, and 252°C for SIAZO-2V, SIAZO-2P, and SIAZO-VP1, respectively. The order parameters ($\phi = 1 - A_1/A_0$, A_0 and A_1 are the absorbances of the film before and after corona poling) of chromophores in these hybrid films are used to characterize the poling efficiency. Under the conditions of a 5 kV poling voltage applied to the corona needle at 200°C for 1 hr, the order parameter values for SIAZO-2V, SIAZO-2P, and SIAZO-VP1 were estimated to be 0.31, 0.25, and 0.24, respectively. The second-order NLO properties of the poled films were characterized by second harmonic generation (SHG) at 1064 nm fundamental wavelength, with a Y-cut quartz crystal ($d_{11} = 0.5 \text{ pm V}^{-1}$) as the reference. We obtained d_{33} values of 58, 50, and 53 pm V^{-1} for SIAZO-2V, SIAZO-2P, and SIAZO-VP1, respectively. The SHG coefficient (d_{33}) of SIAZO-2V calculated from the angular dependence of the SHG intensity was about 58-60 pm V^{-1} for 1 hr and 5 hrs at 160°C and for 1 hr at 200°C. However d_{33} of the SIAZO-2V poled for 5 hrs at 200°C reduced to 15.4 pm V^{-1} due to thermal breaking of the azo-chromophore.

To the thermal stability studies, temperature dependent SHG experiments were carried

Scheme 1. Synthetic routes for organic-inorganic hybrid materials



out *in-situ* by monitoring the SHG signal while heating at a rate of $2^{\circ}\text{C min}^{-1}$. SIAZO-VP1, which has higher cross-linking sites, showed better stability than SIAZO-2V and SIAZO-2P. Fig. 1 shows that the SHG signal remained stable for SIAZO-VP1 until reaching 90°C , where the SHG signal starts to decay rapidly. It completely disappeared as the temperature went above 200°C . These results are understandable because the thermal relaxation of oriented dipoles is related to the free volume in the silica bond. In addition, it was found that the thermal stabilities of the films were greatly enhanced as a poling time increased and a poling temperature became higher.

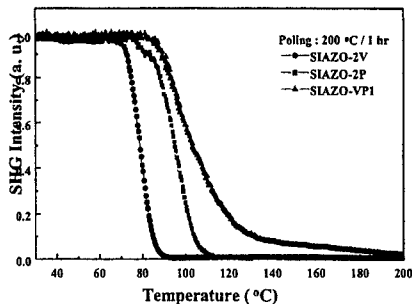


Fig. 1. Thermal stability of NLO activities for three organic-inorganic hybrids.

References

[1] D. M. Burland, R. D. Miller, C. A. Walsh, *Chem. Rev.*, **94**, 31 (1994).
 [2] Y. H. Min, K.-S. Lee, C. S. Yoon, *J. Mater. Chem.*, **8**, 1225 (1998).
 [3] K.-S. Lee, S.-W. Choi, H. Y. Woo, K.-J. Moon, H.-K. Shim, M.-Y. Jeong, T.-K. Lim, *J. Opt. Soc. Am. B*, **15**, 393 (1998).

Refractive index volume grating fabrication by photo-bleaching of azo-dye functionalized polymer waveguides

Toshikuni Kaino, Tomoaki Shibata, and Toshiaki Hattori

Laboratory of Optical Materials Chemistry

Institute for Chemical Reaction Science

Tohoku University

2-2-1 Katahira, Aoba-ku, Sendai, 980-8577 Japan

A polymer waveguide grating was fabricated by combining following two simple methods. One was the waveguide fabrication by using groove-shaped epoxy resin substrate where the grooves are shaped by dicing saw. The other was the grating formation on the waveguide by photobleaching technique in which periodical refractive index change was induced by two-beam interference pattern. Using the methods, polymer waveguide grating of 10.2% output coupling efficiency was successfully fabricated.

Large-capacity optical communications systems based on time division multiplexing (TDM) or wavelength division multiplexing (WDM) require wavelength-filtering devices for the selection of ultra fast pulses and for optical switching. Waveguide grating will be one of the promising devices for that purpose. In past a few years, a variety of polymer waveguide gratings have been proposed. The advantage of using polymeric materials is that they are easy to fabricate waveguides, low in cost, and possible to create many optical functions by adding organic dyes. A polymer containing azo dye is one of the candidates for holographic grating materials through the photochemical reaction of azo dye. With large laser irradiation energy, irreversible photobleaching occurs where π -conjugated system in azo compounds is broken and the dye becomes to be colorless. As a result, refractive index of the polymer changes permanently.

Poly (methyl methacrylate) (PMMA) was used as a host polymer of waveguide core. A mono-azo-dye, Disperse Red 1 (DR1 for short), was doped into the PMMA or bis-azo-dye, 3RDCVXY, was attached to the polymer as a side-chain of it (hereafter named as 3RDCVXY polymer) to functionalize the polymer waveguide. PMMA, DR1, and 3RDCVXY polymer could be dissolved in chlorobenzene. In this study, all sample films were made by spin-coating from the azo-dye chlorobenzene solution.

The waveguide was fabricated as follows. UV-curable epoxy resin was spin-coated on a silicon wafer as a lower cladding, and this layer was cured by UV light irradiation. The thickness of the lower cladding is approximately 90 μm . Onto this cladding layer, grooves, 41 μm in width and 44 μm in height, were shaped by a dicing saw. In order to make core structure, PMMA containing 10 wt% DR1 (DR1(10 wt%)/PMMA for short) solution was spin-coated on the groove-shaped substrate. Then, an epoxy resin that is equal composition with that of the lower cladding was spin-coated as an over cladding layer with about 80 μm in thick.

To evaluate the optical propagation loss of the fabricated waveguide, a cut-back method was used.

Invited Talks

For the measurement, endfaces were cut and polished by the dicing saw. Light from 1.3 μm laser diode was coupled to optical fiber and the fiber was butt-jointed to the waveguide endface. The waveguide length was varied from 0.7 cm to 1.6cm and the loss was estimated to be 1.3 dB/cm.

Refractive index grating was formed into the DR1(10 wt %)/PMMA film or 3RDCVXY polymer film on glass substrate by simple two-beam interference. Grating formation process was monitored by a 0.5 mW He-Ne laser at 633 nm measuring the +1 order diffracted light power. Diffraction efficiency of the grating with a 1.6 μm period was shown in Fig. 1. The efficiency saturated after 200 min. irradiation and reached 36%. The thermal stability of the refractive index grating was examined by keeping it at 120 degree, higher temperature than that of glass transition of the polymer. Though keeping in a high temperature for 240 h, no change of diffraction efficiency was observed. From the results, it was evident that photobleaching by two-beam interference could be used to form thermally stable refractive index grating.

By using the same procedure, refractive index grating was inscribed into the fabricated buried waveguide mentioned above. Irradiation intensity, time and grating period were the same as that for the thin film grating fabrication. The optical characteristics of the fabricated waveguide grating were investigated by the experimental set-up shown in Fig. 2(a). To detect output-coupled light via grating, 1.3 μm laser diode light was coupled into the waveguide via optical fiber. By rotating a photodiode, output-coupled light intensity and its angle were detected. As shown in Fig. 2(b), the output-coupled light was detected around 70 degree. The output coupling efficiency was 10.2% that was defined as the intensity ratio of light output from the grating to light from the endface.

In conclusion, we have succeeded in fabricating polymer waveguide grating by combination of two simple methods, i.e., to use a groove-shaped substrate for fabricating the waveguide and a photobleaching technique for the grating fabrication. This simple fabrication method will be widely applicable to a variety polymer system in which refractive index change can be induced by photobleaching.

We would like to thank Dr. S. Tomaru of NTT Photonics Laboratories for his cooperation in fabrication groove-shaped substrates.

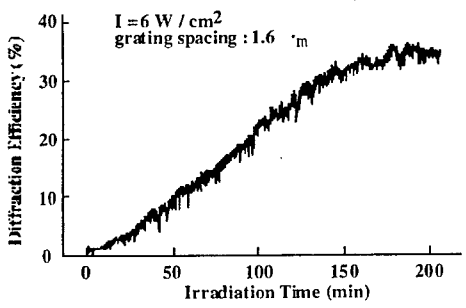


Figure 1 Diffraction efficiency dependence on irradiation time coupling of a 3RDCVXY polymer film

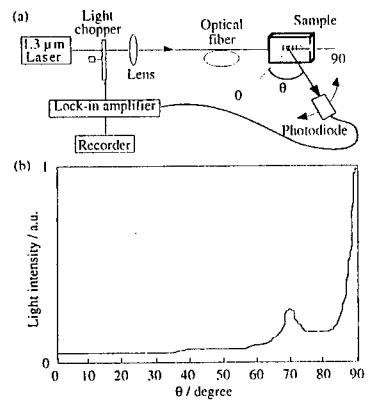


Figure 2 (a)Experimental set-up for output characteristics and (b) its result

Memory Applications of Novel Organic Materials

D. Haarer
Bayer AG
ZF-FP, Q 18
51368 Leverkusen

Polymers have always played a dominating role as substrate materials for optical data storage and polycarbonate (PC) has been the preferred polymeric material due to its unique optical and mechanical properties. For optical write – once applications organic dye layers as functional layers on PC substrate materials are rapidly penetrating the market for optical storage media. Parallel to these market developments more advanced materials are being synthesized for future applications.

In our presentation we will discuss more advanced optical schemes for possible future applications such CD-like discs with rewritable organic functional layers implementing gray-scale (multiplexing) capabilities and materials suitable for holographic applications (PAP - Photo Addressable Polymer materials). For the holographic applications one would have to abandon the CD-format and configure new reading and writing schemes. We will also discuss in the outlook complementary optical storage systems based on photorefractive materials in which optical and opto-electric properties of a completely new class of storage materials have to be balanced in a rather sophisticated fashion.

Invited Talks

High Density, High Performance Data Storage Via Volume Holography

William L. Wilson, K. Curtis, M. Tackitt, A. Hill, T. Richardson, A. Hale, L. Dhar, C. Boyd, and M. Schilling, and A. Harris
Bell Laboratories, Lucent Technologies
600 Mountain Avenue, Murray Hill, NJ 07974

It has long been known that volume holography allows multiple *pages* of data to be stored in the same volume, therefore allowing densities exceeding the diffraction limit for 2-dimensional optical storage. The attraction, is storage of individual Mbit data pages addressed by changing either the angle^[1,2], wavelength^[3,4], or phase code^[5,6] of the reference beams, resulting in the rapid parallel storage and retrieval of digital data. Although this technology has been proposed since the 1970's it has failed to become viable because of five key reasons.

1. **Methods:** Previously proposed methods have been complex and difficult to implement. More importantly, real geometrical constraints limit the maximum density.
2. **Material:** There has been no viable material and moreover material requirements were vague at best.
3. **Lasers:** Initially proposed laser sources were expensive, complex and unreliable.
4. **Detectors:** Fast frame rate, large array detectors needed for readout have had relatively poor performance for this application and are generally low yield, high cost devices.
5. **Data Input Devices, (Spatial Light Modulators SLM):** Suitable SLM's, have only recently come into existence with their performance characteristics for storage applications not adequately tested.

Our team has made great strides toward resolving the five problems illustrated above. First, a new series of methods for recording multiplexed holograms has been developed. These techniques can be implemented with an uncomplicated mechanical geometry, individual holograms are addressed by a simple translation of the media allowing drive strategies similar to current drive technologies. In addition, for one particular technique, phase correlation multiplexing (PCM), figure 1, the method is not dependent upon the Bragg effect, therefore the hologram selectivity is independent of the thickness of the recording media. Storage densities in excess of 350 channel bits/ μm^2 have been demonstrated in 4mm Fe doped LiNbO₃ at a capacity of the order of 4 Gbits, (14,000 holograms), while densities of ~48 channel bits/ μm^2 have been demonstrated for photopolymer films^[7].

Many of the other technical challenges have been addressed and substantially reduced.

(a) Using a organic, visibly initiated, photopolymer based strategy, a WORM material has been developed. Currently the material's dynamic range supports 45-50 Gbytes of user density in a 5-1/4 disk format. A new material supporting in excess of 100 Gbytes is in development. In addition we have developed techniques for making high quality, optically flat media using inexpensive glass or polycarbonate substrates.

(b) Nearly all the parts needed for design of a commercial device are readily available. Compact low cost, reliable, high power solid state lasers have been and are being developed. Newly developed CMOS active pixel detectors, (APD) are the ideal readout solution for holographic storage. These devices which have lower cost and higher performance than CCD detectors, will allow functionality on a pixel level for data processing or buffering. In addition, they inherently support high data transfer rates. The New Digital Micromirror, DMD technology developed by Texas Instruments appears to resolve the input device need. DMD technology will permit 2000 frame/sec data presentation rates, with 1000:1 bit contrast at 1280x1024 pixels per data page.

We have developed a demonstration storage system based on the new multiplexing method using the components listed above^[8], figure 2. The ~480Kb/page system is the first of it's kind using a photopolymer as media. Raw bit error rates of the order of 10^{-5} have been observed for recorded data pages recovered in 280 μm polymer films. Simple error correction codes, (ECC), have allowed error free recovery of a wide variety of stored data types, (text, video, etc.), from photopolymer films.

References

1. D. L. Staebler, W. J. Burke, W. Phillips, J. J. Amodei, Appl. Phys. Lett. 26, 182 (1975).
2. F. H. Mok, M. C. Tackitt, and H. M. Stoll, Opt. Lett. 16, 605 (1991).

Invited Talks

References

1. D. L. Staebler, W. J. Burke, W. Phillips, J. J. Amodei, *Appl. Phys. Lett.* **26**, 182 (1975).
2. F. H. Mok, M. C. Tackitt, and H. M. Stoll, *Opt. Lett.* **16**, 605 (1991).
3. G. A. Rakuljic, V. Leyva, A. Yariv, *Opt. Lett.* **17**, 1471 (1992).
4. F. T. S. Yu, S. Wu, A. W. Mayers, and S. Rajan, *Opt. Comm.* **81**, 343 (1991).
5. J. E. Ford, Y. Fainman, and S. H. Lee, *Opt. Lett.* **15**, 1088 (1990).
6. C. Denz, G. Pauliat, G. Roosen, *Opt. Comm.* **85**, 171 (1991).
7. L. Dhar, C. Boyd, S. Campbell, K. Curtis, A. Harris, A. Hill, N. Levinos, M. Schilling, M. C. Tackitt, and W. L. Wilson; *Optical Data Storage*, **8**, OSA Technical Digest Series, pp. 113 - 115 (1998).
8. S. Campbell, K. Curtis, A. Hill, T. J. Richardson, M. C. Tackitt, W. L. Wilson; *Optical Data Storage*, **8**, OSA Technical Digest Series, pp. 168 - 170 (1998)

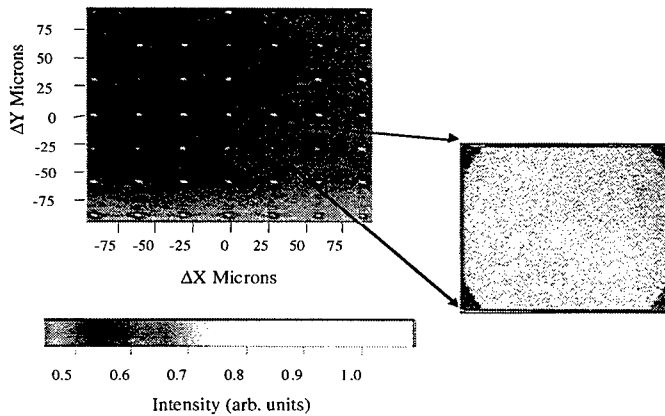


Figure 1: Array of PCM holograms; Scan of hologram diffraction efficiency as a function spatial position. At each maximum, (dot), a greater than 480Kbit data page is stored, as shown. (Note: includes ECC overhead). The sample was a 250 μ m polymer film.



Figure 2: Demonstration System; this 1x2ft device is fully functional and allows for digital data storage and recovery from a polymeric media.

**Recent Advances in Fast Photorefractive polymers and Highly Efficient
OLEDs**

N. Peyghambarian, G. E. Jabbour, S. R. Marder and B. Kippelen
Optical Sciences Center, University of Arizona
Tucson, Arizona 85721

Multifunctional polymers and organic compounds are being developed for various optoelectronic applications including display, storage, optical communication, and electro-optic modulation. This talk will review the recent advances of our group in two of these areas, namely the photorefractive polymers and electroluminescent light emitting diodes. Developments of fast photorefractive polymers with a 2 millisecond response time will be described. We will summarize our results on photogeneration efficiencies reaching 100% with 55 V/micrometer applied voltage. We also report on two-photon induced photoconductivity in polymeric materials yielding photocurrents of up to 0.4 μ A quadratic with the incident intensity based on the photoconductor poly(N-vinylcarbazole) sensitized with three different organic dyes using 80 fs pulses.

In the OLED area we describe our hybrid polymer-small molecule organic light-emitting devices with an aluminum cathode having an external quantum efficiency approaching 9% at pure red color brightness of 14 cd/m^2 and an operating voltage of 5.4 V. At an operating voltage of 8.2 V, the external quantum efficiency is 6.8% at brightness of about 100 cd/m^2 . A phosphorescent dye namely, 2,3,7,8,12,13,17, 18-octaethyl-21H,23H-porphine platinum(II) (PtOEP), is used as the red light emitter. The high efficiency in these hybrid devices is obtained by controlling both the hole injection and exciton diffusion.

Invited Talks

**Organic photorefractive materials
with sub-millisecond response and large dynamic range**

K. Meerholz¹⁾, E. Mecher¹⁾, R. Bittner¹⁾, F. Gallego¹⁾, and H.H. Hörhold²⁾

¹⁾ Physical Chemistry Department, University of München
Butenandtstr. 5-13, Building E, 81377 Munich, Germany

²⁾ Institute of Organic and Macromolecular Chemistry, University of Jena
Humboldtstr. 10, 07743 Jena, Germany

We report on new organic photorefractive (PR) materials with outstanding properties in both, steady-state performance and response time. They are based on the π -conjugated copolymer containing units derived from the common organic photoconductor TPD and poly[1,4-phenylenevinylene] (PPV), the so-called TPD-PPV. After adding the appropriate sensitizer, plasticizer, and electrooptic chromophore, the composite displayed sub-millisecond response times at intensities of $I \approx 5 \text{ W/cm}^2$ and electric fields of $E = 65 \text{ V}/\mu\text{m}$ (Fig. 1). This is among the fastest response times reported to date in organic PR materials, which will allow holographic optical computing at video rate and faster.

At the same time, the material maintains large index modulation ($\Delta n > 6 \cdot 10^{-3}$) which allows for complete internal diffraction even in thin film devices, unlike for the other "fast" organic PR materials reported so far [1,2]. The physical origin of the speed enhancement is discussed by comparing the new material with more traditional organic PR materials containing isolated charge-transport moieties for hopping such as the commonly used photoconductor poly(N-vinylcarbazole) (PVK), but also with other PPV-derivatives. The influence of light intensity and electric field on the PR performance is investigated. We will also incorporate the high-FOM ATOP chromophore [3] and extend the investigation into the NIR. This approach should yield an outstanding organic PR material.

1. D. Wright et al., *Appl. Phys. Lett.*, **73**, 1490 (1998).
2. U. Hofmann et al., *Chem. Phys. Lett.*, **311**, 41 (1999).
3. a) F. Würthner et al., *Angew. Chem. Int. Ed. Engl.*, **36**, 2765 (1997);
b) K. Meerholz et al., *Appl. Phys. Lett.*, **73**, 4 (1998).

Invited Talks

SUB-5-fs NONLINEAR OPTICAL PROCESSES IN POLYDIACETYLENES

Takayoshi Kobayashi

Department of Physics, University of Tokyo, Hongo, Bunkyo-ku, Tokyo 113-0033, Japan

Tell. +81-3-3812-2111, Fax. +81-3818-7812, E-mail takakoba@phys.s.u-tokyo.ac.jp

Using sub-5-fs visible pulses the real-time observation of the formation of a self-trapped exciton in polydiacetylenes has been observed for the first time. The stretching mode vibration ($C=C$, 23fs and $C\equiv C$, 16fs) coupled with the exciton transition drives the coherent vibration of the backbone structure from an acetylene(A)-like ($=CR-C\equiv C-CR'=$)_n to a butatriene(B)-like ($-CR=C=C-CR'-$)_n configuration

Ultrafast dynamics of conjugated polymers such as polydiacetylenes(PDA) have been attracting many scientists because they are model systems of quasi-one dimensional semiconductors with large nonlinearity. From our extensive studies [1] the initial kinetics after photo-excitation can be explained by a relaxation of a free exciton (FE) to a self-trapped exciton(STE) within 150fs. The recent achievement of sub-5-fs visible pulse generation based on a novel noncollinear optical parametric amplification (NOPA)[2] has enabled the real-time observation of the formation of a STE in a PDA for the first time. The stretching mode vibration ($C=C$, 23fs and $C\equiv C$, 16fs) coupled with the exciton transition drives the coherent relaxation of the backbone structure from an acetylene(A)-like ($=CR-C\equiv C-CR'=$)_n to a butatriene(B)-like ($-CR=C=C-CR'-$)_n configuration.

The pulse-front-matched NOPA generates transform-limited(TL) 4.7-fs, 5- J 1-kHz pulses centered at 650nm with a 250-nm bandwidth[2]. The PDA studied is a novel ladder-polymer, PDA4BCMU(8)), with two PDA-backbones linked with methylene chains[3]. The transition energy to a 1^1B_u FE is peaked at 1.96eV, which is classified to a typical blue-phase A-like PDA[1]. The 370-nm-thick film sample prepared by spin-coating was pumped and probed with the visible sub-5-fs pulses at room temperature. The real-time spectrum is given by the transient differential transmittance, which clearly shows a coherent molecular motion composed of several modes over the whole probe spectral range. The integrated Fourier analysis of the real-time spectrum reveals two main modes of $C=C$ ($\sim 1455cm^{-1}$) and $C\equiv C$ ($\sim 2080cm^{-1}$) stretching, in addition to weaker modes around 220, 700, and $1220cm^{-1}$, of which intensities are dependent on the probe wavelength. These modes are also observed in the static Raman spectrum. The vibration persists for longer than 1ps(Fig.1).

Recent experimental and theoretical studies manifest the lowest singlet state in a blue-phase PDA to be a forbidden 2^1A_g state lying $\sim 0.1eV$ below a 1^1B_u FE state[1]. The fast 60-fs decay observed around $E_{probe}=1.96eV$ is attributed to the internal conversion(IC) from a photoexcited 1^1B_u FE to a 2^1A_g FE. The long-lived wavepacket in the bleaching signal is thus exclusively assigned to a ground-state motion driven by impulsive stimulated Raman scattering. The stimulated emission from a 1^1B_u FE observed at $E_{probe}<1.8eV$ is suppressed rapidly by the IC, followed by the relaxation to a STE which causes the excited-state absorption of the biexcitons-<STE transition[1]. The net formation time of STE is determined to be about 80fs and the lifetime is 1.5ps. The wavepacket motion in a STE is transferred coherently from the 1^1B_u FE via IC, which indicates the coherent motions of the $C=C$ and $C\equiv C$ stretching along the backbone act as the driving force of the geometrical relaxation to a

Invited Talks

butatriene(B)-like structure where the exciton is self-trapped. The A(acetylene)->B isomerization and following thermalization of STE is visualized by a real-time frequency analysis using a spectrogram[4](Fig.1). The interesting feature is the $\sim 230\text{-cm}^{-1}$ oscillation (145fs-period) of the mode frequency, which indicates the coupling of the stretching modes with the C-C-C bending mode in the backbone. After the energy exchange the STE is thermalized, and the $\sim 20\text{-cm}^{-1}$ red-shift of each mode indicates the thermal B-like backbone creation. Thus we could for the first time, time resolve the vibrational mode coupling in molecular system.

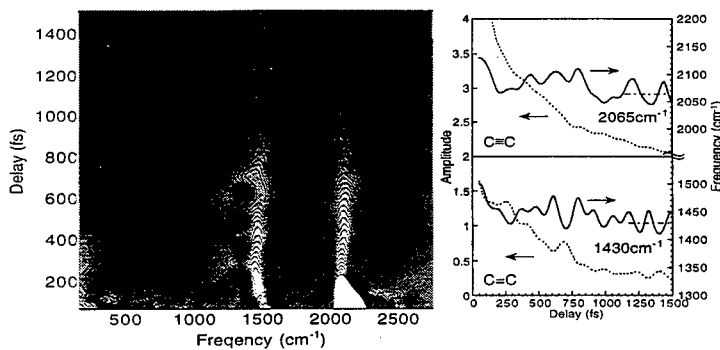


Fig.1. Spectrogram of the coherent motion probed at 1.75eV. The Fourier amplitude increases from black to white. The red-shifts of the mode frequencies are accompanied with an oscillation. The transient amplitude and center-of-mass frequency of each stretching mode obtained from the spectrogram are shown on the right.

References

- [1] E.g. T. Kobayashi, M. Yoshizawa, U. Stamm, M. Taiji, and M. Hasegawa, *J. Opt. Soc. Am. B*, **7**, 1558(1990); M. Yoshizawa, Y. Hattori, and T. Kobayashi, *Phys. Rev. B* **123**, 121(1994); T. Kobayashi, M. Yasuda, S. Okada, H. Matsuda, H. Nakanishi, *Chem. Phys. Lett.* **267**, 472(1997).
- [2] A. Shirakawa, I. Sakane, and T. Kobayashi, *Opt. Lett.* **23**, 1292(1998); A. Shirakawa, I. Sakane, M. Takasaka, and T. Kobayashi, *App. Phys. Lett.*, submitted.
- [3] H. Matsuzawa, S. Okada, H. Matsuda, and H. Nakanishi, *Chem. Lett.*, 1105(1997).
- [4] M. J. J. Vrakking, D. M. Villeneuve, and A. Stolow, *Phys. Rev. A* **54**, 37(1996).

Organic crystal growth and epitaxy

N. Karl

3. Physikalisches Institut Pfaffenwaldring 57, D-70569 Stuttgart, Germany

A review will be given on the different crystal growth methods that were successfully applied to organic molecular materials. For this class of substances specific problems arise from their typically weak (van der Waals) binding forces and from their frequently limited thermal stability. Purification as well as crystal growth from the melt or from the vapor phase require special attention. Single crystals of stoichiometric molecular complexes can often be obtained by nearly isothermal cosublimation techniques. Controlled doping, and growth of higher concentration mixed crystals usually need assistance by phase diagram data.

Following modern technological requirements in information technology considerable attention is presently being focussed on the growth of epitaxially ordered organic thin films on both, inorganic and organic substrates.

Ionic crystals with the cation or the anion, or both, organic are forming a special group among which a number of optically nonlinear materials exist. Growth techniques are limited to crystallization from solution in most cases.

The relevance of crystal purity and perfection for optical applications will be analyzed and suitable analytical methods presented.

Invited Talks

Growth of High Quality DAST Crystal by Using Slope Nucleation Method

Yusuke Mori, Yoshinori Takahashi, Takashi Iwai, Yoke Khin Yap,

Masashi Yoshimura, Takatomo Sasaki

Department of Electrical Engineering, Graduate School of Engineering, Osaka University

2-1 Yamadaoka, Suita, Osaka 565-0871, Japan

We have developed a new technique called Slope Nucleation Method for controlling the position and the orientation of spontaneous organic nuclei. This method combined nucleation and subsequence crystal growth and was applied to grow organic nonlinear optical (NLO) crystal 4-dimethylamino-N-methyl-4-stilbazolium tosylate (DAST). Many single crystals can be grown simultaneously. X-ray diffraction indicates that Slope Nucleation Method is effective for growing high quality DAST crystals as compared to the ordinary spontaneous nucleation method. DAST crystals with X-ray rocking curve as narrow as 20.2 arcsec. full width at half-maximum (FWHM) were obtained.

1, Introduction

The use of seed crystal is necessary for growing high quality single crystals. For inorganic materials, it is generally easier to extract the first seed crystal from solid-state sintering. Such a seed crystal usually has sufficient dimension and hardness to be handled for growing single crystals. The successfully grown crystal provides many high quality seed crystals for subsequence crystal growth with further improved quality. The repeat of this process continually improved quality of seed crystal for the growth of single crystals.

On the other hand, organic materials are usually soft and difficult to be grown to sufficient dimension and quality. Presently, tiny organic seed crystals are first prepared by spontaneous nucleation and then are used for growing single crystals. However, it is difficult to prepare good organic seed by ordinary spontaneous nucleation. It is also not easy to handle such a small seed for subsequence growth of good quality single crystals. Such an obstacle in the growth process reduces the reproducibility and increases the cost for crystal growth.

In order to obtain high quality organic crystals with low processing cost, it is necessary to develop new seeding and growing process. We aimed to combine preparation of good organic seed and subsequence crystal growth by means of a new technique called Slope Nucleation Method. This method can control position and orientation of spontaneous crystals and was used to grow organic nonlinear optical (NLO) crystal 4-dimethylamino-N-methyl-4-stilbazolium tosylate (DAST) [1].

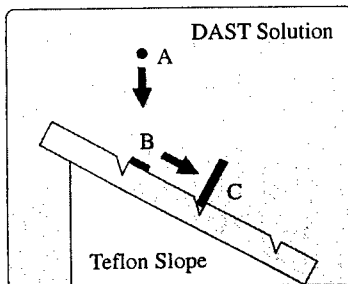


Fig. 1. Slope Nucleation Method

Invited Talks

2, Slope Nucleation Method

Before developing Slope Nucleation Method, we have grown DAST crystals from ordinary spontaneous nucleation method in a Teflon™ vessel [2,3]. However there have been some troubles on controlling position and orientation of nucleation. DAST crystals tend to stick at the bottom of the vessel. These crystals also tend to joint together and result in the formation of poly-crystals. Slope Nucleation Method is then developed to prevent these problems. We introduced a Teflon™ plate into the solution with many grooves on the plate surface as shown in Fig.1. The nucleation and growth process is described as follow. First, small nuclei in the solution (A) condensed on the Teflon™ plate. As it grows to a large size (B), DAST crystals slide downward along the slope until arriving at one of the groove (C). At C, DAST crystals stand up and continue to grow to a larger size as shown. There are several advantages in this method. The most important one is that the largest (001) plane of the DAST crystal doesn't stick to the vessel. This allows the improvement of DAST crystallinity. Besides, we can grow several high quality DAST crystals simultaneously as in Fig. 2. The overall growth process is very simple, high yield and thus reduced the manufacturing cost.

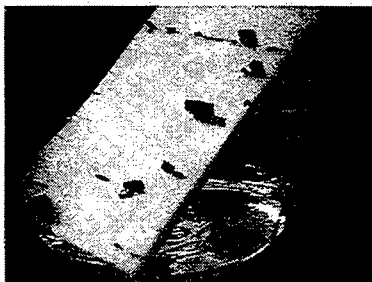


Fig. 2. DAST crystals standing on the Teflon slope

3, Characterization

The DAST (001) X-ray diffraction (XRD) peaks in the ω scan mode were used to characterize crystallinity. The XRD peaks of DAST grown by our new method are between 20.2~57.6 arcsec full width at half maximum (FWHM). DAST crystals grown by ordinary spontaneous nucleation induced XRD peaks between 50~130 arcsec. Note that Si(111) induced XRD peak of about 10 arcsec. This result indicates that Slope Nucleation Method is effective to obtain high quality DAST crystal. Besides, our DAST crystals were tested for electro-optic sampling (EOS) experiment. Note that KTiOPO_4 (KTP) is presently the best materials for EOS in many electric field sensors. EOS sensitivities of DAST crystals grown by our Slope Nucleation Method is about 4 times higher than that of KTP.

References

- [1] H. Nakanishi, H. Matsuda, S. Okada and M. Kato, Mater. Res. Soc. Int. Mtg. Adv. Mater., **1** (1989) 97
- [2] H. Adachi, Y. Takahashi, J. Yabuzaki, Y. Mori, T. Sasaki, Journal of Crystal Growth, **198/199** (1999) 568.
- [3] Y. Takahashi, J. Yabuzaki, H. Adachi, Y. Mori, T. Sasaki, Nonlinear Optics, **22** (1999) 267.

Molecular Engineering of DAST Family

Hachiro Nakanishi
 Institute for Chemical Reaction Science, Tohoku University
 Sendai 980-8577, Japan

Two categories of DAST derivatives were synthesized. For EO application, the polyene analogues with increased double-bond number between two aromatic rings of DAST and fused-ring derivatives of DAST were prepared for larger β than DAST cation. For frequency conversion of laser diodes, 4-substituted pyridiniums were investigated to obtain crystals better than inorganics. By choosing proper counter anions, several SHG active crystals without visible absorption have been found. The research project on DAST to be used as EO sensors is being progressed in Japan.

Organic ionic crystals have several advantages over conventional organic non-ionic crystals. For example, ionic chromophore orientation in crystals can be varied by substituting its counter anion [1]. High melting points and hardness are expected due to Coulombic attraction of the species in crystals. Hyperpolarizability (β) larger than that of non-ionic species, which originates from charged π -conjugated system [2], can be realized. Among such compounds, 1-methyl-4-(2-(4-(dimethylamino)phenyl)ethenyl)pyridinium *p*-toluenesulfonate (DAST) was first discovered by our group as an organic ionic NLO crystal [3,4] and was also investigated by Marder and colleagues [5]. It is now recognized as one of the best organic materials for second-order NLO applications.

Our recent research on DAST family is directed to the following two categories. One is for larger β than DAST cation for EO application. The other is for larger β than *p*-nitroaniline (*p*NA) without visible absorption for frequency conversion of laser diodes. The chemical structures of the synthesized compounds are displayed in Figure 1.

Derivatives with extended π -conjugation system

Polyene analogues **2a-5a** and fused-ring analogues **6a, 8a, 9a** and **11a** of DAST derivative **1a** were synthesized. For the polyene analogues, bathochromic shift of absorption maximum wavelength (λ_{max}) in methanol almost saturated from **4a** to **5a**. Thus, the counter anion exchange to obtain crystals with noncentrosymmetric structures was performed for the **1a-4a**. When (dimethylamino)azobenzene-4-sulfonate was introduced as a counter anion, SHG active

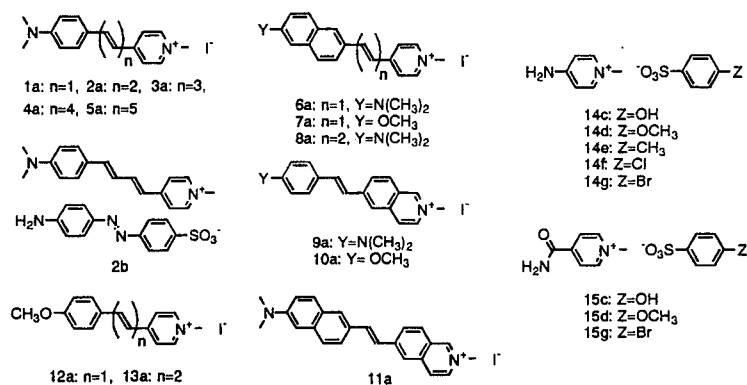


Figure 1 Chemical structures of the compounds synthesized.

Invited Talks

crystals containing one water to an ion pair of **2b** were obtained. By applying the oriented gas model, its d value was estimated to be about 1.3 times as large as that of DAST.

In the case of fused-ring systems, calculated β values become larger when compared with polyene analogues with calculated transition energy (E_{eg}) similar to that of the fused-ring derivative [6]. Actually, λ_{max} s in methanol solution of **6a**, **9a** and **11a** were found to be shorter than those of **1a**, although these fused-ring compounds were calculated to have 1.2-1.4 times of β of **1a**. However, absorption bands of fused-ring compounds tend to be broad resulting in cutoff wavelength in relatively longer region. The order of experimental β_0 for methoxy derivatives determined by the HRS method were **13a** > **10a** > **7a** > **12a**. For both systems, anion exchange for SHG-active crystals are being studied.

Derivatives with shrunk π -conjugation system

Since p -toluenesulfonate, i.e. anionic species of DAST, was found to have a large β value comparable to that of p -nitroaniline [7], simple pyridinium derivatives were investigated as pairing cation species without absorption in visible region. Among them, 4-(dimethylamino)pyridinium cation was evaluated to have more than twice of β_0 of p NA [8], though SHG-active crystals have not been attained so far. Several SHG-active crystals could be grown 4-aminopyridinium salts **14** and 4-carbamoylpyridinium salts **15** [9]. By use of the oriented gas model, the maximum d value of this series of salts was estimated for **14c** to be about one-fourth of that of 2-methyl-4-nitroaniline irrespective of no visible absorption.

Toward device application of DAST

If the using purpose of NLO crystals was limited to the EO sensing, DAST would be the best compound at present both from its large r value exceeding that of lithium niobate and good crystal-growth ability. Thus, we have launched a regional research-and-development project on photonics sensing using DAST crystals sponsored by NEDO, Japan. Three groups from Tohoku University, one national college of technology, two governmental institutes and three companies joined in this program. DAST powder in high purity is now supplied by Daiichi Pure Chemical Co., Ltd. Tokin Corp. and Tohoku Electronic Industrial Co., Ltd. are aiming to develop high-sensitivity and high-frequency EO sensors, respectively, using adequately fabricated DAST crystals. Some of the results of this project will be introduced in the conference.

References

- [1] G. R. Meredith, *ACS Symp. Ser.*, **233**, 27 (1983).
- [2] X.-M. Duan, H. Konami, S. Okada, H. Oikawa, H. Matsuda, and H. Nakanishi, *J. Phys. Chem.*, **100**, 17780 (1996).
- [3] Japanese Patent Application 61-192404 (1986); Japanese Patent 1716929 (1992).
- [4] H. Nakanishi, H. Matsuda, S. Okada, and M. Kato, *Mater. Res. Soc. Int. Mtg. Adv. Mater.*, **1**, 97 (1989).
- [5] S. R. Marder, J. W. Perry, and W. P. Schaefer, *Science*, **245**, 626 (1989).
- [6] X.-M. Duan, N. Nishimura, H. Konami, S. Okada, H. Oikawa, H. Matsuda, and H. Nakanishi, *Nonlinear Opt.*, **20**, 105 (1999).
- [7] X.-M. Duan, S. Okada, H. Oikawa, H. Matsuda, and H. Nakanishi, *Jpn. J. Appl. Phys.*, **33**, L1559 (1994).
- [8] Anwar, X.-M. Duan, K. Komatsu, S. Okada, H. Matsuda, H. Oikawa, and H. Nakanishi, *Chem. Lett.*, **1997**, 247.
- [9] Anwar, K. Komatsu, S. Okada, H. Oikawa, H. Matsuda, H. Nakanishi, *Proc. SPIE*, **3796**, 219 (1999).

Photodegradation of Various Electro-Optic Polymer Families

George I. Stegeman and Adriana Galvan-Gonzales

School of Optics and CREOL, University of Central Florida, Orlando, FL 32826, USA

Michael Canva

Laboratoire Charles Fabry de l'Institut d'Optique, IOTA-Université d'Orsay-Paris XI, 91403 Orsay Cedex France.

Robert Twieg

*Dept. of Chemistry & Liquid Crystal Institute, Kent State University
Kent, OH 44242, USA*

Tony C. Kowalczyk, Xuan Q. Zhang, and Hilary S. Lackritz
Gemfire Corporation, Palo Alto, CA 94303, USA

Seth Marder and Sankaran Thayumanavan

Dept. of Chemistry, University of Arizona, Tucson, AZ 85721, USA

Kwok Pong Chan

Molecular OptoElectronics Corporation (MOEC), Watervliet, NY 12189-1903, USA

Alex K-Y. Jen and Xiaoming Wu

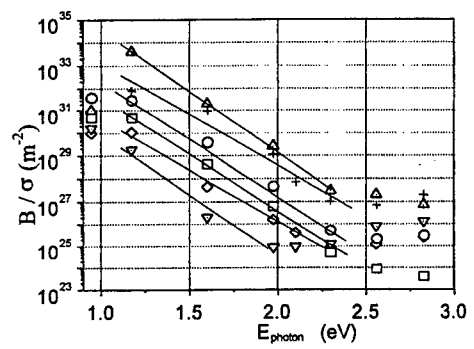
Dept. of Materials Science, University of Washington, Seattle, WA 98195-2120, USA

The photostability of different chromophore families has been studied as a function of probe light wavelength in the spectral range 400 to 1320 nm. Multiple donor and acceptor groups have been attached to the main bridge structures associated with stilbene, azobenzene, aniline, thiophene and aniline-thiophene structures. The figure of merit B/σ was measured and the quantum efficiency B^{-1} was evaluated for over 40 polymers, including both side-chain and guest-host systems.

Photonic devices based on polymers are promising for a number of applications. However, it is well-known that electro-optic polymers under continuous illumination lose their nonlinearity with time due to a number of different mechanisms. We have quantified this process in terms of a figure of merit B/σ where B^{-1} is the quantum efficiency for an absorbed photon to photodegrade a molecule and σ is the molecular absorptivity. In this paper we describe our measurements of this figure of merit for a large range of electro-optic chromophores over the spectral range 400 to 1320 nm.

The experimental protocol used is to measure the transmission change in the tail of the dominant charge transfer absorption line as a polymer film is illuminated with radiation of different wavelengths. The typical observed variation in B/σ is shown in Figure 1 for 6 of the different chromophores studied. The wavelength variation shown, including the straight line approximation in the Near-IR, is typical of all 45 polymers investigated. Such data, when coupled with measurements of the absorption spectrum, yields the quantum efficiency parameter B listed in the table for the 6 chromophores shown in Figure 1, along with their chemical structures. Note that the 2 values for B for DANS indicate that two charge transfer states are photo-active with different quantum efficiencies.

Invited Talks



The major trends in photodegradation associated with stilbene, azobenzene, aniline, thiophene and aniline-thiophene structures, and a variety of different donor - acceptor groups will be discussed, as well as the dominant mechanisms.

#	Symbol	Chromophore	B	$\lambda_{max}(nm)$
1	□	<chem>CN(C)c1ccc(/C=C/c2ccc([N+](=O)[O-])cc2)cc1</chem>	$2 \times 10^4, 8 \times 10^4$	430
2	○	<chem>OCCN(c1ccc(/N=N/c2ccc([N+](=O)[O-])cc2)cc1)</chem>	5×10^6	475
3	△	<chem>CCOC(=O)C=CN(CCC)C1=CC=C(N=N2C=CC(=C2)[N+](=O)[O-])C=C1</chem>	1×10^8	470
4	▽	<chem>CCCCc1ccc(cc1)N(c2ccc(cc2)/C=C/c3sc(C#N)c(C#N)c3)C#N</chem>	3×10^6	640
5	◇	<chem>CN(C)c1ccc(/C=C/C=C/C=C/C#N)cc1</chem>	1×10^6	510
6	+	<chem>c1ccc(cc1)N(c2ccc(cc2)/C=C/C#N)C#N</chem>	2×10^7	520

Nonlinear Optics and Photorefractivity of Polymer Composites

N. Kim, W. S. Jahng, S. Song, D.-H. Shin, H. Chun, and M. Joo
Center for Organic Photorefractive Materials
Korea Institute of Science and Technology
P.O. Box 131, Cheong-ryang, Seoul, 130-650, Korea

Photorefractive composites were prepared from polysiloxane with pendant carbazole (PSX) as photoconducting host, TNF as photosensitizer, and a series of indole-derivatives as NLO chromophores. The influence of chromophores on electro-optics and photorefractive properties were discussed. Response for *2BC* gain buildup was found to be very fast and the composites showed great stability toward phase separation.

Introduction

Since the first discovery of photorefractive effect in polymers in 1991, polymeric materials have been extensively studied due to the potential optical applications [1]. However, the understanding of photorefractive mechanism in polymeric system has been still limited. Furthermore, the response time of photorefractive composites is not sufficient enough for real-time application, even though several photorefractive composites have been reported to have excellent steady-state performance[1]. This work focuses on the influence of NLO chromophore on electro-optics and photorefractive performance of composite system.

Results and Discussion

Carbazole-substituted polysiloxane (PSX) and NLO chromophores were synthesized and the chemical structures are given in Figure 1. The composites consisted of PSX (79 or 69 wt %), chromophores (20 or 30 %), and TNF (1 wt %, Kanto Chemical Co.). And this composites exhibit the better phase stability than the corresponding plasticized PVK system.

The electro-optic properties of composites were determined by transmission ellipsometric method. The transmitted intensity of composites is in the order of IN-DC30>IN-SB30>IN-IO30>IN-BO30>IN-CE30, as in Figure 2. The performance of chromophore embedded in low Tg medium can be evaluated by figure-of-merit (*FOM*) defined as $[9\mu\beta + 2\mu^2 \Delta\alpha/kT]/M$ where μ , β , $\Delta\alpha$, and M are dipole moment, hyperpolarizability, polarizability anisotropy and molar mass, respectively [1]. *FOM* of indole-based chromophore, which was derived from MOPAC calculation (Table I), is in the order of IN-DC, IN-SB > IN-IO>IN-BO > IN-CE. It is in good accord with experimental observation in Figure 2. However, in the case of composites containing 20 % of chromophores, only IN-DC20 composite shows the appreciable electro-optic response (Figure 3). The much lower intensity in ellipsometric measurement for IN-SB20 composite than that of IN-DC20 composite is probably related to the limited mobility of medium, as can be expected from Tg of composites (Table I). This observation illustrates that Tg is of significant importance for EO performance, especially for *in-situ* poled material.

Photorefractive properties of composite systems were studied by *2BC* experiment (Figure 4). IN-DC20 composite exhibits the highest gain among composites studied in this work. IN-DC30 and IN-SB30 composites, of which EO properties are better than IN-DC20 composite, show the inferior photorefractive properties. This may result from the fact that, in addition to EO response, chromophores influence the formation of E_{sc} . Even though chromophores are embedded in same photoconducting host, they probably experience different space-charge field, depending on molecular structure of NLO.

Invited Talks

All polymer composites show very fast response time in the gain growth of $2BC$ measurement. Even at low intensity (20 mW/cm^2), time constant (τ_g) obtained by fitting the evolution of the gain growth with a single-exponential function is in the order of sub-second at $70 \text{ V/}\mu\text{m}$, which is comparable to that of fastest polymer composites reported previously[2].

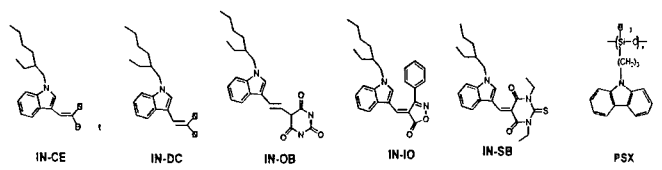


Figure 1. Chemical structures for chromophores and polysiloxane with carbazole

TABLE I Molecular parameters of NLO chromophores and composites

NLO	μ^a	β^a	$\Delta\alpha^a$	T_g^b	
	(D)	(10^{-30} esu)	(10^{-23} esu)	(20%)	(30%)
IN-CE	6.83	8.67	1.78	25	17
IN-DC	6.95	15.0	3.64	25	15
IN-OB	5.10	14.0	4.08	38	34
IN-IO	5.52	16.7	3.99	38	34
IN-SB	7.08	16.0	5.59	42	36

^a Calculated from MOPAC, ^b Composites

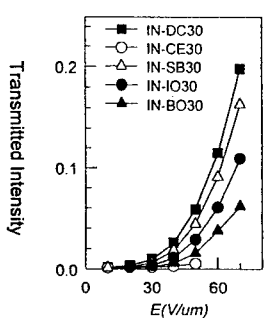


Figure 2: Electro-optic properties of composites ([NLO] = 30%)

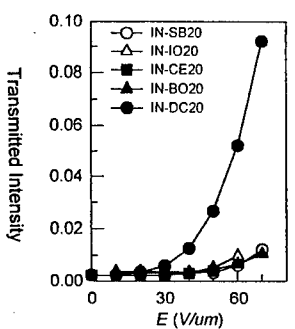


Figure 3: Electro-optic property of composites ([NLO]=20%)

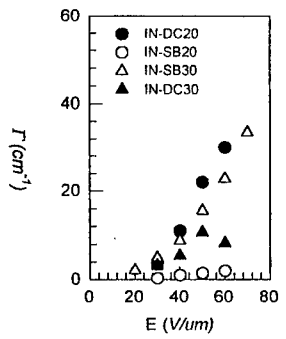


Figure 4. 2BC gain coefficient vs. applied electric field

References

1. E. Hendrickx, J. Herlocker, J. L. Maldonado, S. R. Marder, B. Kippelen, A. Persoons, and N. Peyghambarian, *J. Appli. Phys.*, **72**, 1679-1681 (1998).
2. D. Wright, M. A. Diaz-Garcia, J. D. Caspersen, M. DeClue, W. E. Moerner, and R. J. Twieg, *J. Appli. Phys.*, **73**, 1490-1492 (1998)

Periodically structured polymer films and applications.

Jean-Michel Nunzi^{a,b}, Licinio Rocha^a, Vincent Dumarcher^a, Christine Denis^a, Paul Raimond^a,
Céline Fiorini^a, Frank Sobel^b, Bouchta Sahraoui^b, Denis Gindre^b

^a LETI (CEA - Technologies Avancées), DEIN/SPE, Groupe Composants Organiques,
CEA Saclay, F-91191 Gif-sur-Yvette Cedex, France

^b Laboratoire des Propriétés Optiques des Matériaux et Applications, Université
d'Angers, 2 Boulevard Lavoisier, 49045 Angers Cedex, France

Reversible holographic recording of surface-relief gratings in azo-dye polymers was recently evidenced using atomic force microscopy. Irradiation with an interference pattern between polarized laser beams was observed to lead to quantitative mass-transport. The origin of such efficient photo-driven mass transport comes from chromophore migration from the high to low intensity regions, in an inchworm like motion. In their motion, the chromophores work as molecular trucks, they track the whole polymer chain to which they are attached. As an application, we present a study of Distributed Feedback (DFB) laser emission in various polymer materials. The device permits to control the stimulated emission in dye doped polymer materials. Confinement and wave-guiding effects are evidenced.

Patterning and micro-structuring of functional polymers are key technologies to fabricate organic devices. A recent achievement in this respect is the patterning of photoinduced surface-relief gratings using the interference pattern between optical beams.^{1,2} This opens the route to molecular translation control using optical fields, in the same way as dual-frequency irradiation using appropriate combinations of circular beam polarizations have been demonstrated to enable a full control of the molecular polar order.^{3,4} The well-known azo-dye aromatic polymers have been shown to be among the most efficient materials for such structuring processes using light matter interactions. A simple microscopic model accounting for the essential features of photoinduced surface-relief grating formation has been developed⁵ and some of its peculiar features have verified experimentally⁶.

A challenging issue today is to pattern and micro-structure organic devices in order to control the emission properties of polymer thin films such as the one used for electroluminescent diodes. A control of the radiation modes of electroluminescent diodes has already been demonstrated using planar microcavities^{7,8}. We propose here the use of a periodical excitation in a distributed feedback (DFB) scheme⁹ to investigate the luminescence and lasing properties of dye-doped polymer thin films. The so-called organic lasers^{10,11,12,13} have recently been revisited with an aim at building an organic semiconductor laser diode¹⁴.

In 1971, Kogelnik and Shank first demonstrated DFB dye-laser operation using a dye doped gelatin film in which a grating had been previously printed optically.⁹ They also showed that DFB laser action was possible by making a dynamic grating using the interference fringes from two pump beams inside a dye cell.¹⁵ Narrow-band emission was tuned simply by changing the angle between the pump beams incident onto the dye cell. Efficient feedback is obtained from a spatial modulation of both gain and index of refraction of the polymer film. Modulation is photo-induced with the interference pattern produced by the two coherent laser beams.

Different interference schemes have already been proposed for DFB laser excitation: the so-called Lloyd's mirror which permits stable operation in a compact set-up¹⁶ and a more sophisticated interferometer which permits a better control of the pump beam

Invited Talks

characteristics¹⁷. We used both schemes to study DFB polymer dye laser characteristics. In particular, effects related to waveguiding of the laser emission into the polymer thin film were investigated. This appears as a very important feature in order to control stimulated emission using optically confined structures.

References

- ¹ P. Rochon, E. Batalla, A. Natansohn, *Appl. Phys. Lett.*, **66**, 136 (1995).
- ² D.Y. Kim, L. Li, J. Kumar, S.K. Tripathy, *Appl. Phys. Lett.*, **66**, 1166 (1995).
- ³ C. Fiorini, F. Charra, J.-M. Nunzi, P. Raimond, *J. Opt. Soc. Am. B*, **14**, 1984 (1997).
- ⁴ A.-C. Etilé, C. Fiorini, F. Charra, J.-M. Nunzi, *Phys. Rev. A*, **56**, 3888 (1997).
- ⁵ P. Lefin, C. Fiorini, J.-M. Nunzi, *Pure Appl. Opt.*, **7**, 71 (1997).
- ⁶ C. Fiorini, N. Prudhomme, A.-C. Etilé, P. Lefin, P. Raimond, J.-M. Nunzi, *Macromol. Symposia*, **137**, 105 (1999); C. Fiorini, N. Prudhomme, G. de Veyrac, I. Maurin, P. Raimond, J.-M. Nunzi, to be published in *Synthetic Metals* (1999).
- ⁷ N. Takada, T. Tsutsui, S. Saito, *Appl. Phys. Lett.*, **63**, 2032 (1993).
- ⁸ H.F. Wittmann, J. Gruner, R.H. Friend, G.W.C. Spencer, S.C. Moratti, A.B. Holmes, *Adv. Mater.*, **7**, 541 (1995).
- ⁹ H. Kogelnik, C.V. Shank, *Appl. Phys. Lett.*, **18**, 152 (1971).
- ¹⁰ M. Kuwata-Gonokami, R.H. Jordan, A. Dodabalapur, H.E. Katz, M.L. Schilling, R.E. Slusher, S. Ozawa, *Opt. Lett.*, **20**, 2093 (1995).
- ¹¹ A. Schülzgen, Ch. Spiegelberg, M.M. Morell, S.B. Mendes, B. Kippelen, N. Peyghambarian, M.F. Nabor, E.A. Mash, P.M. Allemand, *Appl. Phys. Lett.*, **72**, 269 (1998).
- ¹² V.G. Kozlov, G. Parthasarathy, P.E. Burrows, S.R. Forrest, Y. You, M.E. Thompson, *Appl. Phys. Lett.*, **72**, 144 (1998).
- ¹³ D. Fichou, S. Delysse, J.M. Nunzi, *Advanced Materials*, **9**, 1178 (1997).
- ¹⁴ D.G. Lidzey, D.D.C. Bradley, S. F. Alvarado, P. F. Seidler, *Nature*, **386**, 135 (1997).
- ¹⁵ C.V. Shank, J.E. Bjorkholm, H. Kogelnik, *Appl. Phys. Lett.*, **18**, 395 (1971).
- ¹⁶ M. Maeda, Y. Oki, K. Imamura, *IEEE J. Quant. Electr.*, **33**, 214 (1997).
- ¹⁷ G.M. Gale, P. Ranson, M. Denariez-Roberge, *Appl. Phys. B*, **44**, 221 (1987).

Applications of Molecules with Large Two-Photon Absorption Cross Sections

V. Alain, S. Ananthavel, J. K. Cammack, M. Halik, S. Kuebler, S. Marder, J. W. Perry,
M. Rumi, S. Thayumanavan, W. Wenselers

*University of Arizona
Department of Chemistry
Tucson, AZ 85747*

B. Cumpston, M. Dickinson, S. E. Fraser, A. Heikal, M. Lipson

*California Institute of Technology
Beckman Institute
Pasadena, CA 91125*

Molecules with large two-photon cross sections have recently been reported. The development of materials for optical limiting applications based upon two-photon absorption followed by either excited state absorption or excited state electron transfer reactions, creating strong absorbing species will be discussed. It has also been shown that such molecules can be used to initiate the polymerization of acrylate monomers. We will also discuss the application of these highly sensitive two-photon absorbing molecules to excited state charge transfer mediated processes and biological imaging applications

We have developed structure-property relationships for two-photon absorbing conjugated organic materials and on the understanding of the underlying physical mechanisms. [1] As a result of this effort, a strategy for the design of molecules with large two-photon absorption cross sections, δ , has been developed. The strategy is based on the concept that symmetric charge transfer upon excitation, from the ends to the middle (or vice versa) of a properly substituted conjugated molecule is correlated with increased δ . This has led to the synthesis of molecules with δ up to 20 times larger than previously available chromophores. In a recent paper, [1], we reported that 4,4'-bis(di-*n*-butyl)amino-*E*-stilbene (**2**, Figure 1) exhibits a value of $210 \times 10^{30} \text{ cm}^4 \text{ sec/photon}$ at 605 nm, which is almost 20 times larger than that of *trans*-stilbene. From this initial observation, we conjectured that the large increase in the two-photon absorption for **2** relative to **1** was related to a symmetrical charge transfer from the amino nitrogens to the conjugated bridge of the molecule. Accordingly we, synthesize the molecules shown in Figure 1 and examined their two-photon cross sections. As can be seen in Table 1 molecules can be realized using this strategy.

These molecules show efficient optical limiting properties, because of the combined effect of large two-photon absorptivity and two-photon induced excited-state absorption. Two-photon excitation can be used to activate a variety of chemical and physical processes with high 3D spatial resolution. The electron richness of D- π -D molecules has been exploited to activate two-photon induced polymerization of acrylate monomers with high efficiency. Such materials and

Invited Talks

processes hold great potential for high-density optical data storage and 3D microfabrication applications, as we have demonstrated in initial experiments (Figure 2). [2]

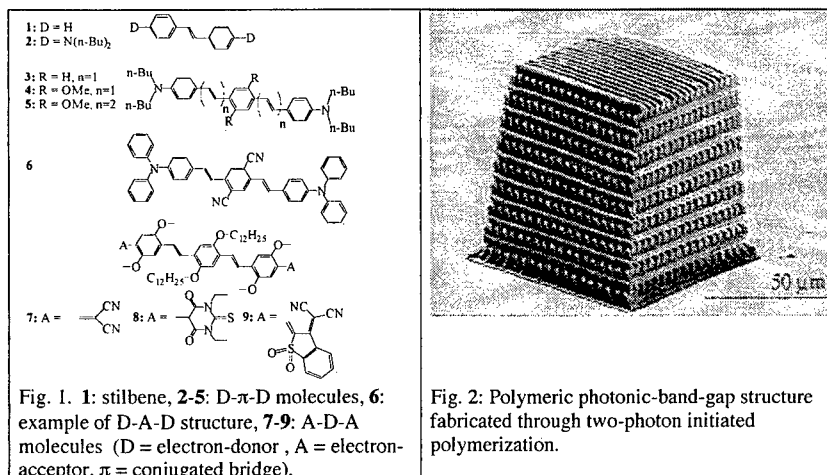


Table 1. Two-photon optical data (wavelengths for the two-photon fluorescence excitation maxima, $\lambda_{\text{max}}^{(2)}$, and two-photon excitation cross sections, δ) for compounds 1-9. Two-photon fluorescence data were measured using nanosecond pulses with a two-photon excited fluorescence method.

Compound	$\lambda_{\text{max}}^{(2)}$ (nm)	δ (10^{-50} cm ⁴ s/photon)
1	514	12
2	605	210
3	730	995
4	730	900
5	775	1250
6	835	1940
7	825	480
	940	620
8	970	1750
9	975	4400

[1] M. Albota, et al. "Design of Organic Molecules with Large Two-Photon Absorption Cross Sections" *Science* **281**, 1653-1656 (1998).

[2] B. H. Cumpston, et al. "Two-Photon Polymerization Initiators for Three Dimensional Optical Data Storage and Microfabrication" *Nature* **398**, 51-54 (1999).

Dimensionality Aspects of Two-Photon Absorption in Conjugated Chromophores

J.L. Brédas, H. Vogel, J.W. Perry, and S.R. Marder
Department of Chemistry
The University of Arizona
Tucson, Arizona 85721-0041

and

D. Beljonne
Center for Research in Molecular Electronics and Photonics
University of Mons-Hainaut
Place du Parc 20, B-7000 Mons, Belgium

A unified picture of linear and nonlinear polarization in π -conjugated chromophores has been recently obtained via derivation of structure/nonlinear optical response relationships. These relationships can now be exploited to probe mechanisms of enhancement of specific nonlinear optical processes. Here, we focus on two-photon absorption (TPA), a process by which a chromophore simultaneously absorbs two photons (of the same or different energy) and which results in various relaxation pathways.

Two-photon absorption (TPA) can be exploited as a gateway to several important applications including two-photon fluorescence spectroscopy, optical limiting, three-dimensional optical memory, or two-photon-induced biological caging studies. In many instances, very large TPA cross-sections are required in a range of fundamental excitation wavelengths on the order of 0.6-1.0 μm (*i.e.*, ca. 2.0 to 1.2 eV fundamental energy). Our goal is to develop strategies helping in the design of chemical structures with enhanced two-photon absorptions in this energy range.

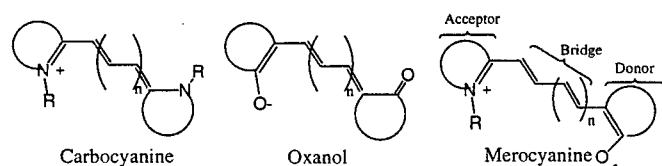
We first focus on quasi-one-dimensional noncentrosymmetric structures. In order to derive structure-property relationships, we have evaluated theoretically, via correlated quantum-chemical calculations, the evolution of TPA as a function of the degree of ground-state polarization in a typical donor-acceptor conjugated molecule, the stilbene derivative, 4-dimethylamino-4'-formylstilbene, DAFS. The degree of ground-state polarization in DAFS depends on the relative contributions of the neutral (aromatic-like) resonance form and the charge-separated zwitterionic (quinoid-like) form; for equal contributions of the two forms, one reaches what we refer to as the cyanine limit.

We have analyzed TPA into the lowest excited state of DAFS, S_1 (whose wavefunction has characteristics similar to the $1B_u$ state of stilbene). The evolution for the TPA is calculated to closely follow the evolution of β and peaks between the neutral structure and the cyanine limit. At the peak, the TPA is enhanced by a factor of nearly 50 with respect to that of the neutral structure. However, in the regime where TPA peaks, the transition energy gets significantly reduced so that the excitation wavelength falls beyond the 1 μm limit. For a number of applications, it will then be desirable to work at higher excitation frequencies.

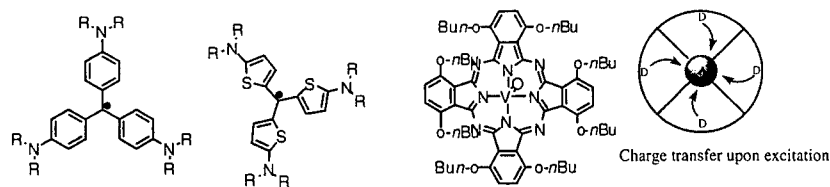
Invited Talks

We have also investigated TPA into the second excited state of DAFS, S_2 (whose wavefunction has characteristics similar to the $2A_g$ state of stilbene). Huge TPA values, representing a 500-fold increase with respect to the neutral structure of DAFS, are obtained near the cyanine limit. It is interesting to note that such large TPAs are related to a near double-resonance process: around the cyanine limit, $E(S_0-S_2)$ is approximately twice as big as $E(S_0-S_1)$; as a result, two-photon resonance to S_2 is accompanied with near one-photon resonance to S_1 , a feature which strongly enhances the TPA response.

Two strategies can thus be followed to enhance TPA in donor-acceptor stilbenes and related conjugated compounds. One is to optimize the conditions (donor-acceptor strength, medium polarity, nature of conjugated segment) to have the structure leading near the maximum of β with TPA into the lowest excited state. A second strategy is to consider TPA into the second excited state while driving the structure towards the cyanine limit. In this framework, we discuss the results of correlated calculations performed on several types of cyanine-like compounds:



The role of molecular dimensionality on the TPA response is then addressed by looking at establishing the structure-property relationships in compounds with several axes of charge transfer, in the present case, octupolar compounds with three-fold symmetry and hexadecupolar compounds with four-fold symmetry:



Waveguides of PPV-Derivatives with Large Cubic Nonlinearities

C. Bubeck, K. Koynov, J. Ziegler, H. Eichner, F. Fitrilawati,¹ H.-H. Hörhold²

Max-Planck-Institute for Polymer Research, Ackermannweg 10, 55128 Mainz, Germany

¹Dept. of Physics, Institut Teknologi Bandung, Bandung 40132, Indonesia

²Inst. for Organic and Macromolecular Chemistry, Friedrich-Schiller-Univ. Jena, 07743 Jena, Germany

Picosecond nonlinear optical spectroscopy is applied to study third-order nonlinearities of poly(p-phenylenevinylene) (PPV) and its derivatives. Thin films on fused silica substrates are prepared by spin coating. Third-harmonic generation spectroscopy is applied to measure $\chi^{(3)}$ values of PPVs and their corresponding oligomers. Their comparison yields the effective conjugation lengths of conjugated polymers. Slab waveguides of substituted PPVs show attenuation losses as low as 1 dB/cm. We use intensity dependent prism coupling of waveguides to obtain *signs and absolute values* of nonlinear refractive index and nonlinear absorption coefficient, respectively. We demonstrate fully reversible Δn as large as +0.002 at 910 – 950 nm with unsubstituted PPV. We conclude that PPVs are highly promising for all-optical devices because of their excellent figures of merit.

The realization of optical signal processing requires materials with large cubic nonlinearity and the possibility to prepare thin film waveguides with low attenuation losses. Applications usually demand a figure of merit $W = n_2 I / 2\alpha_0 \lambda > 1$, where $\Delta n = n_2 I$ denotes the intensity dependence of the refractive index, α_0 is the attenuation coefficient and λ is the wavelength.

Third-harmonic generation (THG) has become a popular method to determine the third-order susceptibility $\chi^{(3)}(-3\omega; \omega, \omega, \omega)$. We have performed many studies of poly(p-phenylenevinylene) (PPV) and its oligomers [3]. New results of various PPV derivatives that have substitutions at the main- and sidechains will be presented. We succeeded to prepare high quality thin films of substituted PPVs that can favourably be used as waveguides that show attenuation losses in the order of 1 dB/cm at 1064 nm. The comparison of $\chi^{(3)}(-3\omega; \omega, \omega, \omega)$ of the polymers with their corresponding oligomers allows us to determine the effective conjugation lengths of the polymers. However, THG data can only be used to make rough estimates of static i.e. nonresonant electronic contributions to n_2 .

In order to obtain n_2 directly at λ with high detection sensitivity, we use intensity-dependent prism coupling of waveguide modes [4]. The principle and an example of the measurement are shown in Fig. 1. Picosecond laser pulses of an OPG are used in the range 700 – 2000 nm. The intensity-dependent shifts of the coupling curves are fully reversible. We performed model calculations to obtain the average guided wave intensity $\langle I_{\text{gw}} \rangle$ and the thickness of the air-gap between prism and film. We succeeded to calculate the shifts of the coupling curves quantitatively by using Δn and $\Delta \alpha$ as the only fit parameters. Fig. 2 shows that Δn increases linearly with $\langle I_{\text{gw}} \rangle$ that is typical for a cubic nonlinearity. From such plots we obtain the *signs and absolute values* of n_2 and α_2 . We observe $\Delta n = +0.002$ of PPV at 910 - 950 nm on a picosecond timescale corresponding to $n_2 = +5 \cdot 10^{-12} \text{ cm}^2/\text{W}$. Such extremely large values were not anticipated from THG experiments [3]. We obtain W in the order of 10 for MEH-PPV.

We conclude that intensity-dependent prism coupling is a highly useful technique. We perform nonlinear waveguide spectroscopy in the near infrared and demonstrate that the cubic nonlinearities of conjugated polymers can be much larger as expected previously.

Invited Talks

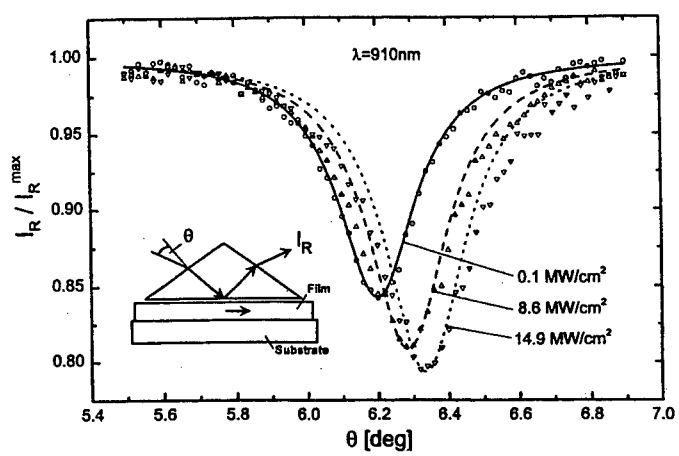


Fig. 1: Experimental setup and example of intensity dependent prism coupling of a waveguide of unsubstituted PPV (TE0 mode). If waveguiding occurs the reflected intensity I_R has a minimum that shifts reversibly at higher peak intensities of the incident beam.

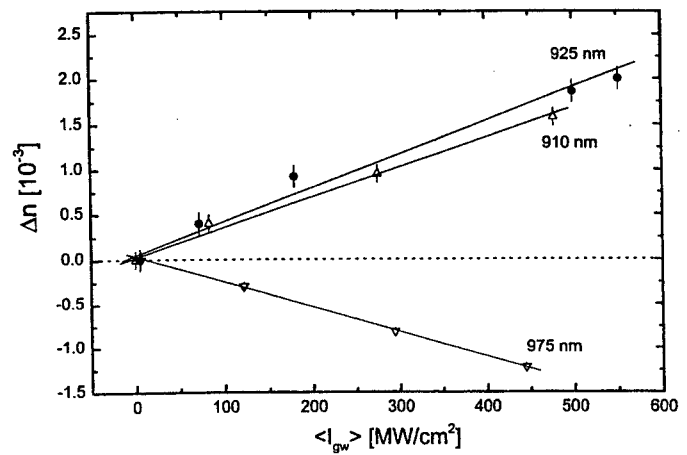


Fig. 2: Changes in refractive index of PPV as a function of the average intensity in the waveguide.

References

[1] G.I. Stegeman, R.H. Stolen, J. Opt. Soc. Am. B 6, 652-662 (1989).
 [2] J.L. Brédas, C. Adant, P. Tackx, A. Persoons, B.M. Pierce, Chem. Rev. 94, 243-278 (1994).
 [3] A. Mathy, K. Ueberhofen, R. Schenk, H. Gregorius, R. Garay, K. Müllen, C. Bubeck, Phys. Rev. B 53, 4367-4376 (1996).
 [4] K. Ueberhofen, A. Deutesfeld, K. Koynov, C. Bubeck, J. Opt. Soc. Am. B 16, No. 11 (1999).

Multifunctional macrocycles and polymers with carbazole oligomeric units

Tatsuo Wada, Atsushi Gunji, Yoshihiro Imase, Tetsuya Aoyama, Hiromi Kimura-Suda and

Hiroyuki Sasabe

*Biopolymer Physics Laboratory, RIKEN, 2-1 Hirosawa, Wako, Saitama 351-0198,
Japan*

We have developed efficient photorefractive carbazole trimers which provide the molecular level tuning of optoelectronic property based on their well-defined structure. Fully functionalized polymers successfully suppressed the phase separation and crystallization. We introduced the trimer units into the polymer main chain and macrocycles. These main-chain polymers with oligomer units can be expected to provide the both advantages of oligomer and polymers. In this paper we discuss the difference of oligomer and polymer in terms of their photorefractive and electroluminescence properties and propose the molecular systems with oligomer units as a new photonic material.

Invited Talks

The Current in Organic Light-Emitting Diodes

M. Schwoerer

*Physikalisches Institut und Bayreuther Institut für Makromolekülforschung
(BIMF), Universität Bayreuth, D-95440 Bayreuth, Germany*

Within only 10 years light emitting diodes or devices (LEDs) with thin films of polymers (PLEDs) or with vapor deposited low molecular mass organic thin films (OLEDs) have been developed to a high technical standard. In both classes the organics materials play the active role in the two fundamental properties of any LED: current and light. Two of the most prominent properties of these organic LEDs are the tunability of their color within the entire visible range and the large area of the thin organic films. - After a few historical remarks I will report on recent experiments by which the charge transport and the potentials across the interfaces and within the organic bulk in these organic LEDs have been analyzed. The experiments which I will report on in detail have been performed by Dr. W. Brütting together with PhD students.



Invited Talks



Charge Transport in Oligothiophene Single Crystals

B. Batlogg, J. H. Schön and Ch. Kloc

Bell Labs, Lucent Technologies, Murray Hill, NJ 07974 USA

The intrinsic charge transport properties have been studied on several oligothiophenes in single crystal form. Depending on temperature and crystal direction, either coherent band-like or incoherent hopping transport is observed in these distinctly layered structures.

Thin film transistors made of thiophenes or pentacene have reached performance levels comparable to that of amorphous Si, yet the intrinsic capabilities of most organic semiconductors are not well established. A main goal of our studies is to shed more light onto the charge transport in oligothiophenes, and the dependence on crystal direction, packing arrangement of the molecules, electric field strength, temperature and conjugation length. The basis of our studies are high quality single crystals, grown from the vapor phase, with electrically active centers below a concentration of $10^{14}/\text{cm}^3$. The electrical properties are probed by space-charge-limited-current spectroscopy, and by fabricating field-effect-transistors.

The carrier mobility is highly anisotropic in these compounds with a layered structure. Within the layers the charge transport is coherent, band-like. Mobilities at room temperature are as large as $\sim 0.9 \text{ cm}^2/\text{Vs}$ in the high-temperature modification of hexathiophene. Upon cooling the mobilities increase, following an inverse power law in temperature, and are ultimately limited at low temperature by shallow trap states. These results can be described as coherent motion of polaron-like quasiparticles with a temperature-dependent effective mass. Estimates of the low-temperature effective mass range from ~ 2 to ~ 20 , and an effective bandwidth ranging from $\sim 450 \text{ meV}$ to $\sim 50 \text{ meV}$ can be deduced. We observe a clear trend towards higher mobilities in compounds with longer molecules, indicating a decreased interaction between the charge carriers and the polarizable surrounding.

The charge transport perpendicular to the layers is incoherent and of hopping type, resulting in anisotropies of ~ 70 at room temperature and > 10000 at 100K. Typical activation energies for hopping are 80-130 meV. Microscopically, the incoherent transport is suggested to arise from the very weak wave function overlap across the ends of molecules in the adjacent layers. This is in contrast to, e.g., pentacene, where the transport is also anisotropic, but with coherent motion in all crystallographic directions.

Particularly noteworthy is the temperature-induced change of the transport characteristic within the molecular layers: it crosses over from band transport below room temperature to hopping motion well above ambient. This might be seen as the clearest evidence for the importance of the strong dynamic interaction between the charge carrier and its polarizable environment in an organic molecular crystal.



Invited Talks



1

Hypercubic octupolar molecular crystals for quadratic nonlinear optics

Joseph Zyss

Laboratoire de Photonique Quantique et Moléculaire, Ecole Normale Supérieure de Cachan,
61 Avenue du Président Wilson, 94235-Cachan, France

Tél. : 33-1-47 40 55 63 ; Fax : 33-1-47 40 55 67 ; zyss@lpqm.ens-cachan.fr

A « hypercubic » network connecting prototypical octupolar cubic templates in a H-bonded helicoidal strand is evidenced as the so-far elusive benchmarking octupolar crystalline lattice for quadratic NLO. Actual crystals are confronted to this target and NLO implications discussed

1. Introduction

Recognition in the early nineties of the enlarged potential for nonlinear optics of octupolar and more generally of multipolar systems at the molecular level has enlarged the earlier 1-D molecular diode template and triggered the exploration of new research avenues exploiting the so-far untapped reservoir of 3-D chemical structures [1]. A subsequent challenge has been the organization of such multipolar units into relevant and possibly optimized macroscopic assemblies and materials with an overall multipolar symmetry capable of revealing the properties of the underlying multipolar building blocks. Such « optimal » blueprints and the associated hierarchy of crystal structures have been recognized in the case of dipolar rods [2] but have failed so far to be generalized to octupolar crystalline lattices. We will report on recent advances in this domain and propose optimal octupolar crystalline templates following a general hypercubic lattice.

2. Hypercubic lattices as templates for optimal octupolar crystalline order

As far as quadratic nonlinear properties are concerned, the generic template for octupolar molecules has been shown to be amenable to a cube with alternating charges at the edges such as accounting for donor and acceptor substituents [1]. Various molecular implementations of this model have been demonstrated such as tetraphenylphosphonium and related tetraphenyl metallorganic moieties, substituted biphenyls and paracyclophanes. Further assemblies of octupolar cubes require the definition of optimal « hypercubic » lattices whereby the underlying molecular unit is fully promoted at the crystalline level.

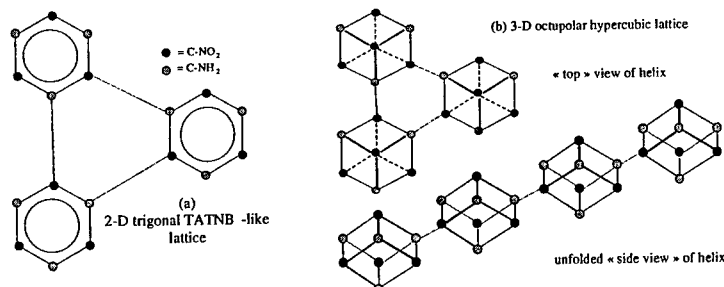


Fig.1: extension of the lamellar TATNB structure (a) onto an hypercubic arrangement in (b). 3-D octupolar molecules represented by cubes are arranged in an helical structure with

Invited Talks

hydrogen-bonded staircase geometry. The skew angle, in-keeping with specific steric considerations prevents overlap between the "upper" atom (in black) of the lowest left-hand side octupole and the "lowest" one the upper right octupole. The folded structure wraps-up in a helicoïdal strand.

In the general case of a fully substituted cube with eight alternating donor and acceptor edges, the optimal 3-D hypercubic structure, as shown in Fig.1(b), can be inferred from the optimal TATNB (1,3,5 trinitro-2,4,6 triaminobenzene) blueprint [3] structure in Fig.1(a) whereby intermolecular hydrogen bonds provide the required 3-fold symmetry 2-D network by connecting complementary donor amino and acceptor nitro groups from adjacent units. A strongly interlocked 3-D lattice with interplanar connectivity is ensuring both perfect octupolar alignment together with a strongly cohesive lattice.

3. A hierarchy of current state-of-the-art octupolar crystals for NLO

Proximity to such optimal template architectures will depend on specific steric as well as electronic affinity features. Various material implementations, some of them approaching closely this organizational blueprint, will be discussed and a quantitative ranking will be proposed, based on an adequately defined normalized tensorial distance between the nonlinear $\chi^{(2)}$ susceptibility of the actual structure and that of the reference template structure. Potential of hypercubic crystalline materials for nonlinear optics in terms of efficiency, transparency, quasi-phasemarching potential and polarization independence will be emphasized in view of their built-in linear and nonlinear isotropy features.

References

- [1] J.Zyss, J. Chem. Phys. **98**, 6583(1993)
- [2] J.Zyss and J.L.Oudar, Phys. Rev A. **26**, 2028(1983)
- [3] I.Ledoux et al., Chem. Phys. Lett. **172**, 440(1989)

Molecular Chirality as a Tool for Second-order Nonlinear Optics

A. Persoons, M. Kauranen, B. Busson, S. Van Elshocht, T. Verbiest
*University of Leuven, Laboratory of Chemical and Biological Dynamics
 Celestijnenlaan 200 D, B-3001 Heverlee, Belgium*

T.J. Katz, K. E. S. Phillips, C. Nuckolls
*Columbia University, Department of Chemistry, New York
 NY 10027, USA*

In this paper we describe the use of chirality as a tool to create macroscopic noncentrosymmetric structures for second-order nonlinear optics. We demonstrate quasi-phase matching in Langmuir-Blodgett films of chiral molecules and discuss the possibility of an electro-optic effect in chiral isotropic media

Chirality is equivalent to the lack of mirror planes in a molecule or a material. In linear optics, chiral molecules give rise to optical activity or circular-difference effects, i.e., the interaction with left- and right-hand circularly-polarized light is different. Such effects exist also in nonlinear optics. For example, second-harmonic generation (SHG) from chiral, isotropic surfaces is sensitive to the handedness of incoming circularly-polarized light. Hence, nonlinear techniques can provide new probes of chirality for applications in biomedical and pharmaceutical sciences [1]. In addition, due to their low symmetry chiral materials can be useful for second-order nonlinear optics because macroscopic assemblies of a single enantiomer of a chiral molecule are necessarily noncentrosymmetric.

We have studied second-harmonic generation from Langmuir-Blodgett (LB) films of a series of chiral molecules and polymers. The second-harmonic technique we use relies on measuring several second-harmonic signals as functions of the rotation angle of a quarterwave plate that controls the state of polarization of the fundamental. This technique allows us to determine all second-order susceptibility components of the chiral LB films.

One particularly exciting material we investigated was a chiral helicene Langmuir-Blodgett film. Such a film has a twofold rotational symmetry (C_2) and an extremely strong second-harmonic response, dominated by second-order susceptibility components associated with chirality (xyz-type components). The magnitude of these (chiral) susceptibility components was estimated to be on the order of 50 pm/V. Since the xyz-type components are only allowed by chirality, racemic samples of the same helicene have a second-harmonic response that is orders of magnitude lower than that of the chiral films. The quality and structure of the LB films can be influenced by heating. After a heat treatment at 220°C the films are more anisotropic in the plane of the film and their quality (as seen by AFM) is greatly improved. As a consequence, the susceptibility components that are connected to the anisotropy of the sample increase. However, the chiral susceptibility components are not affected by the heat treatment.

The chiral components of the second-order susceptibility of the helicene films reverse their sign between the enantiomers. Therefore, structures of alternating layers of the enantiomers could provide a new approach to quasi phase matching. In fact, we have experimentally demonstrated lowest-order quasi phase matching in the reflected direction, using LB films composed of alternating stacks of equal thickness of the R and S enantiomers [2,3].

Invited Talks

Films of the same chiral helicene can also be spincoated on glass substrates yielding high quality films (thicknesses from 0.1 to 1 micron) with a noncentrosymmetric D_{∞} symmetry. The samples have one nonvanishing susceptibility component of the xyz type. The magnitude of this component was found to be a few pm/V and the resulting second-harmonic response from the samples was found to be stable up to temperatures of 220°C.

Another interesting topic that we will discuss is the possibility of observing an electro-optic response from chiral isotropic media. Such materials would be inherently stable and could therefore be extremely useful for the development of electro-optic devices. Contrary to usual electro-optic materials, index (absorption) modulation in such media is due to the imaginary (real) part of the electro-optic susceptibility. The response relies on the damping of the material response. In addition, the response contains also dephasing-induced terms that could give rise to gain for the optical field. This possibility is extremely important for developing active components for electro-optic signal processing [4].

References

- [1] M. Kauranen, T. Verbiest, E.W. Meijer, E.E. Havinga, M.N. Teerenstra, A.J. Schouten, R.J.M. Nolte, A. Persoons, *Adv. Mater.*, **7**, 641 (1995).
- [2] T. Verbiest, S. Van Elshocht, M. Kauranen, L. Hellemans, J. Snauwaert, C. Nuckolls, T.J. Katz, A. Persoons, *Science*, **282**, 913 (1998).
- [3] B. Busson, M. Kauranen, C. Nuckolls, T.J. Katz, A. Persoons, *Phys. Rev. Lett.*, in press.
- [4] D. Beljonne, Z. Shuai, J.L. Brédas, M. Kauranen, T. Verbiest, A. Persoons, *J. Chem. Phys.*, **108**, 1301 (1998).

**SPECTROSCOPY OF EXCITED STATES IN ORGANIC MOLECULES
STUDIED BY OPTICAL LIMITING**

P-A. Chollet*, B. Paci, V. Hully, A. Sorin, J-M. Nunzi, F. Kajzar
CEA (LETI-DTA), DEIN/SPE/GCO, CEA-Saclay, F-91191 GIF CEDEX (France)
**pierre-alain.chollet@cea.fr*

Y. Morel, P.L. Baldeck
Dept of Spectrometry, Univ. Grenoble I, BP87, F-38402 St Martin d'Heres CEDEX (France)

M. Maggini, G. Scorrano, A. Bianco,
Dept of Organic Chemistry, Univ. of Padova, Via Marzolo 1, I-35131 Padova (Italy)

M. Prato, T. Da Ros,
Dept of Pharmaceutic Science, Universita di Trieste, Piazzale Europa I, I-34127 Trieste (Italy)

Optical limiting of nanosecond laser pulses has been measured in the visible range (450-700 nm) in solutions of a two-photon absorbing dye (stilbene3) and reverse saturable absorbers (functionalized fullerene). With the laser beam collimated inside the sample it was possible to fit the dependence of the transmission with the incident energy (0-3 mJ) using a multi-level models which enabled the determination of the wavelength dependence of the two-photon and excited state cross-sections of the various transitions. The results were in agreement with those determined by two-photon fluorescence and optical Kerr ellipsometry.

Nonlinear optical limiting can originate from different phenomena. Some are based on induced refractive index changes deviating (beam fanning in photorefractive crystals) or induced refractive inhomogeneities which generate beam scattering. Others take place at the molecular level and are connected with level population and transition between them. One kind of molecules are transparent at the incident wavelengths and are excited via two-photon absorption (TPA); the other kind absorbs partially the laser beam. In both cases, excited state absorption (ESA) is present. It enhances optical limiting in the case of TPA-molecules and is necessary for the absorbing molecules with the necessity that the ESA cross-section is larger than the ground state's one (Reverse Saturable Absorption, RSA). Thus, optical limiting gives insight into the different cross-sections and enables to perform spectroscopy of excited states. We describe experiments performed in the visible range with nanosecond laser pulses in TPA and RSA molecules.

Two-photon absorbing molecules

Two-photon absorbing molecules have the advantage of being transparent. TPA cross-sections in of organic chromophores have been predicted by quantum chemistry calculations and the general trends have been cleared up. We have analyzed the dependence of optical limiting in a dye (stilbene-3) within a three level model (figure 1). The connection between the population rate variation and the intensity absorption has enabled the determination of the TPA and excited state cross-sections, whose values agree with those determined by other techniques (two-photon fluorescence and optical Kerr effect).

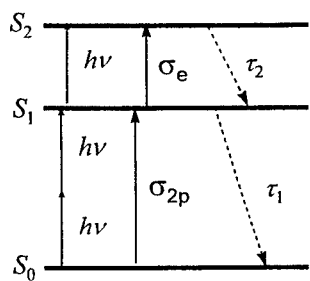


Figure 1. Two-photon absorption of the ground state S_0 , and one-photon reabsorption of the excited state S_1 .

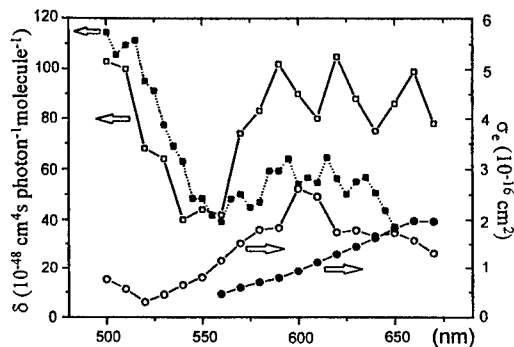


Figure 2. Wavelength dependence of the two-photon cross-sections δ (squares, left scale) and excited state absorption σ_e (circles, right scale) in stilbene 3. The open symbols are the value determined by optical limiting. The solid symbols are determined by two-photon fluorescence for δ and Kerr ellipsometry for σ_e . The line are for guiding the eyes.

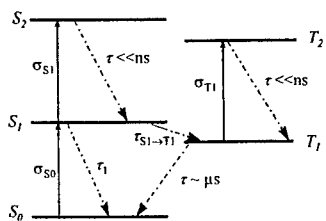


Figure 3. Five level model describing for the functionalized fullerene.

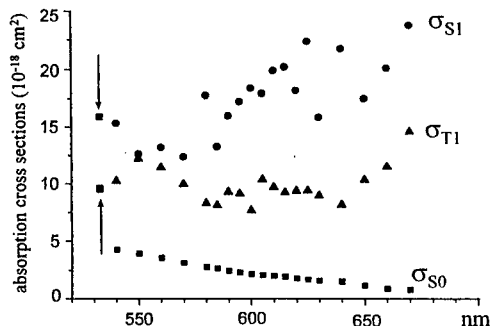


Figure 4. Cross sections of the different transition. The two arrows point values determined in fullerene by other authors.

Reverse saturable absorber

We have also studied reverse saturable absorbers (functionalized fullerene), whose electronic levels are shown in Figure 3. We have deduced from nonlinear transmission the absorption cross-sections of the singlet and triplet excited states (Figure 4), which appear clearly to be much larger than the ground state's one. This is the necessary fulfillment for optical limiting.

Acknowledgments

This work was partially supported by the French «Délégation Générale pour l'Armement» (contract n° 98364) and the Brite Euram Program (contract n° BRPR-CT97-0564).

Synthesis and Photonic Properties of Some Novel Heterocyclic Molecules

R. J. Twieg, S. Gu, M. He, F. You, A. Semyonov, L. Sukhomlinova,
Department of Chemistry
Kent State University
Kent, OH 44240

G. G. Malliaras R. Fan; D. Culjkovic
Department of Materials Science and Engineering,
Cornell University,
Ithaca, NY, 14853-1501

W. E. Moerner, D. Wright
Department of Chemistry
Stanford University
Palo Alto, CA

K. D. Singer, R. G. Petschek, V. Ostroverkhov, O. Ostroverkhova
Department of Physics
Case Western Reserve University
Cleveland, OH 44106

Conjugated organic molecules comprise the most interesting class of organic systems when one considers their potential applications as electronic and optical materials. The properties of the parent carbon based conjugated systems can be modified by the introduction of other elements (heteroatoms) or groups of heteroatoms as endgroups or as a part of the conjugated chain. Currently, a focus of our research effort involves the introduction of heterocyclic rings (especially oxadiazoles) into conjugated organic molecules. For example, we will describe heterocycle containing transport materials for nonlinear optical (NLO), photorefractive (PR), organic light emitting diode (OLED) and liquid crystal (LC) applications.

Heterocyclic organic materials play an important but often generally unrecognized role in the function of electronic and optical materials. Here we would like to discuss our current work on applications of heterocycles in a range of different types of electronic and optical materials. These molecules are loosely grouped together here as "photonic" materials but, in fact, have liquid crystal (LC) properties as a primary unifying theme.

In the area of LCs we have underway a program for the identification and preparation of high birefringence materials. A general working principle entails design of the LCs with minimal optically isotropic aliphatic content and so we usually try to work with materials with only one aliphatic tail. The cyanobiphenyls are very well known LCs and we have found that the substitution of a five member ring heterocycle for the cyano group gives rise to novel class of LCs (1b-1c). Notably, and in contrast, the analogous substitution by benzene (a simple alkoxyterphenyl) does not give rise to a derivative with mesogenic activity (1a).

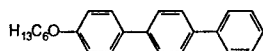
Again in the area of LCs we have been studying materials which also have charge transport and/or luminescent properties so as to prepare LC OLED devices. Of course heterocycles are already much appreciated for their utility in glassy and polymeric OLED devices usually in the capacity of charge transport of either holes or electrons. Our effort has concentrated on 1,3,4-oxadiazole (2a) and 1,3,4 thiadiazole (2b) type LCs. In the glassy state working bilayer and multilayer OLED devices have been prepared from these compounds. Studies of these molecules in the LC state are presently difficult because of the high

Invited Talks

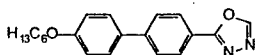
temperatures of the mesophases in available molecules. So, we are trying to design molecules with lower temperature LC ranges and we are looking at special "microcells" for evaluation of the LCs. Our strategy entails typical tail modifications as well as building multiple heterocycles, such as bis-oxadiazoles, into these materials (3a-3b).

Heterocycles such as thiophene and oxadiazole have some very disparate electronic properties due to their relative electron rich and poor character and therefore can serve simultaneously not only as π -conjugators but also as donor or acceptor (4). The exact location and number of heterocycles influences the overall shape of the molecule along with a variety of additional interesting consequences. In the center of a molecule a single heterocycle installs a kink which may inhibit conventional calamitic liquid crystal activity but, on the other hand, may produce special multidimensional contributions to the nonlinearity.

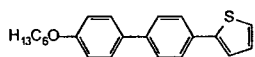
We have recently successfully built high birefringence LCs based on pyridine heterocycles that were originally designed as photorefractive chromophores. This was first accomplished with methylene dihydropyridines (such as 5a) but has now been extended to methylene tetrahydropyridine (5b) and methylene hexahydropyridine (5c) LCs. The electronic and optical properties of these and related heterocyclic compounds are now being actively investigated. We also wish to acknowledge here other collaborators involved in these studies.



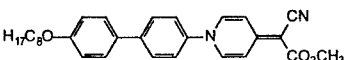
(1a) K 203 I



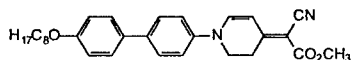
(1b) K 152 S_A 163 I



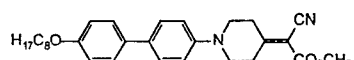
(1c) K 150 S_B 198 I



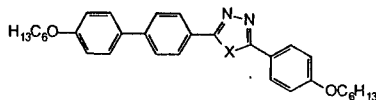
(5a) K 139 K 186 S_A 277



(5b) K 155 S_A 222 N 228 I

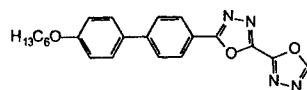


(5c) K 142 S_A 150 I

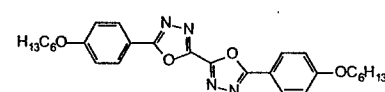


(2a) X = O K 116 K 125 K 127 S_A 170 N 180 I

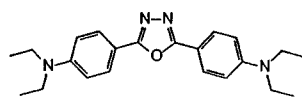
(2b) X = S K 115 S_A 288 N 339 I



(3a) K 172 S_A 175 N 195 I



(3b) K 176 S_A 178 N 189 I



(4)

Polarization State Sensitive Processes in Chiral Molecular Systems and Gyrotropic Materials

F. Jonsson, M. Haddad, R. Frey and C. Flytzanis
Laboratoire d'Optique Quantique, Ecole Polytechnique
 91128 Palaiseau cedex, France

We analyze nonlinear optical effects in gyrotropic media that show specific polarization state sensitivity and can be used to develop techniques for the study of dynamical processes in chiral molecular systems and organic spin complexes. We assess some nonlinear propagation aspects for polarization state control in such media as well as the impact of the time reversal operation and nonreciprocity in gyrotropic cavities and periodic structures with particular emphasis in magneto-optic parametric interactions.

The polarization state of the light reflects the vector nature of the electromagnetic field and introduces specific aspects that drastically effect the discrimination and robustness of certain electromagnetic interaction. Optical birefringence and dichroism, intrinsic or photoinduced, play a key role there. These aspects have been extensively addressed in the case of media with optical anisotropy, natural or photoinduced through the optical Kerr effect, and have led to important applications in beam coupling, and spectroscopic diagnostics.

The case of circular birefringence and dichroism or gyrotropy is related to a quite distinct physical origin and its impact is manifested in strikingly different way⁽¹⁾ from that of the linear birefringence or optical anisotropy. In particular circular birefringence is an intrinsically transverse effect resulting from the interplay of the electric and magnetic field-matter interactions and can even occur in effectively isotropic media. In the linear regime⁽¹⁾ circular birefringence (and dichroism), natural or artificial, as exemplified by the optical activity and Faraday rotation, can be traced to the relation

$$\underline{D} = \epsilon \underline{E} + i(\underline{G} \wedge \underline{E}) \quad (1)$$

between the electric induction \underline{D} and the electric field \underline{E} where ϵ is the dielectric constant, a scalar for an isotropic medium, and \underline{G} is the gyration vector, a material vector property. In the nonlinear regime⁽²⁾ along with the dielectric constant ϵ the gyration vector \underline{G} also becomes field intensity dependent leading to photoinduced modifications of the gyrotropy.

We discuss⁽²⁻⁶⁾ the two beam coupling and degenerate four wave interaction in nonlinear gyrotropic media and compare their efficiencies, specific symmetry features and conservation laws related to gyrotropy. In particular we compare the cases of natural and artificial gyrotropic materials, such as chiral molecules (and polymers) and magneto-optic systems respectively, and we show that in certain configurations the nonreciprocity and time reversal symmetry introduce drastic differences between the two classes.

This is most evident in the presence of inhomogeneities or interfaces^(7,8) and is particularly striking in the nonlinear interactions in gyrotropic, cavities, gyrotropic Fabry-Perot resonators and gyrotropic periodic structures. Here we show that gyrotropy together with non-reciprocity introduce subtle patterns in their transmission and reflection characteristics. Thus the analysis of the nonlinear gyrotropic Fabry-Perot cavity shows that

Invited Talks

one can have a polarization controlled multistable and instable behavior of the transmitted intensity. In addition nonreciprocity can be switched on/off with appropriate choice of the cavity and gyrotropic material parameters. Similar effects occur in periodic gyrotropic guides and structures.

We show that polarization state controlled three-wave parametric interactions in nonlinear gyrotropic media can be very efficient for parametric amplification and oscillation by cavity feedback if circular birefringence can be used for phase matching. Here an extension of the Manley-Rowe relations is presented to also include electromagnetic angular momentum conservation along with the Poynting vector (or flux) conservation. This has some drastic consequences on the polarization state and frequency combinations of the output beams.

All these processes are enhanced close to resonances which in addition introduce dynamical effects related to the relaxation processes.

References

- [1] L.D. Landau and E.M. Lifshitz, *Electrodynamics of Continuous media*, Butterworth and Heinemann Oxford 1984
- [2] M. Haddad, F. Jonsson, R. Frey, C. Flytzanis, *Nonlinear Optics*, to be published
- [3] H. Rabin and P.P. Bey, *Phys. Rev.* **156**, 1010 (1967)
- [4] S.A. Ahkmanov, G.A. Lyakhov, V.A. Makarov and V.I. Zharikov, *Opt. Acta* **29**, 1359 (1982)
- [5] P. Unsbo and C. Flytzanis, *J. Opt. Soc. Am.* **B14**, 560 (1997)
- [6] S. Wabnitz, E. Westin, R. Frey and C. Flytzanis, *J. Opt. Soc. Am.* **B13** (1996) ; *Opt. Comm.* **158**, 97 (1998)
- [7] F. Jonsson, C. Flytzanis, *Phys. Rev. Lett.* **82**, 1426 (1999) ; *Opt. Lett.* **24**, 1514 (1999) and to be published
- [8] M. Haddad, R. André, R. Frey and C. Flytzanis, *Sol. St. Comm.* **111**, 61 (1999)

Frequency conversion through parametric interaction and cascaded processes in a NPP crystal

G. P. Banfi, P. K. Datta, V. Degiorgio and D. Fortusini,

*Istituto Nazionale per la Fisica della Materia and Dipartimento di Elettronica,
Università di Pavia, 27100 Pavia, Italy*

E. E. A. Shepherd and J. N. Sherwood

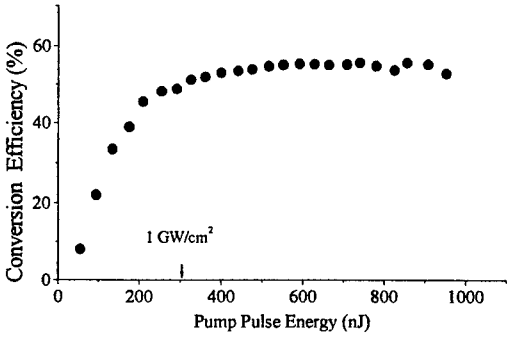
*Department of Pure and Applied Chemistry
University of Strathclyde, Glasgow G1 1XL, UK*

We present measurements performed on a 2.8-mm-thick crystals of N-(4-nitrophenyl)-L-prolinol. The specimen, obtained by cleaving a thick slice parallel to the (101) plane, allows access to the dominant phase matching orientation, including the noncritical one. Various frequency conversion processes (second harmonic, parametric generation and nearly-degenerate frequency conversion through cascading) were produced at a very low input intensity. In particular, at wavelengths around 1.15 μm , all optical frequency conversion with unit gain is obtained with a pump intensity as low as 9 MW/cm^2 , while parametric generation from quantum noise, with 10% conversion efficiency, is obtained in a single pass of a 100 MW/cm^2 pump pulse.

The organic crystal N-(4-nitrophenyl)-L-prolinol (hereafter called NPP), developed by Zyss and coworkers¹ through a molecular engineering approach, is known to possess one of the largest usable second-order nonlinear optical susceptibility in the near infrared. In our experiment we took advantage of the larger size and improved optical quality of the crystals obtained through a new growth procedure.² Our specimen was 2.8 mm-thick, with a clear aperture of 5x15 mm. In the measurements we employed tunable picosecond pulses. We first derived the value of the nonlinear coefficient d_{21} of NPP by comparison with the SH yield of 1-mm-thick BBO crystal. Correcting for Fresnel and scattering losses, we obtain, at $\lambda_p = 1.15 \mu\text{m}$, $d_{21}(\text{NPP}) = 48 \text{ pm}/\text{V}$.

We operated the NPP-based traveling wave parametric generator under noncritical phase-matching, with a pump spot-size around 30 μm . Tuning was accomplished by changing the pump wavelength. By changing the latter from 560 nm to 574 nm, the generated signal and idler covered the IR range from 837 to 1672 nm. It is a remarkable property of such a kind of generation that a given change in the pump wavelength yields a variation of signal and idler wavelengths which can be 10-20 times larger. The conversion efficiency (internal,

Invited Talks



hence correcting for Fresnel losses) from pump to signal+idler is shown in the figure. We find that, starting from quantum noise, conversion to 0.8-1.6 μm radiation with 10 % efficiency only requires 160 MW/cm^2 intensity, or 50 nJ for the energy of the 20 ps pump pulse. This is an exceptionally

low pump requirement, well consistent with the expectations based on the high d_{21} value of NPP.

We then show that the high second-order nonlinearity of NPP can be exploited in a cascaded process for the efficient generation of a frequency shifted beam.³ We used nearly-degenerate-frequency-mixing (NDFM): a pump p at frequency λ_p and a signal s at λ_s , with λ_s close to λ_p , are made to interact in the nonlinear material to generate a frequency shifted signal f at $\lambda_f = 2\lambda_p - \lambda_s$. NDFM can be exploited to realize a wavelength shifter, an interesting device for wavelength division multiplexing in optical networks. Defining by η the ratio of the energy of pulse f at the output to s at the input, the challenging aim is to obtain $\eta=1$ with a moderate pump intensity. Also in this case, we made use of the noncritical p-m and we set pump and signal wavelengths at $\lambda_p=1.148 \mu\text{m}$ and $\lambda_s=1.158 \mu\text{m}$, respectively. We find that $\eta=1$ can be obtained at a pump intensity of only 9 Mw/cm^2 . In the low intensity regime, the cascading process in our NPP crystal can be described in terms of an effective third order nonlinearity $|\chi_{eff}^{(3)}|=2.4 \times 10^{-17} \text{ m}^2/\text{V}^2$, which we believe to be the largest nonresonant electronic third-order nonlinearity measured so far in the near infrared. We shall also present a numerical simulation of the cascading experiment which describes satisfactorily the experimental results and is used to give a perspective of the potentiality of the crystal.

1. J. Zyss *et al.*, *J. Chem. Phys.* **81** (1984) 4160; I. Ledoux *et al.*, *J. Opt. Soc. Am. B* **4** (1987) 987.
 2. B.Y. Shekunov *et al.*, *J. Phys. Chem.* **99** (1995) 7130; J. N. Sherwood, *Pure Appl. Opt.* **7** (1998) 229.
 3. G. P. Banfi *et al.*, *Opt. Lett.* **23** (1998) 439.

Quantum mechanical limits of the nonlinear optical susceptibility

Mark G. Kuzyk

Department of Physics, Washington State University, Pullman, WA 99164-281, USA

The goal of structure-property relationship studies has been to build the required knowledge to design molecules with enhanced nonlinear-optical susceptibility. These have included the two- and three-level models of Dirk, Garito, Kuzyk, and Pierce and the bond-alternation models of Bredas, Marder, Meyers, and coworkers. While these have led to the design and synthesis of better materials, the interesting question remains, "What is the largest nonlinear-optical susceptibility allowed by quantum mechanics." We apply simple principles of quantum Physics to show that nature does indeed set an upper limit. The theory is verified by comparing its predictions with extensive nonlinear-optical measurements.

Invited Talks

Molecular Considerations for Optimizing the Second-Order Nonlinear Optical Response in Chiral Media

V. Ostroverkhov, O. Ostroverkhova, R.G. Petschek, and K.D. Singer
Department of Physics
Case Western Reserve University
Cleveland, OH 44106

L. Sukhomlinova, R.J. Twieg, X.-Y. Wang, and L.C. Chien
Liquid Crystal Institute and Department of Chemistry
Kent State University
Kent, Ohio 44242

Molecular properties leading to second harmonic generation in chiral media in the electric dipole approximation for the cases of axial and biaxial symmetry are described. The components of the hyperpolarizability tensor that transform like a second-rank pseudotensor ($L=2$) and a third-rank tensor ($L=3$) contribute. A quantum two-level model illuminates the molecular features necessary for optimizing the second-rank pseudotensor for dipolar molecules. Results of the measurements of these components in representative molecules using hyper-Rayleigh scattering are presented. Two compounds in which the delocalized π -system is two-dimensional, a camphorquinone derivative and crystal violet are found to exhibit large $L=2$ and $L=3$ components.

Second order nonlinear optics requires a noncentrosymmetric material. Consequently, much effort has gone into developing polar materials that exploit the dipolar (vector) component of the molecular hyperpolarizability. However, it has been recognized for a long time that even isotropic fluids containing chiral molecules can exhibit second order nonlinear optical effects.[1] Second harmonic generation is not observed in such isotropic chiral media, but may be observed in materials with minimal additional imposed symmetries. Since one would like to avoid the difficulties of fabricating and maintaining polar structures, one would like materials with symmetries that allow the easiest fabrication of macroscopic media exhibiting second harmonic generation. The symmetry group D_∞ , which consists of a nonpolar axis and no mirror planes, is the simplest. The group D_2 , which has three two-fold axes and no mirror planes, is also a candidate. The D_∞ symmetry can be fabricated by a single axial stretch of a polymer containing chiral molecules, and is characteristic of a nematic or smectic A liquid crystal. The D_2 symmetry can be attained using a two-axis stretch or shear alignment of a polymer containing chiral molecules, and the closely related C_2 symmetry is characteristic of a smectic C or other biaxial phases of liquid crystals. Thus, these symmetries may be easily and robustly fabricated.

The question then arises as to how to optimize molecular properties in these chiral media. To analyze this we examine how the molecular hyperpolarizability is expressed in terms of the irreducible rotation group. It is found that a second-rank pseudotensor ($L=2$) component makes the only contribution in the case of D_∞ symmetry while both the $L=2$ and $L=3$ contribute in the D_2 case. This $L=2$ component exists in non-Kleinman symmetric materials, and chiral, multidimensional π -electron containing chromophores.[2]

In this study, we describe our efforts aimed at measuring and understanding the features of appropriate chromophores exhibiting this $L=2$ character. We have looked at a quantum mechanical model in the two-level approximation in order to elucidate the basic

Invited Talks

design features for active chromophores. We find that molecules with transition moments perpendicular to the change in dipole moment between the ground and excited state maximize this optical nonlinearity and that the magnitude of the $L=2$ component generally depends on the sine of the angle between the dipole moment difference between the first excited and ground states and the transition moment associated with these states.

We have measured figures of merit for the rotational invariants associated with Kleinman disallowed components using nonlinear light (hyper-Rayleigh) scattering. The intensity of second harmonic light scattered from isotropic solutions of the nonlinear molecules is defined by the rotational average of squared molecular hyperpolarizability tensor $\langle \beta\beta^* \rangle$. The latter can be rewritten as a sum of rotationally invariant tensors multiplied by scalar figures of merit that characterize the hyperpolarizability tensor and are essentially the values being measured in the experiment. The rotationally invariant tensors are solely functions of incoming and outgoing polarization vectors, which are controlled by appropriate polarizer and retarder orientations. The intensity of the scattered light is measured as a function of the polarization state of the incoming and generated light. The raw data is then Fourier-transformed, and the set of invariants are found by fitting the measured Fourier components to ones calculated theoretically. These invariants describe figures of merit for $L=1$ polar (vector), $L=2$ (second-rank pseudotensor), and $L=3$ octupolar (traceless, symmetric third-rank tensor) processes, and thus fully characterize second-order nonlinear optical interactions.

The compounds measured include pNA, camphorquinone derivatives, and crystal violet. The spectral content of the scattered light was measured to verify that multiphoton fluorescence was not problematic at the measured wavelengths. We find that the molecular features for large $L=2$ response are generally consistent with the quantum model. For example, the nearly one-dimensional pNA is nearly Kleinman symmetric and exhibits no $L=2$ component. The chiral camphor derivatives are largely dipolar. Thus, the angle between the dipole moment change and the transition moment are somewhat different but not large enough to provide for a large $L=2$ component. However, these are chiral π -electron systems and may be combined to form more active chromophores. Crystal violet exhibits large $L=2$ and $L=3$ components relative to a nonzero dipolar component. The somewhat resonant values for the $L=2$ and $L=3$ figures of merit are $359 \pm 61 \times 10^{-30}$ esu and $518 \pm 695 \times 10^{-30}$ esu respectively. The large magnitudes of the crystal violet figures of merit indicates that crystal violet is an interesting candidate for use in chiral materials if it can be constructed into an appropriate macroscopic symmetry. These results point out directions for optimization of the chiral molecular nonlinear response.

Support by the NSF under Science and Technology Center Advanced Liquid Crystalline Optical Materials grant DMR89-20147 is acknowledged.

References

- [1] J. A. Giordmaine, "Nonlinear Optical Properties of Liquids", *Phys. Rev.* **138**, 1599-1606 (1965).
- [2] S.F. Hubbard, R.G. Petschek, K.D. Singer, N. D'Sidocky, C. Hudson, L.C. Chien, C. Henderson, and P.A. Cahill, "Measurements of Kleinman-disallowed Hyperpolarizability in Conjugated Chiral Molecules", *J. Opt. Soc. Am. B* **15**, 289-301 (1998).

THz Wave Sensors and Their Applications

P. Y. Han, M. Tani, F. Pan, and X.-C. Zhang

Physics Department, Rensselaer Polytechnic Institute Troy, NY 12180

Terahertz electro-optic sensors make it possible to see images of electric fields, abnormal tissue, and chemical composition of plants that cannot be detected by other imaging systems. Organic DAST will play an important role in THz optoelectronics.

Electro-optic (EO) crystals could be ideal materials for generating and detecting free-space ultra-broadband THz waves. We report recent results on the material selection of THz emitters and sensors for THz image applications. Organic DAST crystal is a promising candidate with high applicable frequency bandwidth up to 20 THz and large EO coefficients. We also report the development of a novel scheme with DAST as an ultrafast THz wave sensor for the first time.

Characterization of DAST by THz reflection and transmission spectroscopy

A *c*-cut DAST sample with a dimension of $4 \times 6 \times 1 \text{ mm}^3$ is used in experiments. Due to the strong birefringence, separate measurement is done with THz polarization parallel to *a* and *b* axis of DAST. For THz transmission geometry, useful data is limited to less than 1 THz due to the strong absorption at higher frequency. While for reflection geometry, the whole spectrum from 0.2 THz up to 3 THz can be resolved. Fitting the data with an oscillator model yields a complete characterization of dielectric constant[1] of DAST. Fig. 1 shows the experimental reflectivity of DAST and the fitting curves using oscillator model. At *a* axis, one phonon is observed, while two phonons are observed in *b* axis.

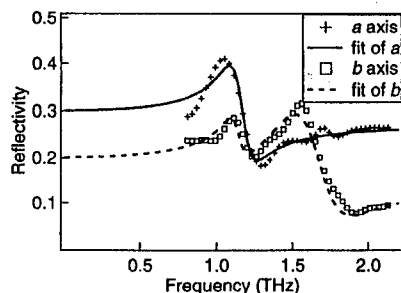


Fig. 1: Experimental reflectivity of DAST and the fitting curves using oscillator model along *a* and *b* axis.

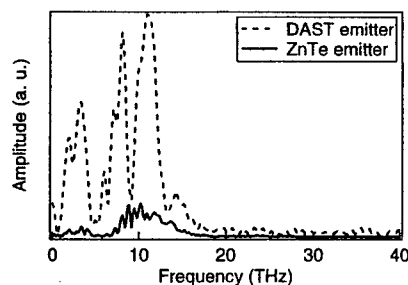


Fig. 2: High frequency THz spectra generated from an 100- μm DAST and a 30- μm ZnTe emitter.

High frequency THz emitter and EO sensor

With the development of THz spectroscopy, it is often necessary to study materials and phenomena at 6-20 THz. DAST was demonstrated as an excellent emitter at less than 5 THz.[2] Here, we present the experimental THz spectrum of DAST as emitter with bandwidth up to 20 THz in Fig. 2, showing a six-fold increase comparing with that of a thin ZnTe sample at the same condition. A novel scheme is employed to compensate the intrinsic birefringence of DAST as a THz sensor, as shown in Fig. 3. A quarter waveplate is aligned so that *s* polarization becomes *p* polarization and vice versa after going through it twice. Thus, optical components along both *a*

Invited Talks

and *b* axes goes through the same DAST twice with two orthogonal polarization states and have the same phase path. Experimental THz waveform is shown in Fig. 4, together with result obtained using a 0.5 mm ZnTe sensor at the same condition. The amplitudes, waveforms and spectra (not shown) are all comparable indicating that DAST is a good EO sensor up to the frequency detected. From the known EO coefficients, the THz amplitude from DAST should be several times larger than that of ZnTe. We attribute the deviation from theory to the imperfection of optical quality of DAST, such as unflatness, inhomogeneity, scattering, and depolarization.

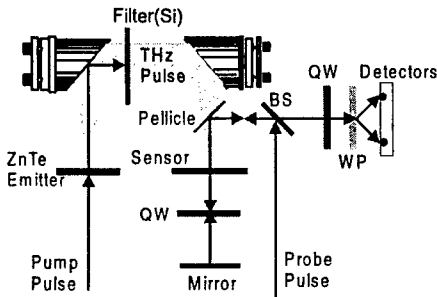


Fig. 3: Schematic setup. QW: quarter waveplate; WP: Wollaston prism; BS: beamsplitter.

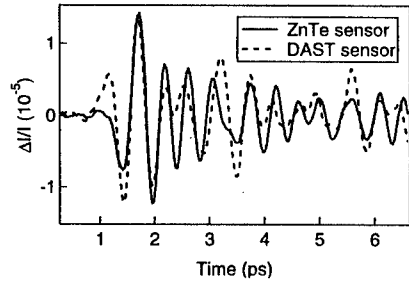


Fig. 4: THz waveform obtained using DAST and ZnTe as EO sensor at the same condition.

Conclusions

We have completely characterized the complex dielectric constant of DAST by oscillator model at THz frequency. DAST has been shown a good THz emitter up to 20 THz. DAST as an ultrafast EO sensor at THz frequency has been realized for the first time. With the improvement of the optical quality, higher response is expected. This technique extends the frequency response of DAST from GHz to THz and opens the door for its applications in high frequency EO waveguide modulator, THz imaging and other ultrafast EO devices at THz frequency region.

References

1. S. Keiding, in private communication.
2. Zhang, X.-C. et. al. Applied Physics Letters **61**, 3080-3082 (1992). K. Kawase et. al. Optics Letters **24**, 1065-1067 (1999).

Growth and Processing of DAST crystal and Its Application toward Tera-Hertz

Hiromasa Ito*,**

**Research Institute of Electrical Communication, Tohoku University
2-1-1, Katahira, Sendai 980-8577, Japan*

Tel : +81-22-217-5518, Fax : +81-22-217-5521

***RIKEN Photodynamics Research Center (PDC)*

19-1399 Koeji, Nagamachi Sendai, 980-0868 Japan

E-mail : hiromasa@riec.tohoku.ac.jp

Among many nonlinear crystals, the organic ionic salt crystal of 4-dimethylamino-N-methyl-4-stilbazolium-tosylate (DAST) is known for its huge nonlinearity. We established reproducible crystal growth method of large and high quality DAST. Due to the fragile nature of organic crystal, it is also so important to establish the processing. We are developing it by the ablation using an excimer laser. Varieties of application are feasible using DAST. As one of the high-frequency applications, the coherent terahertz-wave generation is reported by means of the difference frequency generation between two simultaneously oscillating signal wavelengths of quasi-phases-matched parametric oscillator.

Organic nonlinear optical crystal DAST, which excels over other nonlinear optical materials in its abilities, was first invented and patented by H. Nakanishi et. al[1]. DAST crystals with relatively large dimensions are grown in a saturated methanol solution from seed crystals by controlled temperature lowering or controlled solution vaporization using a temperature programmable incubator / water bath. We have been challenging these several years to establish reproducible and stable DAST crystal growth[2]. Three cascaded runs of growth are adopted, and for the final growth seeds are fixed to a holder and placed in a DAST solution. Fig. 1 shows a grown DAST crystal using this method at a 2.0deg/day cooling rate, $12 \times 11 \times 2 \text{mm}^3$ of dimensions, and a 1.6mm/day growth rate.

DAST crystal, which is harder among other organic one, is still not easy to cut and polish directly. A laser ablation using an excimer laser (248nm) was developed for manipulating DAST crystals. Fig. 2 shows an example of processed ones. The pattern of the metal mask was transferred with high fidelity.

Organic nonlinear materials, especially DAST, have lots of advantages to use for high frequency applications such as millimeter and sub-millimeter wave; in other words, sub-Tera Hertz to Tera Hertz regions. Due to the a large second-order nonlinearity ($d_{11}^{\text{DAST}} \sim 100 d_{31}^{\text{LiNbO}_3}$), it could generate coherent tunable THz-waves efficiently[3]. We demonstrated the difference frequency generation (DFG) of THz-wave by using two simultaneously oscillating signal wavelength lines from quasi-phases-matched optical parametric oscillator. We specially prepared the periodic poled LiNbO₃ (PPLN), which has two different domain periods integrated in a sample. The insert of Fig. 3 shows the experimental setup of THz generation from DAST using a dual signal-wave parametric oscillation. PPLN sample had two domain periods of 29.3 and 29.5 μm , and OPO oscillates at two signal waves of 1.529 and 1.546 μm . About 100 μJ /pulse of two signal outputs at 1 kHz were introduced to 1mm-thick DAST sample to produce the DFG. The THz wavelength was measured by a scanning Fabry-Perot etalon consisting of two metal mesh plates, and the displacement between two periods was 139 μm , which corresponds directly to the

Invited Talks

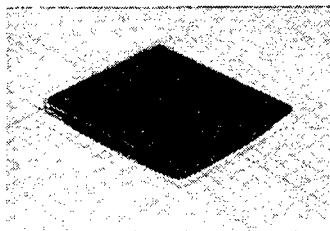


Figure 1: Examples of grown DAST crystals.

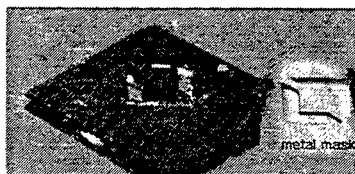


Figure 2: Processed DAST by excimer ablation.

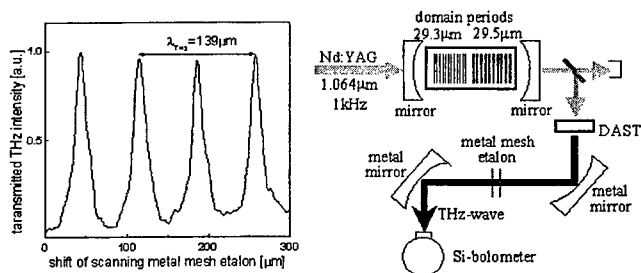


Figure 3: Experimental setup and THz-wave measurement from dual signal-wave QPM-OPO with cascaded domain grating.

generated wavelength. Under the same condition, we obtained the THz signal only from DAST, but not from LiNbO_3 , GaAs and ZnSe.

Further development and improvement for crystal quality and its applications are expected. This work has been performed with numerous people's efforts: T. Takahashi, Y.-M. Son, N. Osaki, T. Hatanaka, M. Mizuno, T. Taniuchi (RIEC), H. Nakanishi and S. Okada (ICRS) of Tohoku University, K. Kawase of RIKEN PDC, S. R. Keiding of Univ. of Aarhus.

- [1] H. Nakanishi, H. Matsuda, S. Okada, and M. Kato, Proc. the MRS Int. Mtg. Adv. Mater., **1**, 97 (1989); Japan Patent No. 1716929 (1986).
- [2] S. Sohma, H. Takahashi, T. Taniuchi, and H. Ito, J. Chem. Phys., **245** (1999).
- [3] K. Kawase, M. Mizuno, S. Sohma, H. Takahashi, T. Taniuchi, Y. Urata, S. Wada, H. Tashiro, and H. Ito, Optics Lett., **21**, 1065 (1999).

Poster Session I

Spatial Solitons in Dye-Doped Nematic Liquid Crystal

G. Abbate

*INFN unità di Napoli and Università di Napoli Federico II
Via Cintia Monte S. Angelo, 80126 Napoli, ITALY*

J.F. Henninot, F. Derrien, M. Warengem
*LPCIA, Université d'Artois, Faculté J. Perrin
rue J. Souvraz, 62307 Lens, FRANCE*

(2D+1) Optical spatial solitons were observed in standard Kerr materials and in photorefractive ones. Owing to their giant nonlinearity, liquid crystals (LC) can be a good candidate for their observation. We describe here the observation of a spatial soliton in a dye doped nematic LC, at very low laser power (mW). The soliton is sustained for thousands of coherence lengths. A semi-phenomenological model explains the competition of thermal and reorientational nonlinearities and how thermal effects could induce a waveguide structure, even without reorientation. Moreover, using the optical waveguide theory, we show how the beam, emerging out of a single-mode fiber, can create a self-induced waveguide supporting the same intensity profile.

Since 15 years, optical spatial solitons have been exciting many researchers in the world. This fascinating object is interesting not only due to its large theoretical development but also through its very promising field of application: all-optical switching, light guided by light, new types of laser cavities and parallel signal processing. Nevertheless, most of the published works is up to now dealing with photorefractive devices, thanks to their low power requirement and their ability to generate solitons even with non-coherent light. The drawback is their low time constant (> 1 s) and their cost. Solitons have been also discovered in gas, glass and semiconductors, but sometimes it requires an high pump intensity. In Kerr media, (2D+1) solitons were found to be unstable, and in photorefractive media, the very low power required to obtain the soliton is correlated to the application of a DC field to the crystal. In 1993, MacLaughlin and co-workers [1] performed experiments on self-trapping of a beam in a nematic liquid crystal (LC) confined in a capillary tube, taking into account the enormous optical non-linearity of such a material (6 to 10 orders higher than doped glass). They observed self-focusing and filamentation of the beam for a moderate laser power (< 1 Watt). It seems that they have not observed spatial solitons, probably because the self-focusing was too strong over the transverse plane of the input beam, leading to filamentation. We describe here the observation of what we call a spatial soliton in a dye doped nematic liquid crystal confined in a capillary tube.

As a beam emerging out of a single mode fiber propagates into a capillary filled with dye doped liquid crystal (DDLDC), it induces an index gradient due to both a thermal indexing and a reorientation of the director. This leads to a complex non linear system, which we have explored experimentally [2]. It is worth noting that the CW laser power employed in our experiments was always in the mW range (up to 10 mW). The DDLDC is initially aligned in the capillary in such a way that the optical axis is parallel to the capillary axis. A single mode fiber is aligned in order to have the beam entering into the capillary parallel to its axis. Due to the experimental geometry, at very low power the DDLDC is seen as an isotropic material, then the optical Fréedericksz effect, enhanced by the Jánossy effect [3], occurs above an intensity threshold. As the input power is increased, we report the sequence of events which we have observed. In this sequence, there are two specific ranges of

Poster Session I

input power which allow a 2D + 1 spatial soliton-like propagation. The soliton observed for the low power range is attributed mainly to a thermal focusing effect, whereas the other one, which occurs at larger power is a combination of both thermal indexing and a director reorientation. Apart from these observations, several complimentary experiments are reported to confirm the soliton nature of these specific modes of propagation. The profiles of the beam are analyzed and found to be constant over millimeters (to be compared with a few microns diffraction length), showing the non divergence of the beam. Collision experiments show that two thermal solitons almost ignore each other, whereas the orientational ones have a more complex behavior. The role of the polarization of the input beam has been studied and the reorientation of the DDLC is also explored via the phase shift experienced by a probe beam transversally crossing the capillary.

Examining the equations, which rule the beam and its interaction with matter, namely the Maxwell's and the thermal transfer (Laplace) equations, we searched the experimental conditions that may lead to a pure thermal soliton, i.e. without any reorientation or, equivalently, at input light power below the Jánossy effect threshold. The results of the model are then compared with the experimental thermal solitons observed in the DDLC. Finally, the most recent observations seem to show a large robustness of the thermal soliton, whose behaviour is almost independent of power variations, of temperature and polarization changes, of the optical axis perturbation in DDLC region at the exit of the glass fiber. Even the occurrence of a small isotropic bubble between the fiber exit and the nematic DDLC does not affect significantly the soliton shape. The latter situations, in which the beam propagates through a region of randomly distributed optical axis, should avoid the spatial soliton formation, at least of the coherent type. Recently, Mitchell and Segev [4] have demonstrated the possibility of spatial soliton formation with incoherent light, so we could classify the thermal soliton observed in DDLC as an incoherent soliton.

References

- [1] E. Braun, L. Faucheux, A. Libchaber, D.W. McLaughlin, D.J. Muraki, M.J. Shelley, "Filamentation and undulation of self focused laser beams in liquid crystals" *Europhys. Lett.*, **23** (4), 239 (1993).
- [2] M. Warengem, J.F. Henninot, G. Abbate, "Non linearly induced self waveguiding structure in dye doped nematics liquid crystals confined in capillaries" *Optics Express*, **2**, 483 (1998).
- [3] I. Jánossy, A.D.Lloyd, B.S. Wherret, "Anomalous Optical Fréedericsz Transition in an Absorbing Liquid Crystal" *Mol. Cryst. Liq. Cryst.* **179**, 1 (1990)
- [4] M. Mitchell, M. Segev, "Self-trapping of incoherent white light" *Nature* **387**, 880 (1997)

Molecular engineering for optical limiting in the visible

C. Andraud, R. Anémian, A. Collet

École normale supérieure de Lyon, UMR CNRS 5532, 69364 LYON Cedex 07, France.

J.F. Nicoud

Institut de Physique et Chimie des Matériaux de Strasbourg-GMO, 23 rue du Loess, 67037 Strasbourg Cedex, France.

B. Paci, P.A. Chollet, J.M. Nunzi

LETI-CEA, DEIN-SPE, Groupe Composants organiques, 91191 Gif sur Yvette, France.

N. Sanz, A. Ibanez

Laboratoire de Cristallographie, CNRS Rhône-Alpes associé à l'Université Joseph Fourier et à l'Institut National Polytechnique de Grenoble, BP 166, 38042 Grenoble Cedex 09, France.

Y. Morel, P.L. Baldeck

**Laboratoire de Spectrométrie physique, Université J. Fourier, UMR CNRS 5588, 38402 St Martin d'Hères, France.*

In this work, we develop a molecular engineering approach to optimize both TPA and ESA phenomena for optical limiting. Several structures (one-dimensional or octupolar systems, monomers or oligomers) exhibiting promising optical power limiting properties, have been obtained. Experimental results are discussed from semi-empirical and sum-over states calculations for the different organic systems.

For nanosecond pulses, optical power limiting can be obtained by different nonlinear absorption processes, such as two-photon absorption (TPA).[1] In this regime, the nonlinear absorption of transparent organic materials is in fact a three-photon process, i.e. a two-photon initiating step followed by a transient absorption during the pulse duration as shown on Figure 1.[2] The nonlinear absorption resulting from this two-step process is governed by the three-photon absorption coefficient α_3 . In the case of a singlet S_1-S_n transition and of an instantaneous molecular response ($\tau_{01} < \tau_p$), α_3 is given by the following relationship:

$$\alpha_3 = \frac{N}{V} f^6 \frac{\sigma_{TPA} \sigma_{1n} \tau_{01}}{2(h\nu)^2} \quad (1)$$

in which N/V is the concentration, σ_{TPA} and σ_{1n} are respectively the two-photon and excited state absorption cross-section ; τ_{01} is the transient absorption lifetime and f the local field factor ($f = \frac{n^2 + 2}{3}$). Thus the design of more efficient materials require the optimization of all parameters involved in eq. (2).

Poster Session I

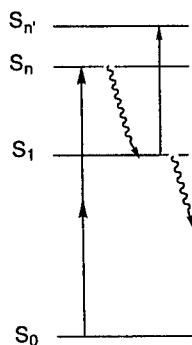


Figure 1 : Four-level model for the three absorption process.

The search of criteria to optimize the three-photon nonlinear absorption of molecules is just beginning. One-dimensional or octupolar systems, monomers or oligomers were studied. Experimental results were discussed from semi-empirical and sum-over states calculations for the different organic systems. We present some molecules satisfying the maximum permissible exposure for the retina.

We present in Figure 2 the three-photon coefficient in the visible range for bis-donor stilbene derivative.

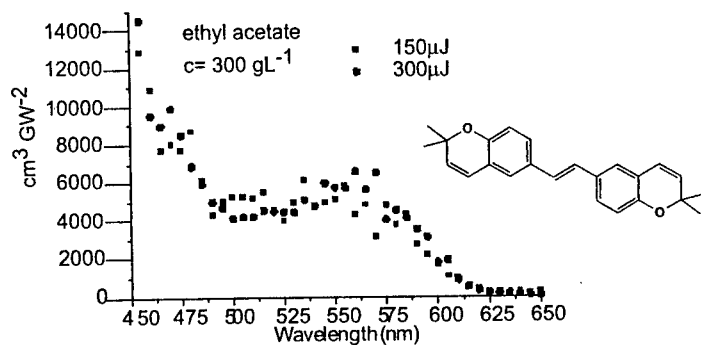


Figure 2 : Three-photon absorption spectra of a bis-donor stilbene derivative.

Acknowledgements : We are grateful to DGA for financial support.

References

- [1] L.W. Tutt, T.F. Boggess, Prog. Quant. Electr. **17**, 299 (1993).
- [2] P.L Baldeck, Y. Morel, C. Andraud, J.F. Nicoud, A. Ibanez Photonics Science News **4**, 5 (1999).

Nonlinear optical properties of octupoles

C. Andraud, T. Zabulon, R. Anémian, X. L. Yang, A. Collet
 École normale supérieure de Lyon, STIM, 69364 LYON Cedex 07, France.

S. Brasselet, I. Ledoux-Rak, J. Zyss
 École normale supérieure de Cachan, LPQM, 94235 Cachan Cedex, France.

The linear and nonlinear optical properties of these octupolar systems are studied and compared to those of their 1D counterparts. In order to reveal interactions within the different branches of the octupoles, the hyperpolarizability was dissected in an additive term β^A representing the tensorial sum of the constituting octupole 1D units hyperpolarizabilities and a term β^I representing interactions between these units. The generalization of this model to multipoles systems is also presented.

This paper discusses the linear and nonlinear optical properties of polyoctupoles of C_{3h} symmetry (Figure 1). This analysis rests on Harmonic Light Scattering (HLS) measurements and CNDO/S calculations. It is shown that, for the same conjugation length, octupoles exhibit a better hyperpolarizability-absorption trade-off, and that laws valid for 1D-dipolar polyenes hold for octupolar polyenes (linear variations of β with \sqrt{n} , exponential variations of $\|\beta\|$ with n). The macroscopic depolarization ratio D is estimated experimentally and is in line with the molecular symmetry. The results are explained in the light of CNDO/S calculations.

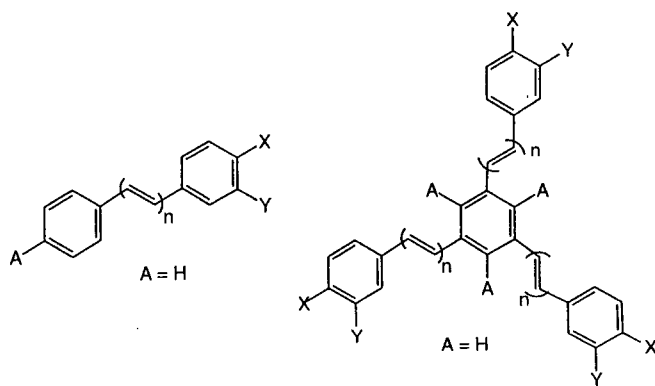


Figure 1 : Polyoctupoles and their 1D-dipolar analogues.

Finally, we present a multipolar interaction concept within the frame of irreducible representation, in which the b tensor of a multipolar system is dissected in two separate components [1]: one (β^A) representing the sum of the contributions of the individual dipole subunits, the other (β^I) reflecting interactions (charge transfer or coulombic) between the dipole units constituting the multipole. The interaction term β^I could be determined in magnitude and in direction in the irreducible $J = 3$ space. In large polyoctupoles, interactions between the octupoles subunits has been evidenced (up to

Poster Session I

20-30% of β^A). The generalization of this model to more conjugated octupoles and multipoles systems is also presented .

References

[1] C. Andraud, T. Zabalou, A. Collet, J. Zyss, Chem. Phys. **245** (1999) 243.

Biphenyl derivatives for optical limiting in the visible

R. Anémian, C. Andraud, A. Collet

École normale supérieure de Lyon, UMR CNRS 5532, 69364 LYON Cedex 07, France.

B. Paci, J.M. Nunzi

LETI-CEA, DEIN-SPE, Groupe Composants organiques, 91191 Gif sur Yvette, France.

Y. Morel, P.L. Baldeck

Laboratoire de Spectrométrie physique, Université J. Fourier, UMR CNRS 5588, 38402 St Martin d'Hères, France.

In this work, we developed a molecular engineering approach to optimize both TPA and ESA on diaminobiphenyl derivatives ; highly concentrated solutions of these compounds present promising properties for optical limiting in the visible. The different parameters involved in the expression of α_3 were determined and discussed in terms of relaxation.

Efficient protection of opto-electronic devices and vision sensors against damage caused by high power lasers can be performed by optical limiting materials.[1] Two-photon absorption (TPA) is an attractive mechanism for optical limiting in the visible range, since the material has an instantaneous response and presents no saturation effect. It has been shown that the nonlinear absorption phenomenon corresponds in fact to a three-absorption process, in which the TPA step is followed by an excited state absorption (ESA).[2] The resulting α_3 can be written as follows in the case of an instantaneous response and of a S_1 - S_n transition :

$$\alpha_3 = \frac{\beta \tau_1 \sigma_{1n}}{2\hbar\omega} \quad (1)$$

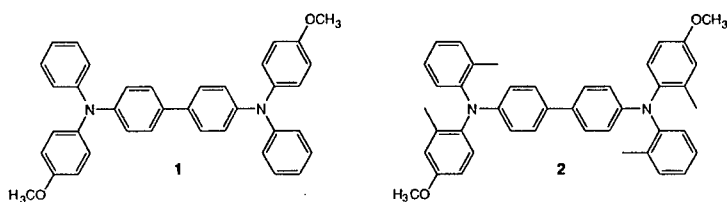
where β is the two-photon absorption coefficient, τ_1 the lifetime of the state S_1 and σ_{1n} , the S_1 - S_n absorption cross-section.

In this work, our molecular engineering was based on the diaminobiphenyl **1**, which presents promising TPA properties in the visible range for nanosecond pulses. From this molecule, we developed a strategy in order to optimize excited state parameters involved in eq. (1), i.e. τ_1 and σ_{1n} . The molecule **2**, which was expected to present reduced rotational relaxation paths, was also prepared according to an Ullmann type coupling from 4,4'-diiodobiphenyl and the corresponding amine. The phenomenological three photon absorption α_3 , the two photon absorption β , the excited state cross section σ_{1n} and lifetime τ_1 were respectively measured from nonlinear transmission, fluorescence up-conversion and Kerr ellipsometry experiments.

The investigated compounds, which satisfy the transparency requirement, show broadband nonlinear absorption spectra in the visible region. The position of the resonance depends on the nature of the substituents. The S_1 - S_n absorption spectra present an intense broad band which overlap the nonlinear absorption spectra in agreement with the three photon absorption phenomenon. The compound **2** appeared to be twice as much more efficient than **1** for optical limiting. As these compounds presented identical two photon absorption spectra, this result couldn't be attributed to any electron delocalization or coupling effect. The introduction of substituents on the peripheral benzene rings inhibits a rotation degree of freedom. This

Poster Session I

induces a more strictly defined molecular geometry and a diminution of the relaxation process, which is experimentally observed by a slightly increase of the excited state lifetime.[3]



We are currently considering substituted fluoren analogs, which could allow a different charge transfer due to their planar geometry. This work opens the way to a molecular engineering approach via the optimization of the excited state dynamics.

We are grateful to DGA for financial support.

1 J.W. Perry et al., *Science* **273** 1533 (1996)

2 P.L. Baldeck et al., *Photonics Science News*, Volume 4, Issue 4 (1999)

3 B. Paci, J.M. Nunzi, R. Anémian, C. Andraud, A. Collet, Y. Morel and P. Baldeck, submitted at *Pure And Applied Optics*.

Theoretical investigation of the nonlinear circular dichroism in a liquid of chiral molecules

F. Hache, M. C. Schanne-Klein, H. Mesnil
Laboratoire d'Optique Quantique
CNRS - Ecole Polytechnique
F-91128 Palaiseau cedex, France

Introducing nonlocal effects such as magnetic dipolar and electric quadrupolar ones in the time-dependent perturbation theory, we show that a liquid of chiral molecules should exhibit a nonlinear circular dichroism, i.e., a difference in the nonlinear absorption depending on the handedness of the light polarization. General expressions are given, and it is shown that such an effect should be measurable experimentally.

In this paper, we are interested in the third-order nonlinear response of chiral molecules. Let us recall that chiral molecules can exist under two mirror-symmetrical (enantiomeric) forms and that they have the property of rotating the polarization of a linearly-polarized light or of absorbing differently right and left circularly polarized ones [circular dichroism (CD)]. In this paper, we investigate the nonlinear effects that exist in the CD.

Linear response

To derive the linear CD, one must calculate the energy-transfer between the molecules and the light beam. In a local approximation (where one neglects the retardation effects in the electric field \mathbf{E} associated to the light), it is given by $Im[\mu \cdot \mathbf{E}^*]$, where μ is the electric dipole moment. This moment can be calculated through the use of the time-dependent perturbation theory by considering the light-matter perturbation hamiltonian $H = -\hat{\mu} \cdot \mathcal{E}$. Once this derivation is carried out, one must average over an isotropic distribution of molecules to obtain the response of the liquid. Note that one must also introduce the local-field correction to take the polarization effects into account. This is however not sufficient to access the CD, as such chiral effects are a direct consequence of the *nonlocality* of the interaction [1]. One must therefore go beyond the local approximation and consider the next terms, namely the magnetic dipole and the electric quadrupole moments, in the energy transfer as well as in the calculation of the different moments through the perturbation theory. In the linear case, one can show that the quadrupole contribution vanishes for an isotropic distribution of molecules [2] and one can calculate the CD, defined as the difference in the absorption for a right (Δ_R) and a left (Δ_L) circularly-polarized light [3]:

$$CD \equiv \Delta_R - \Delta_L = -\frac{4}{3\hbar} EB \sum_a \frac{R_{ga}\Gamma}{(\omega_{ag} - \omega)^2 + \Gamma^2}. \quad (1)$$

In this expression, g and a denote the quantum states of the molecules and $R_{ga} = Im\mu_{ga} \cdot \mathbf{m}_{ag}$ is the Rosenfeld rotational strength [1].

Nonlinear response

Two-level system

It is possible to extend this calculation to the third-order response of a two-level system. One can show by introducing the nonlocal effects that the nonlinear response will be different if, for example, one shifts the polarization of the light from right to left and consider

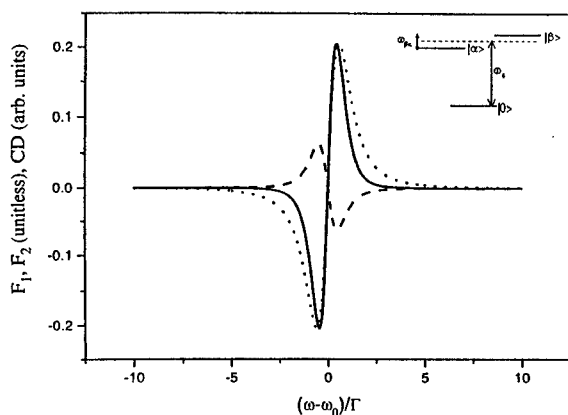


Figure 1: Linear and nonlinear CD of a three-level system.

the absorption saturation. The corresponding nonlinear CD (NLCD) is calculated as:

$$NLCD = \frac{64}{45\hbar^3} R_{01} |\mu_{01}|^2 E^3 B \frac{T_1 \Gamma^2}{[(\omega_{10} - \omega)^2 + \Gamma^2]^2} \quad (2)$$

This calculation can be easily extended to more general cases such as pump-probe experiments or optical phase conjugation by degenerate-four-wave-mixing. In this latter case, one must consider the polarization of the four different beams impinging onto the sample. Several polarization configurations allow to observe a NLCD [3].

Three-level system

The description of a chiral molecule by a two-level system is not satisfactory, as such a model does not obey the general sum rule for the rotational strengths [1] and it is more realistic to consider a three-level system as depicted in the inset of figure 1 giving rise to a linear CD (dotted line). In that configuration, beside the contributions due to the two two-level systems, there exists another one that mixes the three levels. The former is depicted in figure 1 by F_1 and the latter by F_2 (see [3]). It is however possible to check that only the former (two-level effect) is dominant.

References

- [1] S. F. Mason, *Molecular Optical Activity and the Chiral Discriminations* (Cambridge University Press, 1982),
- [2] G. Wagnière, *Linear and Nonlinear Optical Properties of Molecules* (VCH, New-York, 1993)
- [3] F. Hache, H. Mesnil, and M. C. Schanne-Klein, *Phys. Rev.* **B60**, 6405 (1999)

New properties of COANP-polyimide compound: Optical limiting effect

Natalie V. Kamanina*, Lev N. Kaporskii
Vavilov State Optical Institute
St.-Petersburg, 199034, Russia
* E-mail: kamanin@fm.ioffe.rssi.ru

Alex Leyderman, Alfonso Barrientos
Department of Physics, UPR-RUM
Mayagüez, Puerto-Rico 00680-9016

Optical limiting effect in 2-cyclooctylamino-5-nitropyridine (COANP)-polyimide thin films doped with C₇₀ fullerene was studied using second harmonic of pulsed Nd-laser as an irradiation source. The optical limiting was observed in these films that was caused by an additional interaction between electron subsystems of COANP and fullerene molecules. It was established the films investigated could be applied for limiting laser power density of more than 10 J cm⁻².

At present time the optical limiting effect is widely used as a very sensitive characterization method of nonlinear optical organic materials doped with fullerenes. In particular, this effect was investigated in C₆₀-poly [(disilanylene) oligophenylenes] structures [1], C₆₀-2,6-bis(2,2-bicyanovinyl)pyridine thin films [2] and polyimide-fullerene system [3, 4]. 2-cyclooctylamino-5-nitropyridine (COANP) is of nonlinear optical properties [5, 6]. Loosely bound π -electrons in COANP allow the properties to be modified with ease.

In the present paper the optical limiting effect has been first investigated in COANP-polyimide thin films doped with C₇₀ fullerene. 2.5% and 5% solutions of COANP in 1,1,2,2-tetrachloroethane were used. The C₇₀ concentration was varied from 0.1 wt.% to 5 wt.%. Non-photosensitive polyimide 81A was used as a film-forming base. 1-5 μ m thick COANP-polyimide films were spun on glass substrates. The second harmonic (532 nm) of a pulsed Nd-YAG laser was applied as a radiation source in the experiment. A pulsewidth was 15 ns and a laser spot on the sample surface was 3 mm in diameter.

A dependence of the output energy (E_{out}) on the input one (E_{in}) is shown in Fig. 1 for four samples.

The optical limiting effect is observed for all fullerene-containing samples at E_{in} more than 600-700 mJ, corresponding to the incident power density of 8.5-10 J cm⁻². A difference in transmission between samples 2 and 3 is determined by the fullerene concentration. However, the difference between samples 4 and 3 is twice as more at the same fullerene concentration. The result is caused not only by a more COANP concentration, but a possible complex formation between a donor fragment of a COANP molecule and fullerene as well.

The following evidences can be used. First, electron affinity of fullerene is 2.65 eV, that is more than the one for acceptor fragments of most organic molecules. Specifically, the acceptor fragment of the COANP molecule is a NO₂ group, which is bound to the donor fragment by the benzene ring. For a separate NO₂ molecule or radical, the electron affinity is 2.3 eV, while the NO₂ group bound to the benzene ring has the electron affinity is only 0.54 eV [7], that is, it is smaller than the one of fullerene by a factor of 4. Second. We have investigated absorption spectra, which show that the fullerene-containing samples are of very different spectral features from the COANP-polyimide and polyimide-C₇₀

Poster Session I

systems. There are two additional absorption peaks at 490 nm and 810–820 nm. Third, photosensitivity of fullerene-containing samples is one order of magnitude more than the one of fullerene-free sample. The photosensitivity has been measured by the electro-photograph technique [8].

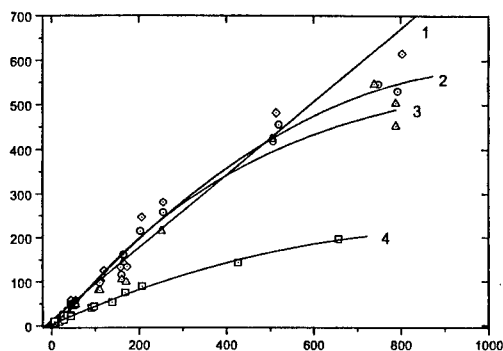


Figure 1: Dependence of E_{out} on E_{in} for the COANP-polyimide structure with the C_{70} concentration: 1 — 0; 2 — 0.5 wt.%; 3 and 4 — 5 wt%. The relation between COANP and polyimide was 1:1 (curves 1–3) and 2:1 (curve 4)

In conclusion, the optical limiting effect and spectral peculiarities have been studied in the fullerene-containing COANP-polyimide system. The films obtained are of spectral features in near IR-region and can be applied as effective non-linear absorber.

The authors wish to acknowledge Dr. N.A. Vasilenko for the help in this work and the Organizing Committee of ICONO'5 Conference for his support.

References

- [1] K. Hosoda, K. Tada, M. Ishikawa, and K. Yoshino, "Effect of C_{60} doping on electrical and optical properties of poly [(disilanylene) oligophenylenes]," *Jpn. J. Appl. Phys. Part 2*, **36**, L372-L375, (1997).
- [2] M. Ouyang, K.Z. Wang, H.X. Zhang, Z.Q. Xue, C.H. Huang, and D. Qiang, "Study of a novel C_{60} -2,6-bis(2,2-bicyanovinyl)pyridine complex thin film," *Appl. Phys. Lett.* **68**, 2441-2443 (1996).
- [3] N.V. Kamanina, L.N. Kaporskii, and B.V. Kotov, "Absorption spectra and optical limiting of the fullerene-polyimide system," *Opt. Commun.* **152**, 280-282 (1998).
- [4] N.V. Kamanina, "Reverse saturable absorption in fullerene-containing polyimides. Applicability of the Förster model," *Opt. Commun.* **162**, 228-232 (1999).
- [5] Ch. Bosshard, K. Sutter, P. Günter, and G. Chapuis, "Linear- and nonlinear-optical properties of 2-cyclooctylamino-5-nitropyridine," *J. Opt. Soc. Am. B*, **6**, 721-725 (1989).
- [6] A. Leyderman and Y. Cui, "Electro-optical characterization of a 2-cyclooctylamino-5-nitropyridine thin organic crystal film," *Opt. Lett.* **23**, 909-911 (1998).
- [7] L.V. Gurvich, G.V. Karachevtsev, V.N. Kondrat'ev, Yu.A. Lebedev, V.A. Medvedev, V.K. Potapov, and Yu.S. Khodoev, "Energies of Chemical Bond Breaking, Ionization Potentials and Electron Affinity," Nauka, Moscow, 1974 [in Russian].
- [8] I.A. Akimov, Yu.A. Cherkasov, and M.I. Cherkashin, "Sensitized Photoeffect," Nauka, Moscow, 1980 [in Russian].

Optical limiting effect in polymer organic system

Natalie V. Kamanina* and Lev N. Kaporskii
Vavilov State Optical Institute
St.-Petersburg, 199034, Russia
*E-mail: kamanin@ffm.ioffe.rssi.ru

Optical limiting effect in both polyimide-fullerene films and polyimide-fullerene solutions has been investigated. The malachite green and coumarin dyes were applied as alternative polyimide matrix impurities. For the investigations the second harmonic of a pulsed Nd-YAG laser was applied. The optical limiting effect was observed for all fullerene-doped systems. The most optical limiting was shown in the polyimide simultaneously doped with fullerene and dye. The laser radiation was attenuated by the factor 20. The Förster model was used to interpret the experimental results.

Optical limiting effect (OLE) is an important characterization technique of polymers doped with fullerenes. Investigations of OLE in fullerene-containing polymer media allowed a value of optical nonlinearity to be estimated [1], generation of second and third harmonics to be studied [2], as well as potentialities to be determined for applications of these media both for recording holograms and for optical limiting of a laser radiation [3, 4, 5]. Optical limiting studies showed fullerene-doped organic materials could be used as nonlinear absorbers in the wide spectral region.

In the present work OLE has been investigated in the systems based on fullerene-doped polyimide. The tetrachloroethane and chloroform were applied as solvents of polyimides. Polyimide was doped with a fullerene mixture (C₆₀:C₇₀=87:13) and/or dyes. Two types of structures, namely, 1 μm thick films and polyimide solutions replaced in 1 cm thick quartz cells, were studied. A pulsed Nd-YAG laser at wavelength of 532 nm was used as an irradiation source. The most OLE was observed in the polyimide structures doped with the fullerene mixture simultaneously with the dyes (see figure, curves 4 and 6).

Since the absorption spectrum of the fullerene-polyimide system is overlapped with the fluorescence spectrum of malachite green and coumarin at the wavelength of the excitation radiation (532 nm), resonance conditions are fulfilled in the polyimide-dye-fullerene structure. This fact allows the OLE peculiarities of that structure to be explained in the framework of the Förster model [6]. In this case overlapping the electron shells of the dye and the fullerene molecules provides the favourable conditions for the formation of the charge transfer complexes as the result of the free electron exchange between donor (dye) and acceptor (fullerene).

It should be noticed somewhat less OLE was observed in the fullerene-doped polyimide solution. This result was determined by the cluster formation causing fluctuations of a solution density. The fluctuations resulted in irregular irradiation absorption through the beam diameter.

In conclusion, OLE has been investigated in the fullerene-containing polyimide systems. The most OLE was shown in the polyimide simultaneously doped with fullerene and dye. The peculiarities observed were explained in the Förster model framework.

The authors wish to acknowledge Dr. N.A. Vasilenko and Dr. B.V. Kotov for helpful discussions and the Organizing Committee of ICONO'5 Conference for the support.

Poster Session I

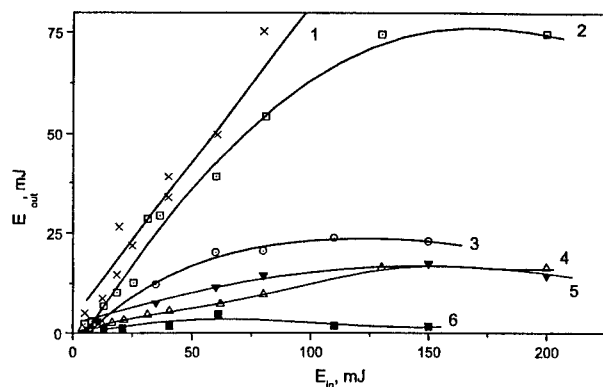


Figure 1: A dependence of the output energy (E_{out}) on the input energy (E_{in}) in films: (1) Pure polyimide; (2) polyimide with the 0.5 wt.% fullerene mixture; (3) polyimide with 0.5 wt.% malachite green; (4) polyimide with 0.15 wt.% malachite green and 0.5 wt.% fullerene mixture; (5) polyimide with 0.2 wt.% coumarin; (6) polyimide with 0.2 wt.% coumarin and the 0.5 wt.% fullerene mixture.

References

- [1] S. Couris, E. Koudoumas, A.A. Ruth, and S. Leach, "Concentration and wavelength dependence of the effective third-order susceptibility and optical limiting of C_{60} in toluene solution," *J. Phys. B: At. Mol. Opt. Phys.*, **28**, 4537-4554, (1995).
- [2] H. Hoshi, N. Nakamura, Y. Maruyama, T. Nakagawa, S. Suzuki, H. Shiromaru, and Y. Achiba, "Optical second- and third-harmonic generations in C_{60} film," *Jap. J. Appl. Phys., Part 2*, **30**, L1397-L1398, (1991).
- [3] V.P. Belousov, I.M. Belousova, V.P. Budtov, V.V. Danilov, O.B. Danilov, A.G. Kalintsev, and A.A. Mak, "Fullerenes: Structural, physical-chemical, and nonlinear optical properties," *J. Opt. Technol.*, **64**, 1081-1109, (1997).
- [4] A. Kost, L. Tutt, M.B. Klein, T.K. Dougherty, and W.E. Elias, "Optical limiting with C_{60} in polymethyl methacrylate," *Opt. Lett.*, **18**, 334-336, (1993).
- [5] N.V. Kamanina, L.N. Kaporskii, B.V. Kotov, "Absorption spectra and optical limiting of the fullerene-polyimide system," *Opt. Commun.* **152**, 280-282 (1998).
- [6] T. Förster, "Transfer mechanisms of electronic excitation," *Disc. Farad. Soc.*, **27**, 7-17, (1959).

In-situ Observation of Thermochromic Behavior in Merocyanine J-aggregate Monolayer Using the Multipurpose Nonlinear Optical Microscope

Noritaka Kato* Kentaro Saito* and Yoshiaki Uesu**

*Department of Physics, **Advanced Research Institute for Science and Engineering, Waseda University, 3-4-1 Okubo, Shinjuku-ku, Tokyo 169-8555, Japan

We found the reversible thermochromic transition between different J-aggregate states of merocyanine dye (MD) in the MD monolayer on the subphase, which contains two kinds of counter-ions; Cd^{2+} and Mg^{2+} . During the transition, the interaction exchange occur between MD- Mg^{2+} and MD- Cd^{2+} , and the absorption band of the J-aggregate at 620 nm for low temperature phase changes abruptly to 595 nm for high temperature phase. We performed the in-situ observation of the transition using the multipurpose nonlinear optical microscope, and the drastic morphological change during the transition was revealed.

Amphiphilic merocyanine dye (MD) (Fig 1) forms the second harmonic (SH)-active two-dimensional crystallite at the air-water interface [1], which are characterized as the J-aggregate assembly (JA). JA exhibits the sharp excitonic absorption band (J-band) at longer wavelength than isolated dye molecule and possesses a high and ultrafast third-order optical nonlinearity [2]. In the case of MD-JA, the second order nonlinear optical property is also large [3] as well as the third order one [4]. The cigar-shaped SH-active domains of JA spreading to several tens μm length in the MD monolayer mixed with arachidic acid (AA) at the air-water interface were observed by the multipurpose nonlinear optical microscope (M-NLOM), which enables us to take the images of SH and fluorescence (FL) signals, and the spectra of FL, absorption and reflection at the same part of the monolayer [1, 5]. The pulsed Nd^{3+} : YAG laser of 1064 and 532 nm was used for SH and FL images, respectively.

The formation of MD-JA is influenced by MD's counter-ion species. On the subphase containing Mg^{2+} , J-band appears at 620 nm, and on the subphase containing Cd^{2+} , at 595 nm (Fig 1). When the subphase contains both Mg^{2+} and Cd^{2+} , the thermochromic transition between the J-band at 620 and 595 nm occurs due to the interaction exchanging between MD- Mg^{2+} and MD- Cd^{2+} at the definite temperature. In Fig 2, the J-band peak position is plotted as a function of the subphase temperature. The molar fraction of Cd^{2+} to Mg^{2+} of the subphase is 20 % (subphase[20 %]). The peak position exhibits thermal-hysteresis. The transition behavior depends on the molar fraction of two ions. As the molar fraction of Cd^{2+} to Mg^{2+} decreases, the transition temperature increases and the width of the hysteresis decreases.

The in-situ observation of the present transition was performed by the M-NLOM. We monitored the aggregate-state by the reflection spectra. For observing the JA, we took SH images instead of FL one, because the FL excitation wavelength located near the J-band causes a damage of the dye molecules much more than SH generation. All images were taken with parallel polarization-state of incident and signal beams. In Fig. 3 (a), the SH image of the MD/AA mixed monolayer on subphase[20 %] with 620 nm J-band at 14 °C is indicated. The homogeneous SH signals are observed from the monolayer and does not show the polarization dependence. Therefore the small JAs whose size is below the microscope resolution are randomly distributed in this stage. When the JA transforms

Poster Session I

to high temperature phase with the band at 595 nm, almost no SH signal is observed. In Fig. 3 (b), the SH image after the restoration of the band at 620 nm on cooling is shown. The large SH-active domains are formed and the contrast of the image is reversed by 90 degree rotating of the polarization direction. This means that the domain is the uniform single JA. These facts indicate that the drastic morphological change occurs during the transition through the ion-exchange process.

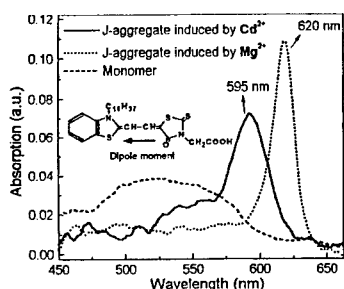


Figure 1: Amphiphilic merocyanine dye and its absorption spectra at different aggregate-states.

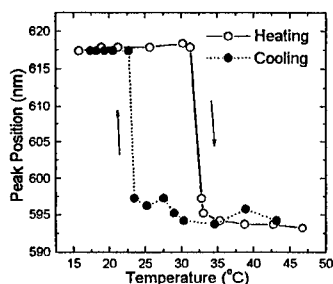


Figure 2: Thermal-hysteresis loop of the J-band.

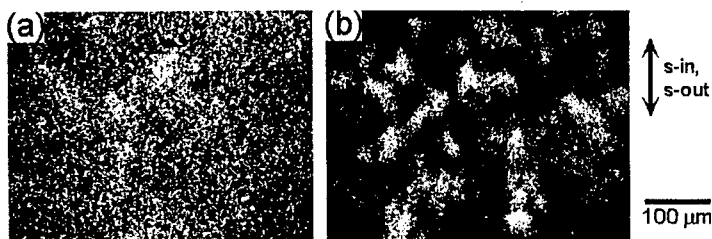


Figure 3: SH images of MD/AA mixed monolayer at the air-water interface. (a) Low temperature phase before heating. (b) Low temperature phase after cooling from the high temperature phase.

References

- [1] N. Kato, K. Saito, H. Aida, and Y. Uesu, *Chem. Phys. Lett.* **312**, 115 (1999).
- [2] *J-Aggregates*, edited by T. Kobayashi (World Scientific, Singapore, 1996).
- [3] K. Kajikawa, H. Tkezoe, and A. Fukuda, *Jpn. J. Appl. Phys.* **30**, L1525 (1991).
- [4] H. Matuda, E. V. Keuren, A. Masaki, K. Yase, A. Mito, C. Takahashi, H. Kasai, H. Kamatani, S. Okada, and H. Nakanishi, *Nonlinear Optics* **10**, 123 (1995).
- [5] N. Kato, K. Saito, and Y. Uesu, *Ferroelectrics*, inprint.

Time-domain transmission spectroscopy with ultrashort THz pulses

P. Kužel, A.V. Pashkin and J. Kroupa

*Institute of Physics, Academy of Sciences of the Czech Republic
Na Slovance 2, 182 21 Prague 8, Czech Republic*

Until recently the terahertz frequency domain (submillimeter wavelength, situated between optical and microwave regions) had been relatively unexplored due to the lack of the accessible radiation sources. The situation has changed with the development of techniques employing ultrashort optical pulses for generation of the THz radiation. Two methods are currently used for the THz radiation emission: The first one is based on a current surge mechanisms in a photoconductive material (photoconducting antennas, typically biased GaAs)[1] while the other one employs optical rectification (more precisely difference frequency generation) in an electro-optic material (e.g. the organic crystal DAST, one of the most efficient materials for THz generation)[2]. In the first case the spectral width of the THz pulses is given by the properties of the antenna material (in usual case when the optical pulse duration is significantly shorter than the carrier recombination time of the photoconductor). For the optical rectification, on the other hand, the spectral width (and therefore also the duration) of the applied optical pulse directly determines the maximal frequency component of the resulting terahertz pulse and the bandwidth of the terahertz radiation is inversely proportional to the pulse width of the incident optical radiation in this case.

Analogical approaches (photoconduction or electro-optic effect) are also used for the THz radiation detection [3]. Necessary time resolution is obtained by sampling with the original optical pulses. The possibility to measure the amplitude of the electric field of the THz pulses (and not only their electromagnetic intensity) with sufficient time resolution is the basis for their time-domain spectroscopic application.

In our contribution we shall discuss some problems connected with the THz transmission measurement set-up and the data evaluation. The first complex of problems is related to the spatio-temporal changes of the THz pulses during their propagation through the optical system [4]. In the main part of our contribution the analysis of the measured amplitude of the THz pulses after transmission through the sample will be presented. The data evaluation is based on numerical solution of the equations for the beam propagation through absorptive and dispersive medium. The experimental data provide the complex transmission function of a sample which is then used to calculate at the same time both refraction and absorption index in the range of 3 - 80 cm^{-1} ; moreover, the procedure also allows to evaluate precisely the sample thickness. The periodicity of the phase can in some particular cases (e.g. in materials with strong dispersion due to a phonon or a relaxation in the THz region) lead to an ambiguity in the refractive index determination. Several possibilities for the choice of the correct branch of the general solution will be suggested. Application of the Kramers-Kronig relations and the oscillator analysis for this task will be discussed in detail. As examples, the complex refractive index spectra obtained from the measured time profiles of the transmitted THz pulses for several materials (e.g. TSCC, LGO) will be presented.

Poster Session I

References

- [1] J. T. Darrow, B. B. Hu, X.-C. Zhang, and D. H. Auston, "Subpicosecond electromagnetic pulses from large-aperture photoconducting antennas", *Opt. Lett.* **15**, 323-325 (1990).
- [2] X.-C. Zhang, X. F. Ma, Y. Jin, T.-M. Lu, E. P. Boden, D. P. Phelps, K. R. Stewart, and C. P. Yakymyshyn, "Terahertz optical rectification from a nonlinear organic crystal", *Appl. Phys. Lett.* **61**, 3080-3082 (1992).
- [3] Q. Wu, M. Litz, and X.-C. Zhang, "Broadband detection capability of ZnTe electro-optic field detectors", *Appl. Phys. Lett.* **68**, 2924-2926 (1996).
- [4] P. Kužel, M.A.Khazan, J.Kroupa "Spatiotemporal transformations of ultrashort terahertz pulses" *J. Opt. Soc. Am. B* **16**, 1795-1800 (1999).

Nonlinear optical phenomena in turbid media of living tissue

Asatur Lalayan

Yerevan State University, Physics Department, A. Manoogian 1, Yerevan, 375025, Armenia

E-mail: alalayan@physdep.r.am

Nonlinear optical phenomena in strong turbid media of living tissue under picosecond laser irradiation have been studied. Second harmonic generation which was more effective in tissue contained 60-70 % of collagen macromolecules (cartilages, tendons, fasciae et al) was observed. By comparison of the intensity of SH in KDP crystal and thin film of fascia the second order nonlinear coefficient has been estimated. The dependencies of SHG on conventional and laser heating were obtained. Two-photon fluorescence and two-quantum decomposition of sensitizer molecules after tissue photosensibilization by hematoporphyrin derivative, chlorin e_6 and fluorescein tumor-seeking drugs were studied.

Nonlinear effects can give unique possibilities for investigations and treatment in biomedicine [1,2]. However, the optical phenomena, which are nonlinearly depend on intensity and conventionally observed in transparent media can be strong limited because of strong scattering of optical beam in turbid media of biotissues.

In present work some optical phenomena, which quadratically depend on intensity have been investigated in biotissue under the picosecond pulses train irradiation with 20-100 MW single pulse peak power at 1064, 532 and 355 nm wavelengths of Nd:YAG laser.

Second harmonic generation. Second harmonic (SH) generation in the different types of animal tissue under 1064nm and 100MW irradiation has been studied. The SH signal was registered in the reflection scheme and also for thin samples in the pass scheme. The peak at 532nm with less than 1nm (resolution of registration system) spectral width was observed. Effectiveness of SH generation has been correlated with the amount of the collagen molecules, which form the oriented longitudinal birefringence macrostructure in the animal and human tissues. Sizes of these native quasi-crystals reach 7x40 microns that are in order of second harmonic generation coherence length, and allows to observe effective SH signal. In the different investigated samples the SH was more effectively generated in tissue, contained the higher amount of collagen, in particularly, cartilages, tendons, fasciae (about 60-70 %). The dependencies of SHG on angles of the signal registration were obtained. By comparison of the intensity of SH in KDP crystal and thin film of fascia (0.09 mm) the second order nonlinear coefficient has been experimentally estimated: $d_{\text{eff}} = 0.3 d_{\text{KDP}}$.

In the case of the nanosecond irradiation, when conditions of registration scheme and energy density are remained the same, but the intensity is decreased in about three orders, SHG was not observed. In this case, the effective formation of the plasma emission contained spectral lines of the Ca, Na, Ca ions, etc. was registered.

During heating of collagen contained different types of tissue (excepting bone tissues) the SH was decreased more than 30 times at temperature interval 59-64°C, which is corresponded to spiral - coil transitions of collagen, and not recovered after cooling. It means, that the method of SHG allows monitoring of the conformational changes of collagen molecules during heating process in real time. The same conformational changes were observed during the laser heating of tissue samples under 200mW microsecond Er: YAG laser irradiation.

Two-photon absorption. Two-photon excited fluorescence from tissues, colored by chlorin e_6 , and hematoporphyrin derivative (HpD) tumor photosensitizers has been registered during excitation at 1064 nm. These spectra coincided with fluorescence spectra at 532nm one-photon excitation, however, the background autofluorescence was practically absent. The

Poster Session I

value of signal/ background relation was more than 1000 at two-photon excitation since at one-photon excitation was ≈ 2 . Two-photon fluorescence scans with high contrast of normal tissue - cancer border allowed to increase the sensitivity of fluorescence method and can be applied in optical biopsy of malignant tissue.

Two-quantum absorption. It is well known, that the generation of reactive photoproducts from the chromophores and destruction of biomolecules can be realized with the high efficiency in the solution under the intense laser irradiation, when two-step light absorption and photoreactions from highly excited electronic states of molecules are taken place [3]. We have observed nonlinear decomposition of some tumor localizing photosensitizers in tissues under laser radiation with wavelength 355 and 532 nm (20-50 MW/cm², 5 Hz) using fiberoptic laser spectrofluorometer. The fluorescence spectra of tissues sensitized by fluorescein, HpD and chlorin e₆ were registered with 355nm low intensity nanosecond probing beam during intense picosecond irradiation. It has been shown that the initial rates of photobleaching depend quadratically on the laser irradiation intensity. The initial level of fluorescence after 1.5 min. of irradiation reduced to 40% and after that became stable. Because the maximal penetration of the probing beam into tissue depth was 2mm, we can conclude, that the effective decomposition of the injected molecules takes place only in superficial (<1mm) sensitized tissue layer. The subsequent change of the autofluorescence spectra of sensitized tissues has been observed, which can be explained by changing of quenching process stipulated by changing of balance between endogenous and exogenous chromophores.

Application of nonlinear mechanisms of photodestruction and free radicals formation make larger sensitizers candidates for cancer photochemotherapy, since there are number sensitizers which have good ability to be accumulated in tumor, but the low phototoxicity (low singlet oxygen yield) at one-photon absorption. In addition, the applying nonlinear method of malignant neoplasms treatment, gives possibility to almost completely avoid main deficiency of PDT method - residual skin photosensitivity.

References.

- [1] N.I. Koroteev "New schemes of nonlinear spectroscopy for chiral biological molecules solutions", *JETP* **106**, 1261-1277, (1994) (in Russian)
- [2] Leopold D., Freyer W., "Proposal of modified mechanisms for photodynamic therapy", *J. Photochem. Photobiol.*, **12**, 311-314, (1992).
- [3] A. Andreoni "Two-step photoactivation of hematoporphyrin by eximer - pumped dye laser pulses", *Photochem. Photobiol., B: Biology*, **1**, 181-193, (1987)

Optically controlled reversible structuring of doped polymer thin film waveguides

Steve Lecomte, Ulrich Gubler, Matthias Jäger¹, Christian Bosshard, and Peter Günter
*Nonlinear Optics Laboratory, Institute of Quantum Electronics
Swiss Federal Institute of Technology, ETH Hönggerberg
CH-8093 Zürich, Switzerland*

Luca Gobbi and François Diederich
*Laboratory of Organic Chemistry, Swiss Federal Institute of Technology, ETH Zürich,
CH-8092 Zürich, Switzerland*

We demonstrate that polymeric thin films doped with the photochromic molecule 1,8a-dihydro-2(4-iodophenyl)-1,1-azulenedicarbonitrile can be reversibly structured by light. We discuss the relevant material properties of the photochromic molecule in solution as well as in polymer films and demonstrate light-induced waveguides at the telecommunication wavelength of 1.313 μm .

The characterization and applications of organic doped polymer thin films have already obtained a lot of attention. The main advantages of this kind of material include the media's low cost, ease of processing, customizable and tailorable properties and compatibility with integrated-optics technology. Several techniques to optically structure a polymer film already exist [1]. Such techniques are well mastered and give devices which are useful in integrated optics. But all these techniques use processes to create waveguides which are irreversible.

In order to create structures which are reversible, we use thin polymeric films doped with the photochromic molecule 1,8a-dihydro-2(4-iodophenyl)-1,1-azulenedicarbonitrile (Figure 1) [2].

Photochromic molecules are systems undergoing structural changes upon illumination. Associated with these chemical reactions the optical properties can be modified significantly. The molecule used in this study is based on a thermally reversible photoretrocyclization (Figure 1) [2]. The photoreaction is activated by illumination with a wavelength near 360 nm while the relaxation is purely thermal. The absorption peak of the form 1 is at 365 nm whereas the accumulation of form 2 is accompanied by a significant color change from light yellow to red according to the appearance of the absorption peak at 480 nm (Figure 3).

By repeated absorption spectroscopy we have characterized the thermal back reaction from form 2 to 1 in solution (chloroform) (Figure 3). The thermal relaxation is very well described by an exponential decay, in agreement with a two state system, with a time constant of 5.4 hours at 300 K.

We have also characterized the back reaction. To describe the relaxation in an inhomogenous medium we consider the KWW function [3] and we obtain time constant of

¹Present address: Agilent Technologies, D-71034 Böblingen, Germany

Poster Session I

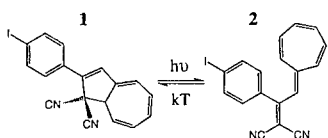


Figure 1: Chemical structure of the photochromic molecules.



Figure 2: Output of the Y-branch waveguide.

about 22 hours.

To accurately measure the refractive index change in polymer films, we used two complementary techniques: The holographic grating technique and the grating coupling technique. The holographic grating technique provided a refractive index change of $\Delta n = (5.9 \pm 0.6) \times 10^{-3}$ at 633 nm with 15.05 weight percent (w%) loading of photochromic molecules in polymer [3]. It also yielded the excitation time in function of the intensity as well as the relaxation time. The grating coupling technique gave the following refractive indices at 1.55 μm and with 13.9 w% loading: In the state 1, $n = 1.609 \pm 0.004$ and in the state 2, $n = 1.618 \pm 0.004$ leading to $\Delta n = (9 \pm 5) \times 10^{-3}$ which is in agreement with the results of the holographic grating technique.

Because of the sufficient index change, we have prepared samples to demonstrate the waveguiding at the telecommunication wavelength of 1.313 μm . We structured the sample with contact mask lithography. The mask contained Y-branch channel waveguides we used to demonstrate the waveguiding. Figure 2 shows the output of the sample which clearly demonstrates the waveguiding.

We want to acknowledge Germano Montemezzani for fruitful discussions. This research was supported by a grant from the ETH Research Council.

References

- [1] L.A. Hornak, *Polymers for Lightwave and Integrated Optics: Technology and Applications*, (Marcel Dekker, New York, 1992).
- [2] L. Gobbi, P. Seiler, F. Diederich, *Angew. Chem. Int. Ed.*, **38**, 674 (1999).
- [3] S. Lecomte et al, *to be submitted to Appl. Phys. Lett.*

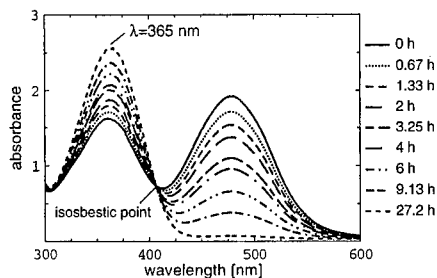


Figure 3: Thermal relaxation of form 2 to form 1 in chloroform with a time constant of 5.4 hours at 300 K.

Quantum and semi-classical modeling of NLO properties in organic systems

Yi Luo¹, Patrick Norman², Peter Macak³, and Hans Ågren³

¹. FYSIKUM, University of Stockholm, Box 6730, S-113 85 Stockholm, Sweden

². Department of Physics, Linköping University, S-581 83 Linköping, Sweden

³. Theoretical Chemistry, Royal Institute of Technology, S-100 44 Stockholm, Sweden

The implementation of reaction field response theory in quantum chemical calculations enables analytical solutions for solvent effects on nonlinear optical (NLO) properties. It provides a tool for exploring the role of electron correlation, dynamical dispersion and vibrational contributions on the NLO properties of molecules in solutions or in solid organic environments. With efficient computational schemes within the Random Phase Approximation one obtains solvent effects on the NLO properties of molecules of the size of the fullerenes and of oligomers of such lengths that the polymer values easily are extrapolated. A semi-classical model is described that gives transparent connections between microscopic and macroscopic optical properties.

Reaction field response theory

Current models of solvent properties using cavity reaction field methods have been analyzed and categorized in two groups according to the use of local fields or cavity fields as the perturbing fields [1]. Analytical connections between the two approaches have been derived to display the ambiguous notion of solvent properties. For example, in the case non-oscillating (static) perturbing fields, we have

$$\alpha_{ij}^C = l_{ia} \alpha_{aj}^{L_i}, \quad \beta_{ijk}^C = l_{ic} l_{aj} l_{bk} \beta_{cab}^{L_i},$$

$$\gamma_{ijkl}^C = l_{id} l_{aj} l_{bk} l_{dl} \gamma_{abcd}^{L_i} \beta_{ija}^{L_i} f_{ab}^R \beta_{bkl}^C + \beta_{ika}^{L_i} f_{ab}^R \beta_{bjl}^C + \beta_{ila}^{L_i} f_{ab}^R \beta_{bjk}^C,$$

where $l_{ij} = (\delta_{ij} + f_{ia}^R \alpha_{aj}^C)$. Here solute molecular properties are labelled with superscripts L_i and C , referring to those defined with respect to the internal local and the cavity fields, respectively. Clearly, different so-called local field factors are needed when computing the corresponding macroscopic quantities, and it has been demonstrated that the cavity properties are those which are computed by standard quantum chemical reaction field methods.

Semi-classical models

Most simplistic, although highly effective, semiclassical methods have been developed to directly relate molecular properties for the isolated species (gas phase) to the corresponding values of the solute molecule [2, 3]. With molecular properties we here refer to the electronic as well as the vibrational contributions, we have for example

$$\gamma_{ijkl}^{e,\text{sol}} = \gamma_{ijkl}^e + \sum_{mnl} \left[\alpha_{im}^e f_{mn}^R \gamma_{njk}^e + \alpha_{jm}^e f_{mn}^R \gamma_{nikl}^e + \alpha_{km}^e f_{mn}^R \gamma_{nijl}^e + \alpha_{lm}^e f_{mn}^R \gamma_{nijk}^e + \beta_{ijm}^e f_{mn}^R \beta_{nkl}^e + \beta_{ikm}^e f_{mn}^R \beta_{njl}^e + \beta_{ilm}^e f_{mn}^R \beta_{njk}^e + \mu_m f_{mn}^R \delta_{nijkl}^e \right],$$

for the electronic contribution to the second hyperpolarizability and

$$\alpha_{ij}^{v,\text{sol}} = \alpha_{ij}^v + \sum_{kl} \left(\alpha_{ik}^v f_{kl}^R \alpha_{lj}^e + \alpha_{ik}^e f_{kl}^R \alpha_{ij}^v \right) + \sum_{klmn} \alpha_{ik}^e f_{kl}^R \alpha_{lm}^v f_{mn}^R \alpha_{nj}^e$$

for the vibrational contribution to the linear polarizability of a nonpolar molecule.

Poster Session I

Applications

Fullerenes

Results for nonlinear optical susceptibilities of the fullerenes, including C_{60} , C_{70} , and C_{84} , in the condensed phase have been obtained from large-scale *ab initio* calculations using self-consistent reaction field theory and an analytical local field method [4]. It has been shown that the intermolecular polarization interaction has significant effects on the nonlinear properties of the fullerenes. Based on the theoretical and experimental results for the polarizability of C_{60} in the gas phase, a general local field factor for C_{60} film has been obtained, which is found to be quite different from the classical Lorentz local field factor. The calculated and experimental nonlinear optical susceptibilities of C_{60} are in good agreement provided the comparison is made on the same basis, *viz* at non-resonant frequencies and considering the relevant macroscopic quantities. The dielectric and density dependence of the nonlinear optical susceptibilities of C_{70} has been investigated as well.

Conjugated Polymers

Solvent effects on the static polarizabilities of conjugated polymers have been studied by means of the semi-classical solvation model using results from *ab initio* calculations [5]. The solvent induced changes of the static polarizabilities show maxima at fairly short oligomer lengths, with the main axial contribution decreasing rapidly to a zero value at the geometrically nondistorted polymer limit. Different saturation behaviors of the static polarizabilities of conjugated oligomers in gas phase and in solution are observed. It is concluded that the dipole-dipole interaction is responsible for the solvent-induced property changes of the oligomers.

References

- [1] P. Macak, P. Norman, Y. Luo, and H. Ågren, *J. Chem. Phys.* in press (2000).
- [2] Y. Luo, P. Norman, and H. Ågren, *J. Chem. Phys.* **109**, 3589 (1998).
- [3] P. Norman, P. Macak, Y. Luo, and H. Ågren, *J. Chem. Phys.* **110**, 7960 (1999).
- [4] Y. Luo, P. Norman, P. Macak, and H. Ågren, *Phys. Rev. B*, Jan. 15, (2000).
- [5] Y. Luo, P. Norman, P. Macak, and H. Ågren, *J. Chem. Phys.*, **111**, 9853 (1999).

Membrane imaging by simultaneous second-harmonic generation and two-photon microscopy

L. Moreaux[†], O. Sandre[‡], M. Blanchard-Desce[§], J. Mertz[†]

[†]Laboratoire de Physiologie ESPCI, 10 rue Vauquelin, 75005 Paris, France

[‡]Laboratoire Physico-Chimie Curie, 11 rue Pierre et Marie Curie, 75005 Paris, France

[§]Département de Chimie ENS, 24 rue Lhomond, 75005 Paris, France

We demonstrate that simultaneous second-harmonic generation (SHG) and two-photon excited fluorescence (TPEF) can be used to rapidly image biological membranes labelled with a styryl dye. We develop a model based on the theory of phased-array antennas which shows that the SHG radiation is highly structured and can be roughly of the same power as TPEF. This model provides a definition of a SHG cross-section which can be directly compared to the TPEF cross-section. Because of its sensitivity to local asymmetry, SHG microscopy promises to be a powerful tool for the study of membrane dynamics.

Second-harmonic generation (SHG) and two-photon excited fluorescence (TPEF) are non-linear optical phenomena which scale with excitation intensity squared, and hence give rise to the same intrinsic 3-dimensional resolution when used in microscopic imaging. SHG microscopy at high resolution has only recently been demonstrated as a tool for biological imaging [1]. Because SHG is a coherent phenomenon involving radiative scattering while TPEF is an incoherent phenomenon involving radiative absorption and re-emission, the two provide intrinsically different contrasts. We study the possibility of combining these contrasts in a single microscope. By using the dipolar charge transfer styryl dye Di-6-ASPBS [3], and exciting near its absorption band, we benefit from a large SHG signal and also a significant two-photon absorption which allows simultaneous and rapid SHG and TPEF imaging of biological membranes.

When imaging molecules in a membrane with SHG microscopy, only a small area about the focal center is active. Given the length scales involved, this area may be considered essentially flat and oriented parallel to the excitation propagation direction. We develop a model specifically tailored to this geometry to characterize SHG in a membrane. Our model is based on the theory of phased-array antennas, in which the dye molecules are regarded as elemental dipole radiators driven at the second-harmonic frequency of the excitation beam, in proportion to their hyperpolarizability [2]. The SHG radiation pattern is derived by taking the excitation polarization to be along the charge transfer axis and coherently summing the far-field amplitudes. The radiation is found to be symmetrically peaked into well-defined forward directions which critically depend on the phase anomaly of the focussed excitation beam. By integrating the radiation pattern over all solid angles, the total SHG power can be expressed in the simple form:

$$P_{SHG} = \frac{1}{2} \sigma_{SHG} N^2 \Theta \bar{I}^2, \quad (1)$$

where N is the number of molecules contributing to SHG, \bar{I}^2 is the excitation mean square intensity, Θ is a parameter dependent on the geometry involved in the coherent summation, and σ_{SHG} is the SHG cross-section for a single molecule which is proportional to its hyperpolarizability squared [2]. We predict a large near-resonance hyperpolarizability for Di-6-ASPBS at an 880 nm excitation wavelength which leads to $\sigma_{SHG} \approx 1 \times 10^{-4}$ GM. In

Poster Session I

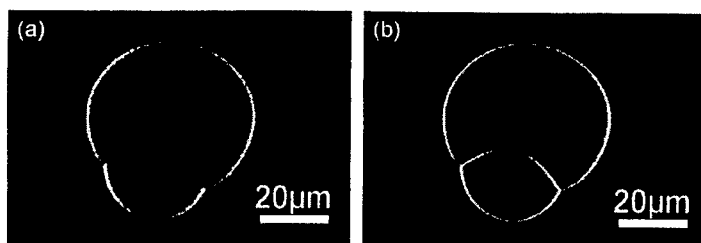


Figure 1: . SHG (a) and TPEF (b) images of two adhering vesicles labeled with Di-6-ASPBS (equatorial slice), excited at 880 nm. The total acquisition time for the images was 1.5 s, for an excitation power at the sample <1 mW. The adhesion area where the membranes are fused exhibits a centrosymmetric molecular distribution wherein TPEF is allowed but SHG is not.

turn, the TPEF cross-section of Di-6-ASPBS in membrane at the same excitation wavelength is estimated to be $\sigma_{TPEF} \approx 30GM$. Although, σ_{SHG} is small compared to σ_{TPEF} for a single molecule, the ratio P_{SHG}/P_{TPEF} scales with N and is significantly enhanced for a large number of molecules owing to the coherent summation of SHG field amplitudes. In our case, and this ratio approaches 0.1. This ratio is even further enhanced if we consider that SHG power, because of its directional nature, can be more efficiently collected than TPEF power.

For simultaneous SHG and TPEF imaging we use a homebuilt TPEF microscope using a mode-locked Ti:Sapphire laser and transmitted light detection. The laser light is focussed into the sample and the resultant SHG is collected in the forward direction while the TPEF is collected in the backward direction. The sample consists of giant unilamellar vesicles made of a phospholipid in water. The vesicles are labeled at 1 mol% with the lipophilic styryl dye Di-6-ASPBS.

Figure 1 illustrates SHG and TPEF images of Di-6-ASPBS molecules under the conditions described above. Near-resonance excitation combined with the coherent summation of SHG resulted in approximately equal measured powers in both images, allowing these to be acquired simultaneously. The measured powers were high enough that we could operate with integration times of only $10 \mu s$ per pixel, meaning that both SHG and TPEF can be used here to probe relatively rapid membrane dynamics. A feature of SHG is that it is a sensitive monitor of local molecular asymmetry. In particular, it is well known that SHG vanishes in the case of symmetric dipole distributions, as illustrated in Fig.1. This sensitivity to local asymmetry is inaccessible to TPEF and promises to be a powerful tool for the study of molecular dynamics in biological membranes.

References

- [1] G. Peleg et al., Proc. Natl. Acad. Sci. USA 96, 6700 (1999).
- [2] L. Moreaux et al., Optics Letters (submitted).
- [3] L. M. Loew et al., Biophys. J. 34, 353 (1981).

Narrow line laser emission from dendrimer doped polymer waveguides

Akira Otomo, Shiyoshi Yokoyama, and Shinro Mashiko
*Kansai Advanced Research Center
Communications Research Laboratory
Kobe 651-2492 Japan*

Extremely narrow-line laser emission is observed in mirrorless polymer waveguides containing Rhodamine B cored dendrimers. The spectrum linewidth of the emission is found to be 0.7 nm which is limited by the resolution of the spectrograph used. Although there have been much interest and study on lasing in scattering media, to the best of our knowledge, the linewidth we observed is the smallest ever reported in the mirrorless polymer systems. Phenomenon of the narrow line emission is based on amplified emission self-seeded by localized light. Anderson localization of light is formed by scattering in the dendrimer/PMMA waveguides.

Organic polymer mirrorless lasers have been investigated in various organic material systems, such as dye doped polymers [1], conductive polymers [2, 3], and scattering pigment solutions [4]. Phenomenon of most of observed mirrorless lasing is amplified spontaneous emission (ASE), excepting a few cases claimed as superfluorescence. The bandwidths of the emission spectrum obtained from these mirrorless systems are rather broad (≈ 10 nm), even in long gain waveguide systems (1.7 nm) [3]. Narrow line emission from mirrorless systems has been reported in strongly scattered semiconductor films [5], and here we report amplified narrow line laser emission from weakly scattered PMMA waveguides containing Rhodamine B(RhB) cored dendrimers.

Dendrimers have attracted attentions because their branching architecture makes their three dimensional structures highly controllable. We synthesized RhB cored dendrimers in order to isolate the RhB from other molecules (Fig. 1). The RhB molecules in a concentrated solution tend to aggregate and become inactive for fluorescence. Since the shell surrounding a dendrimer core limits the interaction of the RhB molecules, aggregated dendrimers are still fluorescent. Moreover the shell can prevent some degradation reactions of the cored dye if it is covered by antioxidant molecules.

RhB dendrimer waveguides were fabricated by dispersing the dendrimers into host polymer, poly-methylmethacrylate (PMMA), films. The RhB dendrimers and PMMA were mixed and dissolved 10 w% in cyclohexanone and then spun onto fused silica substrates, that had been cut into a 5-mm-wide rectangular shape. The film thickness was adjusted as 700-800 nm for single mode waveguides at the emission wavelengths of the RhB (≈ 600 nm). The waveguides were optically pumped from the film surface using a frequency doubled Nd³⁺:YAG pulse laser (532 nm wavelength, 3 nsec pulse width, 10 Hz repetition rate). The pumping region was a 0.1-mm-wide and 4-mm-long stripe shape formed by focusing with a cylindrical lens through a 4 mm slit. The fluorescence guided along the stripe in the film was collected by a 20x microscope objective and was separated from the substrate guided light by making an expanded image of the waveguide end face on the spectrometer input.

The dependence of the total emission from the waveguides on the pump fluence shows the typical stimulated emission threshold behaviour for all the RhB dendrimer concentrations studied. The evolution of the waveguide emission spectra with increasing pumping fluence is shown in Fig. 2. At low pumping energies the fluorescence spectrum consists

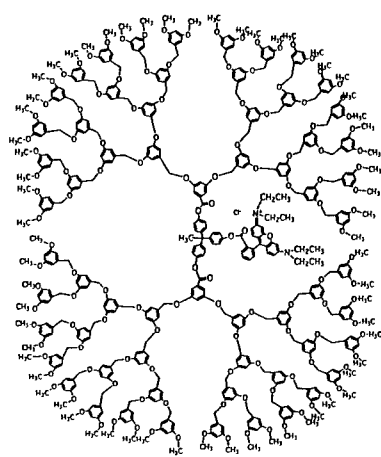


Figure 1: The 4th generation rhodamine B core dendrimer (RhB-G4ether).

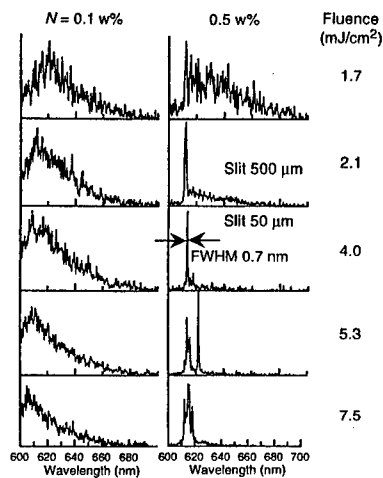


Figure 2: Evolution of the emission spectra from the waveguides with increasing pump fluence.

of a single broad spontaneous emission peak. As pumping energy increases, a narrow line emission appears suddenly and grows rapidly in the spectrum obtained from the film with the higher RhB dendrimer concentration. From its first appearance, the width of the emission line is less than 0.7 nm (FWHM). The observed linewidth is limited by the resolution of the spectrometer used. This behaviour (*i.e.* constant linewidth) is not found in ordinary ASE, in which case the linewidth gradually decreases as the pumping energy increases. The narrow line emission is not due to any macroscopic cavities formed in the waveguides. When the pump energy increases further, other narrow peaks appear and combine together. The RhB/PMMA waveguide, in contrast, does not contain dendrimers and shows the ordinary spectral narrowing behaviour of ASE. Moreover the films with lower RhB dendrimer concentrations show only the normal ASE behaviour. There is some evidence that the scattering of the RhB dendrimers causes the narrow line in the spectrum obtained from films with higher concentrations of RhB dendrimers.

References

- [1] R. E. Hermes, T. H. Allik, S. Chandra, and J. A. Hutchinson, *Appl. Phys. Lett.* **63**, 877 (1993).
- [2] F. Hide, M. A. Diaz-Garcia, B. J. Schwartz, M. R. Andersson, Q. Pei, and A. J. Heeger, *Science* **273**, 1833 (1996).
- [3] C. Zenz, W. Graupner, S. Tasch, G. Leising, K. Müllen, and U. Scherf, *Appl. Phys. Lett.* **71**, 2566 (1997).
- [4] N. M. Lawandy, R. M. Balachandran, A. S. L. Gomes, and E. Sauvain, *Nature* **368**, 436 (1994).
- [5] H. Cao, Y. G. Zhao, H. C. Ong, S. T. Ho, J. Y. Dai, J. Y. Wu, and R. P. H. Chang, *Appl. Phys. Lett.* **73**, 3656 (1998).

Nonlinear Optical Properties of push-pull Stilbenes based on a strong Carbocation Acceptor Moiety

B. PACI, C. SCHMIDT, C. FIORINI and J. M. NUNZI

LETI (CEA - Technologies Avancées), DEIN/SPE Groupe Composants

Organiques, CEA Saclay, F-91191 Gif-sur-Yvette Cedex, France

Tel. : +33 (0) 1 69 08 85 43 ; Fax : +33 (0) 1 69 08 76 79 ; e-mail : barbara.paci@cea.fr

C. ARBEZ-GINDRE, C. G. SCRETTAS

*National Hellenic Research Foundation, Institute of Organic and Pharmaceutical Chemistry,
Vas. Constantinou 48, 11635 Athens, Greece*

Non-linear optical properties of push-pull stilbenes based on an alkylamino donor and a strong carbocation acceptor moieties are analyzed in the present study. The highly electron-acceptor character of the carbocation group makes this kind of molecules promising materials for second-order non-linear optical applications. Photoinduced intramolecular charge-transfer is studied by second harmonic generation in solution using time-resolved non-degenerate six-wave mixing. The fully characterized nonlinear dye Disperse Red 1 is used as a reference. The second-order nonlinear properties of the carbocation molecules are compared to a more standard amino-nitro push-pull stilbene. Kerr ellipsometry measurements aiming at a better understanding of the nonlinear excited state spectroscopy of the molecules are also reported. They reveal a very short excited state lifetime of the molecules. Optimization of this lifetime should lead to an improvement of the six-wave mixing response of such compounds.

Optimization of the second-order non-linear optical properties of organic molecules has been the subject of many studies. Following the classical « push-pull » scheme of paranitroaniline, organic molecules bearing electron donor and acceptor groups separated by large π -electron conjugated systems have been shown to exhibit large molecular hyperpolarizabilities β [1-3]. One challenging prospect is to optimize the relative strength between the electron donor and acceptor groups in order to promote the internal charge transfer along the molecule [4-5], resulting in a further enhancement of the molecular hyperpolarizability.

The aim of this study is to analyze the non-linear optical properties of push-pull stilbenes based on an alkylamino donor and a strong carbocation acceptor groups. The highly electron-acceptor character of the carbocation group makes this kind of molecules promising materials for second-order nonlinear optical applications. The molecular second-order properties are studied by second harmonic generation in solution using time-resolved non-degenerate six-wave mixing [6]. The fully characterized nonlinear dye Disperse Red 1 (4-(N-(2-hydroxyethyl)-N-ethyl)-amino-4'-nitroazobenzene) is used as a reference for the determination of the carbocations second-order properties from the six-wave mixing signal.

Photoinduced anisotropy measurements using nonlinear optical Kerr ellipsometry pump-probe technique [7] have also been performed : they are shown to provide an interesting insight into the molecular excitation dynamics. The second-order nonlinear properties of the carbocation molecules are compared to the more standard dibutylamino-nitro push-pull stilbene.

Poster Session I

In conclusion, although the second-order nonlinear properties of the carbocation studied were shown to be of a comparable order of magnitude than the more classical highly nonlinear dibutylamino-nitro-stilbene dye, the excited state lifetime of the carbocation stilbenes was shown to be extremely short. Optimization of this excited state lifetime should lead to a further increase of the six-wave mixing nonlinear response of such promising compounds. Another issue would be to test the ability of such compounds to orient optically in a solid matrix using all-optical poling [8]. Their short excited state lifetime can be an advantage in this respect, since it implies a weak radiative decay and a strong coupling to the phonon manifold, allowing a more efficient manipulation of the molecules. All the more interesting is that owing to electrostatic interactions with appropriate counter-ions in their host matrix, ionic compounds were shown to exhibit an increased stability of the molecular order, which is essential for efficient second harmonic generation [9].

References :

- [1] D.S. Chemla and J. Zyss eds, Nonlinear optical properties of organic molecules and crystals (Academic, Boston, Mass., 1987).
- [2] Ch. Bosshard et al., Organic nonlinear materials, Advances in nonlinear optics, Gordon and Breach ed. (1995).
- [3] H.S. Nalwa and S. Myata eds., Nonlinear Optics of organic molecules and polymers, CRC press, (1997).
- [4] J.L. Oudar, *J. Chem. Phys.*, **67**, 446, (1977).
- [5] S.R. Marder et al., *Science*, **265**, 632, (1994).
- [6] C. Fiorini, F. Charra, J.-M. Nunzi, *J. Opt. Soc. Am. B*, **11**, 2347 (1994).
- [7] N. Pfeffer, F. Charra, J.M. Nunzi, *Opt. Lett.*, **16** (1991).1987.
- [8] C. Fiorini, F. Charra, J.M. Nunzi, P. Raimond, *J Opt. Soc. Am B*, **108**, 1984, (1997).
- [9] H. Bock, R.C. Advincula, E.F. Aust, J. Käshammer, W.H. Meyer, S. Mittler-Neher, C. Fiorini, J.-M. Nunzi and W. Knoll, *J. Nonlinear Optic. Phys. & Mater.*, **7**, 385 (1998).

All-optically poled polymer microcavities: enhancement of nonlinear optical effects

R. Piron, E. Toussaere, D. Josse, S. Brasselet and J. Zyss

Laboratoire de Photonique Quantique et Moléculaire, (UMR CNRS # 8537),
Ecole Normale Supérieure de Cachan

61 av. du président Wilson, 94235 CACHAN, France

Tel : 33-1-47405563, Fax : 33-1-47405567, e-mail: zyss@lpqm.ens-cachan.fr

All-optical poling is a recent technique which has been successfully used to imprint quadratic nonlinearity patterns in polymer films. Orientation of molecules by the interference of one- and two-photon absorption pathways from mutually coherent fundamental and harmonic beams leads to molecular reorientation and a permanent non-centrosymmetric imprint with a tensorial symmetry pattern controllable via adequate beam polarizations.

Quadratic and cubic phenomena can be further enhanced by insertion of an active polymeric medium inside a resonant cavity so as to take advantage of the confinement of light in the cavity and the associated modal resonances. Significant enhancement of the SHG in all-optically poled polymer microcavities will be reported from these experiments in agreement with comprehensive modelling of the cavity effects.

Over the last several years, there has been considerable interest in the properties of microcavities towards optical telecommunication applications. Less attention has been paid to nonlinear optical microcavities whereby a prerequisite for quadratic effects is an in-plane transverse non-centrosymmetric orientation of the active part. We therefore propose optical poling as a more suitable means to induce such a configuration to a dye-grafted polymer medium than the traditional electric field thermal poling. In the all-optical poling process [1-3], selective excitation of the molecules by the interference of mutually coherent strong fundamental and harmonic beams is capable of breaking centrosymmetry within an initially isotropic medium and subsequent molecular reorientation allow for the imprint of nonlinear second order susceptibility. The macroscopic symmetry and amplitude of the resulting $\chi^{(2)}$ susceptibility can be jointly governed by both the molecular symmetry and the write tensor $\vec{E} = E^{2\omega} \otimes E^{\omega} \otimes E^{\omega}$ controllable via the magnitude, phases, and polarizations of the beams.

The microcavity structure is composed of two Bragg mirrors with a thin Disperse Red-one (DR1) dye-grafted polymer film in between (figure 1). The dielectric multilayer mirror stack is made-up of an alternation of silica and zirconium oxide layers over a BK7 glass substrate, with a reflectivity of 95% centered in the 1300 nm range.

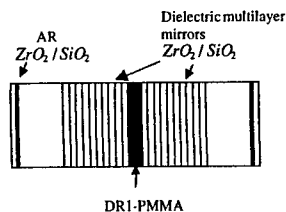


Fig. 1 : Microcavity structure

We have modelled the microcavity transmission (figure 2-a) by means of the transfer matrix method so as to quantify cavity modal resonances and subsequently optimize the design of the multi-stack structure. The measured peak positions and the finesse are found in satisfactory agreement with theoretical values. For a typical 1 μm thick polymer microcavity,

Poster Session I

the calculated finesse from a measured spectrum is of the order of 40, coming close to the theoretical value of 50. Higher values can be reached by controlling the active medium thickness within the cavity.

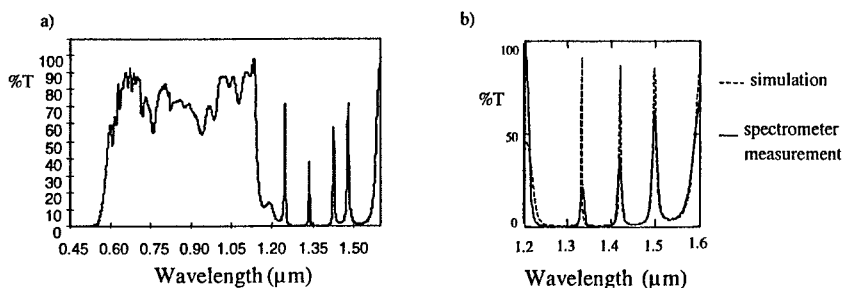


Fig.2: (a) experimental microcavity transmission spectrum.
(b) band gap spectral range of the microcavity: calculated (dotted line) and measured (full line) spectra.

Following linear characterization, the chromophores have been oriented by all-optical poling. The nonlinear efficiency of the resulting active microcavity is tested by spectral scanning through the resonance peaks using a tunable OPO, the signal being converted by the active medium into visible light by second harmonic generation. Significant enhancement by a factor of the order of 20 of the second harmonic generation has been evidenced from our preliminary experiments (figure 3). We have also considered the influence of the polarization states and phases of the write and read beams. Further improvement is expected from currently optimization of these parameters[4].

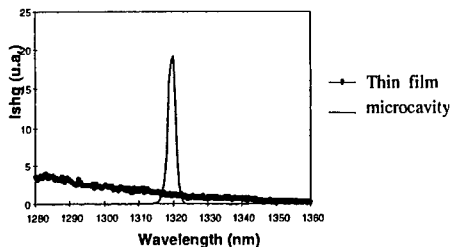


Fig. 3 : Second harmonic signal generated by an all-optically poled polymeric microcavity in comparison with a polymer film oriented in the same conditions.

To sum up, we have provided evidence, for the first time to our knowledge, of all-optical process in a microcavity structure and we have shown how embedding poled polymer film inside a resonant cavity leads to significant enhancement of quadratic nonlinear phenomena as compared to the significantly lower efficiency of plain films without a cavity.

- [1] S. Brasselet and J. Zyss, *Journal of Nonlinear Optical Physics and Materials* **5** (4), 671 (1996).
- [2] S. Brasselet and J. Zyss, *Optics Letters* **22** (19), 1464 (1997).
- [3] S. Brasselet and J. Zyss, *J. Opt. Soc. Am. B* **15** (1), 257 (1998).
- [4] R. Piron, E. Toussaere, D. Josse, S. Brasselet and J. Zyss, "Enhanced second harmonic generation in all-optically poled polymer microcavities", *Appl. Phys. Lett.*, (submitted).

Characterization of Two-Photon Absorption in Symmetric Conjugated Systems with Carbazol end groups

J. Segal¹, Z. Kotler¹, M. Sigalov², A. Ben-Asuly² and V. Khodorkovsky²

¹Photonic Materials Group, Electro-Optics Division, Soreq NRC, Yavne, 81800, Israel

²Department of Chemistry, Ben-Gurion University, Beer-Sheva, 84105, Israel

Large two-photon absorption (TPA) cross-sections were measured in a series of newly synthesized symmetrical di-carbazolyl-polyphenylenes. We report on the spectral properties of these molecules as determined by degenerate two-photon excitation fluorescence and non-degenerate two-photon absorption. The molecules studied are depicted in Figure 1.

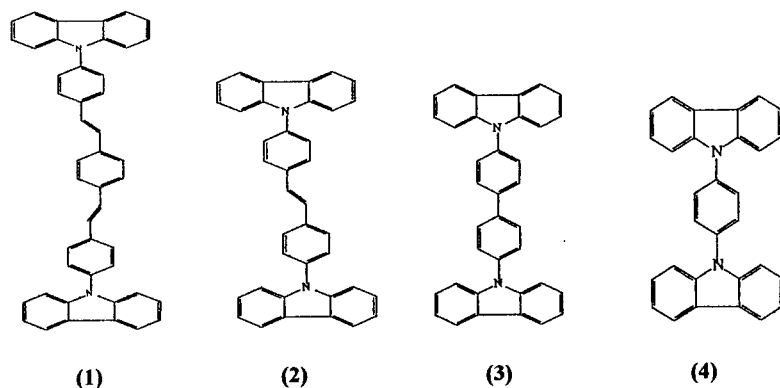


Fig 1: Molecular structures studied in this work

This series of molecules has served in evaluating the dependence of the two-photon absorption spectra on molecular structure (conjugation length and strength, planarity, electron negativity). Solvent effects have been investigated by measuring the solvatochromic shifts of the absorption and fluorescence spectra. While the absorption of (1) shows the expected dispersion dependence the fluorescence spectra reflects a strong dependence on solvent polarity.

We compare the experimentally determined parameters with quantum-chemical calculations of a model molecule (4) for which high level calculations were carried out. The excited state calculations were done using time-dependent B3LYP method on the 6-31G(d) level.

Poster Session I

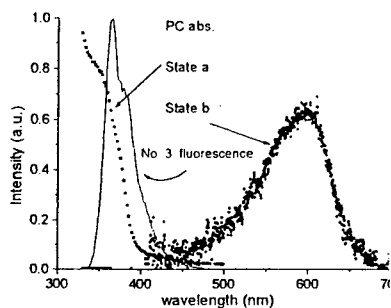
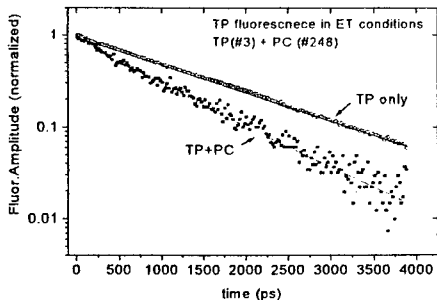


Fig 2: Absorption and fluorescene spectra of the TPA and photochrom species

Finally we present the results of our investigations into the mechanism of resonance energy transfer following two-photon excitation from a donor two-photon absorber (D) to the photochromic acceptor (A). This is done in order to evaluate the energy transfer approach as a mean of writing high resolution optical information in three-dimensions. A model system is depicted in Fig 2. The system comprises molecule (3) as donor and a photochromic molecule (C248), from the spirooxazine family, as an acceptor. The optical change following the TP excitation and energy transfer (ET) is

then retained in the material in the form of a local photochromic change. This results as the PC molecule transforms from state a to state b (peak absorption of state b is $\lambda=590\text{nm}$). Our measurements and calculations show that this process can be very efficient. We find from the fluorescence decay (see figure) following TP excitation a Förster radius, $R_0 = 27$ Ångstroms which ensures efficient ET even for a moderate PC concentration.

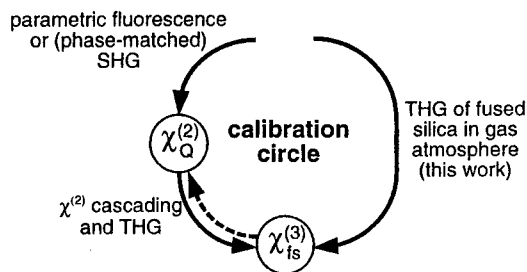


Absolute values of third-order susceptibilities: Third-harmonic generation in the gas phase

U. Gubler and Ch. Bosshard
Nonlinear Optics Laboratory
Swiss Federal Institute of Technology
CH-8093 Zürich, Switzerland

We determined the absolute value of the electronic nonlinear optical third-order susceptibility of fused silica by third-harmonic generation in a well defined gas atmosphere with a new independent method and compare it with results obtained through cascading in third-harmonic generation of single crystals of quartz and KNbO_3 .

One of the great challenges in nonlinear optics is the establishment of reliable absolute values of optical nonlinearities. We here report on a new procedure based on third-harmonic generation (THG) which yields absolute values for the electronic third-order susceptibility [1]. We calibrated the nonlinear susceptibility of fused silica against the established, quantum chemically calculated second-order hyperpolarizabilities of various gases at different pressures and determined reliable absolute values for fused silica. With our gas-phase measurements, we could assess independent standard values and compare them with the values obtained earlier by cascading [2].



Calibration scheme of optical third-order susceptibilities of fused silica. On the left path, the second-order susceptibility of a noncentrosymmetric material (quartz) has to be measured first by parametric fluorescence or (phase-matched) SHG. Afterwards $\chi^{(3)}$ of this noncentrosymmetric material can be calibrated by cascading and finally a comparing THG measurement yields $\chi^{(3)}$ of fused silica. Here we follow the right path, which allows to directly determine $\chi^{(3)}$ of fused silica by comparing it with the nonlinearities of gases in a third-harmonic generation experiment. In the end we can also use the value of $\chi^{(3)}$ determined here to confirm the second-order susceptibility $\chi^{(2)}$ of quartz (dashed arrow).

This comparison with our cascading experiments, which are completely independent to the gas phase THG measurements, disclosed the same results with deviations significantly smaller than the experimental error bars. Combining the results from THG and cascading experiments, we propose as new standard third-order nonlinear optical susceptibilities of fused silica.

Poster Session I

$$\chi^{(3)}(-3\omega, \omega, \omega, \omega) = (2.0 \pm 0.2) \times 10^{-22} \text{ m}^2/\text{V}^2 \text{ at } 1.064 \text{ } \mu\text{m}$$

$$\chi^{(3)}(-3\omega, \omega, \omega, \omega) = (1.6 \pm 0.2) \times 10^{-22} \text{ m}^2/\text{V}^2 \text{ at } 1.907 \text{ } \mu\text{m}$$

Furthermore, we can confirm the second-order susceptibility of quartz to be

$$\chi^{(2)}_{111}(-2\omega, \omega, \omega) = 0.60 \text{ pm/V at } 1.064 \text{ } \mu\text{m and}$$

$$\chi^{(2)}_{111}(-2\omega, \omega, \omega) = 0.56 \text{ pm/V at } 1.907 \text{ } \mu\text{m.}$$

These results obtained by our new method help to finally establish reliable absolute values in nonlinear optics.

References

- [1] U. Gubler and Ch. Bosshard, Phys. Rev. B, in print
- [2] Ch. Bosshard, U. Gubler, P. Kaatz, W. Mazerant, and U. Meier Phys. Rev. B, in print

High Speed PVK-based Photorefractive Polymer Composites

M. A. Díaz-García^a, D. Wright, J. D. Casperson, B. Smith, E. Glazer, W. E. Moerner^b,
Dep. of Chemistry, University of California San Diego, La Jolla, CA 92093-0340 (USA)

^aPresent address: Dep. Física, Universidad Miguel Hernández, Elche-03202, Alicante (Spain)

^bPresent address: Dep. of Chemistry, Stanford University, Stanford, CA 94305-5080 (USA)

L. I. Sukhomlinova, R. J. Twieg

Dep. of Chemistry, Kent State University, Kent, OH 44242 (USA)

The photorefractive properties of polymer composites based on poly(N-vinyl carbazole), doped with the sensitizer C₆₀, the plasticizer butyl benzyl phthalate, and two series of chromophores are presented. These materials exhibit very fast response times (beam-coupling growth times τ_g as small as 60 ms at 50 V/ μ m applied field and 200 mW/cm² intensity and τ_g as small as 5 ms at 100 V/ μ m and 1 W/cm²), of great interest for video-rate optical processing applications. The photorefractive properties are discussed in terms of their structure and oxidation potential of the chromophore.

The properties of photorefractive (PR) materials have been investigated during the last 30 years, mainly motivated by their potential applications in optical processing, phase conjugation, optical storage, etc.¹ Although most of the work has been focused on inorganic crystalline materials, such as LiNbO₃, in 1991 photorefractivity was also demonstrated in polymers. These materials have shown high performance (net gain, overmodulated diffraction efficiencies η , sub-second response times τ and gain coefficients Γ in the 100-200 cm⁻¹ range) in low-cost samples not requiring careful crystal growth. This high performance is mainly due to an orientational enhancement mechanism not present in inorganic materials.

Until now, most of the improvements in the performance of photorefractive polymers have been focused in getting larger gain coefficients and diffraction efficiencies. However, few advances have occurred in the speed of grating formation, with most materials showing grating growth times in the range 0.1-100 s at the canonical 1 W/cm² writing intensity. Very recently, we reported several high-speed PR composites (e.g. PVK:AODCST:BBP:C₆₀) with growth times less than 10 ms at 1 W/cm², while maintaining high net gain coefficients (> 100 cm⁻¹), thus opening new possibilities for video-rate optical processing applications.²

Here we investigate the photorefractive properties of materials of the general composition PVK:Chromophore:BBP:C₆₀, where only the chromophore structure changes.³ Two series of chromophores are described (See Figure 1): a series of dicyanostyrene (DCST) derivatives with varying amine donor, including the previously reported PDCST, AODCST and TDDCST, and a series of cyanoesterstyrene (CEST) derivatives with varying amine donor. We study the effect of the structure and oxidation potential of the chromophore on the PR properties, with particular emphasis on the speed of formation of two-beam-coupling gain.

The photoconductivity of the samples was measured by a simple DC technique. The photorefractive properties (Gain coefficient, maximum index modulation and phase shift) were determined from two wave mixing (TWM) experiments at 647 nm. By fitting the evolution of the growth of the gain, the time constant τ was also obtained. Finally, cyclic voltammetry was performed in all the chromophores, in order to determine their first oxidation potential and the HOMO.

Poster Session I

A comparison of the overall performance of DCSTs and CESTs, at 200 mW/cm^2 of intensity, $\lambda = 647 \text{ nm}$ and under electric fields of $50 \text{ V}/\mu\text{m}$, is illustrated in Fig. 2. Net gain ($\Gamma - \alpha$) is plotted versus the normalized speed (τ_r^{-1}/α). Although both DCSTs and CESTs present very fast response times, the net gain is generally much larger for the DCST derivatives (filled squares), probably due to the larger ground state dipole moment of the DCST derivatives providing higher Pockels and orientational nonlinearity.

CEST	Chemical Structure		DCST	Chemical Structure
	R_1	R_2		
1	C_2H_5	C_2H_5	MFOCST	
2	C_2H_5	$\text{CH}_2\text{CH}_2\text{OCH}_3$	FOCST	
3	C_2H_5	C_2H_5	TDCST	
4	C_2H_5	C_2H_5	7-DCST	
5	C_2H_5	$\text{C}(\text{CH}_3)_3$	DDCST	
6	C_2H_5	CH_3	AOCST	
7	$\text{CH}_3\text{OCH}_2\text{CH}_2$	$\text{CH}_2\text{CH}_2\text{OCH}_3$		
8	CH_3	$\text{CH}_2\text{CH}_2\text{OCH}_3$		

Figure 1: Chemical structures of DCST and CEST derivatives

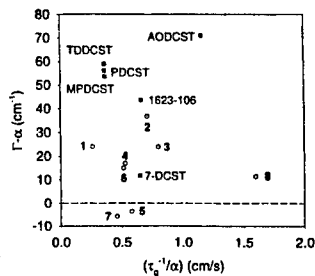


Figure 2: Comparison of the performance of composites of DCST and CEST derivatives.

References

- [1] P. Günter, J-P. Huignard, *Photorefractive Materials and Their Applications I and II*; Springer Verlag: Berlin (1988).
- [2] D. Wright, M.A. Díaz-García, J.D. Casperson, M. DeClue, W.E. Moerner, R. Twieg, "High-speed photorefractive polymer composites" *Appl. Phys. Lett.* **73**, 1490-1492 (1998).
- [3] M.A. Díaz-García, D. Wright, J.D. Casperson, B. Smith, E. Glazer, W.E. Moerner, L.I. Sukhomlinova, R. Twieg "Photorefractive Properties of PVK-Based Composites for High Speed Applications". *Chem. Mater.* **11**, 1784-1791 (1999)

Modelization and Experimental Characterization of Angular Redistribution in Optical Ordering Processes in Dye Containing Polymers

Michel Dumont

*Laboratoire de Photonique Quantique et Moléculaire,
Ecole Normale Supérieure de Cachan, (CNRS UMR # 8537),
61 Avenue du Président Wilson, 94235 Cachan cedex, France
Michel.Dumont@LPQM.ENS-Cachan.fr*

Photoinduced anisotropy (PIA) and all optical poling (AOP) imply an angularly selective resonant excitation of dye molecules followed by angular redistribution (AR). Optical pumping can induce dipolar or octupolar symmetries. In amorphous materials (polymers), without DC field, AR is isotropic and cannot produce order, but it is a necessary process for the permanence of the order created by optical pumping. AR is efficient when photoisomerization occurs. We will discuss AR mechanisms and show that a simple model can predict the final order. Simple PIA experiments can characterize AR dynamics and the ability of materials for AOP, for ONL applications. Examples will be given.

Three different optical methods have been developed for ordering dye molecules in polymer films, for non-linear optics and telecommunication applications.

- Photoinduced anisotropy (PIA) or Weigert effect: birefringence and dichroism are induced by a polarized resonant light excitation.
- Photoassisted electrical poling (PAEP): optical pumping increases the mobility of molecules, which can be oriented by the field at room temperature [1].
- All-optical poling (AOP) is the most recent method: The material is coherently pumped by the fundamental frequency and the second harmonic of a laser beam resonant at 2ω [2]. A $\chi^{(2)}$ can be created with non polar molecules (octupolar molecules) and different macroscopic symmetries can be induced [3].

These three methods can be described by the combination of three mechanisms:

1. A selective optical pumping, or angular hole burning (AHB). In this paragraph, AHB is presented in the case of rod like molecules and of linear polarization of the pumping beams (θ is the angle between the axis molecules and the polarization of light), but the model is valid for any molecular shape and any polarization of light. In PIA, the polarized pumping beam produces an anisotropic depletion of the ground state, according to a $\cos^2 \theta$ law: the pumping has the quadrupolar symmetry. In PAEP the pumping is also quadrupolar, but the anisotropy of AHB plays a secondary role.

In AOP, the depletion of the ground state contains three terms: the 1-photon absorption at frequency 2ω , which is quadrupolar ($\cos^2 \theta$), the 2-photon absorption at frequency ω ($\cos^4 \theta$: quadrupolar and hexadecapolar) and the non centrosymmetric interference term which is dipolar and octupolar ($\cos^3 \theta$). With different polarization configurations, a more sophisticated tensorial hole burning can be produced. For instance two counter rotating circularly polarized beams produce a purely octupolar pumping [3].

2. An angular redistribution (AR) occurring in the optical excitation process and/or during the lifetime of excited levels and/or in the relaxation process, back to the ground state. These angular redistribution is particularly efficient when a change of the geometrical structure of molecules occurs, *i.e.* when molecules are subjected to photoisomerization

Poster Session I

(azo-dyes are the most efficient photoisomerizable molecules). AR is a partial thermalization of molecules orientation during the excitation process.

3. Orientational relaxation in the ground state (thermal diffusion). Of course, to build a permanent orientational order, this relaxation must be avoided.

In PIA and in AOP, the angular redistribution is random and isotropic. The orientational order is produced by the depletion of the ground state through AHB. After several cycles of excitation, molecules are accumulated in the less pumped directions. Finally the geometry of the pumping light is imposed to the material. Conversely, in PAEP, the orientation is produced by the electric field. AR is no more isotropic: the thermalization, during the excitation cycle, occurs in the presence of an electrical torque on polar molecules. The optical excitation increases the mobility of molecules, like heat in the usual thermal poling method.

All these phenomena have been described by a theoretical model [4, 5] and their transient behavior can be computed as a function of the optical pumping geometry and of angular diffusion properties of excitation processes and of the ground state. This model shows that the saturation of the pumping, through multiple excitation cycles, produces a coupling of tensorial orders. The model has been used successfully for PIA and PAEP. It is easy to extend it to AOP in the case of linear polarizations, but it leads to quite heavy computer calculations in the general case. Nevertheless, if the thermal diffusion in the ground state can be neglected, a very simple analytical expression gives the final stationary angular distribution of molecules. This new model is valid for any angular dependence of the probability of optical pumping.

As the angular redistribution is exactly the same in AOP and in PIA, a simple experiment of photoinduced dichroism can determine if a given material can be poled by AOP techniques (provided the chromophores are not centrosymmetric). The optical densities OD_{\parallel} and OD_{\perp} (polarization parallel and perpendicular to that of the pump, respectively) are recorded versus time, at different probe wavelengths. The average optical density, $S_0 = (OD_{\parallel} + 2 OD_{\perp})/3$, related to the population of levels and the anisotropy, $S_2 = (OD_{\parallel} - OD_{\perp})/3$, are built and give information on the dynamics of optical pumping and of angular redistribution [6]. At the beginning of pumping, both signals grow simultaneously, but, if angular redistribution is efficient, the anisotropy signal, S_2 , continues to increase when the population signal, S_0 , has reached a stationary state: in this case, the material is a good candidate for the three methods of optical orientation. On the opposite, if S_0 grows faster than S_2 , the experiment indicates that molecules are unable to rotate and that we observe only the effect of hole burning. The same experiment can monitor the relaxation of the orientation, after the removal of the pump. Several examples will be given, with different azo-dyes.

References

- [1] Z. Sekkat and M. Dumont, *Appl. Phys. B* **54**, 486-489 (1992) and, *Mol. Cryst. liq. Cryst. Sci. Technol. secB: Nonlinear Optics*, **2**, 359-362 (1992).
- [2] F. Charra, F. Kajzar, J.M. Nunzi, P. Raimond and E. Idiart, *Optics Lett.* **18**, 941 (1993). C. Fiorini, F. Charra, J.M. Nunzi and P. Raimond, *Nonlinear Optics* **9**, 339 (1995). J.M. Nunzi, F. Charra, C. Fiorini, *J. Zyss, Chem. Phys. Lett.* **219**, 349 (1994).
- [3] S. Brasselet, *J. Zyss, Opt. Lett.* **19**, 1464-1466 (1997) and, *J. Opt. Soc. Am. B* **15**, 257-288 (1998).
- [4] M. Dumont, in: "Photoactive Organic Molecules, Science and Applications", F. Kajzar, ed., *Nato ASI Series Vol. 9*, 501-511, Kluwer Academic Publishers (1996). M. Dumont, G. Froc and S. Hosotte, *Nonlinear Optics* **9**, 327-338 (1995).
- [5] M. Dumont, *Chemical Physics*, **245**, 437-462 (1999)
- [6] El Osman and M. Dumont, *Proc. SPIE* **3417**, 36 (1998)

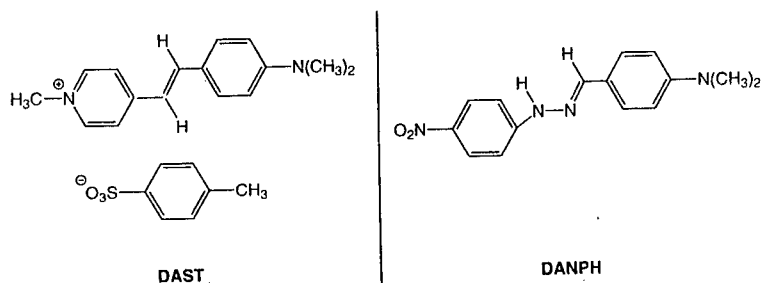
Photorefractive effects in DAST and other organic crystals

S. Follonier, Ch. Bosshard, I. Biaggio, and P. Günter
Nonlinear Optics Laboratory
Swiss Federal Institute of Technology
CH-8093 Zürich, Switzerland

We present a systematic investigation of the photorefractive properties of the organic crystals DAST and DANPH with emphasis on photorefractive gain and charge transport properties.

Organic crystals and polymers are of prime interest for low cost devices based on light-induced changes of refractive indices. Much progress was achieved in terms of photorefractive sensitivity as well as in the design of new compounds optimized for specific needs, like infrared enhanced photorefractive response. Nevertheless, the limits of organic materials have not been reached yet.

In order to improve the photorefractive sensitivity of organic crystals, the photogeneration and charge transport properties of the charge carriers are of prime importance and are investigated in this contribution for the case of the organic salt 4-N,N-dimethylamino-4'-N'-methyl stilbazolium tosylate (DAST) and of 4-dimethylamino-benzaldehyde-4-nitrophenyl-hydrazone (DANPH). DAST is very promising for electro-optic applications due to the almost parallel alignment of the chromophores with the polar a-axis [1]. DANPH is a material with very large nonlinear optical coefficients [2]. Here the chromophores are almost perfectly oriented in the crystal for phase-matched frequency conversion.



Chemical structure of DAST and DANPH.

We report on the photorefractive properties of DAST and DANPH over a large spectral range of incident light (from $\lambda = 632.8\text{nm}$ to $\lambda = 1064\text{nm}$) [3]. Intrinsic parameters such as mobility and lifetime of charge carriers and the quantum efficiency of carrier generation were investigated by DC photoconductivity, two-beam coupling, as well as pulsed photoconductivity experiments in large size DAST crystals and in platelets polished to thicknesses of less than $200\ \mu\text{m}$.

We gained a physical understanding of the mechanisms required for the photorefractive effect to occur: We identified the photogeneration of free charge carriers in DAST with

Poster Session I

an excitonic state of the crystal. We demonstrated the competition of electrons and holes in the crystal and identified the transport process of the photoexcited charge carriers as hopping from stilbazolium chromophore to stilbazolium chromophore. We estimated the mobility of charge carriers, $\mu = 16.5 \pm 10 \text{ cm}^2/\text{Vs}$, and their lifetime, $\tau = 4 \pm 2 \text{ ns}$. We determined the structure-property relationships of the photogeneration and the charge transport in DAST.

Our results show that mobility and lifetime of the photoexcited carriers are comparable to those of the best inorganic crystals such as BaTiO_3 , KNbO_3 , or $\text{Bi}_{12}\text{SiO}_{20}$. Thus, the most important factor limiting the photorefractive sensitivity in organic crystals is the small efficiency of charge carrier photogeneration, described by the quantum efficiency less than 10^{-3} at $\lambda=750\text{nm}$. Improvement of this parameter by, *e.g.*, appropriate doping of DAST with a sensitizer would lead to orders of magnitude improvement of its photorefractive sensitivity.

References

- [1] R. Spreiter, Ch. Bosshard, F. Pan, and P. Günter, *Opt. Lett.* **22**, 564 (1997)
- [2] S. Follonier, Ch. Bosshard, G. Knöpfle, U. Meier, C. Serbutoviez, F. Pan, and P. Günter, *J. Opt. Soc. Am. B* **14**, 593 (1997)
- [3] S. Follonier, Ch. Bosshard, F. Pan, and P. Günter, *Opt. Lett.* **21**, 1655 (1996)

Formation of an Anti-guide Structure in a Photorefractive Polymer by a Pump-light Beam

Takashi Fujihara^a, Takafumi Sassa^b, Kazutoshi Ozawa^a
Shinsuke Umegaki^a, Masaaki Yokoyama^c, Tatsuo Wada^b, and Hiroyuki Sasabe^{b,d}

^aFaculty of Science and Technology, Keio University,
3-14-1 Hiyoshi, Kohoku-ku, Yokohama, Kanagawa 223-8522, Japan

^bThe Institute of Physical and Chemical Research (RIKEN),
2-1 Hirosawa, Wako, Saitama 351-0198, Japan

^cFaculty of Engineering, Osaka University,
2-1 Yamada-oka, Suita, Osaka 565-0871, Japan

^dChitose Institute of Science and Technology,
758-65 Bibi, Chitose, Hokkaido 066-8655, Japan

An anti-guide structure was formed by a pump-light beam in a photo-sensitive nonlinear-optical or photorefractive polymer. The formation was experimentally confirmed by Maker-fringe method, using the polymer which was sensitive to the pump He-Ne laser but not to the fundamental Nd:YAG laser. With a poling electric-field applied, the second-harmonic generation was monitored by changing the temperature, the poling electric-field and the beam radii of the pump and the fundamental wave.

The anti-guide formed in the photorefractive polymer might be applied to light-control by light.

Introduction

Using the thin-film planar waveguide of the photorefractive (PR) polymer, we observed the self-enhancement of the Cerenkov-radiation type second-harmonic (SH) power. It was initially attributed to the gradually formed periodic structure, which satisfied the quasi-phase-matching [1, 2]. After that, however, it was theoretically made clear that the relatively large enhancement experimentally obtained could not be explained by the self-formed quasi-phase-matching but could be explained by the self-formed anti-guide structure[3].

In this paper, we report the results of fabrication of the anti-guide structure by using a He-Ne laser as a pump wave and of its confirmation by monitoring an SH wave of a fundamental Nd:YAG laser in Maker fringes.

Preparation of the PR Polymer

The PR polymer used in the Maker-fringe experiment was composed of 18.9 wt.% nonlinear-optical (NLO) 4-methoxy-4'-nitrostilbene, 0.1 wt.% photosensitizing 2,4,7-trinitro-fluorenone, and 40.4 wt.% plasticizing 1,3-Bis(N-carbazole) propane in a matrix poly(N-vinylcarbazole). Its thin film was sandwiched between the ITO glass substrates whose spacing or the film thickness was 125 μm . Figure 1 schematically shows the anti-guide structure. There, the refractive index of the region irradiated by the pump beam or by the SH beam itself is lower than the surrounding poled

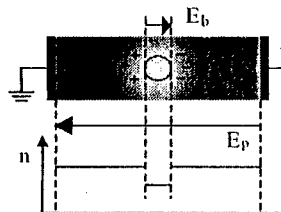


Fig.1 An anti-guide structure

Poster Session I

photorefractive-polymer, since the space charges generated in the beam and trapped outside the beam shields the applied electric field.

Experimental Results

Using a 0.1 mW power-level He-Ne laser (633 nm) as a pump beam and rotating the sample, we obtained Maker fringes of the SH wave generated from a Nd:YAG laser (1064 nm). Figures 2(a) and (b) show the results in case of the poling voltage of 1.5 kV, for almost the same and the smaller pump-beam radius in comparison to the fundamental-beam radius, respectively. Since the pump power was kept constant against making the pump radius smaller, the pump intensity, number of photo-carriers and then, the reduction of the refractive index shown in Fig. 1 increased. As its result, the enhancement of the SH power increased due to the confinement of both the fundamental and its SH power into the core region of the anti-guide.

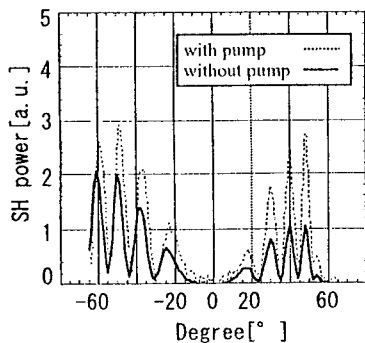


Fig.2(a) Maker fringes for the pump-beam radius same as the fundamental-beam radius.

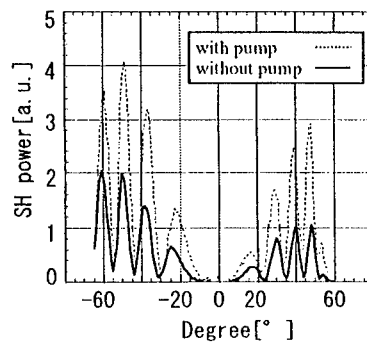


Fig.2(b) Maker fringes for the pump-beam radius smaller than the fundamental-beam radius.

In conclusion, we confirmed that the anti-guide structure was formed by the pump beam. Dependence of the enhancement on the temperature of the polymer and on the poling electric-field and the thermal effect will be discussed.

References

- [1] T. Sassa, W. Sakurai and S. Umegaki, CLEO'96, JTUE6 (1996).
- [2] T. Sassa and S. Umegaki, Opt. Lett., **22**, 856 (1997).
- [3] T. Sassa and S. Umegaki, J. Appl. Phys., **84**, 4071 (1998).

LC SLM based on fullerene doped polyimide

Natalie V. Kamanina
Vavilov State Optical Institute
St.-Petersburg, 199034, Russia
E-mail: kamanin@ffm.ioffe.rssi.ru

Natalie A. Vasilenko
Karpov Research Physical-Chemical Institute
Moscow, 103064, Russia

Liquid crystal spatial light modulator (LC SLM) based on the fullerene-doped polyimide photosensitive layer has been studied. LC SLM diffraction efficiency, sensitivity and temporal characteristics were determined by the holographic technique. The significant improvement (from 10^{-6} to 5×10^{-7} J cm $^{-2}$) in sensitivity was found. This effect is likely to be caused by a creation of additional donor-acceptor complexes in the system used.

A creation of new LC SLM has been stimulated by a development of complicated laser schemes and a design of optical memory devices [1, 2, 3]. Optically addressed LC SLM allows various physical problems to be solved. They are a control of laser directional pattern, an image selection and a phase aberration correction [4, 5]. As the SLM photosensitive layer, soluble polyimides (PIs) hold the greatest promise, because their use allows a high resolution and a high sensitivity to be obtained. This effect is associated with the highly delocalized π -electron states in polyimide that let us to control over its properties.

In the present work dynamic characteristics of LC SLM with the photosensitive layer based on fullerene doped polyimide have been investigated.

LC SLM had the typical structure [6]. For the purpose of sensitization, the polyimide solution in 1,1,2,2-tetrachloroethane was doped with fullerene C $_{60}$ or the fullerene mixture of 87% C $_{60}$ and 13% C $_{70}$. The fullerene concentration in polyimide was 0.25–0.5 wt.%. The compound was poured over a substrate and dried to remove the solvent. The thickness of photosensitive layer was 1–2 μ m. ZhK1289 and E7(BDH) nematic LCs were used as an modulated layer of 5–10 μ m in thickness. Under the Raman-Nath diffraction conditions, a holographic grating was recorded with a pulsed Nd-laser at a wavelength of 532 nm and a pulsewidth of 15 ns. The readout was carried out by the CW He-Ne-laser ($\lambda = 633$ nm) with the power density of 100 μ W cm $^{-2}$ in the collimated beam of diameter 5 mm. Both the grating vector and the vector of the readout beam field were aligned with the LC director during writing and readout. The experimental scheme was analogous to that presented in [7].

The basic characteristics of LC SLM (diffraction efficiency, η , at spatial frequency of 90–100 mm $^{-1}$; sensitivity, S ; temporal parameters) with the fullerene-doped PI photosensitive layer are presented in the Table. The results for other PI LC SLMs are given for comparison.

Poster Session I

Photo-sensitive layer of LC SLM	η %	Switch-on time, ms	Switch-off time, ms	S J cm ⁻²	Supply voltage	Write mode	Ref.
Non-sensitized PI	---	250	700	10 ⁻⁵	dc	dc	[8]
Non-sensitized PI	18*	50	500	5 × 10 ⁻⁶	dc	pulse	[9]
Dye-sensitized PI	10	10	120	10 ⁻⁶	pulse	pulse	[7]
Fullerene-doped PI	7	5	80-100	5 × 10 ⁻⁷	dc	pulse	this work

* This experiment was carried out at spatial frequency of 40 mm⁻¹.

The improvement in sensitivity of LC SLM with fullerene-doped PI is associated with a creation of charge-transfer complex between a donor (triphenylamine) fragment of the matrix PI molecule and fullerene, which has the electron affinity twice as large as that of acceptor PI fragment. The absorption cross section of new complex is several orders of magnitude more than the one of initial PI complex. This peculiarity allows the device sensitivity to be improved significantly. The efficiency of fullerene sensitization for organic PIs was shown by us in the paper [10].

In conclusion, the characteristics of the LC SLM based on fullerene-doped PI were studied using second harmonic of a pulse Nd-laser. The significant improvement (from 10⁻⁶ to 5 × 10⁻⁷ J cm⁻²) in sensitivity was found. This effect is likely to be caused by a creation of additional donor-acceptor complexes in the system investigated.

The authors wish to acknowledge Dr. O.D. Lavrentovich (Kent State University) for the help in this work and the Organizing Committee of ICONO'5 Conference for the support.

References

- [1] F. Pérennès and W.A. Crossland, "Optimization of ferroelectric liquid crystal optically addressed spatial light modulator performance," *Opt. Eng.*, **36**, 2294-2301, (1997).
- [2] A.A. Vasil'ev, D. Casasent, I.N. Kompanets and A.V. Parfenov, "Spatial Light Modulators," *Radio i Svyaz*, Moscow, 1987 [in Russian].
- [3] R.S. McEwen, "Liquid crystal, displays and devices for optical processing," *J. Phys. B: Sci. Instrum.*, **20**, 364-377, (1987).
- [4] F.I. Vladimirov, N.I. Pletneve, I.E. Morichev, and T.O. Reshetnikova, "Optically controlled transparencies for selective recording of moving objects," *Sov. Phys. Tech. Phys.*, **36**, 950-952, (1991).
- [5] N.V. Kamanina, L.N. Soms, and A.A. Tarasov, "Correction of phase aberrations by the holographic method using liquid-crystal spatial light modulators," *Opt. Spectrosc.*, **68**, 691-693, (1990).
- [6] N.V. Kamanina and N.A. Vasilenko, "High-speed SLM with a photosensitive polymer layer," *Electron. Lett.*, **31**, 394-395, (1995).
- [7] N.V. Kamanina and N.A. Vasilenko, "Influence of operating conditions and interface properties on dynamic characteristics of liquid-crystal spatial light modulators," *Opt. Quantum Electron.*, **29**, 1-9, (1997).
- [8] V.S. Myl'nikov, E.A. Morozova, N.A. Vasilenko, B.V. Kotov, and A.N. Pravednikov, "Space-time modulation of light by a liquid crystal-organic polymer photoconductor structure," *Sov. Phys. Tech. Phys.*, **30**, 444-445, (1985).
- [9] M.A. Groznov, V.S. Myl'nikov, A.G. Sinikas, L.N. Soms, "Liquid-crystal light modulator based on S-effect with an organic polymer photoconductor," *Trudy GOI*, **60**, 69-73, (1986) [in Russian].
- [10] Y.A. Cherkasov, N.V. Kamanina, E.L. Alexandrova, V.I. Berendyaev, N.A. Vasilenko, B.V. Kotov, "Polyimides: New properties of xerographic, thermoplastic, and liquid-crystal structures," *Proceed. of SPIE*, **3471**, 254-260, (1998).

Application of phase-modulated beams technique for Bacteriorhodopsin Langmuir-Blodgett films characterization

A. V. Kir'yanov, Yu. O. Barmenkov, A. N. Starodumov
Centro de Investigaciones en Optica, Loma del Bosque #115, Leon, Gto, 37150 Mexico
e-mail: yuri@foton.cio.mx

N. M. Kozhevnikov
St.Petersburg State Technical University, St.Petersburg, 195251, Russia

H. Lemmetyinen
Institute of Materials Chemistry, University of Technology,
PO Box 589, 33101 Tampere, Finland

The phase-modulated beams technique is developed for nonlinear thin photorefractive films characterization. In the Raman-Nath diffraction approximation, the formulas are deduced allowing to measure the amplitude of phase grating recorded in a film and its nonlinear refractive index n_2 . The method is applied for studying Langmuir-Blodgett multilayer thin ($\sim 0.6 \mu\text{m}$) films of Bacteriorhodopsin at wavelength 633 nm.

At present time, the most popular methods for studying photorefractive properties of a medium are the Z-scan technique [1] and measurements of diffraction efficiency. But these methods meet some difficulties in application and the data interpretation for extremely thin films, when an interaction length is limited by the distance of $\sim 1 \mu\text{m}$ or less and therefore the resultant photoresponse is very weak. A number of methods and devices have been developed especially for thin films characterization; among them are the nonlinear distributed gratings or prism couplers [2], the interferometric technique based on an antiresonant ring resonator [3], the DFWM process in waveguides [4]. The main disadvantage of all of them is a necessity to deal with a tested film of high optical quality; in addition, the first two techniques are very sensitive to the temperature variations. Here we present the Phase-Modulated Beams (PMB) technique [5] application for thin films characterization and demonstrate its power for studying the photorefractive properties of multilayer Langmuir-Blodgett films containing Bacteriorhodopsin (BR).

The PMB technique is based on the spectrum analysis of intensity modulation of the output beams in a holographic interferometer resulting from the two phase-modulated beams mixing (Fig.1). The incidence beams are used for simultaneous recording and reading of the gratings. Originally, the PMB technique was developed for measuring a photoresponse from thick photorefractive media, for which the Bragg conditions for the two-waves mixing are fulfilled. Here we obtain such a dependence for a thin film (the Raman-Nath diffraction), when the medium thickness l is much less than the grating period Λ . In the case of equal-intensity incidence beams for a medium with local photoresponse the phase grating amplitude n_1 and the nonlinear coefficient n_2 can be expressed as

$$n_1 = \frac{\lambda}{4\pi l J_1(a)} \delta I_{\alpha}(l), \quad (1)$$

$$n_2 = \frac{n_1}{J_0(a)I_0}, \quad (2)$$

where λ is wavelength, $\delta I_{\Omega}(l)$ is the modulation depth of the output beam intensity at the phase modulation fundamental harmonic Ω , l is the sample thickness, $J_{n,l}(a)$ are Bessel functions of the first and second orders of the phase modulation amplitude a , and I_0 is the incidence beams total intensity.

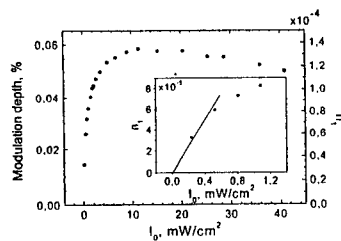
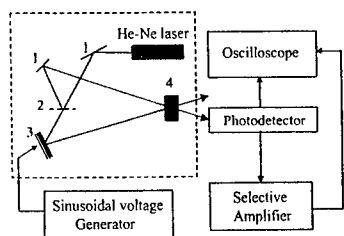


Figure 1: Experimental setup of phase-modulated beams technique. 1 – mirrors, 2 – beam splitter, 3 – mirror attached to electromagnetic modulator.

Figure 2: Dependencies of output beam modulation depth (left scale) and phase grating amplitude (right scale) on total input intensity.

The PMB technique has been applied to characterize the multilayer Langmuir-Blodgett films of BR (total thickness of $\sim 0.6 \mu\text{m}$) at the wavelength 633 nm at steady-state. We measured the dependence of the intensity modulation depth $\delta I_{\Omega}(l)$ against the total input intensity and calculated the phase grating amplitude n_1 using Eq. (1) (Fig. 2). The slope of the curve $n_1(I_0)$ at low intensity (Fig. 2, inset) gives $n_2 = 0.21 \text{ cm}^2/\text{W}$. The area at high intensities (main curve in Fig.2) corresponds to absorption saturation, which results in the phase grating shape distortion and saturation of the curve $n_1(I_0)$. The maximum of the grating amplitude ($n_1 \approx 1.4 \times 10^{-4}$ at $I_0 = 10 \text{ mW/cm}^2$) corresponds to the fundamental spatial harmonic maximum and gives the maximum value of the refractive index variation: $\Delta n \approx 2.8 \times 10^{-4}$. Note that the calculated value of the grating diffraction efficiency in the above circumstances is $\sim 2 \times 10^{-7}$. It is virtually impossible to detect such values experimentally, otherwise one needs to measure powers of the order of 10^{-10} W . Therefore the PMB techniques seems to be an unique method to measure extremely weak nonlinearities.

References

[1] M. Sheik-Bahae, A. A. Said, *et al.*, IEEE J. Quantum Electron. **26**, 760 (1990).
 [2] G. I. Stegeman, E. M. Wright, *et al.*, J. Lightwave Technol. **6**, 953 (1988).
 [3] H. W. H. Lee and R. S. Hughes, Opt. Lett. **19**, 1708 (1994).
 [4] C. Malouin, A. Villeneuve, *et al.*, Opt. Lett. **21**, 21 (1996).
 [5] M. Gertz, J. Pinsl, and Ch. Bräuchle, Appl. Phys. B **43**, 61 (1987).

Influence of rheological properties on photorefractive polymer electrooptic response.

L. Mager*, J.-C. Ribierre*, A. Fort*, S. Méry^o, J.-F. Nicoud^o, *Groupe d'Optique Non Linéaire et d'Optoélectronique, ^oGroupe des Matériaux Organiques, Institut de Physique et de Chimie des Matériaux de Strasbourg, UMR 7504, 23, rue du Loess, 67037 Strasbourg CEDEX, France.

The very large efficiency of low- T_g photorefractive organic materials is known to be connected to reorientation of the chromophores in the space charge field. We show using temperature and frequency resolved ellipsometric measurements that the orientation dynamic is strongly correlated to the material viscosity. A huge decrease of the electrooptic response time from seconds to milliseconds has been observed for a raise of temperature from T_g to $T_g+20^\circ\text{C}$. These results have been fully interpreted with the William-Landel-Ferry formalism. They show that the optimization of these materials must take into account the rheological properties.

The high performances observed in low glass transition temperature (T_g) photorefractive organic materials are connected with the ability of the chromophores to reorient in the space charge field⁽¹⁾. This orientation occurs in a viscous matrix and therefore is connected with the mechanical properties of the medium. When the chromophores move in the polymer matrix, they displace some material and then induce a mechanical stress in the sample. This phenomenon can be considered as a shear stress application experiments similar to these used to characterize viscoelastic behavior of a material and based on mechanical measurement. The orientation rate of the chromophores, which is responsible for the electro-optic (EO) response, gives an induced strain which can be then optically measured.

The measurements are made on a chromophore doped polymer : the polymer matrix is a carbazole functionalized polysiloxane (PS4CZ) which exhibits photoconduction in the visible range when doped with (2,4,7-trinitro-9-fluorenylidene)malononitrile (TNFDM). The chromophore is a push-pull chalcone derivative (CHAL) which does not recrystallize in the polymer matrix after more than six months in the (PS4CZ:TNFDM:CHAL) (80% wt : 0.05% wt : 20 %wt) sample we study⁽²⁾. Its T_g measured by differential scanning calorimetry yields $T_g=23^\circ\text{C}$. The material is pressed between two ITO/glass plates at a 100 microns thickness. We use a transmission ellipsometry setup to characterize the electro-optic behavior of the material depending on the chromophore orientation⁽³⁾. Measurements are performed varying the temperature from 18°C to 50°C .

A 1000 V cw voltage is applied on the sample to induce the centrosymmetry breaking which is needed for the observation of EO response of the material. We add to this constant voltage a sinusoidal tension with an amplitude of 1000 V at Ω frequency. We measure the modulated light intensity variation to determine the EO response versus frequency Ω at a given temperature. We show that these EO response variations strictly follows the William-Landel-

Poster Session I

Ferry equation which describe the time-temperature equivalence principle in viscoelastic materials.

We have also measured the EO response of the materials with 1000 V pulses. The behavior is similar to a viscoelastic liquid showing elastic and viscoplastic responses with a steady state flow at longer time scale. This behavior is strongly temperature sensitive and shows large variations especially around T_g . We demonstrate that the response time of the material varies from 13 s at 26°C to 2 ms at 47°C, i. e. a decrease of 4 orders of magnitude for a 20°C temperature variation.

These results demonstrate the importance of the rheological properties of the material on the EO response and their role in the choice of future polymer matrices for the elaboration of faster photorefractive organic materials.

- (1) W.E. Moerner, S.M. Silence, F. Hache, G. C. Bjorklund, *J. Opt. Am. B*, 11, (2), pp. 320-330, 1994
- (2) L. Mager, C. Melzer, M. Barzoukas, A. Fort, *Appl. Phys. Lett.*, 71, 2248 (1997)
- (3) B. Kippelen, Sandalphon, K. Meerholz, N. Peyghambarian, *Appl. Phys. Lett.*, 68, (13), pp. 1748-1750, 1996

Optical Image Correlators Based on Nematic Liquid Crystals

A. Miniewicz, P. Sikorski, A. Januszko, S. Bartkiewicz,
*Institute of Physical and Theoretical Chemistry, Wrocław University of Technology,
50-370 Wrocław, Poland*

J. Parka
Institute of Technical Physics, Military University of Technology, 00-908 Warsaw, Poland

F. Kajzar
*LETI (CEA - Technologies Avancées) DEIN - SPE, Groupe Composants Organiques,
Saclay, F91191 Gif Sur Yvette, France*

We present an experimental realisation of optical correlation for a real-time pattern recognition by means of a joint-Fourier transform correlator. The correlator operates with a liquid-crystal active matrix spatial light modulator as the input and, designed by us, optically addressed liquid crystalline spatial light modulators at the recording plane allowing both dynamic input and dynamic filtering. We test two different types of optimised liquid crystal cells acting as OA SLM's: (i) nematic liquid crystal doped with 0.4% w/w anthraquinone dye and (ii) hybrid- photoconducting polymer - nematic liquid crystal structure. We discuss performance characteristics of the correlator.

Real-time processing of optical information is nowadays possible because many materials showing capability of dynamic hologram recording has been developed. Among those materials liquid crystals play an important role. One can mention liquid crystalline electrically addressed spatial light modulators (EA SLM) and optically addressed ones (OA SLM). The newly discovered LC OA SLM's [1-5] exhibit high sensitivity and fast photoresponse time, extensive reversibility to permit long-term use and sufficient spatial resolution for processing of complex patterns. We believe that after some maturation of their technology the chosen liquid crystal systems can fulfil the demanding material requirements to be the key elements of real-time image recognition systems.

We assembled a joint-Fourier-transform (JFT) optical correlator where an expanded and collimated laser beam coming from the doubled in frequency cw Nd:YAG laser ($\lambda = 532$ nm) illuminated partially transparent mask where the input objects and the recognition pattern were given. The Fourier lens ($f = 300$ mm) performed a joint-Fourier transform in a back plane where the liquid crystal panel was situated. At light overlap regions the diffraction phase gratings (holograms) were formed. These holograms were reconstructed by another laser beam (He-Ne, $\lambda = 632.8$ nm) and the first order diffracted wave contained the correlation signal of the input objects. The correlation peaks were registered by a CCD camera and transmitted to the computer. The periods $\Lambda = \lambda / (2 \sin \theta)$ of the diffraction gratings recorded in the liquid crystal panel are determined by angles 2θ between the incidence directions of Fourier transforms. In another version of the JFT correlator we replaced an input mask by a transmissive VGA spatial light modulator basing on twisted nematic structure. This EA SLM (15x11 mm in size, 640x480 pixels) steered by a computer could operate at a rate of 25 images per second. However, due to lower contrast and resolution of EA SLM, than that provided by the masks, the correlation peaks were less visible.

We prepared two types of LC panels. First one consisted of a planarly oriented multicomponent nematic mixture (low-angle rubbing, tilt $2 - 3^\circ$) doped with an anthraquinone dye (1 % w/w) [1-3] which acted as a photoconducting dopant. Such LC panel is particularly suitable for optical correlation purposes as the holographic gratings can be written under

Poster Session I

normal light incidence. 6.3 μm thick LC layer made that the system operated within the Raman-Nath light diffraction regime and the written holograms could be read at any incidence angle (no Bragg angle tuning necessary for the readout). The diffraction efficiencies measured in the described panels were of the order of 1% making well visible correlation spots. Long-time operation required frequent voltage reversal (± 10 V) in order to prevent possible memory effects and electrochemical reactions at electrode areas. The total light intensity level entering the LC panel was kept well below 300 mW/cm^2 in order to avoid damage of the system by an excessive heat at the focal point.

The second type panel was a hybrid structure containing a pure nematic liquid crystal (E-7 Merck) sandwiched between two polymeric photoconducting electrodes [4,5]. We employed poly(octylthiophene) as a dual function orienting and photoconducting layer. Two principal effects occur under light illumination: (i) formation of spatially modulated space charge in a photoconducting polymeric layer and (ii) mapping of the space charge electric field into respective changes of an effective refractive index of nematic liquid crystal (via the process of molecular reorientations along the electric field lines). Contrary to the dye-doped liquid crystals, where charge carrier transport and index modulation occur within the same medium, in the latter solution these functions are separated, thus electrode as well as photochemical side reactions are avoided and the durability of the panel is improved. The disadvantageous for optical correlator construction is the necessity of sample tilting for obtaining an efficient hologram recording.

Observation of a rise time of a correlation peak intensities after the laser beam opening allowed us to study the dynamics of the systems. Typically rise times amounted to 20 ms and the decay time of the diffracted signal measured after blocking one of the beams amounted to 30 ms. Then the complete recognition process in our system has been completed within 50 ms, and the system was ready for a new task.

References

1. S. Bartkiewicz, A. Miniewicz, A. Januszko and J. Parka, *Pure Appl. Opt.*, **5**, 799-809 (1996).
2. A. Miniewicz, S. Bartkiewicz, W. Turalski, A. Januszko, in R.W. Munn, A. Miniewicz and B. Kuchta (eds.), *Electrical and Related Properties of Organic Solids*, NATO ASI Series, Vol. **3/24**, Kluwer Academic Publishers, Dordrecht, 1997, pp. 323-337.
3. A. Miniewicz, J. Parka, S. Bartkiewicz and A. Januszko, *Pure Appl. Opt.*, **7**, 179-189 (1997).
4. S. Bartkiewicz, P. Sikorski and A. Miniewicz, *Opt. Lett.*, **23** (22), 1769-1771 (1998).
5. F. Kajzar, S. Bartkiewicz and A. Miniewicz, *Appl. Phys. Lett.*, **74** (20), 2924-2926 (1999).

Influence of the chromophore ionization potential on the magnitude of photorefractive effects in PVK-based polymer composites

D. Van Steenwinckel, E. Hendrickx, and A. Persoons

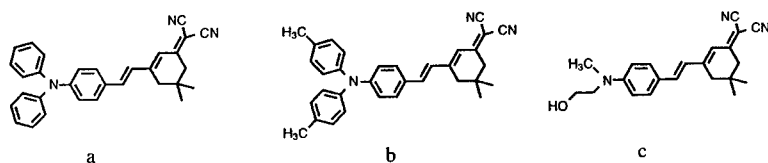
Laboratory for Chemical and Biological Dynamics, Center for Research on Molecular Electronics and Photonics, University of Leuven, Celestijnenlaan 200D, B-3001 Leuven, Belgium

K. Van Den Broeck, C. Samyn

Laboratory of Macromolecular and Physical Organic Chemistry, University of Leuven, Celestijnenlaan 200F, B-3001 Leuven, Belgium

We report on the synthesis of three highly polar chromophores and their use as dopants in poly(N-vinylcarbazole) (PVK)-based photorefractive polymer composites sensitized with (2,4,7-trinitro-9-fluorenylidene)malononitrile (TNFDM). Small alterations in the amino donor group substituents were used to tune the dye's ionization potential (I_p) by 0.2 eV. At 780 nm, 5 °C above the glass transition temperature (T_g), and with an applied field of 59 V/ μ m, we observed complete internal diffraction and a gain coefficient of 167 cm^{-1} . In this temperature range, diffraction efficiency and gain coefficient were found to correlate with the chromophore I_p .

The chromophores that were used for this study as dopants in the PVK-based composites, are shown below. Changing the substituents on the amino donor functionality lead to a change in ionization potential for the chromophores by 0.2 eV.



The Figure of Merit (FOM)¹ for chromophores for photorefractive applications is given by $FOM = A\Delta\alpha\mu^2 + \mu\beta$, where $\Delta\alpha$ is the polarizability anisotropy, μ the dipole moment, β the first hyperpolarizability, and $A = 2/(9kT)$ is a scaling factor. Since $\Delta\alpha\mu^2$ in this equation is the most important factor, the value of this factor was determined for the three chromophores by an ellipsometric technique.² Values for chromophores a, b, and c were 5.1, 5.5, and 6.5 ($\cdot 10^{-57}$ esu), respectively.

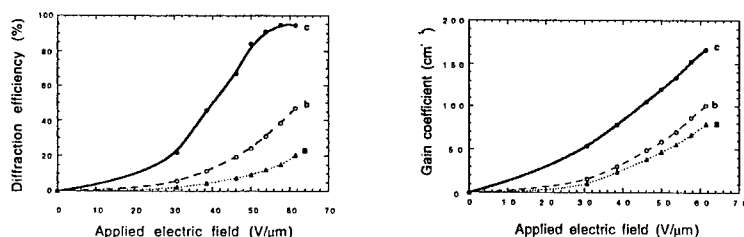
The same tendencies are observed in the values of the ionization potentials of the chromophores. Ionization potentials were calculated out of redox potentials, obtained by cyclic voltammetry. The ionization potentials for chromophores a, b, and c were calculated to be 5.59 eV, 5.46 eV, and 5.40 eV, respectively.

Since the ionization potential of the chromophores is lower than that of the carbazole groups, it is likely that the chromophores will act as hole traps in this mixture. We tested this by measuring photoconductivities in PVK-samples. A large decrease in photoconductivity was measured upon doping PVK with small amounts of chromophore. The photoconductivity then again increases when more chromophore is added. This is similar to what was observed in mobility experiments by Pai et al.³ upon doping PVK with TPD. Also,

Poster Session I

when the chromophores are doped into polycarbonate, photoconductivity and photo-refractivity could be observed. This confirms that the chromophores can act as charge transport species, and hence they can trap holes when doped into carbazole. Knowing the ionization potential for pure N-Ethylcarbazole (ECZ) (5.9 eV) and for the chromophores, the depth of the chromophore traps can be calculated easily.

We have measured diffraction efficiencies and gain coefficients in samples with composition PVK/ECZ/chromophore/TNFD: 42/28.5/28.5/1, containing chromophores a, b, and c, respectively, and we have calculated the refractive index modulation, using Kogelnik's coupled wave theory for thick holograms.⁴ The diffraction efficiencies and gain coefficients for three samples containing chromophores a, b, and c in the same weight concentrations, are shown below.



The birefringence contribution in all samples was equal after adjusting the T_g of the composite by varying the PVK/ECZ ratio. Measurements were performed at the same distances from T_g . The differences in $\Delta\alpha\mu^2$ that were measured for the different chromophores could not explain the large differences that are observed in the diffraction efficiencies and the refractive index modulations of the different samples. A possible explanation is that the refractive index modulation scales with the depth of the chromophore traps and hence with the ionization potential of the chromophore. The holes that are formed in the illuminated parts of the light intensity pattern due to an electron-hole separation migrate towards the darker parts, where they are trapped. Since the possibility of liberation of a hole from a trap with a certain light intensity is inversely proportional to the trap depth, deeper traps decrease the possibility of charge recombination, and increase the total amount of separated charges inside the material. Consequently, both space-charge field and the refractive index modulation can be expected to enlarge with the depth of the traps, as was observed experimentally.

The highest diffraction efficiencies and gain coefficients were obtained for samples containing chromophore c, the chromophore with the lowest ionization potential. For this sample, complete internal diffraction and a gain coefficient of 167 cm⁻¹ were obtained at 780 nm and at an applied field of 59 V/μm.

References

- [1] B. Kippelen, F. Meyers, N. Peyghambarian, S. R. Marder *J. Am. Chem. Soc.* **119**, 4559 (1997).
- [2] Sandalphon, B. Kippelen, K. Meerholz, N. Peyghambarian *Appl. Opt.* **35**, 2346 (1996).
- [3] D. M. Pai, J. F. Yanus, M. Stolka *J. Phys. Chem.* **88**, 4714 (1984).
- [4] H. Kogelnik *Bell. Syst. Techn. J.* **48**, 2909 (1969).

Photorefractive effects in nematic liquid crystals under rigid boundary conditions

G. Zhang, D. Haertle, G. Montemezzani, P. Günter
*Nonlinear Optics Laboratory, Swiss Federal Institute of Technology
CH - 8093 Zürich, Switzerland*

Light-induced space-charge fields and the related orientational photorefractive effects in nematic liquid crystal cells are studied both theoretically and experimentally, showing the importance to consider explicitly the effect of the rigid boundary conditions at the surfaces. Analytical solutions for the refractive index change distribution are obtained under the single-elastic-constant approximation with various configurations of externally applied electric and magnetic fields and of the nematic liquid crystal director. Experimental verifications confirm the expected significant influence of the surface boundary conditions and the applied fields on the optimum geometry for maximum diffraction.

Photorefractive effects induced in doped nematic liquid crystals are attracting considerable interest because of the huge optical nonlinearity that can be induced at very low light levels [1, 2, 3, 4]. The theoretical description of the average molecular orientation and of the optical nonlinearity leading to light diffraction has to include several concurring effects and is therefore rather complicated. One of the key factors is the anchoring of the molecules at the cell surfaces. It influences significantly in which way the nematic molecules can rearrange in the presence of inhomogeneous light illumination and inhomogeneous internal electric fields.

In this work the space distribution of the nematic director and the related optical diffraction efficiency are calculated analytically under the single elastic constant approximation for various configurations of externally applied fields in homeotropic and parallel aligned cells. The rigid boundary conditions are considered explicitly. Besides electric fields, also externally applied magnetic fields are taken into account.

The main results can be summarized as follows. While the quasi-static electric space-charge field, in general, does not point along the grating vector direction, it is its component perpendicular to the cell normal which is responsible for the observable optical effects. This component is phase shifted by $\pi/2$ with respect to the light fringes and gives rise to the well-known possibility to observe two-beam coupling energy transfer in these materials. The effects are strongly enhanced near the Frederick's transition and, in proper geometries, combination of applied electric and magnetic fields permits to enhance the effects further while keeping the fields below the Frederick's threshold values. Under the same conditions the grating spacing Λ_{\max} at which the maximum diffraction efficiency is reached differs strongly between parallel and homeotropically aligned cells. The optimum grating spacing Λ_{\max} also shifts as a function of a combined strength of the externally applied electric and magnetic field, which is a direct consequence of the rigid boundary conditions.

Experimental studies were performed using the nematic mixtures E63 and ZLI 5700-100 of Merck Ltd. Parallel and homeotropically aligned cells of $30 \mu\text{m}$ thickness doped with a small amount of Rhodamine 6G, C₆₀ or Methyl Red were used. The shift of the optimum grating spacing with applied field as well as the expected importance of taking into account the rigid surface anchoring could be verified. As an example Figure 1 shows the grating spacing dependence of the diffraction efficiency of the first order beam for a

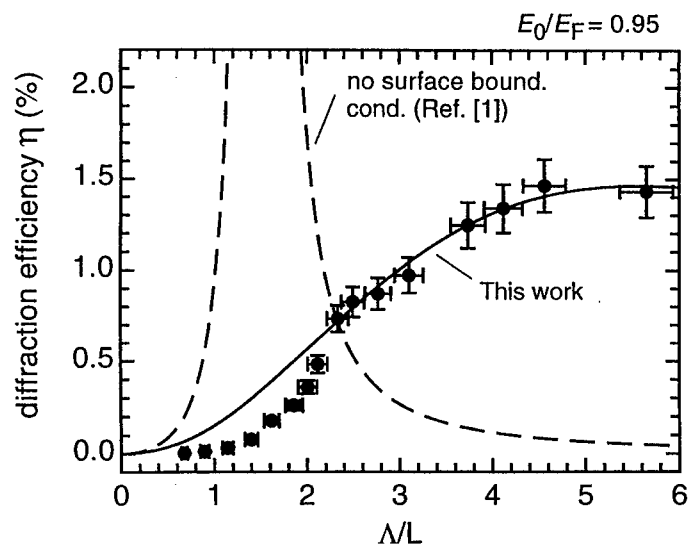


Figure 1: Diffraction efficiency of the first order diffracted beam as a function the grating spacing Λ normalized to the cell thickness L . The solid curve corresponds to the predictions of this work, the dashed curve is derived from Ref. [1], eq. (23). The parameter E_0/E_F is equal to 0.95 in both cases.

E63 parallel aligned nematic cell doped with 0.08 wt% of C₆₀. The applied electric field E_0 is close to the measured Frederick's threshold field E_F , $E_0/E_F = 0.97 \pm 0.12$. The position of the maximum diffraction is well reproduced by our expressions (solid curve) fitted with a value $E_0/E_F = 0.95$. The maximum occurs at a much longer grating spacing than predicted by the theory that neglects the strong surface boundary conditions (dashed curve, Ref. [1], eq. (23)).

In conclusions, this contribution evidences the importance of considering the rigid boundary conditions at the surfaces for predicting light diffraction behaviour in photorefractive nematic liquid crystals.

References

- [1] E. V. Rudenko, A. V. Sukhov, JETP **78**, 875 (1994).
- [2] I. C. Khoo, IEEE J. Quantum Electronics **32**, 525 (1996).
- [3] G. P. Wiederrecht, B. A. Yoon, W. A. Svec, M. R. Wasielewski, J. Am. Chem Soc. **119**, 3358 (1997).
- [4] H. Ono, N. Kawatsuki, J. Appl. Phys. **85**, 2482 (1999).

Surface Mediated Photorefractive Mechanisms in Liquid Crystals

J. Zhang, V. Ostroverkhov, and K.D. Singer
Department of Physics
Case Western Reserve University
Cleveland, OH 44106-7079

V. Reshetnyak
Physics Faculty
Kyiv Taras Shevchenko University
Prosp. Glushkova, 6, Kyiv, Ukraine

Yu. Reznikov
Institute of Physics National Academy of Sciences
Prosp. Nauki, 46, Kyiv, Ukraine

Photorefractive diffraction gratings were studied in cells of homeotropically aligned pentyl-cyanobiphenyl (5CB) liquid crystal. These holographic gratings were induced by the simultaneous and non-simultaneous application of dc and coherent optical electric fields. The observed behavior was consistent with a dominantly surface mediated photorefractive effect. Beam coupling was observed in all cases leading to a model involving screened and unscreened interfacial trapped charge driving a modulation of the easy axis. It was found that holographic gratings could be switched on and off with the application of a small voltage.

The photorefractive effect in nematic liquid crystals (LC) was reported by several groups. This effect is usually attributed to a light-induced modulation of electric charges, in conjunction with an applied dc electric field producing space charge in the bulk of the LC. This inhomogeneous bulk space charge field was described as due either to differential photocarrier diffusion in the LC or to a light-induced electro-hydrodynamic instability. In addition, Khoo et al [1] reported on the recording of persistent photorefractive gratings. The authors believed that these persistent gratings are due to a large perturbation of the surface director axis alignment due to current and nematic flows under the prolonged application of a dc-field. This result implies that the anchoring properties of the aligning surface can be drastically changed during the grating recording and, in turn, the aligning surfaces may play a crucial role in the photorefractive effect.

We report here on new experiments that point to a surface mediated photorefractive effect in homeotropically aligned LC cells. We believe that this effect was due to a light-induced modulation of the easy axis caused by electric charges at the interface of the LC cell and the alignment layer. The effect is marked by the unusual property that the recorded grating can be hidden and then revealed by turning a dc electric field off and then on. This allows for low-voltage switching of the diffraction grating, which may be useful for diffractive beam steering.

Several experiments were carried out as follows:

Writing beams are turned on with no applied electric field. No self-diffraction or diffraction of the test beam was observed at any angle of incidence.

A 2V dc-field was applied for one second, and then the dc circuit was opened. The writing beams were then turned on. Self-diffraction and beam coupling was observed.

Poster Session I

The writing beams were turned on for one second with no electric field applied, and then turned off. A 2V dc-field was then applied. Diffraction of the probe beam was observed.

The three results above suggest a surface-mediated photorefractive effect involving an unknown photo, electrical, and/or chemical process leading to charging at the interfaces. Current induced bulk effects are ruled out.

The following experiment was then performed:

A dc-electric field was turned on followed by the writing beams. At $V_{dc} > 1.2V$, self-diffraction of the writing beams was observed at oblique incidence only. When the dc-field was then switched off, a sharp temporary increase in diffraction of both the probe and recording beams followed, and then disappeared. Despite this, a grating remained in the cell, because, when a dc-field was reapplied, the diffraction grating reappeared, and then slowly disappeared. The grating diffraction can be rejuvenated by turning the dc-field off for up to several hours, and then turning it back on. When a low frequency electric field (0.1-0.5 Hz) was applied, the diffraction intensity appeared in a phase with the maximums of the field. Two-beam coupling was measured verifying the photorefractive nature of the process.

The experimental results can be qualitatively explained by either surface or bulk torque arising from charge modulation at the aligning surface.[2] However, these two mechanisms can be distinguished by observing the characteristics of the grating decay upon switching off the dc-field. The dc-field acts in two different ways. First, it creates the driving force for the director grating, but it also prevents director deviation from the initial homeotropic orientation. If the volume torque was responsible for the observed effect, the director grating would disappear gradually because this torque is proportional to the product of dc- and surface charge field as described above. However, if surface torque or easy axis (anchoring) modulation was responsible for the effect, switching off the dc-field leads to a temporary enhancement of the grating since there is no stabilizing action of dc-field, while there is an easy axis grating at the beginning of the relaxation. Our data demonstrate this behavior. Therefore, we conclude that the second mechanism dominates in our experiments.

Thus, we have demonstrated that the photorefractive effect is surface mediated in homeotropically aligned 5CB liquid crystal cells. Further, we have found that an electrically controlled diffraction grating can be written, which has potential applications in, for example, beam steering.

The authors are grateful to Sergey Shiyankovskii for helpful conversations. This work was partially supported by NRC Twinning Program, Intas Grant 97-635 Grant B29/13 of the National Academy of Sciences of Ukraine, the Air Force Office of Scientific Research (F49620-99-1-0018) and the National Science Foundation under the ALCOM Science and Technology Center (DMR89-20147).

References

- [1] I. C. Khoo, *IEEE J. Quantum Electron.* **32**, 525 (1996).
- [2] N.Tabiryanyan, C Umeton. *J Opt. Soc. Am B* **15**, 1912 (1998).

Theory for Self-enhancement of Second-harmonic Generation in a Photorefractive Polymer Based on Formation of an Anti-guide Structure

Takafumi Sassa ^a, Takashi Fujihara ^b, Kazutoshi Ozawa ^b,
Shinsuke Umegaki ^b, Masaaki Yokoyama ^c, Tatsuo Wada ^a, and Hiroyuki Sasabe ^{a,d}

^a The Institute of Physical and Chemical Research (RIKEN),

2-1 Hirosawa, Wako, Saitama 351-0198, Japan

^b Faculty of Science and Technology, Keio University,

3-14-1 Hiyoshi, Kohoku-ku, Yokohama, Kanagawa 223-8522, Japan

^c Faculty of Engineering, Osaka University, 2-1 Yamada-oka, Suita, Osaka 565-0871, Japan

^d Chitose Institute of Science and Technology, 758-65 Bibi, Chitose, Hokkaido 066-8655, Japan

Enhancement of second harmonic generation by formation of an anti-guide structure is theoretically evaluated. The obtained enhancement explains experimental result in a photorefractive polymer well. Additionally, an enhancement of more than 100 times is shown with refractive index change in the order of 10^{-5} to construct the anti-guide core.

Introduction

Self-enhancement of second harmonic generation (SHG) originating from photorefractive (PR) effect has been shown interest, as it could offer a new technique against conventional one for highly efficient SHG such as quasi-phase-matching and/or introduction of a channel waveguide structure. It yields SH wave increasing in power by itself owing to self-phase matching [1] or to self-waveguide-formation [2] based on the intensity-dependent refractive index change, i.e. PR index change.

Recently, we have found self-enhanced SHG in a PR polymer for the first time, and explained the mechanism by formation of an anti-guide structure which is caused by the PR index change in the medium.[3] Increase of the SHG is introduced by a gradual construction of the anti-guide core, which is induced by the SH wave itself, to strengthen the optical confinement.

In this report, the degree of the SHG enhancement is theoretically evaluated. In the theoretical approach, change of the transversal wavenumber spectrum for lightwave with the anti-guide formation is focused. Finally, the theory is applied to the PR polymer previously reported, where refractive index change accompanies reduction of the nonlinear optical coefficient for SHG ($\chi^{(2)}$), due to molecular reorientation. In addition, it is also applied to a PR crystal to take full advantage of the enhancement effect.

Wavenumber spectrum in an anti-guide structure

Structure of the anti-guide is different from an ordinary waveguide such as an optical fiber, having a core with lower refractive index than a clad. Figure 1 shows the index profile. The depressed part by Δn shows the constructed core region due to the PR effect. In our

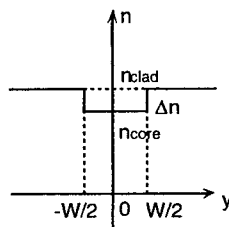


Fig. 1 Index profile.

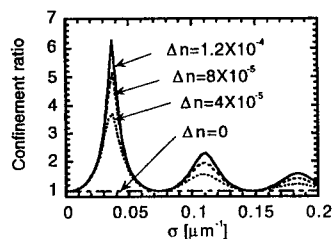


Fig. 2 Confinement factor calculated with $W=85 \mu\text{m}$.

Poster Session I

model, the core has a width (W) which is equal to that of the fundamental wave. The optical confinement induced by the core originates from reflection at the core-clad boundary, and the degree of the confinement can be analyzed by comparing amplitude of lightwave in the core and the clad. In the structure, any lightwave belongs to radiation-mode and the mode-distribution function can be expressed as:

$$f(x) = \begin{cases} \cos(\sigma x) & \text{for } |x| < W/2 \\ -(\sigma/\rho)\sin(\sigma W/2)\sin\{\rho(|x| - W/2)\} + \cos(\sigma W/2)\cos\{\rho(|x| - W/2)\} & \text{otherwise.} \end{cases} \quad (1)$$

σ and ρ correspond to component of wavenumber vectors along y direction in the core and the clad, respectively. Some calculated spectra of degree of the confinement, or the confinement ratio are shown as Fig. 2. The confinement ratio increases resonantly with Δn , which is similar to an etalon. In the spectra, two points are important: one is that the ratio of several times can be obtained even with rather small Δn , and the other is that the largest resonance is achieved by very small σ ($\ll k_0 \sim 10 \mu\text{m}^{-1}$: wavenumber in vacuum).

SHG enhancement ratio

To obtain the SHG enhancement ratio, or to compare the SH power before and after the core formation, spatial overlap of the field between the nonlinear polarization and the SH waves should be evaluated considering phase-matching condition, which might be changed due to the core formation. However, when Δn is small enough and change in the phase-matching condition is negligible, the phase-matching term can be excluded. As a result, the SH power can be written with the following relation, assuming $\chi^{(2)}=0$ at $|y| > W/2$:

$$P(\Delta n) \propto \int_{-\Delta\sigma^{2\omega}}^{\Delta\sigma^{2\omega}} \int_{-W/2}^{W/2} \left\{ \int_{-\Delta\sigma^{\omega}}^{\Delta\sigma^{\omega}} B(\sigma^{\omega}) f^{\omega}(\sigma^{\omega}; y) d\sigma^{\omega} \right\}^2 f^{2\omega}(\sigma^{2\omega}; y) dy d\sigma^{2\omega}. \quad (2)$$

$B(\sigma^{\omega})$ is the coefficient reflecting the coupling of the fundamental wave into the anti-guide. $\Delta\sigma^{\omega}$ corresponds to the divergence of the focused fundamental wave and can be described as $\sim 4/W$ for the Gaussian case. $\Delta\sigma^{2\omega}$ represents the divergence of the generated SH wave and can be shown as $\sim 4/W$. In our experimental condition, the highest resonance peak in the spectrum is included in the integrals for both the fundamental and the SH waves to contribute to the enhancement of SHG.

Figure 3 shows the calculated SHG enhancement ratio $G(\Delta n)$. The result for the polymer well explains the measured value, $G(10^{-5}) \sim 7$. When the reduction of the nonlinearity is excluded, as in PR crystals, the enhancement of more than 100 times can be obtained with $\Delta n \sim 5 \times 10^{-5}$.

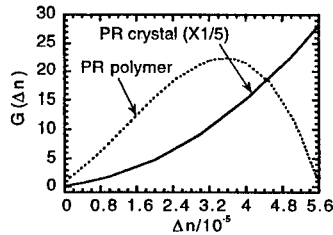


Fig. 3 SHG enhancement ratio calculated with $W=85 \mu\text{m}$.

References

- [1] S. Orlov, A. Yariv, and M. Segev, *Appl. Phys. Lett.* **68**, 1610 (1996).
- [2] S. Lan, M-f. Shih, G. Mizell, J. A. Giordmaine, Z. Chen, C. Anastassiou, J. Martin, and M. Segev, *Lett.* **24**, 1145 (1999).
- [3] T. Sassa and S. Umegaki, *J. Appl. Phys.* **84**, 4071 (1998).

Three dimensional $\chi^{(2)}$ -Analysis of High Field Poled Polymers

Robert Blum, Kersten Pfeifer, Gerrit Schoer, and Manfred Eich

Techn. Univ. Hamburg-Harburg

AB 4-09, Eissendorferstr. 38

21071 Hamburg, Germany

We present a novel method to analyze the three dimensional inhomogeneities in the spatial distribution of the electric field induced $\chi^{(2)}$ -susceptibility in poled polymer films. The $\chi^{(2)}$ distribution in two dimensions and its phase can be measured by Scanning Second Harmonic Microscopy (SSHM) and Scanning Kelvin Microscopy (SKM), respectively. By means of wavelength dependent SSHM we are also able to probe the orientational order parameter in three dimensions. We find that strong inhomogeneities are present near the electrodes.

Electric field poling of NLO polymer films at very high electric fields or with nonoptimized electrode designs can lead to $\chi^{(2)}$ distributions with poor spatial homogeneity, making such films unsuitable for optical devices [1][2]. Various techniques for measuring the two-dimensional homogeneity of the induced susceptibility in NLO films were introduced, which are based on SSHM, scanning electro-optical and pyroelectrical microscopy, and SH imaging using a charge coupled device camera. We propose a method to analyze the $\chi^{(2)}$ homogeneity in NLO polymers in three dimensions [3]. This can be accomplished by measuring the second harmonic response of the polymer film at various wavelengths. The possible resolution in depth is determined by the absorption maximum of the polymer film. For the films investigated this resolution is about 150 nm. We observe strong inhomogeneities in depth, which are most likely due to injected and trapped charges during poling. We also present the scanning Kelvin microscopy (SKM) as a method for measuring the magnitude *and the direction* of the field induced polarization in poled NLO polymer films [4].

References

- [1] M. Adameck, R. Blum, and M. Eich, "Scanning second harmonic microscopy techniques with monomode and near field optical fibers", *Appl. Phys. Lett.* **20**, 2884 (1998).
- [2] R. Blum, M. Sprave, J. Sablotny, and M. Eich, "High electric field poling of nonlinear optical polymers", *J. Opt. Soc. Am. B* **15**(1), 318-328 (1998).
- [3] R. Blum, M. Adameck, T. Elken, and M. Eich, "Analyzing the $\chi^{(2)}$ -distribution in poled polymers", *Nonlinear Optics* **22**, 19-24 (1999)
- [4] R. Blum, A. Ivankov, S. Schwantes, and M. Eich, "Analyzing the Polarization Distribution in Poled Polymer Films by Scanning Kelvin Microscopy", *Appl. Phys. Lett.*, accepted (1999)

Poster Session I

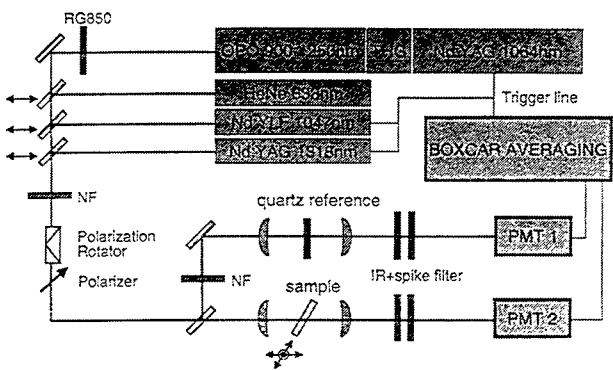


Figure 1: Experimental setup used for the multi wavelength SSHM measurements.

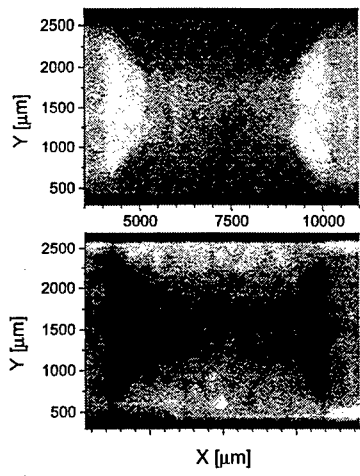


Figure 2: SSHM measurements of the front and the rear side of a 5 microns thick sample. The $1/e$ thickness for the SH wavelength was chosen to be 1 micron. Complementary distributions are observed.

Polymer based electro-optic inline fiber modulator with 1 GHz bandwidth

M. Bösch, I. Liakatas, C. Cai, Ch. Bosshard, and P. Günter
Nonlinear Optics Laboratory
Swiss Federal Institute of Technology
CH-8093 Zürich, Switzerland

Poled organic polymer films show great promise for use in integrated photonic devices such as amplitude or phase modulators for telecommunication. We use these polymers in a novel, low loss electro-optic inline fiber modulator. The modulator consists of a fiber half coupler, i.e. a curved fiber which is incorporated into a glass block and polished down close to the core. The light in the fiber can evanescently couple into the polymer overlay depending on the effective refractive index matching between polymer and fiber core which can be modulated through the electro-optical effect. Preliminary results of our first inline fiber modulators indicate a bandwidth of 1 GHz.

The use of active and passive inline fiber optic components has recently gained a lot of interest [1-3] due to the low optical losses involved and the simplicity in design. Especially the combination of inline components with polymers is very attractive, bringing together the high bandwidth of organic materials (> 100 GHz) with the cost effectiveness of polymers. Generally inline components based on fiber half couplers consist of an optical single mode fiber epoxied into the arcing groove a glass block (Fig. 1).

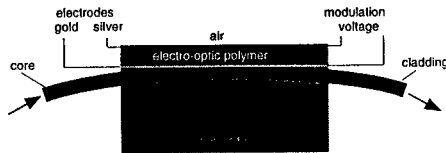


Figure 1: Schematic drawing of inline fiber modulator.

The block containing the fiber is polished until the cladding is partially removed and access to the evanescent field can be achieved through the residual cladding. An overlay, e.g. a polymer film, deposited onto the coupler causes light to couple from the fiber into the overlay provided that the following coupling requirement is fulfilled [4]

$$2 d (n_o^2 - n_{ef}^2)^{1/2} = m \lambda_0 + 2 \frac{\lambda_0}{\pi} \arctan \zeta \left(\frac{n_{eo}^2 - n_c^2}{n_o^2 - n_{eo}^2} \right)^{1/2}$$

where d is the overlay thickness, n_o the overlay refractive index, n_{eo} the mode effective index, n_{ef} the effective index of the fiber, n_c the index of the fiber cladding, λ_0 the input wavelength, m the order of the excited mode in the overlay, $\zeta = 1$ for TE and $\zeta = (n_o/n_c)^2$ for TM polarized light. By changing the refractive index of the polymer overlay due to the electro-optic effect the coupling condition is modified and the intensity passing the half coupler can be modulated. The fiber half couplers on which the modulators are based were fabricated in-house. This allows more control over the optimization of design parameters, such as the radius of curvature of the groove in the glass block and consequently the interaction length (exposed region of the fiber core). Furthermore, the use of a Corning

Poster Session I

SMF-28 fiber (single mode from 1260 - 1600 nm) allows access to both telecommunication windows as opposed to commercial half couplers.

As polymer material we used a guest-host system of highly nonlinear bithiophene chromophores [5] and polymethylmethacrylate. The chromophore concentration was 20 % by weight and the poling field of 120 V/ μm yields an electro-optic coefficient of 15 pm/V.

Deposition of the polymer layer onto the half coupler was achieved both, using direct spin coating and, alternatively, employing the free floating technique (decal deposition). In any case, the semitransparent bottom electrode has to be deposited onto the coupler previously. The top electrode was structured to allow a traveling wave configuration as well as a 50 Ω termination. The measured electric bandwidth of 1 GHz will be further improved if an impedance matched microstrip electrode design is employed.

Fig. 2 shows the transmission spectrum of the inline fiber device in the wavelength range between 1250 and 1350 nm. The dip in transmission is due to coupling into the polymer overlay. The coupling wavelength shifts by 26 nm if a voltage of 200 V is applied. The relatively large switching voltage is less critical since the intended application of inline fiber modulators is mainly for analog modulation. Here, however, these devices offer a very good linearity (superior to those of Mach-Zehnder modulators) and good power handling [2].

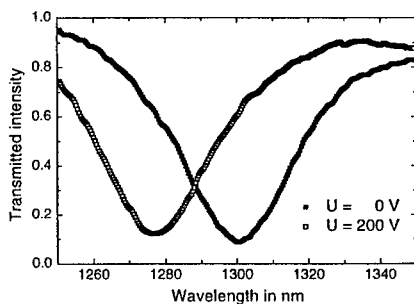


Figure 2: Transmission with and without applied voltage.

Further optimization to reduce the half-wave voltage and increase the modulation efficiency as well as the modulation bandwidth is currently in progress.

References

- [1] J. McCallion and M. Shimazu, *Optoelectronics World*, Sep 1998
- [2] S. A. Hamilton, D. R. Yankelevich, A. Knoesen, R. T. Weverka, R. A. Hill, G. C. Bjorklund, *J. Opt. Soc. Am. B* **15**, 740 (1998)
- [3] M. Bösch, I. Liakatas, M. Jäger, Ch. Bosshard and P. Günter, *Ferroelectrics*, **223**, 405-412 (1999).
- [4] C. A. Millar, M. C. Brierley, S. R. Mallinson, *Opt. Lett.* **12**, 284 (1987)
- [5] C. Cai, I. Liakatas, M-S. Wong, M. Bösch, Ch. Bosshard, P. Günter, S. Concilio, N. Tirelli, and U. Suter, *Org. Lett.* **1**, 1847 (1999)

Photostability of highly nonlinear chromophores for electro-optic applications

M. Bösch, C. Fischer, C. Cai, I. Liakatas, Ch. Bosshard, and P. Günter
*Nonlinear Optics Laboratory
Swiss Federal Institute of Technology
CH-8093 Zürich, Switzerland*

The photochemical stability of highly nonlinear optical bithiophene chromophores is investigated. Experiments in guest-host systems were performed in different atmospheres at visible and infrared wavelengths indicating that these chromophores are excellent candidates for electro-optic applications. Lifetime estimations of electro-optic devices using these chromophores will be presented.

As nonlinear optical polymeric materials begin to enter the market in e.g. electro-optic modulators, stability issues become more and more important. Whereas the orientational stability of poled polymer systems has been studied extensively over the last decade, the photochemical stability of the chromophore dopants in the polymers under working conditions has not been investigated until recently [1]. These measurements revealed that estimated device lifetimes are not yet suitable for practical applications. Therefore chromophores with high nonlinearities and sufficient photochemical stability have to be identified.

In our group we synthesized a group of different phenyl-bithiophene chromophores with different donors and acceptors [2]. Here we report on the photochemical stability of CC172, a molecule based on the phenylbithiophene bridge and a tricyano acceptor, which exhibits excellent microscopic nonlinear optical properties [2]. We determined B/σ , i.e. the inverse photodegradation quantum efficiency B (average number of photons that a molecule absorbs before decomposition) over the absorption cross section σ for the incoming photons, which is the main figure of merit to describe photochemical stability based on one photon processes. Our measurement setup uses different laser sources allowing investigations at wavelengths from 458 nm up to 1552 nm. For probing we use a He-Ne laser operating at 633 nm which is very close to the main absorption peak of CC172. A silicon detector monitors the transmission change of the probe laser as a function of the pump laser photon fluence.

The measurements were performed at different atmospheres (oxygen, air, nitrogen) to study environmental effects on the photodegradation. For data evaluation and calculation of B/σ , we used the model developed by Dubois et al. [3] based on a one photon absorption process. In this model, the dependence of the light transmission $T(E)$ on the pump energy per unit area E is given by

$$T(E) = \frac{T(\infty)}{1 + \left(\frac{T(\infty)}{T(0)} - 1\right) e^{-\frac{E}{h\nu} \frac{\sigma}{B}}}$$

where $T(0)$ and $T(\infty)$ are initial and final transmission, respectively, h is Planck's constant, ν is the frequency of the bleaching beam, and σ is the absorption cross section at the bleaching wavelength.

As can be seen from the figure the change in photochemical stability when using nitrogen instead of oxygen atmosphere is roughly one order of magnitude over the whole

Poster Session I

wavelength range. Furthermore the stability increases by four orders of magnitude when changing the wavelength from the main absorption peak towards telecommunication wavelengths. The photochemical stability is expected to be even higher at 1.5 μm compared to 1.3 μm due to the smaller two photon absorption.

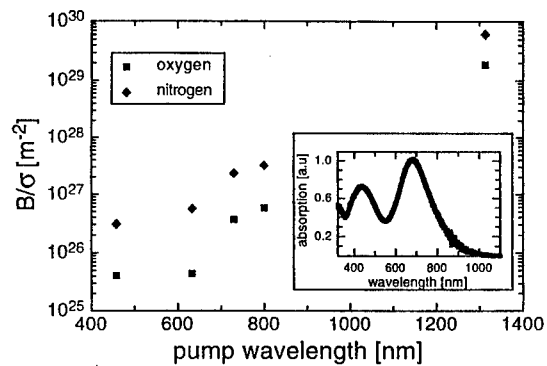


Figure of merit for the photochemical stability for the molecule CC172 measured at different wavelengths and atmospheres. The inset shows the absorption spectrum of the molecule in PMMA.

References

- [1] A. Galvan-Gonzales, M. Canva, G. Stegeman, R. Twieg, T. Kowalczyk, and H. Lackritz, *Opt. Lett.* **24**, 1747 (1999)
- [2] C. Cai, I. Liakatas, M-S. Wong, M. Bösch, Ch. Bosshard, P. Günter, S. Concilio, N. Tirelli, and U. Suter, *Org. Lett.* **1**, 1847 (1999)
- [3] A. Dubois, M. Canva, A. Brun, F. Chaput, J.P. Boilot, *Appl. Opt.* **35**, 3193 (1996)

Towards stable hybrid materials for electro-optic modulation and photorefractive applications

F. Chaput, K. Lahlil, J.-P. Boilot

Laboratoire de Physique de la Matière Condensée (UMR CNRS 7643D), Ecole Polytechnique
91128 Palaiseau, France

M. Mladenova, L. Ventelon, M. Blanchard-Desce

Département de Chimie, Ecole Normale Supérieure (UMR CNRS 8640)
24, rue Lhomond, 75231 Paris Cedex 05, France

B. Darracq, J. Reyes, Y. Levy

Laboratoire Charles Fabry de l'Institut d'Optique (UMR CNRS 8501)
Bâtiment 503, B.P. 147, 91403 Orsay Cedex, France

We have developed new *hybrid organic-inorganic materials* based on the incorporation of push-pull chromophores in an amorphous inorganic matrix. Functionalized thin films have been prepared using the *sol-gel* route allowing for mild synthesis conditions. Orientation of the dipolar chromophores was performed using the Corona or contact electrodes techniques. By combining both optimized chromophores and photoconductors grafted on the matrix, poled thin films with large electro-optical coefficients (up to 53 pm/V) and photoconductive properties have been designed.

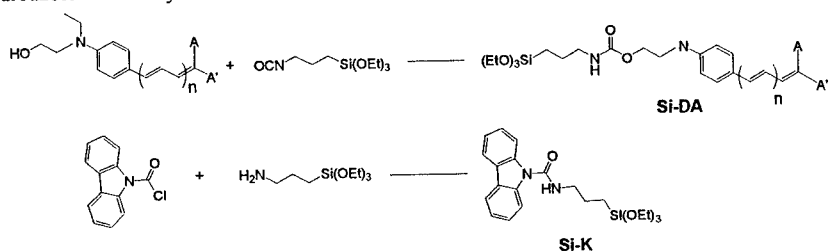
A large effort have been devoted to the preparation of organic polymeric materials for electro-optic modulation. These materials contain push-pull chromophores, either incorporated as guests (doped polymers) or grafted onto (or into) the polymeric matrix (functionalized polymers). These dipolar chromophores can be orientated by application of a strong external electric field while heating above the glass transition temperature (T_g) of the polymer. After cooling to room temperature, noncentrosymmetrical poled-polymeric materials are obtained. Such materials are interesting in view of both their processability and their chemical flexibility. In particular, chromophores having a large figure of merit $\mu\beta$, (where μ is the dipole moment and β the quadratic polarizability), can in principle lead to materials with a large electro-optic coefficient. Issues such as dipolar interactions between chromophores and orientational stability of the polar order have to be considered if materials with both large and permanent nonlinear responses are wanted.

We have implemented the *sol-gel* approach for the design of stable *organic-inorganic hybrid materials* exhibiting large electro-optic coefficients. In order to elaborate materials with excellent nonlinearities and good orientational stability, we have synthesized *sol-gel* systems wherein push-pull chromophores combining large $\mu\beta$ values and suitable thermal stability are covalently attached to the rigid backbone of a silica-based matrix also containing carbazole units grafted as pendant side groups. These moieties could both act as charge-carriers and screen dipolar interactions.

Based on previous work on push-pull polyenes, we have used the push-pull functionalization of the polyenic backbone to engineer very large molecular nonlinearities [1]. We have selected phenylpolyenes or diphenylpolyenes of middle length [1, 2], in order to ensure enhanced $\mu\beta$ values and maintain suitable thermal stability, solubility and poling ability. We have synthesized derivatives bearing terminal hydroxyl groups [3]. By reacting these chromophores with 3-isocyanatopropyltriethoxysilane (ICPTEOS), push-pull molecular

Poster Session I

precursors Si-DA were then obtained. The molecular precursor Si-K was prepared by reacting carbazole-9-carbonyl chloride with 3-aminopropyltriethoxysilane (APTES) :



Coating solutions were prepared by copolymerisation of the functionalized triethoxysilane monomers with the tetraethoxysilane (TEOS) cross-linking agent. The TEOS/(Si-K + Si-DA) ratio was adjusted to 1/6 and Si-K/Si-DA ratios were modulated in order to control the dipolar interactions in the material [4]. Films of several micrometers in thickness were elaborated by spin-coating then cured for 12-24 h at 100-160 °C. Orientation of the push-pull chromophores within the material was performed using either the single-point corona or the contact electrodes poling technique. Electro-optic coefficients r_{33} measurements were carried-out at 830 nm using a reflection method.

Experimental investigation of the linear and nonlinear properties of the hybrid films made from different chromophores and with varying Si-DA/Si-K ratio provides evidence that intermolecular interactions play a significant role in determining the nonlinear optical responses of the sol-gel materials. The bare molecular μ and β values are not sufficient to account for the macroscopic nonlinearities.

Ultimately, by combining a molecular engineering approach towards large nonlinearity-stability characteristics with a strategy aiming at controlling the intermolecular interactions, we have designed *hybrid thin-films with very large electro-optic coefficients* (up to 53 pm.V^{-1}).

Photoconductivity experiments provide indication of the existence of a strong internal electric field in the poled sol-gel materials [5-6]. This is of special interest since combination of photoconductivity and large electro-optic coefficients hold promise for the design of stable hybrid materials exhibiting *photorefractivity* without externally-applied electric field.

References

- [1] V. Alain, S. Rédoglia, M. Blanchard-Desce, S. Lebus, K. Lukaszuk, R. Wortmann, U. Gubler, C. Bosshard, P. Günter, *Chem. Phys.*, **245**, 51-71 (1999) and references cited therein.
- [2] V. Alain, L. Thouin, M. Blanchard-Desce, U. Gubler, C. Bosshard, P. Günter, J. Müller, A. Fort, M. Barzoukas, *Adv. Mater.*, **11**, 1210-1214 (1999).
- [3] M. Mladenova, L. Ventelon, M. Blanchard-Desce, *Tetrahedron Lett.*, **40**, 6923-6926 (1999).
- [4] A. W. Harper, S. Sun, L. Dalton, S. M. Garner, A. Chen, S. Kannuri, W. H. Steier, B. H. Robinson, *J. Opt. Soc. Am. B*, **15**, 329-337 (1998).
- [5] B. Darracq, F. Chaput, K. Lahlil, J. -P. Boilot, Y. Levy, V. Alain, L. Ventelon, M. Blanchard-Desce, *Optical Materials*, **9**, 265-270, (1998).
- [6] L. Ventelon, M. Mladenova, V. Alain, M. Blanchard-Desce, F. Chaput, K. Lahlil, J.- P. Boilot, B. Darracq, J. Reyes, Y. Levy, *Proc. SPIE*, **3623**, 184-193 (1999).

POLARIZATION-INSENSITIVE POLYMER AMPLITUDE MODULATOR

A. Donval, E. Toussaere, R. Hierle and J. Zyss

Ecole Normale Supérieure de Cachan, Laboratoire de Photonique Quantique Moléculaire (UMR CNRS # 8537), 61 av. du président Wilson, 94235 CACHAN, FRANCE.

Polarization insensitivity is a crucial pre-requisite towards insertion of electrooptic waveguiding devices in optical telecommunication systems. The inherent flexibility of polymers allows to monitor different polar axis directions according to the poling geometry. We propose a novel Mach-Zehnder devices based on monolithic integration within one arm of balanced in- and out- of plane poled electrooptic sub-units. Optimization issues related to the electrode configuration, the nature of the cladding layers and the overlap between both poling and modulating field distributions with the waveguide cross-section have been addressed. The design procedure including modelling, fabrication steps and performances, of the two integrated sub-units in the polarization-insensitive polymer device will be also reported.

We address here the issue of polarization insensitive modulators with built-in ability to process random polarization states as a result of uncontrollable statistical perturbations along a fiber communication system. Control of the polarization polymer based devices can be reached by setting the orientation of their polar optical axis by adequate design of the poling electrodes [1,2]. We propose and demonstrate a new configuration for an EO polymer amplitude modulator in an original integrated optics format based on monolithic integration, within a single Mach-Zehnder (MZ) interferometer structure, of a sandwich (SN) electrode phase modulator (PM) together with a transverse (TR) electrode PM, so as to ensure polarization insensitivity.

In polymer waveguide devices the poling as well as the modulation fields are distributed over the entire cross-section of the three stack multilayer device, including the lower and upper buffers as well as the guiding core. It is furthermore crucial to concentrate both DC (static) and high frequency (dynamic) electric field distributions mainly within the active layer portion of the stack so as to optimize both poling and modulation efficiencies. We purposely designed a new double transverse electrode configuration (DT) (see Fig.1) in order to improve the field distribution within the active layer made of 30% molar DR1 grafted PMMA. We then compared the results of finite element calculation [3] of the dynamic and static electric field distributions for a simple single bottom electrode configuration (SBT) (see Fig.1) with the new DT structure. Addition of the upper transverse electrodes has consequently enhanced the static (dynamic) dimensionless field distribution from 0.36 (0.64) to 0.93 (0.91).



Fig.1 Transverse structures: a. single bottom transverse electrodes (SBT). b. double transverse electrodes (DT)

The polarization insensitive amplitude modulator results from monolithic integration of a SBT phase modulator with the subsequent SN configuration (Fig.2). The transverse (resp. sandwich) electrodes being 1 (resp. 0.5) cm long with a gap of 11 (resp. 5.3) μm . The half-wave voltage of the full device is measured as a function of the parameter $\alpha = V_{m,TR}/V_{m,SN}$

Poster Session I

defined in [4] as the potentiometric ratio between the transverse and sandwich dynamic modulation potentials. By tuning the α ratio of the modulation potentials applied on the two SN and TR portions by an appropriate voltage division circuit, one can monitor in real time the polarization dependence and set it to satisfy polarization independence (see Fig.2). The average half wave voltage of the full device has been measured to be $70V \pm 11\%$ with an α parameter of 8 corresponding an expected improved efficiency by a factor of 8 for the SN portion as compared to the TR portion.

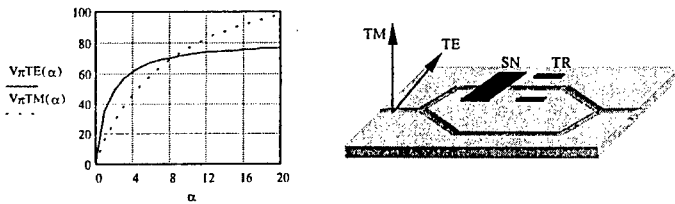


Fig.2 Balanced combinations of transverse and sandwich electrode configurations, reached for $\alpha=8$, result in equalized TE/TM (left) polarization efficiencies

Further work is in progress to lower V_{π} based on a push-pull double-arm version of the single-arm device and the use of improved EO polymer.

-
- [1] T.Gase, A.Bräuer and W.Karthe, ECI'95 Proceedings, 7th European Conference on Integrated Optics with Technique Exhibition 85 (1995)
 - [2] J.J.Kim, W.Y.Hwang, M.C.Oh and S.Y.Shin, SPIE 2527, 397 (1995)
 - [3] DENEb a static electric field distribution program developed at CNET - France Telecom.
 - [4] A.Donval, E.Toussaere, R.Hierle and J.Zyss, to be published in the Journal of Appl. Phys

**Doped planar and channel sol-gel waveguides
for nonlinear devices operating at telecommunication wavelengths**

Anne-Claire Le Duff, Michael Canva, Yves Lévy and Alain Brun

*Laboratoire Charles Fabry de l'Institut d'Optique, CNRS-UMR 8501, IOTA
Université d'Orsay-Paris XI, Orsay, France*

Frédéric Chaput and Jean-Pierre Boilot

*Laboratoire de Physique de la Matière Condensée, CNRS-UMR 7643,
École Polytechnique, Palaiseau, France*

Tomas Pliska and George I. Stegeman

*School of Optics / Center for Research and Education in Optics and Lasers (CREOL),
University of Central Florida, Orlando, FL 32816-2700, USA*

Thin films of DR1-doped sol-gel material were investigated to design multi-layer waveguide structures for second-harmonic generation at 1.55 μm . Optical propagation loss measurements were performed between 0.70 μm and 1.65 μm .

Photobleached channel waveguides were formed and a good lateral confinement of the light was observed.

Organic molecules exhibit large optical nonlinearities and are attractive for electro-optics, frequency conversion... In the past years, doped all-organic polymers proved to be attractive materials to achieve nonlinear integrated optical components. On the other hand, hybrid organic-inorganic sol-gels are exciting alternative systems for applications.

We report on material characterization, thin film deposition process and channel waveguides fabrication. The system under investigation here is a Disperse Red 1 doped hybrid organic-inorganic silica based sol-gel.

Sol-gel process was used to prepare hybrid thin films incorporating both push-pull chromophores (DR1 molecules) and carbazole units covalently attached to the rigid backbone of the silica-based matrix (SiK/DR1/TEOS). Appropriate functionalized triethoxysilane monomers were copolymerized with the tetraethoxysilane (TEOS) cross-linking agent in a mutual cosolvent¹. Thin films (0.2-3 μm) were then spin-coated and cured for 12 h at 120°C.

The absorption spectrum of a SiK/DR1/TEOS film is shown on Figure 1 (plain line). In the red tail of the absorption peak where transmission spectroscopy through a thin film does not provide enough resolution, we used a straight-line approximation (dash line), as suggested by first order development of a Voigt profile^{2,3}. In the 0.70-1.65 μm range, we measured the optical propagation losses in 2.5 μm thick SiK/DR1/TEOS slab waveguides spincoated on oxidized silicon wafers (rotation speed: 1500 rpm). The incoming light was coupled in the waveguide either with a high refractive index prism or with an end-fire coupling set-up. The scattered streak was then imaged on a CCD camera and further analyzed. The results of the measurements are shown in Figure 1 (up triangle symbol). They provide an upper limit of the absorption coefficients. They are comparable to absorption coefficients for common side-chain polymers. For example, at 0.78 μm , the absorption coefficient is $\alpha = 1 \pm 0.3 \text{ cm}^{-1}$.

The remaining losses around 1.55 μm ($1-1.5 \text{ cm}^{-1}$) could be related to the scattering at the upper interface (film-air or film-cladding layer). In order to optimize the general quality of the waveguides, we performed a systematic study of the films' surface roughness and optical propagation losses as a function of the spin coating conditions. The surface roughness was measured with a ZYGO heterodyne profilometer. Those experiments proved that a

Poster Session I

compromise must be found in the viscosity - rotation speed parameters couple and should yield a definitive spin coating procedure to fabricate low losses sol-gel waveguides.

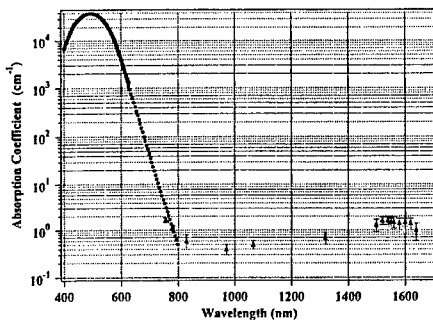


Figure 1: Absorption spectrum and propagation losses in a SiK-DR1-TEOS film.

Traditionally, ultraviolet photobleaching has been the technique of choice for fabricating waveguides in nonlinear all-organic polymers. We used this method with our cross-linked sol-gel material. A good confinement of the light was observed after 3 hours exposure through a mask using a 20 mW/cm² broadband UV lamp centered around 420 nm. A picture of a 1.064 μ m beam coupled out of a 2 μ m x 5 μ m waveguide is shown on Figure 2.



Figure 2: Outcoupled 1064 nm beam of a 5 μ m wide photobleached waveguide. Scattered light is guided in the bleached layer on both sides of the channel waveguide.

With the prospective use of chromophores with enhanced photostability, alternative channel waveguide fabrication techniques are required and a plasma etching process is currently under development.

References

- ¹ F. Chaput, D. Riehl, J.P. Boilot, T. Gacoin, M. Canva, Y. Lévy and A. Brun "Photorefractive sol-gel materials", Better Ceramics Through Chemistry VII, Mat. Res. Soc. Symp. Proc., **435**, 583-588 (1996).
- ² A. Otomo, M. Jäger, G. Stegeman, M. Flipse and M. Diemeer, "Key trade-offs for SHG in poled polymers", Appl. Phys. Lett. **69**, 1991-1993 (1996).
- ³ A.-C. Le Duff, V. Ricci, T. Pliska, M. Canva, G. Stegeman, K. P. Chan and R. Twieg, "The importance of chromophore environment on the near infrared absorption of polymeric waveguides", Applied Optics, in press, (1999).

Second Harmonic Generation in a Photobleached PU1-C4B Film Channel Waveguides

Suguru Horinouchi^{****}, Kwang-Sup Lee^{**}, Je-Hyun Lee^{**},
Primoz Kerkoc^ˆ, Junichi Yoshida^ˆ and Keisuke Sasaki^ˆ

^{*}TAO (Telecommunications Advancement Organization of Japan) Chitose Photonics
Research Center, Chitose-Shimin-Gallery 4F, 5-7-1 Chiyoda-cho, Chitose-shi,
Hokkaido 066-0062 JAPAN

^{**}Department of Polymer Science & Engineering, Hannam University, Taejeon, KOREA

(Tel & Fax) +81-123-27-6090

(Email) THSNhori@aol.com

Many interests have been paid to potential applications of organic materials for the future photonics devices. Organic materials have a lot of advantages; fast operation, easy fabrication process, low cost and so on.

In this study channel waveguide of PU1-C4B film was fabricated via photo-bleaching process and phase matched second harmonic generation (SHG) at 415nm was observed in the waveguide.

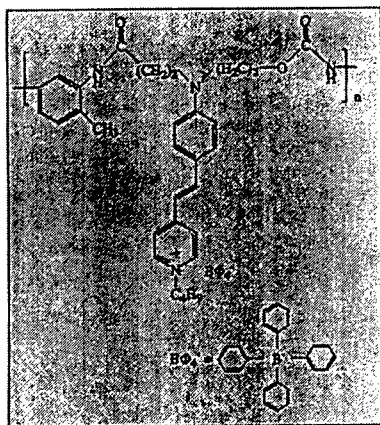


Fig.1 Molecular structure of PU1-C4B

Permanent Address of the first author^{****}
(Affiliation) Chitose Institute of Science and Technology
(Address) 758-65 Bibi, Chitose-shi, Hokkaido 066-8655 JAPAN

Poster Session I

A molecular structure is shown in Fig.1. PU1-C4B film was spin-coated on a Pyrex glass substrate and He-Cd laser operating at 442nm was irradiated on the film.

This process lowered the absorption at 490 nm and the refractive index of the PU1-C4B film. This result is shown in Fig.2 and Fig.3. When He-Cd laser with 9 kJ/cm² was irradiated, the refractive index change of 0.1 was observed.

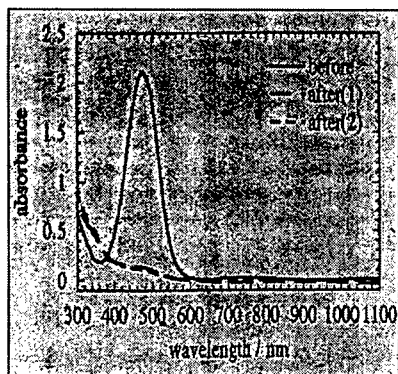


Fig.2 The relation between the absorbance of the film and the wavelength. Before, after(1) and after(2) indicate the film before the irradiation, irradiation of 15 minutes and irradiation of 30 minutes respectively

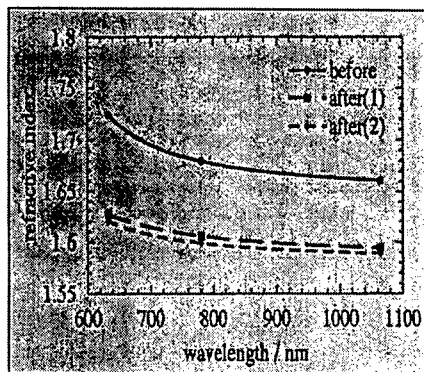


Fig.3 The relation between the refractive index of the film and the wavelength. Before after(1) and after(2) indicate the film before the irradiation, irradiation of 15 minutes and irradiation of 30 minutes respectively

Cerenkov-type phase-matched second harmonic generation at 415 nm was observed in the slab, channel(1)(50 μ m width) and channel(20 μ m width) PU1-C4B film waveguide respectively. Better conversion efficiency was achieved the channel waveguide with narrower width. In this study it was shown that this photo-bleaching process had advantages of precise index control of nonlinear optical polymers, versatile applicability, simple and low cost process.

New SCLCPs Based on 3,3'-Bipyridine Chromophores for Applications in NLO.

N. Lemaître, A.-J. Attias

Office National d'Etudes et de Recherches Aéronautiques
29 Avenue de la Division Leclerc
F- 92322 Châtillon Cedex, France

I. Ledoux, J. Zyss

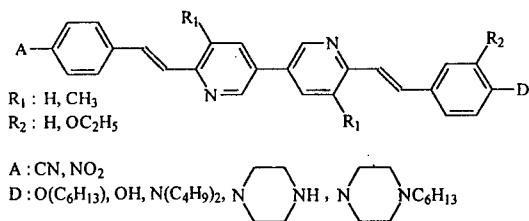
ENS Cachan, LPQM
61 Avenue du Président Wilson
F-94235 Cachan, France

We report on the synthesis, and mesogenic as well NLO properties of a new series of push-pull molecules based on 3,3'-bipyridine. These chromophores have been grafted on polyepichlorohydrine to give SCLCPs that have been characterized.

Progress in telecommunications, optical information processing and data storage aroused the interest in optoelectronic compounds. In quadratic nonlinear optics field, inorganic crystals were traditionally used but have shown their limitations due to their low response time. So studies have been carried out to realize organic materials with highly polarizable electron systems. Among such materials, polymers in particular, allow the preparation of thin films with good optical qualities and good mechanical properties. Moreover, it has been shown recently that the axial order present in side-chain liquid crystal polymers (SCLCPs) can be used to enhance field-induced polar ordering of the films, therefore improving the efficiency of these materials [1].

The present work deals with the synthesis and characterization of mesogenic chromophores, efficient in nonlinear optics, and of their corresponding side-chain polymers.

The new class of chromophores presented were synthesized from 6,6'-dimethyl-3,3'-bipyridine and 5,5',6,6'-tetramethyl-3,3'-bipyridine by Knoevenagel condensation under acid conditions [2]. They have the following formula :



Their liquid crystal character has been determined with DSC, RX, and optical microscopy technics. The second-order nonlinear optical properties of these *push-pull* molecules have been characterized with EFISH measurements. The influence of the nature of attractive or donating groups and of the lateral substituent of the bipyridine core on NLO and mesogenic properties of chromophores have been studied.

Poster Session I

The active molecules have then been grafted with different substituent rates on polyepichlorhydrine. Two series of side-chain polymers, one liquid crystal and the other not, have been obtained. Their comparative study will allow exhibiting the influence of the liquid crystal character of the material on its NLO response.

References

[1] B. Guichard, C. Noël, D. Reyx, F. Kajzar, *Macromol. Chem. Phys.* **197**, 2185-99 (1996).

[2] A. -J. Attias, B. Bloch, C. Cavalli, N. Guillou, C. Noël, *Chem. Mater.* **11**, 2057-68 (1999)

Photobleaching mechanism studies of side-chain polyimides

I. Liakatas, M. Jäger, Ch. Bosshard, and P. Günter
Nonlinear Optics Laboratory
Swiss Federal Institute of Technology
CH-8093 Zürich, Switzerland

T. Kaino
Institute for Chemical Reaction Science
Tohoku University
2-1-1 Katahira, Sendai, 980-8577 Japan

The effect of ultra-violet illumination on the absorption spectrum, the refractive index, and the scattering losses of side-chain polyimides is investigated. The photobleaching mechanism is monitored through visible and infrared absorption spectra and the transition rates between the involved molecular states are derived using a simple model.

We investigate the effect of ultraviolet illumination on the visible and infrared absorption, on the refractive index, and on the scattering losses of the side-chain polyimide A-95.11 [1] (Fig. 1) used for electro-optic applications. Furthermore, we use the UV-Vis absorption spectrum to monitor the evolution of the *trans* and the *cis* state under UV illumination. By using a simple model which takes into account three molecular states (*trans*, *cis*, and *stable*) we determine the value of both *trans* \rightarrow *cis* and *cis* \rightarrow *stable* transition rates, and material parameters such as the ratio of the molecular absorptivities of the *trans* and the *cis* states.

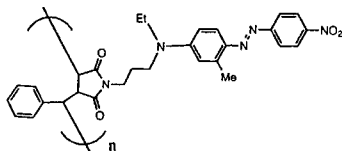


Figure 1: Chemical structure of the A-95.11 polyimide.

The TE and TM refractive indices were measured at $\lambda=1552$ nm in-situ during unpolarized UV illumination with a mercury lamp and using the grating coupling technique. Scattering loss measurements were performed using the prism coupling method at $\lambda=1313$ nm by imaging the light scattered from a planar waveguide before and after illumination. The experimental results will be presented and discussed.

A thin film (60nm) of polyimide A-95.11 has been illuminated for 190 min with a mercury lamp ($I = 117$ mW/cm²) and its spectrum was recorded at several time intervals. The spectrum changes significantly during illumination, as shown in Fig. 2a. We attribute the peak at 497 nm to the *trans* isomer of the molecules which is the dominant one for unbleached films. The peak arising at 377 nm is attributed to the *cis* isomer whereas the absorption at the deep UV wavelengths should arise from shorter or non-conjugated species which are in a photostable state. The FT-IR spectra of bleached and unbleached

Poster Session I

thin films were measured and the absorbance of the N=N peak at 1600 cm^{-1} and the NO_2 peak at 1336 cm^{-1} was determined. We observed that photobleaching has a larger influence on NO_2 than on the N=N bond. This result gives an indication that the *stable* state of the molecules may be the one where the nitro group is missing.

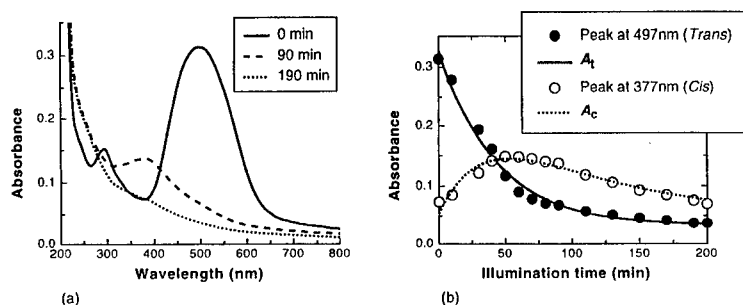


Figure 2: (a) Absorption spectrum of the unbleached (0 min), partially bleached (90 min) and totally bleached (190 min) polyimide A-95.11 thin film. (b) Absorbance of the *trans* (filled circles) and the *cis* (open circles) peaks of the same sample. The full and dotted lines are the theoretical curves using a three-state model.

To check the validity of our assumption that the photobleaching process involves three different molecular states (*trans*, *cis* and *stable*) which contribute independently to the absorption spectrum and in order to gain qualitative insight to this process we developed a three states model which allows the simulation of the time evolution of the wavelength of maximum absorption of each state and the determination of the involved transition rates.

We assume that all molecules are initially at the *trans* state and that, when illuminated, they go to the *cis* state and from there to a *stable* state. A *cis* \rightarrow *trans* transition is not considered, as no relaxation of the *trans* peak is observed even after heating the samples. We also assume that no direct transition from the *trans* to the *stable* state is possible. By solving the set of differential equations for the population of each state, relating the solutions to the relevant absorbance of each state and assuming that light intensity is constant in the material (valid for thin films) we derive equations which express the peak absorbance of the *trans* and *cis* state, respectively, as a function of illumination time. Fig. 2b shows the evolution of the *trans* and *cis* absorption peaks as a function of illumination time and the theoretical curves predicted by our model. In this way, the *trans* \rightarrow *cis* and *cis* \rightarrow *stable* transition rates could be determined.

We thank Dr. Tomaru at the NTT Opto-electronics Laboratories for performing the losses measurements and Mr. Tomoaki Shibata at the Tohoku University for his help with the FT-IR measurements. Financial support by the ETH research council, the Tohoku University and the Swiss-Asia Foundation is gratefully acknowledged.

References

- [1] P. Prêtre, U. Meier, U. Stadler, Ch. Bosshard, P. Günter, P. Kaatz, C. Weder, P. Neuenschwander, U. W. Suter, *Macromolecules* **31**, 1947 (1998).

Measurement of Relative Electrical Resistivities for Optimized Poling of Nonlinear-Optical Polymeric Waveguides

Tomas Pliska*, Vincent Ricci, Joachim Meier, Arne Eckau**, Anne-Claire Le Duff***, Michael Canva***, and George I. Stegeman

*School of Optics / Center for Research and Education in Optics and Lasers,
University of Central Florida,
P.O. Box 162 700, 4000 Central Florida Blvd., Orlando, FL 32816-2700, USA*

** present address: JDS Uniphase AG, Binzstr. 17, 8045 Zürich, Switzerland,
tomas.pliska@ch.jdsunph.com*

*** permanent address: Institut für Schicht- und Ionentechnik ISI-2,
Forschungszentrum Jülich, 52425 Jülich, Germany*

**** permanent address: Laboratoire Charles Fabry, Institut d'Optique Théorique et
Appliquée, Université d'Orsay / Paris-Sud, 91403 Orsay Cedex, France*

Paul Raymond and François Kajzar
*Commissariat à l'Énergie Atomique, Centre d'Études de Saclay, 91191 Gif sur Yvette Cedex,
France*

Kwok Pong Chan

*Molecular OptoElectronics Corporation (MOEC), 877 25th Street,
Watervliet, NY 12189-1903, USA*

Maker fringe measurements of nonlinear-optical coefficients were performed on double-layer samples composed of one nonlinear and one linear (cladding) polymer. The measured nonlinearity allows to conclude on the effective poling field strength in the nonlinear layer. This technique can be used to identify low resistivity linear cladding materials for optimized electric field poling of nonlinear-optical polymeric waveguides. Moreover, it allows to measure the relative electrical resistivities of the investigated polymers. A series of polycarbonate, poly(methyl methacrylate), and polystyrene based polymers was studied, and their resistivity was found to span more than one order of magnitude.

Organic materials, both in single crystal and poled polymer form, can exhibit large optical nonlinearities and are thus attractive for many applications¹. Guided-wave configurations are particularly suitable for nonlinear optics because of the high optical intensity in the waveguide.

Nonlinear polymer waveguides are usually composed of several linear and nonlinear cladding and core layers, respectively. For electric field poling in the parallel plate geometry, the poling voltage is applied across all layers in the structure and will therefore divide according to their resistances. Thus, the effective poling field across the nonlinear core layer will depend on the thicknesses and relative resistivities of the materials used in the waveguide structure. High resistivity cladding layers will severely reduce the poling field in the core layer resulting in a reduction or complete loss of the optical nonlinearity.

In this work we have used a nonlinear optical method to determine relative poling efficiencies². Samples are composed of two polymer layers, one of which is a nonlinear polymer while the other one is a linear cladding polymer. A dc voltage is applied across this two-layer structure. The nonlinearity induced by the poling process is a direct measure of the effective poling field across the nonlinear layer during poling since thermodynamic

Poster Session I

considerations predict a linear dependence of the nonlinearity on the field in the low field limit³. A straightforward calculation using Ohm's law allows then to conclude from the effective poling field on the relative electrical resistivities of the linear and nonlinear polymer.

We used two different nonlinear-optical polymers, namely 4-[N-ethyl-N-(2-hydroxyethyl)amino-4'-nitroazobenzene] (disperse red 1, DR1; glass transition temperature $T_g = 131$ °C, number density of chromophores $N = 0.5 \times 10^{27} \text{ m}^{-3}$, poling temperature $T_{pol} = 120$ °C) and 4-diethylamino-1-nitrobenzyl (DANB; $T_g = 100$ °C, $N = 2.6 \times 10^{27} \text{ m}^{-3}$, $T_{pol} = 100$ °C), both covalently attached to a poly(methyl methacrylate) backbone forming a side chain polymer. Standard Maker fringe measurements at 1.58 μm fundamental wavelength were used to measure the nonlinear coefficients of poled polymer layers. First, we measured the nonlinearity of single-layer samples of these two polymers in order to calibrate the nonlinearity vs. poling field curve. Then, several combinations of these two nonlinear polymers with linear cladding polymers (polycarbonate PC, polystyrene PS, poly(methyl methacrylate) PMMA, PS-PMMA co-polymers) were investigated for their nonlinearity. The effective poling field in the two-layer samples was deduced from the comparison to the single-layer calibration curve.

Results of our measurements are listed in Table I where the relative resistivities of the linear-nonlinear polymer combinations are indicated. It is apparent that the resistivity of PMMA is about one order of magnitude smaller than that of PS. Therefore, we performed a measurement where co-polymers of PMMA and PS with varying molar ratio of the two components were used as cladding layers. The result is shown in Fig. 1, clearly indicating the decrease of resistivity with increasing PMMA content.

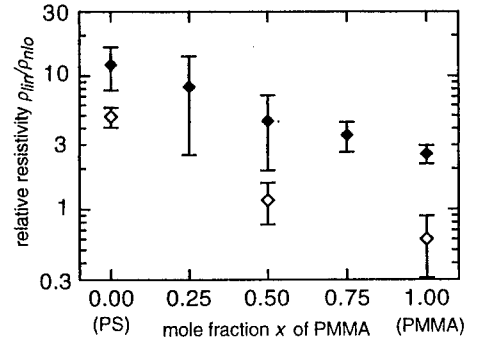
In conclusion, we have used a nonlinear-optical method to study the dc electrical properties of linear and nonlinear-optical polymers with respect to their implementation in waveguide devices. In particular, the method probes directly the effective poling field without measurement of the absolute electrical resistivity.

¹ Zyss, J., Ed., *Molecular Nonlinear Optics* (Academic Press, Inc., San Diego, CA, 1994).
² Pliska, T., Meier, J., Eckau, A., Ricci, V., Le Duff, A.-C., Canva, M., Stegeman, G.I., Raymond, P., Kajzar, F., and Chan, K.P., *Appl. Phys. Lett.*, Jan. 2000 (2000).
³ Singer, K.D., Kuzyk, M.G., and Sohn, J.E., *J. Opt. Soc. Am. B* 4 (6), 968-976 (1987).

Table I: Measured relative electrical resistivities ρ_{lin}/ρ_{nlo} of linear and nonlinear-optical polymers.

PC / DANB	0.9 ± 0.3
PMMA / DANB	2.6 ± 0.4
(PMMA) _{0.75} -(PS) _{0.25} / DANB	3.6 ± 0.9
(PMMA) _{0.5} -(PS) _{0.5} / DANB	4.6 ± 2.6
(PMMA) _{0.25} -(PS) _{0.75} / DANB	8.3 ± 5.7
PS / DANB	12.1 ± 4.3
PMMA / DR1	0.6 ± 0.3
(PMMA) _{0.5} -(PS) _{0.5} / DR1	1.2 ± 0.4
PS / DR1	4.7 ± 0.9

Fig. 1: Relative resistivity of (PMMA)_x-(PS)_{1-x} co-polymers and DANB (♦) and DR1 (◇), respectively, as a function of the PMMA mole fraction x in the co-polymer. The poling temperature was 100 °C for the DANB and 120 °C for the DR1 samples.



Second-Harmonic Generation at Telecommunication Wavelengths in Polymeric Waveguides

Tomas Pliska*, Wook-Rae Cho, Vincent Ricci, Joachim Meier, Anne-Claire Le Duff**, Michael Canva**, and George I. Stegeman

*School of Optics / Center for Research and Education in Optics and Lasers,
University of Central Florida,
P.O. Box 162 700, 4000 Central Florida Blvd., Orlando, FL 32816-2700, USA*

** present address: JDS Uniphase AG, Binzstr. 17, 8045 Zürich, Switzerland,
tomas.pliska@ch.jdsunph.com*

*** permanent address: Laboratoire Charles Fabry, Institut d'Optique Théorique et Appliquée,
Université d'Orsay / Paris-Sud, 91403 Orsay Cedex, France*

Paul Raymond and François Kajzar

*Commissariat à l'Énergie Atomique, Centre d'Études de Saclay, 91191 Gif sur Yvette Cedex,
France*

The linear and nonlinear-optical properties of 4-dimethylamino-4'-nitrostilbene (DANS), 4[N-ethyl-N-(2 hydroxyethyl)] amino-4'-nitroazobenzene (disperse red 1), and 4-diethylamino-1-nitrobenzyl (DANB) based side-chain polymers were investigated in order to design multiple-layer polymeric waveguide structures for modal-dispersion-phase-matched second-harmonic generation at 1.55 μm . Channel waveguides were formed by plasma etching and photobleaching, and second-harmonic generation in waveguides of several millimeter length was demonstrated. We will discuss material requirements, design, electric field poling, fabrication, and optical characterization of these waveguides.

Organic materials exhibit large optical nonlinearities and, hence, are attractive for parametric interactions ¹. We envision using polymers in $\chi^2:\chi^2$ -cascading based optical processes at telecommunication wavelengths.

Cascading of second-order nonlinear-optical processes has been shown to provide new possibilities for all-optical signal processing as $\chi^2:\chi^2$ -cascading can mimic third-order (Kerr-type) nonlinearities ². Because the figure-of-merit for the cascaded nonlinear phase shift is identical to the one for second-harmonic generation given by d_{eff}^2/n^3 where d_{eff} denotes the effective nonlinear-optical coefficient and n the index of refraction, devices exhibiting large second-harmonic conversion efficiencies are also candidates for cascading.

Here we report on material characterization, waveguide fabrication, and second-harmonic generation measurements using three different nonlinear side-chain polymers, namely 4-dimethylamino-4'-nitrostilbene (DANS), 4[N-ethyl-N-(2 hydroxyethyl)] amino-4'-nitroazobenzene (disperse red 1, DR1), and 4-diethylamino-1-nitrobenzyl (DANB). The absorption spectra of these three polymers are shown in Fig. 1 with fitted inhomogeneously broadened absorption profiles ³. While DANS shows a relatively high loss of 2.5 cm^{-1} at the second-harmonic wavelength, DR1 and DANB are essentially transparent at this wavelength. The nonlinear optical coefficient d_{33} , measured by the Maker fringe method at 1.58 μm , were 14.2, 7.3 and 6.8 pmV^{-1} for DANS, DR1, and DANB, respectively.

Two different methods were utilized to form channel waveguides: UV photobleaching and O_2 plasma etching. Modal-dispersion-phase-matching was shown to be a suitable scheme for efficient parametric processes in polymer waveguides ⁴. This type of phase matching, schematically displayed in Fig. 2, is based on an interaction between the lowest order mode at the fundamental wavelength and a higher order mode at the second-harmonic. Therefore,

Poster Session I

special multiple layer structures need to be devised for each material in order to avoid interference effects across the waveguide that cancel the overlap integral for second-harmonic generation (inverse effective cross section). Figure 2a shows the basic structure for the $TM_0^{\omega} \rightarrow TM_1^{2\omega}$ interaction. The core is composed of the nonlinear polymer layer and an index matched linear layer, sandwiched between low index buffer and cladding layers. Figures 2b and 2c schematically show the field profiles of the TM_0^{ω} and $TM_1^{2\omega}$ modes and the nonlinearity, respectively. When the electric field of the second-harmonic mode changes sign across the waveguide, the nonlinearity is turned off resulting in a nonvanishing overlap integral.

Test samples for second-harmonic generation were prepared for all three nonlinear polymers discussed. Normalized conversion efficiencies of $0.25 \%W^{-1}$ were obtained in samples of several millimeter length with propagation losses of a few $dBcm^{-1}$. Based on these results, we estimate for improved waveguide structures that conversion efficiencies of more than $25 \%W^{-1}$ in 1 cm long guides are attainable.

Fig. 1: Absorption spectra of DANS, DR1, and DANB, showing data obtained by transmission spectroscopy using a photospectrometer (circles) and by loss measurements in a planar waveguide (diamonds). The full lines indicate fitted inhomogeneously broadened absorption spectra.

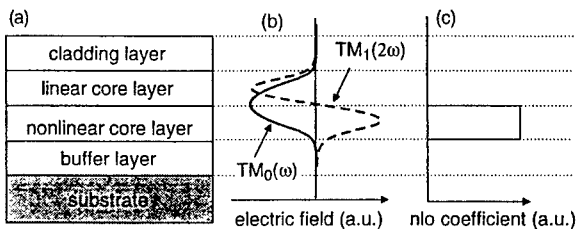
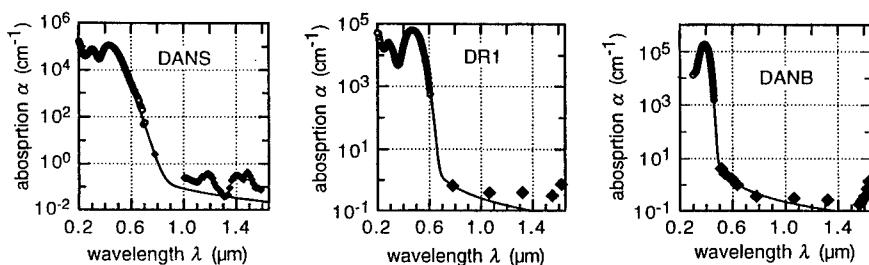


Fig. 2: (a) Basic waveguide structure for modal-dispersion-phase-matched second-harmonic generation. (b) Schematic of the optical fields for the $TM_0^{\omega} \rightarrow TM_1^{2\omega}$ interaction. (c) Schematic of the optical nonlinearity.

¹ Nalwa, H.S., and Miyata, S., Eds., *Nonlinear Optics of Organic Molecules and Polymers* (CRC Press, Boca Raton, 1997).

² Stegeman, G.I., Hagan D.J., and Torner, L., *Optical and Quantum Electronics* **28**, 1691-1740 (1996).

³ A. Otomo, Jäger M., Stegeman, G.I., Flipse, M., and Diemeer, M., *Appl. Phys. Lett.* **69** (14), 1991-1993 (1996).

⁴ Wirges, W., Yilmaz, S., Brinker, W., Bauer-Gogonea, S., Bauer, S., Jäger, M., Stegeman, G.I., Ahlheim, M., Stählin, M., Zysset, B., Lehr, F., Diemeer, M., and Flipse, M.C., *Appl. Phys. Lett.* **70** (25), 3347-3349 (1997).

Relaxation behaviour of the second-order nonlinear response of spin-coated polyphosphazenes films

¹G. Rojo, ¹G. Martín, ¹F. Agulló-López, ²G. A. Carriedo, ²F. J. García-Alonso, ²J. I. Fidalgo
¹Departamento de Física de Materiales, Universidad Autónoma de Madrid, E-28049 Madrid, Spain.
²Departamento de Química Orgánica e Inorgánica, Facultad de Química, Universidad de Oviedo, E-33071 Oviedo, Spain

The relaxation behaviour of the second-harmonic (SHG) response of 4-[(4'-nitrophenyl) azophenoxy]-doped polyphosphazene (PPZ) films with high glass-transition temperatures ($T_g \sim 150$ °C) has been investigated. The nonlinear chromophore has been incorporated into the PPZ as: i) a guest molecule (system I), ii) a side-chain group (system II) and iii) attached to a triphosphazene molecule and then dissolved in the PPZ (system III). At variance with previous work the SHG response of our three PPZ systems is very stable and has been comparatively investigated for various temperatures in the range RT-120 °C.

Introduction

Polyphosphazenes (PPZ) are inorganic-backbone polymers resulting from the repetition of the $-P=N-$ monomer unit and appear as an interesting alternative to organic polymers^[1]. Unfortunately, reported glass-transition temperatures for PPZ are quite low (< 100 °C) so that the electrooptic and SHG responses of the polymers become rapidly degraded^[2]. Recently, a new synthetic route has been developed for the preparation of highly soluble and rigid novel polyphosphazenes with high glass-transition temperatures ($T_g \geq 145$ °C)^[3].

In order to induce SHG activity the group 4-[(4'-nitrophenyl)azo] phenoxy has been incorporated into the polymer. Three strategies have been followed for the incorporation of the chromophore (Fig. 1). A comparison of the relaxation behaviour of the SHG response of the guest-host and side-chain polymers containing the same chromophore has been performed.

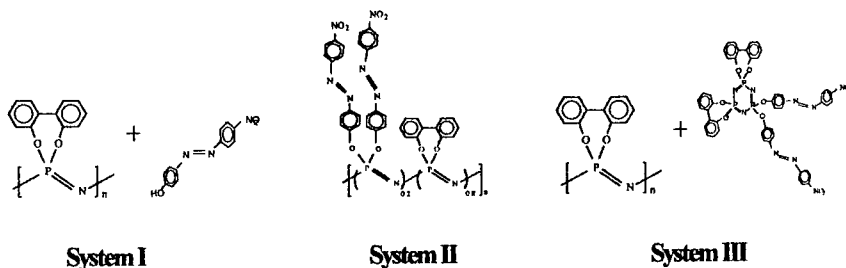


Fig. 1.- Chemical structure of the three system investigated. Systems I and III are guest-host polymers and System II is a side-chain polymer.

Poster Session I

Experimental

The glass-transition temperatures measured by DSC were as follows: $T_g \approx 144$ °C for guest-host system I, $T_g = 145$ °C for side-chain system II, and $T_g = 139$ °C for guest-host system III. On the other hand, the transition temperature for the undoped PPZ polymer was $T_g = 156$ °C.

Spin-coated films of the three systems incorporating the NLO chromophore have been prepared and then corona poled ($V_p = 9$ kV, $T_p \sim 140$ °C) to achieved the order needed for the second-harmonic generation.

Results

The three components $\chi_{11}^{(2)}$, $\chi_{31}^{(2)}$ and $\chi_{33}^{(2)}$ of the second-order nonlinear susceptibility tensor have been measured for corona poled films of our three systems^[4]. Values for $\chi_{33}^{(2)}$ are in the range $5-15 \cdot 10^{-9}$ esu.

The relaxation behaviour of the $\chi_{33}^{(2)}$ at various temperatures are shown in Fig. 2 for the three systems. At RT the second-order response decrease less than 10% for systems II and III in two months whereas for system I the diminution is 20%. It is also shown in Fig. 2 that for temperatures ≤ 105 °C system I relaxes faster than systems II and III. Curiously, guest-host system III shows a lower relaxation rate than side-chain system II (see $T = 80$ °C). However, the differences in relaxation times are relatively modest and decrease with increasing temperature. At 120 °C all systems essentially present the same relaxation behavior. The decay curves can be reasonably well fitted to a biexponential kinetics and also to an stretched exponential or Kohlrausch-Williams-Watts (KWW) law. The relevant parameters for these fittings will be given and discussed in the light of previous work on organic polymers^[5].

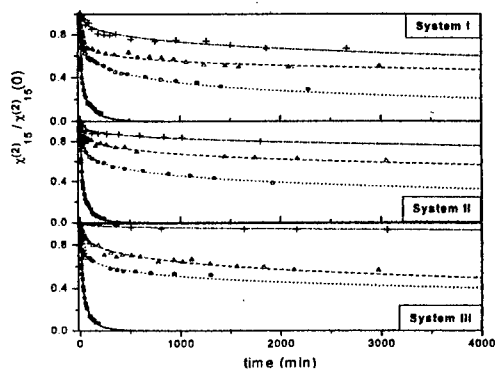


Fig. 2.- Relaxation behaviour for the three systems at different temperatures:

- (Cross): 80 °C (Dashed and dotted)
- (Triangle): 95 °C (Dashed)
- (Circle): 105 °C (Dotted)
- (Square): 120 °C (Solid)

References

- (1) Allcock, H.R., *Inorganic-Organic Polymers*, *Adv. Mater.* **6**, 106 (1994).
- (2) Allcock, H.R., Dembeck, A.A., Kim, C., Devine, R.L.S., Shi, Y., Steier, W.H., and Spangler, C.W., *Macromolecules* **24**, 1000 (1991).
- (3) Carriedo, G.A., García Alonso, F.J. and González, P.A., *Macromol. Rapid Commun.* **18**, 371 (1997).
- (4) D.M. Burland, R.D. Miller and C.A. Walsh, *Chem. Rev.* **94**, 31 (1994).
- (5) G. Rojo, F. Agulló-López, G.A. Carriedo, F.J. García Alonso and J.I. Fidalgo, *Synthet. Met.* (in press).

Synthesis and Nonlinear Optical Properties of High Glass Transition Polyimides and Poly(maleimide-styrene)s

C. Samyn and K. Van den Broeck

Laboratory of Macromolecular and Physical Organic Chemistry,
University of Leuven, Celestijnenlaan 200F, B-3001 Leuven, Belgium

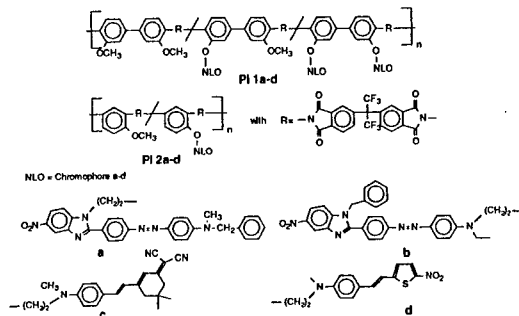
T. Verbiest and A. Persoons

Laboratory of Chemical and Biological Dynamics and Center for Research on Molecular Electronics and Photonics, University of Leuven, Celestijnenlaan 200D, B-3001 Leuven, Belgium

Nonlinear optical side-chain polyimides and poly(maleimide-styrene)s were prepared and investigated for their nonlinear optical effect. Glass transition temperatures from 207–275°C for the polyimide systems and from 178–228°C for the copolyimides were measured. Stability measurements of the Second Harmonic Generation effect (1064 nm) were achieved at 125°C. Both polymer systems showed up to 90% of remaining nonlinear optical response, which did not significantly change over 1000h of heating.

Organic nonlinear optical (NLO) polymers are of considerable interest in the development of second-order nonlinear optical materials, because of their potential applications for frequency doubling, optical storage devices, electro-optic switches and modulators [1]. Long term stability of the NLO response is a major objective in the search for new polymer materials. The common method to suppress the reorientation of the aligned chromophores is to synthesize polymers exhibiting high glass transition (T_g) temperatures [2].

Polyimides show excellent thermal stabilities combined with good (nonlinear) optical properties, they were prepared by covalent binding of a chromophore (a-d) onto the polymer backbone of hydroxyl polyimide precursor polymers.

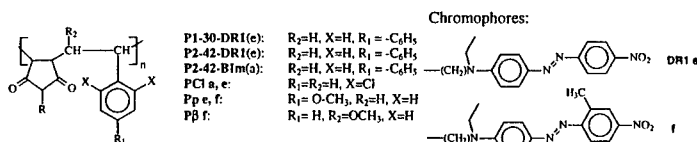


Glass transition temperatures for PI 1a-d polymers: 207–247°C and for PI 2a-d polymers: 264–275°C were obtained. The polymers were loaded with 34–62 wt% of chromophore. Six from the eight polymer systems could be spincoated onto ITO glass substrates, yielding high quality films. Noncentrosymmetry was induced by corona poling at a temperature of 10°C below T_g . Nonresonant $d_{33}(0)$ values up to 10 pm/V were

Poster Session I

obtained at 1064 nm of induced light. Polyimides **PI1b** and **PI 2b** show the highest NLO-effect stability at 125°C, after an initial decrease (28h) the nonlinearity does not significantly change over 1,000 h, which finally results in 78% respectively 90% remaining NLO efficiency.

Poly(maleimide-styrene) copolymers were prepared by polymer analogous reaction of maleic-anhydride copolymers with aminoalkyl-functionalized azo-chromophores **a**, **e**, **f**. Glass transition temperatures from 178–228°C could be obtained. The polymers were loaded with 36–54 wt% of chromophore.



Poled films of the copolymers were measured for their second harmonic generation effect at 1064 nm of induced light, the highest obtained value of $d_{33}(0)$ was 12.5 pm/V. This copolymers show a poling order stability of 90% for the nitrobenzimidazole chromophore loaded copolymer, while the Disperse Red 1 loaded copolymers show stabilities up to 75% respectively 64% this depending on the chromophore content after 1,000 h of heating at 125°C. The other copolymer systems give mostly a larger initial decrease (200h), which does not significantly change over 1,000 h. From the original value of the nonlinear optical response in polymer **Pp e**, 76% of the second-harmonic signal remained, while for **PCl e** only 40% remained, the other copolymers show poling order stabilities from 55–64%.

Our studies have shown that chromophore functionalized polyimides and copolyimides exhibit high glass transition temperatures, which result in a stable NLO-response at elevated temperatures. In addition the magnitude of the NLO-response suggests that these polymers could be useful for NLO-applications.

References

- [1] D. M. Burland, R. D. Miller, C. A. Walsh, *Chem Rev.* **94**, 31 (1994)
- [2] (a) H.-J. Lee, M.-H. Lee, S. G. Han, H.-Y. Kim, J.-H. Ahn, E.-M. Lee, Y. H. Won, *J. Polym. Sci., Part A: Polym. Chem.* **36**, 301 (1998).
- (b) D. Yu, A. Gharavi, L. Yu, *Macromolecules* **29**, 6139 (1996).
- (c) T.-A. Chen, A. K.-Y. Jen, Y. Cai, *Macromolecules* **29**, 535 (1996).
- (d) T. Verbiest, D. M. Burland, M. C. Jurich, V. Y. Lee, R. D. Miller, W. Volksen, *Macromolecules* **28**, 3005 (1995).
- (e) M. Ahlheim, F. Lehr, *Macromol. Chem. Phys.* **195**, 535 (1996).
- (f) T. Verbiest, C. Samyn, M. Van Beylen, A. Persoons, *Macromol. Rapid Commun.* **19**, 349 (1998).

Second Harmonic Generation in Molecular-Doped Poly(ethylene oxide)/*atactic*-Poly(methyl methacrylate) Blends

A.V. Vannikov, A.D. Grishina, L.Ya. Pereshivko, and T.V. Krivenko
A.N. Frumkin Institute of Electrochemistry, Russian Academy of Science
117071 Moscow, Russia

J. Vernel and R.W. Rychwalski
Department of Polymeric Materials, Chalmers University of Technology
SE-41296 Göteborg, Sweden

SHG in *atactic*-PMMA containing *para*-nitrosodimethylaniline (NDMA), and in poly(ethylene oxide) (PEO) /PMMA blends containing 2, 6, 16 and 25 vol. % PEO, doped with 4-anilino-4-nitroazobenzene (DO-3) has been studied in-parallel with measurements of surface potential. Dependence of the SH signal on NLO molecule concentration, temperature and blend composition has been measured. Positive information regarding a mechanism governing kinetic characteristics of the SH signal decay in the corona poled polymer systems can be obtained only in the course of parallel temporal measurements of both the SHG signal and the surface potential.

In PMMA doped with NDMA, the $(I/I_0)^{0.5}$ and U/U_0 decay curves completely coincide and can be represented by the same equation:

$$(I/I_0)^{0.5}(\text{or } U/U_0) = \alpha \text{EXP}(-t/\tau_{e1}) + (1 - \alpha) \text{EXP}(-t/\tau_{e2}), \quad (1)$$

where I_0 and U_0 are the SH intensity and the surface potential immediately after switching off the corona, τ_{e1} and τ_{e2} are the relaxation times for the fast and slow terms, respectively. Thus, the surface potential controls the SH kinetic characteristics in these compositions, and therefore the DC electric-field-induced SH (EFISH) takes place. The coefficient α and the relaxation times τ_{e1} and τ_{e2} in Eq. (1) for different concentrations of NDMA are represented in Table 1.

Table 1: Dependence of α , τ_{e1} , and τ_{e2} in Eq. (1) on NDMA concentration.

NDMA, M	α	τ_{e1} , s	τ_{e2} , s
0.42	0.4	80	1800
1.75	0.8	20	360
3.0	1.0	6	

As shown in Table 1, the SH signal relaxation time shortens as the NDMA concentration in PMMA increases. The mean distance between adjacent NDMA molecules, r , is less than 15Å at given in Table 1 concentrations. In this case the NLO molecules act as electron transport centres, increase the conductivity and determine both, the mechanism of relaxation of the surface potential and SH signal. The time τ_e is related to the conductivity, σ , by the equation τ_e (s) = $8.85 \times 10^{-14} \epsilon / \sigma$ (S cm⁻¹), where ϵ is the dielectric constant of a polymer film.

In the following, the well-known PMMA / chromophore NLO system has been extended by blending with PEO. Several compositions with 2, 6, 16 and 25 vol. % PEO

Poster Session I

in the blend containing 0.4 M DO-3 have been measured. The PEO/PMMA blends have ionic conductivity that increases with the increasing PEO content. It has been shown for a blend with small amount of PEO (2%) that alignment of chromophores under corona is dramatically affected when the temperature is increased to the lower bound of the T_g -region namely, to the point where the cubic coefficient of thermal expansion starts to increase. This temperature is much lower than the enthalpic T_g (by mid-point construction). It has been shown at using the 25% PEO samples that the SH signal under corona disappeared on heating at T_g . This effect is induced by the surface potential sharp decay as the surface potential depends on σ , $U_0 = A/(B + C\sigma)$, and σ exponentially increases at temperature increase.

The common bi-exponential dependence (Eq. (1)) fits well both, the $(I/I_0)^{0.5}$ and U/U_0 experimental decay curves at room temperature. The surface potential and SH signal relaxation time, τ_e , decreases more than 5×10^4 times at transition from 2% to 25% PEO in the blend, whereas the rotation diffusion time remains always less than τ_e . Addition of the electron transporting 4-diethylamino-benzaldehyde-diphenylhydrazone molecules (DEH) into the based on 2% PEO NLO composition having the lowest conductivity and the smallest free volume allows to speed up the U/U_0 decay and to reveal the process of the DO-3 rotational relaxation. For the composition containing 0.7 M DEH the U/U_0 decay is distinctively faster than that of $(I/I_0)^{0.5}$. The surface potential decay corresponds to Eq. (1) with τ_{e1} and τ_{e2} given in Table 2. $(I/I_0)^{0.5}$ decay curves after corona switch-off can be represented by the equation:

$$(I/I_0)^{0.5} = \alpha \text{EXP}(-t/10) + (1 - \alpha) \text{EXP}(-t/\tau). \quad (2)$$

The fast exponent relaxation time equals 10 s and coincides with τ_{e1} for the U/U_0 decay. The slow relaxation times are longer than τ_{e2} and hence should be identified with rotational diffusion relaxation time, τ_{rot} . In Table 2, the slow exponent time constant τ_{rot} are given as a function of the aging time.

Table 2: Dependence of τ_{e1} , τ_{e2} , and τ_{rot} on the aging time. The 2 vol.% PEO/PMMA blend contains 0.4 M of DO-3 and 0.7 M of DEH.

Time of aging	U/U_0		$(I/I_0)^{0.5}$	
	τ_{e1} , s	τ_{e2} , s	τ_{e1} , s	τ_{rot} , s
38 hours	10	200	10	800
3 weeks: before heating			10	800
after heating at 75°C, 5 min			10	1000
5 weeks	10	300	10	3500

The relaxation time τ_{rot} increases in the course of the aging. This effect can be associated with the well known free volume collapse frequently measured as the external volume contraction on aging. The fast EFISH component contribution into the SH signal α is decreased almost down to the DC electric-field-induced third-order effect contribution (within the experimental error) after 5 weeks of aging at room temperature.

We gratefully acknowledge the grant from the International Center for Science and Technology (No. 872-98), the grant from the Royal Swedish Academy of Science (No. 1337), and the grant from the Russian Foundation for Basic Research (No. 99-03-32111).

Organized Organic Multilayer Structures for Frequency Doubling and Electro-Optics

V.Zauls, S.Schrader, B.Dietzel, B.Schultz

*Universität Potsdam, Institut für Physik, Lehrstuhl Physik kondensierter Materie
Am Neuen Palais 10, D-14469 Potsdam, Germany*

C.Flueraru, H.Motschmann

*Max-Planck-Institut für Kolloid- und Grenzflächenforschung
Am Mühlenberg 2, D-14476 Golm, Germany*

G.Decher

*Université Louis Pasteur and C.N.R.S. Institut Charles Sadron
rue Boussingault 6, 67083 Strasbourg Cedex France*

Organised organic multilayers prepared by means of Langmuir-Blodgett (LB) technique based on various polymers and low-molecular amphiphiles have been compared with respect to their linear and non-linear optical properties. New material tested for multilayer preparation is maleic acid anhydride (AMS) polymer carrying NLO chromophores at the side chain and due to high LB film anisotropy demonstrating efficient second harmonic generation (SHG) and electro-optic coefficient up to 20 pm/V. Detailed ellipsometric studies and SHG measurements of obtained structures on various substrates were carried out to characterise thick LB multilayers and the results are comparable to the respective data of docosylamino-5-nitropyridine (DCANP) and spin-coated corona-poled polymer films such as DR-PMMA.

Organised organic multilayers of new maleic acid anhydride (AMS) polymer carrying NLO chromophores in side chains [1] has been regarded as promising candidates for SHG and EO applications. We report here on chromophore orientation studies of thick multilayer AMS films, obtained by LB multilayer deposition technique on hydrophobized silicon wafers and quartz glass substrates using water as a subphase at surface pressure 25 mN/m, dipping speed 5 to 10 mm/min and subphase temperature 21 °C (see [2] for more details on AMS synthesis and LB deposition conditions).

For linear optical characterisation of the samples multiple angle ellipsometric measurements at 632.8 nm wavelength have been performed to obtain averaged LB layer thickness and refractive index of multilayered films. We obtained film thickness growth around 1.6 nm per monolayer within first 5 to 10 deposited monolayers, 0.6 nm for the next 30 monolayers and only about 0.1 nm above 40 deposited layers while the value of refractive index $n=1,557$ was found to be the same for these layers independently on the type of substrate.

Nonlinear optical SHG studies of films were made in transmission or reflection geometries using an actively-passively mode locked Nd:YAG laser emitting 30 ps pulses at 1064 nm wavelength with a repetition rate of 10 Hz. Computer controlled rotation mounts of polarizer, analyzer and sample stage allowed us to perform in various combinations different SHG characterisation methods Maker fringe technique in transmission, incidence beam polarization rotation with detection of p- or s-polarized reflected SH signal and substrate rotation around surface normal to test in-plane anisotropy of film. In addition, interference method [3] has been used for phase sensitive SHG measurements to reveal orientational direction of the active chromophores. Using Y-type LB layers of DCANP as

Poster Session I

reference substance we found $d_{21} = 8.2$ pm/V, $d_{22} = 21.3$ pm/V, $d_{23} = 4$ pm/V, molecular tilt angle 70° and azimuth angle 31° in good agreement with literature data [4].

SHG tests of AMS Z-type multilayers showed remarkable value of $d_{33} = 20$ pm/V of the first deposited layers. However, quadratic growth of SHG intensity with number of layers N was observed only until 30 layers. In the same time SHG polarization measurements indicated significant increase of the molecular tilt angle above 40 deposited layers. These results are supported by ellipsometric data.

Obviously, multilayers the chromophores of the first 10 monolayers are oriented at small tilt almost perpendicular to the substrate plane but become more and more tilted as the number of monolayers increases, as reported for other polymers [5]. This behaviour can be explained by insufficient interaction of the strong chromophore dipoles and substrate surface field with increasing of the film thickness. Therefore, alternating LB layers prepared from the azo-polymers and other amphiphiles could be promising candidates for fabrication of thicker LB layers with high anisotropy and high nonlinear optical susceptibility. Investigations on these materials are in progress. Typical values of nonlinear bulk optical susceptibility range between 15 and 20 pm/V depending on sample thickness and are comparable to the respective data of DCANP.

References

- [1] S. Schrader, D. Prescher, V. Zauls, "New Chromophores and Polymers for Second Order Nonlinear Optics," in M. Eich (ed.), *Second-Order Organic Nonlinear Optics*, Proc. SPIE, **3474**, 160-171 (1998).
- [2] S. Schrader, V. Zauls, B. Dietzel, C. Flueraru, D. Prescher, J. Reiche, H. Motschmann, L. Brehmer, "Linear and Nonlinear Optical Properties of Langmuir-Blodgett Multi-layers from Chromophore Containing Maleic Acid Anhydride Polymers," *Materials Science and Engineering C*, at press (1999).
- [3] R. Stolle, G. Marowsky, E. Schwarzberg, G. Berkovic, "Phase measurements in nonlinear optics," *Appl. Phys. B* **42**, 491-498 (1996).
- [4] C. Bosshard, M. Küpfer, M. Flörsheimer, T. Borer, P. Günter, Q. Tang, F. Zahir, "Investigation of chromophore orientation of docosylamino-5-nitropyridine and derivatives by nonlinear optical technique," *Thin Solid Films* **210-211**, 198-201, (1992).
- [5] T. Verbiest, C. Samyn, A. Persoons, "Second harmonic generation from floating Langmuir layers of an azobenzene functionalized copolymer," *Thin Solid Films* **242**, 139-141 (1994).

Ultra-Efficient Electro-Optic Polymer Modulators for Short-Distance High-Speed Optical Interconnects

N. S. Lagali¹, D. J. W. Klunder¹, G. J. Gerritsma², and A. Driessen¹
MESA+ Research Institute

¹*Lightwave Devices Group,* ²*Low Temperature Division*
Faculty of Applied Physics, University of Twente
P.O. Box 217, 7500 AE Enschede, The Netherlands

The possibility of realizing electro-optic polymer modulators with driving voltages in the millivolt regime is investigated. By utilizing efficient polymeric waveguide devices such as active ring resonators, gratings, and resonant superconducting electrodes, ultra-low modulation voltages can be achieved. This narrows the gap between present-day modulator technology and the low driving voltages typically available in superconducting electronics.

Introduction

The tremendous bandwidth of optical fiber is poised to fully exploit the advantages of the THz-regime data processing speeds and low power dissipation levels that can be provided by superconducting electronics [1]. The first realization of such high bit-rate signal transport is expected to occur over short-distances, for applications in distributed computing or local area network architectures.

Interfacing of cryogenically-cooled superconducting circuits with room-temperature optical fiber transport systems, however, presents a number of practical challenges. For instance, a fundamental limitation of superconducting circuits operating at low temperatures is that the maximum AC voltage available is on the order of a few millivolts. This voltage must be sufficient to drive a high-speed optical modulator, whose modulation depth must be large enough to ensure error-free detection after transport through a few meters of optical fiber. A practical optical detection scheme for a BER of 10^{-9} at 10 GHz imposes a limit of about 1 % on the signal modulation depth at a wavelength of 850 nm.

In this paper, we propose designs for efficient electro-optic polymer waveguide modulators operating with millivolt driving signals. The devices are compact enough to allow for dense integration of arrays of devices on a single substrate. In this manner, multiplexing techniques can be used to achieve aggregate bandwidths approaching the THz level.

Optical Device Design

One modulator design possibility is illustrated in Fig. 1. An applied voltage induces a grating in the electro-optic polymeric core, thereby converting a launched TM mode into a TE mode. The electro-optic polymer, however, is highly birefringent [2] so the TE mode is absorbed by the electrodes. With a grating length of 69 μm , a 2 mV driving signal results in a calculated intensity modulation depth of 1.6 %.

A second possibility is to use a Mach-Zehnder interferometer with enhanced phase sensitivity. The enhancement is achieved by coupling a portion of the light from one branch of the interferometer to a microcavity resonator as shown in Fig. 2 [3]. The fundamental microcavity mode is designed to be resonant with the waveguide mode, thereby inducing a π phase shift in the branch. By tuning the resonance condition by means of an electro-optic polymer coating, the waveguide mode experiences a sensitive phase modulation over extremely short distances due to the high finesse of the resonator.

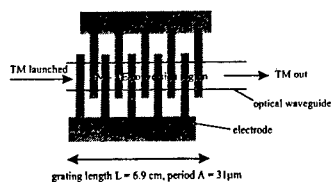


Figure 1: Diagram of mode converter/attenuator intensity modulator.

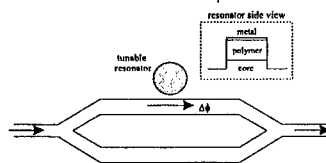


Figure 2: Schematic diagram of Mach-Zehnder ring resonator intensity modulator.

For example, coupling 5 % of the waveguide mode to a ring resonator with a radius of only $12 \mu\text{m}$ can provide a finesse factor of 90. This results in a calculated intensity modulation of 1 % with an applied voltage of 100 mV.

Resonant Superconducting Electrodes

Additional reduction in modulation voltage can be achieved using a superconducting resonant electrode design. The ring resonator or a conventional Mach-Zehnder interferometer realized in electro-optic polymer technology can be operated using superconducting Nb electrodes. In addition to the very low loss of Nb, thin films of this metal can be deposited at room temperature conditions, and a variety of substrate materials are feasible. These properties are attractive as they are compatible with standard integrated optical polymer technology.

The electrode is part of an impedance-matched high-Q resonance circuit designed to achieve microwave or millimeter wave field enhancement through the use of a resonant standing wave voltage signal. For a high Q factor (typical of extremely low-loss Nb electrodes and low dielectric losses in the polymer layers), a voltage reduction of more than an order of magnitude for the modulators is expected. This results in operating voltages in the region 1 - 10 mV, compatible with superconducting circuits currently being fabricated.

Presently we are realizing the first designs of the optical modulators and determining the compatibility of the Nb electrodes with the polymeric thin films. The fiber-pigtailed devices will subsequently be tested for high-speed ($>10 \text{ GHz}$) operation in a cryo-cooled environment. Through modifications in optical device design, other non-linear optical materials (e.g., electro-optic crystals) are also foreseeable for use in ultra-low voltage modulators.

References

- [1] W. Chen, A. V. Rylyakov, V. Patel, J. E. Lukens, and K. K. Likharev, "Rapid single flux quantum T-flip flop operating up to 770 GHz," *IEEE Trans. on Appl. Supercond.* **9**, 3212-3215 (1999).
- [2] M. H. Lee, H. J. Lee, S. G. Han, H. Y. Kim, K. H. Kim, Y. H. Won, S. Y. Kang, "Fabrication and characterization of an electro-optic polymer waveguide modulator for photonic applications," *Thin Solid Films* **303**, 287-291 (1997).
- [3] B. E. Little, S. T. Chu, H. A. Haus, "Track changing by use of the phase response of microspheres and resonators," *Optics Letters* **23** (12), 894-896 (1998).

Second harmonic generation at near resonance of a functionalized pDR1A thin film oriented by corona poling

V. Rodriguez*, C. Sourisseau

Laboratoire de Physico-Chimie Moléculaire UMR 5803 CNRS
 Université de Bordeaux I, 351, cours de la Libération
 Talence 33405, France

* email: vincent@morgane.lsmc.u-bordeaux.fr

Polarized second harmonic generation transmission spectra at near the two photon absorption have been recorded on a p(DR1A) thin film oriented by corona poling, using a 1064 nm Nd/Yag laser pump. Experimental results were interpreted within a multi-layered SHG model including the two photon absorption contributions. The three $\langle P_1 \rangle$, $\langle P_2 \rangle$ and $\langle P_3 \rangle$ Legendre polynomials or orientational order parameters, which describe the chromophore distribution orientation after poling, were thus obtained. Then, a complete molecular orientational distribution function of the chromophores has been estimated from a mean field potential approach.

Thin films of poly{4'-[2-acryloyloxy-ethyl]ethylamino]-4-nitroazobenzene-metacrylate} (p-DR1A or 100 and DR1-covalently bonded polymer) were spun coated onto standard microscope slides. The films were corona poled with a wire held parallel to and above (5.0 mm) the film. A performant SHG experimental setup for collecting transmitted waves has been used to collect p-p and s-p Maker fringes of these films (thickness between 0.15 and 0.20 μm) after corona poling, using a 1064 nm Nd/Yag laser pump.

A multi-layered SHG model, including an anisotropic NL intermediate medium, has been developed which allows the experimental determination of resonance-enhanced mean values of the nonlinear optical coefficients d_{33} , d_{31} as well as the anisotropic two photon absorption coefficients at 532 nm.

Assuming uniaxial symmetry for the poled films, it is thus shown that polarized SHG measurements, under near resonance conditions, lead to quite relevant Legendre orientational order parameters $\langle P_1 \rangle = \langle \cos\theta \rangle$, $\langle P_3 \rangle = \langle 5\cos^3\theta - 3\cos\theta \rangle / 2$ and, more particularly, $\langle P_2 \rangle = \langle 3\cos^2\theta - 1 \rangle / 2$, where θ is the polar angle between the DR1 long molecular axis and the direction of the applied static electric field. Usually, the latter even-order $\langle P_2 \rangle$ parameter is estimated from a comparison of the absorption spectra of the films before and after poling. We have systematically checked the validity of the $\langle P_2 \rangle$ values obtained from SHG measurements, using our multi-layered model, and from the absorption spectra recorded over the 300-700 nm range.

From a set of the three relevant order parameters $\langle P_1 \rangle$ to $\langle P_3 \rangle$, it is thus possible to determine an orientational distribution function,

$$G(\theta) = \frac{\exp(-U_i/kT)}{\int \exp(-U_i/kT) d\cos\theta} \quad (1)$$

described by a mean-field potential $U_i = U_P + U_E$, where U_P is the potential due to the poling field and U_E is the potential that accounts for external forces. Assuming an homogeneous spatial Landau-type "effective" potential for each value of $\cos\theta$, i. e. a constant density number of chromophores, U_E can be expressed as a function of a

Poster Session I

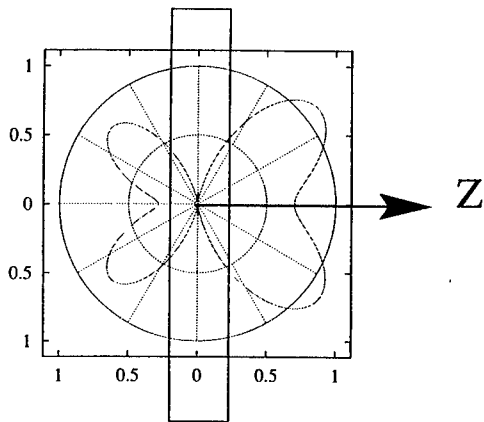


Figure 1: Polar plot of the distribution function, $G(\theta)$. The Z direction is that of the static electric field, and the curves shown are for the starting isotropic film (solid circular curve) and for the poled film (dashed curve).

macroscopic homogeneous spontaneous polarization $P(\cos\theta)$:

$$U_E = a.P^2(\cos\theta) + b.P^4(\cos\theta). \quad (2)$$

Therefore, other higher order parameter values can be estimated and a complete orientational distribution function can be either analytically or numerically computed. As an illustrative example, a polar representation of such a distribution function $G(\theta)$ obtained for a functionalized pDRIA -poled film is shown in figure 1.

References

- [1] W. N. Herman, L. M. Hayden, J. Opt. Soc. Am. **B/Vol. 12**, No. 3, 416-427 (1995).
- [2] M. G. Kuzyk, K. D. Singer, H. E. Zahn and L. A. King, J. Opt. Soc. Am. **B/Vol. 6**, No. 4, 742-752 (1989).
- [3] M. Braun, F. Bauer, Th. Vogtmann and M. Schwoerer, J. Opt. Soc. Am. **B/Vol. 15**, No. 12, 2877-2884 (1998).
- [4] D. K. Martinez, K. Koch, F. K. Ratsavong and G. O. Carlisle, J. Appl. Phys. **75** (8), 4273-4275 (1994).

Poster Session II

Rationalising the SHG Response in DCNP through Anomalous Atomic Thermal Motion and Hydrogen-bonding

J. M. Cole

Chemistry Department, University of Cambridge, Lensfield Road, Cambridge, CB2 1EW. UK

C. C. Wilson

The ISIS facility, Rutherford Appleton Laboratory, Chilton, Didcot, Oxon, OX11 0QX. UK

J. A. K. Howard

Department of Chemistry, University of Durham, South Road, Durham, DH1 3LE. UK

A single-crystal neutron diffraction study of the organic non-linear optical material, 3-(1,1-dicyanoethenyl)-1-phenyl-4,5-dihydro-1H-pyrazole (DCNP) is presented. The study was conducted in order to relate the structural characteristics of the compound to its physical properties. DCNP exhibits a very large second harmonic generation (SHG) output, an extremely large linear electro-optical effect and photoconductive and pyroelectric properties. The nature of the hydrogen-bonding revealed by the study, in part, accounts for the first two of these phenomena. The neutron study also shows that some unusual atomic thermal motion is present in part of the molecule. With the aid of a variable-temperature single-crystal X-ray diffraction study, in conjunction with the neutron study, the atypical thermal motion is attributed to libration and is fully characterized. This libration is shown to enhance the SHG effect.

Introduction

3-(1,1-dicyanoethenyl)-1-phenyl-4,5-dihydro-1H-pyrazole (DCNP) shows exceptional non-linear-optical (NLO) potential, giving powder second-harmonic-generation (SHG) signals of approximately 100 times that of urea when using a fundamental wavelength, λ_f , of 1.9 μm [1-3]. Moreover, the compound exhibits photoconductive and pyroelectric properties and produces a very high linear electro-optical effect, due to the very planar and layer-like solid-state packing of the compound [2]. In light of such favourable attributes, the three-dimensional structure of DCNP was studied in greater detail, in order to try to relate more fully the structure to the physical properties observed. The investigations took the form of a 100K neutron derived structural determination and variable temperature (90K, 100K, 200K, 290K) X-ray diffraction measurements.

Experimental

The neutron diffraction study of monoclinic DCNP [$\text{C}_{13}\text{H}_{10}\text{N}_4$, $M_r = 220.0$, $F(000) = 464$, space group, Cc, $a = 11.571(2)\text{\AA}$, $b = 12.258(3)\text{\AA}$, $c = 7.868(2)\text{\AA}$, $\beta = 90.11(3)^\circ$, $Z = 4$] was performed on the single-crystal diffractometer, SXD, at the ISIS facility, Chilton, U.K. The single-crystal variable-temperature X-ray diffraction studies were all carried out using the Bruker SMART-CCD diffractometer at the temperatures 90(2)K, 100(2)K, 200(2)K and 290(2)K. This instrument is ideal for a variable temperature study since, by nature of its large area detector, data can be recorded at several different temperatures in just a few days.

Results and discussion

The 100K neutron study yielded much better defined hydrogen atom positions than those obtained from the original X-ray study [2]. The presence of two C-H...N hydrogen-bonds was indicated as a result of this greater accuracy. The contacts are considered to be fairly weak [at distances of 2.513(8) \AA and 2.49(1) \AA] but even so, they are thought to dictate the three-dimensional packing of the compound. The hydrogen-bonds hold the molecules together in a

Poster Session II

corrugated layer formation. Hydrogen-bonding thus may be considered to be responsible for the extremely large electro-optic coefficient reported, since the magnitude of the phenomenon is largely dependent upon the parallel alignment of the molecules [1]. Moreover, hydrogen-bonding is known to strongly enhance the SHG effect (e.g. [4]). This is because the electrostatic nature of these intermolecular interactions provide a facile route for charge transfer between molecules. Furthermore, close proximity and good relative alignment of molecules with respect to each other promote charge transfer and hydrogen-bonding often encourages such features, as in this case. The powerful combination of this hydrogen-bonding with the aforementioned high potential of the isolated molecule, thus helps explain the high SHG output observed in the bulk material.

The uncertainty in the weaker hydrogen-bond is markedly greater than that for the other hydrogen-bond. This is due to the rather striking peculiar anisotropic thermal behaviour in the phenyl ring with which it is involved. The variable temperature X-ray diffraction studies showed that this motion was due to libration. Such libration was primarily concentrated in the phenyl ring and was subsequently characterised through a thermal motion analysis program, THMA11 [5] which provided suitable corrections to bond distances and atomic thermal displacement parameters.

Results show that this libration perturbs the ring current in the phenyl group as is evident from the bond lengths of the phenyl group which show a marked tendency towards quinoidal character, i.e. the polarization of a phenyl unit into a quinoidal structure is less energetically costly than it would normally be in the absence of libration. This will provoke a greater ease of charge transfer within the molecule and so libration must be an enhancing factor in terms of SHG. Moreover, the presence of libration in the nitrile groups will result in a greater susceptibility of the triple bonds to vary slightly in bond order with time. A reduction in triple bond character at a time, t , will result in a lower bond-length alternation value which is favourable for SHG effects [6,7].

A more detailed description of this work will be reported elsewhere [8].

Acknowledgements

The authors wish to thank the Institut Laue Langevin, Grenoble, France, for financial support (JMC), the Royal Society for a Leverhulme Senior Research Fellowship (JAKH), the EPSRC for access to neutron beam-time at ISIS, J. N. Sherwood and E. E. A. Shepherd for supplying the crystals and the late K. N. Trueblood for scientific advice.

References

- [1] A. Miniewicz, K. Palewska, J. Lipinski, R. Kowal, B. Swedek, *Mol. Cryst. Liq. Cryst.*, **253**, 41-50 (1994).
- [2] S. Allen, T. D. McLean, P. F. Gordon, B. D. Bothwell, M. B. Hursthouse, S. A. Karaulov, *J. Appl. Phys.*, **64**, 2583-2590 (1988).
- [3] S. N. Black, R. J. Davey, P. R. Morley, P. Halfpenny, E. E. A. Shepherd, J. N. Sherwood, *J. Mater. Chem.*, **3**, 129-132 (1993).
- [4] J. A. R. P. Sarma, F. H. Allen, V. J. Hoy, J. A. K. Howard, R. Thaimattam, K. Biradha, G. R. Desiraju, *J. Chem. Soc., Chem. Commun.*, 101-102 (1997).
- [5] K. N. Trueblood, K. N. THMA11. *Program for Thermal Motion Analysis*. University of California, Los Angeles, U.S.A (1990).
- [6] L. Cheng, C. B. Gorman, S. R. Marder, B. G. Tiemann, *Proc. SPIE*, **1775**, 19-31 (1993).
- [7] S. R. Marder, J. W. Perry, *Adv. Mater.*, **5**, 804-815 (1993).
- [8] J. M. Cole, C. C. Wilson, J. A. K. Howard, F. R. Cruickshank, *Acta Crystallogr. B* (submitted, 1999).

Preparing Polydiacetylene Single Crystal Thin Films

A. Feldner, Th. Fehn, Th. Vogtmann, and M. Schwoerer
*Lehrstuhl Experimentalphysik II and
Bayreuther Institut für Makromolekülforschung (BIMF)
Universität Bayreuth,
Universitätsstr. 30,
D-95440 Bayreuth*

Polydiacetylene (PDA) single crystals show extremely high and anisotropic values of the third order susceptibility. Here we describe a method to prepare polydiacetylene single crystal thin films of about a micrometer thickness and several square millimeters surface area. It is shown how to grow single crystals of the monomer and how to avoid crystal cleaving or other damages during the polymerization process that usually occur due to a slight contraction of the crystal. Being a one-pass crystallization process, the resulting optical quality is very good, and the films are well suited as wave guides.

The polydiacetylene (PDA) polymer can be prepared in single crystals. Their preparation is based on the unique feature of many diacetylene derivatives to polymerize in a crystal without destroying the crystal structure. The polymer backbones are aligned in these crystals so that PDA single crystals show extremely high and anisotropic values of the third order susceptibility. The polymerization process can be driven e.g. by gamma ray treatment or even, with some derivatives, by modest heating. The polymerization reaction causes a contraction in the chain direction. This results in a strain in the monomer crystal, once a certain amount of polymers have been induced. The crystal strain drives the polymerization reaction of the remaining monomer. The contraction in the direction of the reaction is especially high for the thermally polymerizable polydiacetylenes, e.g. 5% for TS-6.

Preparation crystals of polydiacetylene therefore is a two-step process. First, a crystal of diacetylene monomer is grown, then this monomer crystal is turned into a polymer crystal by gamma ray treatment or heating. However, there is a major problem involved with this polymerization, as there's a slight contraction of the crystal in the direction of the forming polymer chains. This causes cracks in the crystals that inhibit any use as nonlinear-optical waveguides.

To address this problem, the monomer crystals should be removed from the substrate before polymerization. Although it is possible to remove them partially, only smaller crystals, or small parts of the larger ones, will detach from the substrate surfaces, involving quite some mechanical stress and damage to the surfaces.

The general idea that allowed us to successfully circumvent this problem is, instead to remove the crystals from the substrate, to dissolve the substrate itself. As our method is a one-pass crystallization process, the resulting optical quality is very good, and the films are well suited as wave guides. No difference of optical properties were found in these thin film single crystals when compared to macroscopic PDA crystals.

Poster Session II

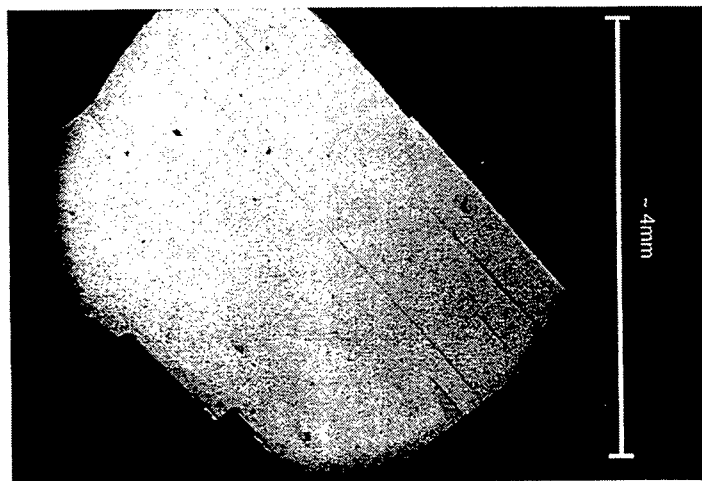


Figure 1: p-TS-6 crystal between two crossed polarizers. The crystal axes are turned 45° against the polarizer direction, so that the crystal destroys the polarization by its birefringence and lights up. Any inhomogenities, defects, cracks, and zone boundaries can be seen very clearly in this view.

Linear Optical Properties of p-Toluene-Sulfonate (PTS)

Lars Friedrich¹, Tomáš Pliška¹, Mingguo Liu¹, George I. Stegeman¹, Seung-Han Park²,
Andreas Feldner³, Thomas Vogtmann³, and Markus Schwoerer³

¹CREOL School of Optics, University of Central Florida, Orlando, FL, U.S.A., 4000 Central Florida Blvd.,
P. O. Box 162700, Orlando FL 32816, U.S.A., email george@mail.creol.ucf.edu

²Yonsei University, Dept. of Physics, Seoul, Korea

³Lehrstuhl Experimentalphysik II and Bayreuther Institut für Makromolekülforschung (BIMF), Universität
Bayreuth, Germany

Abstract – We report measurements of the dispersion in the linear index and absorption coefficient of Para-Toluene-Sulfonate single crystal waveguiding films and bulk material prepared by different growth techniques and evaluate the coefficients for a one-resonance Sellmeier fit. These are, to the best of our knowledge, the first index data that extent well into the near infrared, to 1.55 μm wavelength. The bulk data, obtained by ellipsometry, agree well with data previously published in the visible region of the spectrum. We found the PTS films to have lower absorption coefficients, and the index data, obtained by m-line spectroscopy, are also lower.

Poly[bis(p-toluene-sulfonate)] of 2,4-hexadiyne-1,6-diol (PTS) is a promising material for applications in ultrafast all-optical switching. PTS is a one-dimensional conjugated polymer single crystal and exhibits one of the largest non-resonant, ultrafast nonlinearities reported to date ($n_2=2.4 \times 10^{-12} \text{ cm}^2/\text{W}$ at 1600 nm), combined with low linear and nonlinear loss in this wavelength region [1,2].

However, to date there were only few and perfunctory data published on the linear properties of PTS [1,3]. These properties can be expected to be very different for light polarized either parallel or perpendicular to the polymer chain direction (b-axis). For the polarization parallel to the b-axis, an absorption peak in the visible spectral region is expected, resulting in normal dispersion in the near infrared (NIR). For the other polarization, no such peak is present and thus the index in the NIR should be lower and the expected dispersion smaller.

The PTS single crystal films were prepared by two different methods: They were either grown free floating in a solution of the monomer and afterwards attached to the substrate by adhesion or the monomer solution was thermally polymerized between two

Poster Session II

substrates separated by spacers [4]. The single crystal bulk PTS was grown by the first technique.

The film indices of refraction were measured using m-line-spectroscopy. For coupling, a grating was holographically patterned onto the PTS film, using plasma etching. For the absorption measurements, very thin films had to be used because of the large absorption coefficient for light polarized parallel to the b-axis. Using plasma etching, a PTS film was etched to a thickness of about 200 nm. The transmission of this film was then measured for both polarizations in the visible and NIR region of the spectrum using an optical multichannel analyzer (OMA). All bulk data were obtained by ellipsometric measurements.

The results, summarized in Figs. 1 and 2 below, show lower values of both the refractive index and the absorption coefficient for the PTS films than for the bulk material. We used the data to fit a one oscillator Sellmeier equation to the film refractive index data parallel to the b-axis, assuming only one resonance at $\lambda_0=620$ nm (see Fig. 1).

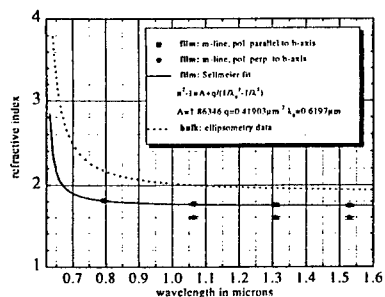


Fig. 1: Refractive index measurements for PTS films and bulk PTS, obtained by m-line spectroscopy and ellipsometry, respectively.

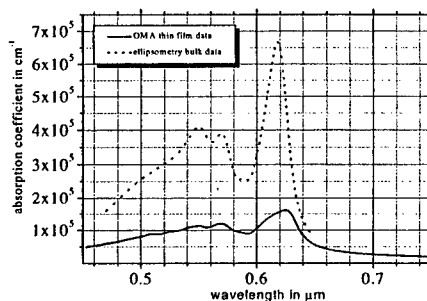


Fig. 2: Absorption coefficient measurements of PTS films and bulk PTS, obtained with an optical multichannel analyzer and ellipsometry, respectively.

1. C. Sauteret et al., *Phys. Rev. Lett.*, vol. 36, no. 16, pp. 956-959 (1976)
2. B.L. Lawrence et al., *Phys. Rev. Lett.*, vol. 73, no. 11, pp. 597-600 (1994)
3. M. Thakur et al., *Appl. Phys. Lett.*, vol. 56, no. 12, pp. 1187-1188 (1990)
4. M. Liu et al., *Organic Thin Films for Phot. Appl. 1997*, paper WC2-1 (Long Beach 1997)

Molecular Recognition Concept in the Growth of Polar Organic Nonlinear Optical Crystals

Hyung-ki Hong, Jaewoo Park, Choon Sup Yoon
Department of Physics, KAIST
Daeduck Science Town, Taejeon 305-701, Korea

Most of organic nonlinear optical crystals are composed of molecules of large dipole moments. The condition of antisymmetric crystal structure for quadratic nonlinear optical effects requires the polar arrangements of the dipole moments in the crystal lattice. This polar nature influences not only linear and nonlinear optical properties, but also crystal growth processes significantly. The polar structure quite often inevitably leads to the unidirectional growth in solution which could be an adverse effect for the growth of high quality organic crystals for both characterization of nonlinear optical properties and device applications.

The observed unidirectional growth in meta-nitroaniline (mNA), 3-methyl-4-methoxy-4'-nitrostilbene (MMONS) and other organic crystals is presented and discussed in terms of molecular recognition concept [1, 2]. The influence of polar arrangement of dipoles on linear and nonlinear optical properties is also discussed.

The unidirectional growth was observed both in meta-nitroaniline (mNA) and 3-methyl-4-methoxy-4'-nitrostilbene (MMONS) crystals, and the mechanism for the unidirectional growth was investigated.

The morphology of the mNA crystals grown in acetone:benzene (50:50 in volume) solution exhibits circular cone shape while the morphology of the supercooled melt grown mNA crystals looks more close to a polyhedral cone with the $[0\ 1\ 0]$ along the cone axis. A close examination of mNA crystal structure indicates that hydrogen-rich faces containing amino groups are exposed along the $(0\ 0\ 1)$ plane and oxygen-rich faces containing nitro groups are exposed along the $(0\ 0\ \bar{1})$ plane. In solution grown mNA crystals, solvent-crystal interactions may play a significant role. Even if benzene has no dipole moment, acetone has a strong dipole moment of 2.88 Debye due to large electronegativity of oxygen atoms in carbonyl group. Thus the carbonyl groups of acetone molecules would interact repulsively with the nitro groups of mNA molecules since the oxygen atom in both groups are electrically negative. However the carbonyl groups of acetone molecules could have attractive interactions with the NH_2 and CH groups at the $(0\ 0\ 1)$ faces by forming $(\text{mNA})\text{C}-\text{H} \cdots \text{O}(\text{acetone})$ and $(\text{mNA})\text{N}-\text{H} \cdots \text{O}(\text{acetone})$ bonds. The observed unidirectional growth in the $[0\ 0\ \bar{1}]$ direction could be explained by the growth inhibition at the $(0\ 0\ 1)$ faces due to the adsorption of solvent acetone molecules at the hydrogen-rich faces. However the origin of the unidirectional growth observed in the mNA crystals grown from the supercooled melt is different. Since there is no solvent involved in this case, the solvent-crystal surface interactions cannot explain the unidirectional growth of mNA from the supercooled melt at all. This could be explained by poisoning of the faces of the $[0\ 0\ 1]$ direction by the oxidized material of mNA, 1,3-dinitrobenzene (DNB) on melting. Since a DNB molecule has two nitro groups, it is obvious that DNB molecules cannot be attached on the faces of the $[0\ 0\ \bar{1}]$ direction due to the strong repulsive interactions between the electron acceptor nitro groups of mNA and DNB molecules. In the $[0\ 0\ 1]$ directions, however, electron donor amino groups are exposed on the surface and therefore DNB molecules can be easily fitted onto the surfaces as mNA molecules do. Once the DNB molecules attach to the faces of the $[0\ 0\ 1]$ direction, the repulsive interactions between the nitro group of a DNB molecules and the nitro group of an oncoming mNA

Poster Session II

molecule prevent further growth along the $[0\ 0\ 1]$ direction while mNA molecules continue to attach to the faces of the $[0\ 0\ \bar{1}]$ direction, which results in the observed unidirectional growth along the $[0\ 0\ \bar{1}]$ direction.

The overall morphology of MMONS crystals grown in methyl-ethyl-ketone (MEK) solution is represented by a truncated octahedra, which is a consequence of the unidirectional growth along one direction of the polar axis. A MMONS molecule has a nitro group at one end and two methyl groups at the other, and the MMONS molecules are placed in such a manner that the nitro groups and the methyl groups face each other in the crystal lattice. Since a MEK molecule also has two methyl groups at one end, MEK molecules can fit in place of MMONS molecules on the $(0\ 0\ \bar{1})$ plane where nitro groups are exposed, but are highly unlikely to be adsorbed on the $(0\ 0\ 1)$ face where methyl groups are exposed. Once MEK molecules occupy the MMONS sites, no more MMONS molecules can attach on the $(0\ 0\ \bar{1})$ face, which leads to the observed unidirectional growth in the $[0\ 0\ 1]$ direction. A number of different solvents were attempted for the growth of MMONS crystals, such as hexane, methanol, toluene, acetonitrile, benzene, dichloromethane, ethyl acetate, acetone, chloroform as well as MEK. Only MEK, acetone, ethyl acetate that have two methyl groups at one end in common resulted in the unidirectional growth, which confirms that the mechanism of the unidirectional growth is caused by the selective adsorption of solvent molecules on the nitro group ends and the growth inhibition on the $(0\ 0\ \bar{1})$ face thereafter.

Linear and nonlinear optical properties were measured along the polar c-axis and the nonpolar b-axis. The linear and two photon absorption coefficients in the nonpolar b-direction are $2.24\ \text{cm}^{-1}$ and $7.37\ \text{cm/GW}$ at 532 nm, respectively and those values in the polar c-direction are $4.95\ \text{cm}^{-1}$ and $34.2\ \text{cm/GW}$, respectively. The nonlinear refractive index, $n_2(1.04 \times 10^{-10}\ \text{esu})$ in the polar c-direction at 532 nm is about twenty times larger than that in the nonpolar b-direction. Much larger values of the two photon absorption coefficient and nonlinear refractive index of MMONS along the polar c-axis than the b-axis reflect the fact that the molecular dipole moments are cancelled each other in the a-b plane, but the large macroscopic polarization is established along the polar axis.

In summary, the unidirectional growth observed in the polar organic nonlinear optical crystals, mNA and MMONS is explained by the molecular recognition concept and the strong polar nature in these crystals not only affects the crystal growth processes, but also overall linear and nonlinear optical properties significantly.

References

- [1] I. Weissbuch, L. Addadi, M. Lahav, L. Leiserowitz, *Science*, **253**, 637 (1991).
- [2] I. Weissbuch, M. Lahav, L. Leiserowitz, G. R. Meredith, H. Vanherzeele, *Chem. Mat.*, **1**, 114 (1989).

SHG-active p-nitroaniline thin films grown by dip-coating

Hiroyuki Kobayashi, Hiroyuki Okuyama and Masahiro Kotani
*Faculty of Science, Gakushuin University
Mejiro, Tokyo 171-8588, Japan*

A strongly second-harmonic active thin film is grown when p-nitroaniline is dip-coated on a glass plate. The intensity of the second harmonics is as high as that from a film of MNA (2-methyl-4-nitroaniline). The SHG-active phase is metastable and undergoes a transition into a SHG-inactive phase, the transition rate being dependent on the temperature and the solvent used. Observation with second harmonic microscopy are also reported.

p-Nitroaniline is a compound which has a large second-order polarizability. However, it crystallizes in a centrosymmetric structure and the crystal is considered to be inactive in SHG. Effort has been made to realize a SHG-active system by arranging p-nitroaniline moiety in a favourable way— by electrical poling, co-crystallization, epitaxy, etc.

We have reported an observation that an intense second harmonic is generated at etch pits developed on a single crystal surface. It is supposed that a microcrystal having an acentrosymmetric structure grows at the etch pits [1].

Here we report another example in which a SHG-active arrangement of p-nitroaniline molecules is realized: Thin films are formed by dip-coating of a glass plate with a solution of p-nitroaniline. Several different organic solvents have been tested. Thin films prepared with a saturated benzene solution exhibit intense SHG, comparable to MNA (2-methyl-4-nitroaniline) thin films. Interestingly, the SHG activity of films prepared with different organic solvents differ in durability, as well as its magnitude. The SHG-active phase seems to be metastable and changes into a nonactive structure, with a half life which depends both on the temperature and the solvent used. Results of X-ray diffraction measurements indicate that the SHG-active powder has a structure different from the ordinary crystal. The (202) diffraction peak, which is strong in the ordinary crystal, is much weaker in the SHG-active powder, and gains intensity as the SHG-activity deteriorates.

The spatial pattern of SHG is monitored, after magnified with an objective lens, with a CCD camera. A film is illuminated with a 1064 nm pulse from a Q-switched Nd:YAG laser. The image, monitored at 532 nm, shows that the film is composed of needle crystals, several microns wide.

Polarized second-harmonic is generated when the polarization of the laser light is parallel to the needle axes. A distribution, among crystal grains, in half life of SHG-activity has been observed.

References

- [1] H. Kobayashi and M. Kotani, *Mol. Cryst. Liq. Cryst.* **278**, 125-130 (1996).

Poster Session II

DAST Thin Film Growth: Seven Exploratory Methods

S. Manetta, M. Ehrensperger, Ch. Bosshard, and P. Günter
Nonlinear Optics Laboratory, Institute of Quantum Electronics
Swiss Federal Institute of Technology, ETH Hönggerberg
CH-8093 Zürich, Switzerland

Seven different exploratory methods to grow organic single crystalline thin films from the solution are presented. We focus on the DAST (4'-dimethylamino-N-methyl-4-stilbazolium tosylate) / methanol system, because of the exceptionally high optical nonlinearities of DAST. The travelling cell method lead to c-plate single crystals of $2 \times 2 \times 0.02 \text{ mm}^3$. The undercooled flow cell method lead to $3 \times 3.7 \times 0.04 \text{ mm}^3$ monocrystals. $2 \times 2 \times 0.03 \text{ mm}^3$ single crystals were grown by solution epitaxial growth.

Molecular engineering for the optimization of microscopic optical properties and crystal engineering for non-centrosymmetric packing are foregoing steps to growth engineering and final integration. These are all decisive steps to reach any prototypical device. We here concentrate on the growth engineering since the two first steps have been successfully carried out until now, providing excellent nonlinear optical efficient materials for potential integration [1]. In particular, one will have to optimize the growth methods and conditions for a bulk- and defect-free monocrystal. Tailored two-dimensionnal growth techniques have to be developed for organic thin film growth. We focus on the DAST / methanol system, because of the exceptionally high nonlinearities of DAST [2].

Already-existing planar growth methods may start with simple mechanical treatment of a bulk defect-free crystal, like cutting & polishing, or etching. Direct methods especially efficient for highly concentrated solutions and melts are the shear method and the two-dimensionnal Bridgman-Stockbarger growth. This may be followed by a planar refinement step, in the case of meltable material. Finally, isothermal solvent evaporation in between two plates showed good results for planar growth from the solution.

We present seven new methods to grow planar organic crystalline thin films from solutions containing less than 5% of solute, which is the case of the DAST/methanol solution.

The two-dimensional ΔT method is basically the same as the common ΔT bulk growth, but confined to a two-dimensionnal space. The bottom of a thin hermetic cell is placed in an aluminium holder at 42°C . The rest of the cell is surrounded with an air bath at 36°C .

The travelling cell method showed very good results. A thin hermetic cell is moved through a heating element at 50°C . The whole set-up is in a stabilized environment at 36°C . The solute concentration within the cell is at its highest when inside the local heater. The cell is then undercooled as soon as it has passed this element. Growth occurs then mainly by thermal undercooling but also to some extend by solutal undercooling. Figure 1(a) shows the cell after the experiment. A high-quality monocrystal is shown in figure 1(b).

The capillary and the ΔT aided capillary methods consist of placing two substrates in a closed system filled with 2 cm saturated solution. The solution flows in between the

Poster Session II

substrates by capillary force. Nucleation occurs by slow cooling and further growth occurs by slow solvent evaporation. If the system is placed in a temperature gradient, solute supply is eased. The largest single crystals were in the range of $2 \times 6 \times 0.02 \text{ mm}^3$.

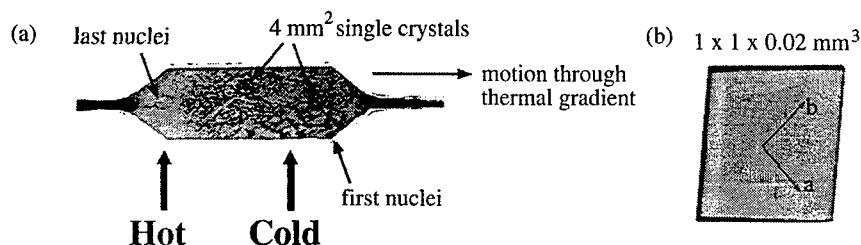


Figure 1: (a) Growth cell after the travelling heater zone refiner experiment, (b) Microscope picture of a high-quality single DAST crystal in between crossed polarizers.

In the **undercooled flow cell** method, a just saturated solution flows through a thin hermetic cell. A micropump provides a slow enough (1 cm/s) constant flow rate. The cell is locally undercooled, implying a local undercooling and therefore local controlled nucleation. The largest crystal grown by this method was of $3 \times 3.7 \times 0.04 \text{ mm}^3$.

Fabrication using laminar flow take advantage of the fact that streams in microcapillaries are laminar. The interface of two different streams flowing in the same capillary (in the same direction) stays planar. Thin films are expected to grow at the planar interface between a DAST/methanol stream and a pure methanol stream.

Growth by **solution epitaxy** requires on a surface-treated quartz substrate (see figure 2(a)). The substrate was placed in the saturated solution and the steering force to growth was slow cooling. Large thin crystals were obtained, as illustrated in figure 2(b).

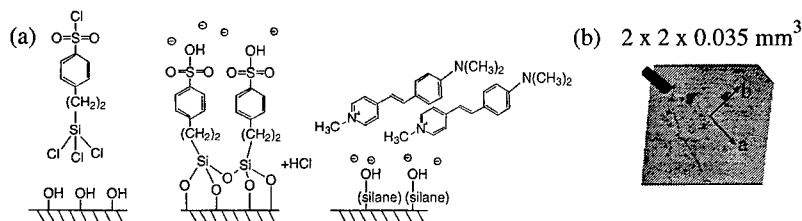


Figure 2: (a) The surface of a quartz substrate is first treated with 2-(4-chlorosulfonylphenyl)-ethyltrichlorosilane molecules. The acidic substrate is then brought in contact with pure 4'-dimethylamino-N-methyl-4-stilbazolium (the cation of DAST). (b) Microscope picture with crossed polarizers of a 4 mm^2 DAST single crystal grown by solution epitaxy.

References

- [1] S.R. Marder, J.W. Perry, Ch.P. Yakymyshyn, *Chem. Mater.*, 1137-1147 (1994).
- [2] U. Meier, M. Bösch, Ch. Bosshard, F. Pan and P. Günter, *Journal of Applied Physics*, **83** (7), 3486-3489, (1998)

Observations of 180° polar domains in molecular crystals using phase-sensitive second harmonic microscopy

P. Rechsteiner and J. Hulliger

*Department of Chemistry and Biochemistry, University of Berne,
Freiestrasse 3, CH-3012 Berne, Switzerland*

The non-destructive characterisation of polar materials with designer properties is a fundamental target of contemporary materials research. New types of polar molecular materials resulting from the co-crystallisation of perhydrotriphenylene (PHTP) with nonlinear optical guest molecules form a nanotube-like crystal architecture. A stochastic mechanism of alignment, more generally described by a Markov chain model, produces crystals composed of adjacent macro-domains featuring an opposite polarisation. Phase-sensitive second harmonic generation microscopy (PS-SHGM) allowed to distinguish between the macro-domains of μm thin molecular crystals using the interference effect between the second harmonic waves of the sample and a reference crystal. The nonlinear optical characterisation is in agreement with a precedent analysis using scanning pyroelectric microscopy (SPEM).

1. Introduction

Recently, we have introduced a *general principle* of spontaneous polarity formation in molecular crystals [1]. A stochastic process of alignment of dipolar components during crystal growth has been identified as the driving-force for producing polarity. In this general model the phenomenon of polarity formation is related to the degree of orientational disorder of dipole moments within a topologically organised structure of aligned molecules. A feasible representation of the basic principles are given by channel-type inclusion compounds e.g. perhydrotriphenylene (PHTP) and prolate A- π -D nonlinear optical guest molecules (A and D are acceptor and donor substituents respectively, attached to linear, π -conjugated frameworks). In the host-guest crystal architecture, PHTP host molecules pack into columnar stacks forming parallel channels. The guests align as molecular chains within the well separated channels. As a result of the stochastic growth mechanism, needle-like crystals (channels parallel to the needle axis), consist of two adjacent macro-domains with opposite polarity. The bipolar structure of PHTP inclusion crystals is in agreement with measurements using scanning pyroelectric microscopy (SPEM, see Ref. [1]). As a result of the nature of collinear intermolecular interactions of guest molecules in channels, A or D group preferably cover the capping faces of the needles. When using A = -NO₂, theory predicts, that A groups cover the surface. The polarity of capping faces as determined by pyroelectric measurements is in agreement with theoretical predictions using realistic values for interaction energies.

2. Nonlinear optical proof for a bipolar growth mechanism

Optical techniques able to visualise 180° domains are of importance for example for the fabrication of quasi-phase matched devices. In this respect, second harmonic microscopy (SHGM) has demonstrated its effectiveness as a non-destructive and non-contact probing technique for the characterisation of a number of materials showing domains within e.g. thin layers. Phase-sensitive second harmonic microscopy (PS-SHGM) is of particular interest in order to identify the polarity of domains [2]. In principle, domain mapping is

Poster Session II

achieved by using the interference effect between the SH waves from a sample and from a single-domain SHG plate. Interference between SH waves converts the phase information into an SH contrast.

Here, for the first time we present PS-SHGM results from organic single crystals. We have used a congruently melting inclusion compound PHTP-DMNA (DMNA: N,N-dimethyl-p-nitroaniline). Thin layer single crystals have been prepared from the melt placed between glass plates to provide a uniform thickness below the characteristic coherence length l_c (sample thickness $\approx 1-2 \mu\text{m}$). A change in the sign of the effective NLO coefficient d_{333} (channel direction) when considering each of the domains, is related to a phase shift of π for SH waves emerging from either domains. The phase difference can be imaged (see Figure 1) using the interference effect between SH waves from the sample and those from a uniform SHG reference plate. In order to obtain a high contrast, an optically linear phase plate is inserted between the reference plate and the sample. For testing the conditions for l_c , a Maker fringe experiment was carried out. The thickness was found to be below the coherence length.

In agreement with scanning pyroelectric microscopy for crystals grown from solution (see Ref. [1]), the present procedure using PS-SHGM opens up the possibility of imaging 180° twinning in thin PHTP-DMNA crystals. Theory predicts, that only a few attachment steps along the growth direction are necessary in order to reach a constant average polarity. This is in agreement with the observed, rather constant SH intensity seen across both domains (Figure 1). Future work will concentrate on a qualitative use of PS-SHGM to identify the absolute polarity of unknown samples by comparison with materials of known polarity.

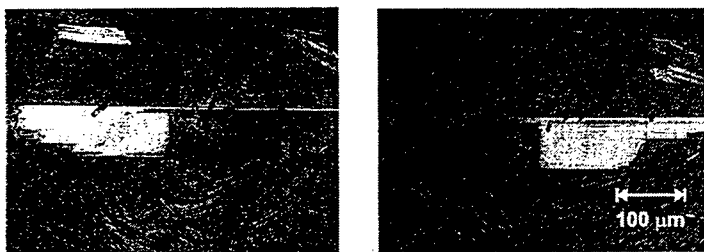


Figure 1: Phase-sensitive second harmonic microscopy: To the left the SH intensity of one domain is enhanced while being attenuated at the other side. In the right picture SH light is emitted from the oppositely orientated domain.

References

- [1] J. Hulliger, S. W. Roth, A. Quintel, "The prediction and production of polarity in crystalline supramolecular materials", in D. Braga et al. (eds.), *Crystal Engineering: From Molecules and Crystals to Materials*, Kluwer Academic Publishers, NATO Series C 538, 349-368 (1999).
- [2] Y. Uesu, "SHG Microscope: Principle and its Application", *J. Korean. Phys. Soc.* **32**, S461-S463 (1998).

Organic nanocrystals in sol-gel glasses: a new type of nonlinear organic material

I. Wang, P. L. Baldeck

*Laboratoire de Spectrométrie Physique, Université J. Fourier,
CNRS (UMR 5588) BP 87, 38402 Saint Martin d'Hères cedex, France.*

N. Sanz, A. Ibanez

Laboratoire de Cristallographie, CNRS BP 166, 38042 Grenoble cedex 09, France.

We have designed a new type of composite materials for optical applications: organic nanocrystals embedded in sol-gel glasses. The nanosized control of crystallization allow us to obtain optical grade samples with very high (>30wt.%) concentrations of active molecules. Depending on the preparation method, we can reproducibly obtain bulk or thin film samples, with monodisperse sizes as small as 20 nm. Currently, we have succeeded in designing nanocomposite materials with molecules selected for their second harmonic efficiency (oriented nanocrystals) and their nonlinear absorption at visible wavelengths (for optical power limiting applications).

We have prepared a new type of hybrid organo-mineral material that is composed of organic nanocrystals embedded in sol-gel glasses [1]. By this technique, crystals of different organic molecules can be included in an inorganic matrix that affords better stability and easier elaboration. The resulting material is solid, transparent, and highly concentrated in active compounds (e.g. nonlinear, fluorescent, photorefractive, photochrome, or photomagnetic) that can fulfill one or several functions. In this paper we report on materials that have been elaborated for their nonlinear optical properties. Recent results in second harmonic generation and optical power limiting are presented.

Preparation method

Monodisperse crystallization proceeds in two steps: instantaneous nucleation and controlled growth of the nuclei. The first step is performed at very high supersaturation (200 to 300%) by an abrupt lowering of the temperature. The second step occurs in the gel pores which act as nanoscale growth reactors. Growth is inhibited by both the low diffusion rate expected in this medium and the small size of gel pores. This method provides monolithic transparent xerogels with nanocrystals size ranging from 20 nm to 80 nm, depending on the preparation conditions. We have extended the technique to the elaboration of thin films by spin coating.

Second harmonic generation with oriented nanocrystals

For applications based on the second order nonlinear response, such as electro-optic modulation and second harmonic generation (SHG), it is necessary to create a noncentrosymmetric media. This entails that we should be able to compel nanocrystals' orientation during the growth step. Recently, we have prepared nanocrystals of N-(4-nitrophenyl)-(L)-prolinol (NPP). During the growth process, a 16 T magnetic field was applied to achieve orientation. A weak SHG was obtained from these samples. Figure 1 shows how the SHG efficiency depends on the linear polarization angle of the laser beam ($\lambda = 1.04\mu\text{m}$ and propagation perpendicular to the direction of the applied magnetic field). This polarization dependency indicates a strong $\chi^{(2)}$ anisotropy that confirms the nanocrystals' orientation. Orientation under electric field using the corona technique is also in progress.

Poster Session II

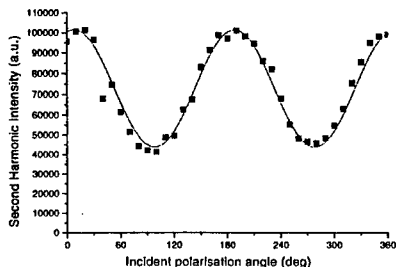


Figure 1: Polarization measurement on SHG of NPP nanocrystals

Optical power limiting

The development of optical power limiting devices requires solid material displaying high nonlinear absorption and polarization-independent response. Our nanocomposite material appears to be especially well-fitted to this application since high concentrations of active compound can be included in the gel and random dispersion of the nanocrystals ensures the isotropic response of this material. We have grown nanocrystals of stilbene3 that exhibits a strong nonlinear absorption in solution. Typical optical limiting curves for a sol-gel glass doped with stilbene3 to 30% in weight are displayed in figure 2.

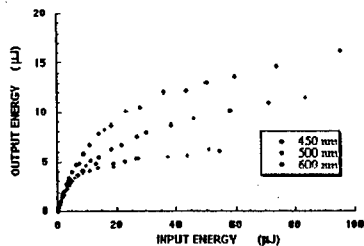


Figure 2: Optical limiting curves of stilbene3 nanocrystals recorded at several wavelengths

The optical power limitation effect is broadband over most of the visible range. These results are encouraging, but stilbene3 nanocrystals are slightly colored and the output energy is still too high for implementation in practical devices. We are testing new molecules to improve these features.

References

[1] A. Ibanez, S. Maximov, A. Guiu, C. Chaillout and P.L. Baldeck, *Advanced Materials* **18**, 1540-1543 (1998).

**Phase-matching properties of
(S)-3-Methyl-5nitro-N-(1-phenylethyl)-2-pyridinamine**

M.Rini, G.P. Banfi, V. Degiorgio
*Istituto Nazionale per la Fisica della Materia and Dipartimento di Elettronica,
Università di Pavia, via Ferrata 1, 27100 Pavia, Italy*

J.N. Sherwood
*Department of Pure and Applied Chemistry
University of Strathclyde, Glasgow, G1 1XL, Scotland, UK*

From refractive indices measurements obtained by the minimum deviation method we derive a set of Sellmeier coefficients for (S)-3-Methyl-5-nitro-N-(1-phenylethyl)-2-pyridinamine (S3MeMBANP). By using our Sellmeier set, whose accuracy has been confirmed by a second harmonic generation experiment, we calculate the phase matching properties of S3MeMBANP for all the principal planes.

The molecular organic crystal MBANP, (S)-5-nitro-N-(1-phenylethyl)-2-pyridinamine, is a material which was developed since the early 1980's and possesses strong second order optical nonlinearities, but the disposition of the dielectric axes and refractive indices is not particularly favourable to the production of large phase-matched SHG signals in the near infrared [1]. In the past years, a number of derivatives of MBANP have been synthesised in order to investigate if compounds similar to MBANP may crystallise in more advantageous ways [1]. Among them, one of the most promising is S3MeMBANP, (S)-3-Methyl-5-nitro-N-(1-phenylethyl)-2-pyridinamine, a methyl-substituted derivative of MBANP, identified as having large second-order d coefficients: d_{14} , d_{25} , $d_{36} \cong 20 \text{ pmV}^{-1}$ [1]. Ease of crystal growth is also an attractive feature of S3MeMBANP and, in general, of this family of derivatives of MBANP [2]. The availability of large, high quality, single crystals of S3MeMBANP allowed us to carry out a linear and nonlinear characterisation of this crystal for almost the entire transmission range of the crystal. The measurements were taken by mean of a tunable source, a β -barium borate (BBO) type-I optical parametric oscillator (OPO) synchronously pumped by a frequency doubled, 30 ps active/passive mode-locked, 10 Hz, Nd:YAG laser.

By using two prisms of S3MeMBANP with different cut we measured the three principal refractive indices n_x , n_y and n_z by the minimum deviation method. The measured values were fitted to a four-parameter, one-pole Sellmeier equation. The values of the coefficients we obtained by a least-square fitting are reported in the following table:

Coefficients of the Four-Parameter Sellmeier Equation

$$n_i^2 = A + \frac{B\lambda^2}{\lambda^2 - C} - D\lambda^2$$

	A	B	C/ μm^2	D/ μm^{-2}
n_x	2.48696	0.15890	0.16193	0.01138
n_y	2.33345	0.60733	0.15030	0.01342
n_z	2.54969	0.20019	0.15513	0.02693

This set of coefficients for the Sellmeier equations should be regarded as valid in the range of wavelengths from 500 to 1600 nm, where the measurements have been taken.

Poster Session II

The accuracy of our refractive indices measurements has been confirmed by a second harmonic generation (SHG) experiment in the xy principal plane of the crystal. The PM in this plane is of type I. The cut of the samples did not allow SHG on the yz plane. The internal PM angle θ , measured as function of the wavelength of the fundamental beam λ is plotted in Fig. 1. The prediction given by our Sellmeier set, plotted in solid line, shows a good fitting of the data.

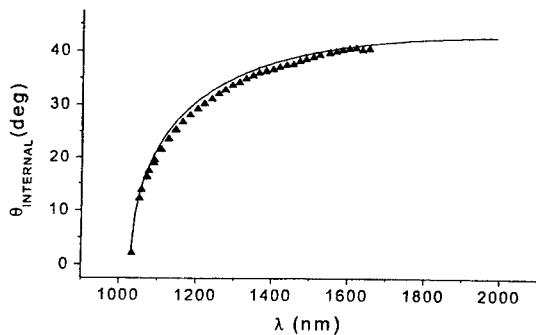


Fig 1. The dependence of the phase matching angle θ on the incident wavelength λ for SHG in S3MeMBANP with type-I "eo" phase-matching in the xy plane. The solid curve is calculated from our Sellmeier formula.

By using our set of Sellmeier equations, whose accuracy in the wavelength range of interest has been confirmed by the SHG experiment, we calculate the complete phase-matching criticality curve, reported in Fig. 2, showing the dependence of phase-matching wavelength on angle for all the principal planes of the crystal.

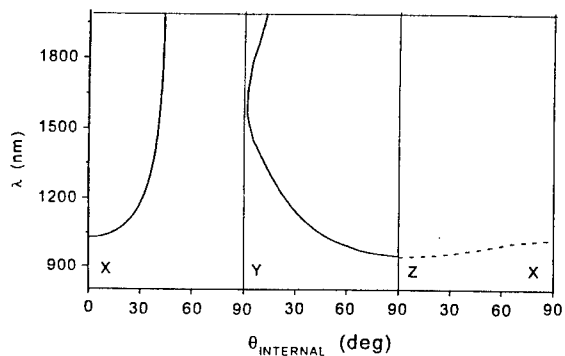


Fig 2. Phase matching criticality curves, as predicted by our Sellmeier set. Only type-I PM is possible. The dashed line represents a symmetry-forbidden interaction. The effective d coefficient vanishes under angle-noncritical PM conditions.

References

- [1] R.T. Bailey, F.R. Cruickshank, D. Pugh, J.N. Sherwood, P. J. Langley, J.D. Wallis. To be published.
- [2] S. Lochran, R.T. Bailey, F.R. Cruickshank, D. Pugh, J.N. Sherwood, G.S. Simpson, J.D. Wallis, P.J. Langley, "Refractive Indices of the Optically Nonlinear Organic Crystal (S)-3-Methyl-5-nitro-N-(1-phenylethyl)-2-pyridinamine", *J. Pys. Chem. A* 1998, 102, 8520-8525.

ANHARMONISITY EFFECTS IN SPECTRA OF ALCOHOLS.

N.A. Atamas ^{a)}, A.M. Yaremko ^{b)*}, L.A. Bulavin ^{a)}, V.E. Pogorelov ^{a)},
S. Berski ^{c)}, Zd. Latajka ^{c)} H. Ratajczak ^{c)} and J. Leszczynski ^{d)}

- a) Department of Physics, Kiev Taras Shevchenko's University : 6, Glushkov
prospect, Kiev-252127, Ukraine
- b) Institute of the Semiconductor Physics of NAS of Ukraine : Prospect Nauki,
45, Kiev 252028, Ukraine
- c) Faculty of Chemistry, University of Wroclaw, 14, F. Joliot-Curie, 50-383,
Wroclaw, Poland.
- d) Department of Chemistry, Jackson University: O. Box 17910, Jackson, MS
39217, Jackson, MS, USA

The vibrational Raman spectra of liquid alcohols (methyl, ethyl, buthyl and amil) were studied experimentally at room temperature in wide frequency region (1000- 4000) cm^{-1} . Special attention was paid to investigation of high frequency region ($\geq 3000\text{cm}^{-1}$) containing the OH-vibration. The numerical ab-initio calculations of frequencies and corresponding intensities of transitions of the molecules studied substances were made. It is shown that features of spectrum in the region of $\sim 3000 \text{ cm}^{-1}$ and appearance of very broad bands in this region can be explained in the framework of Fermi resonance and very strong interaction of hydrogen bond vibrations with low frequencies vibrations of own molecule.

The vibrational spectra of alcohols are investigated during many years. These spectra are enough complicated what due to both as many atomic structure of corresponding molecules so anharmonic effects giving rise to mixing of vibrations. In particular very important for structure of high frequency region the occurrence of the hydrogen bond vibrations. Beside for many alcohol molecules overtones of some vibrations of CH_3 group are located very close to the fundamental vibrations CH_3 and CH_2 groups (the same symmetry) what result in the Fermi resonance (FR) effects.

Poster Session II

Important is also intermolecular interaction which responsible for some structural features of condensed phase. The last allows use these objects as model ones at study the formation of mesophases (for example the plastic crystals).

Very positive factor, however, for studying the optical properties of alcohols can be the homological series, which is generated by the different alcohols $\text{CH}_3(\text{CH}_2)_n\text{OH}$ ($n=0,1,2,\dots$) elements of which is differed only by addition to chemical formulae the CH_2 group. Therefore studying the spectroscopical properties of such homological series we can make **important conclusion about mechanisms** responsible for forming of spectrum.

The enough detail spectral investigation were made up to now only for **methyl** and **ethyl** alcohols ($n=0,1$). For members with $n>2$ the optical information is poor.

Therefore in present communication we fulfill experimental and theoretical investigations for more wide row of alcohols (methyl, ethyl, buthyl and amil)

- We have made *ab-initio* calculations of frequencies of the corresponding molecules;
- We have studied the influence of anharmonic interaction and FR effect on the shape band of high frequency vibrations.
- Special attention was spared to position of $\nu\text{-OH}$ vibration and its shape band which generated by strong interaction with the low frequency vibrations of complex molecules.

CONCLUSION

- We have shown that complication of Raman spectra for series alcohols depends not only on the member of atoms in molecule but also due to anharmonic interactions giving rise to such effects as:
 - Fermi resonance;
 - transformation $\nu\text{-OH}$ vibration into broad band, shifted significantly into low frequency region and overlapping with other part of spectrum.

REFERENCES

1. B. Schrader, Raman/ Infrared Atlas of Organic Compounds, (Second Editions), Germany, 1989
2. H. Ratajczak, A.M. Yaremko, Chem. Phys. Letters, 243 (1995) 348
3. D.I. Ostrovskii, H. Ratajczak, A.M. Yaremko et al., Optics and Spectroscopy, 78, N 3, (1995) 378.

Photosensitive Media on the Base of Bacteriorhodopsin

I. K. Bandrovskaya, Z. I. Batori-Tartzi, A. A. Grabar, O. I. Korposh,
N. P. Frolova and J. P. Sharkany

*Institute of Solid State Physics and Chemistry of Uzhgorod State University
Pidhirna 46, 294000, Uzhgorod, Ukraine*

It is demonstrated that the kinetic of bacteriorhodopsin's photocycle can be modified by introduction of triethanolamine in a composition of a bacteriorhodopsin film. Investigation of optical parameters of BR films in gelatin matrix with TEA shows that light sensitivity increased and the photocycle of BR slows in two order of magnitude. The optimal concentration of additive were determined on the base of optical absorption kinetics and holographic measurements.

Bacteriorhodopsin (BR) is a retinal protein found in the purple membrane of *Halobacterium halobium*. Absorption of light energy by light-adapted BR initiates a photochemical cycle of reactions. BR undergoes through several spectroscopy distinct intermediate states (K, L, M, N, O) and translocated one proton across the membrane [1]. The transition of BR570 to a most long living intermediate M412, is most important for applications. It is known that optical properties of BR films can be changed by addition of different chemical additives or with modification of the structure of BR molecules. Partially, it is possible to slow the kinetic of BR photocycle with additives such as guanidine-hydrochloride [2] or triethanolamine, dodecyl trimethylammoniumbromide [3]. In the present work we have focused on chemically enhanced films containing the BR, triethanolamine (TEA) in gelatin (GE) matrix.

Purple membranes were obtained from *Halobacterium halobium* by the well-known method [4]. The samples were prepared by drying of suspension of BR, BR + GE and BR+GE +TEA on a clean glass surface at room temperature. The thickness of BR film was determined by an interference method $\sim 40 \mu\text{m}$, the optical density OD ~ 1 . The optical kinetic measurements were performed at 410 nm on different composition BR film, excited by second harmonic of YAG:Nd laser (532 nm) with energy up to 10 mJ/cm^2 and pulse duration 6 ns. It was found that gelatin does not change the photocycle of BR. The light absorption kinetics of dried BR and BR+GE films are similar. Adding TEA (200 molecules TEA/BR) to BR+GE increments the half-life time of intermediate M412 and the amplitude of absorption increased. The both amplitude and half-time of decay as a function of TEA/BR showed a saturation at a ratio between 200 and 250 (Figure 1). Further increasing of TEA concentration leads to decreasing of above parameters.

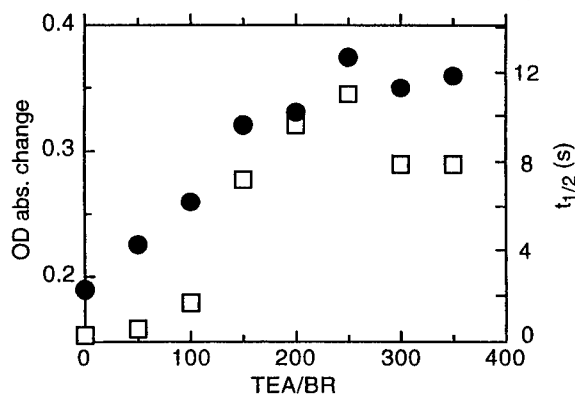


Figure 1. Optical density changes of the dried BR+TEA+gelatin films. measured at 410 nm after laser (532 nm) pulse as a function of TEA content. Circles - amplitude, squares - half-time of the excited state.

Obtained films of BR+TEA+gelatin were studied also as holographic media in two- and four-beam schemes. It was observed that the hologram writing can be realized using He-Ne laser irradiation (633 nm), partially, with ortogonally polarized beams, and the decay kinetic in various modified samples strongly depends on the light intensity.

References\

- [1] M. P. Krebs, H. G. Khorana, "Mechanism of light-dependent proton translocation by bacteriorhodopsin", *J. Bacteriol.* **175**, 1555 -1560 (1993).
- [2] Y. Yoshida, K. Ohno, Y. Takeuchi, Y. Kagawa, "Prolonged lifetime of the 410-nm intermediate of bacteriorhodopsin in the presence of guanidine hydrochloride", *Biochem. Biophys. Res. Commun.* **75**, 1111-1116 (1977).
- [3] I. K. Bandrovskaja, Y. D. Shershun, Z. I. Batori-Tartsi e.a., "Special photochrome material on the base of bacteriorhodopsin", *SPIE Proc.* **3055**, 91-94 (1997).
- [4] D. Oesterhelt, W. Stoeckenius, "Isolation of the cell membrane of *Halobacterium halobium* and its fractionation into red and purple membrane", *Method Enzymol.* **31**, 667 - 678 (1974).

Investigation of the Third-order Optical Susceptibility of Chromophores Through Broadband Electrooptic Spectroscopy

B. K. Canfield, R. J. Kruhlak, and M. G. Kuzyk
Nonlinear Optics Laboratory
Dept. of Physics, Washington State University
Pullman, WA 99164-2814 USA

We present an investigation of the nonlinearity of several chromophores through quadratic electroabsorption (QEA) and electrooptic measurements on thin film samples. The practicality of the experimental setup used, a Mach-Zehnder interferometer, is discussed. The QEA data obtained is fitted to the inhomogeneously broadened electronic transition theory. This theory enables us to determine the real part of the third-order susceptibility from the electroabsorption data which we can then compare to the susceptibility experimentally determined from the electrooptic data to characterize the molecular excited states.

Introduction

The identification of effective nonlinear chromophore dopants for polymer optical communications fiber and waveguide devices is of considerable interest. Nonlinear guest-host polymer systems are relatively inexpensive and easy to fabricate compared to their glass counterparts. We present an investigation of the nonlinearity of several chromophores through quadratic electroabsorption (QEA) and electrooptic measurements on thin film samples throughout the visible and near infra-red wavelengths.

Experiment

The electrooptic experiments are performed using a Mach-Zehnder interferometer, as shown in Fig. 1. The laser source is a Ti:Sapphire ring laser tunable from 705 nm to 1100 nm, and with active frequency stabilization to less than 500 KHz rms. The reference arm contains a glass slide driven by a stepper motor under computer control to adjust the phase of the interferometer. A sinusoidal modulation voltage at a frequency Ω much lower than optical frequencies is applied to the thin film sample. The intensity of the 2Ω Fourier component of the transmitted beam, $I_{sig}^{2\Omega}$, is then measured with a photodetector and lock-in amplifier (not shown). Using the interferometer output intensity, I_{out} , measured by chopping the beam incident on a second photodetector (lock-in amplifier also not shown), the magnitude of the third-order electrooptic coefficient, s_{1133} , and hence $|\text{Re } \chi^{(3)}|$, can be determined from the experimental data [1].

Infrared QEA measurements can also be performed using the same Mach-Zehnder setup with a few simple modifications. We place a third photodetector in the reference arm following the first beamsplitter (shown in shaded gray) for the incident intensity measurement. The sample absorption due to the applied modulation voltage can then be measured by using the original two photodetectors from the electrooptic experiment. In place of the interferometer output I_{out} , we measure the transmitted intensity with no applied voltage, I_0 . The other detector still measures the 2Ω Fourier component. The data thus obtained is fitted to the inhomogeneously broadened electronic transition theory to model the excited states of the chromophore molecules and determine $\text{Im } \chi^{(3)}$. Using Kramers-Kronig relations, we can also calculate $\text{Re } \chi^{(3)}$, which we can then compare

Poster Session II

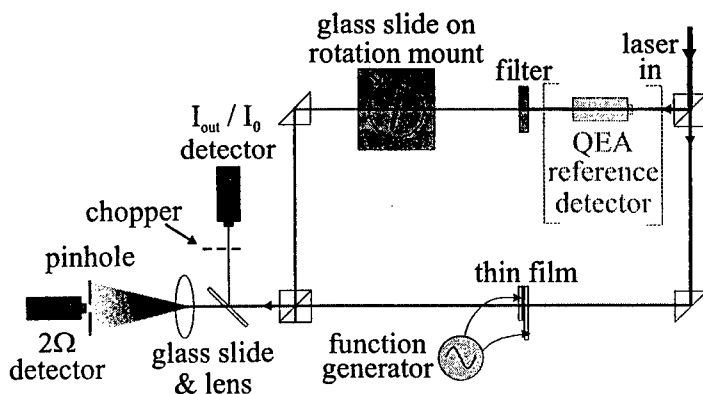


Figure 1: Mach-Zehnder interferometer used for electrooptic and QEA measurements.

to the electrooptic measurement results. A similar setup using a xenon arc lamp and monochromator as the light source is used to perform QEA measurements in the visible region.

Discussion

The Mach-Zehnder interferometer coupled with the tunable IR laser source provides a versatile experimental setup for investigating the nonlinearity of various chromophores. Our preliminary results are encouraging, and in the case of ISQ, show good agreement with previous investigations carried out by Kuzyk *et al* [1]. The electrooptic experiments may also be performed using electrooptic fibers (dye-doped polymer fibers with electrodes along the core) [2] in place of the thin films. In fact, the thin film thickness, and hence electrode separation, averages $4 \mu\text{m}$. However, a 20 cm-long single-mode ($8 \mu\text{m}$ diameter core) electrooptic fiber would have an electrode separation of about $40 \mu\text{m}$. Since the electrooptic signal is proportional to the ratio of interaction length to electrode separation, the electrooptic fiber should yield a signal enhancement factor of about 5000 over a thin film.

References

- [1] M. G. Kuzyk, J. E. Sohn, C.W. Dirk, "Mechanisms of quadratic electro-optic modulation of dye-doped polymer systems," *J. Opt. Soc. B* 7, 842-58 (1990).
- [2] D. J. Welker, J. Tostenrude, D. W. Garvey, B. K. Canfield, and M. G. Kuzyk, "Fabrication and characterization of single-mode electro-optic polymer optical fiber," *Opt. Lett.* 23, 1826-8 (1998).

Second-harmonic generation in chiral smectic liquid crystals

M. Copic, I. Drevensek Olenik, and M. Zgonik

*University of Ljubljana, Dept. of Physics, Jadranska 19, SI-1000 Ljubljana
and J. Stefan Institute, Ljubljana, Slovenia*

Nonlinear optical second harmonic generation in helically twisted SmC* liquid crystals has some interesting properties. The spatial periodicity of the helical structure allows several special phase-matching situations in which the optical wave-vector mismatch is compensated by the vector of the helical pitch. In addition, spatial resonance can appear when the second harmonic wave is close to the edge of the Bragg reflection band. These resonances can substantially enhance frequency doubling for a given length of SmC* material.

During the last decade several techniques have been developed to construct various periodic dielectric structures on the scale of optical wavelengths. These media, known as photonic band materials, exhibit optical properties very similar to the properties of electrons in periodic lattices. Their optical dispersion spectrum has a characteristic band structure with gaps at certain photon energies. Chiral liquid crystalline phases represent an example of inherent periodic dielectric structures with a smooth continuous modulation of the optical properties. The set of reciprocal lattice vectors needed to expand the modulation into Fourier components is small and the optical eigenmodes are given with relatively simple analytic expressions. This allows the analysis of linear and nonlinear optical processes in manageable form.

In the equilibrium bulk phase, the SmC* liquid crystal has a superstructure in which the molecular tilt and the spontaneous electrical polarization form a helix in the direction normal to the smectic layers. The dispersion relation for light propagating along the helix direction has two branches which are at most frequencies separated by approximately twice the grating-vector of the helix q . In a small frequency interval one of the branches has a gap in which the corresponding light wave cannot propagate, but is Bragg reflected. The phase-matching condition for SHG can include a multiple of the grating-vector providing several new possibilities.

Optical second harmonic generation (SHG) in the ferroelectric SmC* phase of liquid crystals is interesting both for fundamental studies and for applications.

For propagation along the helical axis these phenomena were discussed in previous papers [1, 2, 3, 4, 5]. The possibility of resonant SHG enhancement in periodic medium was also discussed in Refs. [6, 7]. Enhanced generation of SHG around the Bragg reflection band in SmC* liquid crystals was also experimentally observed [8, 9, 10]. This poster presents the analysis of a general case of SHG or sum frequency generation in the nondepletion approximation. The problem can be treated analytically for the case of propagation along the helical axis. Using coupled wave theory good analytical solution can also be obtained for the approximate ordinary waves propagating at large angles with respect to q direction [11]. In the intermediate case of propagation at moderate angles the reflection bands at q and $2q$ overlap and the solution is more complex since in the general case 12 coupled waves must be taken into account. One prominent feature of the optical SHG in the helical SmC* phase is the interference oscillation of the second-harmonic intensity which originates primarily from the helical modulation and not from

Poster Session II

the refractive index dispersion which is the case in homogeneous media. Close to the edge of the selective reflection band these oscillations lead to an enhancement of the SHG conversion efficiency.

For applications, materials with large optical anisotropy and large tilt should be used. The molecular hyperpolarizability of some materials forming the SmC* phase is relatively large. With thick and well oriented samples of the appropriate helical pitch practical SHG devices could be built.

References

- [1] M. Copic and I. Drevensek Olenik, *Liq. Cryst.* **22**, 233 (1996).
- [2] I. Drevensek Olenik and M. Copic, *Phys. Rev. E* **56**, 581 (1997).
- [3] I. Drevensek Olenik and M. Copic, *Mol. Cryst. Liq. Cryst.* **320**, 265 (1998).
- [4] S. V. Shiyanovskii, *Ukr. Fiz. Zhurn.* **27**, 361 (1982).
- [5] S. V. Shiyanovskii, *Proc. SPIE*, **2795**, 2 (1996).
- [6] V. A. Belyakov and N. V. Shipov, *Phys. Lett.* **86A**, 94 (1981).
- [7] V. A. Belyakov and N. V. Shipov, *Zh. Eksp. Teor. Fiz.* **75**, 1589 (1987) [*Sov. Phys. JETP* **55**, 647 (1982)].
- [8] K. Kajikawa, T. Isozaki, H. Takezoe, and A. Fukuda, *Jpn. J. Appl. Phys.* **2**, Lett. **31**, L679 (1992).
- [9] T. Furukawa, T. Yamada, K. Ishikawa, H. Takezoe, and A. Fukuda, *Appl. Phys. B* **60**, 485 (1995).
- [10] J. G. Yoo, S. W. Choi, H. Hoshi, K. Ishikawa, H. Takezoe, and M. Schadt, *Jpn. J. Appl. Phys.* **2**, Lett. **36**, L1168 (1997).
- [11] V. A. Belyakov and M. Copic, *Mol. Cryst. Liq. Cryst.* **328**, 151 (1999).

Modelling and characterisation of nonlinear materials for optical limiting. Mononuclear and binuclear platinum ethynyls

Anders Eriksson

*Department of Physics and Measurement Technology, Linköping University
S-581 83 Linköping, Sweden*

Cesar Lopes, Mikael Lindgren and Sören Svensson

*Defence Research Establishment, Department of Sensor Technology
PO Box 1165, S-581 11 Linköping, Sweden*

Tim McKay and Julianne Davy

*Electronic Warfare Division, Defence Science and Technology Organisation
PO Box 1500 Salisbury South Australia 5108, Australia*

Platinum ethynyls for optical limiting applications were synthesised and optically characterised. Both mononuclear and binuclear compounds were investigated. The Z-scan technique was used to characterise third order optical nonlinearities. Optical limiting measurements in a f#5 system have also been performed. A previously reported modelling tool relying on a Gaussian decomposition of the laser beam was used to model the experiments. This numerical tool, which allows for non-Gaussian laser beams and thick samples exhibiting both nonlinear refraction and absorption, was used to model the optical limiting experiments.

A number of different platinum ethynyls have been synthesised for optical limiting purposes. Mononuclear platinum ethynyls have shown some interesting features; which includes acting over a large range of pulse lengths, and showing evidence of being a broadband optical limiter[1]. Both mononuclear and binuclear compounds (Fig. 1) with different ligands were synthesised in order to improve the nonlinear effect as well as stability and solubility.

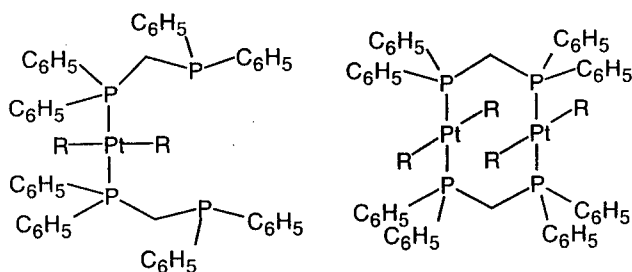


Figure 1. Mononuclear and binuclear platinum ethynyls.

Poster Session II

The capability for protecting an optical sensor was investigated in a test-bed where a top-hat laser beam was used in a f#5 geometry. The focus was centered to the middle of a 2 mm cell. The sample was several Rayleigh lengths thick, and the irradiance was much lower at the surface than at the focus. The laser was a frequency-doubled YAG operating at a wavelength of 532 nm. The pulse length was 5 ns. The laser energy was varied from below μJ to some 150-200 μJ . Fig. 2 and fig. 3 show the optical limiting for the samples.

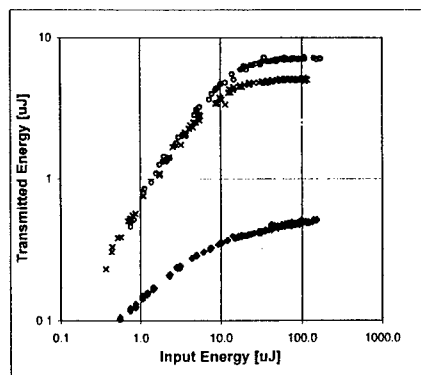


Figure 2 Optical limiting with SiNC (\diamond) and a mononuclear platinum ethynyl. (\circ) and (\times) are the same but with 50 mM and 100 mM concentrations respectively.

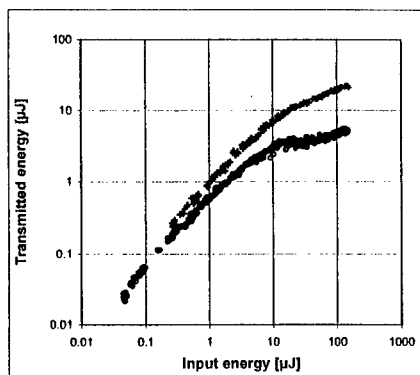


Figure 3. Two different solutions of platinum ethynyls. (+) is a dinuclear compound (5 mM in THF) while (\circ) is mononuclear (100 mM in CHCl_3).

The linear transmission, including the cell, was only 40 % at 532 nm for the sample with Silicon-Naphthalocyanine (SiNC), while the linear transmissions for the other samples shown in the figure were between 70 and 90 %.

A previously reported numerical modelling tool for Z-scans with thick samples and nonlinear absorptive and refractive optical properties [2] was used to model the optical limiting measurements.

References

- [1] J. Staromlynska, T. J. McKay, J. A. Bolger and J. R. Davy, "Evidence for broadband optical limiting in a Pt:ethynyl compound," *J. Opt. Soc. Am.* **B15**, 1731-1736 (1998)
- [2] A. Eriksson, M. Lindgren, S. Svensson, T. Bubner, T. McKay and J. Staromlynska "Numerical modeling of z-scans of thick nonlinear absorbers," *SPIE* **3472**, 144-150 (1998)

Electronic defects and conjugation length in mesoscopic π -system

Luca Del Freat¹, Anna Painelli¹, Alberto Girlando¹, and Z.G. Soos²

¹*Dipartimento Chimica G.I.A.F., Università di Parma I-43100 Parma, Italy*

²*Department of Chemistry, Princeton University, NJ-08544 Princeton, US*

The NLO properties of π -conjugated materials strongly depend on the coherence length of the delocalized electronic system. We theoretically investigate the effect of a local conjugation defect, as a sp^3 defect or a para-conjugated phenyl ring in a polyene chain, on the conjugation length and NLO responses. Even in the case of a phenyl ring, the defect reduces the conjugation length and effectively decouples the two polyenes. We introduce the concept of mesoscopic π -conjugated material: systems long enough to define local defects, but short enough to have NLO properties modified by the defect.

Introduction

Among organic materials, π -conjugated molecules have attracted much attention due to their large non-linear optical (NLO) responses that make them prominent candidates as new non-linear media [1]. Delocalized π -electrons account for their peculiar properties. A central problem is the relation between electronic and optical properties and the coherence length of π -electron fluctuations. Conjugated polymers are amorphous and interchain contacts depend on sample preparation. Conformational and structural defects interrupt the conjugation and lead to current models based on segments. We exploit the non-linearity of physical properties with increasing segment length to study defects that limit the conjugation, as seen in electronic or vibrational spectroscopy. The two defects discussed here are an sp^3 carbon or a para-conjugated phenyl ring in a polyene chain.

Conjugation Defects

We consider two polyenic strands of length $2N$, connected by a para-conjugated phenyl, and study the perturbation induced by the benzene on the polyene in a Hückel approach. The six π -orbitals of benzene originate two local states that, being localized on the ring, are irrelevant to our problem. The remaining benzene orbitals are rigorously equivalent to those of a butadiene fragment with hopping integrals fixed to: $\sqrt{2}t$, t , $\sqrt{2}t$. Our model then correspond to $4N+4$ sites chain, with one π -electron per site. The $2N$ bonding polyene orbitals give a degenerate set of N even, N odd states. Benzene generates two occupied states: the even one is split off from the bottom of the valence band and stays as a localized state with almost pure benzene character, the odd state mixes with the middle of the polyene band. Overall states of polyene at the top of the valence band have negligible benzene character. Electron-hole symmetry guarantees equally weak benzene contributions at the bottom of the conduction band.

A central benzene ring effectively breaks electronic conjugation of the polyene system and reduces the extent of π -electron fluctuations. To confirm this counterintuitive result, we investigate the benzene's effect on the optical gap, on the linear polarizability α , and on the second hyperpolarizability γ . As expected for reduced coherence length of π -electrons, the defect reduces α , and γ relative to an uninterrupted chain of the same length.

It is interesting to investigate how the defect affects the properties of chains as a function of chain length. For long enough chains, intensive properties become independent

Poster Session II

of length and the presence of a defect becomes irrelevant. On the other hand, short chains correspond to substituted benzenes whose electronic structure is far from polyenic. Intermediate chains or segments are more interesting: we can define a mesoscopic regime, where a defect does not disrupt polyenic behavior but effectively reduces the coherence length of π -electron fluctuations.

We define an effective chain length for a $4N+4$ chain with a benzene ring, based on intensive properties. Specifically we match the intensive value of electronic properties calculated in the presence of benzene to the length N' of a pristine chain with the same values. The most notable result is that, for a given $4N+4$ chain we estimate different N' depending on the property we consider (either α or γ or the electronic gap). Although N' is always less than $4N+4$, the reduction depends on the property considered and the system is qualitatively different from a polyene of any length.

For the vibrational part of the problem, we calculate the normal modes of the system using an appropriate reference force field (without π -electron fluctuations)[2]. We impose the actual trans-transoid structure for the polyene chain and hexagonal shape of the phenyl ring. We consider only modes with a great contribution of Extended Conjugation Coordinate, considered the most relevant coordinate [3], and we find that modes are quite completely decoupled by the benzene. Benzene defect then disrupts conjugation also in the vibrational properties.

In addition we consider a sp^3 defect in the conjugated chain: in the Hückel scheme this defect can be replaced by a single bond with a hopping integral weaker than a single bond. We find that a single bond with a hopping integral $0.6t$, has an essentially equivalent effect on the polyene as a benzene. The similarity between the weak-bond and the benzene is further confirmed by vibrational calculations. Interrupted conjugation due to a weak-bond is expected. The surprise is that the stronger ($\sqrt{2}t$) bonds of benzene act the same way.

Since both benzene and weak-bond defects affect in a non trivial way the properties of π conjugated strands, we conclude that care has to be paid in extracting information on the behavior of polyenic chains from experimental and/or theoretical studies performed on defect chains. The inductive effects of nonconjugated substituents that, for example, confer rigidity or solubility probably affect the π -system to a lesser extent.

References

- [1] Handbook of Conducting Polymers; Marcel Dekker, New York (1998)
- [2] Z.G. Soos, A. Painelli, A. Girlando and D.Mulkopadhyay in [1]
- [3] A.Painelli, L. Del Freato, A. Girlando and Z.G.Soos *Phys. Rev. B* **60**, 8129-8137 (1999)

Improved Photogeneration Efficiency of C₆₀ Sensitized Arylamines

E. Hendrickx, B. Kippelen, S. R. Marder,⁽¹⁾ A. P. Persoons,⁽²⁾ and N. Peyghambarian

Optical Sciences Center, The University of Arizona, Tucson, AZ 85721.

⁽¹⁾ *Department of Chemistry, The University of Arizona, Tucson, AZ 85721.*

⁽²⁾ *Laboratory for Chemical and Biological Dynamics, Center for Research on Molecular Electronics and Photonics, Leuven, Belgium.*

Photogeneration of carriers was measured at 633 nm in a series of polymer composites based on polystyrene doped with a triphenylamine derivative and C₆₀. Light absorption and carrier generation was achieved through the charge-transfer (CT) complex formed between the hole transport molecule and the sensitizer. We demonstrate the influence of the ionization potential of the donor molecule on the photogeneration efficiency of the CT complex it forms with the acceptor C₆₀. Photogeneration efficiency of unity at an applied electric field of 55 V/μm is found in one composite.

The structure of the arylamine derivatives used in this study and their ionization potentials are shown in Fig. 1. The ionization potential of molecules 1-5 could be varied by 0.25 eV by substitution with the electron withdrawing fluorine atoms and the electron donating alkoxy groups. All the molecules shown in Fig. 1 were found to form a CT complex with C₆₀ in the solid state when doped in a polystyrene (PS) matrix. By subtracting the absorption of a C₆₀/PS reference sample to the absorption spectrum of PS-based samples doped with 1-5 and C₆₀, broad complexation bands with maxima at 610 nm, 630 nm, 790 nm, 790 nm, and 730 nm, respectively, could be found. The position of these maxima scales with the arylamine Ip.

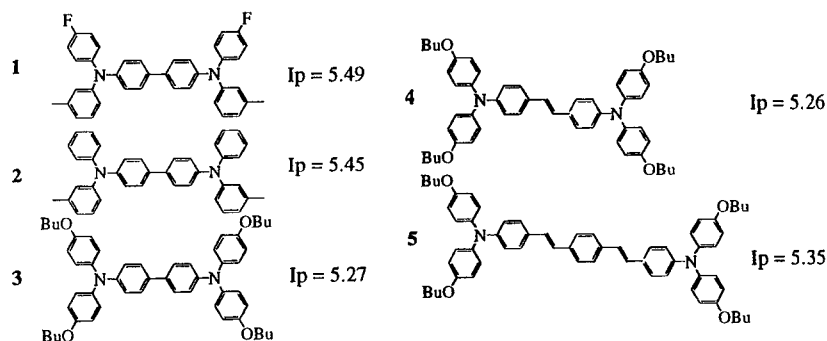


Figure 1: Molecular structures and ionization potentials (eV) of the studied arylamines.

Poster Session II

We have studied the field dependence of the photogeneration efficiency of PS-samples doped with 30 wt. % of molecules 1-5 and sensitized with 1 wt. % C_{60} at 633 nm. The experimental data for the samples doped with molecules 1, 2, 5 and a reference polyvinylcarbazole (PVK)/N-ethylcarbazole (ECZ) sample are shown in Fig. 2.

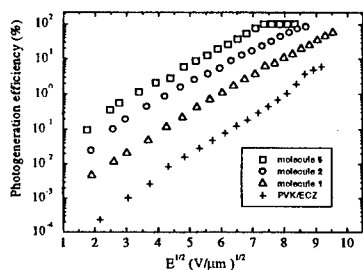


Figure 2: Field-dependence of the photogeneration efficiency.

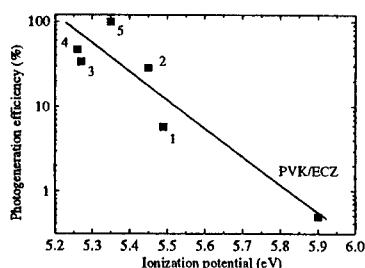


Figure 3: Photogeneration efficiencies at 55 V/μm.

As shown in Fig.2, samples containing donor molecules with the highest ionization potential have the lowest photogeneration efficiency, the CT complex PVK/ECZ/ C_{60} having the lowest. For the samples with a high I_p the photogeneration efficiency keeps increasing with electric field for field values up to 90 V/μm. In contrast, for the sample with molecule 5 it reaches a maximum value of unity at a field value of 55 V/μm and stays constant at higher fields. To the best of our knowledge, this is the highest photogeneration efficiency reported in an organic photoconductor at 633 nm. For the sample doped with 4 (not shown in Fig. 2), the photogeneration efficiency reached 0.61 at an applied field of 70 V/μm and saturated at this value. Fig. 3 shows the photogeneration efficiency of samples with molecules 1-5 measured at the saturation field of the sample doped with 5 (55 V/μm) as a function of the ionization potential of the dopant donor molecule. Within the experimental errors, the correlation between ionization potential of the donor and photogeneration efficiency of the CT complex is clear.

The results can be rationalized within the geminate recombination model for photogeneration efficiency in organic amorphous materials. In this model, the steps leading to photogeneration of charges in the polymer composite involve: (1) the optical excitation of the CT-complex; (2) electron transfer from an uncomplexed donor to the excited CT-complex; and (3) the dissociation of the electron-hole pair. Hence, a higher photogeneration efficiency can be obtained by a faster electron transfer, or a more rapid electron-hole dissociation. A change in the arylamine I_p will simultaneously affect steps 2 and 3.

Acknowledgements: This work was supported by the Office of Naval Research (ONR) through the MURI Center (CAMP), by the Air Force Office of Scientific Research (AFOSR) and by the national Science Foundation (NSF). E. H. is a postdoctoral fellow of the Fund for Scientific Research-Flanders (Belgium).

Control of the First Hyperpolarizability of Functionalized Mesostructures through Cation Binding

Stephan Houbrechts*, Tatsuo Wada, Hiroyuki Sasabe

Frontier Research Program, The Institute of Physical and Chemical Research (RIKEN),
2-1 Hirosawa, Wako, Saitama 351-01, Japan

* Laboratory of Chemical and Biological Dynamics, Catholic University of Leuven, Belgium

Yuji Kubo

Department of Applied Chemistry, Faculty of Engineering, Saitama University, 255 Shimo-ohkubo, Urawa, Saitama 338-8570, Japan

The effect of cation complexation on the nonlinear optical properties of a functionalized crown ether and calixarene has been addressed by means of hyper-Rayleigh scattering.

For years, the photophysics and photochemistry of fluorophores and chromophores linked to cyclic structures as crown ethers or calixarenes has been an area of growing interest. Particularly these compounds where insertion of a cation into the ligand cavity substantially alters the optical properties have been the subject of profound investigations.^[1-3] Herein, one can distinguish two main groups (Fig. 1): compounds of type (I) that interact with the ion through the acceptor site of the chromophore and chromophores of type (II) that interact through the donor site. For the first group, complexation will enhance the internal charge transfer (ICT) and thus induces a bathochromic shift. Type(II) interactions on the other hand reduce the ICT which results in a hypsochromic shift of the charge transfer band.

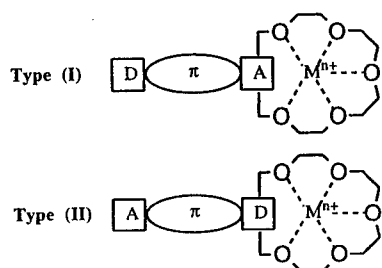


Figure 1: Types of complexation between chromoionophores and cations.

In like manner, elaborate studies have been performed on the relationship between the molecular structure and the nonlinear optical (NLO) response for organic and organometallic compounds.^[4] Moreover, the molecular hyperpolarizability has been shown to depend on the CT transition between donor and acceptor for dipolar structures.^[5] As such, cation complexation with donor or acceptor is expected to alter the molecular hyperpolarizability.

In this regard, we have studied the second-order nonlinear optical properties of NLO functionalized mesostructures and determined the changes in the first hyperpolarizability upon binding of alkaline and alkaline-earth ions. The results reveal that cation complexation is an excellent tool to modify the NLO response "after synthesis", and a potential alternative to photochemical and electrochemical tuning.^[6-9] Moreover, the molecular hyperpolarizability

Poster Session II

is shown to increase (decrease) in case the electron acceptor (a) (donor (b)) is involved in the complexation (Fig. 2).

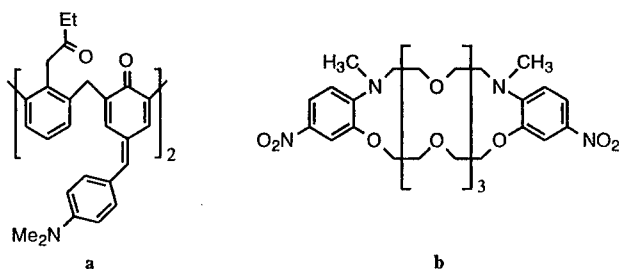


Figure 2: NLO functionalized ionophores of type (I) (a) and type (II) (b).

In addition, hyper-Rayleigh scattering was used to monitor the NLO response upon titration of the NLO-functionalized ionophore. The experiments demonstrate for the first time that the NLO properties can be used to determine the stability constant of ion complexation in solution for 1:1 complexes.

References

- [1] H. G. Löhr, F. Vögtle, *Acc. Chem. Res.* **18**, 65-72 (1985).
- [2] B. Valeur, in J. R. Lakowicz (Ed.): *Topics in fluorescence spectroscopy: Probe design and chemical sensing, Vol. 4*, Plenum Press, New York 1994, p. 21-48.
- [3] T. Hayashita, M. Takagi, in J. L. Atwood, J. E. D. Davies, D. D. MacNicol, F. Vögtle, G. W. Gokel (Eds.): *Molecular Recognition: Receptors for Cationic Guests, Vol. 1*, Elsevier Science Ltd., Oxford 1996, p. 635-669.
- [4] T. Verbiest, S. Houbrechts, M. Kauranen, K. Clays, A. Persoons, *J. Mater. Chem.* **7**, 2175-2189 (1997).
- [5] J. L. Oudar, D. S. Chemla, *J. Chem. Phys.* **66**, 2664-2668 (1977).
- [6] H. Sakaguchi, T. Nagamura, T. Matsuo, *Jpn. J. Appl. Phys.* **30**, L377-L379 (1991).
- [7] A. Persoons, K. Clays, M. Kauranen, E. Hendrickx, E. Put, W. Bijnens, *Synthetic Metals* **67**, 31-38 (1994).
- [8] K. Alagesan, P. C. Ray, P. K. Das, A. G. Samuelson, *Current Science* **70**, 69-70 (1996).
- [9] B. J. Coe, S. Houbrechts, I. Asselberghs, A. Persoons, *Angew. Chem.* **38**, 366-369 (1999).

Ellipsometric Polarization Contour Measurement for Anisotropy in Organic Materials

Minsoo Joo and Nakjoong Kim
 Center for Organic Photorefractive Materials
 Korea Institute of Science and Technology
 P.O. Box 131, Cheong-ryang, Seoul, 130-650, Korea

Ellipsometric Polarization Contour Measurement (EPCM), which consists of conventional ellipsometric measurement system with rotational mode of an analyzer, is newly introduced. Anisotropic properties of organic photorefractive materials are studied using EPCM. EPCM technique was first tested by optical components such as wave plates and then applied to the organic photorefractive materials to study about the poling process with applied voltage. Comparing to conventional ellipsometric measurement, EPCM makes the anisotropic properties of materials more directly characterized by analyzing the polarization state of light.

Introduction

Orientation in polymers is of great technical and theoretical importance and therefore, the measurement of orientation in polymers provides valuable information to understand the structures and properties of polymers. The information about molecular orientation in polymeric samples is to be reflected on the polarization state of light which travels through the samples. Ellipsometric technique is widely used for the measurement of polarization state and the anisotropic properties of materials are analyzed in terms of optical birefringence. Ellipsometric Polarization Contour Measurement (EPCM), which consists of conventional ellipsometric measurement system with rotational mode of an analyzer, can directly measure the polarization characteristics of light passing through samples. EPCM gives not only the information about the polarization state of light but other useful information such as the optic axis of samples.

Theory and Experimental

By adopting rotational mode of an analyzer in conventional ellipsometric measurement system, the anisotropic properties of materials can be directly characterized. As light propagates through materials, the polarization ellipse of light changes and the change of the polarization state can be described by the Jones matrix as Eq.(1) [1]:

$$E_{out} = M_A M_S E_{in} \quad (1)$$

where E_{in} , M_S , and M_A are the Jones vector for the polarization state of input beam and the Jones matrices for a sample and for a rotating analyzer, respectively.

If input beam is linearly horizontally polarized (LHP), then output beam intensity can be described by Eq.(2) and if input beam is right circularly polarized (RCP), then output beam intensity can be described by Eq.(3).

$$I_{LHP} = I_0 \left\{ \cos^2 \frac{\Delta\phi}{2} \cdot \cos^2 \theta + \sin^2 \frac{\Delta\phi}{2} \cdot \cos^2 (\theta - 2\alpha) \right\} \quad (2)$$

$$I_{RCP} = \frac{I_0}{2} \{ 1 + \sin \Delta\phi \cdot \sin 2(\theta - 2\alpha) \} \quad (3)$$

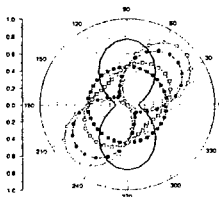
Poster Session II

where I_0 , θ , $\Delta\phi$, and α are input beam intensity, rotation angle of an analyzer, phase difference due to birefringence of a sample, and tilt angle of a sample, respectively. Therefore, if light passing through a sample is scanned by a rotating analyzer, then the polarization state of light can be determined and the information about the optical state of a sample can be obtained from Eq.(2) or Eq.(3).

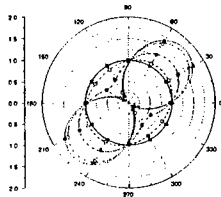
The intensities of light passing through a sample at various rotating angles of an analyzer are detected and the data collected as a function of analyzer angles were fitted by Eq.(2) or Eq.(3) according to the input beam polarization state. EPCM with LHP input beam was first tested by optical components such as tilted wave plates and then applied to the organic photorefractive materials, PDCST20 and PDCST30, with RCP input beam. PDCST20 consists of 20% of PDCST, 79% of carbazole-substituted polysiloxane, and 1% of TNF. PDCST30 consists of 30% of PDCST, 69% of carbazole-substituted polysiloxane, and 1% of TNF.

Results and Discussion

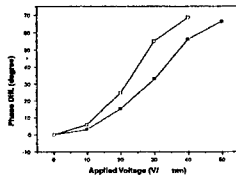
The validity of Eq.(2) was confirmed by the experiment with a tilted half-wave plate. The polarization contour diagram calculated from simulation with Eq.(3) is given in Fig.1. The lines with symbols in Fig.1 are for the cases of no tilt with various phase differences (filled-square for 0° , empty-square for 15° , filled-circle for 45° , and empty-circle for 90°) and the solid line is for the case of 45° tilt with 45° phase difference. The tilt effect is obvious in the EPCM diagram. The experimental data for PDCST30 obtained from EPCM are shown in Fig.2 (filled-square for $0V/\mu m$, empty-square for $10V/\mu m$, filled-circle for $20V/\mu m$, empty-circle for $30V/\mu m$, and filled-triangle for $40V/\mu m$). The fitting results for PDCST30 with Eq.(3) are also shown in Fig.2 by lines (solid line for $0V/\mu m$, dash for $10V/\mu m$, dash-dot for $20V/\mu m$, dash-dot-dot for $30V/\mu m$, and short-dash for $40V/\mu m$). No tilting of the optic axis is observed either in PDCST20 or PDCST30, as applied voltage increases. Phase differences of light passing through the organic samples, PDCST20 and PDCST30, due to the electric field are given in Fig.3 as a function of voltage.



EPCM diagram for the simulation results from Eq.(3).



Experimental data for PDCST30 obtained from EPCM and fitting results.



Phase differences for PDCST20 (filled square) and for PDCST30 (empty square).

References

- [1] D. Clarke and J.F. Grainger, *Polarized Light and Optical Measurement*, Pergamon Press (1971).

Determining the nature of excited states using an inhomogeneous-broadening analysis of third-order processes in guest-host systems

R. J. Kruhlak, M. G. Kuzyk¹
Department of Physics
Washington State University
Pullman, WA, USA 99164-2814

In guest-host systems, the electronic properties of the ensemble of guest molecules are normally inhomogeneous due to the polymer host environment. First- and second-order theories have been developed to treat the inhomogeneous-broadening (IB) of the electronic transitions. We extend the theory for inhomogeneously broadened electronic transitions to third-order systems. Since the theory must be developed for each specific process, as in the second-order case, we discuss the theory in terms of pump-probe, Kerr, third harmonic generation, and quadratic electrooptic processes. Finally we compare this theory with the standard Lorentzian (L) theory by describing squaraine-doped poly(methylmethacrylate) (PMMA) thin film quadratic electroabsorption results.

Introduction

Guest-host polymer optical systems are currently of great interest for nonlinear optical devices due to the ease of processing, the low cost, and the numerous potential dopant molecules. However, doping polymer systems with dye molecules complicates the analysis of the electronic properties of the dyes due to the matrix nature of the polymer host. To effectively model the electronic properties of the ensemble of dye molecules we extend an inhomogeneous-broadening theory, developed by Toussaere for second-order systems [1], to third-order systems.

Inhomogeneously Broadened Transitions

$$D_{11}(-\omega_\sigma; \omega_1, \omega_2, \omega_3) = \hat{I}_{1,2,3} \left\{ [(\Omega_{1g} - \omega_\sigma)(\Omega_{1g} - \omega_3)(\Omega_{1g} - \omega_1)]^{-1} + [(\Omega_{1g} - \omega_3)(\Omega_{1g}^* + \omega_2)(\Omega_{1g} - \omega_1)]^{-1} + [(\Omega_{1g}^* + \omega_\sigma)(\Omega_{1g}^* + \omega_3)(\Omega_{1g}^* + \omega_1)]^{-1} + [(\Omega_{1g}^* + \omega_3)(\Omega_{1g} - \omega_2)(\Omega_{1g}^* + \omega_1)]^{-1} \right\} \quad (1)$$

An example of a Lorentzian denominator for a general third-order transition between the ground and first one-photon excited state is given in Equation (1), where $\hat{I}_{1,2,3}$ is the intrinsic permutation operator, ω_i are the incident frequencies, $\omega_\sigma = \sum \omega_i$, $\Omega_{1g} = \omega_{1g} - i\Gamma_{1g}$, * denotes complex conjugation, ω_{1g} is the transition frequency, and Γ_{1g} is the linewidth.

To completely determine the inhomogeneous-broadening version of the third-order susceptibility $\chi_{IB}^{(3)}$, for a specific process, the Lorentzian denominators, like Equation (1), making up $\chi_L^{(3)}$ are expanded using partial fractions in terms of the three basic Lorentzian quantities in Table 1. Each basic Lorentzian contribution is transformed to an inhomogeneous-broadening contribution by convolving it with Gaussian (often referred to as a Voigt Profile). This convolution models the statistical nature of the dye molecules in the polymer matrix. The three most basic inhomogeneous-broadening contributions

¹and Material Science Program

Poster Session II

are written in terms of a complex error function, $W(z)$, to facilitate numerical integration. Thus we write $\chi_{IB}^{(3)}$ by replacing each basic Lorentzian contribution in $\chi_L^{(3)}$, with its corresponding inhomogeneous-broadening contribution in Table 1.

Lorentzian (L)	Inhomogeneous-Broadening (IB)
$\frac{C_1}{\omega_{ng} \mp i\Gamma_{ng} \mp \omega}$	$\frac{i\sqrt{\pi}C_1}{\gamma_{ng}} W\left(\frac{-\omega_{ng} \pm i\Gamma_{ng} \pm \omega}{\gamma_{ng}}\right)$
$\frac{C_2}{(\omega_{ng} \mp i\Gamma_{ng} \mp \omega)^2}$	$\frac{i\sqrt{\pi}C_2}{\gamma_{ng}} \left\{ \frac{2(\omega_{ng} \mp i\Gamma_{ng} \mp \omega)}{\gamma_{ng}^2} W\left(\frac{-\omega_{ng} \pm i\Gamma_{ng} \pm \omega}{\gamma_{ng}}\right) + \frac{2i}{\sqrt{\pi}\gamma_{ng}} \left(1 + \frac{\mp i\Gamma_{ng} \mp \omega}{2\sqrt{\pi}\gamma_{ng}}\right) \right\}$
$\frac{C_3}{(\omega_{ng} \mp i\Gamma_{ng} \mp \omega)^3}$	$\frac{i\sqrt{\pi}C_3}{\gamma_{ng}} \left\{ \left(\frac{2(\omega_{ng} \mp i\Gamma_{ng} \mp \omega)^2 - \gamma_{ng}^2}{\gamma_{ng}^3} \right) W\left(\frac{-\omega_{ng} \pm i\Gamma_{ng} \pm \omega}{\gamma_{ng}}\right) + \frac{2i(\omega_{ng} \mp i\Gamma_{ng} \mp \omega)}{\sqrt{\pi}\gamma_{ng}^2} \right\}$

Table 1: The three most basic denominator contributions to $\chi^{(3)}$, for Lorentzian (L) and inhomogeneously broadened (IB) electronic transitions (γ_{ng} = Gaussian linewidth, $W(z) = \frac{i}{\pi} \int_{-\infty}^{\infty} \frac{\exp(-t^2)}{z-t} dt$).

Unfortunately, the transformation from the Lorentzian model to the inhomogeneous-broadening model is specific to each third-order process like, pump-probe, Kerr, third harmonic generation (THG), or quadratic electrooptic (QEA), and thus very time consuming, so we provide the detailed transformations for each process in this poster.

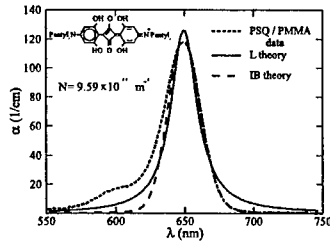


Figure 1: Lorentzian (L) and inhomogeneous-broadening (IB) models of the dominant excited state for a bulk sample of PSQ/PMMA.

Discussion

Figure (1) shows the two models for linear absorption in a PSQ/PMMA bulk sample [2]. Since the IB model is a much better description of the guest-host system in a linear process, we expect inhomogeneous-broadening to be important in describing third-order processes. Currently the IB model shows promise in comparison to the Lorentzian model for QEA data of an ISQ/PMMA thin film.

References

- [1] E. Toussaere, "Polymer electrooptiques pour l'optique non lineaire caracterisation optique et modeles statistiques," Ph.D. Dissertation, (University of Paris, Paris, 1993)
- [2] R. J. Kruhlak and M. G. Kuzyk, Side-illumination fluorescence spectroscopy. II. Applications to squaraine-dye-doped polymer optical fibers, J. Opt. Soc. Am. B 16, 1756 1767 (1999).

Application of the optical and positron spectroscopy to the study of structural transformations in milk fat and its simple purified fractions

V. Y. Kudryavtsev, S. M. Yablochkov
Taras Shevchenko Kyiv University, Physics Dept.
252127, Kyiv, Ukraine

S. P. Likhatorovich, M. M. Nishchenko
Institute of Metal Physics, National Acad. Sci of Ukraine,
252680, Kyiv, Ukraine

T. A. Rashevskaya, I. S. Gulyi
Ukraine State University of Food Technologies,
252033, Kyiv, Ukraine

The structural transformations in milk fat (MF) from amorphous to crystalline state as well as in simple purified fractions (SPF) were investigated by using optical and positron spectroscopy. The crystallization of amorphous MF leads to appearance of the prominent peak in the luminescence spectra of MF. The transmission and excitation of the luminescence spectra were also investigated at different temperatures. The results of optical study of MF and SPF are supplemented by the results of the positron spectroscopy of MF and SPF.

Introduction

Long chain compounds, such as MF, contain a various fractions, which can be occurred in different crystal forms, a phenomenon is known as polymorphism. It is widely acknowledged that the habit (size and shape) of crystals in a fat is related to the polymorphic state of the fat [1].

The most widely used method for studying of lipid polymorphism is X-ray diffraction. There are other well-known methods for studying of polymorphism such as low temperature infrared spectroscopy, differential scanning calorimetry, microscopy. In this work the photoluminescence and positron spectroscopy were employed in order to obtain an additional information on the influence of the structural transformations in milk fats and their simple purified fractions on their physical properties .

Experimental details

Amorphous phase of MF was obtained by the quenching of the melted MF from 340 K into the liquid nitrogen. Structural relaxation of amorphous phase to more equilibrium crystalline phase was obtained due to aging of this amorphous samples at different (273 and 293 K) temperatures during 90 days. Besides MF, two SPF were also investigated. SPF were extracted from MF by using fractional crystallization from its solution in acetone by separation at 286 and 273 K on the so-called "high-melting-point" (HM) and "low-melting-point" (LM) fractions, respectively.

Results and discussion

The luminescence spectrum of as-quenched amorphous MF is characterized by an intense peak with a maximum at 3.1 eV and several weak features on its low-energy shoulder

Poster Session II

located at 2.6 and 2.8 eV. The aging of amorphous MF at 273 K as well as room temperatures during 90 days has led to an appearance of an additional prominent luminescence peak with a maximum at 2.38 eV. The relative intensity of this additional peak as well as weak features on the low-energy shoulder of main peak (in respect with main peak) is higher at the larger temperature of aging. It can be supposed that such a transformation of the luminescence spectrum of MF due to aging reflects the structural relaxation of amorphous structure towards the crystalline phase or crystallization of MF. Indeed, the structural study of MF by using microphotography as well as results of electron-positron annihilation confirms this supposition. An observed changes in the luminescence spectra are reversible, i. e. heat treatment of the aged MF to the liquid state (up to 340 K) nearly completely restores the primary luminescence spectrum measured in solid state (at 293 K). The intensity of the luminescence in the liquid state (measured at 340 K) is significantly lower than in the solid state. This decrease in intensity can be caused by several mechanisms, for example, temperature quenching. Even without an additional peak in the luminescence spectrum of aged MF which is located at 2.38 eV, main peak exhibits rather complicated structure and contains at least 3 components. It can be supposed that these peaks occur from the different SPF of MF. LM and HM SPF have a complicated luminescence spectra with maximums at 2.6 and 3.0 eV, respectively.

The transmission spectra of MF were investigated at room and elevated temperatures. All this spectra are characterized by absorption peaks at 3.9, 4.4 and 4.6 eV on the background. Transition from the solid state to the liquid one (with the increasing of the temperature up to 340 K) has led to the remarkable decrease in value of background, while the intensity and location of the 4.4 and 4.6 eV absorption peaks have not changed. The excitation spectrum of the luminescence for the MF exhibits intense peak at 3.9 and two weak peculiarities at 4.4 and 4.6 eV. The location of the components in the excitation spectrum exactly corresponds to the locations of the peculiarities in absorption spectra.

According to the results of the positron spectroscopy study the radius of nanopores depends on structural state of triglycerides of MF and its SPF and for all the investigated samples varies from 2.3 to 3.9 Å. The correlation dependence between an average radius of pores, R_p , and the probability of the positronium annihilation, S , was established that the larger R_p , the smaller S . The maximum value of radius for various structural states is changed in a very narrow range and varied from 3.6 to 3.9 Å. These values are rather close to the distances between chains in fat acids for different modifications of triglycerides (α , β and β'), that are 4.14, 3.78 and 3.68 Å, respectively [2]. Long term aging of HM SPF at room temperature during 90 days leads to a decrease in R_p from 3.6 to 2.2 Å. This decrease in average pore radius may reflect the structural ordering (crystallization) due to aging.

References

- [1] A. E. Baily, "Melting and Solidification of Fats and Fatty Acids, Interscience," New York, pp. 117 - 178, (1950).
- [2] W. W. Walker, W. G. Merrit, and G.D. Cole, "Phase dependence of positron annihilation in tristearin, Physics Letters," 40, 157, (1972).

Strong field poling of multipolar structures : fundamentals and device implications

Isabelle Ledoux, Irène Cazenobe, Sophie Brasselet, Eric Toussaere and Joseph Zyss
*LPQM – UMR 8537 – Ecole Normale Supérieure de Cachan
61 avenue du Président Wilson 94235 Cachan Cedex - FRANCE*

The electro-optic anisotropy of a polymer containing nonlinear multipolar molecules is experimentally shown to decrease from 3 to 2.3 in strong electric field poling conditions. Implications as to the introduction of multipolar systems in the elaboration of polarization-independent optoelectronic devices are discussed.

Polarization independence is a crucial prerequisite towards actual use of polymer-based electro-optic devices in optical telecommunication systems. Polymers containing highly dipolar chromophores oriented under a weak external electric field E_p (i.e. $\mu \cdot E_p < kT$, where μ is the ground state dipole moment and T the temperature of poling) leads to an electro-optic anisotropy ratio $\alpha = r_{33}/r_{13} = 3$ or more, corresponding to different modulated refractive index respectively parallel and perpendicular to the poling and modulation field axis (3). The need for adapted architectures using a less effective in-plane transverse electrode configuration [1] requires the availability of highly efficient electro-optic polymers, involving new molecules with $\mu \cdot \beta$ values 3 to 5 times higher than those of the currently used Disperse Red 1 (DR1) chromophore.

Another approach is to implement polarization independence at the core molecular level. We show that a departure from the low field 3 value of the α nonlinear anisotropy can be obtained in strong poling field conditions. Such departure is positive for dipolar molecules ($\alpha > 3$) and negative ($\alpha < 3$) in the presence of strong octupolar contributions to the β tensor, and may be decreased to 1 in this latter case[2]. Such possibility of controlling the nonlinear anisotropy ratio has been experimentally evidenced for different values of the corona poling field in the case of polycarbonate matrices doped with the DR1 dipolar chromophore and the multipolar dinitro-di-(n-butylamino)-benzene (DNDAB) compound. The corresponding Langevin coefficient $p = f_0 \mu \cdot E_p / 5kT$ (f_0 being the local field factor) is inferred by an independent linear spectroscopic method on poled and unpoled samples[3]. The nonlinear anisotropy factor $\alpha' = d_{33}/d_{31}$ for second harmonic generation (SHG) has been evaluated by frequency doubling at 1.34 μm in different polarization configurations of the fundamental wave.

Poster Session II

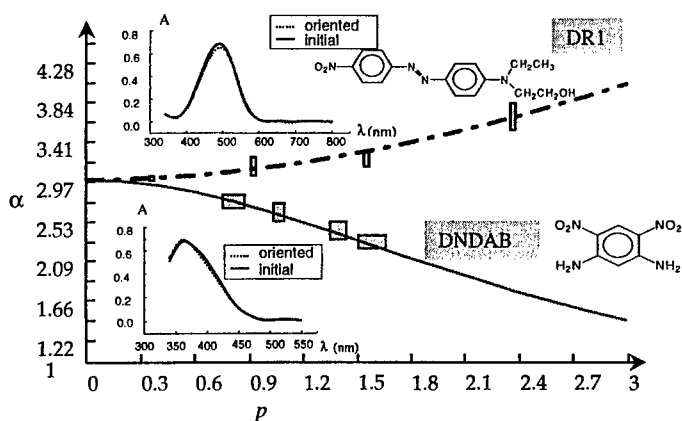


Fig. 1 : Calculated values (continuous line) and measured ones (rectangular boxes accounting for experimental errors) for the nonlinear SHG anisotropy $\alpha' = d_{33}/d_{31}$ of a dipolar (DR1) and multipolar (DNDAB) doped polycarbonate matrix, as a function of the Langevin factor p . The latter is determined by comparison of their UV-Visible absorption spectra (see inserts) before and after electric field poling [3].

The poling field dependence of the α value as from a statistical oriented gas model is sketched in Figure 1. The observed behavior is in good agreement with the theoretical model of Ref.[2]. Whereas α increases up to 3.6 for DR1-doped matrix, it decreases down to 2.3 for the DNDAB doped polymer. As the poling field remains in the range of currently used values for electro-optic devices oriented under electrodes ($150 \text{ V} \cdot \mu\text{m}^{-1}$), the possibility to reach $\alpha = 1$ and hence polarization independence by use of multipolar molecules becomes a realistic target. Perspectives towards a more elaborated engineering strategy of multipolar molecules, combining a high static dipole moment with a strong octupolar $\beta_{J=3}$ component, will be discussed in that respect.

[1] A. Donval, PhD Thesis, Orsay, 1999. A. Donval, R. Hierle, E. Toussaere and J. Zyss, submitted to *Journal of Applied Physics*.
 [2] S. Brasselet, PhD Thesis, Orsay, 1997. S. Brasselet, E. Toussaere, J. Zyss, submitted to *Phys. Rev. A*
 [3] S. Brasselet and J. Zyss, *J. Nonlinear. Opt. Phys. Mater.*, **5**, n°4, 671-693 (1996).

Second Order Nonlinear Optical Response at the Two-Photon Resonance in a Two Dimensional NLO Molecule

Guilia Meshulam, Garry Berkovic, Zvi Kotler
*Photonic Materials Group, Soreq NRC,
 Yavne 81800, Israel*

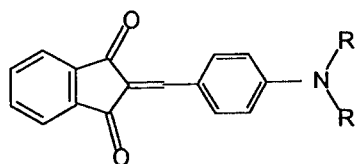
Amos Ben-Asuly, Royi Mazor, Lev Shapiro and Vladimir Khodorkovsky
*Department of Chemistry, Ben-Gurion University of the Negev,
 Beer-Sheva 84105, Israel*

Organic nonlinear optical molecules, having a carbazole group as electron donor, exhibit special "2-dimensional" second harmonic behavior due to the development of two β components. Quantum Chemical calculations indicate that this results from the presence of two overlapping transitions that contribute to β . The experimental verification is based on the frequency dependence of β . Measuring second harmonic in the two-photon resonance shows a much larger enhancement of β for the two-dimensional molecule than for a one-dimensional molecule, in agreement with predictions.

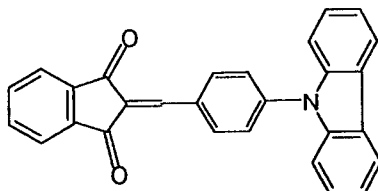
Introduction

The second order nonlinear optical response of π -conjugated organic molecules depends on their electronic structure. We have recently shown [1] that there is a large difference in the second harmonic response of very similar molecules **I** and **II**. Molecules of type **I** with dialkyl or diaryl amino donor groups are typical one-dimensional (1-D) rod shaped NLO molecules, whose β tensor is dominated by the long axis β_{zzz} component. These molecules show strong SHG when measured by either EFISH or HRS. The corresponding molecule **II** having carbazole in the donor site, develops two β components, and is consequently a 2-D NLO molecule. Since these two components are opposite in sign, but approximately equal in magnitude, the molecule gives only a negligible low frequency EFISH response, but a strong HRS signal [1].

We will now compare the SHG frequency dependence of these molecules using EFISH, showing further unusual behaviour by molecule **II**.



I R = C_nH_{2n+1}, phenyl



II

Results and discussion

Expected frequency dependence of β^{EFISH} in the two-dimensional molecule

Quantum chemical calculation on molecule **II** have suggested that the two β components developed in the molecule are a consequence of the following: a charge transfer band gives a positive β_{zzz} contribution along the long axis of the molecule, and an almost degenerate transition

Poster Session II

involving the carbzole group provides an off-diagonal β_{zx} hyperpolarizability. Measuring the SHG using the EFISH technique at low frequencies (where 2ω of the laser is much lower than the absorption energy of the molecule) gives the sum of these components, which yields a very small total β value. If EFISH is measured in the two-photon resonance regime each β will be resonantly enhanced and consist of a real part and an imaginary part. A typical simulation is presented in Figure 1, showing the real and imaginary parts of the two β components. The measured EFISH signal will depend on the total absolute value $|\beta_1 + \beta_2|$. It is seen that the EFISH enhancement from the non-resonant to the resonant regime (thick line) can be a factor of several hundred. On the other hand, a 1-D molecule shows only the enhancement given by β_1 , which is given by the ratio of the absorption peak to its linewidth – typically 10-20.

A second unique feature of the resonance enhancement in the 2-D molecule is that there will exist a frequency in the resonance peak where the hyperpolarizability will be purely real, as a result of cancellation of the imaginary parts of β_1 and β_2

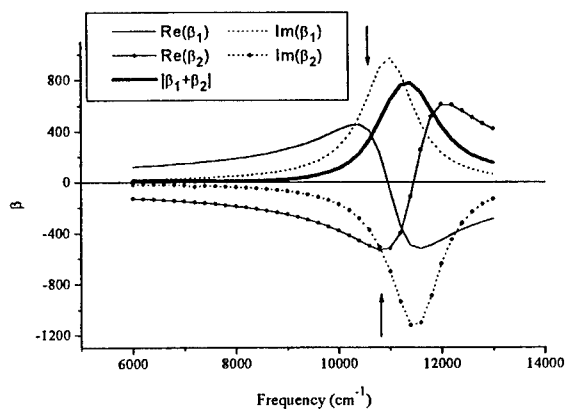


Figure 1: Model of EFISH β frequency dependence for a “2-D” molecule with two different β components originating from different excited states. The thin lines represent the frequency dependence of the individual β components (full lines = real parts; dashed lines = imaginary parts) and the thick line represents the *amplitude* of the total β . The arrow represents a frequency where the imaginary β 's cancel, and the hyperpolarizability is purely real.

Experimental Results

As expected, we see a “normal” resonance enhancement of about 15 for 1-D molecules. For molecule II we observe an EFISH resonance enhancement of about 200, in agreement with Figure 1. We also found that the resonance hyperpolarizability is dominated by its real part, again in agreement with expectations, and contrary to behavior of 1-D molecules.

References

- [1] G. Meshulam, G. Berkovic, Z. Kotler, A. Ben-Asuly, R. Mazor, L. Shapiro and V. Khodorkovsky, Proc. SPIE 3796, 279, 1999.

Enhanced two-photon absorption in phenyl and fluorene oligomers

Y. Morel, O. Stephan, P.L. Baldeck

*Laboratoire de Spectrométrie Physique, Université Joseph Fourier,
CNRS (UMR 5588) BP87, 38402 Saint Martin d'Hères Cedex*

C. Andraud

*Laboratoire de Stéréochimie et Interactions Moléculaires,
ENS Lyon, 69364 Lyon cedex 07*

We have studied the two-photon absorption (TPA) spectra of fluorene and phenyl oligomers. At resonance, the large TPA amplitude increases when changing the oligomer size. This TPA enhancement is in agreement with semi-empirical quantum chemistry calculations.

We present the two-photon absorption spectra of fluorene and phenyl oligomers. When changing the oligomer size, an enhancement of the TPA amplitude and a red-shift of the resonance have been observed. The TPA spectra are deduced from nanosecond fluorescence measurements using an Nd:YAG pumped optical parametric oscillator in the visible range (450-650nm). Calibration of the cross section is obtained by comparison with a TPA standard reference : p-Bis(o-methylstyryl)-benzene.

An example of TPA cross section for the bifluorene is presented figure 1. The compound exhibits a strong resonance at 530nm with a large value of $900.10^{-50} \text{ cm}^4 \cdot \text{s}/\text{photon-molecule}$. The TPA cross section of the fluorene was too weak and too blue-shifted to be characterized with our set-up.

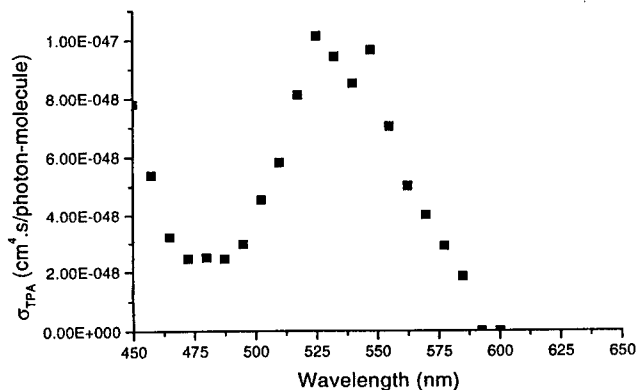


Figure 1: Measured TPA cross section of bifluorene in chloroform.

These experimental results are analysed using semi empirical quantum chemistry calculations. Figure 2 shows that the theoretical TPA spectra are in good agreement with the

Poster Session II

experimental ones. Indeed, going from fluoren to bifluoren, a strong red-shift and an increase in the TPA amplitude is observed.

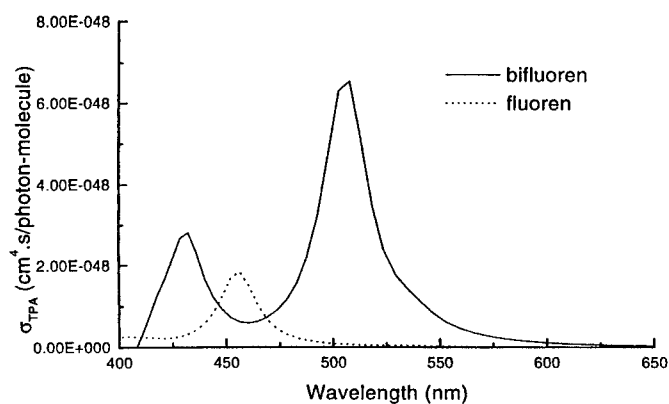


Figure 2: Calculated TPA cross sections of fluoren and bifluoren.

Oligomers are of great interest in the design of molecules with enhanced TPA amplitude. Moreover, the intermolecular interaction between the monomers allows new excited states to be created. This effect could be useful for nonlinear applications in the nanosecond regime, such as optical power limiting, where molecules need to be optimized for both two-photon absorption and excited state absorption.

Response theory calculations of optical limiting processes

Patrick Norman¹, Yi Luo², Peter Cronstrand³, Peter Macak³, and Hans Ågren³

¹. Department of Physics, Linköping University, S-581 83 Linköping, Sweden

². FYSIKUM, University of Stockholm, Box 6730, S-113 85 Stockholm, Sweden

³. Theoretical Chemistry, Royal Institute of Technology, S-100 44 Stockholm, Sweden

An analytical and efficient computational toolbox based on *ab initio* quadratic and cubic response theories has been developed and applied to optical limiting processes, including ground state multiphoton absorption and excited state optical absorption of organic molecules and conjugated polymers.

Optical limiting devices have a wide range of applications in many areas. The aim with the present research is to find new materials that possess large two-photon absorption and excited state absorption in desirable optical regions, and to understand the effects of electronic and geometrical changes, media, and vibronic coupling on the performance of these materials.

Two-photon absorption

Length dependence: Several conjugated oligomers, such as, *trans*-polyenes, *cis*-polyenes, *diphenyl*-polyenes, polyacenes, polythiophenes, polypyrroles, and polyfurans, have been studied. It has been shown that there exists a common localization length for these conjugated oligomers, longer than which the TPA spectrum is completely dominated by a single state, mA_g . The position of that state is dependent on the system, varying in the range 1.4 to 1.8 times the band gap energy. Strong correlations between the intensity of the maximum two-photon mA_g state and the length of the oligomers are found.

$$\begin{aligned} \delta_{tp}^{mA} &\propto L^{6.2} \text{ (trans-polyenes),} & \delta_{tp}^{mA} &\propto L^{5.0} \text{ (cis-polyenes),} \\ \delta_{tp}^{mA} &\propto L^{7.0} \text{ (oligothiophenes),} & \delta_{tp}^{mA} &\propto L^{6.2} \text{ (oligofurans),} \\ \delta_{tp}^{mA} &\propto L^{4.0} \text{ (oligopyrroles),} \end{aligned}$$

where L denotes the molecular head-to-tail length. Among the conjugated oligomers so far investigated [1, 2], we find the ring systems to show the stronger nonlinear absorption; the oligothiophenes show the strongest TPA, while the TPA of oligofurans are comparable to that of the *trans*-polyenes.

Dimensionality: One-dimensional charge-transfer (CT) stilbene-derivatives have been the focus of recent experimental as well as theoretical investigations. We have shown that the TPA cross section can be efficiently enhanced by extending the dimensionality of the CT network. Two series of compounds, representing the two- and three-dimensional CT systems, have been studied. The two-dimensional CT system is based on 1,2-di(9H-9-fluorenylidene)ethene [3] whereas the three-dimensional CT system is built from a triphenylamine donor center (see Figs. 1a and 1b). With donor-acceptor substituents on the two-dimensional structure, the TP cross section can be enhanced in the visible region to take on values as high as $1732 \times 10^{-50} \text{ cm}^4 \text{ photon}^{-1}$, which is a number quite comparable to those for rather complicated stilbene based systems.

Poster Session II

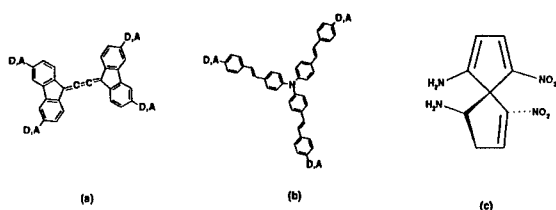


Figure 1: Structures of some CT molecules studied in present work: (a) cumulene, (b) triphenylamine, (c) spiro-conjugated dimer.

Medium effects: We have studied the solvent effects on the TPA of CT molecules using both self-consistent reaction field and internal finite field approaches [4]. It is shown analytically and numerically that the results from the two methods can be connected through induced local reaction field factors. In general, the solvent effects on the TPA cross section are quite moderate, e.g. much smaller than those for the first hyperpolarizability β .

Vibrational contribution: The importance of the vibrational contributions to the TPA cross sections has been illustrated by a spiroconjugated dimer [5], 1,1'-diamino-4,4'-dinitro-5,5'-spirobicyclopentadiene (ANSC). The vibrational contributions increase the electronic part of the TPA cross section by a factor of 10, and the maximum of the TPA spectrum is blue-shifted by as much as 1600 cm^{-1} from the electronic original. It can be expected that similar effects should be observed for multi-dimensional CT molecules.

Excited state absorption

Single determinant formulation: The oscillator strength for linear absorption of light from one electronically excited state to another has been investigated for diatomic and polyatomic molecules. Special attention has been given to the possibility of doing so in a single-determinant framework through a residue analysis of the ground state response functions, that is to say, neither of the two states involved in the absorption process are explicitly optimized. The approach is evaluated against results based on multi-determinant wave functions where the coupling matrix element is directly computed with the excited state as reference state. Preliminary calculations, addressing the first few singlet excited states, show a fair reliability of these properties in the single-determinant approximation. Relaxation effects are presently not taken into account.

References

- [1] P. Norman, Y. Luo, and H. Ågren. *Chem. Phys. Lett.*, **296**, 8, (1998).
- [2] P. Norman, Y. Luo, and H. Ågren. *Opt. Commun.*, **168**, 297 (1999).
- [3] P. Norman, Y. Luo, and H. Ågren. *J. Chem. Phys.*, **111**, 7758 (1999).
- [4] Y. Luo, P. Norman, P. Macak, and H. Ågren. *J. Phys. Chem.*, submitted.
- [5] Y. Luo, P. Macak, P. Norman, and H. Ågren. *J. Chem. Phys.*, submitted.

Theoretical Study on the Third-Order Nonlinear Optical Properties of Thiophene Derivatives

Koji Ohta, Ryo Shikata, Kenji Kiyohara, Keiko Tawa, Kenji Kamada
Department of Optical Materials, Osaka National Research Institute
1-8-31 Midorigaoka, Ikeda, Osaka 563-8577, Japan

Second hyperpolarizabilities of the thiophene homologues and their oligomers are calculated by *ab initio* molecular orbital methods. It is found that substitution of the hetero atom with heavier one of these homologues can contribute to the enhancement of the third-order nonlinear optical effects by the theoretical calculation. By including both effects of electron correlation and frequency dispersion for the monomers, the calculated results give excellent agreements with the experimental values observed by the optical Kerr effects. The effects of conjugation length and difference in the linkage type on the nonlinear optical properties are compared for the oligomers.

Thiophene and its derivative have been recognized as important organic materials not only in the field of nonlinear optics, but also in other fields of molecular photonics like electroluminescence. The nonlinear optical property, especially the chain length dependence of nonlinear properties of thiophene oligomers was well examined by Prasad's group [1]. In this study, we have made theoretical calculation of second hyperpolarizability, γ , of thiophene homologues and their oligomers by using *ab initio* molecular orbital methods.

Calculation Method

The Gaussian program [2] was used for calculating the static second hyperpolarizability, γ , of the thiophene derivatives by the finite-field (FF) method, where the effect of electron correlation were included using the CCSD(T) method or density functional theory (DFT). The frequency dispersion of the hyperpolarizability was also examined for monomers by the TDHF method using the HONDO 95.3 program [3]. The 6-31G+*pd* or 6-31G+*pdd* basis set was used [4]. For the heavy atoms like selenium or tellurium, Wadt-Hay's effective core potential (ECP) method [5] was employed to treat inner electrons.

Monomers of Thiophene Homologues

Table 1 summarizes the calculated γ values for monomers of thiophene homologues. At any kind of approximation levels, the calculated results show that the substitution with heavy atoms is effective for the increase of second hyperpolarizability. The γ values calculated including both effects of electron correlation and frequency dispersion are in good agreement with the recent observed values of nonlinear optical susceptibilities obtained using the optical Kerr effect (OKE) experiments, which have been done in our laboratory [6].

Oligomers of Thiophene Homologues

From the analysis of the results of monomers, the transition moment along the molecular axis is found to be important for the heavy atom effect on the γ values of the thiophene homologues. Therefore, we compare the effects of difference in the linkage type on the γ values for their oligomers. As shown in Figure 1, for the homologues with heavier atoms, the dimers with 2,3-linkage can give larger hyperpolarizability than the usual dimers with 2,2-linkage. This is ascribed to simultaneous contribution of the effects of heavy atom substitution and π -conjugation to the enhancement of the same tensor component of the γ

Poster Session II

Table 1. Comparison between the orientationally averaged second hyperpolarizabilities obtained by the present *ab initio* calculations and OKE experiment. Basis set used is the 6-31G+*pd* set. Numbers in parentheses are ratios to the values for furan.

Molecule	Calculation						Experiment 10 ⁻³⁶ esu
	HF		CCSD(T)		CCSD(T) + TDHF		
	a.u.	10 ⁻³⁶ esu	a.u.	10 ⁻³⁶ esu	a.u.	10 ⁻³⁶ esu	
C ₄ H ₄ O	11096	5.6 (1.0)	14750	7.4 (1.0)	18200	9.2 (1.0)	7.5 (1.0)
C ₄ H ₄ S	15040	7.6 (1.4)	20000	10.1 (1.4)	24400	12.3 (1.3)	13.2 (1.7)
C ₄ H ₄ Se	18978	9.6 (1.7)	25480	12.8 (1.7)	31700	16.0 (1.7)	17.2 (2.3)
C ₄ H ₄ Te	29515	14.9 (2.7)	38890	19.5 (2.6)	51690	25.5 (2.8)	37.5 (5.0)

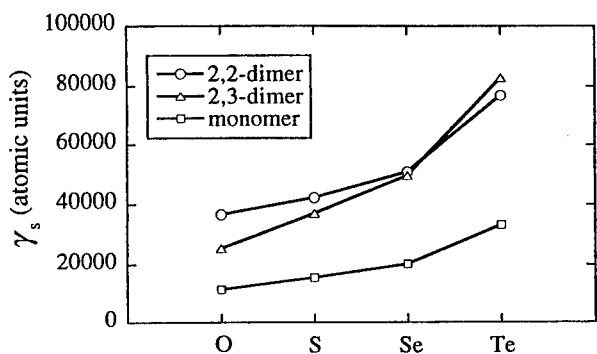


Figure 1: The second hyperpolarizabilities of the 2,2-dimer, 2,3 dimer, and monomer calculated with the 6-31G+*pd* basis set by the Hartree-Fock method.

values concerning molecular axis. Further extension of the conjugation length is discussed. The effect of electron correlation using DFT will also be discussed at the conference site.

References

- [1] M. T. Zao, et al., J. Chem. Phys. **89**, 5535 (1988).
- [2] M. J. Frisch, et al., Gaussian 98, Revision A.6, Gaussian, Inc., Pittsburgh PA, 1998.
- [3] M. Dupuis, et al., HONDO 95.3, IBM Corporation, 1995.
- [4] K. Kamada, et al., Int. J. Qunt. Chem. **70**, 737 (1998).
- [5] W. R. Wadt and P. J. Hay, J. Chem. Phys. **82**, 284 (1985).
- [6] K. Kamada, et al., Chem. Phys. Lett. **302**, 615 (1999).

Polarization Recording and Reconstruction in a Photoinduced Anisotropic Medium

Yoshiko Okada-Shudo
 Dept. of Electronic Engineering
 The Univ. of Electro-Communications
 182-8585 Tokyo, Japan

We have derived the polarization state of the wave which is diffracted at two types of polarization gratings; one is recorded with two orthogonally linear polarized waves, the other with two orthogonally circular polarized waves. The corresponding experiments using bacteriorhodopsin films are interpreted in terms of this simplified model.

Polarization grating

Spatially variable anisotropic transparencies such as polarization gratings are potential use in polarization control and splitting [1, 2]. The aim in this paper is to determine the selectivity dependence on the diffracted wave polarization by the polarization thin gratings. We consider two types of polarization interference pattern formed by two plane waves R and S with equal intensity. The grating \mathbf{a} is recorded by orthogonal linear (R :vertical, S :horizontal) and \mathbf{b} by circular (R :right-hand, S :left-hand) polarized waves on the xy plane. The resulting light field are described respectively for the case \mathbf{a} and \mathbf{b} by

$$E_a = \begin{pmatrix} E \\ E \exp(2\delta i) \end{pmatrix}, E_b = \begin{pmatrix} E \cos \delta \\ -E \sin \delta \end{pmatrix},$$

where $\delta = 2\pi x \sin \theta_w / \lambda_w$, 2δ is the phase shift between R and S whose wavelength is denoted by λ_w and the angle between two waves by θ_w . The period of these gratings $d = \lambda_w / 2 \sin \theta_w$. The Jones matrices for the gratings are

$$JM_a = \frac{1}{2} \begin{pmatrix} \frac{t_o + t_e}{2} + \frac{t_o - t_e}{2} \cos 2\delta & -\left(\frac{t_o + t_e}{2} - \frac{t_o - t_e}{2} \cos 2\delta\right) \\ \frac{t_o + t_e}{2} - \frac{t_o - t_e}{2} \cos 2\delta & \frac{t_o + t_e}{2} + \frac{t_o - t_e}{2} \cos 2\delta \end{pmatrix}, \quad (1)$$

$$JM_b = \begin{pmatrix} t_o \cos^2 \delta + t_e \sin^2 \delta & (t_o - t_e) \sin \delta \cos \delta \\ (t_o - t_e) \sin \delta \cos \delta & t_o \sin^2 \delta + t_e \cos^2 \delta \end{pmatrix}, \quad (2)$$

where t_o and t_e are the amplitude transmissions of the ordinary and extraordinary wave, respectively. The Jones vector for the incident wave (a general elliptic) can be written as

$$P = \frac{a}{\sqrt{a^2 + b^2}} \begin{pmatrix} 1 \\ i \end{pmatrix} + \frac{be^{i\varphi}}{\sqrt{a^2 + b^2}} \begin{pmatrix} 1 \\ -i \end{pmatrix}, \quad (3)$$

where a and b are the length of the principal axes. The amplitude distribution on z_1 plane in case \mathbf{a} is obtained by multiplying Eqs.(1) and (3);

$$U_{a1}(x_1) = \frac{t_o + t_e}{2} \left\{ \frac{a}{\sqrt{a^2 + b^2}} \begin{pmatrix} 1 \\ i \end{pmatrix} + \frac{be^{i\varphi}}{\sqrt{a^2 + b^2}} \begin{pmatrix} 1 \\ -i \end{pmatrix} \right\} + \frac{t_o - t_e}{4} (e^{\frac{2\pi i}{d} x_1} + e^{-\frac{2\pi i}{d} x_1}) i \left\{ \frac{a}{\sqrt{a^2 + b^2}} \begin{pmatrix} 1 \\ -i \end{pmatrix} - \frac{be^{i\varphi}}{\sqrt{a^2 + b^2}} \begin{pmatrix} 1 \\ i \end{pmatrix} \right\}. \quad (4)$$

Poster Session II

In case **b**, it is obtained by multiplying Eqs.(2) and (3);

$$U_{b1}(x_1) = \frac{t_o + t_e}{2} \left\{ \frac{a}{\sqrt{a^2 + b^2}} \begin{pmatrix} 1 \\ i \end{pmatrix} + \frac{be^{i\varphi}}{\sqrt{a^2 + b^2}} \begin{pmatrix} 1 \\ -i \end{pmatrix} \right\} + \frac{t_o - t_e}{2} \left\{ e^{\frac{2i\pi x_1}{d}} \frac{a}{\sqrt{a^2 + b^2}} \begin{pmatrix} 1 \\ -i \end{pmatrix} + e^{-\frac{2i\pi x_1}{d}} \frac{be^{i\varphi}}{\sqrt{a^2 + b^2}} \begin{pmatrix} 1 \\ i \end{pmatrix} \right\}. \quad (5)$$

Polarization property of diffracted wave

The amplitude distributions on z_1 plane as shown in Eqs.(4) and (5) are regarded as the pupil functions. After some manipulations the basic integral for Fraunhofer diffraction on z_2 plane, $U_{a2}(x_2)$ and $U_{b2}(x_2)$, turn out to take the forms (we omit here a constant factor) as,

$$U_{a2}(X) = \pi(t_o + t_e) \left\{ \frac{a}{\sqrt{a^2 + b^2}} \begin{pmatrix} 1 \\ i \end{pmatrix} + \frac{be^{i\varphi}}{\sqrt{a^2 + b^2}} \begin{pmatrix} 1 \\ -i \end{pmatrix} \right\} \delta(X) + \frac{\pi(t_o - t_e)i}{2} \left\{ \frac{a}{\sqrt{a^2 + b^2}} \begin{pmatrix} 1 \\ -i \end{pmatrix} - \frac{be^{i\varphi}}{\sqrt{a^2 + b^2}} \begin{pmatrix} 1 \\ i \end{pmatrix} \right\} \delta(X + \frac{2\pi}{d}) + \frac{\pi(t_o - t_e)i}{2} \left\{ \frac{a}{\sqrt{a^2 + b^2}} \begin{pmatrix} 1 \\ -i \end{pmatrix} - \frac{be^{i\varphi}}{\sqrt{a^2 + b^2}} \begin{pmatrix} 1 \\ i \end{pmatrix} \right\} \delta(X - \frac{2\pi}{d}), \quad (6)$$

$$U_{b2}(X) = \pi(t_o + t_e) \left\{ \frac{a}{\sqrt{a^2 + b^2}} \begin{pmatrix} 1 \\ i \end{pmatrix} + \frac{be^{i\varphi}}{\sqrt{a^2 + b^2}} \begin{pmatrix} 1 \\ -i \end{pmatrix} \right\} \delta(X) + \pi(t_o - t_e) \frac{a}{\sqrt{a^2 + b^2}} \begin{pmatrix} 1 \\ -i \end{pmatrix} \delta(X + \frac{2\pi}{d}) + \pi(t_o - t_e) \frac{be^{i\varphi}}{\sqrt{a^2 + b^2}} \begin{pmatrix} 1 \\ i \end{pmatrix} \delta(X - \frac{2\pi}{d}). \quad (7)$$

where $X \equiv 2\pi x_2 / \lambda_i l$. Here l denotes the distance between z_1 and z_2 , and λ_i the incident wavelength. Equation (6) shows that diffracted waves at the polarization grating **a** is split into three plane waves, the direction of which are λ_i/d , $-\lambda_i/d$, 0, respectively. 0-th order beam has the same polarized state as the incident wave *P*, and ± 1 order diffracted waves are polarized orthogonal to the incident wave. From Eq.(7), it is noticed the diffracted waves at the grating **b** are split into the same direction as the case **a**. The state of polarization of the order +1 is left-circular and that of the order -1 is right-circular, no matter what the polarization state of the incident wave. It is remarkable that the grating **a** and **b** play respectively the role of a half-wave plate and polarization compensator without wavelength dependence of the incident wave.

The corresponding experiments using photoinduced anisotropic media bacteriorhodopsin films are interpreted in terms of this simplified model.

References

- [1] P. Rochon, V. Drnoyan, and A. Natansohn, Proc. of SPIE **3491**, 306 (1998).
- [2] Franco Gori, Opt. Lett. **24**, 584 (1999).

Optical properties of composite materials

Anatoliy O. Pinchuk
Radiophysical Faculty
Kyiv T. Shevchenko University
Volodymyrska 64, Kyiv, Ukraine

Optical properties of nonlinear metal-polymer composites were theoretically studied. A metal fraction of spherical or ellipsoidal inclusions causes a surface plasmon resonance absorption. The dielectric permeability of nonlinear polymer matrix depends on the intensity of the local electric field. The effective dielectric permeability of the composite was calculated in quasi-electrostatic approximation for the inclusions much smaller than the incident wavelength. It is shown, that the optical transparency of thin film made from such composite can be changed from zero up to 40% when applying a moderate electric field. Such films can be used for optical signal processing devices.

Introduction

The optical properties of nonlinear metal-dielectric composites have been extensively studied in recent years [1]-[3]. It was theoretically shown that these composites have large nonlinearities in refractive indexes and can be used for purely optical signal processing devices. A bulk effective dielectric permeability $\tilde{\epsilon}$ of such composites is very sensitive to their microstructure. Moreover, $\tilde{\epsilon}$ depends on a dielectric permeability of a metal fraction $\epsilon_m = \epsilon'_m + i\epsilon''_m$ and on a nonlinear dielectric permeability $\epsilon_d = \epsilon_0 + \chi|E_0|^2$, where E_0 is the external electric field, χ , ϵ_0 are positive constants. The effective dielectric permeability also depends on a bulk fractions of a metal f_m , a dielectric f_d and a binder f_0 . It is obviously that $f_m + f_d + f_0 = 1$.

The metal fraction of a composite causes a resonant absorption of an electromagnetic radiation on Frolish's modes ω_s [3] corresponding to frequencies of surface plasmons in these systems within a frequency range ω smaller than a plasma frequency ω_p of a metal component where $Im\epsilon < 0$. A number of ω_s and their magnitudes strongly depends on the inclusions shape. In the simplest case of spherical metallic inclusions in a nonlinear dielectric, the frequency ω_s can be found from the relation [4]

$$\epsilon'_m(\omega_s) + 2\epsilon_d = 0 \quad (1)$$

In this equation the dielectric permeability of a nonlinear component ϵ_d depends on an intensity of the local electric field $I_d = |E_d|^2$ which in its turn is a function of the external field $I_0 = |E_0|^2$. Therefore in this case at $\omega \approx \omega_p$ the external electric field E_0 can considerably change a character of absorption of the electromagnetic radiation by the composite.

The correctly made film using such material can be changed over from a regime of complete nontransparency to a high transparency at $\omega \sim \omega_p$ by increasing the external electric field applied to the film. At the film thickness of 1mm we need the applied voltage of the order $\sim 10V$. The effect magnitude strongly depends on the composite content and structure. The same effect can be observed in many-component compounds. It is worth noting availability of a nonlinear component and a component having a negative magnitude of a real part of a dielectric permeability are the necessary conditions. The latter means that metals can be substituted with a dielectric having surface polaritons and excitons.

Poster Session II

Matrix disperse system with ellipsoidal inclusions

Consider the metal-dielectric nonlinear composite consisting of a nonlinear dielectric matrix and ellipsoidal metallic inclusions. Calculation of the effective dielectric permeability in general case is rather complex procedure[3]. The situation becomes simpler in the continuous approximation when the radiation wavelength traveling in the system is much larger than typical sizes of inclusions and average distances between them. In this case we can use the effective dielectric permeability in the next view

$$\frac{\bar{\epsilon} - \epsilon}{\epsilon + (\bar{\epsilon} - \epsilon)L_m} = N\alpha_m \quad (2)$$

where N is the inclusion concentration, α_m is the inclusion dipole polarization. This quantity for a double-layer ellipsoid was found in [4]. Therefor, determining $\bar{\epsilon}$ we can calculate the effective refraction index of the composite media \bar{n} . A detailed consideration of a calculation of a transmission coefficient will be published somewhere.

Summary

Thus we have considered the tuning effect of electric properties of nonlinear metal-dielectric composites by an external electric field. Considerable variations of these properties take place near the sharp resonance corresponding to the surface plasmon frequencies. To observe this effect the composite must contain the two components - metal and nonlinear dielectric. The effects are most conspicuous when: - $Im\epsilon$ is minimum (a semiwidth of the resonance line is minimum); - the coefficient χ is maximum that provides a wide tuning diapason at small electric fields. A possible application of the effect under consideration can be high resolution displays. For examples, the film of a width 3000\AA needs only $3V$ to obtain the value $E - 0 \sim 10^7 V/m$ when the clarification effect becomes significant.

References

- [1] D. Ricard, in Nonlinear Optics: Materials and Devices, edited by C. Flytzanis and J.L. Oudord, Springer-Verlay, Berlin, 154 (1986).
- [2] N. Kalyaniwalla, J.W. Hays, R. Inguva, and M.N. Birnboim, Phys.Rev.A **42**, 5613-5619 (1990).
- [3] L. G. Grechko, V. G. Levandovskii, V.M. Ogenko, A.O. Pinchuk "Effective Dielectric Properties of Metallic Particles Aggregates", Proceedings SPIE, USA, **3055**, 111-118, (1996).
- [4] C.F. Bohren, D.R. Huffman, "Absorption and Scattering of Light by Small particles", John Wiley & Sons, New York, (1983).

Femtosecond Spectroscopy of Polymethine Dyes in Liquid and Polymeric Media

Olga V. Przhonska*, Mikhail V. Bondar*, Yuriy L. Slominsky^o,
Raluca Negres, JinHong Lim[†], David J. Hagan, and Eric W. Van Stryland

School of Optics / CREOL, University of Central Florida
Orlando, FL 32816-2700

* Institute of Physics, National Academy of Sciences of Ukraine, Prospect Nauki 46, Kiev-22, 252650, Ukraine

^o Institute of Organic Chemistry, National Academy of Sciences of Ukraine, Murmanskaya 5, Kiev-94, 253660, Ukraine

[†] Present address: Dept of EE & Computer Science, Univ. of Michigan, 1124 EECS Bldg, 1301 Beal Avenue, Ann Arbor, MI 48109-2122

We report measurements of the excited state absorption spectra and dynamics in a series of polymethine dyes. We find extremely large excited-state absorption cross-sections, up to 200 times the ground state value in some materials. The combination of long lifetimes in PUA and broadband strong ESA is attractive for optical limiting applications.

We have studied nonlinear absorption in a series of polymethine dyes (PD) in ethanol solution and in an elastopolymeric material, polyurethane acrylate. (Fig. 1.) In the wavelength region 450-620 nm the dominant nonlinearity is excited-state absorption (ESA). Using picosecond Z-scan and pump-probe techniques, a relatively large ground-state absorption cross-section of these dyes has been measured, which effectively populates an excited state that possesses an extremely large ESA cross-section of up to 200 times the ground state value at 532 nm. Using a femtosecond white-light continuum spectrometer we studied the spectral and temporal dependence of the nonlinear absorption. Picosecond Z-scan and pump-probe techniques were used to measure the ground state absorption cross section, σ_0 , and ESA cross section, σ_1 , at specific wavelengths to calibrate the continuum measurements. The ratio of $\sigma_1/\sigma_0 = 200$ is the largest we know of at 532 nm.^{1,2}

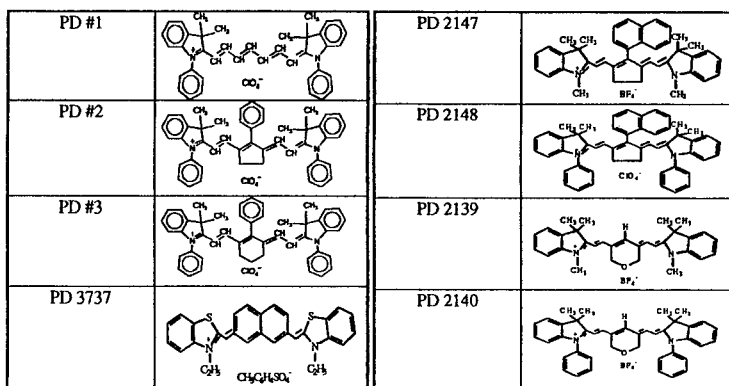


Figure 1. Molecular structure of polymethine dyes (PD's).

Poster Session II

Using our femtosecond white-light continuum pump-probe apparatus, we were able to record the ESA spectra of several PD samples as a function of delay time between the pump and probe pulses. We used 696 nm as the pump wavelength, which is resonantly absorbed within these dyes. Fig. 2 illustrates the ESA cross-sections of PD's in PUA over the visible region. One can easily see that the PD3 sample has a large cross-section σ_{ex} along with the broadest spectrum.

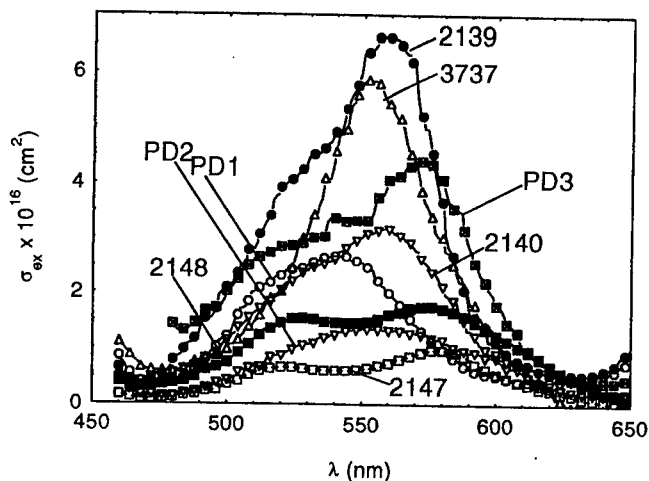


Figure 2. ESA cross-section spectra of PD's in PUA host material obtained with 696 nm excitation and probed with visible WLC at a delay of 60 ps.

Being a pump-probe experiment, our nonlinear spectrometer also gives information on the dynamics of the nonlinearity. By studying the time evolution of the ESA in PD3 in ethanol and in PUA, we observe a difference in the relaxational kinetics for low viscosity solvents like ethanol (5-7 ps) and the elastic polymer PUA (30 ps). We believe that the relaxation may be related to conformational changes to the dye in the excited state. However, these data require additional investigations to fully understand the relaxation dynamics of these types of molecules. To our knowledge, such relaxation processes for molecules in elastic hosts have not yet been investigated.

The broadband strong ESA is attractive for optical limiting applications, however, a longer lifetime is desired for applications. The longer lifetime observed in PUA is promising. In this respect, the combination of PD3 in PUA is attractive for device applications

References:

1. Olga V. Przhonska, J. H. Lim, D. J. Hagan, E. W. Van Stryland, M. V. Bondar and Y. L. Slominsky, "Nonlinear light absorption of polymethine dyes in liquid and solid media", *J. Opt. Soc. Amer. B* **15**, no. 2, 802-809 (1998).
2. J. H. Lim, Olga V. Przhonska, S. Khodja, S. Yang, T. S. Ross, D. J. Hagan, E. W. Van Stryland, Mikhail V. Bondar and Vuriy L. Slominsky "Polymethine and squarylium molecules with large excited-state absorption", *Chem. Phys.*, **245**, 79-97 (1999).

Microscopic and Macroscopic Third-Order Nonlinear Optical Properties of Organobimetallic compounds

G. Rojo¹, J. A. Campo², J. V. Heras², M. Cano² and F. Agulló-López²

¹Departamento de Física de Materiales, Universidad Autónoma de Madrid, 28049 Madrid, Spain.

²Departamento de Química Inorgánica I, Facultad de Ciencias Químicas, Universidad Complutense, 28040 Madrid, Spain.

The third-harmonic (THG) macroscopic and microscopic responses of a family of push-pull organobimetallic compounds with ferrocene as donor end, linked through a (HN- π -bridge) to the acceptor group, [Mo(Tp^{An})(NO)(Cl)], have been investigated. Compounds having NO₂ as acceptor end were also studied as references. Some trends for the role of conjugation length, substituents in the bridge and molecular characteristics have been determined. Design criteria for the optimization of the THG response have been obtained and compared to those derived for the second-order phenomena.

Introduction

Organometallics are a particular class of compounds offering a promising route for NLO studies that has not been sufficiently explored yet^[1]. The objective of this communication has been to investigate the THG responses of a family of push-pull organobimetallic molecules (1-5, 7), together with two compounds containing NO₂ as acceptor group (6, 8), shown in Fig. 1. Experiments to determine the molecular (solution) and macroscopic (films) THG response have been carried out.

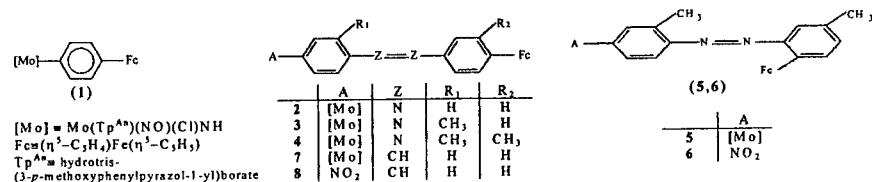


Fig. 1.- Chemical structure of compounds 1 - 8.

Experimental

The measurements, both in chloroform solution and dispersed into PMMA films, were performed at 1907 nm fundamental light obtained by shifting the wavelength of the 1064 nm emission of a Nd:YAG laser through a Raman cell containing hydrogen at high pressure.

From the solution data, both the real γ_r and imaginary γ_i parts of the molecular cubic hyperpolarizability $\chi(-3\omega; \omega, \omega, \omega) = \gamma_r + i\gamma_i$ were determined. Moreover, the magnitude and phase of $\chi^{(3)}(-3\omega; \omega, \omega, \omega)$ were obtained from the measurements in films.

Results

The real and imaginary components of the complex cubic hyperpolarizability for compounds 1-5 and 8 are listed in Table 1. Highest values $|\gamma| \cong 5 \times 10^{-33}$ esu have been obtained for 'straight' aza-bridged derivatives 2-4 having the [Mo(Tp^{An})(NO)(Cl)] fragment

Poster Session II

as acceptor group as expected from the dominant contribution of a 3ω resonance. A significant decrease in γ is observed for compound **1** and 'bent' molecule **5**.

The results for the macroscopic nonlinear susceptibility are also listed in Table 1. After normalization to equal concentration, the $\chi^{(3)}$ data show the similar trends (aside from data dispersion) found for the $|\gamma|$ ones, the highest values being obtained for compound **2** and slightly smaller for **3** and **4**. Substantially lower values are measured for the 'bent' organobimetallic molecule **5** and the nitro-compounds **6** and **8**.

Table 1: Microscopic and macroscopic third-order nonlinear optical properties of compounds **1-8**.

Compound	Microscopic nonlinear properties			Macroscopic nonlinear properties	
	γ_r (10^{-34} esu)	γ_i (10^{-34} esu)	$ \gamma $ (10^{-34} esu)	N (10^{19} cm $^{-3}$)	$ \chi^{(3)} $ (10^{-14} esu)
1	-4.50	4.60	6.40	18	30.2 (1.7)
2	-34.5	32.1	47.1	7.1	89.6 (12.6)
3	-4.67	13.2	14	7.3	64.4 (8.8)
4	-4.28	57.7	57.9	6.9	50.4 (7.3)
5	-1.80	4.10	4.48	10.7	13.4 (1.25)
6	-	-	-	15	14.6 (0.97)
7	-	-	-	9	50.4 (5.6)
8	6.05	8.60	10.5	6	7.8 (1.3)

Discussion

The main conclusions derived from the comparison between the γ and $\chi^{(3)}$ values measured for the different compounds and films are:

- (i) *Conjugation length:* Both the third-order NLO susceptibility, $\chi^{(3)}$, and the cubic hyperpolarizability, γ , strongly increase with the extension of the π -conjugated bridge, i.e. from **1** to **2**. The enhancement is even larger than that found for the second-order NLO susceptibility.^[2]
- (ii) *Substituents in the bridge:* A significant decrease in γ_r and also in $\chi^{(3)}$ is observed when moving from **2** to **4**, i.e. when substituents are attached to the bridge. However, the SHG yield was essentially insensitive to the presence of substituents at the bridge.^[2]
- (iii) *Bridging group:* The nonlinear response decreases when the stilbene group is substituted for the aza group in the bridge, **7** vs **2**. This effect was also observed for the $\chi^{(2)}$ and it was associated to the higher polarizability of the aza group in comparison to the stilbene one.²
- (iv) *Molecular bending:* 'Bent' compound **5** shows lower $|\gamma|$ and $|\chi^{(3)}|$ than the corresponding 'straight' compound **4**. The same conclusion can be also derived from the comparison between the susceptibilities of the 'straight' **8** and 'bent' **6** nitro-compounds, although the effect is here reduced due to the lower polarizability associated to the stilbene group in **8**. A similar trend with molecular bending was measured for the $\chi^{(2)}$ and attributed to a breaking or shortening of the conjugation path,² in agreement with (i).
- (v) *Acceptor group:* The [Mo(Tp^A)(NO)(Cl)] acceptor group causes a clear enhancement in the $\chi^{(3)}$ with respect to the nitro group (**7** vs. **8** or **5** vs. **6**). This is a key difference in relation to the second-order NLO responses where the opposite behavior was observed^[2,3].

References

- (1) Whittall, I. R.; McDonagh, A. M.; Humphrey, M. G.; Samoc, M. *Adv. Organomet. Chem.* **43**, 349 (1998).
- (2) López-Garabito, C.; Campo, J. A.; Heras, J. V.; Cano, M.; Rojo, G.; Agulló-López, F. *J. Phys. Chem. B* **102**, 10698 (1998).
- (3) Campo, J. A.; Cano, M.; Heras, J. V.; López-Garabito, C.; Pinilla, E.; Torres, R.; Rojo G.; Agulló-López, F. *J. Mater. Chem.* **9**, 899 (1999).

Quantum Chemical *ab initio* Search for Novel Molecular Technologies

A. Tamulis^a, J. Tamuliene^a, M.L. Balevicius^b, J.-M. Nunzi^c, R. Abdreimova^d, M. Peruzzini^e,
A. Graja^f

^aInstitute of Theoretical Physics and Astronomy, A. Gostauto 12, 2600 Vilnius, Lithuania;

^bFaculty of Physics, Vilnius University, Lithuania; ^cGCO-LETI-CEA, Saclay, France; ^dIOCE,
Almaty, Kazakhstan; ^eISSECC, Florence, Italy; ^fIFMPAN, Poznan, Poland

Quantum chemical *ab initio* density functional theory (DFT) and Hartree-Fock configuration interaction singlet (CIS-HF) methods are used for the investigations of *trans-cis* transitions in both stilbene and disperse orange 3 (DO3) azo-dye molecules during excitation and for the design of molecular logically controlled multivariable anisotropic random-walkers. These methods are also using for quantum chemical investigations of tetraphosphorus activation within coordination sphere of transition metal complexes and for finding of geometrical and electronical structure of fullerene C₆₀, CS₂, benzene, tetrafulvalene molecules, Li atom and their complexes.

1. Quantum Chemical Design of Molecular Logically Controlled Multivariable Anisotropic Random-Walkers^{a,b,c}

DFT and CIS-HF methods are used for the geometry optimization in ground and first excited states of both stilbene and DO3 azo-dye molecules. The results of light induced internal molecular motions in these molecules have been used for the design of light driven molecular machines.

Two-, three-, four- and six-variable anisotropic random-walk molecular motor devices are designed from photoactive organic molecules such as carbazole, 1,4-phenylenediamine (PhDA), TeMePhDA, stilbene, DO3 azo-dye, 4,5-dinitro-9-(dicyanomethylidene)-fluorene (DN9(CN)₂F), TCNB and TCNQ molecules joined with -C₂H₂- or -N=N- bridges.

Molecular implementation of organic derivatives based two-, three-, four-variable logic functions, summators of neuromolecular networks, cells of molecular cellular automata, molecular trigger - molecular logic devices and molecular devices for electronically genome regulation were designed based on results of semiempirical and *ab initio* HF, DFT quantum chemical calculations of the above mentioned electron-donors, electron-insulators, electron-acceptors as well as fullerene molecules.

Poster Session II

The molecular logical devices joined to multivariable anisotropic molecular random-walkers should be capable of moving under light exposure and therefore represent a new kind of logically controlled molecular motors. Two examples of such molecular logically controlled motors have been designed and calculated using HF\6-31G method: (1) (Cz-C₂H₂-)(NH₂-)(C₆H₃)-C₂H₂-(DN9(CN)₂F)-N=N-(C₆H₄-NO₂) and (2) (Cz-C₂H₂-)(PhDA-C₂H₂-)(NH₂-)(C₆H₂)-C₂H₂-(DN9(CN)₂F)-N=N-(C₆H₄-NO₂) and analogous compounds with the more flexible bridge -N=N-. (1) random-walker is two variable AND logically controlled molecular device and (2) is three different ways two variable AND controlled molecular random-walker.

2. Quantum Chemical Investigations of Tetracosphorus Activation within Coordination Sphere of Transition Metal Complexes^{a,b,d,e}

The ecologically friendly catalytic P-O coupling reaction for the synthesis of trialkyl phosphates is proposed. A slightly distorted octahedral symmetry was used for the design of the initial starting geometry in different transition metal (M = Pt, Pd, Ni) complexes:

- (1) [MX₃(CH₃OH)(η²-P₄)]⁻¹, (2) [MX₃(CH₃OH)(η²-P₄)]⁺¹,
(3) [MX₃(CH₃OH)(H₂O)(η¹-P₄)]⁻¹, (4) [MX₃(CH₃OH)(H₂O)(η¹-P₄)]⁺¹,
(5) [MX₃(CH₃OH)(η²-P₄)]⁻¹, (6) [MX₃(CH₃OH)(η²-P₄)]⁺¹,
(7) [MX₃(CH₃OH)(H₂O)(η¹-P₄)]⁻¹, (8) [MX₃(CH₃OH)(H₂O)(η¹-P₄)]⁺¹, (X = Cl, Br).

Suitable conditions for the intersphere nucleophilic attack of the tetracosphorus P₄ molecule by the alkoxide-ion RO⁻ are better matched with cationic complexes with highly oxidized M(IV) transition metals.

3. Quantum Chemical Methods for Investigations of Fullerene C₆₀, CS₂, Benzene, Tetrafulvalene Molecules, Li Atom and their Complexes^{a,b,f}

The geometry and energy of formation of single molecules such as fullerene C₆₀, CS₂, benzene and tetrathiofulvalene (TTF) and of their complexes like C₆₀+CS₂, C₆₀+benzene, C₆₀+TTF, C₆₀+Li were obtained using HF and DFT methods with the aim to search for new high conducting organic thin films. Weak chemical interactions were estimated satisfactorily by using HF\6-31G for a comparison of various geometrical conformations of these complexes. The energy of formation of the charge-transfer complex C₆₀+TTF has been performed calculating the complex with far-separated molecules.

This Research was supported by CEA-Saclay, France, EC contract ERBIC15CT960746, Lithuanian Research and Education Foundation, Dr. N.A. Kotov, Oklahoma State University, Vilnius Technical University and Poznan's Supercomputing and Networking Centers.

Understanding non-linearity: a toy model for push-pull chromophores

Francesca Terenziani, Luca Del Freato, Anna Painelli

*Dipartimento di Chimica Generale ed Inorganica, Chimica Analitica e Chimica Fisica
Università di Parma, I-43100 Parma, Italy*

We extend the two-state model for push-pull chromophores to account for electron-phonon coupling and the interaction with the environment. The model offers a simple and comprehensive picture for static NLO responses, electronic (absorption and emission) and vibrational spectra. The complex spectral behavior of push-pull chromophores is well understood within the simple model, accounting for few relevant interactions, provided its intrinsic non-linearity is fully exploited: standard perturbative approaches are proved to fail when applied to non-linear materials.

Introduction

Push-pull chromophores are an interesting class of π -conjugated molecules for advanced applications. They are currently investigated for their large β responses, as molecular rectifier, or as active chromophores for tunable light emitting devices. These diverse and fascinating properties originate from the intrinsic non-linearity of these materials. Experimental and numerical evidences are accumulating, proving the important role of vibrations and of the environment on NLO responses of push-pull chromophores [1, 2]. Large environment effects are also observed in absorption and emission spectra [3]. Vibrational frequencies, intensities and band-shapes show an impressive dependence on the embedding medium. All these seemingly unrelated phenomena are naturally understood based on a simple two-state model self-consistently accounting for the coupling of the electrons to molecular vibrations and to the surrounding medium.

A non-linear model for electronic and vibrational solvatochromism

An isolated push-pull chromophore can be modeled as a DA dimer with Holstein coupling to molecular vibrations [1]. Polar chromophores dispersed in a solvent also generate a reaction field, F_R , proportional to their dipole moment. A component of F_R originates from the polarization of the electronic cloud of solvent molecules. This fast component can be dealt with in the antiadiabatic approximation, simply renormalizing the effective model parameters [2]. In polar solvents, a second component of F_R appears, F_{or} , related to the orientation of the solvent molecules around the solute. The orientational dynamics is slow: F_{or} is introduced as an adiabatic boson field, so that the hamiltonian for a push-pull molecule in a polar solvent reads [2]

$$H = 2z_0\hat{\rho} - \sigma_x + \sum_{i=0}^N \frac{1}{2}\omega_i^2 Q_i^2 - \sum_{i=0}^N \sqrt{2\epsilon_i\omega_i} Q_i \hat{\rho} \quad (1)$$

where the first two terms describe the DA dimer; $\rho = (1 - \langle\sigma_z\rangle)/2$ measures the polarity of the chromophore; σ_x and σ_z are the Pauli spin operators, and the coefficient of σ_x is fixed to energy unit. Out of the boson coordinates, Q_0 accounts for F_{or} , $Q_{i>0}$ for internal vibrations. ϵ_0 is the relaxation energy due to solvent orientation, whereas $\epsilon_{i>0}$ measures the small polaron binding energy.

The above hamiltonian can be solved exactly. The coupling between electronic and slow degrees of freedom, treated in the adiabatic approximation, amplifies the non-linearity of the system, as evidenced by the large enhancement of static NLO responses [1, 2].

Poster Session II

But non-linearity also affects linear spectral properties. Within our model we calculate exact absorption and emission frequencies and demonstrate a non-linear dependence of the Stokes-shift on the solvent polarity, thus proving the failure of standard perturbative approaches to solvatochromism [3]. The non-linearity of push-pull chromophores implies a large and non-trivial dependence of molecular properties on the reaction field, and more generally on the configuration of slow variables. In striking agreement with experimental data, our model predicts solvent-dependent absorption and emission band-shapes, as well as narrower emission than absorption bands. It also naturally accounts for the narrowing of emission bands, as observed in time-resolved emission experiments [3].

Exact results are also obtained for vibrational properties. The frequencies and IR and non-resonant Raman intensities of coupled modes depend on ρ , and therefore on the solvent polarity. We can calculate exact ground- and excited-state potential energy surfaces, to get reliable simulations of resonant Raman spectra. Inhomogeneous broadening effects are well apparent in vibrational spectra of push-pull chromophores dispersed in polar solvents [4]. The orientational component of the reaction field slowly oscillates around its equilibrium value and the chromophore instantaneously readjusts its polarity to the local field. ρ -dependent vibrational properties are then the key to understand the inhomogeneous broadening of vibrational spectra as observed in polar solvents. In agreement with experimental data, we get solvent-dependent IR and Raman frequencies and band-shapes, and reproduce the dispersion of resonant Raman frequencies with the exciting line, as observed, e.g., in phenol blue [4].

Conclusions

The DA dimer model plus Holstein coupling, as reported in (1), offers a simple description of static NLO responses of push-pull chromophores and accurately reproduces their spectral behavior in terms of a few microscopic parameters. Linear and non-linear optical properties of push-pull chromophores cannot be caught, even at a qualitative level, without accounting for the intrinsic non-linearity of the system. Perturbative approaches to electron-molecular vibration coupling and/or to the interaction with the solvent are bound to fail if applied to NLO materials.

References

- [1] A. Painelli, Chem. Phys. Lett. **285**, 352 (1998).
- [2] A. Painelli, Chem. Phys. **245**, 183 (1999).
- [3] A. Painelli, F. Terenziani, Chem. Phys. Lett. **312**, 211 (1999).
- [4] T. Yamaguchi, Y. Kimura, N. Hirota, J. Chem. Phys. **109**, 9075 (1998).

Establishing the Optical Parameters of the thin Films in the Case of Bacteriorhodopsin Molecules

R.Todoran, D.Todoran,
North University of Baia Mare
Str. Victor Babes Nr. 62/A,
4800 Baia Mare, Romania

J.Sharkany
Uzhgorod State University
Pidhirna St. 46, Uzhgorod, Ukraine

The use of organic optical sensors has become increasingly frequent in the field of signal conversion and transmission. Rhodopsin plays an important role in this respect. This paper presents briefly results concerning the determination of the values of the optical functions of some bacteriorhodopsin thin films. Knowledge of these functions contributes to knowledge of some optoelectronic properties of the bacteriorhodopsin.

Bacteriorhodopsin are of great interest due to their photochromic properties, the ability to generate potential when illuminated, and the availability of the photoinduced anisotropy and dichroism [1].

The bacteriorhodopsin molecules are fixed on the amorphous support with the help of organic chemical additive with a transparency in the optical domain UV-VIS as good as possible. Gelatin, polyvinyl alcohol and polyvinylpyrrolidone were used.

Using the Kramers-Kronig formalism and with the aid of the optical reflection spectra UV-VIS, we could calculate the following optical functions for the bacteriorhodopsin layer: the optical absorption coefficient α ; the refraction index n ; the absorption index k ; the effective valence number n_{ef} ; the real part ϵ_1 of the dielectric constant; the imaginary part ϵ_2 of the dielectric constant; the functions of the characteristic losses of the electrons $-\text{Im}\epsilon^{-1}$ and $-\text{Im}(1+\epsilon)^{-1}$; the effective dielectric constant ϵ_{ef} ; the function $\epsilon_2 E^2$ [2]. The first three coefficients are used to determine the depth of the penetration of the optical beam in the interaction medium at the interface, thus providing information regarding the dimensions of the absorption layer. ϵ_1 gives information about the structure of the electronic cover of the interface whereas ϵ_2 gives information on the mechanism of the light and charge carriers interaction. The function $\epsilon_2 E^2$ gives information on the spectral evolution of the energetic states. The effective valence number n_{ef} characterizes the average valence number of the compound composition of the compound. The energetic losses could be characterized by the functions $-\text{Im}\epsilon^{-1}$ and $-\text{Im}(1+\epsilon)^{-1}$ according to the nature of the refraction index. In those spots where they show extreme values represented by the van Hove points, the functions characterise the shape of the energetic bands and the dispersion of the effective masses of the carriers of the structure analyzed.

These parameters allow an optoelectronic evaluation of the thin bacteriorhodopsin layer, leading to a better use of the bacteriorhodopsin in optical devices.

Obtaining the above optical functions on the basis of the reflection spectrum of the bacteriorhodopsin thin film was achieved owing to the use of a computer software designed for the processing of the Kramers-Kronig functions, which eliminates the states of mathematical indetermination [3].

The results of the determinations were the following: the optical function α shows an increase on the interval 1,9 eV–4,8 eV and a decrease on the interval 4,8 eV–6,3 eV, the

Poster Session II

maximum value of this function being 0,11 for 4,8 eV; the optical function k shows an increase on the interval 2,4 eV-2,9 eV and a decrease on the interval 2,9 eV-6,1 eV, the maximum value of this function being 2,4 for 2,9 eV. For the optical function $-\text{Im}\varepsilon^{-1}$ and $-\text{Im}(1+\varepsilon)^{-1}$ there exists two van Hove points. The function n_{ef} present a variation between -2,5 and -3,5 for the evaluated optical interval.

References

- [1] Z. Bathory Tarczy, O. Korposh, N. Frolova, V. Jarosh, "Modification of Properties of Light-Sensitive Bacteriorhodopsin Layers", International Workshop on Advanced Technologies of Multicomponent Solid Films and Structures, 53-55 (1994).
- [2] M. I. Karaman, V. A. Litchman, V. P. Mushinski, Im. Smirnov, "Dispersia Opticheskikh Konstant Kristallov Paratelurita", Nauch. Journ., Pr. Spektroskopji **49**, 825-829(1988).
- [3] R. Todoran, J. Sharkany, "An "in Situ" Kinetics Studying Method by Optical Reflection in VIR-IR of the Xanthate Adsorption on the Surface of Sulfuric Minerals", J. Min. **34**, 57-65 (1998)

Second Harmonic Spectroscopy and SHG Microscopic Observation of J-aggregate Domains in Merocyanine at the Air-Water Interface

Yoshiaki Uesu***, Noritaka Kato* and Kentaro Saito*

**Department of Physics,*

***Advanced Research Institute for Science and Engineering,*

Waseda University, 3-4-1, Okubo, Shinjuku-ku, Tokyo 169-8555, Japan.

Optical second harmonic(SH) spectrum of merocyanine dye(M D) at the air-water interface was investigated in the SH wavelength region from 300 to 635nm. Three peaks were observed at 620, 314 and 310nm. The spectrum of 620nm is the resonant J-band of the fundamental wave, the spectrum at 310nm the resonant J-band of the SH wave and the spectrum observed at 314nm is probably the bi-exitonic spectrum. 2D-SH images were taken using the multi-purpose nonlinear optical microscope at several wavelengths. Careful comparisons revealed that the whole spectra originate from the J-aggregate states of MD.

Certain kinds of dye molecule are known to form the J-aggregate, which is characterized by a red-shifted sharp absorption band and Stokes-shift-free fluorescence[1]. Our recent investigations using the second harmonic generation (SHG)/fluorescence(FL) microscope clarified the morphological structure of MD/arachidic acid (AA) mixed monolayer at the air-water interface and the merocyanine dye (MD) was found to form mesoscopic J-aggregate domains which are SHG-active[2,3]. The purpose of the present study is to clarify the active site which produces the characteristic nonlinear optical properties of the MD/AA monolayer system. For this purpose, we first measured the SH spectrum in the wide wavelength range including the resonant spectra and took the SHG images of MD/AA mixed monolayer at the air-water interface around the resonant spectra and compared them.

Monolayer specimens containing large SHG-active JA domains were prepared with aqueous ammonia (<0.03 wt.%, >pH10) as a subphase [3]. AA of molar fraction of 60% was mixed to stabilize the MD monolayer. The mixture compound was solved in chloroform (1mmol/l) and the solution was gradually spread on the subphase. Surface pressure was less than 14.7mN/m.

The optical parametric oscillator (OPO) was used for changing fundamental wavelength from 600nm to 1269nm. The average power of the output wave from OPO is 2~23mW and the repetition frequency is 20Hz. SHG spectrum was detected by a polychromator equipped with semiconductor detector array. The exposure time was 4 seconds. Reflection spectrum was also detected by the polychromator. SHG image was taken by ICCD (Integrated charge coupled device) with gating image intensifier synchronized with the laser oscillation [4]. The exposure time is 20~30 seconds.

Poster Session II

K. SAITO, N. KATO and Y. UESU

The formation of the J-aggregate of each specimen was examined by observing the characteristic J-band reflection and fluorescence spectra at 620nm[3]. In the SH spectrum of the MD/AA monolayer system, three distinct peaks were observed: One at 620nm is the resonant spectrum of the J-band for the fundamental wave and another sharp peak at 310nm is the resonant J-band for the SH wave. It should be noted that the third peak is also observed near the SH resonant peak of the J-band. The spectrum is located at 314nm and would be due to the resonance with excitonic 2-strings, which is the bound state of two Frenkel excitons [5]. The more precise examination is necessary for clarify the origin.

SHG images of the MD/AA system were observed at several wavelengths. During the observation, the optical geometry should have been rearranged when the wavelength is shorter than 867.4nm (shorter than 433.7nm for SHG) and we had to prepare a new sample under same condition. Thus we choose the SHG image taken at 433.7nm as the reference to compare the image for all spectrum range. In whole wavelength rage, no significant change in the image was observed. Thus we can safely conclude that SH spectra are generated from the JA forming MD domain.

References

- [1] T. Kobayashi, J-aggregates, (World Scientific, Singapore, 1996).
- [2] N. Kato, K. Saito, and Y. Uesu, Chem. Phys. Lett., in print.
- [3] N. Kato, K. Saito, and Y. Uesu, Ferroelectrics, inprint.
- [4] N. Kato, K. Saito, and Y. Uesu, Thin Solid Films, **338**, 5 (1999).
- [5]. Tokihiro, M. Kuwata-Gonokami, R. Shimano, K. Ema, E. Hanamura, B. Fluegel, K. Meissner, S. Mazumdar, N. Peyghambarian, Solid State Commun., **88**, 211 (1993).

Longitudinal and Transverse Dynamics of Soliton Excitations on a Multileg Ladder Lattice

Oleksiy O. Vakhnenko

Bogolyubov Institute for Theoretical Physics Kyiv 252143, Ukraine

Engineering Science Department, University of Patras, Patras 26110, Greece

The exactly integrable model of nonlinear excitations on a multileg ladder lattice and its continuous counterpart are proposed. The models are closely related to the nonlinear Schrödinger model on the same lattice with linear and nonlinear couplings between the chains explicitly taken into account. The models permit a number of interesting physical applications related to the strip-like and bunch-like biological and condensed matter systems as well as to the arrays of linearly and nonlinearly coupled optical fibers. The soliton solutions of two-chain and three-chain models are found and analyzed. Apart from the spatially constricted translational mode typical to the traditional one-chain soliton, the interchain beating mode and the circular travelling modes redistributing the excitations between the chains are revealed.

The models of a nonlinear Schrödinger type have played an exceptional role in physical applications for more than three decades. They arise in rather different physical systems where the balance between dispersion and nonlinearity produces the fundamental entity known as a soliton. The most intriguing ones are the multicomponent nonlinear models supporting linear or nonlinear couplings between their components thereby prompting rather sophisticated effects of mode-mode interactions. Here it is worth noticing the exactly integrable models of Manakov type [1-3]. Though being very useful for the nonlinear optics these models [1-3] become hardly suitable for the needs of biological and condensed matter systems inasmuch as they do not describe the effects of linear (tunneling) couplings between the excitations belonging to the different chains. In this communication we will try to fill this gap by presenting the new integrable model of intramolecular excitations on a multileg ladder lattice with linear and nonlinear interchain couplings between the excitations explicitly taken into account. The extended reports of our investigation was published elsewhere [4,5].

Following the terminology of nonlinear transport phenomena we prescribe the quantities $q_\alpha(n)$ and $r_\alpha(n)$ to be the excitation amplitudes of molecule sited on α -th chain within n -th unit cell. The longitudinal numerical coordinate n is supposed to run from minus to plus infinity, whereas the transverse one α from unity to the number of chains (legs) M . The exactly integrable evolution model dealing with the intramolecular excitations on M -leg ladder lattice reads as follows:

$$\begin{aligned}
 & i\dot{q}_\alpha(n) + \sum_{\beta=1}^M t_{\alpha\beta} q_\beta(n) + [q_\alpha(n+1) + q_\alpha(n-1)] \left[1 + \sum_{\beta=1}^M q_\beta(n) r_\beta(n) \right] = \\
 & = \sum_{\beta=1}^M [q_\alpha(n-1) q_\beta(n) - q_\alpha(n) q_\beta(n-1)] r_\beta(n) \quad (1)
 \end{aligned}$$

$$\begin{aligned}
 & -i\dot{r}_\alpha(n) + \sum_{\beta=1}^M r_\beta(n) t_{\beta\alpha} + [r_\alpha(n+1) + r_\alpha(n-1)] \left[1 + \sum_{\beta=1}^M r_\beta(n) q_\beta(n) \right] = \\
 & = \sum_{\beta=1}^M [r_\alpha(n+1) r_\beta(n) - r_\alpha(n) r_\beta(n+1)] q_\beta(n), \quad (2)
 \end{aligned}$$

Poster Session II

where $\alpha = 1, 2, 3, \dots, M$ and $t_{\alpha\beta}$ is the interchain linear coupling constants. The dot stands for the derivative with respect to dimensionless time. Being rather general, the model (1) and (2) permits a number of physically interesting ramifications obtainable by merely imposing appropriate restrictions on the coupling constants $t_{\alpha\beta}$. Thus we are able to model the nonlinear excitations on a multileg ladder lattice unrolled into the two-dimensional strip or combined into the three-dimensional bunch of tightly bound chains. Moreover, in the latter case we are in a position to apply an external magnetic field parallel to the ladder legs without the integrability of the model to be lost.

In particular, we have studied the transverse and longitudinal dynamics of nonlinear excitations on two-leg ladder lattice and have shown the existence of transverse beating mode periodically redistributing the soliton density between the chains. Depending on the initial conditions, the relative amplitude of beating can be varied from zero to unity. On the other hand the frequency of beating has a fundamental origin and is determined by the value of interchain coupling constant.

In the case of charged nonlinear excitations on bunch-like three-leg ladder lattice we have managed to describe exactly the effect of constant magnetic field directed along the chains. Thus it has been shown that the magnetic field breaks the symmetry of soliton dynamics with respect to clockwise and anticlockwise propagation across the chains and gives rise to three different circular travelling modes redistributing the soliton density in transverse direction. Moreover at some fixed values of magnetic field these modes could be transformed into two circular modes or even into one standing mode.

Except of these transverse breathing-like modes our models support the purely translational soliton-like modes typical to the models without interchain linear coupling.

In some problems and in particular those dealing with nonlinear optics the discretization of amplitudes $q_\alpha(n)$ and $r_\alpha(n)$ with respect to n becomes unnecessary. Then it is reasonable to replace the discrete nonlinear model (1) and (2) by its partially continuous equivalent [5], which also happens to be integrable. Nevertheless, the general features of transverse dynamics of such partially continuous model coincide with those of completely discrete one (1) and (2) inasmuch as the terms responsible for the interchain linear coupling are the same in both models.

Summarizing, we have developed an exactly integrable nonlinear model on multileg ladder lattice strongly related to a wide range of physically important phenomena from nonlinear transport in low-dimensional biological, polymeric and condensed matter systems to electric pulse propagation in nonlinear transmission lines and light pulse propagation in tunnel- and nonlinearly coupled arrays of optical fibers. In doing so we have suggested the systematic analytical approach suitable for the needs of nonlinear physics in more than one spatial dimension and have studied the structure of simplest nonlinear excitations on two- and three-leg ladder lattices.

References

- [1] S.V. Manakov, JETP **38**, 248 (1974).
- [2] T. Tsuchida, H. Ujino and M. Wadati, J. Phys. A **32**, 2239 (1999).
- [3] M.J. Ablowitz, Y. Ohta and A.D. Trubach, Phys. Lett. A **253**, 287 (1999).
- [4] O.O. Vakhnenko, Phys. Rev. E **60**, R2492 (1999).
- [5] O.O. Vakhnenko, J. Phys. A **32**, 5735 (1999).

Orientation and nonlinear optical properties of DAN crystals on PTFE substrates

R. Vallée, P. Damman, M. Dosiere
*Laboratoire de physicochimie des polymères
Université de Mons
B-7000 Mons
Belgique*

E. Toussaere, J. Zyss
*Laboratoire de photonique quantique et moléculaire
Ecole normale de Cachan
UMR CNRS # 8537
61, Avenue du président Wilson
94235 CACHAN Cedex
France*

The growth of DAN crystals on nano-structured PTFE substrate has been investigated by means of X-ray, FTIR and NLO ellipsometry. Two types of structural arrangements were detected, depending on the growth conditions. In both cases, the (001)_{DAN} plane contacts the (100)_{PTFE} substrate plane. The major difference between both types of samples lies in the presence of azimuthal orientation at the interface. The comparison between the various techniques used in this study to characterize the obtained thin films showed a remarkable agreement. With respect to this, the Second Harmonic Generation revealed once again as a powerful technique for the study of orientation effects in crystalline layers of NLO organic materials.

Organic materials presenting huge nonlinear optical (NLO) property are generally made-up of molecular structures consisting of a conjugated π -electron system, with electron donor and acceptor groups attached at opposite sides of the molecule so as to induce an intramolecular charge transfer and consequently enhance the first-order hyperpolarizability tensor β . In this respect, p-nitroaniline (p-NA) is usually considered as a benchmark molecule. However, due to the centrosymmetry of the p-NA crystal, its second-harmonic nonlinear coefficients d_{ij} vanish.

Therefore, closely related molecules such as 4-(N,N-dimethylamino)-3-acetamidonitrobenzene (DAN) which maintain an important charge transfer but hinder the centrosymmetric crystal packing have been widely investigated.[1][2][3][4]

DAN crystals were grown by sublimation on nanostructured poly(tetrafluoroethylene) (PTFE) substrates prepared by the friction transfer method.[5] For such a growth procedure, a large number of tiny crystals are deposited on the substrate. But are those numerous crystals oriented in the same manner on the substrate? Investigations were performed by means of X-ray, micro-FTIR and nonlinear optical ellipsometry techniques.

Two types of structural arrangements were identified, depending on the growth conditions. In both cases, the (001)_{DAN} plane contacts the (100)_{PTFE} substrate plane. Nevertheless, while a uniform extinction is observed at the polarizing microscope, indicating the presence of an azimuthal orientation in this plane, for the thinnest samples, the thickest ones do not exhibit such an extinction.

In fact, for the thinnest samples, the average direction of the crystallographic axes of the DAN crystals lie parallel to the [001]_{PTFE} direction with a broad angular distribution,

Poster Session II

while the thick samples are characterized by a uniaxial orientation with an isotropic random distribution in the plane of the layers.

Indeed, the thinnest samples exhibit a very large lattice mismatch, $\Delta = 15\%$, between the substrate and the overlayer lattices, quantified on the basis of GIXD measurements.

Furthermore, assuming a box-like distribution of angular aperture $[-\alpha_0, \alpha_0]$ to account for an hypothetic uniform disorientation of the a parameter with respect to the PTFE sliding directions, leads to an average α_0 value of around 20° , deduced from FTIR measurements.

Finally, considering that the numerous DAN crystals of the layers are characterized by a broad distribution of orientation allows to reproduce the experimental data obtained for the nonlinear SHG ellipsometry technique, since a matching between the simulated graphs and the experimental results has been found for an angular range spreading over a $[-34^\circ, 34^\circ]$ broad interval.

Contrarywise, the thickest samples lack peaks in GIXD measurements (ϕ scan), indicating the absence of azimuthal orientation in the $(001)_{DAN}$ plane of contact. Moreover, interpretations of experimental data obtained from SHG ellipsometry measurements agree with this latter observation, thus comforting the lack of in-plane orientation.

In this context, Second Harmonic Generation revealed once again as a powerful technique towards the study of orientation effects in crystalline layers of NLO organic materials, much beyond the possibilities of traditional linear polarization. methods.[6][7]

References

- [1] R. J. Twieg and K. Jain, in *Nonlinear Optical Properties of Organic and Polymeric Materials*, edited by D.J. Williams, ACS Symposium Series No. 233 (American Chemical Society, Washington, D.C., 1983), pp. 57-80.
- [2] P.A. Norman, D. Bloor, J.S. Obhi, S.A. Karaulov, M.B. Hursthouse, P.V. Kolinsky, R.J. Jones, S.R. Hall, *J. Opt. Soc. AM. B* 4(6), 1013 (1987).
- [3] J-C Baumert, R.J. Twieg, G.C. Bjorklund, J.A. Logan, and C.W. Dirk, *Appl. Phys. Lett.* 51(19), 1484 (1987).
- [4] P. Kerkoc, M. Zgonik, K. Sutter, Ch. Bosshard, and P. Günter, *Appl. Phys. Lett.* 54(21), 2062 (1989).
- [5] J.C. Wittmann, P. Smith, *Nature*, 352, 414 (1990).
- [6] P. Damman, R. Vallée, M. Dosière, J.C. Wittmann, E. Toussaere, J. Zyss, *Opt.Mat.*, 9, 423 (1998).
- [7] R. Vallée, P. Damman, M. Dosière, E. Toussaere, J. Zyss, *J. Am. Chem. Soc.* (submitted).

Holographic Time-Of-Flight for the sub-nanosecond investigation of charge transport

M. Wintermantel, I. Biaggio, and P. Günter
Nonlinear Optics Laboratory
Swiss Federal Institute of Technology
CH-8093 Zürich, Switzerland

Holographic Time-Of-Flight (HTOF) is a contactless optical method for the investigation of charge-transport in materials with low charge carrier mobilities and lifetimes where classical Time-Of-Flight (TOF) measurements are difficult or impossible to apply. It can be used without any applied fields (diffusion mode) or by letting the photoexcited carriers drift in an applied electric field (drift mode). When used with pump & probe techniques in a degenerate four wave mixing set-up, it can detect charge transport on the picosecond time-scale. We discuss the applicability and the advantages of this methods for investigations in organic and inorganic materials.

In many materials fundamental charge transport parameters like the mobility of charge carriers and the free carrier lifetime are difficult to determine using conventional Time-of-Flight (TOF) methods. The reason is often to be found in low mobility values and short free carrier lifetimes (of the order of some nanoseconds or less) which render electronic-detection of a current difficult. Moreover, many TOF-measurements (which use relatively long transport lengths) do not determine a well-defined mobility because of dispersive charge-transport, or because of the existence of shallow traps: many trapping/thermal excitation steps take place during the TOF measurement, which leads to an average non-intrinsic value of the mobility.

Holographic Time of Flight (HTOF) allows the the all-optical and contact-less determination of the carrier mobility in the bulk of an electro-optic and photoconductive sample. The transport length is set by the period of a photoinduced interference pattern, and its time-resolution is only limited by the duration of the optical pulses employed, allowing the sub-nanosecond study of charge transport.

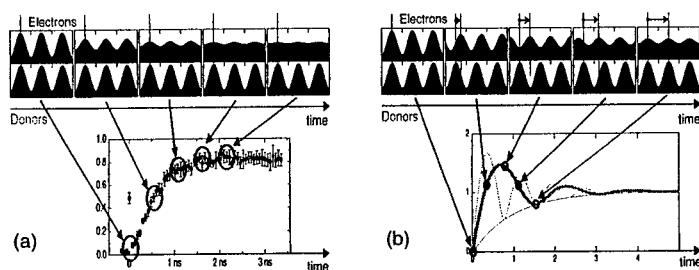


Figure 1: Movement of the charge carriers (in this case electrons) away from their counter-charges (donors) and the resulting time-dependant diffraction efficiencies for (a) diffusion-mode and (b) drift-mode HTOF.

HTOF uses two interfering short laser pulses of adequate wavelength to excite a spatially sinusoidal pattern of charge carriers in the bulk of a sample. The evolution of this pattern is measured optically by diffracting a probe beam from the space-charge-induced

Poster Session II

index-change caused by the separation of the free carriers from their excitation point. This separation is caused by drift in an external electric field for *drift-mode* HTOF (Fig. 1b), and is simply caused by thermal diffusion for *diffusion-mode* HTOF (Fig. 1a). In diffusion-mode HTOF the carrier migration leads to a perfect exponential build-up of the signal (Fig. 1a). The build-up time gives the carrier diffusion time and therefore the mobility. In drift-mode HTOF the space-charge field reaches a maximum when the mobile carriers have drifted to a position of anticoincidence with the immobile distribution of the donors from where they were photoexcited. Further drift causes a decrease of the space-charge field until coincidence is reached again and so on (Fig. 1b).

When the transport lengths (*i.e.* the spatial period of the photoexcited charge pattern) are long and the mobility is small, charge-transport can be observed using a continuous wave probe beam. For short transport lengths (which can be as small as a fraction of a μm) and larger mobilities, charge migration must be followed using a delayed probe pulse in a pump & probe, degenerate four-wave mixing set-up. This allows time resolutions from nanoseconds down to the duration of the optical pulses used.

HTOF was first demonstrated in drift-mode with relatively large transport lengths of several $100\ \mu\text{m}$ by Partanen *et al.* [1]. They thus determined the average electron mobility caused by shallow traps in $\text{Bi}_{12}\text{SiO}_{20}$. Diffusion-mode HTOF was first used in a pump & probe set-up to determine the intrinsic electron mobility in KNbO_3 [2, 3].

In order to determine the intrinsic band-mobility in $\text{Bi}_{12}\text{SiO}_{20}$, it was necessary to move to shorter transport lengths and observe charge migration on the nanosecond time scale [4]. The measurements of electron-mobility vs. temperature demonstrated that the intrinsic electron band-mobility in $\text{Bi}_{12}\text{SiO}_{20}$ corresponds to large polarons [4].

The HTOF method was first applied to a photorefractive polymer by Malliaras *et al.* [5] in its drift-mode variant, with a continuous wave probe beam. These measurements lack the typical oscillatory behavior shown in Fig. 1b. This is a consequence of dispersive charge transport, which leads to a smearing out of the oscillations [6].

In the present contribution, we will make an overview of HTOF techniques, discuss their applicability and advantages in organic materials, and show several examples of HTOF measurements in different materials.

References

- [1] J. P. Partanen, P. Nouchi, J. M. C. Jonathan, and R. W. Hellwarth, *Phys. Rev. B* **44**, 1487 (1991).
- [2] I. Biaggio, M. Zgonik, and P. Günter, *J. Opt. Soc. B* **9**, 1480 (1992).
- [3] M. Ewart, I. Biaggio, M. Zgonik, P. Günter, *Phys. Rev. B* **49** (8), 5263-5273 (1994).
- [4] I. Biaggio, R. W. Hellwarth, and J. P. Partanen, *Phys. Rev. Lett.* **78**, 891 (1996).
- [5] G. G. Malliaras, V. V. Krasnikov, H. J. Bolink, and G. Hadziioannou, *Phys. Rev. B* **52**, 14324 (1995).
- [6] G. G. Malliaras, H. Angerman, V. V. Krasnikov, G. ten Brinke, and G. Hadziioannou, *J. Phys. D: Appl. Phys.* **29**, 2045 (1996).

Influence of conjugation length on first hyperpolarizability of fluorescent hemicyanine (DAST) derivatives

Kurt Wostyn, Geert Olbrechts, Koen Clays and André Persoons¹
*Laboratory of Chemical and Biological Dynamics, Center for Research on Molecular Electronics and Photonics, University of Leuven
Celestijnenlaan 200 D, B-3001 Leuven, Belgium*

Akira Watanabe, Kyoko Nogi, Xuan-Ming Duan, Shuji Okada, Hidetoshi Oikawa, and Hachiro Nakanishi
*Institute for Chemical Reaction Science, Tohoku University
Katahira, Aoba-ku, Sendai 980-8577, Japan*

Henryk Vogel, David Beljonne, and Jean-Luc Brédas¹
*Laboratory for Chemistry of Novel Materials, Center for Research on Molecular Electronics and Photonics, University of Mons-Hainaut,
place du Parc 20, B-7000 Mons, Belgium*

¹also at University of Arizona, Tucson, AZ 85721, USA.

The influence of the conjugation length upon the first hyperpolarizability for a series of five fluorescent hemicyanine (DAST) chromophores was studied by hyper-Rayleigh scattering. The fluorescence contribution was eliminated using high frequency demodulation of multiphoton fluorescence.

Ionic chromophores have since long been envisaged as promising precursors for nonlinear optical (NLO) materials. However, their ionic nature precludes the determination of their first hyperpolarizability value β using Electric-Field-Induced Second-Harmonic Generation (EFISHG). The electric field, needed to break the centrosymmetry of the solution, can not be applied over ionic solutions. The introduction of hyper-Rayleigh scattering (HRS) [1, 2] has made it possible to measure the β -value of such ionic chromophores. In the HRS-technique, the temporal and orientational fluctuations of chromophores in the solution break the macroscopic centrosymmetry allowing for second-order processes to be observed. Multiphoton fluorescence (MPF), however, can contribute to the incoherent HRS-signal leading to an overestimated β -value. Recently, a frequency-resolved HRS-setup has been devised to differentiate between the immediate scattering and the time-delayed fluorescence in the frequency domain [3,4].

Technique

The technique relies on the demodulation (decrease in amplitude) of the fluorescence as a function of the amplitude modulation (AM) frequency of the fundamental light beam. The observed demodulation tend to zero at high AM frequencies. This effect, together with the out-of-phase behaviour of the fluorescence versus increasing AM frequency of the laser excitation source, is well known from (multi-frequency) phase fluorometrie [5]. On the contrary, the scattering is immediate, resulting in a constant scattering intensity, irrespective of the AM frequency. Whereas the generic laser type for HRS experiments is a Nd³⁺:YAG laser, a femtosecond Ti³⁺:sapphire laser has to be used for the frequency-resolved HRS measurements. An additional femtosecond OPO has been inserted to shift the fundamental wavelength towards the infrared (1300 nm) resulting in a second-harmonic wavelength of 650 nm. The intrinsic high harmonic content of the repetitive femtosecond pulse can then be used as an amplitude modulation source of high frequency.

Measuring at a very high modulation frequency (several GHz) would enable us to only measure the scattering, leading immediately to the inherent first hyperpolarizability of the chromophore, not overestimated by fluorescence. Unfortunately, this very high modulation

Poster Session II

frequency cannot be attained experimentally. We have resolved this problem by measuring the demodulation of the fluorescence as a function of the modulation frequency. As a result, multiple HRS experiments at various modulation frequencies have to be performed. The obtained demodulation curve (β versus modulation frequency) is then fitted. The fitting equation includes the MPF intensity, the fluorescence lifetime(s) and the intrinsic fluorescence-free β -value. The latter is obtained as the high-frequency limit of the fitted demodulation curve.

Experimental results

The technique was used to measure the first hyperpolarizability of five fluorescent ionic hemicyanine homologues (DAST) of increasing conjugation length (see fig. 1). The influence of the conjugation length on the first hyperpolarizability was studied. In earlier studies on non-ionic and non-fluorescent chromophores, a large influence of the conjugation length on the β -value has been observed initially and a levelling off behaviour afterwards [6-9]. This observation is in good agreement with theoretical predictions on these chromophores.

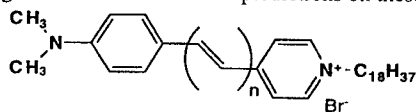


Figure 1. Structure of the hemicyanine homologues. $n=1-5$

Theoretical calculations of the effect of increasing conjugation length on the ionic and fluorescent DAST chromophores predict a similar behaviour.

However, the experimentally obtained values of the first hyperpolarizability show a different dependence upon the conjugation length. Initially, as predicted by the theoretical calculations, the conjugation length has a large influence on the first hyperpolarizability (from $\beta=107 \times 10^{-30}$ esu for $n=1$ to $\beta=1670 \times 10^{-30}$ esu for $n=2$). Nevertheless, as the conjugation length is further increased, the β -value reaches a maximum at $n=3$ ($\beta = 2070 \times 10^{-30}$ esu) and then falls back to lower values (β for $n=4$ and 5 is 780 and 1200×10^{-30} esu, respectively).

The experimentally observed maximum as well as the theoretical predictions can be explained by considering the possibility of excited-state isomerization. If isomerization takes place in the excited state (which can be reached since we observe fluorescence), then the all-trans configuration is lost and a less conjugated cis-isomer is generated leading to a reduced β -value. The theoretical calculation on the other hand consider only the all-trans isomers of the chromophores. If, however, isomerization takes place, the calculation should incorporate several cis-isomers as well.

References

- [1] K. Clays, A. Persoons, "Hyper-Rayleigh scattering in solution," *Phys. Rev. Lett.*, **66**, 2980-2983, (1991)
- [2] K. Clays, A. Persoons, "Hyper-Rayleigh scattering in solution," *Rev. Sci. Instrum.*, **63**, 3285-3289 (1992)
- [3] G. Olbrechts, R. Strobbe, K. Clays, A. Persoons, "High-frequency demodulation of multi-photon fluorescence in hyper-Rayleigh scattering," *Rev. Sci. Instrum.*, **69**, 2233-2241 (1998)
- [4] G. Olbrechts, K. Wostyn, K. Clays, A. Persoons, "High-frequency demodulation of multi-photon fluorescence in long-wavelength hyper-Rayleigh scattering," *Opt. Lett.*, **24**, 403-405 (1999)
- [5] K. Clays, J. Jannes, Y. Engelborghs, A. Persoons, "Instrumental and analysis improvements in multi-frequency phasefluorometry," *J. Phys. E: Sci. Instrum.*, **22**, 297-305, (1989)
- [6] R. A. Huijts, G. L. J. Hesselink, "Length dependence of the second-order polarizability in conjugated organic molecules," *Chem. Phys. Lett.*, **126**, 209-212 (1989)
- [7] J. L. Oudar, H. L. Person, "Second-order polarizabilities of some aromatic molecules," *Opt. Comm.*, **15**, 258-262 (1975)
- [8] J. L. Oudar, "Optical nonlinearities of conjugated molecules. Stilbene derivatives and highly polar aromatic compounds," *J. Chem. Phys.*, **67**, 446-457 (1977)
- [9] A. Dulcic, C. Flytzanis, C. L. Tang, D. Pépin, M. Fétizon, Y. Hoppilliard, "Length dependence of second-order optical nonlinearity in conjugated hydrocarbons," *J. Chem. Phys.*, **74**, 1559-1563 (1981)

Preparation of the Anisotropic Thin Film on an ITO Substrate for Application to Opto-electronic Device

T. Tano, T. Kodzasa, H. Ushijima, T. Kamata,
National Institute of Materials and Chemical Research
1-1 Higashi, Tsukuba, Ibaraki 305-8565, Japan

We have examined the possibility if the column structure of bis-(diphenylglyoximate)platinum(II) orients perpendicular to the film surface on ITO substrates. It was shown for the first time that a control of substrate temperature permits the fabrication of a thin film with perpendicular orientation of the metal chains on ITO substrates.

There has been many proposals to improve the performance of the organic electroluminescence (OEL) devices. One example is to utilize wave guides for collecting emitted light which radiates three dimensional space. Another is to use high photoluminescence quantum-yield molecules for an emission layer. However, it has not been investigated for the increase in emission efficiency to enhance probability of encounter between electrons and holes. To study this, we considered that it would be useful to prepare paths through which electrons and holes are carried from electrodes. It has been known that bis(diphenylglyoximate)platinum(II), $\text{Pt}(\text{dpg})_2$, (Figure 1), in the evaporated thin film has a square planar configuration and stacks face-to-face, forming a one-dimensional columnar structure [1-3]. In the columnar structure, the central metal ions interact strongly with those of the adjacent molecules to give a linear metal chain. Since electrons are delocalized in the linear chain, this chain can be a good candidate for paths mentioned above. Therefore, it is necessary to investigate the conditions for the fabrication of high quality thin films, in which molecules stack in a line. In a previous study[4], we have found that perpendicular orientation of the metal chains of $\text{Pt}(\text{dpg})_2$ films on a glass substrate could be obtained by controlling substrate temperature although it was not in the lattice matching condition between deposited molecules and substrate surface. In this study, we examined the effect of substrate temperature on the molecular structures of $\text{Pt}(\text{dpg})_2$ in a film by UV-vis spectroscopy and Atomic Force Microscope (AFM) measurements. Thin films of $\text{Pt}(\text{dpg})_2$ were prepared by conventional vacuum-evaporation onto an ITO substrate at several temperatures. In order to investigate the orientational effect, a *p*-polarized UV beam through a polarizer was incident upon the film at angle of 70° .

Figure 2 shows absorption spectrum of $\text{Pt}(\text{dpg})_2$ films on an ITO substrate prepared at -110°C with an evaporation rate of 1.5 nm/min. At normal incidence, one band was clearly observed at 380 nm, assigned to the metal-to-ligand charge transfer transition [1,5]. In case of $\text{Pt}(\text{dpg})_2$ film made with the same deposition rate at 20°C , a strong absorption band was observed at 570 nm. This band is assigned to the $5d_z^2-6p_z$ transition of platinum that originates in the d-orbital overlap between adjacent platinum ions in the linear metal chain [1,5]. The transition moment of 570 nm band is parallel to the metal chain. Therefore, molecular orientation change of $\text{Pt}(\text{dpg})_2$ in the film is a possible explanation for absence of this absorption in

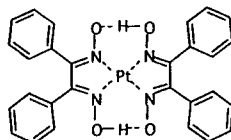


Figure1. Molecular structure of $\text{Pt}(\text{dpg})_2$.

Poster Session II

Figure 2. To investigate this, polarized absorption spectra with oblique incidence of source beam were measured. Obtained result is shown in Figure 2 (dotted line). A strong broad band could be observed at 570 nm. This shows that the Pt(dpg)₂ molecules are stacked as its axis is almost perpendicular to the substrate surface.

To investigate the molecular arrangement of Pt(dpg)₂ film in further detail, we applied AFM measurements. In the film prepared at -110 °C, its film surface was relatively flat and definite structure was not clearly observed. To confirm the film structure well, we annealed the film at 100 °C for ten minutes. Figure 2 displays a topographic image of Pt(dpg)₂ film after annealing at 100 °C. The left side of the column could be seen because the cantilever was obliquely swept over the surface from left to right. The topographic image clearly shows that almost all column has the same size in diameter and orients the same direction to the surface.

From the obtained results, we concluded that the fabrication of high quality thin films, in which molecules stack in a line onto an ITO substrate, is possible by controlling the substrate temperature.

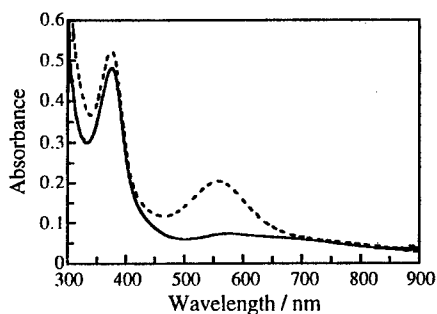


Figure 2. Absorption spectra of Pt(dpg)₂ film prepared at -110 °C. The solid line is the spectrum of normal incidence; the dotted line is that of 70° incidence from the surface normal.

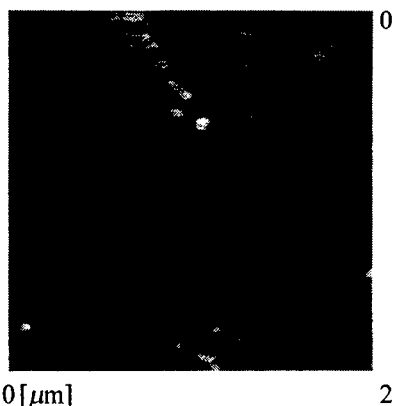


Figure 3. AFM image of Pt(dpg)₂ film after 10 minutes annealing at 100 °C prepared at substrate temperature of -110 °C.

References

- [1] T. Kamata, T. Fukaya, H. Matsuda, F. Mizukami, M. Tachiya, R. Ishikawa, and T. Uchida; *J. Phys. Chem.*, **99**, 13239 (1995).
- [2] K. Yamamoto, T. Kamata, Y. Yoshida, K. Yase, F. Mizukami, and T. Ohta; *Adv. Mater.*, **10**, 1018 (1998).
- [3] S. Isoda, M. Tsujimoto, K. Yoshida, T. Kobayashi, and T. Kamata; *Mol. Cryst. Liq. Cryst.*, **316**, 15 (1998).
- [4] T. Tano, T. Kodzasa, H. Ushijima, T. Kamata, *Mol. Cryst. Liq. Cryst.* in press.
- [5] Y. Ohashi, I. Hanazaki, and S. Nagakura; *Inorg. Chem.*, **9**, 2551 (1970).

Influence of the molecular orientation on the stimulated emission and gain dynamics of Phenylene Vinylene oligomers

T. Barisien, T.-A. Pham, L. Guidoni, M. Albrecht and J.-Y. Bigot
*Institut de Physique et Chimie des Matériaux de Strasbourg,
 Unité Mixte CNRS-ULP-ECPM, 23 rue du Loess, 67037 Strasbourg Cedex, France*

The amplified spontaneous emission and gain dynamics have been studied in oriented thin films of a model oligo(p-phenylene vinylene). It is shown that the molecular orientation present in crystalline films is a key parameter for obtaining low amplification thresholds and minimum induced absorption in the spectral region of fluorescence.

The lasing properties of conjugated polymers depend on the gain characteristics in the transparent region of fluorescent emission [1, 2]. In most cases, a major drawback to obtain efficient devices is a decrease or a complete quenching of the fluorescence which is observed for instance in many derivatives of the para-phenylene vinylene family. This quenching has been attributed to several mechanisms like a photo-induced oxidation, an inter-molecular energy transfer or an exciton annihilation. In the present contribution we show that an important factor to consider is the molecular orientation of the emitting species.

The amplified spontaneous emission (ASE) and the gain dynamics of crystalline thin films of the oligomer 5-ring n-octyloxy-substituted oligo(p-phenylene vinylene) are shown in figures 1 and 2. The crystalline thin films are obtained by a thermally induced re-crystallization of spin coated films deposited on a glass substrate. The crystalline order, determined by transmission electron microscopy (TEM), depends on the sample thickness. The dynamics is performed with a time resolved femtosecond pump-probe set-up delivering 100 fs pump pulses (400 nm) and chirp compensated continuum probe pulses (100 fs in the 500–700 nm spectral range). Figure 1 (a) shows the intensity of the time

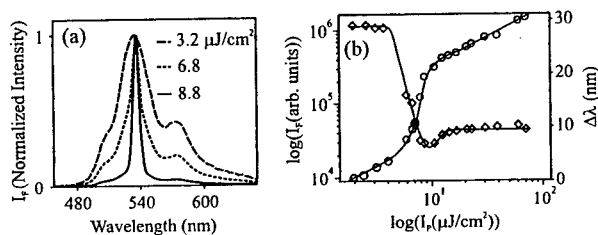


Figure 1: (a) Time integrated emission spectra of the oligomer thin film.
 (b) Details of the corresponding fluorescence intensity (circles) and line width (diamonds) as a function of the pump energy density.

integrated fluorescence I_F measured as a function of the absorbed density of energy of the incident pulse. The corresponding spectral narrowing due to the ASE is reported in figure 1 (b). The polarization of the incident pulse is set parallel to the oligomer chains and the fluorescent emission is also parallel. This behavior is characteristic of the films

Poster Session II

having a thickness less than ≈ 150 nm. For the thinnest samples which we studied, even lower ASE thresholds are obtained (typically $1\mu\text{J}/\text{cm}^2$ is enough for 100 nm thick samples). The differential gain spectra associated to this film is shown in figure 2 (a) for the pump-probe delays 0.1 ps (full curve) and 20 ps (dashed curve). The positive signal in the region 500–700 nm indicates that the emission process is not perturbed by any induced absorption mechanism. The ASE process and gain dynamics behave differently in thicker samples, for which broader TEM peaks are observed, indicating a certain amount of disorder. The stimulation process occurs only with a pump polarization set perpendicular to the oligomer chains (the polarization of the emission remaining parallel to the chains). In this case, the absence of stimulation when the pump is parallel to the chains is due to

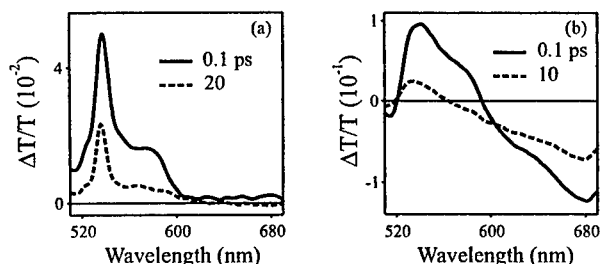


Figure 2: Differential gain spectra of 100 nm (a) and 200 nm (b) thick films, measured for short (full curve) and long (dashed curve) pump-probe delays.

an induced absorption as seen in figure 2 (b) for the delays 0.1 and 10 ps. We attribute this effect to a disorder induced excited state absorption. It prevents the development of an efficient gain which suppresses the stimulated process in the parallel configuration. It is important to emphasize that, in non-oriented films [3, 4], this mechanism would result in a strong reduction of the ASE process since, near the amplification threshold, only the chains perpendicular to the laser polarization are efficient. The above considerations demonstrate that the molecular orientation is a major parameter to consider in order to obtain efficient light emitting devices made of conjugated polymers or oligomers.

References

- [1] N. Tessler, G. J. Denton, R. H. Friend, "Lasing from conjugated-polymer microcavities," *Nature* **382**, 695–697 (1996).
- [2] D. Bradley, "Plastic lasers shine brightly," *Nature* **382**, 671 (1996).
- [3] L. J. Rothberg, M. Yan, F. Papadimitrakopoulos, M. E. Galvin, E. W. Kwock, T. M. Miller, "Photophysics of phenylenevinylene polymers," *Synth. Met.* **80**, 41–58 (1996).
- [4] V. I. Klimov, D. W. McBranch, N. N. Barashkov, J. P. Ferraris, "Femtosecond dynamics of excitons in π -conjugated oligomers: the role of intrachain two-exciton states in the formation of interchain species," *Chem. Phys. Lett.* **277**, 109–117 (1997).

Femtosecond Z-scan measurement of the third order nonlinear optical coefficient of CuPc thin films

H.J. Chang, S.H. Han, and J.W. Wu

Department of Physics, Ewha Womans University, Seoul 120-750, Korea

Tel.:+82-2-3277-2369, Fax.:+82-2-3277-2372

E-mail : jwwu@mm.ewha.ac.kr

We performed the Z-scan experiment varying the repetition rate at 4MHz, 800kHz and 400kHz with a pulse selector. we found that the nonlinear absorption behavior is different for the different pulse. At 4MHz, the sample shows RSA, while it shows saturable absorption. From these, we find that the triplet state lying in between two singlet states plays a role for the different behaviors at the different repetition rates. The sample was irradiated by Ti-sapphire femtosecond laser with pulse of FWHM 100-200fs. CuPc was made in a thin film by a vacuum evaporation. We also get nonlinear refractive property of CuPc thin film by Z-scan measurement. we compared the experiment results with the theory (GD method)

Metallo-phthalocyanine (MPc) possesses a highly conjugated two-dimensional π electron system and an exceptional chemical and thermal stability. This makes MPc a strong candidate for the third-order nonlinear optical materials. The $\chi^{(3)}$ measurement techniques employed for the study of MPc are the third harmonic generation (THG), the degenerate four wave mixing (DFWM), and Z-scan. The $\chi^{(3)}$ value measured in THG experiment can be different from one measured in DFWM or Z-scan. The THG method is sensitive only to the ultrafast distortion of the electronic clouds, while other mechanisms, such as reorientation and optical pumping, can contribute to the DFWM and Z-scan signal, depending on the experimental configurations.[1]

The optical limiting behavior is an important nonlinear optical process, where the nonlinear optical material has a high transmission at a normal light intensity and a less transmission for an intense beam. The optical limiting based on the reverse saturable absorption have been reported using phthalocyanines [2], [3]. The mechanism for nonlinear absorption in phthalocyanine limiters has been usually the optical pumping of the low lying electronic states of the molecule.

In the experiment, we employed the femtosecond Z-scan set-up to identify the mechanism of the saturable absorption and the optical limiting at the ultra-high fast time regime. The focused spot size ω_0 was in the range 6-10 μ m, and CS_2 was employed as a reference for Z-scan alignment. The sample employed for the measurement was the copper-phthalocyanine (CuPc) thin film, prepared by a vacuum evaporation. The sample was irradiated by Ti-sapphire femtosecond laser with pulse widths of FWHM 150 fs. Without changing the pulse width, the pulse repetition rates of the femtosecond laser were varied at 4MHz, 800kHz, and 400kHz with a pulse selector in the laser system. We found that the nonlinear absorption behavior is different for the different pulse repetition rates. At 4MHz, for example, the sample exhibits a reverse saturable absorption behaviour (Fig. 1), while at other pulse repetition rates it exhibits the saturable absorption behavior (Fig. 2). From these, we find that the triplet state lying in between two singlet states plays a role for the different behaviors at the different repetition rates. At the high repetition rate, the electrons on the triplet state are optically pumped to the high lying states before intersystem-crossing to the singlet ground state. On the other hand, at the low repetition rates, the electrons have enough time to get down to the singlet ground state before the

Poster Session II

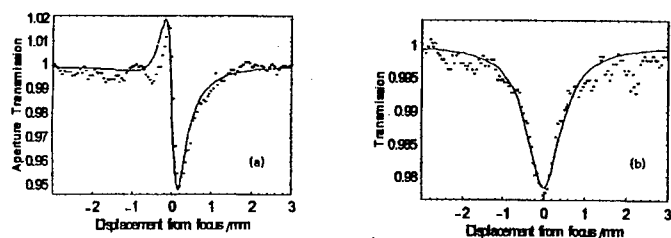


Figure 1: Open (a) and closed (b) aperture Z-scan experimental results for CuPc at 4MHz, the dotted curve: experiment data, the solid curve : theory

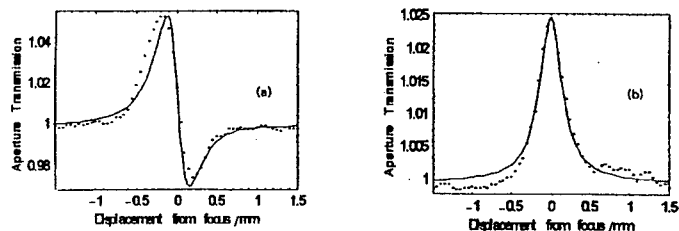


Figure 2: Open (a) and closed (b) aperture Z-scan experimental results for CuPc at 800kHz, the dotted curve: experiment data, the solid curve : theory

next pulse comes in. From this measurement, we find that the triplet state life time in the CuPc thin film is between $0.25\mu s$ and $1.25\mu s$. We also got the nonlinear refractive index coefficients and found that the nonlinear refractive response of our samples makes a Gaussian beam always defocused, meaning that the sign of γ is negative. The value of γ is $-1.2 \times 10^{-14} m^2/W$ at 800kHz, $3.5GW/cm^2$ pulse peak intensity. At another repetition rate, the results are similar to this. We compared the experiment results with the theory derived from the Gaussian decomposition method [4].

References

- [1] C. C. Leznoff, A. B. P. Lever "Phthalocyanines properties and applications," VCH Publishers, INC. Vol. 4 (1996).
- [2] J. S. Shirk, R. G. S. Pong, A. W. Snow, "Optical limiter using a lead phthalocyanine," Appl. Phys.lett, **63**, 1880 (1993).
- [3] T. H. Wei, D. J. Hagan, M. J. Sence, E. W. Van Stryland, J. W. perry, and D. R. Coulter, "Direct measurements of nonlinear absorption and refraction in solutions of phthalocyanines," Appl. Phys., **B 54**, 46-50 (1992).
- [4] Mansoor Sheik-bahae, Ali A Said, Tai-huei Wei, David J. Hagan, E. W. Van Stryland, "Sensitive Measurement of optical Nonlinearities Using a Single Beam," IEEE J.Quantum Electron., **26**, 760-769 (1990).

Measurement of relations between molecular structure and two-photon absorption spectra in fluorene dye compounds.

David J. Hagan, Kevin D. Belfield, Katherine J. Schafer, Raluca Negres,
Wael Mourad and Eric W. Van Stryland

School of Optics and Department of Chemistry
University of Central Florida, Orlando FL 32816-2700

We report a study of nondegenerate two-photon absorption (2PA) spectra in a series of fluorene derivatives with different electron withdrawing and donating groups, synthesized via transition metal catalyzed coupling reactions. We observe a strong relationship between the strength of electron donors and acceptors and the magnitude of 2PA cross sections.

Considerable effort is focused on designing compounds with large 2PA cross-sections for several practical applications such as two-photon fluorescence imaging and microfabrication.^{1,2} Conjugated systems with alternating double and/or triple and single bonds have given promising results due to the electronic charge transfer that greatly enhances the nonlinearity. This can be further increased by means of donor and acceptor groups intra-chain and/or end-chain substituted. A series of eight *alkyl fluorenes* were synthesized³ and nondegenerate 2PA spectra measured using our nonlinear spectrometer. The molecular structures of four of these compounds are shown in fig. 1. The series was designed to probe the effect of the electronic character of the compounds on nonlinear absorption. The synthetic methodology facilitated a systematic variation of functional groups of differing electronic character, while providing compounds with high photochemical and thermal stabilities. For example, compounds #1 and #6 were designed to investigate the effect of strength of the electron acceptor (withdrawing) group in a D- π -A molecule, while the electron donor functionality is varied somewhat in compounds #2 and #6. Compound #3 is of the A- π -A type with electron acceptor moieties of disparate electronic character.

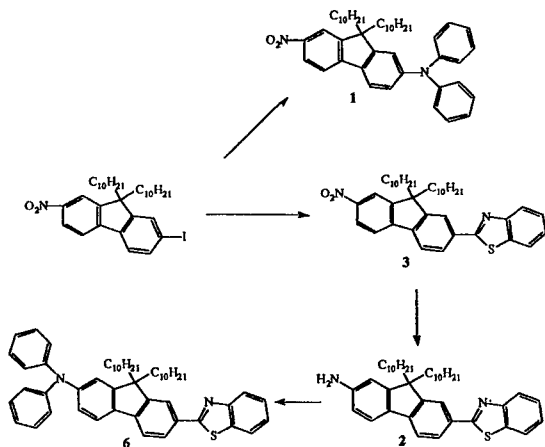


Figure 1. Synthetic scheme for the preparation of end-substituted alkyl-fluorenes 1, 2, 3, and 6. The electron-acceptors are nitro and benzothiazole, while amine and diphenylamine groups are -donors.

Poster Session II

The excitation wavelength used in these experiments was 1210 nm with about 13-15 μJ of energy, provided by the TOPAS OPG/OPA system. From the UV spectra of these molecules (fig. 2(a)), we can assume that 2PA at the pump wavelength (degenerate) is not possible. From energy considerations, the visible part of continuum will be absorbed at the same time the infrared pulse is present in the samples. These organic compounds were dissolved in tetrahydrofuran (THF) and stored in 1 mm path length cells. Fig. 2(b) plots the two-photon absorption cross section, δ , for all four molecules versus continuum wavelength. The estimated experimental error in δ is $\pm 43\%$. The largest cross section value we measured, of over $1600 \times 10^{-50} \text{ cm}^4/\text{s}/\text{photon}$ at the peak of the spectrum for compound #6, is similar in magnitude to the values reported by Albota *et. al.*¹

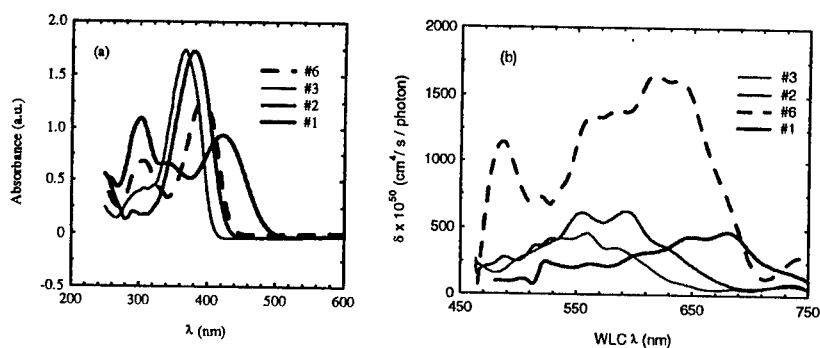


Figure 2. (a) Linear UV spectra of alkyl fluorenes; (b) Spectra of measured TPA cross-section, δ , obtained for an excitation wavelength of 1210 nm and probed with visible continuum. The estimated error in δ is $\pm 43\%$.

Comparing compounds #1 and #6, we observe a strong enhancement of the 2PA cross section by reducing the strength of the electron acceptor group. Conversely, comparison of compounds #2 and #6 reveals that increasing the strength of the donor group enhances the 2PA cross section. As compound #6, with the strongest donor and weakest acceptor, exhibits a considerably larger 2PA cross section than any of the others, it appears that a greater electron density in the π -conjugated central fluorene group leads to a greater 2PA cross section. A logical next step is to study D- π -D molecules of this type. These are currently being synthesized for this purpose. The linear and 2PA spectra are strongly correlated, indicating, as expected for these asymmetric molecules, that the same states are responsible for linear and two-photon absorption in these molecules.

Acknowledgements

This work was carried out under the support of the National Science Foundation (grant #. 9970078), the Naval Air Warfare Center/Joint Service Agile Program (contract #. N00421-98-C-1327), and the Air Force Office of Scientific Research (grant #. F49620-93-C-0063).

References

1. M. Albota, *et. al.*, "Design of organic molecules with large two-photon absorption cross sections", *Science* **281**, 1653-1656 (1998).
2. J. E. Ehrlich, *et. al.* "Two-photon absorption and broadband optical limiting with bis-donor stilbenes", *Opt. Lett.* **22**, no. 24, 1843-1845 (1997).
3. K. D. Belfield, *et. al.* "Synthesis and characterization of new two-photon absorbing polymers", *Polymer Prep.* **40**, no. 1, 127-128 (1999).

Influence of Molecular Orientation and Arrangement to Two-dimensionality of Metallophthalocyanines

Takashi Isoshima and Tatsuo Wada

Biopolymer Physics Lab.

*The Institute of Physical and Chemical Research (RIKEN)
2-1 Hirosawa, Wako, Saitama 351-0198, Japan*

*Core Research for Evolutional Science and Technology (CREST)
Japan Science and Technology Corporation (JST)
2-1 Hirosawa, Wako, Saitama 351-0198, Japan*

Hiroyuki Sasabe

*Chitose Institute of Science and Technology
758-65 Bibi, Chitose, Hokkaido 066-8655, Japan*

*Core Research for Evolutional Science and Technology (CREST)
Japan Science and Technology Corporation (JST)
2-1 Hirosawa, Wako, Saitama 351-0198, Japan*

A metallophthalocyanine molecule has two-dimensionality due to twofold degenerate $\pi\text{-}\pi^*$ transitions, and intermolecular interaction can affect it. Anisotropy of subpicosecond pump-probe responses in various metallophthalocyanine samples are measured to investigate influence of molecular orientation and arrangement to dimensionality. Aggregate metallophthalocyanines in various phases and planary oriented vanadylphthalocyanine grown with organic molecular beam epitaxy are examined. In aggregate metallophthalocyanines, less symmetric intermolecular interaction can provide one-dimensional response at certain wavelength range. In a planary oriented vanadylphthalocyanine, two-dimensionality is kept and almost isotropic response is observed due to the orientation. This feature is useful to photonic device applications such as a polarization-independent all-optical switch.

In order to design a molecular system with a desired function, it is essential to understand the structure-to-property relation. A two-dimensional (2-D) molecule with three-, four-, or higher-fold symmetry is very interesting from this view point, since it has twofold degenerate transitions and thus presents anisotropy of nonlinear optical response different from an ordinary one-dimensional (1-D) molecule. For example, 2-D molecules such as metallophthalocyanines present polarization dependence of 8:1 or 4:3 in pump-probe response, depending on the nature of the probe transition [1], in contrast with 1-D molecules which show 3:1 polarization dependence. This anisotropy is also very important in terms of material characterization and application, such as the optical Kerr-gate measurement and all-optical switches. In this paper, we discuss intermolecular exciton-exciton interaction and the dimensionality of the system composed of 2-D molecules, through the polarization dependence of pump-probe response in evaporated and epitaxially grown vanadylphthalocyanine thin films.

In aggregate state, metallophthalocyanines present polymorphism and "slipped stack" structure is generally observed, in which each phthalocyanines are stacked so that the molecular planes are parallel to each other and that the stacking axis is oblique to the normal of molecular plane. This introduces asymmetry in the molecular plane, resulting into nondegeneracy showing a 1-D response. In addition, such a slipped stack columns are closely packed, resulting in an

Poster Session II

intermolecular interaction which has a rather "coplanar" nature and might introduce a 1-D character. VOPc can also be heteroepitaxially grown on cleaved (001) surface of KBr by means of organic molecular beam epitaxy (OMBE) [2], orientating flat on the surface and forming a square lattice. Since both the molecule itself and the arrangement has fourfold symmetry, it is expected that the anisotropy of pump-probe response for normal incident light is 1:0 or 1:1 (corresponding to 8:1 and 4:3 cases in a randomly oriented system, respectively).

In the experiment, transient absorption change of evaporated VOPc films and of an OMBE-grown VOPc thin film on a KBr substrate were measured using a subpicosecond pump-probe measurement setup. The light source is a Ti-sapphire laser with a Ti-sapphire regenerative amplifier, which provides about 20 $\mu\text{J}/\text{pulse}$ output with a temporal width of 250 fs operating at 1 kHz. The probe beam is a spectral continuum of wavelengths from 450 nm to longer than 1 μm . Polarizer and half-wave plate combinations are used to control polarization and intensity of pump and probe. As shown in Fig. 1, in the evaporated phase-I film the polarization ratio of the transient transmission change is 4:3 at ca. 700nm probe suggesting 2-D character in this transition, and more than 2:1 at 750 nm or longer wavelength probe suggesting contribution of 1-D character. This result suggests that the influence of the intermolecular interaction depends on the wavelength. In the OMBE-grown film shown in Fig.2, the polarization ratio is almost 1:1 at most of the probe wavelengths except for 780 nm at which wavelength there might be a contribution of fluorescence band, as theoretically predicted. This isotropic feature is advantageous in photonic applications such as a polarization-independent all-optical switch. Polarization dependence of transient refractive index change is also investigated.

References

- [1] N. Pfeffer, T. Isoshima, M. Tian, T. Wada, J.-M. Nunzi, and H. Sasabe, *Phys. Rev. A* **55**, R2507 (1997).
- [2] H. Tada, K. Saiki, and A. Koma, *Jpn. J. Appl. Phys.*, **30**, L306 (1991)

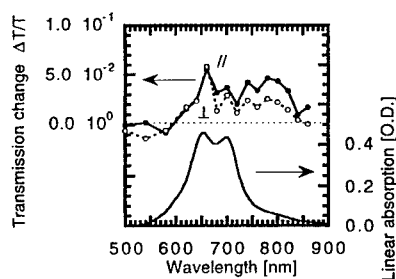


Figure 1: Transient absorption and linear absorption spectra of an evaporated phase-I VOPc thin film. Pump wavelength was 760 nm. Delay time was 5ps.

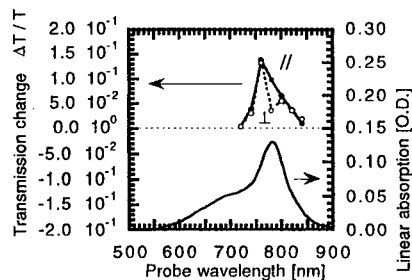


Figure 2: Transient absorption and linear absorption spectra of an epitaxially grown VOPc thin film on KBr. Pump wavelength was 760 nm. Delay time was 0ps.

Optical and nonlinear optical properties of low-dimensional aggregates of the amphiphilic cyanine dyes

R.V.Markov, P.A.Chubakov, A.I.Plekhanov,
Z.M.Ivanova, N.A.Orlova, T.N.Gerasimova, V.V.Shelkovnikov
and J.Knoester

*Institute of Automation and Electrometry, 1 Academician Koptyug Ave., Novosibirsk
630090, Russia*

*Novosibirsk Institute of Organic Chemistry, 9 Academician Lavrentjev Ave., Novosibirsk
630090, Russia*

*Institute for Theoretical Physics, Material Science Center University of Groningen,
Nijenborgh 4, 9747 AG Groningen, The Netherlands*

In the paper thin solid films of well-ordered low-dimensional J-aggregates of the amphiphilic cyanine dyes with different length of the alkyl substituents were obtained. It was found that the length of alkyl substituent of the cyanine dye had impact on the structure and degree of order of the aggregates, which allows for control their optical properties. The films demonstrate a giant third-order optical susceptibility ($\approx 10^{-5}$ esu) and fast switching time ($\sim 0,2$ ps). The spectral behavior features of $\text{Im}\chi^{(3)}$ in the exciton absorption band of the aggregates are measured. The refractive index and absorption coefficient of the films are also measured by the spectral ellipsometry method.

In recent years, there has been increasing interest in the optical and nonlinear optical properties of quasi-one-dimensional J-aggregates of cyanine dyes, which possess a giant nonlinear susceptibility at the exciton absorption band $|\chi^{(3)}| \sim 10^{-5}$ esu with fast response [1]. It is well known that the translational symmetry and interaction of neighboring molecules lead to the delocalization of excitations over the one-dimensional aggregate and to the formation of the exciton absorption band (J-band), and also give large, size-enhanced optical nonlinearities [2, 3]. However the disorder of molecular aggregate, which is caused by breakdown of translational symmetry leads to the localization of exciton on a part of the aggregate [3]. The localization can considerably manifests in optical properties of the J-aggregates [4].

The goal of our work is to study the optical and nonlinear optical properties of molecular J-aggregates constituted by identical molecules but possessed various structural parameters and, accordingly, various degrees of disorder. The change of structural parameters was realized by using the J-aggregates, which are composed of molecules of 1,1'-diethyl-2,2'-cyanine iodide (PIC) with various N-alkyl substituents. The substituents do not change the optical properties of a single molecule but they influence the mutual arrangement of molecules in the J-aggregate. PIC with symmetrical and asymmetrical N-alkyl substituents (**1a** – e, $C_2H_5 - C_2H_5$, $C_6H_{13} - C_6H_{13}$, $C_{10}H_{21} - C_{10}H_{21}$, $C_{15}H_{31} - C_{15}H_{31}$, $C_{18}H_{37} - C_{18}H_{37}$), (**2a** – d, $C_2H_5 - C_6H_{13}$, $C_2H_5 - C_{10}H_{21}$, $C_2H_5 - C_{15}H_{31}$, $C_2H_5 - C_{18}H_{37}$) was synthesized and was used in this work.

The films were obtained by spin-coating of the dye solutions on a glass substrate. The thickness of these films was about 30 nm. Our experiments have shown, that the thin films of ordered quasi-one-dimensional J-aggregates are formed only for PIC with a series of N-alkyl substituents **1a**, **b**, **2a-d**. Also it was found, that the films are formed in

Poster Session II

a monomeric phase for PIC with substituents **1c-d**. The dye with substituent **1e** gives so-called H-aggregates which is characterized by a wide exciton absorption band shifted to the high-frequency side from the peak of the monomer dye.

It has been found experimentally that with an increase in the length of substituent **2a-d** a legible tendency to spontaneous formation of J-aggregates with magnification of conversion from monomeric form of dye to the J-aggregate form is observed. The process of the J-aggregate formation increases with increasing relative humidity of air. Apparently, the reason of such an effect is due to change of amphiphilic nature of dye, i.e. its hydrophobic properties are amplified with the length of substituent.

It was found that the films of PIC J-aggregates with substituents **2b-d** are the most stable. Their optical properties practically do not vary within several months. The optical constants of the complex index of refraction $n = n_o - ik$ of these films in the region of 500-650 nm are measured by a method of spectral ellipsometry. At the maximum of J-band the typical values of n_o equals ≈ 2.7 , and $k \approx 1.3 - 1.4$.

The optical spectra of these films are measured at room temperature and approximately the same air humidity. Absorption spectra of these films reveal that the wavelength of the maximum of J-band monotonically moves to the long-wave region with an increase in the length of N-alkyl substituent. This apparent shift can be assigned to the change of the geometrical arrangements of the aggregate. Thus it leads to change the value of a dipole - dipole interaction between the neighboring molecules in the J-aggregate.

The nonlinear absorption spectra of these films were studied by Z-scan technique [1]. In these measurements we have used a pulsed ($\tau \approx 5$ ns) dye laser. In the vicinity of the maximum of exciton absorption the dynamic bleaching of J-band about 10-15 % is observed at a laser intensity ≈ 2 MW/cm², which corresponds to $Im\chi^{(3)} \approx -7 \cdot 10^{-6}$ esu. The maximum of bleaching coincides with the maximum of J-band with precision of 15 cm⁻¹. The nonlinear spectra have an asymmetrical shape. The low-frequency side of these spectra decreases approximately twice faster than the high-frequency side. For some films at the low-frequency side of the exciton absorption band, one can observe induced darkening that is Stokes shifted by $\sim 130-160$ cm⁻¹ from the J-band. These spectral features have quite well described by four-level model of exciton transitions. However, the half-width of the nonlinear absorption spectrum of the J-aggregates of PIC with substituents **2c, d** occurs to be narrower than that is expected in the model of saturation of the homogeneously broadening transition. At the same time such disagreement is not observed for the sample with substituent **2b**. A half-width of nonlinear darkening increases by $\sim 40\%$ with an increase in the length of substituent.

This work was supported by grant of INTAS 97-10434 and grant of " Laser physics " 6.35 of the Ministry of Science of the RF.

References

- [1] R.V.Markov, A.I.Plekhanov, S.G.Rautian et al., Optics and Spectroscopy **85**, 588-594 (1998).
- [2] F.S.Spano, S.Mukamel, Phys.Rev.A **A40**, 5783-5801 (1989).
- [3] H.Fidder, J.Knoester, K.Wiersma, J.Chem.Phys., **95**, 7880-7890 (1991).
- [4] J.Knoester, Chem.Phys.Lett., **203**, 371-377 (1993).

**Picosecond Optical Limiting Action through a Thin MMA-Octupole
Copolymer Layer near the Total Reflection State**

R. Mountasser*, M. Ayadi

*Département de Physique, Faculté des Sciences
Université Hassan II
Route d'Eljadida, Casablanca, Maroc*

H. Maillotte

*Laboratoire d'Optique P.M. Duffieux, UMR CNRS/Université de Franche-Comté n°6603
Institut des Microtechniques de Franche-Comté
UFR Sciences et Techniques, 16 route de Gray
F-25030 Besançon cedex, France*

F. Chérioux

*Laboratoire de Chimie et Electrochimie Moléculaire
Université de Franche-Comté
16 route de Gray, F-25030, Besançon cedex, France*

Non-resonant optical transmission near the critical angle of incidence, through a new nonlinear thin polymer layer surrounded by two linear glass slabs, is studied experimentally in the picosecond range. The thin film is a spin-coated MMA polymer reticulated by a new octupolar molecule displaying off-resonant third order susceptibility. The optical transmission through the layer is switched by more than 40 % with microjoule pulses, from a high transmission state to a weak transmission state when increasing the input intensity. The switching behavior is completely reversible and exhibits long-term stability.

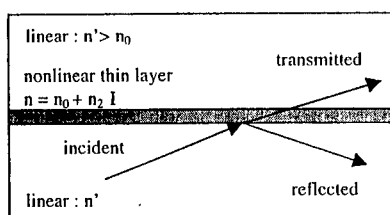
Intensity-dependent transmission, near the total reflection state, through a nonlinear Kerr thin film surrounded by two linear slabs (fig.1) has been introduced as a potential tool for ultrafast switching and optical limitation. As shown in the relevant theoretical studies [1-3], the main advantages of this nonlinear sandwich, when compared to the single nonlinear interface case, come from the lower switching energy and the stability. Previous experimental works [1,4,5] dealt with nonlinear refraction induced by absorption and thermal effects in the sandwich, *i.e.* in a rather slow diffusive regime. The present study focuses on the non-resonant transmission in the picosecond range through a thin nonlinear layer made up from a new copolymer MMA-octupole.

Figure 1 illustrates the principle of the experiment. At low intensity, the incident beam is adjusted either slightly higher than the critical angle of incidence θ_c (low transmittivity, positive n_2 case) or slightly lower than θ_c (high transmittivity, negative n_2 case). By increasing the incident intensity, the value of $\theta_c = \sin^{-1}[(n_0 + n_2) / n']$ changes. If n_2 is positive, θ_c is increased beyond the incident angle. Therefore, from a threshold intensity, the layer switches from a weak transmission state (0) to a high state (1). On the contrary, if n_2 is negative, the

Poster Session II

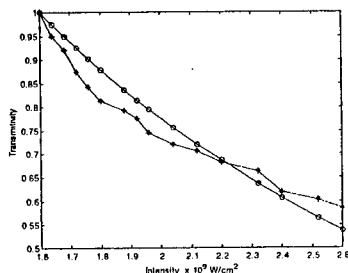
transmittance of the layer decreases gradually from a relatively high state (1) to a low state (0).

Fig. 1. Principle of the nonlinear optical transmission through a thin film ($n = n_0 + n_2 I$) near the critical angle of incidence. The thin film is surrounded by two identical linear media ($n' > n_0$).



The octupolar monomer was synthesized via a triple aromatic nucleophilic substitution of dithienyl derivatives on cyanuric chloride [6]. The new copolymer MMA-octupole was synthesized with quantitative yield by copolymerisation of the allyl monomer with ethylacrylate. A thin layer of 5 μm thickness was spin-coated on one of the glass slabs (with $n' = 1.501$) from a dichloro-methane (CH_2Cl_2) solution of the copolymer. The linear refractive index n_0 of the thin solid film, measured by an optical refractometer, is 1.477 at 1064 nm. Its nonlinear picosecond response was found to be negative at this wavelength. The second glass slab was then carefully adjusted on the top of the layer. The critical angle of incidence is $\theta_c = 79.74^\circ$ at low intensity. The experiments were performed with linearly polarized 50 ps pulses at 1064 nm with a repetition rate of 10 Hz. The TEM_{00} beam was focused on the layer with a waist radius of nearly 40 μm and its incidence angle was adjusted at 79.6° . Figure 2 presents the normalized transmittivity of the sandwich versus the incident intensity. The experimental data (stars) are obtained by measuring the intensity ratio of the transmitted beam to the incident one on a single laser shot.

Fig. 2. Normalized transmittivity of the nonlinear thin copolymer (MMA-octupole) layer versus the incident intensity. The experimental data are represented by stars (*). The theoretical values (open circles-o) are obtained from a plane-wave model by fitting the measurements with $n_2 = -7.5 \cdot 10^{-17} \text{ m}^2/\text{W}$ and the other parameters listed in the text.



The optical transmission through the layer is switched by more than 40 % with microjoule pulses, from a high transmission state to a weak transmission state, when increasing the input intensity. One-shot and cumulative measurements were carried out to check the reversibility and the stability of the results with successive increases and decreases of the incident intensity. The optical limiting behavior is completely reversible and stable, without parasitic long-term effects due to pulse accumulation.

- [1] Th. Peschel, P. Dannberg, U. Langhein, F. Lederer, *J. Opt. Soc. Am. B* **5**, 29-36 (1988).
- [2] E. Lantz, D. Métin, H. Cornet, A. Lacourt, *J. Opt. Soc. Am. B* **11**, 347-354 (1994).
- [3] H. Mitchinel, *Opt. and Quantum Electron.* **30**, 79 (1998).
- [4] I.C. Khoo, P. Zhou, *Opt. Lett.* **17**, 1325-1327 (1992).
- [5] K. Strobl, I. Golub, *IEEE J. Quantum Electron.* **28**, 1435-1438 (1992).
- [6] F. Chérixoux, H. Maillotte, P. Audebert, J. Zyss, *Chem. Commun.*, 2083-2084 (1999).

Resonant nonlinearities in an organic material: irradiance dependence

R. Rangel-Rojo
Optics Department

*Centro de Investigación Científica y Educación Superior de Ensenada
Apartado Postal 2732, Ensenada B.C. 22860, México
e-mail: rrangel@cicese.mx*

H. Matsuda
Molecular Photonics Group

*National Institute of Materials and Chemical Research
1-1 Higashi, Tsukuba 305-8565, Japan*

H. Kasai, and H. Nakanishi
*Institute for Chemical Reaction Science
Tohoku University,
Sendai 980-77, Japan*

We present experimental data for the irradiance dependence of the optical nonlinearity of an organic material at different wavelengths across resonance. The material studied was a suspension of vanadyl-phthalocyanine nano-crystals in cyclohexane, and the refractive and absorptive contributions to the nonlinearity were resolved using the z-scan technique with a tunable picosecond laser source. The observed dependence of the nonlinearity with irradiance is explained by excited-state absorption, and a three-level model is used to describe the nonlinear response. A fit to the experimental data is made, allowing the extraction of molecular parameters which are of interest for a full characterisation of the nonlinearity.

The optical nonlinearities of organic materials have been studied extensively, due to, among other things, their potential use in optical information processing devices. The manipulation of molecular structure and aggregation state in an almost infinite fashion, gives scope to the optimization of the nonlinear response for the intended applications. The desired characteristics are: a reasonably large nonlinearity, small linear and nonlinear absorption, an ultrafast response, along with others such as processability, durability, etc.

Recently, a systematic study of the spectral dependence of nonlinear refraction and nonlinear absorption has been carried out on different materials in nanocrystalline form in the on- and near-resonance regime [1, 2] using the z-scan technique. By using materials in nanocrystalline form, some of the issues of material processability and control of aggregation state were addressed. These studies allowed the identification of spectral ranges where the nonlinearity is dominantly refractive, and therefore free of nonlinear absorption effects which are in general deleterious for the proposed applications.

Independently of the experimental technique employed, resonant interactions usually show a nonlinear response that is not purely of third-order, and the contribution of higher order terms, or some non-perturbative nonlinearity, needs to be considered. In either case, a study of the irradiance dependence of the nonlinear response becomes imperative to determine the proper figures of merit and quantify effects such as the saturation of refractive index change, for example.

In this paper we present experimental results for the nonlinear response of a vanadyl-phthalocyanine nanocrystal aqueous suspension at different wavelengths across resonance

Poster Session II

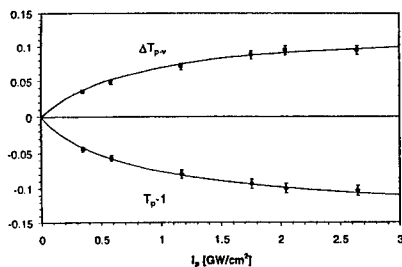


Figure 1: Irradiance dependence of z-scan results at 580 nm. $T_p - 1 < 0$ indicating the presence of induced absorption. The points are the experimental data, and the full lines the best fits obtained using the three-level model for the nonlinearity.

using the z-scan technique with a tunable picosecond laser source. The z-scan technique allowed the simultaneous determination of the refractive and absorptive contributions to the nonlinearity. We also present a study of the irradiance dependence of the z-scan results at two different wavelengths where saturable and reverse saturable absorption are observed. A three-level model for the nonlinear response of the nano-crystals is used to explain the observed irradiance dependence of the nonlinear signals, which is explained in terms of excited state absorption.

Figure 1 shows the experimental z-scan results obtained for the VOPc microcrystals as a function of irradiance for $\lambda = 580\text{nm}$. For the open aperture z-scan, the measured $T_p - 1$ value, which is the difference between the peak transmittance T_p found at the focal plane and the linear transmittance measured far away from focus (normalized to 1), is shown. For the closed aperture z-scan we plot ΔT_{p-v} , the difference between the normalized peak and valley transmittance: $T_p - T_v$.

In order to explain the observed irradiance dependence, a microscopic model for the response of the material is needed. A three-level model has been successfully used to describe the spectral dependence of the nonlinearity of polydiacetylene nano-crystals [1], and since this model results in a nonperturbative expression for the susceptibility, it can be used to describe the irradiance dependence of the response. Figure 1 shows the fit to the experimental data obtained using this model, for the case where induced absorption is present. The model worked well for the different wavelengths studied, and allowed the extraction of material parameters such as excited state absorption cross-sections which are difficult to determine by other means.

References

- [1] R. Rangel-Rojo, S. Yamada, H. Matsuda, H. Kasai, H. Nakanishi, A.K. Kar, B.S. Wherrett, *J. Opt. Soc. Am. B* **15**, 2937 (1998).
- [2] R. Rangel-Rojo, S. Yamada, H. Matsuda, H. Kasai, Y. Komai, S. Okada, H. Oikawa, H. Nakanishi, *Jpn. J. Appl. Phys. Part 1* **38**, 69 (1999).

Studies of Third-Order Optical Nonlinearity, Nonlinear Absorption and Excited State Dynamics in Tetra Tollyl Porphyrins using Degenerate Four Wave Mixing and Z-Scan

S. Venugopal Rao^a, N.K.M. Naga Srinivas^a, Reji Philip^c, G. Ravindra Kumar^c
L. Giribabu^b and Bhaskar G. Maiya^b, and D. Narayana Rao^a

^aSchool of Physics, ^bSchool of Chemistry

University of Hyderabad, Hyderabad - 500 046, India

^cTata Institute of Fundamental Research, Mumbai - 400 005, India

Abstract

We present our experimental results on the third-order optical nonlinearity, nonlinear absorption and excited state dynamics measurements in tetratollyl porphyrins using DFWM and Z-scan with incoherent light and 35 ps pulses.

Introduction

The last decade has received tremendous interest and witnessed extensive research activity in the nonlinear optical, photophysical and photochemical properties of organic materials in general and metalloporphyrins/related compounds in particular [1]. They are found to possess strong nonlinearity and fast response time, the desired criteria for making photonic devices. Recently we synthesized Tetra Tollyl Porphyrins (TTP) with sixteen different metal ions in the ring and studied the third order optical nonlinearity, nonlinear absorption and excited state dynamics using Degenerate Four Wave Mixing (DFWM) and Z-Scan techniques.

Degenerate Four Wave Mixing and Z-scan

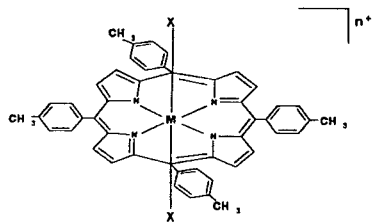
The source for ps $\chi^{(3)}$ measurements is a hybrid mode-locked Nd: YAG laser (35 ps, 532 nm, 10 Hz). The experimental set up is similar to the above, except that the beams are loosely focused by an $f \sim 200$ cm lens to avoid large power densities inside the sample. The angle between the pump and probe beams is $\sim 5^\circ$. For time-resolved measurements, the backward pump is delayed with respect to the temporally coincident forward pump and probe. The intensity ratio of beams 1, 2 and 3 approximately is 1:1:0.2 for nonlinearity measurements and 1:0.2:1 for time-resolved measurements. For the Z-scan studies, dye laser pulses centered at 600 nm wavelength and 6 ns duration also were used for excitation, in addition to the others. The sample is scanned across the focus using a micrometer translation stage, which is controlled by a PC. The transmitted light is collected using a large area lens of $f \sim 100$ mm and focused on to a photodiode for open aperture data.

Results and Discussion

During the DFWM experiments, the cubic dependence of the phase conjugate signal with the input intensity and linear dependence with concentration has been verified for all the samples. It is seen that for ns pulses SnTTP has the largest value of F ($\sim 323 \times 10^{-13}$ cm.esu) whereas for ps pulses H₂TTP has the largest value ($\sim 7.24 \times 10^{-13}$ cm.esu). Obviously, structural modifications to the porphyrin ring can be expected to result in molecules with diverse photophysical and photochemical properties that will in turn affect their optical nonlinearity. Among the various factors involved, the atomic number of the central metal atom, redox potential of the ring and occurrence of excited-state absorption require special mention. On comparing the $\langle \gamma \rangle$ values of our compounds with other porphyrins, the ns values are found to be three orders of magnitude larger than any of them. When the probe

Poster Session II

polarization is made normal to the pump beams, the PC signal gets reduced by only one-third of the original value (when all beams are co-polarized) indicating that the nonlinearity is predominantly electronic in origin and thermal effects are not dominant. However, there should be a significant contribution to this large value of $\langle \gamma \rangle$ from the excited singlet and triplet states, since we observe very strong ESA in all the open aperture Z-scan data. It is well established that ESA is an intensity dependent process and will dominate at higher intensity levels. This is well supported by our $\chi^{(3)}$ measurements at different input intensity levels whereby we observe an enhancement by a factor of three to four in its value. Furthermore, the intensity dependence of PC signal shows a different behavior at high intensities. A log-log plot of input energy versus PC signal gives a slope of < 3 at lower intensities and a slope of ~ 5 at higher intensities suggesting nonlinearity contributions from higher excited states. We observe the two-peak structure for FWM signals in all the porphyrins viz. a sharp, intense peak and a broad, weak peak. The widths of the peaks and the ratio of the peaks give information on the dephasing of the S_n , S_1 states and the population relaxation time (lifetime) of the S_1 state [2,3]. The dephasing time (T_2) for all the samples are < 170 fs, the vibrational relaxation times ($S_{1v} - S_{10}$) are $\sim 3-6$ ps, the population relaxation time (T_1) values are in the range of $\sim 20 - 70$ psec. Figures 2(b) show the PC signal obtained for samples NiTTP as a function of the beam 2 delay using ps 35 pulses. For cross polarization of the probe beam (beam 2) the signal dropped down to $\sim 3-4$ times but the structure remained the same. Solid dots are the experimental data for the sample and the solid line is for the sample CS_2 (to show the auto-correlation function). The results of $\chi^{(3)}$ measurements, excited state dynamics for different samples will be discussed in detail.



M = Zn, n = 0
M = Co, Ni, Cu, Zn, Ag, Cd or Hg, n = 0
M = Cr, Mn, Fe or Au, n = 1, X = Cl
M = In, n = 1, X = OH
M = Ge or Sn, n = 2, X = OH
M = V, n = 2, X = O
M = P, n = 3, X = OH

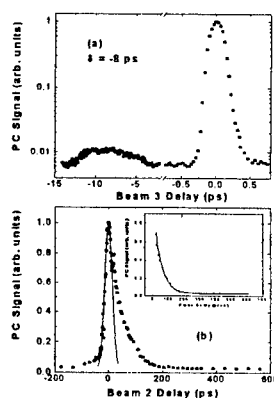


Fig. 1 Structure of the compounds used in the study

Fig. 2 PC signal in CoTTP ($ChCl_3$) (a) using incoherent light and (b) 35 ps pulses

References

- [1] H.S. Nalwa and S. Miyata, Ed.s, Nonlinear Optics of Organic Molecules and Polymers, CRC Press Inc., USA, (1997).
- [2] D.V.G.L.N. Rao, F.J. Aranda, D.E. Remy, J.F. Roach, Int. J. Nonlinear Opt. Phys. 3 (1994) 511.
- [3] S.V. Rao, N.K.M.N.Srinivas, L.Giribabu, B.G.Maiya, R. Philip, G.R. Kumar, and D.N. Rao, Submitted to Optics Communications; *ibid.* submitted to JOSA B

Nonlinear optical properties of model polyenes studied with femtosecond Z-scan at 800 nm

A. Samoc, M. Samoc, B. Luther-Davies

Laser Physics Centre, Research School of Physical Sciences, Australian Photonics Cooperative Research Centre, Australian National University, Canberra, ACT 0200, Australia

C. Andraud, T. Brotin and A. Collet

École normale supérieure de Lyon, Stéréochimie et Interactions moléculaires, 69364 Lyon cedex 07, France

The technique of closed and open aperture Z-scan at 800 nm was used to investigate third-order nonlinear optical properties of five symmetric polyenovanillins, the polyene molecules possessing a sequence of conjugated double bonds: $(-\text{CH}=\text{CH}-)_n$, with $n=3-8$, terminated with phenyl groups substituted with solubilizing agents. Absorption spectra show strong shifts to longer wavelengths with increasing number of double bonds. Z-scan measurements in solutions show strong variations of the real and imaginary part of nonlinear refractive index and third-order hyperpolarisabilities. The two-photon absorption increases with increasing number of double bonds. The cubic nonlinearities depend on solvent environment.

The symmetric *trans* polyenovanillins [1] possessing various number of π -conjugated double bonds (see the formulas in Figure 1) resemble a classic series of diphenylpolyenes whose peculiar optical properties have been recognised since the pioneering work of Hausser et al. [2]. Figure 1 shows a bathochromic shift of linear absorption spectra of polyenovanillins in chloroform solutions to longer wavelength with increasing number of C=C bonds in polyene chains. The presence of the auxochromic groups (OMe, SMe, OBU, SBU) induces a red shift and increases the intensity of absorption in comparison to unsubstituted polyenes and diphenylpolyenes.

Closed and open-aperture Z-scan measurements were performed on series of solutions with varying solute concentrations using 120 fs laser pulses obtained from an amplified Ti:sapphire system at 800 nm. The repetition rate was 30 Hz, the pulse energy was about 0.3 μJ , the beam waist 20 μm . The measurements were repeated using 140 fs laser pulses, the pulse energy 4 μJ and the beam waist 47 μm . The shapes of the Z-scans were fitted with expressions derived in [3] to yield the real and imaginary parts of the nonlinear phase shift. The data obtained from dilute solutions were approximated with linear dependences on the concentration of the solute [4].

Figure 2 shows the real and imaginary parts of the hyperpolarizabilities measured at 800 nm in the substituted diphenylpolyenes. Especially large values of the real and imaginary parts of the third-order nonlinearity have been found for the polyenovanillines with the number of double bonds equal to 7 and 8. This may be because our fundamental wavelength of 800 nm is close to strong two-photon absorption resonances which are tuned by the length of π -electron conjugation. The results emphasise the importance of dispersion for nonlinear optical properties of the conjugated molecules.

We observed variations in linear spectroscopic properties and third-order optical nonlinearities of studied polyenes in various solvents. This might indicate that the measured spectral and photophysical parameters are characteristic for the molecule in its solvent environment rather than for the isolated molecule. The UV absorption spectra

Poster Session II

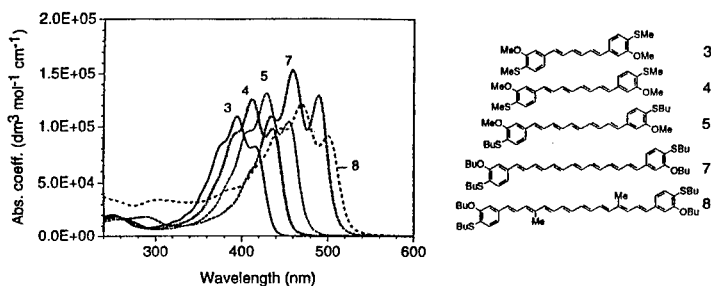


Figure 1: Optical spectra of symmetric polyenovanillins in chloroform and the diagram of their formulas.

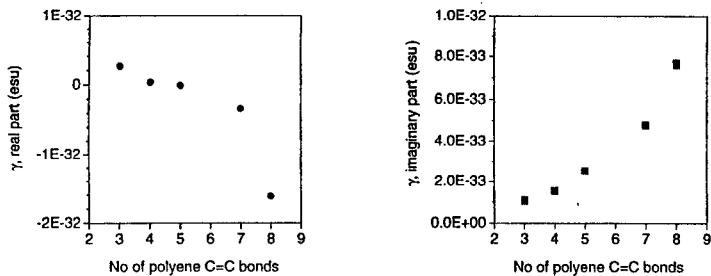


Figure 2: Third-order hyperpolarizabilities of polyenovanillins in chloroform derived from femtosecond Z-scan measurements at 800 nm.

of polyenovanillins and the cubic nonlinearities depended also on the history of the sample, which may result from the susceptibility of the molecules to *trans-cis* thermal and photo-isomerisation.

References

- [1] B. C. Andraud, T. Brotin, C. Garcia, F. Pelle, P. Goldner, B. Bigot, A. Collet, "Theoretical and experimental investigations of the nonlinear optical properties of vanillin, polyenovanillin, and bisvanillin derivatives" *J. Am. Chem. Soc.* **116**, 2094-2102 (1994)
- [2] K. W. Hausser, R. Kuhn, A. Smakula, "Lichtabsorption und Doppelbindung IV. Diphenylpolyene" *Z. phys. Chem. B* **29**, 384-389 (1935)
- [3] M. Sheikh-bahae, A. A. Said, T. Wei, D. J. Hagan, E. W. van Stryland, "Sensitive measurement of optical nonlinearities using a single beam" *IEEE Journ. Quantum Electr.* **26**, 760-769 (1990)
- [4] M. Samoc, A. Samoc, B. Luther-Davies, Z. Bao, L. Yu, B. Hsieh, U. Scherf, "Femtosecond Z-scan and degenerate four-wave mixing measurements of real and imaginary parts of the third-order nonlinearity of soluble conjugated polymers" *J. Opt. Soc. Am. B* **15**, 817-825 (1998)

Thin films of a novel polydiacetylene for applications in all-optical signal processing

S. Sottini, G. Margheri, E. Giorgetti, F. Gelli,
IROE-CNR, Firenze, Italy

A. Cravino, D. Comoretto, C. Cuniberti, C. Dell'Erba, I. Moggio and G. Dellepiane
INFM, Dipartimento di Chimica e Chimica Industriale, Università di Genova, Genova, Italy

The linear and nonlinear characterization of waveguide films, made of a novel polycarbazolyldiacetylene, polyDCHD-HS, is in progress. A preliminary measure of the third order nonlinear susceptibility at $\lambda=1064\text{nm}$ by the Surface Plasmon Resonance method, gave a value of $4.4 \times 10^{-17} + i3.5 \times 10^{-18} (\text{m/V})^2$, which is a particularly promising result.

Future all-optical devices can be based both on a third order nonlinear process and on a cascading of two second order processes (CP). The latter process is practically the most studied at the moment because the CP efficiency, whenever a direct comparison is possible, turns out to be substantially larger than the third order susceptibility $\chi^{(3)}$ [1]. On the other hand, devices based on a CP show serious problems related to the need of noncentrosymmetric nonlinear materials and to severe phase matching requirements since the CP usually includes second harmonic generation. Such considerations suggest that the investigation of new polymers with higher third order nonlinearities and the utilization of waveguide configurations to minimize the operating power are topics of the greatest interest in the present research activity.

Polydiacetylenes show values of $\chi^{(3)}$ which are still the highest available out of resonance. These polymers can be synthesized from monomers where special substituents can be introduced. In particular the synthesis of novel carbazolyldiacetylene monomers has opened a way to the preparation of soluble polydiacetylenes which form two-dimensional highly ordered supramolecular assemblies in the solid state. Such two-dimensional organization has been detected by powder X-ray diffraction for polyDCHD-HS (which is a polycarbazolyldiacetylene having long alkyl groups on the carbazolyldiacetylene substituents), and found to consist of polydiacetylenic columns in a hexagonal array [2]. This result, together with the large solubility of polyDCHD-HS has suggested the investigation of its linear and nonlinear properties in thin spun films.

In order to demonstrate waveguiding, films of thickness ranging from 1 to $3.6\mu\text{m}$ were spun on soda lime microscope slides. The best results were obtained with toluene solutions. The guided streak was clearly visible at 849 and at 1321nm, thus the propagation losses could be measured by the scattered intensity: they resulted to be 8.5 and 5dB/cm, respectively. These values are comparable with those currently obtained with other polydiacetylene guides. It is also remarkable that polyDCHD-HS films show a negligible birefringence. This fact suggests that such insensitivity to polarization, which is highly appreciated in telecommunications, can hold also in the case of the nonlinearity. In addition to waveguiding, also photobleaching of

Poster Session II

polyDCHD-HS films is under investigation as a suitable technique for patterning. Preliminary results obtained under UV light exposure suggest that very low molecular weight degraded species are formed along with some material ablation.

The Kerr nonlinearity of very thin films (10-15nm) of polyDCHD-HS is currently investigated by the Surface Plasmon Resonance technique which has the advantage of being quite insensitive to film inhomogeneities and propagation losses. On the other hand the thermal contributions have been minimized by using short pulses (≈ 20 ps) and low repetition rate (10Hz). Only preliminary results are available, obtained by using the Kretschmann configuration. An example is shown in Fig. 1: two measurements of the plasmon coupling angle were performed at low ($8\text{MW}/\text{cm}^2$) and at high intensity ($0.35\text{GW}/\text{cm}^2$) respectively. A 0.026° angular shift of the reflectivity dip, which indicates just the plasmon coupling, was observed. This shift is related to the refractive component of $\chi^{(3)}$, while the broadening of the curve and the variation of its minimum are related to its imaginary part. In conclusion, in this experiment the complex $\chi^{(3)}$ resulted equal to $4.4 \times 10^{-17} + i3.5 \times 10^{-18} \text{ (m/V)}^2$. Even if these preliminary tests need further confirm they seem to be very promising; in particular, the real part of $\chi^{(3)}$ that we have measured is an order of magnitude greater than that of PTS at the same wavelength.

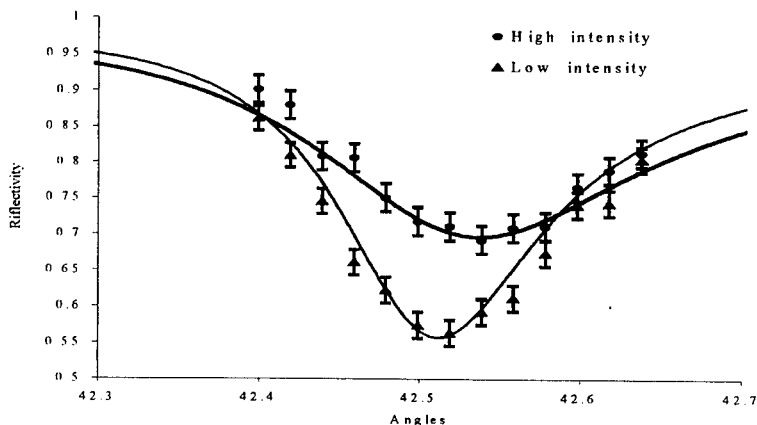


Figure 1: Angular shift of reflectivity dip due to SPR

References

- [1] G. P. Banfi, P. K. Datta, V. Degiorgio, G. Donelli, D. Fortusini, J. N. Sherwood, *Opt. Lett.* **23**, 439, 1998
- [2] B. Gallot, A. Cravino, I. Moggio, D. Comoretto, C. Cuniberti, C. Dell'Erba, G. Dellepiane, *Liquid Crystals* **26**, 1437, 1999

Poster Session III

Drift correction in organic intensity modulator

P. Labbé^{1,2}, A. Clouqueur², R. Hierle², E. Toussaere², J. Zyss²

¹ Centre de Recherche Motorola - Paris, Espace technologique de Saint Aubin
91193 Gif-su-Yvette, France

² ENS-Cachan, LPQM, 61, avenue Président Wilson
94235 Cachan, France.

The maturing of electrooptic polymer based Mach-Zehnder intensity modulators qualifies them as serious contenders for telecom applications. Their manufacturing is now at the quality control level and several outstanding demonstrations of their capacities have been reported (high modulation up to 110GHz [1] and a quenching voltage lower than 2V [2], polarization insensitivity [3] and long term stability [4]). Nevertheless, a slow drift of their characteristics has been observed.

In order to solve this problem, we report an electronic system that is able to follow the evolutions of the modulator characteristics so as to correct the slow variations of the operating point. This approach will further enhance the reliability of this type of components.

Modulator characterization

Electrooptic polymer modulators were made by spin coating different polymer layers on a oxidized silicon wafer with photolithographically patterned gold electrodes [6]. Measured dynamic and static halfwave voltages were 15V and 5V respectively. Since the modulators were characterized on an optical bench without any temperature nor mechanical stabilization, drift of their modulation characteristics could be observed as a shift of the operating point and can be expressed by the addition of a static phase φ^s (ideally null) in the modulated intensity:

$$I_s = \frac{I_e}{2} \left\{ 1 + \sin \left[\varphi^d \sin(\Omega t) + \varphi^s \right] \right\} \quad (1)$$

φ^d is the dynamic phase amplitude; I_e and I_s are the input and the output light signal intensities (defined figure 1). As soon as the drift occurs, φ^s is slowly varying compared to the modulating rate and can be compensated for by the application of a constant voltage. Expressing the output signal as a sum of Fourier harmonics, we obtain:

$$I_s = \frac{I_e}{2} \left\{ 1 + \sin(\varphi^s) J_0(\varphi^d) + 2 \cos(\varphi^s) \sum_{k=0}^{+\infty} J_{2k+1}(\varphi^d) \sin[(2k+1)\Omega t] + 2 \sin(\varphi^s) \sum_{k=1}^{+\infty} J_{2k}(\varphi^d) \cos[2k\Omega t] \right\} \quad (2)$$

$(J_n)_{n \in \mathbb{N}}$ are the first kind n-th order Bessel functions. Equation 2 shows that the dominant term for a correction of the bias voltage is the second order term.

Signal processing

A constant bias field is first added to the modulation signal as a driving voltage. The operating point is obtained when the amplitude of the second order term of the optical signal is minimum. A lock-in detection is therefore used at twice the modulation frequency to yield the amplitude of the second harmonic distortion which is then amplified and mixed back with the driving voltage as a correcting bias signal (global system represented on figure 1).

Poster Session III

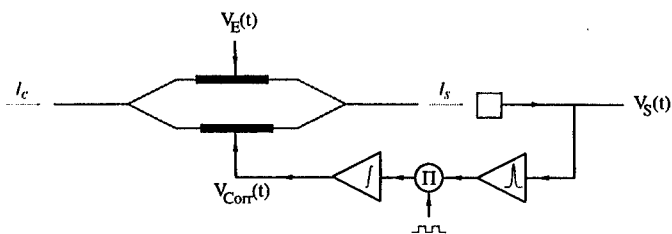


Figure 1: Global scheme of the system. I_e and I_s are the input and output light intensities. $V_E(t)$ is the command voltage and $V_S(t)$ the output voltage. $V_{Corr}(t)$ is the bias voltage.

All amplification stages are calculated in order to minimize the number of iterations and the time constant. Moreover, the bias voltage amplitude is wide enough to follow a shift of twice the extinction voltage. Taking into account the speed of the drift phenomenon, a correction time constant of a millisecond is sufficient.

Conclusion

We have built-up a compact electronic system composed of simple and low-cost electronic devices allowing for analogic processing of the output signal of a Mach-Zehnder intensity modulator. The operating point of an organic intensity modulator could be stabilized. The system shows its robustness to a quicker disruption such as an illumination which usually shifts the operating point within a few seconds.

References

- [1] D. Chen, H. R. Fetterman, A. Chen, W. H. Steier, L. R. Dalton, W. Wang, Y. Shi, "Demonstration of 110GHz electrooptic polymer modulators," *Applied Physics Letters*, **70**(25), 3335-3337 (1997).
- [2] A. Chen, V. Chuyanov, S. Garner, H. Zhang, W. H. Steier, "Low V_π electro-optic modulator with a high- μ_β chromophore and a constant-bias field," *Optics Letters*, **23**(6), 478-480 (1998).
- [3] A. Donval, E. Toussaere, R. Hierle, J. Zyss, "Polarization-insensitive electrooptic polymer modulator," *Journal of Applied Physics*, (to be published).
- [4] H.T. Man, H.N. Yoon, "Long term stability of a poled side-chain nonlinear optical polymer," *Applied Physics Letters*, **72**(5), 540-541 (1998).
- [5] Y. Shi, W. Wang, W. Lin, D.J. Olson, J.H. Bechtel, "Long-term stable direct current bias operation in electro-optic polymer modulators with an electrically compatible multi-layer structure," *Applied Physics Letters*, **71**(16), 2236-2238 (1997).
- [6] R. Levenson, J. Liang, C. Rossier, R. Hierle, E. Toussaere, J. Zyss, "Advances in Organic Polymer-based Optoelectronics" in *ACS Symposium (Series 601, Polymers for Second-Order Nonlinear Optics*, G.A. Lindsay, K.D. Singer Eds, 1995), pp.436-455.

Gaussian profile Bragg gratings in polydiacetylene waveguides: characterization and application in integrated optics

G. Marowsky and M. A. Bader
Laser-Laboratorium Göttingen e. V.
Hans-Adolf-Krebs-Weg 1
D-37077 Göttingen, Germany

Optical nonlinear devices are required to control the processing of fast optical signals. Polymeric materials with high optical nonlinearities are particularly suited to realize novel all-optical switching concepts.

To open up the wide field of device applications in integrated optics based on periodically structured planar polymer waveguides we studied nonuniform Bragg gratings in polydiacetylene channel waveguides. The fabrication, using an optimized photo-bleaching setup, and the optical characterization of shallow Gaussian profile gratings in the polydiacetylene poly(4-BCMU) will be reported. The suitability of the system to nonlinear wave propagation phenomena and nonlinear switching processes based on Bragg soliton generation will be shown.

Novel all-optical switching concepts based on Bragg grating structures in planar waveguides are of still increasing interest for integrated optics [1]. A high third-order nonlinearity of the material causes a detuning of the photonic band gap of the periodic structure which, as a result, changes from its reflective state to a completely transmissive state as intensity in the device is increased and so-called gap solitons are created [2].

Nonlinear propagation effects resulting in all-optical switching or nonlinear optical pulse narrowing have been predicted and observed in both planar and fiber waveguide devices [3, 4, 5]. Organic materials, however, such as conjugated polymers like polydiacetylenes are known to be among the most promising candidates for high-speed photonic switching and signal processing concepts, due to their high third-order susceptibilities and fast response times [6].

We present the fabrication and characterization of high quality nonuniform Bragg gratings in planar poly(4-BCMU) waveguides and show the suitability of our system for all-optical switching phenomena.

Bragg grating fabrication and characterization

Bragg gratings in planar poly(4-BCMU) waveguides of thicknesses of about $1.25 \mu\text{m}$ were fabricated by UV-photobleaching using the third harmonic of a picosecond 1064 nm Nd:YAG laser ($\lambda_{\text{THG}} = 355 \text{ nm}$). A change in the refractive index n is induced in the material when irradiated by UV-light. The decrease dn/n per pulse was deduced from the bleaching behavior of the material, which we investigated by evaluating reflection and absorption spectra during irradiation. A linear dependency of the bleaching rate with respect to the laser energy on the polymer surface was found.

A periodic refractive index modulation in the polymer film was generated by interfering the ± 1 . diffraction orders of a phase mask, which was illuminated by a Gaussian shaped 355 nm laser beam. An optimized setup to define the grating period based on a variable angle of incidence onto two steering mirrors was used. High quality Gaussian profile Bragg gratings could be achieved by applying this method.

Poster Session III

The linear optical characterization of the device was done by scanning a 355 nm Nd:YAG-pumped, continuously tunable optical parametric generator (OPG) across the Bragg wavelength λ_B of the Gaussian profile grating, the infrared idler beam being coupled into and out of the waveguide by identical glass prisms. The transmission spectrum of the device was measured for different incident intensities to allow the detection of intensity-dependent nonlinear effects.

Application in integrated optics

We present device transmission spectra around center wavelengths close to the telecommunication wavelength of 1300 nm. To investigate and characterize the generated nonuniform grating structures, we compare experimental data to theoretical calculations based on coupled mode theory as outlined in ref. [7]. The shapes of the spectra, especially the characteristics of the edges and the flat transmission minima, indicate high quality nonuniform gratings and suggest the suitability of the system to nonlinear pulse propagation or switching applications. Requirements to obtain evidence of nonlinear effects, such as the exact shape of the Bragg grating and the coupling efficiency, are discussed.

References

- [1] G. I. Stegeman, A. Miller in "Photonics in Switching", edited by J. E. Midwinter (Academic Press, San Diego), Vol. 1, 81-145 (1993)
- [2] C. M. de Sterke, J. E. Sipe in "Progress in Optics", edited by E. Wolf (Elsevier Science, Amsterdam), Vol. XXXIII, 203-260 (1994)
- [3] N. D. Sankey, D. F. Prelewitz, T. G. Brown, "All-optical switching in a nonlinear periodic-waveguide structure", *Appl. Phys. Lett.* **60**, 1427-1429 (1992)
- [4] B. J. Eggleton, R. E. Slusher, C. M. de Sterke, P. E. Krug, J. E. Sipe, "Bragg grating solitons", *Phys. Rev. Lett.* **76**, 1627-1630 (1996)
- [5] D. Taverner, N. G. R. Broderick, D. J. Richardson, R. I. Laming, M. Ibsen, "Nonlinear self-switching and multiple gap-soliton formation in a fiber Bragg grating", *Opt. Lett.* **23**, 328-330 (1998)
- [6] G. I. Stegeman in "Nonlinear Optics of Organic Molecules and Polymers", edited by H. S. Nalwa, S. Miyata (CRC Press, Boca Raton), 799-812 (1997)
- [7] J. E. Sipe, L. Poladian, C. M. de Sterke, "Propagation through nonuniform grating structures", *J. Opt. Soc. Am. A*, **11**, 1307-1320 (1994)

Compression of soliton-like pulses in Kerr-type planar waveguides

M. E. Pietrzyk^{1,2}

*Institut für Festkörpertheorie und Theoretische Optik,
Friedrich-Schiller Universität Jena,
Max-Wien Platz 1, D-07743, JENA, GERMANY*

It is known that compressors of optical pulses based on Kerr-type planar waveguides can give rise to large compression of pulses with anomalous dispersion. However, the compression have a local character, i.e., the maximal compression takes place on a certain distance of propagation, thus optimization of the length of the compressor is required. Here we demonstrate that this difficulty can be avoided when a pulse with normal dispersion is introduced to the system. The analysis, based on the variational and numerical solutions of the two coupled (2+1)-dimensional NSE modeling the above proposed configuration, shows that the best parameters of the compression can be achieved in the case of vanishing dispersion of the auxiliary pulse, i.e., when soliton-like solutions arise.

We study a compression of an optical pulse propagating in a Kerr-type planar waveguide into which a second pulse is launched. As the model equation we take two coupled (2+1)-dimensional nonlinear Schrödinger equations (NSEs):

$$i \frac{\partial}{\partial \zeta} \Psi_1 + \frac{1}{2} \sigma_1 \frac{\partial^2}{\partial \tau^2} \Psi_1 + \frac{1}{2} \frac{\partial^2}{\partial \xi^2} \Psi_1 + (|\Psi_1|^2 + 2|\Psi_2|^2) \Psi_1 = 0, \quad (1a)$$

$$i \frac{\partial}{\partial \zeta} \Psi_2 + \frac{1}{2} \sigma_2 \frac{\partial^2}{\partial \tau^2} \Psi_2 + \frac{1}{2} \frac{\partial^2}{\partial \xi^2} \Psi_2 + (|\Psi_2|^2 + 2|\Psi_1|^2) \Psi_2 = 0, \quad (1b)$$

where ζ, τ, ξ denote, respectively, the longitudinal coordinate, the local time, and the transverse spatial coordinate. The wavelengths of the pulses are chosen in such a way that the pulse, which is the subject of the compression propagates in the anomalous dispersion regime, while the second one, treated as an auxiliary pulse, is in the normal regime; it means that $\sigma_1 > 0$ and $\sigma_2 < 0$ (the limiting case of vanishing dispersion, $\sigma_2 = 0$, is also considered). Here σ_j stand for the dispersion-to-diffraction ratio of the j -th pulse, $j = 1, 2$. In the analysis we use the variational method and numerical simulations. As the Ansatz in the variational method we take the Gaussian function:

$$\Psi_j(\zeta, \tau, \xi) = A_j(\zeta) \exp \left[-\frac{\tau^2 (1 + iC_{\tau j}(\zeta))}{2w_{\tau j}(\zeta)} \right] \exp \left[-\frac{\xi^2 (1 + iC_{\xi j}(\zeta))}{2w_{\xi j}(\zeta)} \right] e^{i\phi_j}, \quad (2)$$

which depends on 12 parameters, the temporal (spatial) width, $w_{\tau j}$ ($w_{\xi j}$), the temporal (spatial) chirp, $C_{\tau j}$ ($C_{\xi j}$), the amplitude, κ_j , and the phase, ϕ_j , of the j -th pulse, $j = 1, 2$. As the initial condition we take function (2) and assume that $w_{\tau j}(0) = w_{\xi j}(0) = 1$, $C_{\tau j}(0) = C_{\xi j}(0) = 0$, $\phi_j(0) = 0$, where $j = 1, 2$. Magnitudes of the dispersion-to-diffraction ratio, σ_j , and the parameter $\kappa_j := A_j(0)$, referred here to as the strength of nonlinearity of the j -th pulse, $j = 1, 2$, are varied in the analysis.

The analysis of the variational and numerical solutions of equations (1)a,b can be found in [1]. here we focus on the temporal aspect of the compression, which we characterize

¹On leave from: Faculty of Physics, Warsaw University of Technology, Warsaw, Poland.

²e-mail: monika@nlwl.uni-jena.de

Poster Session III

by three parameters: the maximal compression factor, defined as the ratio of the initial temporal width of the pulse to the minimal width obtained during the evolution of the pulse; the optimal length of the compressor, determined as the distance of propagation on which the minimal temporal width of the pulse takes place; and the compression length, defined as the interval of the propagation distance within which the evolution of the pulse is such that its temporal width is approximately constant and equal to the minimal width. We observe that the best parameters of the proposed compressor, i.e., as large as possible maximal compression factor and compression length, can be obtained for the parameters of the system admitting generation of soliton-like solutions. This occurs when duration of the auxiliary pulse is so large that its dispersion can be neglected and its strength of nonlinearity is above the threshold of soliton generation, while the strength of nonlinearity of the pulse being the subject of the compression is below the threshold of catastrophic self-focusing occurring during its single propagation (formation of soliton-like solutions can be explained as follows: the pulse with negligible dispersion, since its dynamics can be modeled by integrable (1+1)-dimensional NSE, creates a waveguide in the medium in which it propagates and the other pulse gets trapped into this waveguide [2]).

Note that the optimal length of the compressor under discussion is equivalent to the distance of propagation necessary for formation of soliton-like solutions; the compression length, which is associated with the distance of propagation on which soliton-like solutions maintain their shapes, is infinitely large (assuming that soliton-like solutions are stable against small perturbations). The maximal compression factor and the optimal length of such a compressor depend, in general, on initial parameters of the pulses being the subjects of the compression. However, since the compression length is considerably large, then it is possible to choose the length of the compressor in the way which can guarantee that on the output optimally compressed pulses, irrespective of their initial shapes, amplitudes and widths, are obtained. Such a compressor can be, therefore, considered as an universal device. Moreover, the maximal compression factor and the optimal length of the compressor under discussion are much larger than in the case of a single anomalous pulse, e.g., for $\kappa_1 = 1$, $\sigma_1 = 1$, $\kappa_2 = 2$, $\sigma_2 = -1$, they are, respectively, more than 3 times larger and, at least, 10 times greater than the corresponding values of the compressor with a single pulse. To our knowledge, large optimal length of the compressor is the only fact which can be considered as a disadvantage of such a configuration, since a preparation of a large waveguide, which can be problematic in practice, is required in this situation. However, we believe that the proposed configuration have a potential to be realized in practice. For this purpose AlGaAs structures, which have high nonlinear refractive index and large damage threshold, could be used.

Note that we investigated here only the temporal aspect of the compression; however, in the configuration under discussion one obtains pulses, that are confined not only in time but also in space. Such a pulses, compressed temporally and spatially, can be used, e.g., for nanostructuring. Proposed here configuration could be used also as a basic element of optical steering or switching devices.

References

- [1] M. E. Pietrzyk, *J. Opt. A: Pure Appl. Opt.* **1**, 685-696 (1999).
- [2] M. E. Pietrzyk, "Are there soliton-like solutions of coupled (1+1)- and (2+1)-dimensional NSEs?," to be published in *Rep. Math. Phys.*

Functionalized Polymers for Photonic Applications

Claire Pitois, Anders Hult
*Royal Institute of Technology, Department of Polymer Technology
S-100 44 Stockholm, Sweden*

Dorothea Wiesmann
IBM Zurich Research Laboratory, CH-8803 Rüschlikon, Switzerland

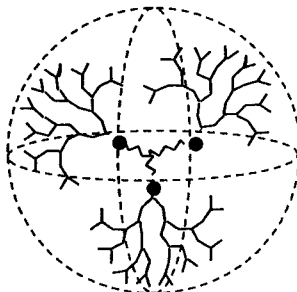
Åsa Claesson
Acree AB, Electrum 233, 164 40 Kista, Sweden

*Mikael Lindgren
*Division of Laser Systems; Defense Research Establishment (FOA32)
P.O. Box 1165; S-581 11 Linköping, Sweden
Fax: + 46 13 378066, Tel: + 46 13 378038, Email: miklin@lin.foa.se*

Optical and opto-electronic functions supporting fiber optic networks can be realized using polymer materials. The main problems to overcome concern index matching between passive and active devices, optical losses, long term stability, and processing of waveguide structures. We present results of hyper-branched polymer materials designed for low-loss optical wave guiding at 1550 nm, based on fluorinated compounds. Optical losses down to 0.1 dB/cm and refractive index matching capabilities for single mode channel wave-guides were achieved at telecommunication wavelengths. We also present spectroscopic evidence for incorporation of Er^{3+} into dendrimer complexes with similar structure to the hyper-branched polymers constituting the passive wave-guiding materials.

A vision for the future is to move from traditional photonics technology with its associated high costs to polymer photonics. By producing wave-guides, light emitters, receivers, that is, both active and passive optical waveguide components in polymers, it should be possible to circumvent many problems associated with e.g.: 1/ the costly precision alignment of e.g. semiconductor lasers and 2/ length & volume demands and cost of optical fiber amplifiers. This provided the effort invested in the processing of the polymers is cost effective.

Here we present results on new hyper-branched polymer materials demonstrating low optical losses (see beside). The principle is to build a material that is flexible with regard to chemical modification. The material is a hyper-branched polymer network build around a trivalent core structure. The bulk material is per-fluorinated to give low optical losses. Certain groups can be replaced by, for example, chlorine, to increase/tune refractive index. The core can house an active function, such as an electro-optic dye, two-photon absorber, or other optically nonlinear function. Here the result of the Er^{3+} cation is demonstrated.



* Corresponding/presenting/participating author.

Poster Session III

The hyper branched fluorinated material can be used to produce wave guiding thin films by spin-coating. Guided wave measurements were made on thin films of approximately 5 μm thickness formed by spin-coating SiO_2/Si wavers. The attenuated total reflection method showed a refractive index of 1.558 at 632.8 nm, and 1.533 at 1550 nm (TE-mode). Preliminary results of optical loss measurement at 1550 nm indicated losses down to 0.1 dB/cm. This is similar or better than optical losses measured previously for pentafluorostyrene/PMMA copolymers (0.4 - 0.5 dB/cm).¹

Dendrimer complexes doped with Lanthanide cations² can give rise to an optical amplifying function.³ The spectroscopic results of a thin film containing Er^{3+} are shown in Figure 1 below. The fluorescence spectrum obtained (right) was obtained by pumping with ca 5 mW at 975 nm using a Argon (514 nm) pumped Ti:Saffire cw-laser.

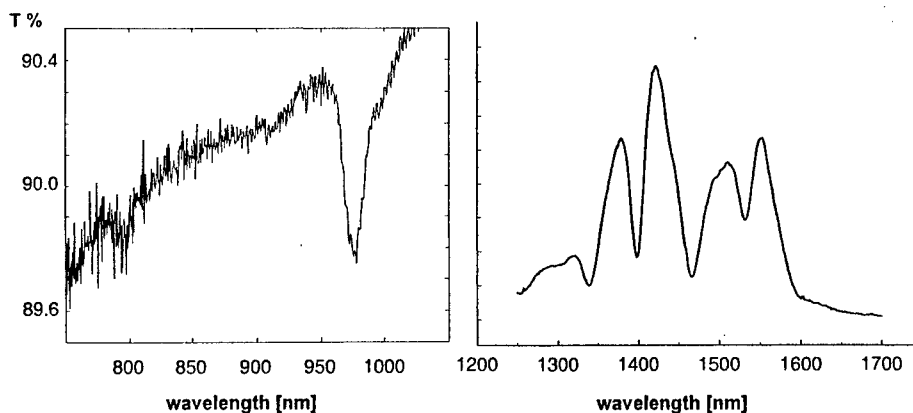


Figure 1. Optical transmission spectrum (left) and fluorescence spectrum (right) of thin film (ca 100 μm) of Er^{3+} -doped dendrimer complexes. The film was sandwiched between two glass plates. The concentration of Er^{3+} -ions was approximately 2 %.

Acknowledgements: We thank Fredrik Karlsson and Per-Olof Holtz for assisting in the measurement of the fluorescence spectrum.

¹ C. Pitois, S. Vukmirovic, A. Hult, D. Wiesmann, M. Robertsson. "Lowloss passive optical waveguides ..."; *Macromolecules* 32, 2903-2909 (1999).

² M. Kawa, M. J. Fréchet. "Self-Assembled Lanthanide-Cored Dendrimer Complexes: ...". *Chem. Mater.* 10, 286-296 (1998).

³ S. Sudo (ed). "Optical Fiber Amplifiers." Artec House Inc. Boston 1997.

Three Dimensional Optical Fiber Simulation

Dennis M. Sullivan
Department of Electrical and Computer Engineering
University of Idaho
Moscow, ID USA 83843-1023

Abstract

The goal of this project is to develop computer simulation methods for ultra-fast optical switching mechanisms using the finite-difference time-domain (FDTD) method [1]. The FDTD method is an explicit method that implements Maxwell's equations, treating light beams as electromagnetic waves. A simulation using this method offers the possibility of studying the propagation of electromagnetic energy through a nonlinear material in minute detail. The accuracy of this method in modeling nonlinear phenomena has been demonstrated [2].

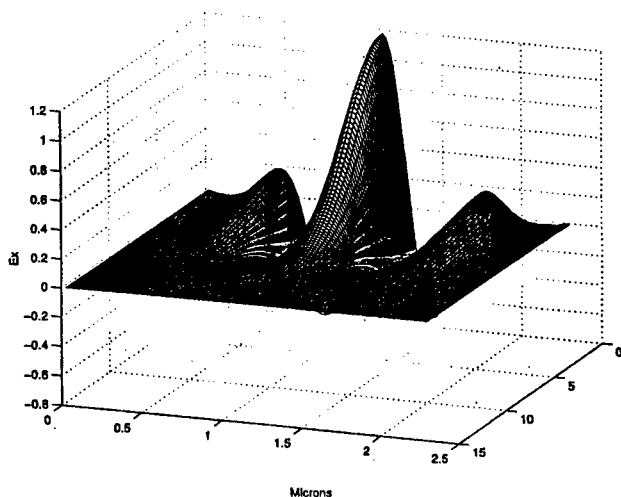


Figure 1. The propagating pulse after 300 time steps. Once it has reached the center of the problem space, it is held there.

Three-Dimensional Optical Fiber Simulation

The three dimensional simulation of an optical fiber via the FDTD method has some substantial logistical problems stemming from the fact that light pulses consist of very small wave lengths. To accurately calculate phase over long distances, it is desirable to have thirty points per wavelength [1]. The computational resources needed to model even a small section of fiber in three dimensions would overwhelm even today's supercomputers. There are three

Poster Session III

things that can be done to make the simulation of an optical fiber a tractable problem [3]: 1. Oblong cells, which are 1/6 as large in the propagation direction as the transverse, are used to maximize resolution where it is most needed. 2. Only one quadrant is simulated, since the optical fibers being simulated are single mode. 3. The propagating pulse is held in the middle of the problem space (Fig. 1).

Analysis of the Pulse

Even though the pulse is being held in the middle of the problem space, its characteristics are being calculated by a Fourier transform at 282 THz to determine the macroscopic properties. In this manner, the amplitude and phase of the propagating pulse can be calculated over distances much larger than the section of fiber being simulated. Furthermore, wavelet analysis of the propagating pulse takes place every $.5 \mu\text{m}$ (Fig 2). The wavelet analysis allows the pulse shape to be stored with a minimum number of variables.

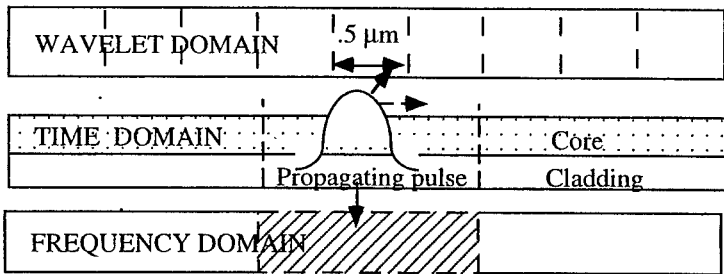


Figure 2. The time domain problem space is assumed to be moving along a fiber. The discrete Fourier transform is being calculated and mapped to another domain. At the same time, wavelet analysis is done at $.5 \text{ mm}$ intervals and the parameters stored.

Discussion

By using the methods described above, simulations over distances of 10 cm have been obtained. This is enough to observe the effects of nonlinear phenomena. Qualitative agreement with experimental results has been obtained [4].

Bibliography

1. A. Taflove, *Computational Electrodynamics, the Finite Difference Time Domain Method*, Boston: Artech House, 1995.
2. D. M. Sullivan, "Nonlinear FDTD formulations using Z transforms," *IEEE Transactions on Microwave Theory and Techniques*, Vol. 43, pp. 676-682, March, 1995.
3. D. M Sullivan, M. Kuzyk, "Three dimensional optical pulse simulation using the FDTD method," *IEEE Trans. on Microwave Theory and Tech.*, accepted for publication.
4. D. W. Garvey, Q. Li, M. G. Kuzyk, C. W. Dirk, "Sagnac interferometric intensity dependent refractive index measurements of polymer optical fibers," *Optics Letters*, Vol. 21, no. 1, pp. 105-107, 1996.

Channel Waveguide Fabrication of Organic Nonlinear Optical Crystal, DAST, by Using Oxygen RIE

K. Takayama, M. Yoshida, H. -H. Deng, K. Komatsu, T. Kaino
Institute for Chemical Reaction Science, Tohoku University
 2-1-1 Katahira, Aoba-ku, Sendai 980-8577 JAPAN

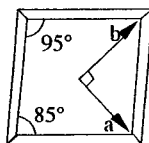
An organic salt, 4-*N,N*-dimethylamino-4'-*N'*-methyl-stilbazolium tosylate, DAST, has been attracting many researchers because of its large second-order optical nonlinearities. The difficulty in fabricating waveguide of DAST crystal is that it easily dissolves in general photoresist solutions. We fabricated its ridge waveguide for the first time to our knowledge by using photolithography and oxygen reactive ion etching (O_2 RIE).

To attain this, poly(methyl methacrylate) (PMMA) was spun on the top of the crystal as a buffer layer to protect it from damage by photoresist solutions. The buffer layer was effective to remove residual photoresist *via* lift-off process. The side-wall of DAST ridge was almost perpendicular to the etched crystal surface. Channels with $34 \times 20 \mu\text{m}$ and $6 \times 6 \mu\text{m}$ and 2mm in length were successfully fabricated by this process.

Introduction

Organic nonlinear optical materials are very promising for practical applications because of their large intrinsic nonlinearities, fast response time, low dielectric constant and high optical damage threshold limits.

DAST crystals have been studied from a wide variety of point of view [1]-[4], such as crystal growth, X-ray crystallography and linear and nonlinear optics. In this work, we will report the fabrication of DAST waveguide by using O_2 RIE. (a)



(b)

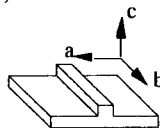


Figure 1 Schematic illustration of (a) DAST crystal habit and (b) DAST waveguide structure.

Experiments

DAST crystals to fabricate a ridge waveguide were grown from a methanol solution by a temperature lowering technique. The grown crystals as thin plates (typically 0.3mm) with the *ab* plane parallel to the largest surface (typically $4 \times 4 \text{mm}^2$) were used to fabricate the waveguide. Figure 1(a) is a schematic illustration of DAST crystal habit.

DAST crystals have large electro-optic coefficient along the *a*-axis. So, the waveguide core ridge was fabricated parallel to the *b*-axis. Figure 1(b) is a schematic illustration of fabricated DAST waveguide.

Schematic diagram of the fabrication process of DAST waveguide is shown in Figure 2. To protect DAST crystal from a photoresist solution, PMMA spin coated thin layers with toluene as a solvent which does not dissolve DAST crystal was used as a buffer layer. An etching mask was patterned from a photoresist by photolithographic technique. A core ridge was then

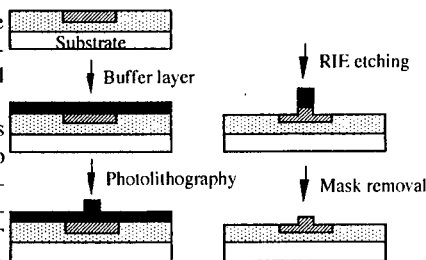


Figure 2 Schematic diagram of the fabrication process of DAST waveguide.

Poster Session III

fabricated by O₂ RIE. After the etching of DAST crystal, the etching mask was removed by dissolving the buffer layer into toluene by heating up to 40°C. The end-faces of the waveguide was made by the cleavage of DAST crystal.

Results and Discussion

The core ridge of DAST crystal waveguide was successfully fabricated by using O₂ RIE. Figure 3 shows a typical cross-sectional polarizing microscope image of the fabricated DAST waveguide. When a 40µm wide etching mask with 5 hours etching time were taken, the core ridge was 34µm in width and 20µm in height as shown in Figure 3(a). When a 8µm wide etching mask with 1.5 hours etching time were taken, the core ridge was 6µm in width and 6µm in height as shown in Figure 3(b). An etching rate of DAST crystal by O₂ RIE with a optimal condition is 4.0µm/h calculated by the ridge height and the etching time. The side-wall of DAST ridge was almost perpendicular to the etched crystal surface.

Figure 4 shows a typical SEM image of DAST waveguide. The side-wall of ridge had vertical stripes due to the etching. We consider that those stripes will not influence the transmission loss into the waveguide. The etched crystal surface was very smooth.

Conclusions

PMMA was used as a lift-off layer and a buffer layer to protect DAST crystal from damage by photoresist solutions. DAST waveguide structure was successfully fabricated by using O₂ RIE and this lift-off layer. The side-wall of DAST ridge was almost perpendicular to the etched crystal surface. The etched crystal surface was smooth enough for waveguide operations.

References

- [1] S. R. Marder, J. W. Perry, and C. P. Yakymyshyn, *Chem. Mater.* **6**, 1137-1147 (1994).
- [2] G. Knöpfle, R. Schlessler, R. Ducret, and P. Günter, *Nonlinear Optics* **9**, 143-149 (1995).
- [3] F. Pan, G. Knöpfle, Ch. Bosshard, S. Follonier, R. Spreiter, M. S. Wong, and P. Günter, *Appl. Phys. Lett.* **69**, 13-15 (1996).
- [4] F. Pan, K. McCallion, and M. Chiappetta, *Appl. Phys. Lett.* **74**, 492-494 (1999).

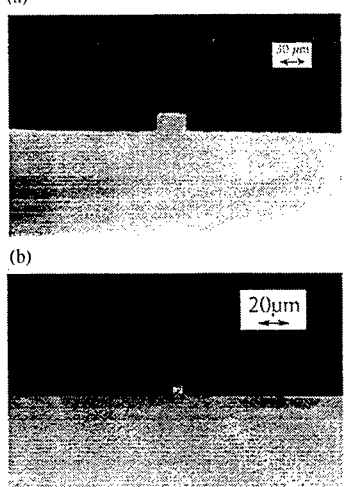


Figure 3 Typical cross-sectional polarizing microscope image of DAST waveguide. The ridge size is (a)34x20µm and (b)6x6µm , respectively.

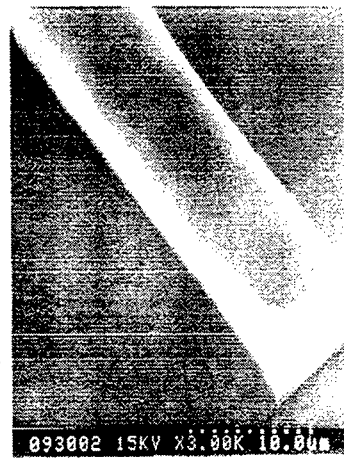


Figure 4 Typical SEM image of the DAST waveguide.

**New disubstituted organic compounds with enhanced non-resonant
nonlinear refraction in the picosecond range**

André-Jean Attias

*DMSC, ONERA, 29 avenue de la Division Leclerc,
BP72, F-92322 Chatillon cedex*

Frédéric Chérioux

*Laboratoire de Chimie et Electrochimie Moléculaire, Université de Franche-Comté,
La Bouloie, 16 route de Gray, F-25030, Besançon cedex*

Hervé Maillotte

*Laboratoire d'Optique P.M. Duffieux, UMR CNRS/Université de Franche-Comté n°6603,
Institut des Microtechniques de Franche-Comté,
UFR Sciences et Techniques, 16 route de Gray, F-25030 Besançon cedex*

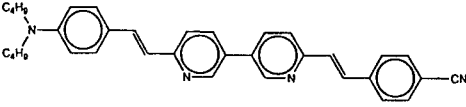
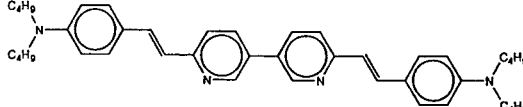
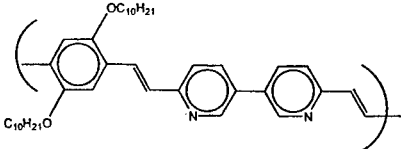
The synthesis and Z-scan measurements of new 3,3'-bipyridine derivatives with off-resonant third order nonlinear optical properties are discussed. We also report the characterization and the nonlinear properties of a polymer based on 3,3'-bipyridine moieties.

Realistic integrated photonic devices suitable for ultrafast all-optical processing systems require materials with a high non-resonant nonlinear refractive index and low absorption losses at infrared wavelengths. In this context, organic molecules and polymers have been the subject of extensive research [1]. However, only a small number of presently available organic materials are suitable for practical implementation, because the high third-order susceptibilities in such materials are mostly achieved via resonant enhancement. Thus, depending on whether essentially one- or two-photon absorption dominates, a high nonlinear refractive index is generally obtained at the expense of large linear or nonlinear absorption losses.

We report in this work the synthesis of different families of new 3,3'-bipyridine derivatives. The table presents one of this family, with dibutylamino (donor) and/or cyano (attractor) substituents. The elaborated compounds are dipolar (push-pull molecules) or apolar (symmetric push-pull-push molecules). Only the latter compounds can be polymerized by polycondensation between aromatic dialdehyde and 5,5'-dimethy-3,3'-bipyridine [2]. This particular chemical property is very attractive for the development of new nonlinear optical (NLO) cubic polymers but there is no report in the literature of the NLO properties of symmetric push-pull-push compounds.

The chemical way is a Knoevenagel reaction between an aromatic aldehyde (substituted with a donor or an attractive group) and 5,5'-dimethy-3,3'-bipyridine. The syntheses of the different compounds are efficient (yield close to 30%) and easy.

Poster Session III

<p style="text-align: center;">Push-Pull</p> 	<p style="text-align: center;">Nonlinear properties in solution</p> <p style="text-align: center;">$C = 0.01 \text{ mol.L}^{-1}$</p> <p style="text-align: center;">$\beta < 3 \cdot 10^{-13} \text{ m/W}$</p> <p style="text-align: center;">Extrapolated $n_2 \approx 3 \cdot 10^{-16} (\text{m}^2/\text{W})$</p>
<p style="text-align: center;">Symmetric Push-Pull-Push</p> 	<p style="text-align: center;">Nonlinear properties in solution</p> <p style="text-align: center;">$C = 0.03 \text{ mol.L}^{-1}$</p> <p style="text-align: center;">$\beta < 4 \cdot 10^{-13} \text{ m/W}$</p> <p style="text-align: center;">Extrapolated $n_2 \approx 1.5 \times 10^{-16} (\text{m}^2/\text{W})$</p>
<p style="text-align: center;">Polymer</p> 	<p style="text-align: center;">Nonlinear properties in solution</p> <p style="text-align: center;">$C = 0.033 \text{ mol.L}^{-1}$</p> <p style="text-align: center;">$\beta < 8 \cdot 10^{-13} \text{ m/W}$</p> <p style="text-align: center;">Extrapolated $n_2 \approx 1 \times 10^{-16} (\text{m}^2/\text{W})$</p>

Both the nonlinear refractive index n_2 and the two-photon absorption coefficient β were simultaneously measured at $\lambda=1064 \text{ nm}$, using a single-shot (50 ps, 10 Hz) multi-channel Z-scan method [3]. For all molecular compounds, Z-scan measurements in dichloromethane solutions show a large nonlinear refractive index, close to that of pure carbon disulfide, without detectable two-photon absorption. This non-resonant n_2 is obtained whatever the electronic structure of the compounds. Hence, apolar symmetric push-pull-push molecules appear to be an interesting new family of NLO dyes.

A polymer was also synthesized from its symmetric molecular analogous by polycondensation and exhibits the same overall NLO properties.

The extrapolated n_2 values of all solutes stand between 1.1×10^{-16} and $3.9 \times 10^{-16} \text{ m}^2/\text{W}$, close to the off-resonant value reported for PTS [4]. Due to the absence of detectable linear and two-photon absorption at 1064 nm in most cases, the figures-of-merit are good ($W > 1500$ and $T < 1$).

These new organic molecules are very promising in terms of their off-resonant third order nonlinear properties. Moreover, we have shown that electronic structures like symmetric push-pull-push molecules may exhibit better figures-of-merit than classical dipolar dyes and lead to the development of a new class of original polymers.

[1] H.S. Nalwa and S. Myata, *Nonlinear Optics of Organic Molecules and Polymers*, CRC Press, Boca Raton, 1997.

[2] A.J. Attias, C. Cavalli, B. Bloch, N. Guillou and C. Noel, *Chem. Mater.*, **11**, 2057-2068 (1999).

[3] A. Marcano O., H. Maillotte, D. Gindre, D. Métin, *Opt. Lett.*, **21**, 101-103 (1996); F.E. Hernandez, A. Marcano O., H. Maillotte, *Opt. Comm.*, **134**, 529-536 (1997).

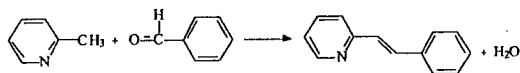
[4] B.W. Lawrence, M. Cha, J.U. Kang, W. Torruellas, G. Stegeman, G. Baker, J. Meth, S. Etemad, *Electr. Lett.*, **30**, 447-448 (1994).

Tuning of the Mesogenic, Electronic, and Optical Properties of New Conjugated 3,3'-Bipyridine derivatives.

A.-J. Attias, B. Bloch, C. Cavalli
Office National d'Etudes et de Recherches Aéronautiques
29 Avenue de la Division Leclerc
F- 92322 Châtillon Cedex, France

We report on the synthesis of a new class of distyryl-3,3'-bipyridine derivatives that display interesting mesogenic, electrochemical and optical properties (especially photoluminescence) that are tuned by using adequate substituents. These compounds are potentially interesting for applications in photonics (NLO, and light-emitting devices).

We have described in a previous paper [1] a strategy to synthesize by means of the Knoevenagel condensation



a series of 6,6'-distyryl-3,3'-bipyridine derivatives (**A1-5**) (Chart 1) as a new class of liquid crystalline conjugated molecules. These compounds are prepared by reaction of 6,6'-dimethyl-3,3'-bipyridine (**A0**) with aromatic aldehydes, e.g., thiophene or benzene rings substituted with electron acceptor or donor groups. These preliminary results have shown that these compounds exhibit, in addition to mesomorphism, absorption in the UV spectral range, and, in solution, intense emission in the blue region.

The major interests for liquid crystals and side chain liquid crystal polymers are motivated by their spontaneous tendency to a high degree of axial ordering and consequently their easy coupling to an external field, more particularly in the case of the less viscous smectic A and nematic phases. However, all the previously investigated compounds exhibit mesophases with high transition temperatures. Specially, nematic phases occur at temperature not very far from degradation or sublimation points. To favor the occurrence of the highly fluid nematic phase, we have to lower the transition temperatures in order to prevent any thermal degradation during macroscopic alignments of liquid crystals.

To achieve this goal, methyl groups have been introduced, as lateral substituents into the pyridinic rings of the molecules of the **A** series into the 5 and 5'-positions of the 6,6'-dimethyl-3,3'-bipyridine, giving the homologous series **B**.

In this poster, we report the synthesis of a series of 5,5'-dimethyl-6,6'-distyryl-3,3'-bipyridine derivatives (**B1-5**) (Chart 1), and compare the mesogenic, electrochemical, and photophysical properties for the two series of molecules (**A1-5** and **B1-5**). Specific properties which are of interest are (i) the changes in the thermal transitions, and liquid crystalline behavior, (ii) redox potentials (used to estimate the relative ionisation potentials and electron affinities), and (iii) optical properties: absorption and emission spectra. In all cases the properties were analyzed and discussed in terms of nature of the conjugated core and end-substituent effects [2].

The high degree of conjugation, absorption in the UV range, and the mesogenic character of these molecules can lead to NLO applications (side chain liquid crystal polymers) for the

Poster Session III

push-pull compounds ($\mu\beta = 1000 \cdot 10^{-48}$ esu). High fluorescence ($\Phi > 75\%$), associated with high electron affinity (-3.2 eV), opens up light emitting diodes applications.

References

[1] A. -J. Attias, B. Bloch, C. Cavalli, N. Guillou, C. Noël, Chem. Mater. **11**, 2057-68 (1999).

[2] A. -J. Attias, P. Hapiot, P. Valat, V. Wintgens, Chem. Mater. Accepted for publication.

Compounds

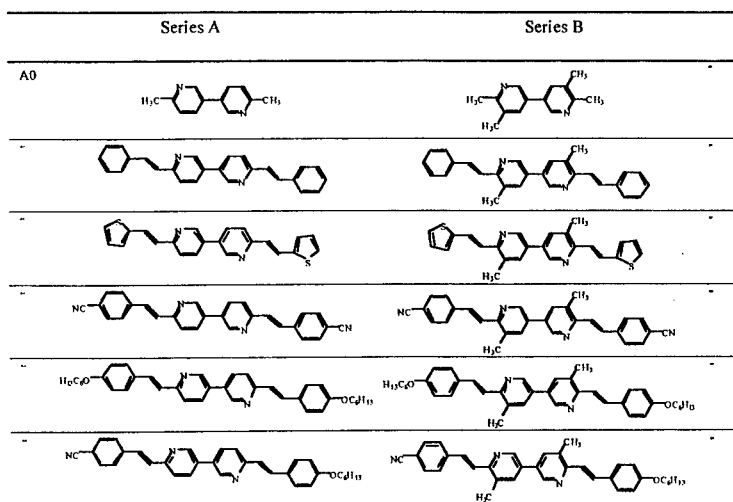


Chart 1

Synthesis of a New Nonlinear Optical Chromophores Based on a Novel N-aryl Carbazole Derivatives

A. Ben-Asuly, L. Shapiro, A. Ellern, V. Khodorkovsky
 Department of Chemistry
 Ben-Gurion University of the Negev
 84105 Beer-Sheva, Israel

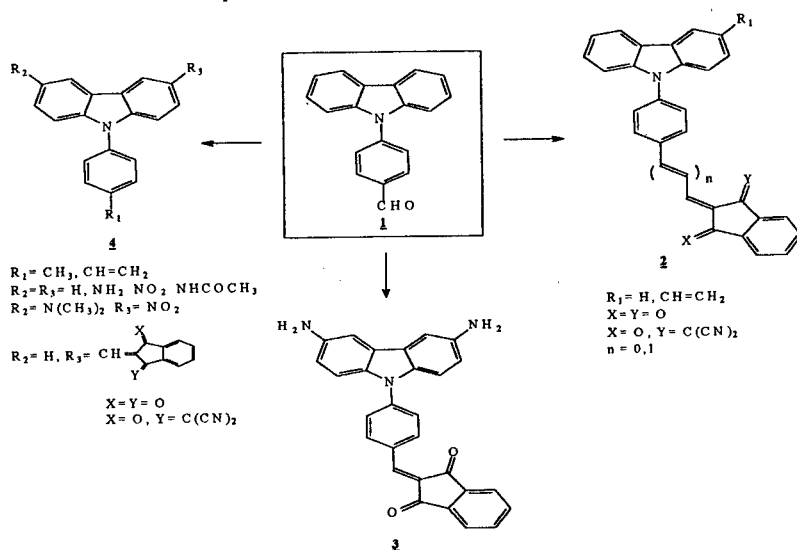
A previously unknown N-aryl carbazole derivative, N-(p-formylphenyl)carbazole, is a key precursor for a series of novel π -conjugated chromophores.

Carbazole derivatives, such as N-alkyl carbazoles has been incorporated as a donor moieties in many nonlinear optical materials. The NLO properties of N-aryl carbazoles derivatives, on the other hand, has much less extensively been investigated.

Recently, we synthesized previously unknown N-(p-formylphenyl)carbazole **1**, a precursor for a series of π -conjugated chromophoric monomers involving 1,3 indandione derivatives as an acceptor moiety attached via the N-aryl bridge **2**, **3** or 3-position on the carbazole moiety **4**.

These novel chromophores can be incorporated into a polymeric chain via appropriate substituent in 3,6 position of the carbazole moiety or trough a N-aryl substituent.

Studying the NLO properties of these novel chromophoric monomers analogs both by EFISH and Hyper-Rayleigh Scattering revealed that these chromophores must be described by "non-classical" two-dimensional NLO chromophore model [1].



References

- [1] G. Meshulam, G. Berkovic, Z. Kotler, A. Ben-Asuly, R. Mazor, L. Shapiro, V. Khodorkovsky, Proc. SPIE, 3796, 279-285, (1999).

Poster Session III

Molecular Engineering of Push-Pull Chromophores for Nonlinear Optics

M. Blanchard-Desce, V. Alain, S. Rédoglia
Département de Chimie, Ecole Normale Supérieure (UMR CNRS, 8640)
 24, rue Lhomond, 75231 Paris Cedex 05, France

M. Barzoukas
Institut Charles Sadron
 6, rue Boussingault, 67083 Strasbourg Cedex, France

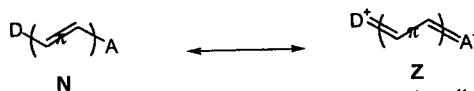
R. Wortmann, S. Lebus, K. Lukaszuk
Institut für Physikalische Chemie der Universität Mainz
 Jakob Welder-Weg 11, W-55099 Mainz, Germany

P. Günter, C. Bosshard, U. Gubler
Nonlinear Optics Laboratory, Institute of Quantum Electronics, ETHZ Hönggerberg, HPF
 E14, CH-8093 Zürich, Switzerland

Design of efficient chromophores exhibiting enhanced nonlinear optical (NLO) responses is required for the elaboration of optimized NLO materials. Within this framework, we have implemented a strategy based upon the molecular engineering of the hyperpolarizabilities of push-pull compounds. By developing an analytical modelization of the push-pull structure, we have opened a new engineering route towards NLO chromophores displaying giant hyperpolarizabilities and large figures of merit for various applications based upon nonlinear processes. For instance push-pull polyenes exhibiting both enhanced quadratic and cubic polarizabilities (up to $\beta(0) = 1200 \cdot 10^{-30}$ and $\gamma(0) = 8000 \cdot 10^{-36}$ esu) and optimized nonlinearity-stability-solubility-transparency characteristics have been designed.

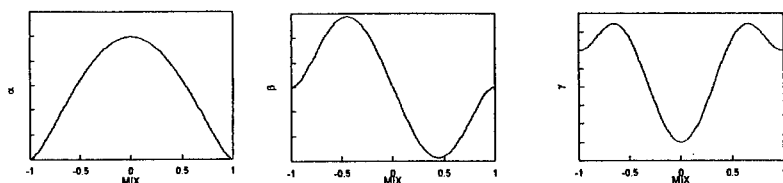
Interest in the study of the non-linear optical (NLO) properties of organic materials has kept growing for the past two decades due to potential applications in various fields such as telecommunications, optical data storage and optical information processing. The design of NLO chromophores exhibiting enhanced molecular quadratic (respectively cubic) responses is a requisite for the design of efficient second-order (respectively third order) NLO materials [1-3]. In particular, much efforts have been dedicated to the optimization of the typical "push-pull" structure (i.e. of molecules that bear an electron-donating group and an electron-withdrawing group interacting through a π -conjugated system).

The two-level two-state (TLTS) model provides a helpful guide for the molecular engineering of such chromophores. This model is based upon the two-level approximation (which takes into account only the ground and the first-excited state) and a simple two-valence bond-state description of the push-pull chromophores :



This simple model yields analytical expressions of the linear and non-linear polarizabilities, as functions of a general coordinate MIX, which characterizes the amount of mixing between the N and the Z forms [1-2]:

Poster Session III

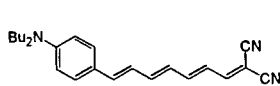


The TLTS model yields interesting clues about the parameters governing the peaks magnitudes α_{max} , β_{max} , γ_{max} and suggests possible routes to increase them. A simple way to achieve large peaks magnitudes is to lengthen the conjugated chain. In addition, the model predicts a steeper enhancement of γ_{max} with respect to β_{max} . In order to obtain molecules having simultaneously large quadratic and cubic polarizabilities, the molecules should lie near its maximum- γ value, where β retains about 75% of its maximum magnitude (i.e. β_{max}).

Within this framework, we have synthesized and investigated several series of soluble push-pull diphenyl- and phenyl-polyenes of increasing length. Their linear and NLO properties have been studied by performing electrooptical absorption measurements (EOAM) and Third-Harmonic Generation (THG) experiments in solution.

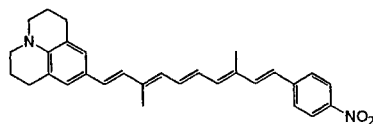
Lengthening the polyenic chain results in a more pronounced enhancement of the cubic hyperpolarizabilities than of the quadratic hyperpolarizabilities [3-4], as expected from the TLTS model prediction. In addition, the peak magnitudes β_{max} and γ_{max} can be significantly modulated by playing on the structure of the donor and acceptor end groups [2, 4].

Ultimately, push-pull polyenes exhibiting very large optical nonlinearities (both quadratic and cubic) but also suitable solubility, satisfactory stability and transparency in the near IR have been designed [3-4]:



$$\lambda_{max} = 571 \text{ nm}$$

$$\gamma(0) = 7400 \cdot 10^{-36} \text{ esu}$$



$$\lambda_{max} = 500 \text{ nm}$$

$$\gamma(0) = 8300 \cdot 10^{-36} \text{ esu}$$

References

- [1] M. Barzoukas, C. Runser, A. Fort, M. Blanchard-Desce, *Chem. Phys. Lett.*, **257**, 537 (1996).
- [2] M. Blanchard-Desce, M. Barzoukas, *J. Opt. Soc. Am. B*, **105**, 302 (1998).
- [3] V. Alain, S. Rédoglia, M. Blanchard-Desce, S. Lebus, K. Lukaszuk, R. Wortmann, U. Gubler, C. Bosshard, P. Günter, *Chem. Phys.*, **245**, 51-71 (1999).
- [4] V. Alain, L. Thouin, M. Blanchard-Desce, U. Gubler, C. Bosshard, P. Günter, J. Müller, A. Fort, M. Barzoukas, *Adv. Mater.*, **11**, 1210-1214 (1999).

**Tetra(4-methoxyphenyl)phosphonium iodide :
a new NLO crystal built-up with tetrahedral-like
octupolar chromophores**

Cyril Bourgogne, Patrick Masson, Jean-François Nicoud
*IPCMS, Groupe des Matériaux Organiques
CNRS et Université Louis Pasteur, 23 rue du Loess
F-67037 Strasbourg, France*

Yvette Le Fur, Patrick Juen, René Masse
*Laboratoire de Cristallographie associé à l'Université Joseph Fourier
CNRS
F-38042 Grenoble, France*

We report the molecular modeling and the synthesis of a new tetrahedral-like phosphonium chromophore, as well as the x-ray characterization of the first crystal obtained from a tridimensional octupolar molecule. The calculated octupolar spherical component $\beta_{(J=3)}$ of the hyperpolarizability tensor is up to 20.1×10^{-30} esu. The colorless material crystallizes in the $P2_12_12_1$ space group. The SHG powder test signal at $1.06 \mu\text{m}$ is equivalent to that of urea even though the crystals are twinned by merohedry.

In the engineering of crystalline materials for quadratic nonlinear optics, most of attention was paid until now to the design of quasi one-dimensional (1D) polar chromophores and the means directing their non-centrosymmetric assemblies. This concept has led to the discovery of very efficient crystals, nevertheless the single high coefficient β_{xxx} of the hyperpolarizability tensor of these rod-like 1D chromophores induces a unique high value for the quadratic susceptibility $\chi^{(2)}$ in optimized crystal structures. To overcome this drawback, J. Zyss has proposed the concept of two-dimensional (2D) and three-dimensional (3D) octupolar chromophores in which every dipolar properties vanish, but that preserve a non-zero β tensor due to several non-diagonal coefficients [1]. Crystal engineering of octupolar molecules has been successfully investigated by G. Desiraju & al. with planar ternary molecules [2] but the even more isotropic tetrahedral symmetry has attracted little attention up to now.

The tetraphenylphosphonium ion is representative of this 3D octupolar class of chromophores. Corresponding salts with various counter anions often crystallize in a non-centrosymmetric pattern [3]. Nevertheless their NLO activity was supposed to be weak despite P^+ is a good electron withdrawing center. We report here the synthesis, modeling, crystal structure and quadratic NLO properties of the tetra(4-methoxyphenyl)phosphonium iodide (MOPPI), a new crystal built-up from tetrahedral-like octupolar phosphonium chromophore with improved charge transfer properties.

Synthesis - Crystal structure

MOPPI is prepared with good yields by palladium-catalysed coupling of 4-iodoanisole with tris(4-methoxyphenyl)phosphine. White crystals are obtained from recrystallization and UV-Visible spectroscopy of MOPPI in solution in methanol shows no absorption in all the visible range.

The material crystallizes in the $P2_12_12_1$ space group (Fig. 1). The phosphonium geometry is weakly distorted and the molecular arrangement is far from the $I\bar{4}$ space group

Poster Session III

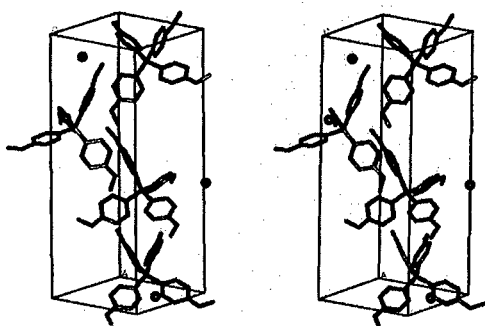


Figure 1: Stereographic view of the unit cell of MOPPI.

observed for the tetraphenylphosphonium iodide [3]. The crystal is twinned by merohedry, with a ratio of 40/60 between the two individuals.

Molecular Modeling

The tetraanisylphosphonium cation (PAn_4^+) has been optimized with the semi-empirical AM1 and PM3 Hamiltonians in MOPAC 6, and with the *ab initio* Hartree-Fock based Turbomole software. Both D_2 and S_4 octupolar point groups have been investigated.

Nonlinear optical properties

The static hyperpolarizability tensor components of PAn_4^+ and the reference PPh_4^+ have been computed from theoretical and experimental structures with the THDF method available in MOPAC 93 and the equivalent CPHF method in Turbomole. All these methods demonstrate the reinforced hyperpolarizability of this new chromophore, in which the most significant β_{xyz} coefficient is up to 9.23×10^{-30} esu. The calculation of the octupolar spherical components $\beta_{(J=1)}$ and $\beta_{(J=3)}$ of the hyperpolarizability tensor [4] on the crystalline geometry shows the octupolar nature of the chromophore despite the observed structure distortions.

Nonlinear optical activity

The SHG Kurtz & Perry powder test signal at $1.06 \mu\text{m}$ on a sample of PAn_4I is slightly less than $1 \times \text{urea}$, although it is much more significant than the one of PPh_4I . Untwinned crystals of MOPPI should exhibit a better $\chi^{(2)}$ response in agreement with β calculations.

References

- [1] J. Zyss, I. Ledoux, *Chem. Rev.* **94**, 77 (1994).
- [2] V. Thalladi & al., *J. Am. Chem. Soc.* **120**, 2563 (1998).
- [3] M. Lloyd, C. Pratt Brock, *Acta Cryst.* **B53**, 780 (1997); E. Schweizer, C. Baldacchini, A. Reingold, *Acta Cryst.* **C45**, 1236 (1989)
- [4] S. Brasselet, J. Zyss, *J. Opt. Soc. Am. B* **15**, 257 (1998).

Nonlinear Optical Thin Films Based on Strong Head-to-Tail Hydrogen Bonding Grown by Oblique Incidence Molecular Beam Deposition

C. Cai, M. Kiy, A. Tapponnier, R. Ono, I. Biaggio, Ch. Bosshard, P. Günter
*Nonlinear Optics Laboratory, Institute of Quantum Electronics,
Swiss Federal Institute of Technology, CH - 8093 Zürich, Switzerland*

We describe a new kind of organic thin films consisting of an oriented supramolecular assembly of specially designed organic molecules. The films are self-assembled in vacuum by Oblique Incidence Molecular Beam Deposition, a recently developed technique that allows setting the preferential molecular orientation in the film by choosing the direction of incidence of the molecular beam that deposits the molecules on the substrate. The individual molecules self-assemble in vacuum into "linear supramolecular polymers" by strong directional hydrogen bonding.

The basic structures of organic molecules with large nonlinear optical hyperpolarizabilities have been identified during the last 15 years. Materials with hyperpolarizabilities exceeding the ones of inorganic compounds by up to three orders of magnitude have been developed. In order to use these materials in optoelectronic applications, the molecules have to be aligned in a predetermined order. Up to now several alignment methods have been tried. They include crystal growth, poling of dipolar polymer films, preparation of thin films by the Langmuir-Blodgett technique, and most recently Molecular Beam Epitaxy.

However, obtaining noncentrosymmetric thin films of oriented dipolar molecules at a reasonably high growth rate has proven to be a very difficult task with many of the techniques described above. A breakthrough has been achieved recently with the development of Oblique Incidence Organic Molecular Beam Deposition (OI-OMBD) [1, 2]. This is a new technology that produces thin films of "supramolecular polymers" with monomers linked in linear head-to-tail chains via hydrogen bonds. The dipolar supramolecular assemblies obtained by OI-OMBD consist of specially designed molecules which are at the same time OMBD compatible, i.e. with proper vapor pressure and high thermal stability, have a molecular dipole, and allow the building of a linear chain connected by head-to-tail hydrogen bonds. During OI-OMBD, such supramolecular "polymers" can be evaporated at elevated temperatures and under ultra-high vacuum by breaking the hydrogen bonds, they form a molecular beam incident on the substrate under an angle (the experiments in Ref. 1 were performed using an angle of about 30° between molecular beam and normal to the substrate surface), and they self-assemble again on the substrate surface [3].

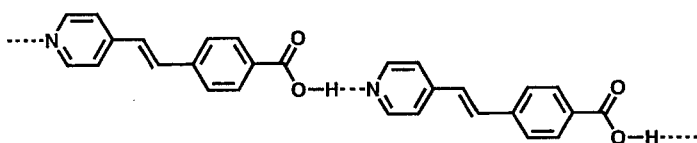


Figure 1: Molecules of 4-[trans-(pyridin-4-ylvinyl)]benzoic acid (PVBA) used in Ref. 1 and their head-to-tail hydrogen bonding.

Poster Session III

The polar direction in self-assembled films was determined using Second Harmonic Generation (SHG) experiments [2], proving that the polar axis is parallel to the substrate plane and directed along the projection of the molecular beam on the substrate. The SHG signal was also measured over the whole film surface of several cm^2 and for different film thicknesses, confirming the high homogeneity of the supramolecular films and the constancy of the polar order up to thicknesses of half a micrometer [2]. For the prototype molecules used in Ref. 1, a nonlinear optical coefficient for SHG of the order of 1 pm/V was achieved.

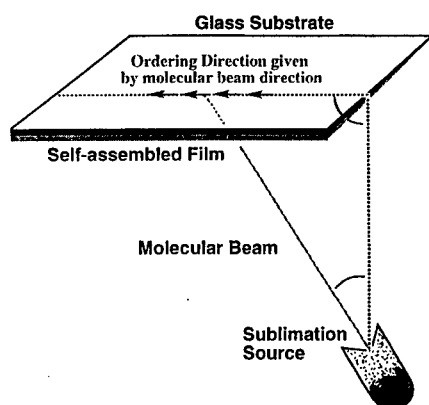


Figure 2: Deposition geometry used in Oblique Incidence Organic Molecular Beam Deposition (OI-OMBD). The polar axis of the self-assembled supramolecular film coincides with the projection of the molecular beam direction on the substrate.

The polar direction in the otherwise amorphous supramolecular films of dipolar molecules is determined exclusively by the direction of the oblique molecular beam with respect to the substrate [2, 3]. The unprecedented advantage of being able to set the direction of the polar order in the thin film by an easy-to-control experimental parameter, coupled with a high growth rate of several nanometers per minute, make OI-OMBD exceptionally interesting for the growth of new, oriented supramolecular structures. It can allow for example the growth of polar films with controllable polar direction both within the film plane and within a stack of differently oriented thin films.

References

- [1] C. Cai, M. M. Bsck, Y. Tao, B. Mller, Z. Gan, A. Kündig, Ch. Bosshard, I. Liakatas, M. Jäger, P. Günter, *J. Am. Chem. Soc.* 120, 8563 (1998).
- [2] C. Cai, M. Bösch, B. Müller, Y. Tao, A. Kündig, Ch. Bosshard, Z. Gan, I. Biaggio, I. Liakatas, M. Jäger, H. Schwer, P. Günter, *Adv. Mater.* 11, 745 (1999).
- [3] C. Cai, B. Müller, J. Weckesser, J. Barth, Y. Tao, M. Bösch, A. Kündig, Ch. Bosshard, I. Biaggio, P. Günter, *Adv. Mater.* 11, 750 (1999).

**New octupolar star-shaped molecules with
non-resonant quadratic optical nonlinearities**

Frédéric Chérioux

*Laboratoire de Chimie et Electrochimie Moléculaire, Université de Franche-Comté, La
Bouloie, 16 route de Gray, F-25030, Besançon cedex*

Pierre Audebert

*PPSM, Ecole Normale Supérieure de Cachan,
61 avenue du Président Wilson, F-94235 Cachan cedex*

Sophie Brasselet and Joseph Zyss

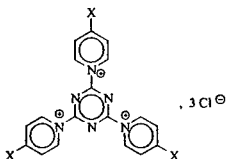
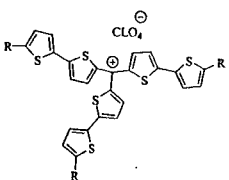
*LPQM, Ecole Normale Supérieure de Cachan,
61 avenue du Président Wilson, F-94235 Cachan cedex*

Two new classes of octupolar nonlinear chromophores, deriving from 1,3,5-triazines and oligothiénylic crystal violet analogues, have been synthesized, and their nonlinear properties investigated using the Harmonic Light scattering experiment. The easy preparation of these molecules makes them attractive candidates for further applications. Off-resonant measurements show high nonlinearities together with an excellent transparency, which make these compounds attractive for emerging nonlinear optical applications whereby the multipolar character of the chromophores is of particular importance.

Octupolar molecules have recently generated increasing interest in the field of quadratic nonlinear optics. At the microscopic level, strategies have been developed during the past decade in order to circumvent the eventual drawbacks of one-dimensional dipolar molecules, for which a strong nonlinearity is often antagonized by a strong absorption at the visible harmonic wavelength. In particular, the large class of octupolar molecules belonging to the T_d , D_{3h} or C_{3v} symmetry groups, has attracted the attention of both physicists and chemists since the early demonstrations that significant second order nonlinear efficiency could be achieved from non-dipolar molecules [1]. The particular interest of octupolar systems is their favorably displaced nonlinearity-transparency trade-off [2], opening therefrom new avenues in the field of molecular engineering for nonlinear optics.

We have recently reported the preparation and electrochemical properties of families of D_{3h} conjugated molecules [3,4]. Nonlinear optical measurements were performed using the harmonic light scattering experiment in off-resonance conditions [5], so as to avoid spurious two-photon fluorescence background which could otherwise arise at the vicinity of the absorption band.

Poster Session III

Compounds 3				Compounds 5			
							
Compd	λ_{max} (nm)	$\langle\beta^2\rangle^{1/2}$ (10^{-30} esu)	$\langle\beta(0)^2\rangle^{1/2}$ (10^{-30} esu)	Compd	λ_{max} (nm)	$\langle\beta^2\rangle^{1/2}$ (10^{-30} esu)	$\langle\beta(0)^2\rangle^{1/2}$ (10^{-30} esu)
a	547	fluo		a	360	17.4	11.8
b	440	18.5	9.4	b	350	20.5	14.3
c	470	45.6	20.3	c	370	22.7	15
d	432	14.5	7.6	d	360	45	29.7
e	310	11	8.2				

The molecular engineering of 1,3,5-triazines and oligothiénylic crystal violet analogues appears as a promising approach to octupolar compounds for nonlinear optics. High off-resonant second order nonlinear coefficient are found for oligothiénylic compounds, while the chemical structure of both families of molecules is of a particular interest for future applications related to all-optical orientation in polymer matrices [6].

- [1] J. Zyss, J. Chem. Phys. **98**, 6583-6599 (1993); C. Dhenaut, I Ledoux, I. Samuel, J. Zyss, M. Bourgaud, H. Le Bozec, Nature, **374**, 339-342 (1995).
- [2] M. Joffre, D. Yaron, R. Silbey and J. Zyss, J.Chem.Phys. **97**,5607-5613 (1992)
- [3] F. Cherioux, P. Audebert and P. Hapiot, Chem. Mater., **7**, 1984-1989 (1998).
- [4] F. Cherioux, L. Guyard and P. Audebert, Adv. Mater., **13**, 1013-1018 (1998).
- [5] S. Brasselet, F. Cherioux, P. Audebert and J. Zyss, Chem. Mater., **11**, 1915-1920 (1999).
- [6] S. Brasselet and J. Zyss, J. Opt. Soc. Am. B, **15**, 257-265 (1998).

Synthesis and characterization of an octupolar polymer and new molecular octupoles with off-resonant nonlinear refractive index

Frédéric Chérioux

*Laboratoire de Chimie et Electrochimie Moléculaire, Université de Franche-Comté,
La Bouloie, 16 route de Gray, F-25030, Besançon cedex*

Hervé Maillotte

*Laboratoire d'Optique P.M. Duffieux, UMR CNRS/Université de Franche-Comté n°6603,
Institut des Microtechniques de Franche-Comté,
UFR Sciences et Techniques, 16 route de Gray, F-25030 Besançon cedex*

Joseph Zyss

*LPQM, Ecole Normale Supérieure de Cachan,
61 avenue du Président Wilson, F-94235 Cachan cedex*

Pierre Audebert

*PPSM, Ecole Normale Supérieure de Cachan,
61 avenue du Président Wilson, F-94235 Cachan cedex*

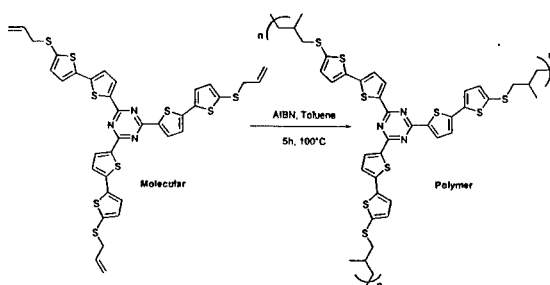
The first synthesis and Z-scan measurements of an octupolar polymer with off-resonant third order nonlinear optical properties are discussed. Two others new molecular thiophene-based octupoles with similar nonlinearities are also reported.

In the quest for materials applicable to all-optical devices, there has been over the last decade an increasing interest in the quadratic nonlinear optical (NLO) properties of organic or organometallic octupolar molecules [1]. Improving the NLO efficiency/transparency (or figure-of-merit) trade-off stands out among the important goals of this approach. Indeed, the particular symmetry of octupoles may lead to a better transparency and improved stability compared with classical dipoles although the question has not been completely elucidated as yet.

In all-optical applications based on the optical Kerr effect, it is also of paramount importance to improve the figures-of-merit (essentially $W=n_2I/\alpha\lambda$ and $T=\lambda\beta/n_2$) of cubic NLO materials because high nonlinear refractive indices n_2 in dipolar organics are generally obtained via resonant enhancement, at the price of large linear (α) or two-photon (β) absorption losses. Moreover, to the best of our knowledge, no synthesis of octupolar polymers displaying enhanced NLO properties has been so far reported in the literature in spite of their potential interest towards further material and device investigations.

Poster Session III

We report in this work the efficient synthesis of the first octupolar polymer [2] and two original octupolar thiophene-based molecules [2,3], which exhibit large non-resonant nonlinear refractive indices.



$\lambda_{max} = 380\text{nm}$, Optical Kerr effect : Extrapolated $n_2 \approx 1.75 \times 10^{-16} \text{ m}^2/\text{W}$, $T < 1$, $W > 2200$

The two molecules were synthesized via a triple aromatic nucleophilic substitution of 3 equiv. of thienyl derivatives on cyanuric chloride. Such reactions are efficient with a yield as high as 90%. The obtained compounds are octupolar, with a D_{3h} symmetry, as confirmed by *ab-initio* or semi-empirical computations as well as by electrochemical characterisation [3]. The new octupolar polymer was synthesised with quantitative yield by homopolymerisation of the allyl monomer with AIBN. All products are very soluble in toluene at concentrations close to 0.1 mol.L^{-1} .

UV-Visible spectra in toluene solutions exhibit a single linear absorption band of 30 nm width, centered at 380 nm and 376 nm for molecular octupoles and polymer, respectively. Both their nonlinear refractive index n_2 and two-photon absorption coefficient β were simultaneously measured at $\lambda = 1064 \text{ nm}$, using a single-shot (50 ps, 10 Hz) multi-channel Z-scan method [4]. The octupoles and the polymer in toluene solution have the same off-resonant nonlinear refractive index, close to that of pure carbon disulfide. The extrapolated value for the solutes is $n_2 \approx 1.75 \times 10^{-16} \text{ m}^2/\text{W}$, close to the off-resonant value reported for PTS [5]. Due to the absence of detectable linear and two-photon absorption at 1064 nm, the figures-of-merit are good ($W > 2200$ and $T < 1$). Moreover, the photo-stability of the polymer in solution has been found very satisfactory up to energies per pulse of 120 μJ .

Nonlinear refraction and absorption measurements on thin solid films of the new polymer are being currently investigated.

- [1] J. Zyss, J. Chem. Phys., **98**, 6583-6599 (1993); C. Dhenaut, I. Ledoux, I. Samuel, J. Zyss, M. Bourgaud, H. Le Bozec, Nature, **374**, 339-342 (1995)
- [2] F. Cherioux, H. Maillotte, P. Audebert and J. Zyss, J. Chem Soc. Chem. Comm., 2083-2084 (1999).
- [3] F. Cherioux, L. Guyard and P. Audebert, J. Chem Soc. Chem. Comm., 2225-2226 (1998).
- [4] A. Marcano O., H. Maillotte, D. Gindre, D. Métin, Opt. Lett., **21**, 101-103 (1996) ; F.E. Hernandez, A. Marcano O., H. Maillotte, Opt. Comm., **134**, 529-536 (1997).
- [5] B.W. Lawrence, M. Cha, J.U. Kang, W. Torruellas, G. Stegeman, G. Baker, J. Meth, S. Etemad, Electr. Lett., **30**, 447-448 (1994).

Structure-property relations in nonlinear optical molecular wires and planar sheets

U. Gubler, Ch. Bosshard, P. Günter

*Nonlinear Optics Laboratory, Swiss Federal Institute of Technology ETH
CH-8093 Zürich, Switzerland*

R. Martin, F. Diederich

*Institute of Organic Chemistry, Swiss Federal Institute of Technology ETH
CH-8092 Zürich, Switzerland*

R. R. Tykwinski

*Department of Chemistry, University of Alberta
Edmonton T6G 2G2, Canada*

We investigated the third-order nonlinear optical properties of the linearly conjugated polytriacetylenes and the two-dimensionally conjugated tetraethynylethenes by means of third-harmonic generation and degenerate four wave mixing. For the one-dimensional polytriacetylenes a scaling of the nonlinearity with a power law upon backbone elongation is observed with an exponent $\alpha \approx 2.5$. For the two-dimensional tetraethynylethenes the importance of low symmetry in the conjugation plane is observed and explained by selection rules for the dipole operator.

The development of structure-property relationships is of prime interest on the path to organic materials with improved third-order nonlinear optical properties. In second-order nonlinear optics the guidelines for the optimization of the first-order hyperpolarizability β are well established whereas in third-order nonlinear optics the situation for the second-order hyperpolarizability γ is less clear.

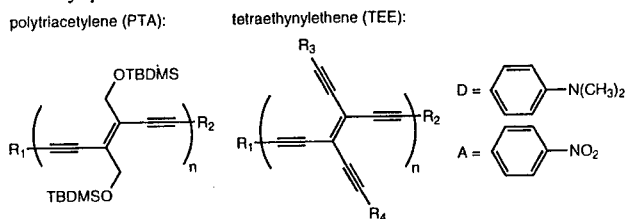


Figure 1: Molecular structure of the linearly conjugated polytriacetylenes and the two-dimensionally conjugated tetraethynylethenes. The end groups R_1 can either be electronically neutral groups (trimethylsilyl or triethylsilyl) or substituted by electron donors (dimethylaniline) and acceptors (nitrophenyl). The OTBDMS ((tert-butyl)dimethylsilyloxy) groups on the polytriacetylenes increase the solubility.

The third-harmonic generation (THG) and degenerate four wave mixing (DFWM) experiments have been performed outside any one-, two-, or three-photon resonance enhancement. In THG a nanosecond Nd:YAG laser is shifted to a fundamental wavelength of 1907 nm by a H_2 -Raman cell. For DFWM a 10 ps Nd:YLF laser at 1047 nm is employed to avoid thermal contributions to the nonlinearity or orientational effects of the dissolved molecules.

The unsubstituted molecular wires polytriacetylene (PTA) disclose a power law scaling of the second-order hyperpolarizability upon conjugation elongation (Fig. 2) with an exponent around 2.5 for THG and DFWM as well [1]. The power law saturates for 60 carbon-carbon

Poster Session III

bonds and an only linear increase follows for longer oligomers. The scaling exponent around 2.5 and the saturation around 60 bonds seem to be a collective characteristic for various conjugated polymers as polyenes, oligothiophenes, and oligothiophenyleneethylenes when measured outside any resonance enhancement [1].

The substituted PTAs show improved nonlinearities for short oligomers compared to the unsubstituted ones and tend to the same values towards the polymeric samples. For the monomer and dimer the asymmetric substitution pattern is best although the double donor dimer comes close to the asymmetric dimer. The guideline of asymmetry for large nonlinearities can be questioned for longer oligomers.

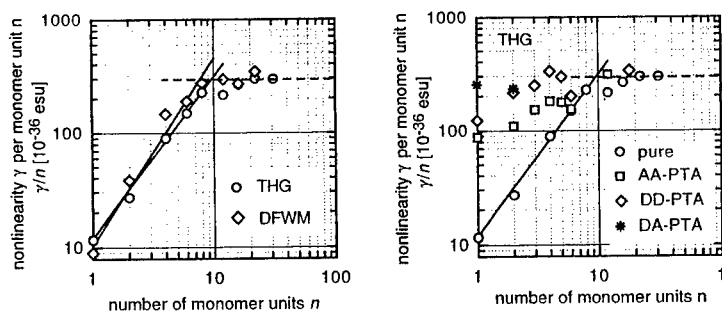


Figure 2: (left) Power law scaling of the second-order hyperpolarizabilities γ vs. number of monomer units n measured by third-harmonic generation (THG) and degenerate four wave mixing (DFWM). The power law saturates around 10 monomer units (60 bonds) and an only linear increase for polymeric samples follows. The power law exponent for THG is 2.46 ± 0.10 and for DFWM 2.64 ± 0.20 . (right) Nonlinearities γ for pure and substituted polytriacetylenes measured by THG.

For the two-dimensionally conjugated tetraethynylethene monomers the molecules with the lowest symmetry yield the largest nonlinearities (Fig. 3) [2]. This can be explained by a dipolar contribution to the nonlinearity which is only present for allowed dipole moments in the conjugation plane [2]. For dimers with donor and acceptor groups on the ends of the polymerization direction and neutral groups connected laterally, the asymmetric substitution pattern exhibits the largest second-order hyperpolarizability γ .

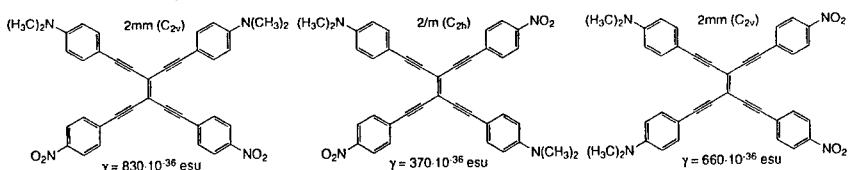


Figure 3: Tetraethynylethene monomers substituted by two donors and acceptors. Above the molecules the symmetry in international and Schönflies notation is given. The molecule in the middle with the highest symmetry in the conjugation plane (two-fold axis) shows the smallest nonlinearity.

References

- [1] U. Gubler, Ch. Bosshard, P. Günter, M. Y. Balakina, J. Cornil, J.-L. Brédas, R. E. Martin, F. Diederich, *Opt. Lett.* **24**, 22, 1599-01 (1999).
- [2] U. Gubler, R. Spreiter, Ch. Bosshard, P. Günter, R. R. Tykwinski, F. Diederich, *Appl. Phys. Lett.* **73**, 17, 2396-98 (1998).

Second-order Nonlinear Optical and Photorefractive Properties of Amorphous Calix[4]arene Containing Carbazole Derivatives

Atsushi Gunji^{a,b}, Hiromi Kimura-Suda^b, Takafumi Sassa^a, Tatsuo Wada^{a,b}
and Hiroyuki Sasabe^{a,b,c}

^a*The Institute of Physical and Chemical Research (RIKEN)*
2-1 Hirosawa, Wako, Saitama 351-0198, Japan

^b*Core Research for Evolutional Science and Technology (CREST), JST*

^c*Chitose Institute of Science and Technology (CIST)*
758-65 Bibi, Chitose, Hokkaido, 066-8655, Japan

As a new class of multi-functional compounds, two novel calix[4]arene molecules in which carbazole derivatives as second-order NLO chromophore are connected with long alkyl chains at the lower rim have been newly synthesized. Those compounds take amorphous state as proved by differential scanning calorimetry and powder X-ray diffraction and they can be made into films without a supporting matrix polymer. Second harmonic generation signals were observed in the calix[4]arene films after electric poling at a temperature above glass transition point. Photorefractive effect was observed in the film of calix[4]arene with carbazole and nitrocarbazole derivatives doped with 2,4,7-trinitro-9-fluorenone.

Organic photorefractive materials are promising candidates for optical data storage materials, optical image processing materials, etc. and many efforts have been made to create new and efficient photorefractive materials.¹ Recently, carbazole-polymers, dendritic carbazoles and macrocyclic carbazole-oligomers have been developed in our laboratory as good candidates for monolithic photorefractive materials.² Compared with other multi-component photorefractive systems such as host-guest ones, monolithic systems have a practical advantage: they are free from phase separation. On the other hand, recently calix[4]arenes have been used intensively for high efficient second-order nonlinear optical (NLO) system, because the systems up to four π -conjugation with donors and/or acceptors are oriented in quasi-one direction in cone conformation. Furthermore, highly ordered films of neat calix[4]arenes have been reported recently.³ So, the use of calix[4]arene molecules as a platform could provide various merits in the developments of novel monolithic photorefractive materials. In this paper we present some results of the properties of the titled compounds.

Novel calix[4]arene containing two 3-nitrocarbazoles as NLO chromophores in the lower rim (**1**), and calix[4]arene containing carbazole as a charge-transporting moiety and 3-nitrocarbazole as a NLO chromophore in the lower rim (**2**) have been successfully synthesized. 1,3-di-*O*-substituted calix[4]arenes **1** and **2** adopt cone conformation in chloroform solution.

From differential scanning calorimetric (DSC) analysis it is proved that **1** and **2** are amorphous with the glass transition temperatures (T_g) of 75 °C and 53 °C, respectively. The powder X-ray diffraction results of **1** and **2** showed there is no sharp signal but only broad signals, indicating that **1** and **2** are amorphous state as shown in Figure 1 for **1**. Moreover, **1** and **2** can be made into thin films without matrix polymer.

Poster Session III

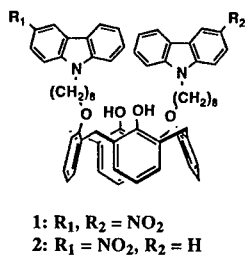


Figure 1 Molecular structures of calix[4]arenes 1 and 2.

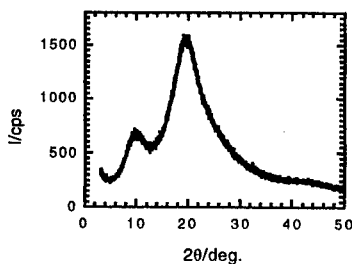


Figure 2. Powder X-ray diffraction data of 1.

To investigate the NLO properties of 1 and 2, second-harmonic generation (SHG) measurement was performed. SHG signals were observed in the thin films of 1 and 2 after electric poling at a temperature above T_g as shown in Figure 2 for 1. The obtained second-order nonlinear susceptibilities, d_{33} of 1 and 2 are 7.9 pm/V and 2.4 pm/V, respectively. The photorefractive properties of film of 2 doped with 0.1 wt.% of 2,4,7-trinitro-9-fluorenone (TNF) were examined by two beam coupling. As shown in Figure 3, asymmetric energy transfer was observed in two beams.

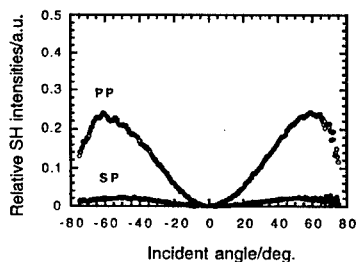


Figure 2. Maker fringe data for a poled 1 film with 621Å thickness.

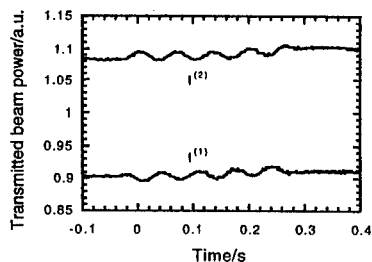


Figure 3. Transmitted intensities of the two coupling beams where the sample was translated.

This result indicates that the film of 2 doped with TNF showed photorefractive effect. This is the first report in which the photorefractive effects were observed in calix[4]arene films.

References

[1] P. Günter, J.-P. Huignard, Eds. *Photorefractive Materials and Their Applications*; Springer-Verlag: New York, 1988; Parts I, II, Topics in Applied Physics Vols. 61 and 62.
 [2] Y. Zhang, T. Wada, and H. Sasabe, *J. Mater. Chem.*, **1998**, *8*, 809.
 [3] E. Kelderman, G. J. T. Heesink, L. Derhaeg, T. Verbiest, P. T. A. Klaase, W. Verboom, J. F. J. Engbersen, N. F. van Hulst, K. Clays, A. Persoons, and D. N. Reinhoudt, *Adv. Mater.*, **1993**, *5*, 925.

Linear and nonlinear optical properties of hypervalent iodine derivatives

K. Kamada, K. Ohta

Department of Optical Materials, Osaka National Research Institute
1-8-31 Midorigaoka, Ikeda, Osaka 563-8577, Japan

R. R. Tykwinski, D. Bykowski

Department of Chemistry, University of Alberta
Edmonton, Alberta T6G 2G2, Canada

Thienyl(phenyl)iodonium triflate salts, hypervalent iodine derivatives with thiophene and bithiophene substituents, have been synthesized and their linear and nonlinear optical properties were explored by UV/visible absorption spectroscopy and femtosecond Z-scan experiment, respectively. The UV/visible absorption spectra of the iodonium salts suggest that electronic communication between the phenyl and thienyl/bithienyl moieties is mediated by the *d*-orbitals of cationic iodine. Preliminary results of open aperture Z-scan experiments show that the bithienyl(phenyl)iodonium salts exhibit strong two-photon absorption at the nonresonant wavelength of 663 nm.

Functionalized derivatives of thiophene and oligothiophenes display unique electronic behavior and have substantial potential as organic materials for *e.g.* nonlinear optics, electroluminescence, and conducting polymers. Whereas thiophene has been incorporated into a variety of iodonium(III) salts, such as aryl(heteroaryl)iodonium salts, the potential of these compounds as organic materials for nonlinear optics has, to the best of our knowledge, been ignored. A number of electronic and/or photonic characteristics of thienyl iodonium compounds intrigued us, including the role of the positively charged iodonium moiety as a π -electron acceptor which links π -electron donating aryl and heteroaryl groups, and its ability to influence linear and nonlinear optical behavior. Here we report the preliminary results of our studies of iodonium salts **1** and **2** (Figure 1), including an examination of their linear (UV/Visible) and nonlinear (Z-scan) optical behavior[1].

Synthesis

Thienyl(phenyl)iodonium triflate salts **1** and **2** were synthesized from a reaction of a CH_2Cl_2 solution of corresponding heteroarylstannanes at -78°C with iodonium transfer reagent $\text{PhI}(\text{CN})\text{OTf}$, as reported previously [2]. Subsequent warming of the reaction mixture to room temperature, followed by the addition of hexanes, gave the crystalline iodonium salts in good yields.

Linear and Nonlinear Optical Properties

The linear electronic absorption spectra of **1** and **2** were measured in CH_3CN , the most

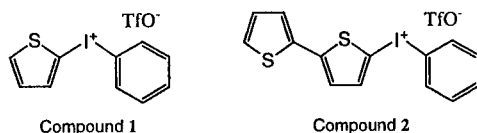


Figure 1: Molecular structure

Poster Session III

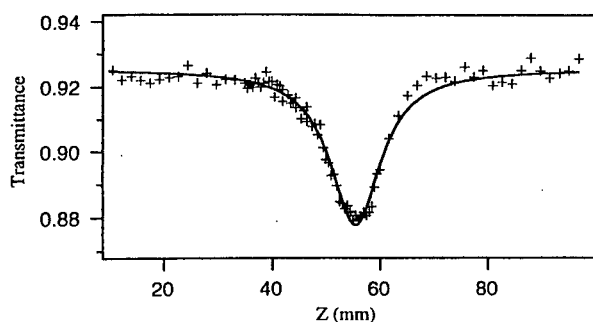


Figure 2: Open aperture Z-scan trace of compound 2

intense absorption (λ_{max}) of **1** (242 nm) is almost the same of 2-iodothiophene (λ_{max} = 243 nm). However, the cut-off energy for **1** at ca. 320 nm is red-shifted about 40 nm versus that of iodobenzene. For bithiophene derivative **2**, the absorption spectrum (λ_{max} = 334 nm), is shifted considerably lower in energy than that of 2-iodobithiophene (λ_{max} = 315 nm). Thus, electronic communication between the bithienyl and phenyl moieties mediated by the *d*-orbitals of the cationic iodine appears more substantial for the bithienyl derivative **2** than thienyl derivative **1**.

The nonlinear optical behavior of **1** and **2** in THF solutions has been explored using the Z-scan technique with femtosecond laser pulses (1 μ J, 130 fs) emitted from an optical parametric amplifier (OPA) operating at 1 kHz and centered at 663 nm, where the both derivatives are non-resonant. For thiophene derivative **1**, no significant signal was recorded even at a concentration of 0.10 M in open and closed aperture configurations. For bithiophene derivative **2**, on the other hand, prominent signals were obtained by both open and closed aperture measurements. The recorded open aperture signal (Figure 2) demonstrates the existence of two-photon absorption (TPA) at this wavelength. The TPA cross section was calculated to be $0.98 \pm 0.22 \times 10^{-50} (\text{cm}^4 \cdot \text{s} \cdot \text{photon}^{-1} \cdot \text{molecule}^{-1})$ by assuming a Gaussian pulse. The closed aperture signal of **2** is deviated in shape and power-dependence from ordinary behavior, which suggests that the TPA-induced thermal effect interferes with the closed aperture measurement at the repetition rate of 1 kHz.

The difference in TPA behavior between **1** and **2** can be related to the linear electronic absorption behavior; the strong linear absorption of **2** at 331.5 nm correlates well with the TPA observed at the wavelength of 663 nm, whereas **1**, with a minimal absorption at 331.5 nm, shows no TPA at 663 nm. The spectral dispersion characteristics for **2** are currently being probed and should provide an estimate of the maximum TPA cross section obtainable for this molecule.

References

- [1] R.R.Tykwinski, K. Kamada, D. Bykowski, K. Ohta, and R. McDonald "Thienyl(phenyl)iodonium triflates — Structural, and linear and nonlinear optical behavior of hypervalent iodine derivatives," *Adv. Mater.* in print (2000).
- [2] R. R. Tykwinski, Ph.D. Thesis, University of Utah, Salt Lake City, 1994.

Nonlinear Optical Properties of the Langmuir-Blodgett Films of an Intermolecular Charge Transfer Complex

J. Kawamata, T. Akutagawa, T. Hasegawa, K. Inoue and T. Nakamura

Research Institute for Electronic Science, Hokkaido University

N12W6, Kita-ku, Sapporo 060-0812, JAPAN

Langmuir-Blodgett (LB) films of a charge transfer (CT) complex, OMTTF (bis(tetramethylene)tetrathiafulvalene)-C₁₀TCNQ (decyltetracyanoquinodimethane) were fabricated and the optical properties were examined. The UV-visible-NIR as well as IR spectra showed the neutral CT state of the complex. The nonlinear optical parameters were evaluated by the electroabsorption measurements and by the Maker-fringe technique. The $\chi^{(2)}$ value of 10 pm/V was obtained by the latter method.

Langmuir-Blodgett (LB) films of charge transfer (CT) complexes have potentials for technological application in the field of photonics, since the molecular orientations and configurations of D and A molecules can be controlled by LB technique. In this paper, we will describe linear and nonlinear optical properties of the LB films of the CT complex, OMTTF (bis(tetramethylene)tetrathiafulvalene) and C₁₀TCNQ. Donor molecules, which do not have any hydrophobic alkyl moieties, are combined with alkylTCNQ to form amphiphilic charge transfer complexes [1,2].

Linear optical properties

Figure 1 shows the electronic absorption spectrum of the LB film. The B-band (0.65 eV) is assigned to the CT transition. The C and D-bands are the intramolecular transitions of the acceptor molecule. These spectral features are characteristic for mixed-stack neutral CT complexes. The neutral CT state of the complex was also confirmed by the CN stretching band of C₁₀TCNQ which appeared at 2214 cm⁻¹.

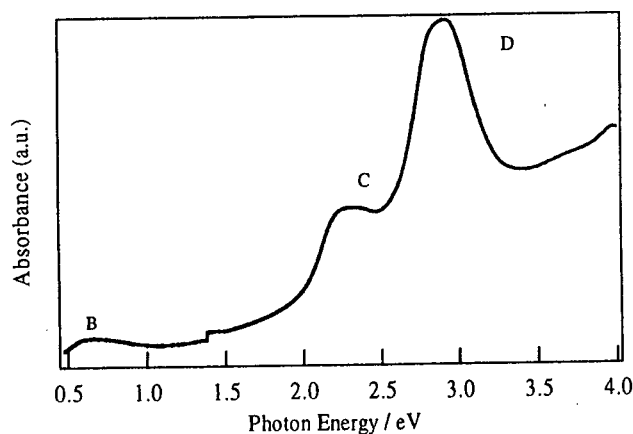


Figure 1. Absorption spectrum of the LB film of OMTTF-C₁₀TCNQ

Nonlinear optical properties

The *NLO* parameters were evaluated from electroabsorption (EA) spectra [3] and by the Maker-fringe method. The electroabsorption spectra over photon energy range from 1.5 to 4.0 eV were measured for 20-layer LB film prepared by the horizontal lifting method. The modulated absorption spectra, $\Delta\alpha = -\Delta T/T$ at electric field E were converted to the imaginary part of the second order electric susceptibility, $\text{Im}[\chi^{(2)}(-\omega; \omega, 0)]$. The $\text{Im}[\chi^{(2)}(-\omega; \omega, 0)]$ reached 0.3 pm/V at 2.2 eV.

The result of the Maker-fringe measurement is shown in Fig. 2. The measurement was carried out on a one-layer LB film. Fundamental light (1064 nm) of Nd-YAG laser (20 mJ, 8 ns) was polarized parallel to the incident plane. The Maker-fringe pattern was analyzed in a similar way as in the case of an LB monolayer of a phenylhydrazone dye [4]. The second order coefficient, d_{33} was 10 pm/V when quartz crystal was used as a reference.

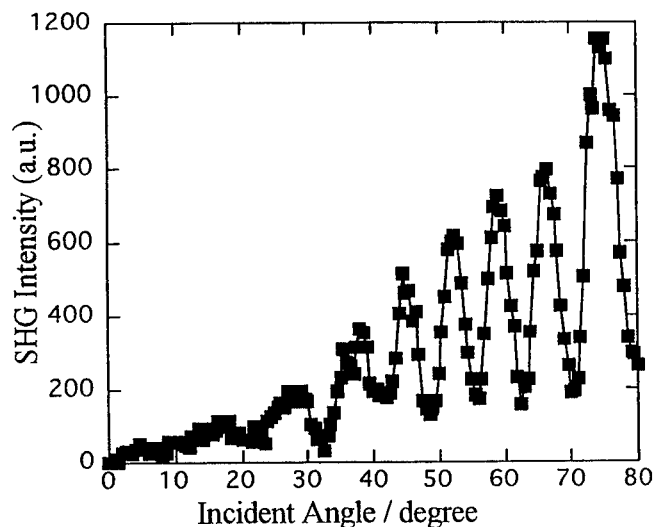


Figure 2. Maker fringe of a one-layer LB film of OMTTF-C10TCNQ

References

- [1] T. Konuma, T. Akutagawa, T. Yumoto, T. Nakamura, J. Kawamata, K. Inoue, T. Nakamura, H. Tachibana, M. Matsumoto, H. Ikegami, S. Horiuchi, H. Yamochi and G Saito; *Thin Solid Films*, **327-329**, 348 (1998).
- [2] T. Nakamura, T. Yumoto, T. Suzuki, T. Akutagawa, T. Hasegawa, H. Tachibana, M. Matsumoto, S. Horiuchi, H. Ikegami, H. Yamochi and G Saito; *Mol. Cryst. Liq. Cryst.*, **327**, 83 (1999).
- [3] T. Hasegawa, T. Akutagawa, T. Konuma, T. Nakamura, J. Kawamata and K. Inoue; *Nonlinear Optics*, **22**, 143 (1999).
- [4] D. Lupo, W. Prass, U. Scheunemann, A. Laschewsky, H. Ringsdorf and I. Ledoux; *J. Opt. Soc. Am. B*, **5**, 300 (1988).

Structural Analyses of Clay-Metal Complex Hybrid Films by Observing Optical Second Harmonic Generation

J. Kawamata, K. Inoue
*Research Institute for Electronic Science,
Hokkaido University, Sapporo, 060-0812, Japan*

Y. Ogata, A. Yamagishi
*Division of Biological Science, Graduate School of Science,
Hokkaido University, Sapporo, 060-0810, Japan*

We observed the optical second harmonic generation (SHG) from clay-metal complex hybrid films. The Langmuir-Blodgett films having non-centrosymmetric molecular alignment were prepared by forming a monolayer of an amphiphilic metal complex (such as tris(7,7-diphenyl-1,10-phenanthroline)ruthenium(II)perchlorate) onto an aqueous dispersion of a clay (such as montmorillonite). The dependence of the SHG signal intensity on the concentration of the clay was examined. In addition, each of the χ^2 tensor components was compared. Basis on the results, we have analyzed the characteristics of the molecular alignment in those films.

INTRODUCTION

Organometallic compounds have been considered to exhibit a large nonlinear optical coefficient owing to a metal-to-ligand and ligand-to-metal charge transfer (MLCT and LMCT) transition [1]. Therefore, the study of organometallic compounds for a nonlinear optical (NLO) material is currently of great technological and scientific interests.

Second-order NLO phenomena are observed only when the component chromophores are aligned in a noncentrosymmetric array. However, organic and organometallic compounds have a tendency to crystallize in a centrosymmetric array in most cases. Therefore, a means of imposing a noncentrosymmetric structure on those materials. The Langmuir Blodgett (LB) technique is one of the various methods that can implement a noncentrosymmetric structure. However, problems such as poor thermal and mechanical stability, and poor optical quality are sometimes encountered with LB films. Thus, we have attempted to make a "stable" LB film by hybridizing a clay and a metal complex. Here a clay is chosen as a component reinforcing a film structure because it consists of two-dimensional ultra-thin layers (1 nm thick). Second-harmonic generation (SHG) properties of the resulting hybrid films were then investigated. As a result, clear SHG responses have been observed [2]. In this study, we have made the further fundamental study on the SHG properties of these hybrid films. Namely, the relationship between their SHG behavior and the structural features was investigated. The results will be reported.

EXPERIMENTS

A monolayer of tris(7,7-diphenyl-1,10-phenanthroline)ruthenium(II)perchlorate (Δ -Ru(dpp)₃; Fig. 1.) were formed onto an aqueous suspension of a clay. A single clay layer that was charged negatively was thought to attach the positively charged monolayer to form a clay-metal complex hybrid film. The Z-Type films were prepared by the horizontal lifting method. The Y-Type hybrid films were prepared by the vertical dipping method. The deposition on a fused silica substrate was achieved at a pressure of 15 mN/m. The procedure was made only one time for both cases. SHG measurements were made by means of the

Poster Session III

Maker-Fringe method [4]. A pulsed beam from a Q-switched Nd-YAG laser was used for excitation.

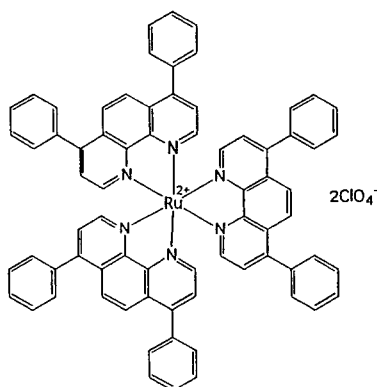


FIGURE 1. Chemical Formula of $[\text{Ru}(\text{dpp})_3](\text{ClO}_4)_2$

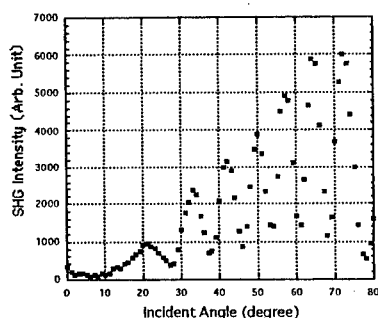


FIGURE 2. Angular dependence of SHG signals from a $[\text{Ru}(\text{dpp})_3]^{2+}$ / synthesized saponite hybrid film deposited at 15 mN/m.

RESULTS

The Maker-Fringe pattern for the Y-Type hybrid film of the synthesized saponite and Δ - $[\text{Ru}(\text{dpp})_3]$ is shown in Fig. 2. Clear fringes of the SHG signal have been observed. The results show that the present hybrid films are "stable enough" to investigate their SHG characteristics. Thus, it should be concluded that the incorporation of a clay into the LB films is very effective for the systematic analyses of NLO properties of metal complexes.

The Maker-Fringe pattern shown in Fig. 2 has been analyzed in a similar way as in the case of phenylhydrazone dyes [5]. As the result, for the present film, the magnitude of d_{33} is estimated to be 30 pm/V by comparing the intensity to that of the Maker-Fringe due to d_{11} observed for a reference crystal of quartz.

The dependence of the SHG signal intensity on the concentration of the clay and other features were investigated. A comparison of the χ^2 magnitude between the respective tensor components was also made. Thus, we have characterized those films. The results will be discussed.

References

- [1] D. S. Chemla and J. Zyss, ed. *Nonlinear Optical Properties of Organic Molecules and Crystals*, Academic Press, New York, (1987).
- [2] S. R. Marder, D. N. Beratan, B. G. Tiemann, L. Cheng and W. Tam, in *Organic Materials for Nonlinear Optics II*, ed. R. A. Hann and D. Bloor, Cambridge, 165-175 (1991).
- [3] S. Allen, T. G. Ryan, D. P. Devonald, M. G. Hutchings, A. N. Burgess, E. S. Froggatt, A. Eaglesham, G. J. Ashwell and M. Malhotra, in *Organic Materials for Nonlinear Optics II*, ed. R. A. Hann and D. Bloor, Cambridge, 51-59 (1991).
- [4] J. Jerphagnon and S. K. Kurtz, *J. Appl. Phys.*, **41**, 1667-1681 (1970).
- [5] D. Lupo, W. Prass, U. Scheunemann, A. Laschewsky, H. Ringsdorf and I. Ledoux, *J. Opt. Soc. Am. B*, **5**, 300-308 (1988).

Dithienothiophene-Based Organic Molecules with Large Two-Photon Absorption Cross Sections

Kwang-Sup Lee, Jong Hyoup Lee

Department of Polymer Science & Engineering, Hannam University, Taejon 306-791, Korea

Oh-Kil Kim, Han Young Woo, Kie-Soo Kim

Chemistry Division, Naval Research Laboratory, Washington, DC, 20375-4532, USA

We have synthesized a novel class of two-photon absorption (TPA) chromophores based on dithienothiophene (DTT) as π -center which is linked through a π -conjugation to electron-donor (D) or electron-acceptor (A) at each end, forming a three segmented structure; D- π -D or D- π -A. Their TPA cross-section (σ) values were measured using 810 nm/8 ns pulsed laser. The σ values attained by DTT-based chromophores are the largest ever known and increase with the D strength and the structural symmetry; D- π -D. Such an outstanding molecular TPA is assumed mainly due to the unique electronic properties of DTT as π -center.

Organic molecules exhibiting a large two-photon absorption (TPA) have drawn a growing interest recently due to the feature that it occurs under the irradiation of sufficiently high intensity of low energy photons, emitting photons of higher energy that allows a deeper penetration into absorbing materials. Thus, TPA materials with a large cross section (or molecular TPA coefficient), σ , have a variety of applications such as for two-photon-excited fluorescence microscopy, optical limiting, three-dimensional optical data storage and two-photon induced biological caging studies¹.

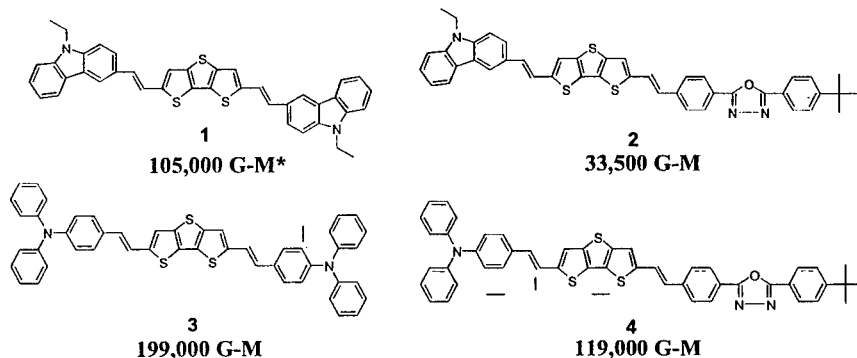
A number of NLO chromophores including commercial dyes have been reported to display TPA behavior but most known two-photon absorptivities were too small to find usage in practical applications. Unfortunately, design criteria for the molecules with large TPA cross-section, σ , have not been well developed. Recent reports²⁻⁴ from two different groups disclosed their design strategies for efficient TPA molecules by a systematic investigation of chromophores with various electron-donor (D) and electron-acceptor (A) moieties, which are attached symmetrically or asymmetrically to a conjugated linker (π -center); D- π -D or A- π -A. The typical difference in their approaches is that the one² deals with *trans*-stilbene as π -center with various D/A pairs, and the other⁴ does with chromophores bearing fluorene as π -center, which is asymmetrically coupled with D and A; D- π -A. While the former emphasizes the importance of conjugation length, D/A strength and molecular symmetry, the latter stresses planarity of π -center (fluorene), the donor strength, and molecular asymmetry. It seems to be that there must be more crucial molecular factors other than structural symmetry and donor strength. The largest σ value⁴ known so far was obtained with an asymmetric structure, D- π -A (where D, A and π -center are N,N-diphenylamino, 4-ethenylpyridine and 9-dialkyl-fluorenyl, respectively), known to be AF-50.

Recently, we have been observed a distinct role of dithienothiophene (DTT) as electron-relay in charge-transfer (CT) of nonlinear optical chromophores and as electron modulator in redox reaction of light-emitting chromophores. These are some of the novel features of DTT.

In this presentation, we report another feature of DTT as π -center of TPA molecules, in that

Poster Session III

DTT induces a large enhancement of TPA, compared with benzenoids counterpart,⁴ such that one of the DTT-centered chromophores produces the largest σ value ever known. There are significant differences in σ values of the chromophores, depending on the structural variations; the symmetric structure (1 and 3) exhibits relatively larger values compared to the respective asymmetric ones (2 and 4) and the stronger donor (triphenylamine > N-ethylcarbazole) seems to be more effective. When a comparison is made among chromophores differing in the π -center, the σ values of DTT-based chromophores are roughly 2-10 times larger than that based on fluorene as well as on stilbene. When the comparison is made with respect to the asymmetric chromophores (e.g., AF-50 and 4) with a nearly comparable A-strength (referring to pyridine and oxadiazole moieties), the σ value of chromophore 4 is 6 times larger than that of AF-50. The σ value of DTT-based asymmetric chromophore 4, for example, is much larger than that of symmetric stilbene-based BDBAS and BDPAS. Part of the role played by DTT is considered contributed by electron-rich heterocycles involving sulfur atoms, known to possess enhanced $\chi^{(3)}$ effects. An enhanced TPA can be also expected as it represents the imaging part of $\chi^{(3)}$.



*1 G-M = $116 \times 10^{-50} \text{ cm}^4 \cdot \text{sec} / \text{photon}$
TPA cross-section values were measured in tetrachloroethane using 810 nm and 8 ns pulse laser
(Measurements: Prof. P. N. Prasad's Lab.)

References

- [1] J. D. Bhawalkar, G. S. He, P. N. Prasad, *Rep. Prog. Phys.*, **59**, 1041 (1996).
- [2] J. Bradas, S. R. Marder, J. W. Perry, et.al, *Science*, **281**, 1653 (1999).
- [3] C. F. Zhao, G. S. He, J. D. Bhawalkar, C. K. Park, P. N. Prasad, *Chem. Mater.*, **7**, 1979 (1995).
- [4] B. A. Reinhardt, L. L. Brot, S. J. Clarkson, A. G. Dillard, J. C. Bhatt, R. Kannan, L. Yuan, G. S. He, P. N. Prasad, *Chem. Mater.*, **10**, 1863 (1998).

New Photoisomerisable Organometallic Chromophores as Precursors of Optically Poled Materials

Olivier Maury^a, Hubert Le Bozec^a, Isabelle Ledoux^b, Michel Dumont^b, Joseph Zyss^b

^a *Laboratoire de Chimie de Coordination et Catalyse, UMR 6509 CNRS-Université Rennes 1, Campus de Beaulieu, 35042 Rennes Cedex, France.*

^b *Laboratoire de Physique Quantique Moléculaire, ENS Cachan, 61 avenue du président Wilson, 94235 Cachan, France.*

Photoassisted electrical poling and all optical poling methods can be used at room temperature to induce macroscopic non centrosymmetric organisation of dipolar and octupolar photoisomerizable molecules. We have previously shown that metalloorganic complexes containing π -donor substituted 4,4'-alkenyl-2,2'-bipyridyl ligands display high microscopic non linearities. As the C=C double bond is poorly photoisomerizable as compared to other moieties such as the N=N double bond, we have designed new bipyridines containing azo transmitters. The preparation of the corresponding zinc(II) complexes, their linear and nonlinear properties as well as their preliminary photoassisted electrical poling behavior are also described.

Poled polymers containing second order nonlinear (NLO) molecules are particularly promising for electrooptic device applications. Usually, dipolar chromophores have to be aligned by using electric-field poling near the glass transition temperature (T_g) of the polymer [1]. Besides this approach, which requires high temperature treatment, new mild optical poling techniques have been recently developed. The so-called photoassisted electrical poling [2] and the "all optical" poling [3], can be used at room temperature for the macroscopic non centrosymmetric organisation of dipolar and octupolar chromophores, respectively. These methods require the presence of chromophores featuring a photoisomerisable moiety and use the "flexibility" of the molecule to break the centrosymmetry of the material. We have previously reported that metalloorganic complexes containing π -donor substituted 4,4'-alkenyl-2,2'-bipyridyl ligands **a** [4] such as and show large dipolar or octupolar microscopic non linearities [5]. As the C=C double bond is known to be poorly photoisomerisable as compared for example to the N=N double bond [6], we design new potentially photoisomerisable bipyridines by introducing nitrogen atoms into the transmitter.

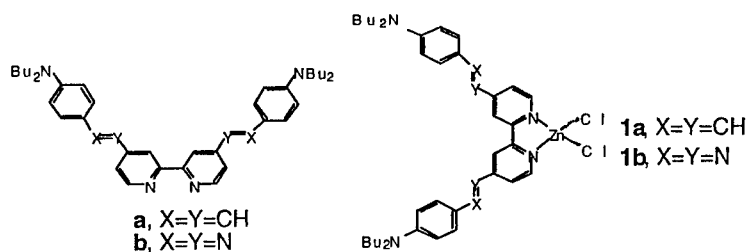
The synthesis of the azo- containing bipyridyl ligand **b** was readily accomplished in two steps from 4,4'-dinitro-2,2'-bipyridine-1,1'-dioxide in 25% yield. The corresponding tetrahedral zinc complexes **1b** (Scheme 1) were easily prepared upon treatment of the ligand **b** with ZnCl₂ in dichloromethane. Their optical spectra and those of the related aminostyryl derivatives **a** and **1a** are displayed in Table 1. Most importantly, a large bathochromic shift of the ICT band is observed by changing the C=C bond by the N=N in the ligand and in the zinc complex.

Table 1. Linear and nonlinear data.

ligand	λ_{\max}^a nm	ϵ mol ⁻¹ .cm ⁻¹	complex	λ_{\max}^a nm	ϵ mol ⁻¹ .cm ⁻¹	$\mu\beta^b$ 10 ⁻⁴⁸ esu ^c	$\mu\beta_o^b$ 10 ⁻⁴⁸ esu ^c
a	397	57000	1a	455	62000	1420	660
b	471	63000	1b	516	63000	2160	700

Poster Session III

Scheme 1: ligand a,b and corresponding zinc complexes.



^a solution in CH_2Cl_2 , ^b solution in CHCl_3 , precision of the measurement is about 10%,
^c correlation between esu and SI unit : β (SI) = $4.172 \cdot 10^{-10} \times \beta$ (esu)

The molecular hyperpolarisabilities $\mu\beta$ of **1a-b** were measured in chloroform using the electric-field-induced second harmonic generation (EFISH) at 1340 nm, and the non resonant $\mu\beta_0$ values were calculated using the two-level model. (Table 1) The results show that these complexes have good nonlinear optical activities which are sensitive to the nature of both the transmitter and donor groups. A slight increase of $\mu\beta$ is also observed on replacing CH by N. However comparison of the zero-frequency $\mu\beta_0$ values reveals that the increase on non-linearity seems to be mainly due to resonant enhancement.

In conclusion we have described the synthesis of new bipyridyl ligands bearing azo substituents. The NLO activity of the chromophore **1b**, which contains the most suitable photoisomerisable azo ligand, can be favourably compared with that of the prototypical azo dye DR1 ($\lambda_{\text{max}} = 480 \text{ nm}$, $\mu\beta_0 = 450 \cdot 10^{-48} \text{ esu}$) [7]. Researches are now in progress to study the photoassisted electrical poling of such dipoles in polymer films. Finally, these ligands open up the access to D_3 octupolar complexes which will be promising candidates for the "all optical" poling method.

[1] T. J. Marks and M. A. Ratner, *Angew. Chem. Int. Ed. Engl.*, 1995, **34**, 155 and references cited therein.

[2] (a) Z. Sekkat and M. Dumont, *Mol. Cryst. Liq. Cryst. Sci. Technol. sect B: Nonlinear Optics*, 1992, **2**, 359. (b) R. Loucif-Saïbi, K. Nakatani, J. A. Delaire, M. Dumont and Z. Sekkat, *Chem. Mater.*, 1993, **5**, 229.

[3] J. M. Nunzi, F. Charra and C. Fiorini and J. Zyss, *Chem. Phys. Lett.*, 1994, **219**, 349.

[4] (a) A. Juris, S. Campagna, I. Bidd, J. M. Lehn and R. Ziessel, *Inorg. Chem.*, 1988, **27**, 4007. (b) M. Bourgault, T. Renouard, B. Lognoné, C. Mountassir and H. Le Bozec, *Can. J. Chem.*, 1997, **75**, 318.

[5] For dipolar molecules see (a) M. Bourgault, K. Baum, H. Le Bozec, G. Pucetti, I. Ledoux and J. Zyss, *New J. Chem.*, 1998, 517. For octupolar molecules see (c) C. Dhenaut, I. Ledoux, I. D. W. Samuel, J. Zyss, M. Bourgault and H. Le Bozec, *Nature*, 1995, **374**, 339. (d) T. Renouard, H. Le Bozec, I. Ledoux and J. Zyss, *Chem. Commun.*, 1999, 871. For a review see (e) H. Le Bozec and T. Renouard, *Eur. J. Inorg. Chem.*, accepted.

[6] V. Wing-Wah Yam, V. Chor-Yue Lau and L. X. Wu, *J. Chem. Soc., Dalton Trans.*, 1998, 1461.

[7] C. W. Dirk, H. E. Katz, M. L. Schilling and L. A. King, *Chem. Mater.*, 1990, **2**, 700.

Synthesis and characterization of a series of NLO chromophores based on indan-1,3-dione derivatives.

R. A. Mazor¹, L. Shapiro¹, A. Ellern¹, V. Khodorkovsky¹, Z. Kotler², G. Berkovic², G. Meshulam²

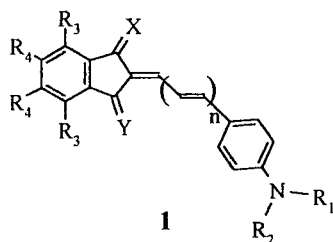
¹Department of Chemistry
Ben-Gurion University of the Negev
84105 Beer-Sheva, Israel

²Photochromic Materials Group
Soreq, NRC
Yavne, Israel

A series of NLO chromophores based on indan-1,3-dione derivatives was synthesized. The influence of the increasing accepting strength on the second polarizability was studied.

The electronic and structural properties of donor-acceptor substituted π -conjugated organic compound are of considerable interest due to the nonlinear optical (NLO) properties they can exhibit with potential application in optical communications. The ability to examine the magnitude of the NLO property through a series of organic compounds can be of a great importance to the contribution of understanding the structure property relationship. The ease of chemical modification of indan-1,3-dione makes this molecule an excellent accepting moiety in push-pull polyenes. Using indan-1,3-dione derivatives as an acceptor moiety enables the investigation of the influence of increasing acceptor strength on the second polarizability.

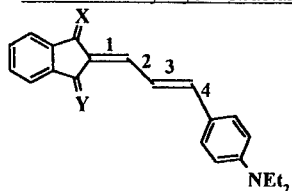
Recently we synthesized a series of push-pull polyenes based on indan-1,3-dione derivatives of the general structure 1.



The effect of the systematic variation of the accepting moiety and the length of the polyene bridge was studied with the aid of X-ray spectroscopy. Some results are shown in Table 1.

Poster Session III

Table 1. X-Ray crystal structure data



structure	T (°C)	1 (Å)	2 (Å)	3 (Å)	4 (Å)
	25	1.355 (6)	1.447 (6)	-	-
	-81	1.363 (4)	1.423 (5)	1.352 (4)	1.439 (4)

Comparison between three methods for estimation of second polarizability: EFISH technique, solvatochromic behavior and quantum mechanical calculation gave us a powerful tool for prediction of the second harmonic polarizability in similar derivatives. Some results are shown in Table 2.

Table 2. $\mu\beta$ values

structure	λ_{vac}^a	λ_{vac}^b	$\mu_g \beta_{\mu}^a$	$\mu_g \beta_{xxx}^a$	$\mu_g \beta_{xxx}^b$	$\mu_g \beta_{(0)}^c$
	398	404	117	120	116	-
	405	415	136	142	196	150

^a quantum mechanical calculation, ^b solvatochromism, ^c EFISH
 $\mu\beta * 10^{-48}$ esu

Nonlinear optical properties of cyanines and oligoenes: influence of bond-length alternation substituents and chain length

D. Scherer, A. Feldner, R. Dörfler, M. Welscher, Th. Vogtmann, M. Schwoerer
*Lehrstuhl Experimentalphysik II and
Bayreuther Institut für Makromolekülforschung (BIMF)
Universität Bayreuth,
Universitätsstr. 30,
D-95440 Bayreuth*

H.-H. Johannes, U. Lawrentz, and W. Grahn
*Institut für Organische Chemie,
TU-Braunschweig,
Hagenring 30,
D-38106 Braunschweig*

Different chemically pure dyes were prepared, that address different aspects of structure-property relationships, especially electron density, bond length alternation and prolonged conjugation by rigidisation. The defined structures make these series of molecules interesting models for the study of nonlinear optical behaviour of conjugated π electron systems. The third order nonlinear optical susceptibilities of dye solutions have been studied using THG, DFWM and pump-probe experiments. The two-photon absorption was studied by excitation scans of the two-photon fluorescence.

The mechanisms of third order nonlinear optical susceptibilities ($\chi^{(3)}$) as the origin of an intensity dependent refractive index as well as of two-photon absorption are still of strong interest, with the background of possible applications e.g. in all-optical switching devices or analysis based on two-photon fluorescence (TPF) [1].

Conjugated π electron systems, as found in various polymers, show very high nonlinear susceptibilities. Increasing the conjugation length lowers the energy of the B_u state and increases its transition moment. So, an increase of the NLO response is achieved, but accompanied by a strong shift of the absorption to longer wavelengths. On the other hand, the behaviour of a chain of fixed length can be influenced by side and end groups of the molecule, e.g. by variation of bond length alternation [2].

For a meaningful analysis and for the possible applications, it is also of high importance to know the energy of the two-photon niveaux A_g . Theoretical studies show that changing BLA and electron density causes relative shifts of the energy niveaux of one- and two-photon excited states [3].

In our co-operation of chemists and physicists, different chemically pure dyes were prepared (fig. 1), that address different aspects of structure-property relationships, especially electron density, bond length alternation and coupling of chromophors with conjugated bridges. The defined structures make these series of molecules interesting models for the study of nonlinear optical behaviour of conjugated π electron systems.

The third order nonlinear optical susceptibilities of dye solutions have been studied using THG, DFWM and pump-probe experiments. The two-photon absorption was studied by excitation scans of the two-photon fluorescence.

Poster Session III

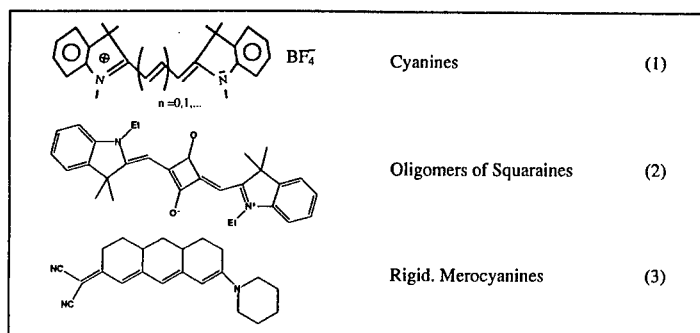


Figure 1: Examples of molecules from each class under investigation. Each substance was chemically pure not only in terms of their substituents, but also in terms of chain length. The cyanines (1) were varied in chain length and symmetrically substituted functional end groups. The squaraines (2) were oligomerized with conjugated bridges, up to the pentamer. By donor and acceptor groups of different strength, rigidized merocyanines (3) were prepared with varying bond-length alternation from oligoionic structures into the cyanine limit.

The concentration dependence of $\chi^{(3)}$ has been measured, yielding the mean value $\langle\gamma\rangle$ of the molecular hyperpolarizability. DFWM measurements at 1064nm have been found to be particularly well suited to compare the molecules, because this wavelength is well off the linear resonances of every molecule under investigation.

$\langle\gamma\rangle = 10^{-35}$ esu was found for the simple cyanine (1) (fig. 1). By attaching an electron donor end group, this value increased by two orders of magnitude to $1.3 \cdot 10^{-33}$ esu, with the absorption peak still below 500nm. The corresponding trimethine (1) shows a shift of the absorption maximum to 550nm and $\langle\gamma\rangle = 7 \cdot 10^{-34}$ esu. Time-resolved measurements did not show any broadening of the 3rd order autocorrelation of the 6ps laser pulse, such excluding slow thermal or reorientational effects on the obtained values.

To get the energy levels of two-photon excited states, excitation scans of the two-photon fluorescence were performed. The two-photon absorption cross section δ was determined by relative measurements versus fluorescein. For example, δ of the rigidized merocyanines (3) could be tuned in the range $(200 \dots 1400) \cdot 10^{-50} \text{cm}^4 \text{s}^{-1}$.

References

- [1] J.D. Bhawalkar, G.S. He and P.N. Prasad, Rep. Prog. Phys **59**, 1041 (1996).
- [2] Ch. B. Gorman and S. R. Marder, Chem. Mater. **7**, 215 (1995).
- [3] Z. Shuai, J.L. Brédas, S.K. Pati and S. Ramasesha, The International Society for Optical Engineering **3145**, 293 (1997)

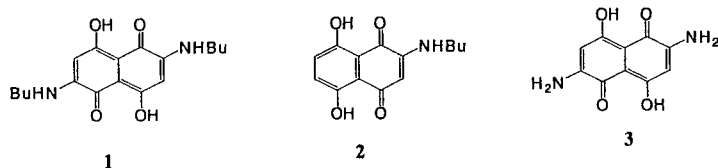
MO calculations of dyes for the solid state absorption spectra

H. Shiozaki, Y. Sakurai, S. Nakao, M. Kimoto
 Technology Research Institute of Osaka Prefecture
 1-18-13 Kishibenaka, Suita, Osaka 564-0002, Japan

Absorption spectral shift of a series of dyes, which have large $\chi^{(3)}$ values in spite of their small π -conjugation systems, was studied. These dyes have both characteristics of large bathochromic shift of λ_{\max} from the solution to solid state, and strong π - π interactions between the molecular layers. CNDO/S and ab initio methods were used to calculate this spectral shift. The resonance integral term of the CNDO/S program was modified for the evaluation of the interaction between the atoms with long interatomic distances.

Organic nonlinear optical (NLO) materials are of interest as key materials in photonics technology. Recently, Matsuoka and co-workers identified a series of dyes, which have large $\chi^{(3)}$ values in spite of their small π -conjugation systems [1]. These dyes have both characteristics of large bathochromic shift of λ_{\max} from the solution to solid state, and strong π - π interactions between the molecular layers. We estimated that the large bathochromic shift is an indication of obtaining a higher $\chi^{(3)}$ value, and tried to evaluate the shifts accurately by MO calculations.

The $\chi^{(3)}$ value of 2,6-dibutylamino-dihydroxynaphthoquinone **1** determined by the third harmonic generation method was 4.8×10^{-11} e.s.u. in vapor-deposited thin film; however, that of 2-butylamino-dihydroxynaphthoquinone **2** was around 10^{-13} e.s.u. [1]. As shown in Fig. 1, dye **1** produced a bathochromic shift about 100 nm of λ_{\max} from solution (541 nm) to solid state (641 nm); however, no bathochromic shift was observed in dye **2**.



In single crystal, the molecules of dye **1** align in the same plane and are parallel to each other with an interlayer distance of 3.3 Å. To study the bathochromic shift in absorption spectra of dye **1**, we used dye **3** as the model compound for dye **1**. We calculated the spectra of the monomer and the dimers of dye **3** by the single excitation configuration interaction (SE-CI) calculations with the 6-31G(d) basis set, implemented in the Gaussian 94 program. The structures of the three dimers for calculations were shown in Fig. 2. The calculated results were shown in Table 1 [2]. The CONH dimer showed a bathochromic shift of 0.101 eV, which corresponds to about 30% of the observed shift for dye **1**. The calculated absorption spectra by a

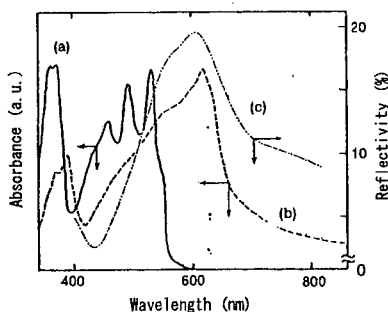


Fig. 1. Spectra of dye **1**: (a) absorption in cyclohexane; (b) absorption of evaporated film; (c) reflection of single crystal

Poster Session III

semi-empirical program, CNDO/S, were also shown in Table 1. The shifts calculated by CNDO/S were smaller than that by ab initio calculations. We estimated that this defect of CNDO/S was derived from the inadequacy in the long range interaction calculation. To correct this defect, the resonance integral term of the CNDO/S program was modified. In the original CNDO/S approximation, the core matrix element $H_{\mu\nu}$ between orbitals μ and ν on atoms r and s respectively, is obtained by

$$H_{\mu\nu} = (1/2)(\beta_r^0 + \beta_s^0)(S_{\mu\nu}^\sigma + \kappa S_{\mu\nu}^\pi) \quad (1)$$

where $S_{\mu\nu}^\sigma$ and $S_{\mu\nu}^\pi$ are the σ component and π component of overlap integrals, respectively, and κ is a constant of 0.585. We added a term, which amplifies the π component of overlap integrals between the atoms having long interatomic distances, to the constant, as follows.

$$\kappa = 0.6 + \exp(2.43 R_{rs} - 5.9) \quad (2)$$

Where R_{rs} is the distance in angstrom unit between atoms r and s . The calculated results by the modified CNDO/S program including equation (2) were also showed in Table 1. The modified CNDO/S gave a bathochromic shift of 0.07 eV for the CONH dimer, indicating that equation (2) corrected the above defect. Our modification is a convenient and simple method to estimate the spectral shift from solution to solid state, although it has no theoretical validity.

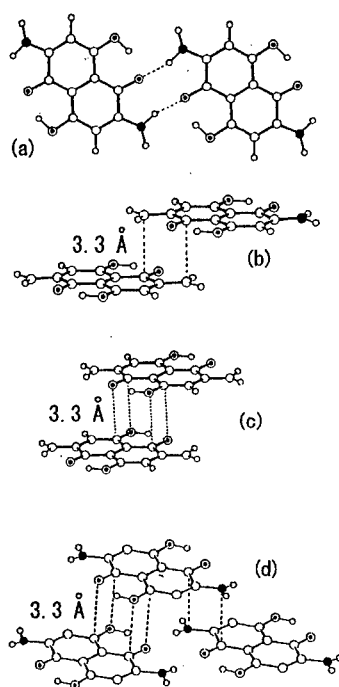


Fig. 2. Structures of **3** for the spectral calculations: (a) H-bond dimer; (b) CONH dimer; (c) parallel dimer; (d) tetramer.

Table 1 Calculated λ_{\max} of the monomer, dimers and tetramer of **3** by Gaussian 94 and CNDO/S

	SE-CI/6-31G(d) λ_{\max}/nm [λ_{\max}/eV]	CNDO/S ^{a)} λ_{\max}/nm [λ_{\max}/eV]	modified CNDO/S ^{a)} λ_{\max}/nm [λ_{\max}/eV]
Monomer	365.2 [3.394]	473.3 [2.620]	554.9 [2.234]
Dimer			
H-bond	374.1 [3.314]	477.9 [2.595]	567.2 [2.186]
CONH	376.5 [3.293]	475.4 [2.608]	572.8 [2.164]
Parallel	351.1 [3.531]	442.0 [2.805]	523.1 [2.370]
Tetramer		473.7 [2.617]	574.1 [2.159]

^{a)} Configuration interaction were made with 100 configurations.

References

- [1] M. Matsuoka, A. Oschida, A. Mizoguchi, Y. Hattori, A. Nishimura, *Nonlinear Optics*, **10**, 109 (1995).
- [2] H. Shiozaki and M. Matsuoka, *J. Mol. Struct. (Theochem)*, **427**, 253 (1998).

**Novel aminopyrazine fluorescent dyes for NLO materials;
their solid state spectra and crystal structures**

Kazuko Shirai and Masaru Matsuoka

Material Science Laboratory, Kyoto Women's University,
Imakumano, Higashiyama, Kyoto 605-8501, Japan

Novel aminopyrazine fluorescent dyes with strong intramolecular charge-transfer character were synthesized for NLO materials and their solid state spectra were correlated with their X-ray crystal structures.

We have been studied the relationship between 3rd order NLO susceptibility and intermolecular π - π interactions of dye chromophores in the solid state, and found that large susceptibility could be obtained from strong π - π interactions [1]. In this paper, a series of 2,5-bis(*N,N*-dialkylamino)-3,6-dicyanopyrazine dyes (1-4) have been synthesized by the alkylation of 2,5-diamino-3,6-dicyanopyrazine. The structures and their spectral properties are shown in the Table. The difference in λ_{\max} from the solid state to the solution is denoted as $\Delta\lambda$, and that in F_{\max} is ΔF . The planarity of π -conjugation systems and the space-filling molecular structure were deduced from the optimized molecular structures calculated by the MOPAC AM1 and PM3 methods and the results are shown in the Figure.

The λ_{\max} values of these dyes 1-4 in the solid state showed quite different behavior which can be evaluated by the $\Delta\lambda$ values. The $\Delta\lambda$ value of dye 1 was 90 nm which indicated strong intermolecular π - π interactions in the solid state but $\Delta\lambda$ for dye 2 was small (5 nm). There is little difference in λ_{\max} of dye 2 between the solution and the solid state, and no intermolecular π - π interactions are proposed from the results of steric requirements of the benzyl groups. Dyes 3 and 4 also showed quite large $\Delta\lambda$ values. From these results, the $\Delta\lambda$ value may be a good indicator to know the intermolecular π - π interactions which can be also deduced from the molecular packing of the optimized structures obtained by the MOPAC methods.

The solid state fluorescence in the powder state exhibited large differences in F_{\max} values which were evaluated by the ΔF values. In the powder state, larger ΔF values were obtained in dyes 1 (60 nm) and 3 (84 nm) but dyes 2 (1 nm), and 4 (36 nm) showed smaller values. In contrast, the relative fluorescence strength of dyes 1 (6930 nm) and 2 (10160 nm) were large, whilst dye 3 gave rise to weak fluorescence indicating strong intermolecular π - π interactions in the powder state. Dye 4 (8230) showed relatively stronger fluorescence than that of dye 3 (610).

It is generally known that a decrease in fluorescence intensity or fluorescence quenching in solution is observed accompanying with an increase of dye concentration and/or the formation of an excimer. Intermolecular interactions of a singlet excited dye

Poster Session III

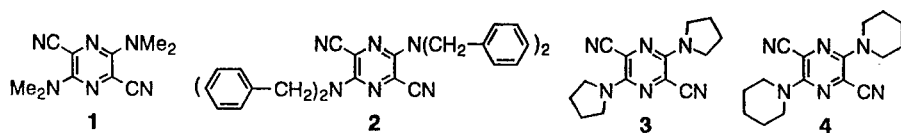


Table. Visible and fluorescence properties of dyes 1 - 4 in the solid states

Compd. No.	λ_{\max} (nm)	F_{\max} (nm)		$\Delta\lambda^d$ (nm)	ΔF^e (nm)
	film ^a	powder ^b	(intensity) ^c		
1	592	643	(6930)	90	60
2	495	575	(10160)	5	.1
3	596	680	(610)	70	84
4	566	633	(8230)	74	36

a, Vapor deposited thin film on glass. b, Solid state F_{\max} excited at λ_{\max} (film) value. c, Measured in powder on the white plate. d, $\Delta\lambda = \lambda_{\max}$ (film) - λ_{\max} (CHCl_3). e, $\Delta F = F_{\max}$ (solid) - F_{\max} (solution).

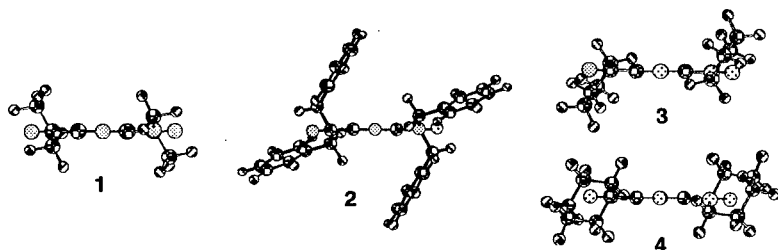


Figure. Optimized molecular structures of dyes 1 - 4 by MOPAC AM1 methods showing the side view from π -plane.

molecule with a ground state dye molecule give rise to the energy-transfer to quench the fluorescence. Solid state fluorescence was determined in the powder state in which dye molecules formed aggregates or stacked strongly, and strong intermolecular interactions between dye molecules are proposed. The interactions can be evaluated in terms of the ΔF value, and also the strength of solid state fluorescence can be correlated with the optimized molecular structures.

From these results, it was found that fluorescence quenching in the solid state occurred in the order of dyes 1 > 2 accompanying with the increase of intermolecular π - π interactions. In a series of dyes 3 and 4, the sterically hindered six membered dye 4 having a dumbbell structure have stronger fluorescence in the powder state than the corresponding dye 3. The X-ray crystal analyses revealed that absorption shift can be evaluated from their optimized structure, and fluorescence quenching will become a new measure to evaluate the intermolecular π - π interactions in the solid state.

Novel carbazole derivatives for two-photon absorption applications

Mark Sigalov, Amos Ben-Asuly, Lev Shapiro, Vladimir Khodorkovsky
*Department of Chemistry, Ben-Gurion University of the Negev,
84105 Beer-Sheva, Israel*

The multi-step synthetic route to the novel highly conjugated carbazole derivatives is developed. These compounds are photostable, strongly fluorescent and according to preliminary measurements have the values of the cross-section of two-photon absorption in the range of 900-4000 (10^{-50} cm⁴/s/photon) and some of them exceed the best known to date values.

During the past time much efforts were directed towards design, synthesis and study of organic fluorescent molecules with large two-photon absorption cross-section. This is stimulated by the growing interest in multiphoton fluorescent imaging, laser scanning microscopy, optical data storage, optical limiting and photodynamic localized treatment.

There are evidences of the very important role which play the stilbene derivatives as the main components for effective materials for many photochemical and photophysical applications. Recently, it was shown that substituting a stilbene moiety by electron donating groups substantially increases the cross-section of two-photon absorption of the molecule [1].

The N-vinyl-carbazole derivatives possess advanced photophysical properties and have found numerous applications in various fields of the modern technology. Their less widespread and investigated N-aryl analogs according to recent data also can be perspective components of advanced materials.

The combination of electron donating and polarizable carbazole unit with the fluorescent stilbene and distyrylbenzene moieties is promising for the synthesis of new compounds with desirable properties.

We have developed the multi-step synthetic route the novel highly conjugated carbazole derivatives which are photostable, strongly fluorescent and, according to preliminary measurements, the values of the cross-section of two-photon absorption for these compounds are in the range of δ 900-4000 x 10^{-50} cm⁴/s/photon and some of them exceed the best known to date values [2].

The key compound for this route was previously unknown 9-(4'-formylphenyl) carbazole. The use of this compound and its ring-substituted derivatives in the Ti-catalyzed aldehyde coupling leads to series of stilbene 1, and in the Wittig reaction with corresponding phosphonates – to series of distyrylbenzene derivatives 2, polyene 3 and polyphenylene 4. According to the measured fluorescence properties some of new compounds are perspective as fluorescent probes for practical applications. Strong dependence of quantum yield and two-photon absorption cross-section on substituent allows fine adjustment of these properties. In addition, the presence of highly reactive centers in carbazole moieties offers the possibility of further substitution on the central aromatic ring, and allows incorporation of novel fluorophores into polymeric backbones.

Poster Session III

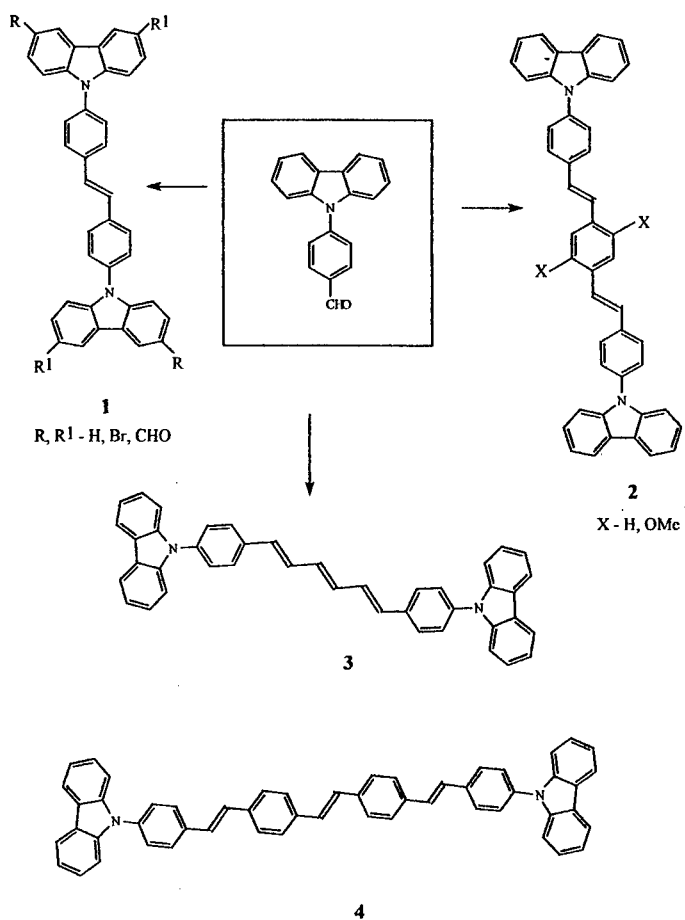


Figure 1: Main synthesized carbazole-based compounds

References

- [1] M. Albota et al., *Science*, 1998, v.281, p. 1653-1656.
- [2] Z. Kotler, J. Segal, M. Sigalov, A. Ben-Asuly, V. Khodorkovsky, submitted

Multifunctional TCNQ Adducts

Marek Szablewski, Mosurkal Ravi, Nancy-Ann Hackman
Graham H.Cross, David Bloor
Department of Physics, University of Durham,
Durham DH1 3LE, England

Bis-amino TCNQ adducts (eg. Fig.1) possess absorption maxima below 420nm in solution, a large ground-state dipole moment and molecular nonlinearity, and fluoresce strongly and electroluminesce in polymer matrices.

Solution absorption and fluorescence spectra, crystal structures and theoretical calculations are consistent with a twisted conformation in the electronic ground state and a more planar excited state with a small dipole moment, which decays non-radiatively. The hindrance of the conformational change in viscous solvents and solid matrices opens a radiative decay channel with a high fluorescence quantum yield.

Preliminary results on application to electro-optical devices will be presented.

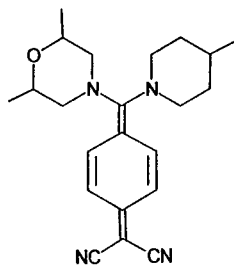


Fig. 1

References

- [1] "Polar TCNQ adducts for nonlinear optics", Yasuki Kagawa, Marek Szablewski, Mosurkal Ravi, Nancy-Ann Hackman, Graham H.Cross, David Bloor, Andrei.S.Batsanov and Judith A.K.Howard, Nonlinear Optics, 1999, Vol. 22, pp 235-240

Poster Session III

Organic / Inorganic Quantum Confinement Structures based on Lead Halide Perovskites

Yuko Tabuchi^{1), 2)}, Keisuke Asai^{1), 2)}, Masahiro Rikukawa^{2), 3)},
Kohei Sanui^{2), 3)} and Kenkichi Ishigure¹⁾

- 1) *Department of Quantum Engineering and Systems Science, University of Tokyo,
7-3-1, Hongo, Bunkyo-ku, Tokyo 1130033, Japan*
- 2) *CREST, Japan Science and Technology Corporation (JST)*
- 3) *Department of Chemistry, Sophia University,
7-1, Kioi-cho, Chiyoda-ku, Tokyo 1028554, Japan*

Organic / inorganic quantum confinement structures based on lead halide perovskites were successfully prepared. The dimension of inorganic part can be easily controlled by intercalating various organic amines into lead halide inorganic layers. In this study, by constructing various organic / inorganic self-organized materials, the optical properties caused by the quantum confinement structures were investigated.

Introduction

Organic / inorganic perovskite-type materials have been known to self-organize into low-dimensional quantum confinement structures. These compounds consist of the unit structure as shown in Figure 1. The inorganic semiconductor part comprised of $[\text{PbX}_6]^{4-}$ octahedra is located at the body center, while the organic ammonium ions $[\text{RNH}_3]^+$ reside the eight corner of the cube being shared by eight unit cells. The

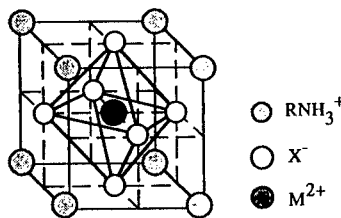


Figure 1 Unit structure of perovskite-type compounds; shaded circle: organic ammonium ion, open circle: halogen ion and closed circle: metal cation.

dimension of the inorganic part can be easily controlled by changing the size or shape of organic amine^{[1], [2]}. Thus, PbX -based perovskite compounds have enormous variety, which may be utilized for studying the physical properties inherent to these materials. In this paper, we try to fabricate two- and lower- dimensional (LD) perovskite-type compounds. The structural and optical properties of these LD semiconductor systems are also investigated.

Experimental

Pyrrolidine ($\text{C}_4\text{H}_8\text{NH}$) and piperidine ($\text{C}_5\text{H}_{10}\text{NH}$) were used as starting organic materials. After bromination, each organic amine was mixed with PbBr_2 in DMF. The products were

Poster Session III

obtained as precipitation by adding poor solvent into the DMF solutions, respectively. Spin-coated films of these products were fabricated on glass slides from DMF solutions.

Results and Discussion

The products were confirmed to be $C_4H_8NH_2PbBr_3$ and $C_5H_{10}NH_2PbBr_3$ by elemental analysis, respectively. Figure 2 shows the X-ray diffraction patterns of these powder samples. In the diffraction profiles, new diffractions, which were not observed for raw materials, were clearly shown in each system. This means that the new self-organized structures were obtained. Spin-coated films also showed similar X-ray diffraction patterns which implies the self-organized structures were maintained in the films.

Optical absorption spectra of spin-coated films were shown in Figure 3. Figure 3 (a) displays the result of $(C_6H_{13}NH_3)_2PbBr_4$ which is known to form typical two-dimensional quantum confinement structure. $(C_6H_{13}NH_3)_2PbBr_4$ show strong, sharp exciton absorption at 395 nm which is assigned to the exciton from the $[PbBr_6]^{4-}$ inorganic layer. In the case of $C_4H_8NH_2PbBr_3$ and $C_5H_{10}NH_2PbBr_3$ spin-coated films, strong and sharp single absorption peaks were observed at 359 and 330 nm, respectively. These exciton peaks were located at lower energy than $(C_6H_{13}NH_3)_2PbBr_4$. This mentions that the lower dimensional structures were formed in $C_4H_8NH_2PbBr_3$ and $C_5H_{10}NH_2PbBr_3$.

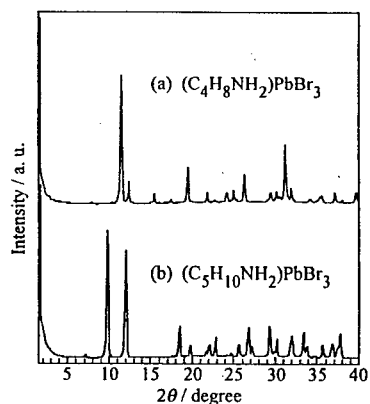


Figure 1 X-ray diffraction patterns of powder samples of (a) $(C_5H_{10}NH_2)PbBr_3$ and (b) $(C_4H_8NH_2)PbBr_3$.

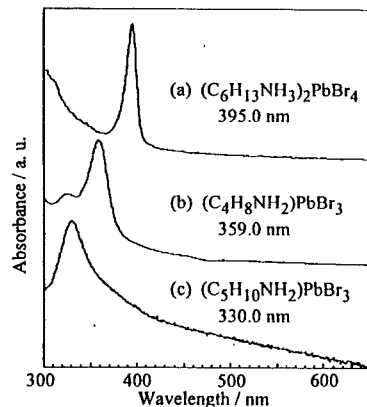


Figure 2 Optical absorption spectra of spin-coated films of (a) $(C_6H_{13}NH_3)_2PbBr_4$, (b) $(C_4H_8NH_2)PbBr_3$ and (c) $(C_5H_{10}NH_2)PbBr_3$.

References

- [1] J. Calabrese et al., *J. Am. Chem. Soc.*, **113**, 2328 (1991).
- [2] G. C. Papavassiliou et al., *Synthetic Metals*, **55**, 3889 (1993).

Acknowledgment

This work is supported by the CREST of the Japan Science and Technology Corporation.

Novel Organic-Inorganic Quantum Confinement Structure (VII)
Structural Characterization and Optical Properties for Low Dimensional
Compounds with PbX₆ Octahedra

K. Teshima¹, S. Kano^{1,2}, M. Kawahara^{1,2}, M. Rikukawa^{1,2} and K. Sanui^{1,2}
JST CREST¹, Department of Chemistry Sophia Univ.²
7-1 Kioi-Cyo, Chiyoda-ku, Tokyo 102-8554, Japan

Ammonium lead halide compounds were reported to form quantum confinement structures with perovskite type crystal lattice, which have different dimensions for inorganic region by control of synthesis conditions. The purpose of this study is a formation of novel low dimensional quantum confinement structure with triamine salts etc. The products are mainly characterized by X-ray diffraction and optical measurements. The result of single crystal X-ray analysis mentioned that the inorganic region of the crystal had a side-sharing PbI₆ octahedral structure between 1 and 2 dimensions. Since the compound showed different optical properties from corner sharing perovskite compound, it expected to have interesting nonlinear optical properties.

Alkylammonium lead halide compounds were reported to form self-organized perovskite type crystal structures. The dimensions of the semiconductor inorganic region constructed by PbX₆ can be controlled easily by changing organic compounds or mixture ratio of raw materials. Primary salts were usually used to prepare perovskite compound and have extremely limited the structures and physical properties. In this report, we discussed about possibility to form novel organic-inorganic quantum confinement structures with triamine salts such as N(C₃H₆NH₃I)₃ [TAPAI], N(C₂H₄NH₃Br)₃ [TAEABr], etc.

TAPAI and PbBr₂ were dissolved into DMF, and the product (TAPAPbI) was obtained by recrystallization from a DMF solution by the solvent diffusion method with H₂O. Spin-coated films of TAPAPbI were prepared from a 10w% DMF solution. The structural characterization of the products and the spin-coated films were performed by X-ray diffraction measurements, and these optical properties were characterized by UV-Vis absorption spectra and fluorescence spectra.

The single crystal X-ray analysis was performed for TAPAPbI. The residual (R) didn't decrease adequately because of unsatisfactory data collections. Therefore, the refinement was carried out for only lead and iodide atoms. The results of single crystal X-ray analysis are

Table 1 Data collection and refinement

Empirical Formula ¹⁾	C ₉ H ₂₈ I ₄ N ₄ Pb ₅
Formula Weight ²⁾	3005
Crystal Color, Habit	Brown, Cubic
Crystal Dimensions	0.10 X 0.10 X 0.10 mm
Crystal System	Monoclinic
Lattice Type	Primitive
Space Group	P2 ₁ /a (#14)
Lattice Parameters	a=33.091 Å b=11.946 Å c=8.017 Å β = 89.86°
Volume	3169 Å ³
Z value	2
Dcalc ²⁾	3.149g/cm ³
μ (MoKα) ²⁾	200.89cm ⁻¹
Structural Solution	Direct Methods (SIR92)
Refinement	Full-matrix least-squares
Residuals: R; Rw	0.102; 0.121
Max Shift / Error in Final Cycle	0.00

1) The formula was predicted from the result of the single crystal X-ray analysis.

2) These values were calculated from the anticipated formula.

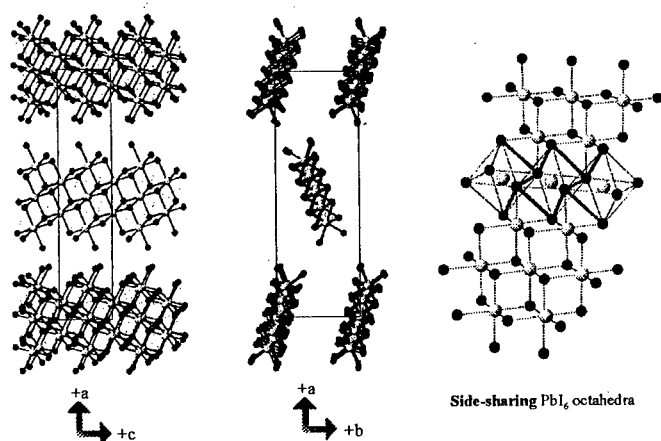


Fig. 1 The inorganic region structure for TAPAPbI determined by single crystal X-ray analysis

summarized in Table 1. As the result of refinement, a value of R finally decreased to 0.102. This value indicates that the calculated structure of inorganic region is reasonable one. Furthermore, the powder X-ray diffraction pattern for TAPAPbI was compared with the pattern simulated by the result of the single crystal X-ray analysis. As these patterns almost coincided with each other, this result also supported above refined structure for inorganic atoms.

The result of single crystal X-ray analysis indicated that the inorganic region of TAPAPbI crystal had a side-sharing PbI_6 octahedral structure between 1 and 2 dimensions as shown in Fig.1. The bandwidth of side-sharing PbI_6 octahedra were three units of the octahedra, and the band extended along the c-axis. Thus, the novel structure with PbI_6 octahedra could be constructed with triamine organic cation, and it is very interesting to have novel dimensions with PbI_6 octahedra.

The TAPAPbI powder prepared from the single crystal had the absorption band around 2.97eV (417nm) and the fluorescence band around 2.65eV (468nm) as shown in Fig.2. As the powder sample showed a fluorescence band, it expected to be a quantum confinement structure. The absorption photon energy took lower value than that of the reported corner-sharing perovskite compounds, though the dimension of the TAPAPbI crystal structure is between 1 and 2. This indicates that the side-sharing PbI_6 octahedral compounds have different optical properties from the corner-sharing compounds.

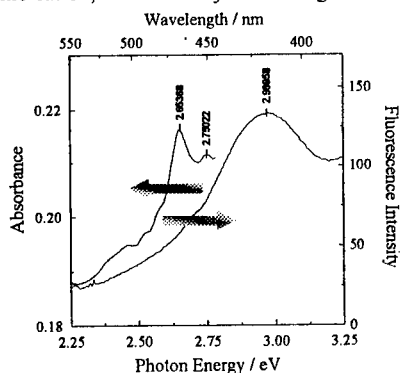


Fig. 2 The absorption and fluorescence spectra of TAPAPbI powder prepared from its single crystals.

This study is supported by CREST of Japan Science and Technology Corporation.

**Novel Organic-Inorganic Quantum Confinement Structure (VIII)
Structural Characterization for Self-Organized Compounds with
Quaternary Ammonium Salt**

K. Teshima¹, S. Kano^{1,2}, M. Rikukawa^{1,2} and K. Sanui^{1,2}
*JST CREST¹, Department of Chemistry Sophia Univ.²
7-1 Kioi-Cyo, Chiyoda-ku, Tokyo 102-8554, Japan*

The perovskite compounds were reported to form quantum confinement structures. The reported compounds were mainly composed of primary amine salts, and these however have disadvantages of instability for oxygen and light. Therefore, we selected quaternary alkylammonium bromide salts as organic materials in order to overcome the disadvantages. In this report, we discussed about quaternary alkylammonium lead bromide systems such as $(C_{12}H_{25})_2(CH_3)_2NBr$ [C12DMNBr] etc. C12DMPbBr have distinguished self-organized properties, which easily provided polycrystalline film by the spin-coat method. Since these films have two absorption peaks and one fluorescence band, a quantum confinement structure seems to be formed by the spin-coated method.

The organic-inorganic hybrid compounds with composition A_2MX_4 consist of alternating structures that have layer of metal halide perovskite (MX_4) sheet with MX_6 octahedra and organic ammonium cation (A^+) layer, and are particularly interesting because of the ability to use the organic layers to control properties of the inorganic perovskite sheets. These perovskite compounds have also received attention due to attractive optical properties. The reported alkylammonium perovskite compounds were only primary amine salt, and these however have disadvantages of instability for humidity, light, and temperature. Therefore, we selected quaternary alkylammonium bromide salts as organic materials instead of primary amine salts in order to overcome disadvantages mentioned above, because these salts have high stability and can be applicable to easy synthesis on further research. In this report, we discussed about possibility to form novel organic-inorganic quantum confinement structures with quaternary alkylammonium bromide salts such as $(C_{12}H_{25})_2(CH_3)_2NBr$ [C12DMNBr], $C_6H_5(CH_3)_3NBr$ [PhTMNBr] etc.

C12DMNBr and $PbBr_2$ were dissolved into NMP, and the product (C12DMPbBr) was obtained by recrystallization from its NMP solution. Spin-coated films of C12DMPbBr were prepared from a 30 mg/ml chloroform solution. The structural characterization of the products and the spin-coated films were performed by X-ray diffraction measurements, and the optical properties were characterized by UV-Vis absorption spectra and fluorescence spectra.

The powder of C12DMPbBr was characterized by powder X-ray diffraction, and the diffraction peaks corresponding to 35\AA , the first peak located at 2.6° , were observed with high order reflections. This result showed that the C12DMNBr system, in particular, formed a layered structure with very high regularity. Furthermore, the elemental analysis performed for the products. The

Table 1 The results of elemental analysis. The calculated value was leaded from $[(C_{12}H_{25})_2(CH_3)_2N]_2PbBr_4$

Atoms	C	H	N	Other
Calcd. / %	48.33	8.74	2.17	40.76
Found / %	48.22	9.08	2.19	40.52

Poster Session III

found value confirmed with the calculated one obtained from the molecular formula $[(C_{12}H_{25})_2(CH_3)_2N]_2PbBr_4$ (Table 1). As this composition ratio is equal to the layered perovskite compounds such as the alkylammonium lead halide, the C12DMPbBr expected to take layered perovskite compounds.

In addition, as the product can be dissolved into several organic solvents such as chloroform, DMF etc., these thin film could be prepared by the spin-coating method. X-ray diffraction measurement was used for the characterization of the film structure. The X-ray diffraction pattern for the spin-coated film was shown in Fig.1. The Bragg reflections at 2.7° , which correspond to 32.7\AA , were observed to high order, and it had a same inclination as its powder X-ray diffraction pattern. The result means that the film takes layered polycrystalline structure, and the product has distinguished self-organized properties.

The UV-Vis absorption spectrum had two absorption bands at around 3.60eV and 3.84eV , on the other hand, fluorescence band was observed at around 3.26eV , as shown in Fig.2. Since the fluorescence arose from the inorganic region, a quantum confinement structure seems to be formed by the spin-coated method. This inorganic region of the products seems to be different structure from the layered perovskite structures because the absorption bands have lower photon energies than those of the layered perovskite structure and another absorption band while the perovskite structure has sharp single absorption band concerned with exciton band. The structure with composition A_2MX_4 except for the layered perovskite structure was reported by Mitzi et al.^[1], which contains $\langle 110 \rangle$ -oriented perovskite sheets. As this compound has anisotropic structure in inorganic region, the absorption band of the inorganic region would take more than two. The optical measurements of our new materials are in progress.

This study is supported by CREST of Japan Science and Technology Corporation.

References

- [1] D.B.Mitzi, S. Wang, C. A. Feild, C. A. Chess, A. M. Guloy, "Conducting layered organic-inorganic halides containing $\langle 110 \rangle$ -oriented perovskite sheets," *Science* 267, 1473-1476 (1995)

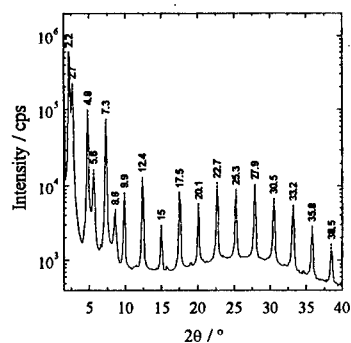


Fig. 1 X-ray diffraction pattern of spin coated C12DMPbBr film prepared from chloroform solution.

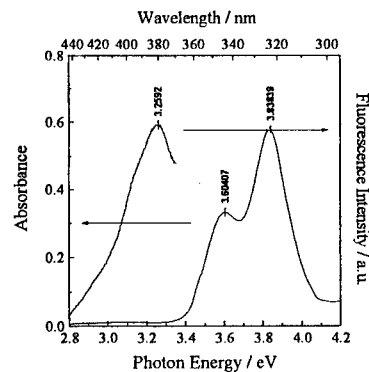


Fig. 2 Absorption and fluorescence spectra of spin-coated C12DMPbBr film.

New Quadrupolar Fluorophores with High Two-Photon Excited Fluorescence

L. Ventelon^a, L. Moreaux^b, J. Mertz^b, M. Blanchard-Desce^a

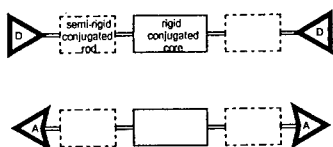
^a*Département de Chimie, Ecole Normale Supérieure (UMR 8640)
24, rue Lhomond, 75231 Paris Cedex 05, France*

^b*Laboratoire de Physiologie, Ecole Supérieure de Physique et Chimie Industrielle
10, rue Vauquelin, 75231 Paris Cedex 05, France*

New quadrupolar fluorophores that combine very large two-photon absorption cross section and high fluorescence quantum yield were prepared and investigated. These molecules were designed according to a molecular engineering approach based on push-push and pull-pull elongated molecules built from a rigid conjugated fluorescent core. As a result, two-photon excited fluorescence (TPEF) cross-sections an order of magnitude larger than those of conventional fluorophores such as fluorescein or rhodamine have been achieved.

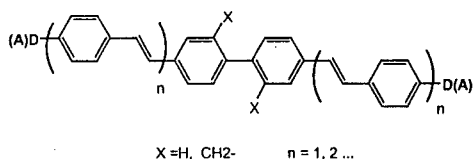
Molecular two-photon absorption (TPA) has found many applications over recent years, including optical power limitation, localised photochemistry, photodynamic therapy, three-dimensional optical data storage, microfabrication, etc. Applications that specifically require excited state fluorescence include two-photon-excited fluorescence (TPEF) microscopy [1] which has gained widespread popularity in the biology community for imaging purposes at an increased penetration depth in tissue with reduced photodamage. In most cases, TPEF microscopy applications have relied on molecules originally designed for one-photon fluorescence. It has become increasingly clear, however, that molecules specifically engineered for TPEF may significantly outperform these more conventional molecules [2]. Key ingredients for efficient molecular TPEF are a large two-photon absorption cross section σ_2 , and high fluorescence quantum yield Φ .

It has recently been reported that symmetrical phenylene-vinylene oligomers bearing electron-releasing (or electron-withdrawing) end groups can display very large σ_2 . Such behaviour seems correlated to a symmetrical quadrupolar charge redistribution occurring between the periphery and the centre of the molecule [2]. Following some of these guidelines, our strategy was to achieve pronounced two-photon absorption while maintaining high fluorescence quantum yields by the symmetrical grafting of two semi-rigid conjugated rods bearing either donor or acceptor terminal substituents onto a rigid conjugated central building block :



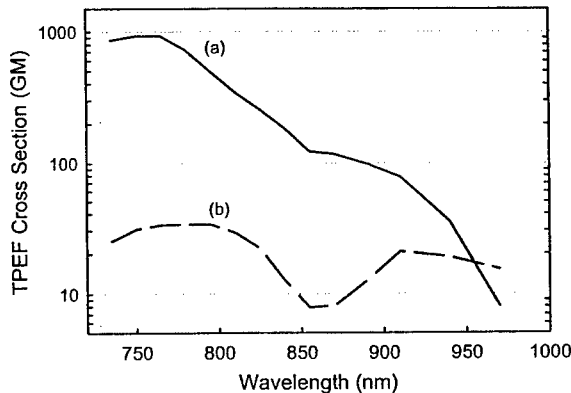
Both push-push and pull-pull elongated derivatives were prepared. Different central conjugated blocks derived from the biphenyl moiety and allowing the variation of the dihedral angle were selected in order to control fluorescence yield and quadrupolar charge redistribution :

Poster Session III



The two-photon excitation cross sections of this class of chromophores were determined by comparing the TPEF of molecules to that of fluorescein using a mode-locked Ti:sapphire laser operating between 730 and 970 nm and delivering 80 fs pulses at 80 MHz, following the experimental protocol described in details by Xu and Webb [3]. This allows the determination of the TPEF action cross section $\sigma_2 \Phi$. Pure σ_2 values can then be derived by determining the fluorescence quantum yield Φ from fluorescence measurements.

Figure 1 : Two-photon excited fluorescence spectrum of optimized quadrupolar fluorophore (D= NBu₂, X=CH₂, n=1) dissolved in DMSO (10⁻⁴ M) (a) and Fluorescein in water (b)



A number of quadrupolar chromophores indeed combine large two-photon absorption cross-sections *and* high fluorescence quantum yields. By playing on the nature of the end groups and tuning the central core, very large TPA cross-section (up to $\sigma_2 = 1.2 \cdot 10^{-47} \text{ cm}^4 \text{ s photon}^{-1}$) could be achieved. Thus, push-push fluorophores having a TPEF cross-section an order of magnitude larger (about $10^{-47} \text{ cm}^4 \text{ s photon}^{-1}$) in the visible red or near NIR than conventional fluorophores such as fluorescein or rhodamine B were obtained [4]. This spectral window is particularly advantageous for imaging in biological tissues. Pull-pull derivatives combining enhanced TPA cross-section *and* excellent transparency in a wide range of the visible region were also obtained. These compounds are particularly interesting candidates for optical power limitation in the visible region.

Finally, we have implemented a successful engineering route towards fluorophores which combine very large two-photon absorption cross sections and high quantum fluorescence yield. This opens interesting prospects for several applications, specially in the fields of two-photon microscopy and optical power limitation.

References

- [1] W. Denk, J. H. Strickler, W. W. Webb, *Science*, **248**, 73 (1990).
- [2] M. Albota *et al.*, *Science*, , **281**, 1653 (1998).
- [3] C. Xu, W. W. Webb, *J. Opt. Soc. Am. B.*, **13**, 481 (1996).
- [4] L. Ventelon, L. Moreaux, J. Mertz, M. Blanchard-Desce, *Chem. Commun.*, 2055 (1999).

Intermolecular Coupling Enhancement of the Molecular Hyperpolarizability in Multichromophoric Dipolar Dendrimers

S. Yokoyama, T. Nakahama, A. Otomo, S. Mashiko
Communications Research Laboratory
588-2 Iwaoka, Nishi-ku Kobe 651-2492, Japan

NLO dendritic macromolecules, called "azobenzene dendrimers", having a branching structure modified with a second-harmonic nonlinear optical chromophore has been synthesized. An electron donor and acceptor azobenzene chromophore, having a large molecular hyperpolarizability of $150\text{e-}30$ esu, was chosen. The electronic structure of synthesized dendrimers, which were expected to become dipolar due to their intermolecular attractive interaction, was proven by second-order nonlinear optical properties. The molecular hyperpolarizability of the dendrimer was measured by the hyper-Rayleigh scattering technique. The highest molecular hyperpolarizability was found to be $3,010\text{e-}30$ esu for an azobenzene dendrimer having 15 chromophoric unit. This level of molecular hyperpolarizability was much larger than that for a monomeric azobenzene chromophore.

Dendritic macromolecules, called dendrimers, are a new category of hyper-structured materials. Their widely branching polymeric chains and the high degree of control over regular molecular weight through stepwise synthesis have led to three-dimensional structures that are roughly spherical or globular [1, 2]. A variety of dendrimers have been studied to determine their characteristic chemical and physical properties. However, only a few reports describing a dendrimer having an electronically dipolar structure, which is essential for NLO activity, have been published. In our previous studies, we found, using the rod-shaped chromophore as the branching unit, that the dendrimers could be assembled in Langmuir-Blodgett monolayer films and that these films exhibited a large second-order susceptibility [3, 4]. In these molecularly assembled thin films, SHG activity was attributed to their microscopic second-order nonlinear susceptibility due to the molecular orientation and molecular packing structure. In this study, we describe our experimental and theoretical approaches to the design, synthesis, and molecular structure of dipolar dendrimers for NLO applications.

The synthesis method involves repeating coupling reactions of high molecular hyperpolarizability chromophore as the dendritic branching unit, and introduction of hydrophobic alkyl chains at exterior position. The chromophore chosen for the branching unit was azobenzene chromophore having an electron system coupled with electron donor and acceptor groups. The starting azobenzene chromophore exhibits SHG efficiency with a static molecular hyperpolarizability of $150\text{e-}30$ esu. This level of SHG response is comparable to or higher than that of the well studied NLO chromophores. The dendritic structure could be built up through a number of generation from one to four, G1-G4. The resulting G4 azobenzene dendrimer constructs of 15 units of chromophore.

For a semiempirical estimation of the molecular hyperpolarizability of azobenzene dendrimers, CNDO/S calculation was made on the optimized structures after molecular mechanics and molecular dynamics calculations. Calculated molecular hyperpolarizabilities were significantly depended on the number of generation and the intermolecular orientation of chromophore units. We made some model structures for calculations, which were

Poster Session III

a rod-shaped structure and a random structure. When the molecular axis of each chromophore was oriented to the chain direction in a rod shaped dendrimer, the molecular hyperpolarizabilities became large as the number of the generation increases. However, a centrosymmetric chromophore-chromophore interaction in a random structure decreased the values.

The experimental result by hyper-Rayleigh scattering measurement supported a rod shaped structure of the azobenzene dendrimers, where their molecular hyperpolarizabilities became large as the number of generation increased. We, further, found an enhancement of the nonlinear optical susceptibility of azobenzene dendrimers for the larger molecular size. On passing from the monomer to G4 dendrimer, molecular hyperpolarizabilities became 3.010×10^{-30} esu, which was much larger than that estimated when corresponding the simple additivity of the monomeric value. For explanation, we assumed cluster and/or molecular assembly model, where a local field corrections due to molecular-molecular interactions clearly began to play a large role in determining the macroscopic nonlinear optical activity. Synthesized linear NLO polymers with a random conformation never showed such an enhancement explained as a cluster model. Thus, enhancement of the nonlinear optical activity was essential for the dendritic structure, where each of the chromophoric unit arranged noncentrosymmetrically and became dipolar. We will discuss molecular conformation and molecular hyperpolarizability of the azobenzene dendrimers from both the theoretical and experimental aspects.

References

- [1] D. A. Tomalia, A. M. Naylor, W. A. Goddard III, *Angew. Chem. Ed. Engl.*, **29**, 138 (1990).
- [2] J. M. Frechet, *Science*, **263**, 1710 (1994).
- [3] S. Yokoyama, T. Nakahama, A. Otomo, S. Mashiko, *Chem. Lett.*, 1137 (1997).
- [4] S. Yokoyama, T. Nakahama, A. Otomo, S. Mashiko, *Thin Solid Films*, **331**, 248 (1998).

Octupolar molecular engineering for nonlinear optics

J. Zyss, I. Ledoux

LPQM – UMR 8537 – Ecole Normale Supérieure de Cachan
61 avenue du Président Wilson 94235 Cachan Cedex - FRANCE

Abstract : Various design strategies for two- and three-dimensional nonlinear octupolar molecules are derived from a general point charge template made-up of alternating charges at the edges of a cube. Applications to organic and organometallic molecules are discussed.

In the early 90's, the experimental evidence of frequency doubling in the 1,3,5-trinitro-2,4,6-triaminobenzene (TATB) crystal[1] based on the simplest octupolar extension of paranitroaniline, has triggered the opening of a broader molecular engineering avenue, whereby symmetry-ensured cancellation of the molecular dipole moment is shown to be compatible with non-zero and significantly larger β tensor coefficients than for the purely dipolar scheme. Moreover, earlier 1-D systems have been embedded in the broader realm of multipolar systems whereby the quadratic nonlinearity of any molecule can be decomposed in rotationally invariant dipolar and octupolar components. Full exploitation of the tensorial character of β has thus permitted to enlarge the pool of candidate molecular structures to more isotropic 2-D and 3-D multipolar systems[2], whereas a n -level model (where $n > 2$) has been shown to adequately describe the frequency dispersion of multipolar β tensors[3].

Point charge templates made-up of alternating charges at the edges of a cube[2] (Fig. 1) embody the essence of octupolar molecular structures, and exhibit T_d (resp. D_{3h}) symmetry features in the 3-D (resp. 2-D) cases. The implementation in real structures of the basic cubic point charge template has followed so far two main avenues in the realm of 2-D structures:

- a central π -electron reservoir mediating intramolecular charge transfer (ICT) interactions between peripheral electro-active side groups (Fig. 2a). Examples are 1,3,5 benzene[4] or triazine derivatives[5].

- a donor (acceptor) atom standing at the cornerstone of the molecular structure mediating a multipolar ICT interaction with three accepting (donating) groups through a conjugated system (Fig. 2b). Typical systems are Crystal Violet[6] and oligothieryl analogues[5], or Ru^{II} (2,2'-bipyridine)₃ complexes[7], or subphthalocyanines[8].

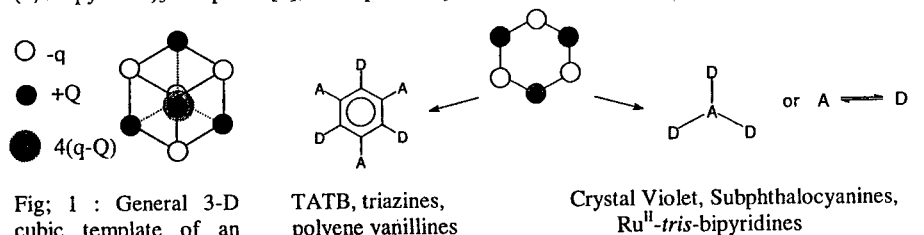


Fig. 1 : General 3-D cubic template of an octupolar system mapped onto a 2-D D_{3h} octupolar structure after projection of the cube along one of its diagonals. The $4(q-Q)$ charge is at the center of the cube

TATB, triazines, polyene vanillines

Figure 2a

Crystal Violet, Subphthalocyanines, Ru^{II} -tris-bipyridines

Figure 2b

Fig. 2 : Various implementations of 2-D octupolar molecular engineering strategies : central π -electron system (2a) and central atom (2b) based structures .

Poster Session III

Design of efficient 3-D structures is mainly illustrated by metal complexes. The structures allow for rich 3-D hybridization schemes, and provide appealing possibilities for the octupolar engineering of 3-D molecules, in view of their potentially available symmetry features, metal core oxidation potential, open-shell electronic structures, and the ability of built-in chirality. Tetrahedral covalent bonding or complexation, as derived from the very general 3-D cubic octupolar scheme made of two intricate donor or acceptor tetrahedral substructures results in efficient T_d octupolar systems such as tetrasubstituted tin derivatives[9] (Fig. 3a), or tetrahedral copper bipyridine complexes (Fig. 3b)[10]. Purely organic alternatives such as based on functionalized biphenyls [11] (Fig. 3c) or paracyclophane derivatives (Fig. 3d)[12] will also be discussed. For all these systems, experimental values mainly based on polarized harmonic light scattering [13] will be presented and discussed in the light of a quantum molecular modeling by a n -level model and a transparency-efficiency figure of merit.

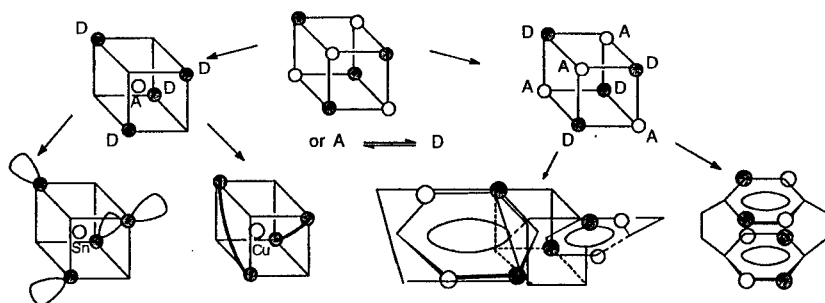


Figure 3a

Figure 3b

Figure 3c

Figure 3d

Figure 3 : Various engineering strategies of octupolar 3-D molecules : centered tetrahedral covalent Sn derivative (3a) , Cu^{II} bis-bipyridine complex (3b), fully tetrahedral purely organic biphenyl (3c) and paracyclophane derivative (3d).

- [1] I. Ledoux, J. Zyss, J.S. Siegel, J. Brienne, J.M. Lehn, *Chem. Phys. Lett.* **172**, 440 (1990)
- [2] J. Zyss, *Nonlinear Optics* **1**, 3 (1991); J.Zyss, *J. Chem. Phys.*, **98**, 6583 (1993).
- [3] M.Joffre, D.Yaron, R.Silbey, J.Zyss, *J.Chem.Phys.* **97**, 5607 (1992); S. Brasselet and J. Zyss, *J. Nonlinear. Opt. Phys. Mater.*, **5**, n°4, 671-693 (1996).
- [4] C. Andraud, T. Zabolon, A. Collet and J. Zyss, *Chem. Phys.*, **245**, 243 (1999).
- [5] S. Brasselet, F. Cherioux, P. Audebert and J. Zyss, *Chem. Mater.* **11**, 1915 (1999).
- [6] J. Zyss, C. Dhenaut, T. Chau Van, I. Ledoux, *Chem.Phys.Lett.*, **206**, 409 (1993).
- [7] C.Dhenaut, I.Ledoux, I.Samuel, J.Zyss, M.Bourgault, H.LeBozec, *Nature*,**374**,339 (1995).
- [8] A. Sastre, T. Torres, M.A. Diaz-Garcia, F. Agullo-Lopez, C. Dhenaut, S. Brasselet, I. Ledoux, J. Zyss, *J. Am. Chem. Soc.* **118**, 2746 (1996).
- [9] M. Lequan, C. Branger, J. Simon, T. Thami, E. Chauchard, A. Persoons, *Chem.Phys.Lett.***229**, 101 (1994).
- [10] T.Renouard, H. LeBozec, S. Brasselet, I. Ledoux and J. Zyss, *Chem. Comm.*, 871 (1999).
- [11] M. Blanchard-Desce, J-B. Baudin, L. Jullien, R. Lorne, O. Ruel, S. Brasselet and J. Zyss, *Opt. Mater.*, **12**, 333 (1999).
- [12] J. Zyss, I. Ledoux, G. Bazan and S. Mukamel, unpublished results (1999).
- [13] J. Zyss and S. Brasselet, *J. Nonlin. Opt. Phys. Mat.*, **7**, 397 (1998).

Nonlinear third-order optical susceptibilities of some metallo-complexes compounds

B. Sahraoui, J. A. Weinstein^(a), M. Ya. Mel'nikov^(a), N. N. Zheligovskaya^(a) and X. Nguyen Phu

Laboratoire des Propriétés Optiques des Matériaux et Applications, CNRS EP 130
Université d'Angers, 2, Boulevard Lavoisier, 49045 Angers cedex (France).

^(a)Departement of Chemistry, Moscow Lomonosov State University, Moscow
117234 (Russia)

Research of new materials which have great potential for use in non-linear optical devices, is one of the current interesting subject of investigations [1-2]. Due to their efficiency, chemical flexibility, metallochromophore have received considerable attention as material for non-linear optics. The syntheses and the study of spectroscopic UV/VIS, resonance Raman of The studied compounds are given in [3]. The chemical structures and their optical spectra are presented in fig .1 and fig .2 respectively.

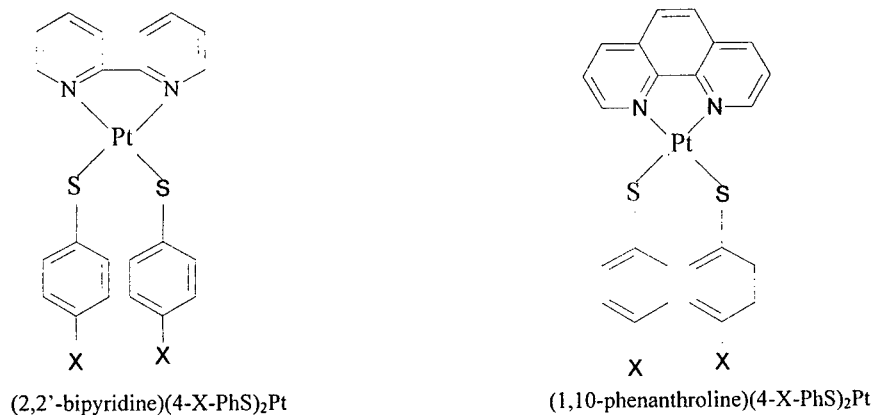


Fig.1 Chemical structures of studies compounds

We will report the measurement of nonlinear third-order optical susceptibilities of metallo-complexes compounds: (2,2'-bipyridine)(4-X-PhS)₂Pt, (1,10-phenanthroline)(4-X-PhS)₂Pt in solutions using the degenerate four wave mixing technique at 532 nm in

Poster Session III

picosecond regime. The obtained value for the best compound in term of $\chi^{(3)}$ (10^{-20} m^2/V^2) is larger than the value obtained for CS_2 , which is a reference material. A correlation between chemical structures and NLO properties will be presented. The merit factor for each compounds will be given and the obtained results will be compared to those obtained previously on analogues of tetrathiafulvalenes [3-5]

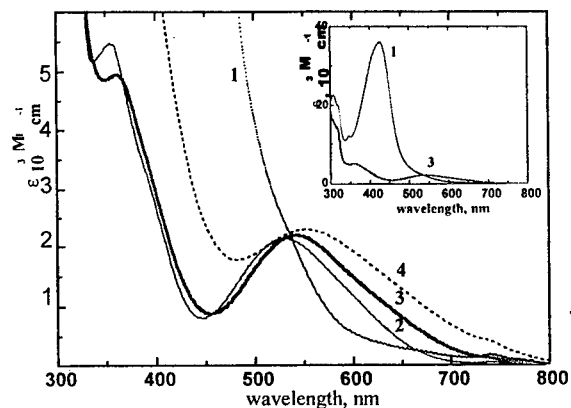


Fig.2 Absorption spectra in THF at 298 K for compounds: 1, 2, 3 and 4.
1, 2, 3, 4 represent respectively, $\text{Pt}(\text{bpy})(4\text{-NO}_2\text{-PhS})_2$; $\text{Pt}(\text{bpy})(\text{PhS})_2$; $\text{Pt}(\text{bpy})(4\text{-CH}_3\text{O-PhS})_2$; $\text{Pt}(\text{bpy})(4\text{-(CH}_3)_2\text{N-PhS})_2$

References

- [1] J. Zyss, ed., *Molecular Nonlinear Optics : Materials, Physics and Devices*, (Acad., Boston, 1994)
- [2] F. Kajzar, C. Taliani, R. Zamboni, S. Rossini, R. Danieli, *Synthetic Metals* 77, 257-263, (1996)
- [3] J. A. Weinstein, N. N. Zheligovskaya, M. Ya. Mel'nikov and Franstisk Hartl, *J. Chem. Soc., Dalton Trans.*, 2459-2466 (1998).
- [4] B. Sahraoui, X. Nguyen Phu, M. Sallé and A. Gorgues, *Optics Letters*, Vol.23, No.23, p.1811, (1998)
- [5] B. Sahraoui, X. Nguyen Phu and G. Rivoire, T. Nozdryn, J. Cousseau, *Synthetic Metals*, Vol. 94/1, 57-60 (1998)

New Quinoline-Based Thermally Stable Polymers

S. Concilio
*Department of Chemical Engineering
University of Salerno,
via ponte Don Melillo I-84084 Salerno*

N. Tirelli
*Institute of Biomedical Engineering
Department of Materials, ETH and University of Zürich,
Moussonstr. 18, CH-8044 Zürich*

P. Pfister, U. W. Suter
*Institute of Polymers, Department of Materials, ETH Zürich,
Universitätstr. 6, CH-8092 Zürich*

New quinoline-based homo- and copolymers have been synthesized and investigated as high-temperature resistant materials for NLO applications. The synthetic method used the acid-catalyzed Friedlaender condensation between a bis(*o*-amino ketone) and two silicon containing bis(ketomethylene) monomers. Starting from these silicon containing polyquinolines, two block-polyamide-polyquinoline materials were also prepared in order to improve the processing properties of the final material without significantly lowering its thermal stability. The combination of good thermal, mechanical, and optical features in the resulting polymers is promising for the development of EO devices.

Conjugated polymers have gained widespread interest as electronic and nonlinear optical materials. Among these, fully aromatic polyquinolines, the synthetic chemistry of which has been developed by Stille in the 70's [1,2], are among the most promising materials due to their high glass-transition temperatures and excellent thermal stability.

Synthesis of homo- and copolymers

We have recently prepared polyquinolines containing quaternary silicon atoms. Silicon enhances the torsional mobility and flexibility of the main chain, possibly contributing to overcoming the usual limits in solubility and processing of fully aromatic polymers.

A series of six new homo- and copolymers, containing quinolines groups linked to a variety of aromatic groups along the main chain, have been prepared from two new bis(ketomethylene) silicon monomers.

These two new monomers have first been condensed with two aromatic bis(*o*-amino ketone) monomers to afford the silicon containing polyquinolines. The polycondensation reaction was acid-catalyzed and carried out in a mixture of *m*-cresol and di-*m*-cresyl phosphate.

Some processing difficulties brought us to design new block copolymers based on a polyamide-polyquinoline structure (see Fig. 1).

This copolymerization results in improving the solubility without significantly lowering the softening temperature of the final material.

Poster Session III

Characterization data

The glass-transition temperatures of the new polymers, measured by differential scanning calorimetry, fall in the range 260-330 °C and thermogravimetric analysis shows that all decomposition temperatures in air are near 600 °C.

The synthesized polymers are all completely amorphous, as confirmed by X-ray diffraction pattern collected on powder samples.

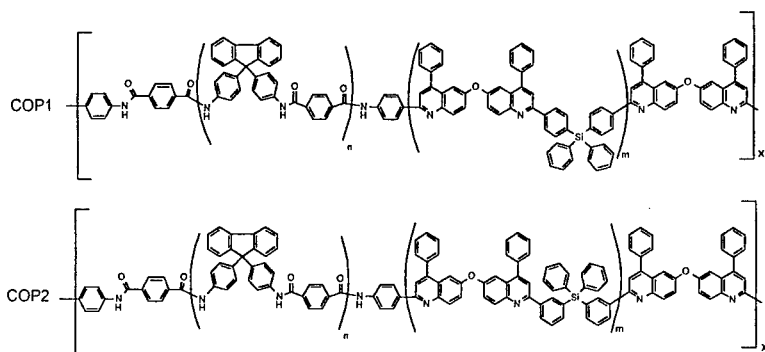


Figure 1: Structures of the two amide-quinoline copolymers.

For the copolymers COP1 and COP2, the structures of which are reported in Figure 1, it was also possible to measure optical properties in solution. Absorption and fluorescence spectra were recorded in the UV-VIS-NIR region and showed intense absorption peaks at 280-396 nm and emissions bands in the violet-blue region (370-420 nm).

Moreover, the good solubility of the copolymers in N-methyl-2-pyrrolidone at room temperature allowed facile processing to thin films of optical quality.

Outlook

Because of their good thermal and processing properties, these new quinoline-based polymers can be used as highly stable materials, e.g., for hosting NLO chromophores, or for photoconductive applications.

References

- [1] J. K. Stille, "Polyquinolines: versatile aromatics with diverse properties", *Pure & Appl. Chem.* **50**, 273-280 (1978).
- [2] W. H. Beever, J. K. Stille, "Polyquinolines: a class of rigid-chain polymers", *J. Polym. Science: Polym. Symp.* **65**, 41-53 (1978).

Performance of Organic Light Emitting Devices Based 8-hydroxyquinolato Boron Emitters

Marie D'Iorio and Ye Tao

*National Research Council Canada, Institute for Microstructural Sciences
Ottawa, Ontario, Canada, K1A 0R6*

Suning. Wang, Qing-guo Wu and James Lavigne

*Department of Chemistry, Queen's University
Kingston, Ontario, Canada K7L 3N6*

Since the realisation that amorphous films of sublimed molecular materials could be used for the fabrication of efficient light emitting devices, there has been a quest for stable and efficient materials emitting in the blue green range of the visible spectrum. Based on the encouraging performance of organoboron compounds based on 7-azaindole, we have investigated boron chelate compounds with 8-hydroxyquinolines. We report on the absorption and emission properties of these materials and their performance when integrated in an organic light emitting device structure as an emitter layer.

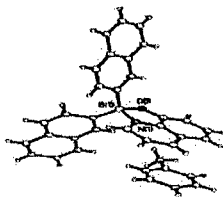
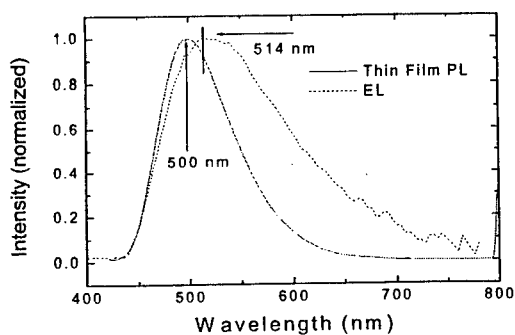
The development of organic light emitting devices (OLEDs) has relied on organic and organo-metallic/coordination compounds as electroluminescent molecular materials of choice [1-3]. One of the best known electron transport material and emitter used in the fabrication of organic light emitting devices is Alq₃ in which three 8-hydroxyquinolato ligands chelate to the Al(III) ion in an octahedral configuration. Studies on long term stability of OLEDs have suggested that performance degradation is linked to the interdiffusion of the Alq₃ layer into the TPD hole transport layer through local Joule heating and subsequent decrease in conductivity and current flux [4]. Recent studies on blue emitters of organo metallic/coordination compounds have used blue emitting chelating ligands bound to a central atom by N and O donors. When boron is used as a central atom, the larger covalency of the boron-ligand bond enhances the stability of the compound as was demonstrated in compounds containing 7-azaindole [5]. In this study we focus on the luminescence properties of a boron (2-naphthalene)₂ 8-hydroxyquinolato compound.

Single-crystal X-ray diffraction analysis reveals a tetrahedral geometry to boron (2-naphthalene)₂ 8-hydroxyquinoline. This compound has a melting point of ~214 C and sublimes at 160 C at 0.1 mm Hg. The 2-naphthyl groups are thought to be responsible for the high melting point by enhancement of the intermolecular π - π interactions and improved packing of the molecules in the solid state. The compound was purified by vapor train sublimation prior to fabrication of EL devices. Our devices were fabricated by thermal evaporation at 1×10^{-7} Torr and the sublimation conditions were similar to that of Alq₃. Light emitting devices were fabricated on patterned ITO on glass substrates with 30 nm of TPD (4,4'-di(n-(2-methyl)phenyl-N-phenylamino)biphenyl) as a hole transport layer, 30 nm of BR₂q (where R=2-naphthalene and q = 8-hydroxyquinolato) as the emitter layer, 10 nm of PBD (2-(4-biphenyl)-5-(4-tert-butylphenyl)-1,3,4 oxadiazole) as an electron transport material, 60 nm of Ca and 120 nm of Al as cathode materials. The current-voltage characteristics were measured using a Keithley 238 current/voltage source while the electroluminescence was obtained using a Photo Research 650

Poster Session III

spectracolorimeter. The thin film photoluminescence measurements were obtained using an ISA Jobin-Yvon-SPEX Fluorolog 3 spectrometer. The devices showed clear rectifying behavior in their current-voltage characteristics with a turn-on voltage between 5-10 V. The emission of the boron(2-naphthalene)₂ 8-hydroxyquinolato compound shown below 2 is centered in the blue-green part of the spectrum at 500 nm. The electroluminescence of the device is centered at 514 nm and a maximum luminance of 55 cd/m² was measured before breakdown at 24 V.

The 8-hydroxyquinoline boron complex provides blue-green photoluminescence and displays excellent electron transport properties. The high melting point is attributed to increased intermolecular interactions in the solid state. Further investigation of boron compounds may lead to a new class of electron transport materials for light emitting display applications.



References

- [1] C.W. Tang, S.A. Van Slyke, *Appl. Phys. Lett.* **51**, 913 (1987).
- [2] Y. Shirota, Y. Kuwabara, H. Inada, T. Wakimoto, H. Nakada, Y. Yonemoto, S. Kawami, and K. Imai, *Appl. Phys. Lett.* **65**, 807 (1994)
- [3] C. Adachi, S. Tokito, T. Tsutsui, and S. Saito, *Jpn. J. Appl. Phys.* **27**, L713 (1988); C. Adachi, T. Tsutsui, and S. Saito, *Appl. Phys. Lett.* **56** 799 (1990); Z. Shen, P. E. Burrows, V. Bulovic, S. R. Forrest, and M. E. Thompson, *Science* **276**, 2009 (1997); H. Aziz, Z. D. Popovic, N.-X. Hu, A.-M. Hor, and G. Xu, *Science* **283**, 1900 (1999).
- [4] M. Fujihira, Lee-Mi Do, Amane Koike, Eun-Mi Han, *Appl. Phys. Lett.* **68**, 1787 (1996).
- [5] W. Liu, A. Hassan, and S. Wang, *Organometallics* **16**, 4257 (1997); J. Ashenurst, L. Brancalione, A. Hassan, W. Liu, H. Schmider, S. Wang, and Q. Wu, *Organometallics* **17**, 3186 (1998); Q. Wu, M. Esteghamatian, N.-X. Hu, Z. D. Popovic, G. Enright, S. R. Breeze, S. Wang, *Angew. Chem.Int.Ed.* **38**, 985 (1999).

Hetero-layer light-emitting devices based on PPQ/PPV/TPQ films

P. Imperia, S. Schrader, M.B. Casu

Universität Potsdam Institut für Physik LS PKM Am Neuen Palais 10 D-14469
Potsdam Germany

M. Jandke, P. Strohrriegl

Universität Bayreuth Makromolekulare Chemie I D-95440 Bayreuth

Polymer hetero-layer structures were realized by combination of hole transporting materials like polyparaphenylenevinylene (PPV) with new electron transporting materials i.e. heterocyclic polymers (PPQs) and heterocyclic low molecular compounds especially phenylquinoxalines (PQs) and trisphenylquinoxaline (TPQ). The PPQs, PQs, and TPQ are studied by combined investigations of thermally stimulated discharge current (TSDC), thermally stimulated current (TSC), dielectric relaxation spectroscopy (DES), ultraviolet photoelectron spectroscopy (UPS), near edge X-ray absorption fine structure (NEXAFS) and optical spectroscopy.

Separating the light-emitting volume from the ones which are assigned to charge injection or transport is one approach to increase the performance of organic light emitting devices. We realised such polymer hetero-layer structures by combination of hole transporting materials like polyparaphenylenevinylene (PPV) with new electron transporting materials, i.e. heterocyclic polymers and heterocyclic low molecular compounds, especially phenylquinoxalines (PQs), polyphenylquinoxalines (PPQs) and trisphenylquinoxalines (TPQs). The PPQs and TPQ, shown in figure 1, suitable as electron-transporting / hole-blocking layer in OLED devices, are studied by several investigation techniques like thermally stimulated discharge current (TSDC), thermally stimulated current (TSC), dielectric relaxation spectroscopy (DES), ultraviolet photoelectron spectroscopy (UPS), near edge X-ray absorption fine structure (NEXAFS) and optical spectroscopy.

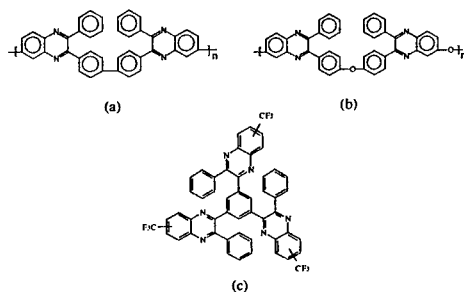


Fig. 1: Chemical structures of two types of polyphenylquinoxaline (PPQ): (a) PPQ 1A, and (b) PPQ 1B and (c) trisphenylquinoxalines (TPQ).

Measurements were carried out both on films (30 μm) and thin layers (20-80 nm). Films were prepared by solution-casting, thin layers by spin-coating and in situ evaporation from pinhole sources for UPS investigations. The UPS measurements were performed using an ADES 400 spectrometer at the TGM2 beamline at BESSY I, Berlin. We also performed a

Poster Session III

theoretical simulation of the valence band region. The results were obtained using a semi-empirical quantum mechanical calculation method (PM3, AM1). The good agreement between the experimental and the theoretical curve allows to assign the different features of the spectra to the related molecular orbitals. PQs and TPQ show electron affinities near 3.5 eV and ionisation potentials near 6 eV. The figure 2 shows the valence electronic structure of TPQ and the quantum chemical simulation.

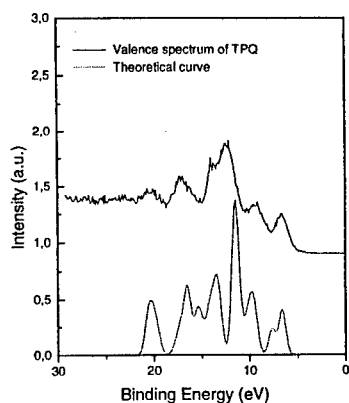


Fig. 2: Valence electronic spectrum of TPQ given with respect to the vacuum level set at zero and theoretical calculation.

The electrical measurements on PPQs and TPQ single layers were performed in order to study the transport properties of the materials. As expected both behave like insulators reaching a conductivity of about 2×10^{-9} S/m at 300 K decreasing with temperature.

Different peaks of TSDC spectra are observed. They originate both from dipolar and from carrier relaxation processes. TSDC peaks were analysed in order to get more detailed information about the processes taking place in the samples. The dipolar processes show activation energies between 0.4 eV and 1 eV which are typical values for small relaxing entities like polymer side groups. Current-voltage (I-V) and current-luminance (EL-V) characteristics were used to study the prepared heterolayer devices. Double and triple layers made of PPV and both PPQ and TPQ are characterised by low onset voltages near 2 V and high luminous efficiency at rather moderate voltages. At a bias of 7 V a brightness of about 250 cd/m² is achieved, which is already well suitable for the application in flat screen displays. The efficiency of these devices at this brightness reaches 0.7 lm/W, which is only slightly lower than the maximum efficiency of 0.75 lm/W obtained for lower driving voltages. More than 1000 cd/m² were reached above a driving-voltage of 10 V. The experimental findings show that PPQs and TPQs are promising materials in the field of organic electroluminescence.

Ultra High Vacuum reveals interface-dependent charge-injection properties of Organic Light Emitting Diodes, and the effects of exposure to impurity gases

M. Kiy*, I. Gamboni, I. Biaggio, and P. Günter

*Institute of Quantum Electronics, Swiss Federal Institute of Technology
ETH-Hönggerberg, CH-8093 Zürich, Switzerland*

*e-mail: kiy@iqe.phys.ethz.ch, [www: http://nlo-serv.ethz.ch](http://nlo-serv.ethz.ch)

We observed the influence of impurity gases on the performance of organic light emitting diodes. Using ultra-high vacuum for the fabrication and characterization we are able to measure the intrinsic performance without any uncontrolled influence of impurity gases.

Despite the fact that Organic Light Emitting Devices (OLEDs) have reached ever better results in terms of their efficiency and lifetime during the last few years, there are still many behaviors and mechanism that are only little known. The influence of trace-gases on the OLED performance and lifetime has not received a great amount of attention yet, but its investigation is very important in order to gain a deeper understanding of the fundamental physical and chemical processes taking place in an OLED structure. Although the best lifetimes to-date have been demonstrated with encapsulated devices, a better knowledge about the effects of impurity gases could allow the development of better encapsulation techniques, or even of OLEDs which are stable enough in air.

In order to systematically control the influence of gases, one must be able to work in as much a gas-free environment as possible to determine the intrinsic "clean" properties of an OLED. We found that only an Ultra-High-Vacuum (UHV) environment, with a impurity gas pressure of 10^{-9} mbar or below, fulfills adequately these conditions. At these levels of pressure/purity, one needs some hours to adsorb a monolayer gas on a surface.

The OLEDs were produced inside this UHV system using evaporation from effusion cells onto Indium Tin Oxide (ITO) coated glass substrates. We patterned the ITO with photolithography and used two masks during the deposition. Never did the devices leave the UHV system, during the different deposition steps, or during any other manipulation. While always staying in UHV, the samples are moved to a special UHV chamber to characterize their electrical and electroluminescent properties of the device.

The injection properties of OLEDs are influenced by the injection barrier heights. For a small electron injection barrier from cathode to organic material, low work function metals are good candidates. Elements like Mg, Ca, Sr, Li, Al have a low work function, but they are very reactive and change there electronic properties under humidity and oxygen environment, another fact that requires the use of a UHV system to study the intrinsic properties of the charge-injection system.

An additional fact to consider at the cathode-organic interface, is that many metals diffuse inside the organic material during the deposition, leading to an non-sharp interface (reported in [1] for Ca on Alq₃ and [2] for Mg on Alq₃). There exists an interdiffusion layer with different electronic properties. In [3] we reported that this diffusion does not deteriorate the device performance in the case of Mg and Alq₃.

For the measurements we produced a very simple bilayer device structure on a glass substrate coated with an Indium Tin Oxide (ITO) anode (~ 30 nm), the hole trans-

Poster Session III

port layer NPB (N,N' -bis-{1-naphthyl}- N,N' -diphenyl-1,1'-biphenyl-4,4'-diamine, ~ 40 nm) and Alq_3 (tris {8-hydroxyquinoline aluminium}, ~ 65 nm) as an electroluminescent layer, and with Mg (~ 200 nm) as cathode material.

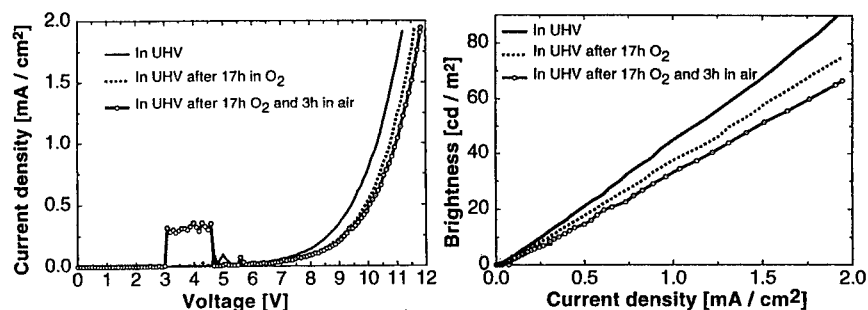


Figure 1: Current density versus. voltage (left) and brightness versus. current density (right) of an OLED running in UHV as deposited and after exposure to different impurity gases.

We measured the current versus voltage characteristic and the brightness versus current characteristic of a device directly after the fabrication, after 17 hours exposure to pure oxygen and after storing 3 hours in air (Figure 1).

The threshold voltage for electroluminescence increases after exposure to oxygen, while the efficiency is lower compared to the performance in the UHV. Also after a short, three hours exposure to air, we observed a degradation of the performance measured in UHV.

If we bring the devices a longer time (17 hours) into contact with air we can also see some black spots in the UHV environment. However, despite the black spots, we observe in this case a higher efficiency accompanied by a higher threshold voltage. The reason for this observation is not yet known.

We conclude that the ability to fabricate and fully characterize OLEDs under the controlled influence of gases, or their almost complete absence in a UHV system, is very important. By measuring electroluminescence data of OLEDs fabricated and operated in the ultra-pure conditions of an UHV system we obtained several interesting results, examples of which are the direct observation that no black spots appear if the sample does not come into contact with impurities. Also, oxydation and reaction within humid atmosphere changes the injection properties and efficiency.

References

- [1] M. Probst and R. Haight, "Diffusion of metals into organic films," *Appl. Phys. Lett.* **70**, 1420 (1997).
- [2] A. Rajagopal and A. Kahn, "Photoemission spectroscopy investigation of magnesium/ Alq_3 interfaces," *J. Appl. Phys.* **84**, 355 (1998).
- [3] M. Kiy, I. Gamboni, U. Suhner, G. Conradin, I. Biaggio, and P. Günter, "Interface dependent electrical properties of organic light emitting devices in ultra-high vacuum," *Synth. Met.* accepted for publication (2000).

Blue Organic Light-Emitting Diode Based on Dipyrvole3

WeiLing Guo*, E. Herbert Li¹ ChiMing Che¹ Yi zhao² and Shiyong Liu²
 (1 Department of EEE and Chemistry, The University of Hong Kong; 2 Jilin University, Jilin 110015, China)

Abstract: We reported a new organic material, Dipyrvole3, which can emit a pure blue light when used as a emitting layer. The blue organic light emitting diode (OLED) was fabricated employing the Dipyrvole3 as a blue dye material doped into a BePP2 host. These devices' peak wavelength are 448nm and the full width at half maximum is 75nm. The maximum luminance is 1400cd/m² at a voltage of 13V. The peak power efficiency is 0.23lm/W at a voltage of 9V.

Organic Light-emitting diodes (OLEDs) have drawn considerable interest due to their potential use as a means for full color display. Much progress has been made and the device performance has increased dramatically since then. Full color display needs integrate light emitting devices of three different colors onto a single substrate[1-2]. In search of blue-light emitting devices, scientists have spent the last few years designing and modifying the architecture of some candidate organic materials, but till now blue light devices have not been as successful as green and red devices[3-5]. In this paper, we present a simple blue light OLED using a new organic dye material Dipyrvole3, the maximum luminance obtained for the device was 1610cd/m².

A new chemical compound Dipyrvole3 is used for emitting layer and the OLED emits a pure blue light. The Device structure were shown in Fig.1, The device structure is Al/Dipyrvole3/NPB/CuPc/ITO. The synthesis and chemical properties of Dipyrvole3 will be reported later. Figure 2 shows the electro-luminescence (EL) spectrum of this device, the Dipyrvole3's emission peak is at 448nm. The device is not very bright due to the "self-quenching".

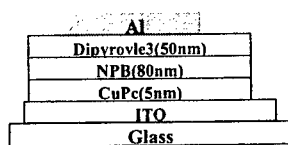


Fig.1 The cell configuration of OLED with a structure as: IO/CuPc/NPB/Dipyrvole3/Al.

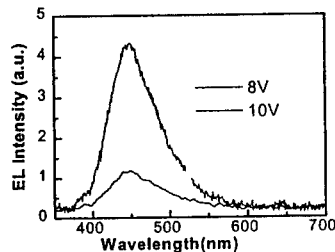


Fig.2 EL emission spectrum of the Al/Dipyrvole3/NPB/CuPc/ITO at two different voltages.

A Doped OLED was fabricated where Dipyrvole3 was used as a blue luminous dye. The device structure was shown in Fig.3. (CuPc) was used as a buffer layer (5nm) and (NPB) was used as a hole transport layer. BePP2 layer doped with

Poster Session III

Dipyrovle3 (blue fluorescent dye) was used as a emitting layer, the ratio of BePP2:Dipyrovle2 is 100:4. The Organic materials were grown by organic molecular beam deposition system, the chamber pressure was maintained below 2×10^{-4} Pa and the thickness were determined by an oscillating quartz thickness monitor. Then samples were transfer to another evaporator in air, and Aluminum(Al) was thermal deposited as cathode. Current-voltage and luminance characteristics of devices were measured in forward bias. All device testing was done in atmosphere.

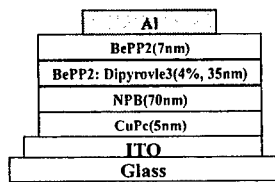


Fig.3 Schematic cross-section of OLED where Dipyrovle3 used as a blue luminous dye.

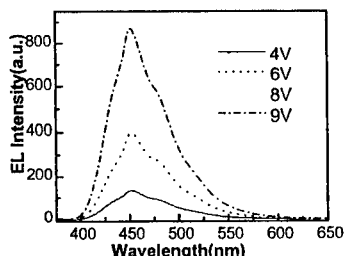


Fig. 4 Electroluminescence device spectrum for ITO/CuPc/NPB/BePP2:Dipyrovle3(4%)-/BePP2/Al devices.

Figure 4 shows the EL emission spectrum of the doped device at different voltage. The peak wavelength of this devices is 452nm and the full width at half maximum is 75nm. There is no wavelength shift as the voltage increasing. In fig.5, we plot luminance and current as functions of voltage. The peak luminous is 1400 cd/m^2 at a voltage of 13V. The peak power efficiency for this devices is 0.23 lm/W at a voltage of 9V.

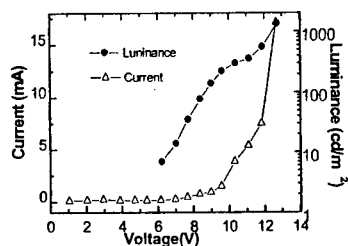


Fig.5 Current and Luminance vs voltage for ITO/CuPc/NPB/BePP2:Dipyrovle3(100:4)/BePP2/Al devices.

We note the device structure has the potential for further optimization. For example, the use of LiF cathodes and novel hole transport materials, the doping density that result in a reduction in operation voltage or increased quantum efficiency are also applicable to this work. So the blue emission from Dipyrovle3 has potential to fabricated some high performance OLED, the work will be continued.

This work was supported by China State Key lab opening project in optoelectronic Lab, Jilin University. The authors would like to thanks Li Feng for his help in fabrication and measurements and thanks Prof. Niu Zhongguo for his help in traveling and living in Changchun.

Organic DFB-lasers with mode emission tuneability by dynamic and permanent photoinduced gratings

G. Kranzelbinder, E.Toussaere, R. Mathevet, D. Josse, J. Zyss

Laboratoire de Photonique Quantique & Moléculaire (UMR CNRS 8537), ENS Cachan, France

email: kranzelb@lpqm.ens-cachan.fr, tel.: ++ 33 147 40 55 60; fax: ++ 33 147 40 55 67

We show continuously tuneable polymeric DFB-lasers (600-640 nm) to be controlled by dynamic and permanent photoinduced in-plane gratings. A "write & read-technique" for multiple solid-state laser mode emission is presented.

1. Introduction

Solid state organic luminescent materials, conjugated polymers and systems based on organic small molecules attract a revival of interest as innovative approaches towards solid-state photonic applications including display and laser technology, as well as telecommunication applications in view of a number of technological and functional assets [1-4].

2. Results and Discussion

Thin film samples are spin-coated from solution onto planar substrates and graded index waveguides are prepared by dye-doping polymeric plates via a solvent assisted in-diffusion process. In our experiment we make use of the Lloyd-mirror configuration to evidence distributed feedback (DFB) laser emission via photoinduced gratings. In this experiment the sample is photo-pumped by the periodic fringing pattern of a two-beam interference configuration (Fig.1a). The optical distributed feedback structure is provided by the in-plane grating which results from the spatial modulation of gain and refractive index. The spectral position of the laser mode emission can be continuously tuned by variation of the interference incidence angle. We observe laser mode emission over a broad spectral range of more than $\Delta\lambda = 40$ nm and with a spectral mode of FWHM width narrower than 1nm (Fig.1b).

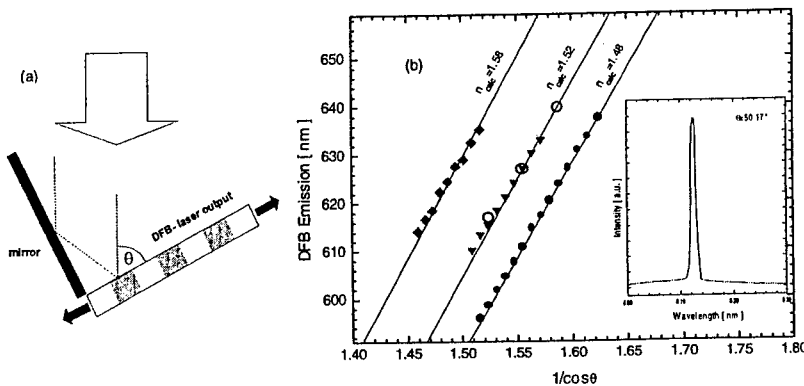


Fig.1 : Distributed feedback laser emission; (a) Lloyd mirror set-up: the angle θ is varied to change the pump grating periodicity ; (b) DFB-laser emission (FWHM<1nm)of DCM doped in different polymer matrices DCM:PC (n=1.58),DCM:PMMA (n=1.52) and in-diffused DCM:plexiglass (n=1.48).

Poster Session III

At high excitation densities the feedback mechanism can be permanently imprinted. In this way one can determine the emission wavelength by setting the writing interference angle θ and imprinting this wavelength results in a laser device that can be pumped from an arbitrary angle (see fig.2).

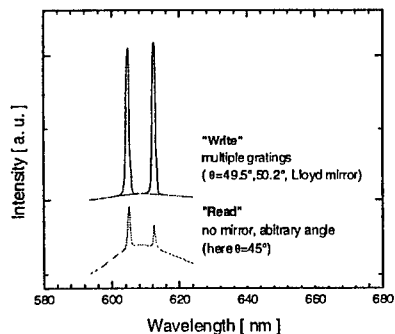


Fig. 2: Writing and Reading of multiple DFB structures;

This optical "write & read technique" can be advantageously combined with the waveguiding properties of different structures. Single and multiple grating devices can be designed following waveguide construction rules and optimized with respect to optical loss and polarization. This property provides a versatile fabrication tool for organic integrated optics and opens new application perspectives in the realm of local network communications.

References

- [1] H. Kogelnik, C.V. Shank, Appl.Phys.Lett. **18** (1971) 152.
- [2] Z. Bor, A. Mueller, B. Racz, F.P. Schaefer, Appl. Phys. B **27**, (1982) 77.
- [3] W.J. Wadsworth, I.T. McKinnie, A.D. Woolhouse, T.G. Haskell, Appl.Phys. B **69**, (1999) 163.
- [4] J.-M. Nunzi, F. Sobel, D. Gindre, B. Sahraoui, C. Denis, V. Dumacher, C. Fiorini, B. Paci, L. Rocha, Proceedings of the SPIE Conf., Denver '99 (in print)

Influence of hole transporting materials on the properties of organic LED

Zugang Liu, Jorge Soares, Estela Peireira

Universidade de Aveiro, Departamento de Física, 3800 Aveiro, Portugal

Email:zugang@fis.ua.pt

We compare the properties of some multilayer organic light emitting diodes based on emission layers (EML) tris-8-hydroxyquinoline aluminium (Alq3) and bis-8-hydroxyquinoline zinc (Znq2) and some hole transport layers (HTL). The HTL materials used are 4,4',4"-tris (3-methyl-phenylphenylamino) triphenylamine (m-MTDATA), N,N'-bis-(1-naphthyl)-N,N'-diphenyl-1,1'-biphenyl-4,4"-diamine (NPB), N,N'-diphenyl-N,N'-bis(3-methylphenyl)-(1,1'-biphenyl)-4,4"-diamine (TPD), and (N-p-methoxyphenyl-N-phenyl)-p-methoxyphenyl-styrylamine (SA). The electroluminescent (EL) spectra of the devices and their current voltage, luminance voltage characteristics have been investigated.

Organic LED made by organic small molecules or polymer is a potential device to be used in planner display in near future after a widely investigation in past decade after Tang and VanSlyke published their paper in 1987(1). Now the works are focused on the mechanism and the stability of device.

Most organic LED are composed by two main organic thin films, one of them is emission layer (EML) and the other is carrier transport layer. The EML may be electron transport (ETL) or hole transport (HTL), depending on the charge transport property of EML material. An electron transport layer or a hole transport layer is used in order to increase the opposite carrier injection efficiency and hence to increase the electroluminescent (EL) efficiency. Besides increasing the EL brightness of device, the carrier transport materials will affect other EL properties of devices such the emission spectrum, the current pass through the devices and the stability.

In this work, we will compare the properties of four double-layer organic LED devices based on emissive tris-8-hydroxyquinoline aluminium (Alq3) and bis-8-hydroxyquinoline zinc (Znq2), and four different hole-transporting layers. The hole transporting layer (HTL) materials used are 4,4',4"-tris (3-methyl-phenylphenylamino) triphenylamine (m-MTDATA), N,N'-bis-(1-naphthyl)-N,N'-diphenyl-1,1'-biphenyl-4,4"-diamine (NPB), N,N'-diphenyl-N,N'-bis(3-methylphenyl)-(1,1'-biphenyl)-4,4"-diamine (TPD), and (N-p-methoxyphenyl-N-phenyl)-p-methoxyphenyl-styrylamine (SA). The electroluminescent (EL) spectra the devices and their current voltage, brightness voltage characteristics have been investigated.

The hole transport layer materials m-MTDATA, NPB, TPD are persuaded from Syntec, and SA get from Shanghai University. Alq3 and Znq2 are synthesised by us.

On the pattern ITO glass, organic hole transport materials and emissive Alq and Znq2 are deposited sequentially by thermal evaporation. The thickness of the organic layers are 400 Å and monitored and controlled by a Sycon Instruments STM-110 thickness/rate monitor, the typical deposition rate are 1-2 Å/s. Finally a aluminium layer of 2000 Å is deposited on the top of Alq layer to form the electrode. The emission area is 5X5 mm². The devices are encapsulated in nitrogen.

The electroluminescent spectra of the devices are measured with Czery-Turner SPEX spectrometer. The current of the device is measured with a multimeter and driven with self-made direct current power supply. The relative brightness is calculated from the measured spectrum. All the measurements are carried in room temperature.

As we know Alq is a green emission material. It emits a very wide band centred at 520nm-530nm, depend on the source. The centre peak of a thermally deposited Alq film synthesised in our group is 525nm. In double layer devices basing on Alq, the emission shift toward to a

Poster Session III

long wavelength when use m-MTDATA as HTL, and shift toward to a short wavelength when use NPB as HTL.

In m-MTDATA/Alq double layer device, the emission band is 0.53eV, wider than the 0.44eV of PL of Alq film. On the other hand, the emission peak varies with the driven voltage from 570nm to 530nm when the voltage increases from 8V to 14V. This indicates that the some new emission exist beside the emission from Alq layer. That emission, as reported elsewhere (2), is an exciplex emission at interface of m-MTDATA and Alq.

In NPB/Alq bilayer device, all the emission peaks at different voltage are at same position of 515nm, a little blue shift comparing to the 525nm of PL Alq film. No significant wideness of band is observed. The origin of blue shift in NPB/Alq double layer device has not confirmed yet and will be investigated further.

No significant changes in emission of double layer devices based on Znq2 have been observed, too. That's mean no interaction occurred at hole transport layer materials and emissive Znq2 in these device. The Znq2 is a yellowish green emission material. It emits a wide band too, but centred at 550nm.

When use different HTL material, the current voltage characteristics (I-V) and brightness voltage (B-V) characteristics of bilayer devices change a lot.

We also investigated the multilayer hole transport films and study which HTL materials is good for hole injection, which one is suitable for hole transport and which is better for forming the heterojunction.

From this work, we can conclude that the hole transport layer not only influence the hole injection in the bilayer device, but also the emission colour. The EL spectra of devices with m-MTDATA and NPB as the HTL are red and a little bit blue shifted comparing to the PL emission at ~525nm of Alq3 layer. The former emits at 550nm and the latter at 515nm. M-MTDATA is suitable for hole injection and NPB is suitable for electron block layer, so a triple layer device with m-MTDATA as hole injection layer and NPB as electron block layer has a very high efficiency and stability.

This work is partly supported by Foundation for Science and Technology (FCT) of Portugal and by Foundation of Calouste Gulbenkian (FCG) of Portugal.

Reference:

1. C. W. Tang and S. A. VanSlyke, *Appl. Phys. Lett.*, 51:913(1987)
2. K. Itano, H. Ogawa, and Y. Shirota, *Appl. Phys. Lett.*, 72(6):636 (1998)

Probing space charge distributions in polymer LEDs by means of an electro-optic technique

Francesco Michelotti, Sebastiano Bussi, Mario Bertolotti
*Università degli Studi di Roma "La Sapienza" - Dipartimento di Energetica
 Via A. Scarpa, 16 I-00161 Roma, Italia*

Zhenan Bao
*Lucent Technologies, Bell laboratories
 600 Mountain Avenue - Murray Hill, New Jersey, USA*

A single wavelength electro-optical reflection technique was used to study the creation of space charge (SC) distributions in an Al/PPV/ITO LED by monitoring the third order NLO response of the electro-luminescent layer. The polymer is a PPV derivative with oxadiazole groups grafted as side chains. The measurements show the creation of SC distributions given by the sum of a ionic contribution close to the ITO, and of a slowly changing and bias dependent one due to charge injection. Taking into account Debye-Hückel screening in the polymer, we estimate the density of the ionic charges to be $\rho_0 = 1.510^{24} \text{ m}^{-3}$, for a uniform distribution in a 110nm thick layer. The real third order susceptibility of the polymer is estimated to be $\chi^{(3)} = 4 \cdot 10^{-21} \text{ m}^2/\text{V}^2$.

We investigated a PPV derivative with electron-deficient oxadiazole sidechains covalently linked to PPV backbones (OXA1PPV). The external quantum efficiency for OXA1PPV has been shown to be about ten times higher¹, compared to similar PPVs. Al/PPV/ITO test LEDs were fabricated, with PPV thickness $h=285\text{nm}$. Due to the relatively large thickness, electro-luminescence was not observed.

A polarisation sensitive single wavelength electro-reflectance experimental technique² (figure 1) was used to check SC distributions in OXA1-PPV. Upon application of a voltage $V(t) = V_{off} + V_{mod} \cos(\Omega t)$ to the electrodes, the reflected intensity can be modulated at Ω and 2Ω , due to either a phase or an amplitude modulation of the p and s components. Due to disorder in the polymer, the modulation can be only attributed to the bulk complex $\chi^{(3)}$ response (Kerr electro-optic effect and electro-absorption) as well as to modulation of the reflectance of the ITO/polymer interface due to modulation of the polymer refractive index². Taking into account only bulk effects, the power modulation at Ω is given by:

$$P_{ac}(\Omega) = \Lambda(\alpha) \cdot P_0 |r_s|^2 \cdot \Gamma_1 \cdot \left[\text{Re}(\tilde{\chi}_{zzz}^{(3)}) \cdot \tan(\Phi) \cdot \sin(\Psi_p + \Psi_c) + \text{Im}(\tilde{\chi}_{zzz}^{(3)}) \cdot [\tan(\Phi) - \cos(\Psi_p + \Psi_c)] \right]$$

where P_0 is the input power, Φ and Ψ_{ps} are defined by $r_p/r_s = \tan(\Phi)e^{i\Psi_{ps}}$, $r_{p,s}$ are the reflection coefficients for the p and s polarisations, $\tilde{\chi}_{zzz}^{(3)}$ is the main third order susceptibility tensor component (z is the stacking direction) for the weakly anisotropic polymer film³; $\Gamma_1 = \int_0^h E_s(z)E_m(z)dz$ is the overlap integral along the polymer thickness; $E_m(z)$

is due to V_{mod} , $E_s(z)$ is due both to V_{off} to the V_{bi} given by the difference of the work functions $\Delta\Phi$ of Al and ITO ($V_{bi} = \Delta\Phi/e = -0.5\text{V}$) and eventually to the presence of trapped charges; $\Lambda(\alpha)$ is the angle dependent reflection coefficient.

In order to eliminate the ITO/PPV interface modulation, it is sufficient to measure the signal in the two bias points $\Psi^{A,B} = (\Psi_p + \Psi_c) = \pm\pi/2$, and evaluate the quantity²:

$$S_{Kerr}(\Omega) = \frac{V_{ac}^{(eff)}(\Omega, \Psi^A) - V_{ac}^{(eff)}(\Omega, \Psi^B)}{2V_{dc}} = 4\Lambda(\alpha) \cdot \frac{\tan \Phi}{1 + \tan^2 \Phi} \cdot \Gamma_1 \cdot \text{Re}(\tilde{\chi}_{zzz}^{(3)}),$$

Poster Session III

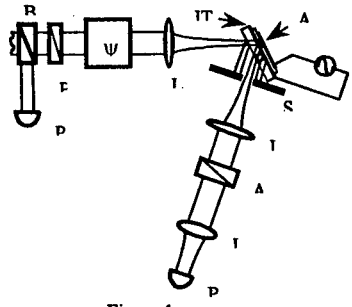


Figure 1

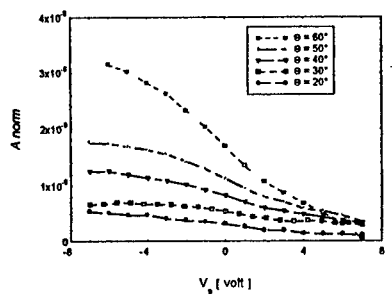


Figure 2

in order to extract the information on Γ_1 and $Re(\chi^{(3)})$.

In Figure 2 we observe that the signal vanishes for V_{off} as high as about +7V, much higher than the $-V_{bi}$ predicted for a perfect and charge free insulator. Such result suggests that a very stable SC distribution $\rho(z,t;V_{off})$ exists in the polymer film, giving rise to an additional $E_p(z,t)$. However such assumption is not sufficient as $\Gamma_1=0$ for $V_{off} + V_{bi} = 0$, in a perfect insulator and if $\rho(z,t;V_{off})$ is slowly-varying with respect to $V_{mod} \cos(\Omega t)$. It is necessary to suppose that the large amount of polarisable oxidazole side-chains in the material gives rise to electrostatic Debye-Hückel screening with characteristic length λ , distorting both the $E_m(z)$ and $E_s(z)$ profiles in the PPV film; $E_m(z)$ is stronger close to the electrodes and acts as a weighting function for $E_s(z)$ in Γ_1 . In a simplified analytical model, considering a space charge distribution of thickness δ close to ITO with an uniform density $\rho(t;V_{off})$ and screening, we obtain:

$$\Gamma_1(t;V_{off}) = \kappa \frac{V_{mod}}{h} [V_{off} + V_{bi} + V_{DH}(t;V_{off})] \quad \text{with} \quad V_{DH}(t;V_{off}) = \frac{\lambda^2 \rho(t;V_{off})}{\epsilon} \left(-\frac{\beta_2 + 1}{2\beta_1} + \frac{\beta_4}{\beta_1\beta_3} \right)$$

$$\kappa = \frac{\beta_1^2 \beta_3 h}{4 \lambda}, \quad \beta_3 = 1 - e^{-2h/\lambda} + 2 \frac{h}{\lambda} e^{-h/\lambda}, \quad \beta_2 = \left[1 + e^{-h/\lambda} - e^{-\delta/\lambda} - e^{-(h-\delta)/\lambda} \right] \cdot \lambda \beta_1$$

$$\beta_1 = \frac{1}{\lambda(1 - e^{-h/\lambda})}, \quad \beta_4 = \frac{\delta}{\lambda} e^{-\delta/\lambda} + \frac{1}{2} e^{-(h-\delta)/\lambda} - \frac{1}{2} e^{-(h+\delta)/\lambda} + \frac{h-\delta}{\lambda} e^{-(h-\delta)/\lambda} + \frac{1}{2} e^{-\delta/\lambda} - \frac{1}{2} e^{-(2h-\delta)/\lambda}$$

The equations show that the condition $\Gamma_1=0$ can be shifted by V_{DH} . $\rho(t;V_{off})$ is the sum of a very stable ρ_0 , due to ionic charges, and of a slowly varying $\rho_{inj}(t;V_{off})$, due to carrier injection in the film. A stationary $\rho(\infty;V_{off})$ can be assumed if V_{off} is kept constant long enough to exhaust the transients. Such circumstance leads to the fact that when the $A_{norm}(\Omega)$ vs V_{off} characteristic is measured, the differential slope is changing during the scan, due to the variation of $\rho(\infty;V_{bias})$ between adjacent stationary states. Assuming $\delta = 110\text{nm}$ and fitting data for three different α (40° , 50° , 60°), we obtain $\rho_0 = (1.5 \pm 0.5) \cdot 10^{18} \text{ cm}^{-3}$ and $\lambda = 100\text{nm}$. The ionic nature of ρ_0 is motivated with the high stability of the charge distribution in time, even for temperatures as high as 120°C under a $\pm 10 \text{ V}$ bias voltage. From the experimental data we obtain $Re(\tilde{\chi}_{zzz}^{(3)}) = (4 \pm 1) 10^{21} \text{ m}^2/\text{V}^2$, in good agreement with values found for other polymers of the PPV family.

1 Z. Bao, Z. Peng, M. Galvin, E.A. Chandross, Chem. Mater., 10 (5), 1201 (1998).
 2 F. Michelotti, G. Nicolao, F. Tesi, M. Bertolotti, Chem. Phys., 245 (1-3), 311 (1999).
 3 P.N. Butcher, D. Cotter, The Elements of Nonlinear Optics, Cambridge University Press, Cambridge (1990).

Impedance Spectroscopy of Alq_3 based-Organic Light Emitting Diodes (OLEDs) measured in Ultra High Vacuum and Air

Rudi Ono, Paulo Losio, Michael Kiy, Axelle Tapponnier
Iris Gamboni, Ivan Biaggio and Peter Günter
*Nonlinear optic Laboratory, Swiss Federal Institute of Technology
CH-8093 Zürich, Switzerland*

The electronic properties of bulk-organic layer and interface behaviour of OLED structures were studied using impedance spectroscopy. To avoid the effect of gas contamination, the measurement was done in Ultra-High-Vacuum (UHV) and the results were compared with those measured in air. The impedance formed due to deflection region at the interface, observed in the air, was not detected in UHV. O_2 gas and oxide thin film were useful to treat interface behaviour.

Electroluminescent (EL) devices based on organic materials are interesting for several applications. These Organic Light Emitting Diodes (OLEDs) have the advantage of a low-cost deposition method, and allow the fabrication of large-area display. Remarkable progress in optimising device performance has been made in recent years. However, the knowledge of the electronic properties of the bulk organic layers and interfaces is still insufficient.

In order to better understand the electronic properties of OLEDs, we use impedance spectroscopy, which allows the investigation of the frequency dependency of the complex impedance of the device. It also allows us to find the equivalent circuit of the individual OLEDs and study the existence of a depletion layer at the interface.

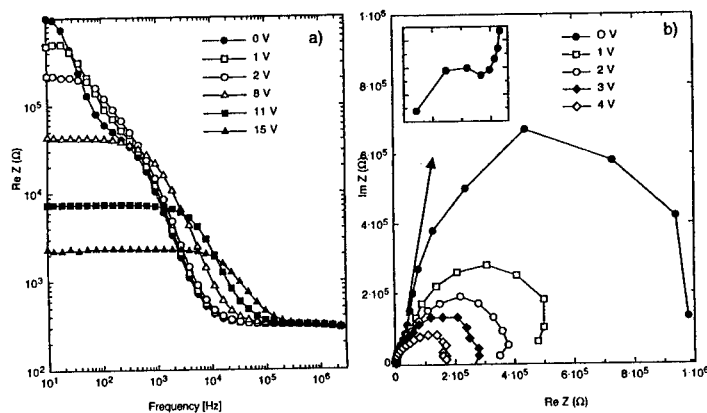


Figure 1: Real part of the impedance (a) and cole-cole plot in the complex plane (b) of an ITO/ Alq_3 /Mg OLED measured in air at different bias voltages. The amplitude of the ac modulation is 0.1 V, with a frequency range from 10 Hz to 10 MHz.

Our research goal is to understand the electronic properties of OLEDs, to obtain information on the internal device structure as well as the behaviour of, *e.g.*, the metal/organic

Poster Session III

interface. To this aim, we have grown the layered structure in a controlled way by molecular beam deposition in a Ultra High Vacuum system (UHV, pressure below 10^{-9} mbar). Since in the UHV-system is also equipped with an electrical measurement chamber and in situ surface characterisation facilities (UPS,XPS), we can measure the electrical characteristic of freshly fabricated devices which never entered into contact with any impurity gas. Thus we can truly exclude the effect of air/gas contamination. The system also allows us to determine the electronic binding energy in each OLED layer and the energy level alignment at the interface. For the impedance spectroscopical measurement, a programmable impedance analyser (Hewlett-Packard, HP 4129A) was used.

The real part of the impedance of a single layer(ITO/Alq₃/Mg) OLED as a function of frequency (f) when the device is exposed to air is shown in Fig. 1a. At the bias voltage of 0 V, it shows 2 structures resembling relaxation, where one of them ($f < 1$ kHz) disappears as the applied voltage is increased. The cole-cole plot (Fig.1b) also supports this observation, because it shows 2 semicircles at low bias voltage. They may be interpreted as the Alq₃-bulk resistance, and one depletion region at the Mg/Alq₃ interface which decreases with increasing bias voltage. The result of UPS measurement may give support for the formation of a depletion region at the interface.

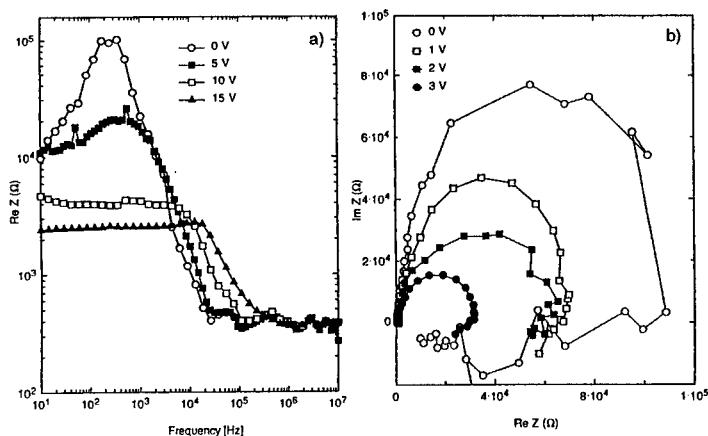


Figure 2: Real part of the impedance (a) and cole-cole plot in the complex plane (b) of an ITO/Alq₃/Mg OLED measured in UHV at different bias voltages. The amplitude of the ac modulation is 0.1 V, with a frequency range from 10 Hz to 10 MHz.

The result in UHV, however, shows only one semicircle (Fig. 2b), indicating that the depletion region due to the energy level-gap at interface is not formed in UHV. Moreover, as shown in Fig.2a, at low ($f < 1$ kHz for low bias) and high ($f > 100$ kHz) frequencies, the impedances are unstable, which may be related to the conductivity and carrier mobility of Alq₃ in UHV-ambient. We have also found that O₂ adsorption at the Alq₃-surface, and also the insertion of MgO or Mg-doped Alq₃ thin layer at the Alq₃/Mg interface, can be used to control either the impedance spectroscopy or EL-performance of OLED both in UHV and air.

A Comparative Study of Photoluminescence Spectra of Chromophores and Semiconducting Polymer Films

J. Shin¹, H. Choi¹, J. Ro¹, H. Kim¹, J. Noh², S. Lee², H. Suh², C. Ha³, K. Lee¹, M. Cha¹

1. Department of Physics and Research Center for Dielectric and Advanced Matter Physics, Pusan National University, Pusan 609-735, S. Korea

2. Department of Chemistry, Pusan National University, Pusan 609-735, S. Korea

3. Department of Polymer Engineering Pusan National University, Pusan 609-735, S. Korea

Photoluminescence(PL) spectra of chromophore-attached polymer and semiconducting polymer thin films are comparatively studied. In the chromophore thin film, we clearly observe that a vibronic subband of the luminescence has been bleached after waveguiding under optical pumping, in strong contrast to the case of the semiconducting polymer film. This provides a direct evidence that the PL mechanisms in short chromophores and semiconducting polymers are different.

Stimulated emission and even lasing have been observed in a variety of organic light-emitting materials. Especially, conjugated polymers have high photoluminescence(PL) efficiency and large cross section for stimulated emission[1]. However, the photoluminescence(PL) mechanisms of the new class of gain materials have been a subject of debate.

In this work, we comparatively studied the PL spectra of a chromophore-attached polymer and a main-chain-active semiconducting polymer thin films. The materials used in our experiment are [N, N-Bis(2-hydroxyethyl)amino]-4'-cyano stilbene attached to a polyurethane main-chain (PU-CN) and poly(2-methoxy -5-(2'-ethyl-hexyloxy)-1-4-phenylenevinylene) (MEH-PPV). Thin films were made by spin-coating. PU-CN film was pumped by the third harmonic(355 nm) and the MEH-PPV by the second harmonic(532 nm), respectively of a Q-switched Nd:YAG laser. The excitation beam was focused on the film to a rectangular shape with a cylindrical lens in order to obtain a long gain pass for the waveguided PL[2]. The edge-emitted PL spectra were measured, and compared with those from the surface.

In the PU-CN thin film, the PL spectrum from the surface exhibits distinct feature from that of the waveguided PL (Fig. 1). In the latter spectrum, we clearly observe that the peak vibronic subband of the PL has been bleached after waveguiding the pumped region. In contrast, the two PL spectra of the MEH-PPV film are not so different (Fig.2). The difference explain that the PL peak vanish because induced absorption occurs in a long.

Such difference between the chromophore and conjugated polymer can be explained by a phenomenological four-level model, at the peak of which either amplified spontaneous emission or induced absorption can occur depending on the relative population of the pump-induced levels.

References

- [1] F. Hide, M. A. Diaz-Garcia, B. J. Schwartz, M. R. Andersson, Q. Pei, A. J. Heeger, *Science* **273**, 1833(1996).
- [2] M. D. McGehee, R. Gupta, S. Veenstra, M. A. Diaz-Garcia, A. J. Heeger, *Phys. Rev.* **B58**, 7035(1998)

Poster Session III

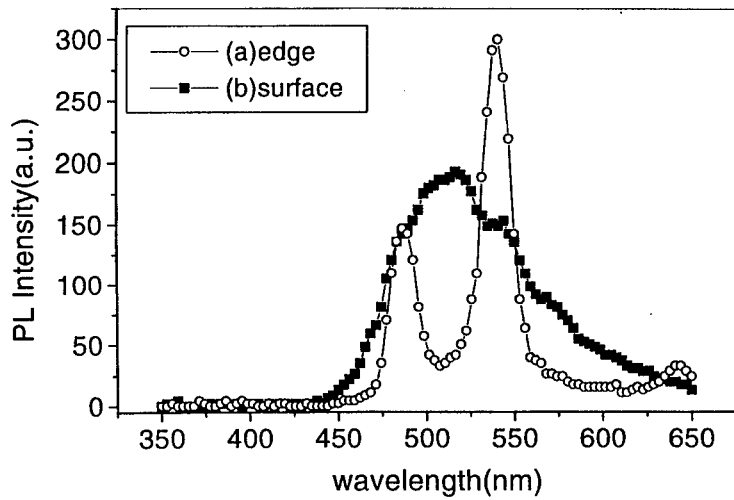


Figure 1: PL spectra of chromophore thin film detected from edge (a), and from surface (b).

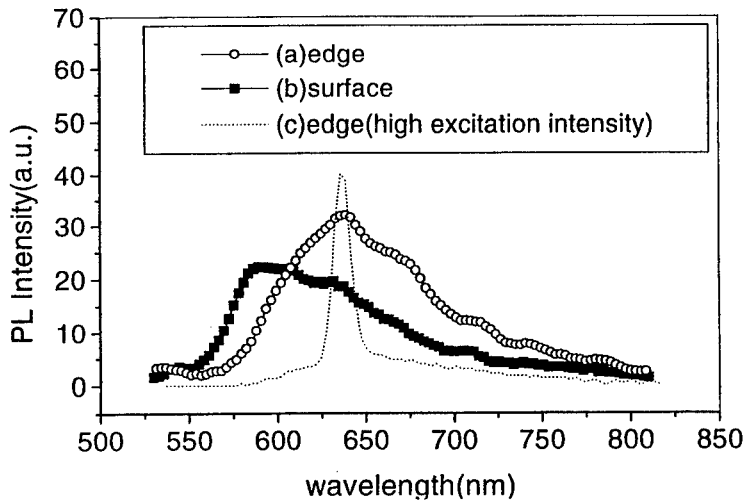


Figure 2: PL spectra of semiconducting polymer thin film detected from edge (a), from surface (b) and from edge at high excitation intensity.

Amplification of Raman Scattering in an Oriented Poly(p-phenylenevinylene) Film

Seungwoo Shin, Jeongmi Shin, Hongki Kim, Jung Hoon Ro, Heayoung Choi,
Kwanghee Lee, and Myoungsik Cha

*Department of Physics and Research Center for Dielectric and Advanced Matter Physics
Pusan National University, Pusan 609-735, Korea*

Photo-excitation of a stretched poly(p-phenylenevinylene) thick film results in a light emission with a narrow linewidth (about 1 nm) when the excitation intensity exceeds a threshold, as compared with that of amplified spontaneous emission (about 10 nm). By performing thorough excitation spectroscopy, we verify that the narrow emission is an amplification of Raman scattering during waveguide propagation. We found that an optimal excitation wavelength exists for a given thickness and loss spectrum of a thick film, and suggest that better emission efficiency can be attained for an appropriate film thickness and excitation wavelength.

Semiconducting polymers such as poly(p-phenylenevinylene)(PPV) and their derivatives are known to have high photoluminescence (PL) efficiency. The possibility of making lasers out of semiconducting polymers as gain media are being challenged. Photoluminescence spectral narrowing (PLSN) due to amplified spontaneous emission (ASE) and even lasing in a variety of semiconducting polymers have been recently reported [1,2].

On the other hand, stretched polymer films are attractive materials for photonic device applications because they are supposed to have larger linear and nonlinear optical responses and better interchain transport properties than spin-cast films due to the molecular orientational order and partial crystallization.

A free-standing PPV film was prepared from a precursor polymer[3]. It was stretched by tensile drawing with a draw ratio of 7:1, which resulted in a thickness of about 10 μm . Our excitation source was an optical parametric oscillator (OPO) pumped by the third harmonic (355 nm) of a Q-switched Nd:YAG laser. The excitation beam was focused on the film to a rectangular shape in order to obtain a long gain pass[2]. The emission from one side of the film was detected. The excitation beam was polarized parallel to the draw direction of the film throughout our experiments.

At low level of excitation intensity we observed a broad PL spectrum that had a typical stokes shift with respect to the absorption spectrum as shown in Fig. 1. At high level of excitation intensity, however, the emission linewidth was only ~ 1 nm. It should be noted that it is much narrower than the typical width of PLSN of ~ 10 nm[1,2]. By varying the excitation wavelength (λ_{ex}), the emission wavelength (λ_{em}) also shifted, as summarized in Fig. 2. From the figure it is clear that they have the relation, $\lambda_{ex}^{-1} = \lambda_{em}^{-1} + \Lambda^{-1}$. The frequency differences (Λ^{-1}) for the two kinds of peaks are 1170 cm^{-1} and 1580 cm^{-1} , which are assigned as the phenylene C-H bending and ring stretch modes, respectively. We verified the two major Raman shifted peaks with a Raman spectrometer.

We also observed that the narrow emissions have well-defined thresholds, depending on the excitation wavelengths. The detailed dependence of the emission intensity on the excitation intensity was measured at several excitation wavelengths. The threshold tends to increase with increasing λ_{ex} .

The above behavior can be explained by the amplification of the Raman-scattered signal by the PL gain exactly in the same way as ASE in conventional PLSN phenomena[2]. The emission efficiency can be improved if the thickness of the stretched film can be controlled.

Poster Session III

We also observed that the narrow emissions have well-defined thresholds, depending on the excitation wavelengths. The detailed dependence of the emission intensity on the excitation intensity was measured at several excitation wavelengths. The threshold tends to increase with increasing λ_{ex} .

The above behavior can be explained by the amplification of the Raman-scattered signal by the PL gain exactly in the same way as ASE in conventional PLSN phenomena[2]. The emission efficiency can be improved if the thickness of the stretched film can be controlled.

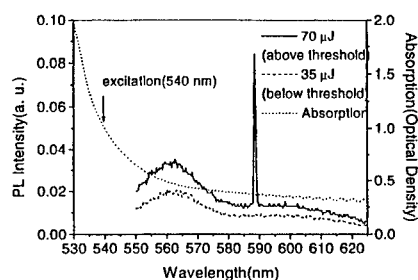


Figure 1: PL spectrum compared with absorption spectrum(dashed curve). Solid curve: PL with strong excitation ($70 \mu J/pulse$), Dotted curve: PL with weak excitation ($35 \mu J/pulse$). Narrow peaks are present only at high excitation intensities. ($\lambda_{ex} = 540 nm$ in this case)

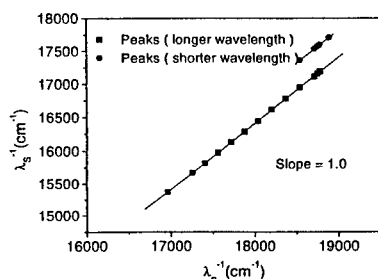


Figure 2: Emission frequency versus excitation frequency.

References

- [1] F. Hide, M. A. Diaz-Garcia, B. J. Schwartz, M. R. Andersson, Q. Pei, A. J. Heeger, *Science* **273**, 1833(1996).
- [2] M. D. McGehee, R. Gupta, S. Veenstra, M. A. Diaz-Garcia, A. J. Heeger, *Phys. Rev. B* **58**, 7035(1998)
- [3] T. Olnishi, T. Noguchi, T. Nakano, M. Hirooka, I. Murase, *Synth. Met.* **4143**, 309 (1991)

Blue-green light-emitting electrochemical cells based on a copolymer derived from fluorene

O. Stéphan, V. Collomb and J.-C. Vial

Laboratoire de Spectrométrie Physique, Université Joseph Fourier Grenoble 1 and CNRS (UMR C5588), 140 rue de la physique, B.P. 87 38402 Saint Martin d'Hères Cedex, France

A copolymer derived from fluorene has been synthesised using a fluorene monomer functionalised with PEO-like segments as comonomer in a poly(dihexylfluorene) main chain. Efficient blue-green polymer light-emitting diodes (LEDs) based on this material and working under ambient atmosphere are reported. Light-emitting electrochemical cells (LECs) are also demonstrated, leading to threshold operating voltages close to the electrochemical gap of poly(fluorene).

Considerable efforts have been carried out in the field of organic light emitting devices to obtain brightnesses and operating voltages suitable for commercial applications. In this field, a promising new advance, based on the development of light emitting electrochemical cells (LECs), has been proposed by Pei *et al.* [1]. In such devices, the phase separation that occurs between the ionic conductor, generally poly(ethylene oxide) (PEO) complexed by a lithium salt, and the non-polar (ionic) luminescent polymer remains the main problem to solve [5,6]. On this basis, our purpose was to improve the compatibility of the solid electrolyte with the conjugated polymer.

With this aim in view [2], we have synthesised a new monomer derived from fluorene, functionalised with PEO-like segments : 2,7-dibromo-9,9-bis(7,10,13,16-tetraoxaheptadecyl)fluorene, denoted dibromo(BTOHF). It must be pointed out that the use of an alkyl spacer-arm between the fluorene units and the PEO-like segments prevents the twist of the conjugated repeating units from planar configuration which usually leads to a drop in fluorescence quantum yield.

The synthesis of the corresponding homopolymer, poly(BTOHF) was successful. Nevertheless, the resulting material was melted at ambient temperature due to its side groups. As a consequence, we investigate the co-polymerisation of the BTOHF moiety with the more simple 9,9-dihexylfluorene one, denoted DHF. The chemical structure of poly(DHF-co-BTOHF) copolymer is shown on Fig. 1.

The copolymer was synthesised using the well-known dihalogenative polycondensation of the dibromo corresponding derivatives catalysed by a Ni(0) complex in

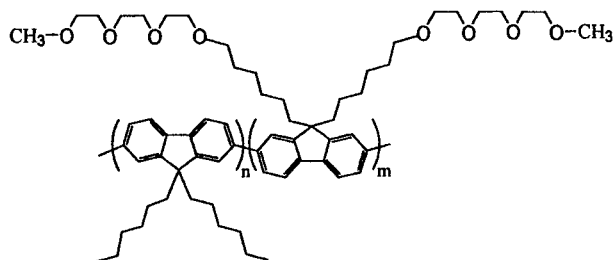


Fig 1 : chemical structure of the copolymer

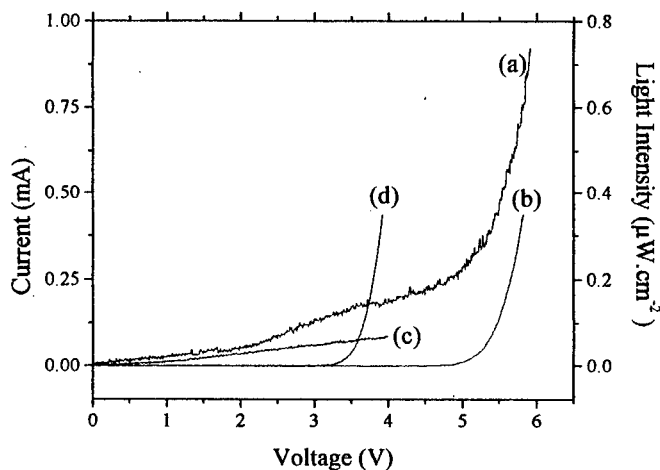
N,N-dimethylacetamide (DMAc) starting with a 4:1 molar ratio for the DHF and BTOHF comonomers. The photoluminescence spectra for films and chloroform solutions of the copolymer display different spectral features, with a red shifted emission for the film. This

Poster Session III

can be attributed to the formation of aggregates leading to inter chain electron-hole recombination. Electroluminescence spectrum exhibits the same feature, i. e. formation of aggregates, but an interesting point is that it shows only a very slight evolution upon device operation. First investigations were based on the use of the classical and simple LEDs device configuration : Indium-Tin-Oxide (ITO)/copolymer/Calcium/aluminium. Thin films (typical thickness 110 nm) were prepared from 10 mg.ml⁻¹ chloroform solution. Light reaches values below 1 $\mu\text{W.cm}^{-2}$, which can be seen under ambient luminosity conditions, for operating voltage higher than 12 V. Typical lifetime for electroluminescence is 10-12 hours at 15 volts polarisation, under ambient atmosphere.

LECs were prepared using a blend of poly(DHF-co-BTOHF) with a solid electrolyte consisting of poly(ethylene oxide) (PEO) and lithium trifluoromethanesulfonate (LiCF₃SO₃). Active layers were spin coated from cyclohexanone solutions containing the mixture at weight ratio of 10 : 0.5 : 1 for copolymer, PEO and lithium-triflate respectively. As shown by Fig.2, the turn on voltage is rather low and close to the electrochemical gap of polyfluorene. When a voltage scan is performed between 0 and 6 Volts in one second on a "fresh" LECs, the apparent threshold voltage for L(V) curve is around 5 Volts as shown on Fig.2 (b).

Fig. 2 :
I(V) and *L(V)* curves of
a "fresh" LECs :
(a) *I(V)* and (b) *L(V)*
compared to the ones
obtain after 5 minutes
of stress at +5V :
(c) *I(V)* and (d) *L(V)*.



Nevertheless, it is noteworthy that once the junction has been formed, for instance after an initial stress at 5 V for few minutes, the subsequent scan exhibits lower threshold, around 3.2 V (Fig. 2 (d)). Furthermore, the linear dependence of the current on the operating voltage (Fig 4 (c)) strongly suggests that polymer/electrode interfaces become, as expected, ohmic contacts. Typical lifetime is 10 hours under 4 V.

These preliminary results on electroluminescence of a copolymer derived from fluorene containing fluorene moieties functionalised by PEO-like segments, clearly show the interest of such a system in which ion conducting segments are incorporated into the poly(fluorene) main chain.

- [1] Q. Pei, G. Yu, Chi Zhang, A. J. Heeger, Science 269 (1995) 1086.
- [2] O. Stephan, V. Collomb and J. C. Vial, M. Armand submitted to Syn. Met.

Luminescent and electronic properties of end-substituted oligo(phenylene vinylene)s

Y. Tao, M. D'Iorio, A. Donat-Bouillud, J. Lam
*Institute for Microstructural Sciences, National Research Council of Canada
M-50 Montreal Road, Ottawa, Ontario, Canada, K1A 0R6*

M. S. Wong, Z. H. Li
*Department of Chemistry, Hong Kong Baptist University
Kowloon Tong, Kowloon, Hong Kong*

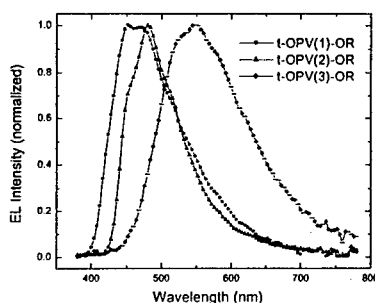
The luminance and electronic properties of a homologous series of highly soluble, symmetrically multi-alkoxy substituted oligo(phenylene vinylene)s containing up to six phenyl rings were investigated. The electron donating groups substituted at the end of oligomer(phenylene vinylene)s were found to lead to a shorter effective conjugation length relative to those of the unsubstituted. The end-substituted oligo(phenylene vinylene)s have potential application in blue light emitting devices.

Electroluminescence in conjugated polymer was first discovered in poly(*p*-phenylene vinylene)(PPV)^[1]. Since then research efforts on polymer-based light emitting devices have increased dramatically, primarily due to their potential application in full color flat panel display and the low fabrication costs associated with this technology. Poly(phenylene vinylene) (PPV) and its derivatives have remained as the material of choice for polymer light emitting diodes (PLEDs). Many researchers are working on the modification of PPV's electronic and mechanical properties by introducing substituents in the molecular structure.

Conjugated polymers derive their semiconducting properties from delocalised π -electrons along the polymer chain. Therefore it is possible to modify the semiconducting properties of the polymer by adding different functional groups to the polymer structure thereby altering the extent of delocalisation of the π -electrons. Understanding how different functional groups in the PPV structure affect its physical properties is an important step towards rational modification of the material. However, a broad molecular weight distribution and the presence of blocks with different conjugation lengths in the polymeric material will complicate the investigation. Therefore, oligomers of PPV are of great interest. Their well-defined chemical structure together with their improved solubility and processibility allow access to high purity materials and facilitates the interpretation and modeling of the experimental results. In addition, many oligomer materials can be thermally sublimed under high vacuum, allowing for the preparation of multilayer OLED structures and devices in an ultra clean and well-controlled environment thus overcoming the uncertainties involved in wet processes.

It is well known that in oligo(phenylenevinylene)s (OPVs), the fluorescence yields and wavelengths for absorption and emission are very sensitive to the conjugated length. This is especially useful in the search for blue light emitting materials. For these reasons, different types of OPVs have been synthesized and their absorption, luminance and electronic properties [2-4] have been investigated. Wong *et al*.^[5] have recently shown that solubilizing substituents such as polyalkyleneoxy and alkylsulfonyl groups incorporated at the ends of the π -conjugated skeleton of distyrylstilbene can improve solubility without disrupting the coplanarity of π -conjugation backbone. We have found that substituents incorporated at the end of the conjugated position of main chain, i.e. 4,4'-positions can shift the HOMO and/or LUMO level and thus alter the HOMO-LUMO energy gap of an oligomer. This provides a

Poster Session III



Electroluminescent spectra of OLEDs using end-substituted oligo(phenylene vinylene)s as emitters.

means to tune the energy gap leading to a change in optical and electronic properties of an oligomer[6].

We herein report luminance and electronic properties of a novel homologous series of highly soluble, symmetrically multi-alkoxy substituted OPVs containing up to six phenyl rings which were shown to have co-planar π -conjugation backbone. Vacuum deposited thin films and light emitting diodes (LEDs) were used in photoluminescence (PL) and electroluminescence (EL) measurements. We have found from the fluorescence spectra of the end-substituted OPVs, that the emission bands are apparently composed of two major emissions. Although the two emission peaks undergo different red shifts, the corresponding peak maxima also exhibit a tendency of saturation as the conjugation length increases. The spectral features of the EL are very similar to those of the solid-state PL of the corresponding oligomer, suggesting that both emissions arise from the same oligomers. The methoxy substituents attached onto the non-conjugated *ortho*-positions of the end-capped phenyl rings have pronounced effect on the solid-state luminescence properties. The emission maxima of both EL and PL are significantly blue-shifted (~ 20 nm) in the three-phenyl-ring oligomer (t-OPV(1)-OR) when compared to that of the corresponding unsubstituted counterparts. The emission from the t-OPV(n)-OR ($n=1-4$) based LEDs covers a spectral range between blue to green (456-542 nm). The t-OPV(1)-OR based LEDs emit at 456 nm with 120 cd/m^2 at a bias voltage of 7V; the best external efficiency and brightness reached so far are 1.3 cd/A and 980 cd/m^2 respectively, which shows the potential for applications as blue LEDs. All the devices showed clear rectifying behavior in their current-voltage characteristics. The turn-on voltages of these LEDs are all around 4-5 volts.

In summary, we have shown that the electron donating groups substituted at the end of OPVs can lead to a shorter effective conjugation length relative to those of the unsubstituted and lateral substituted OPVs. The blue shift caused by introducing methoxy groups to the *ortho*-positions in OPV structure might be used in the search of blue emitters.

References

- [1] J. Burroughs, D. D. Bradley, A. R. Brown, R. N. Marks, K. Mackey, R. H. Friend, P. L. Burns, A. B. Holmes, *Nature* 347 (1990) 539.
- [2] S. Nakatsuji, K. Matsuda, Y. Uesugi, K. Nakashima, S. Akiyama, G. Katzer, W. Fabian, *J. Chem. Soc. Perkin Trans. 2* (1991) 861.
- [3] N. N. Barashkov, D. J. Guerrero, H. J. Olivos, J. P. Ferraris, *Synth. Met.* 75 (1995) 153.
- [4] A. Schmidt, M. L. Anderson, D. Dunphy, T. Wehrmeister, K. Muellen, N. R. Armstrong, *Adv. Mater.* 7 (1995) 722.
- [5] M. S. Wong, M. Samoc, A. Samoc, B. Luther-davies, M. G. Humphrey, *J. Mater. Chem* 8 (1998) 2005.
- [6] Y. Tao, A. Donat-Bouillud, M. D'Iorio, J. Lam, T. C. Gorjanc, C. Py, M. S. Wong, *Synth. Met. (in press)*.

Transient photocurrent investigation of charge transport in electroluminescent organic thin films

A. Tapponnier, I. Biaggio, P. Günter

*Nonlinear Optics Laboratory, Institute of Quantum Electronics
Swiss Federal Institute of Technology
CH-8093 Zürich, Switzerland*

Optimizing the performance of organic light emitting diodes (OLEDs) requires a deep knowledge of the electronic and transport properties of the materials. We used transient photoconductivity induced by short light pulses to study the charge transport processes occurring in Alq₃-based OLEDs on different time-scales. From the temporal variation of the photocurrent transient, information on charge-carrier dynamics and trapping can be extracted.

Photocurrents induced by short light flashes can give information on the response time of the photoconductivity and thus on free-carrier lifetimes, the influence of deep and shallow traps, and the charge-carrier mobility (which is generally strongly electric-field dependent in organics). They can be applied directly to standard Organic Light Emitting Diodes (OLEDs) structures, and offer complementary information to Time of Flight mobility measurements [1] [2].

In our pulsed photoconductivity measurements, a constant voltage is applied to an OLED illuminated by short laser pulses (Nitrogen laser pulses at $\lambda_{ex} = 337.1$ nm with pulse duration < 1 ns) and the current through the sample (with capacitance C_{OLED} and resistance R_{OLED}) as a function of time is determined by measuring the voltage drop over a resistor R .

It is common to measure directly the relaxation of the photoinduced current by using a small measurement resistor R to decrease the response time of the detection system. But, although this method is the most straightforward to analyze the photocurrent signal, it is not possible to apply it in a simple way to OLEDs, which have a relatively large capacitance and therefore make the response time of the current detection system too long.

However, this can be turned to an advantage. When the RC time constant of the detection circuit is much larger than the relaxation time of the photoinduced current pulse, the time-dependence of the voltage drop over the resistance is given by the rate at which charge is accumulated on the capacitor of the OLED, before it has the time to flow through the circuit. Therefore, the detected signal is in this case proportional to the time integral of the current, *i.e.* the total charge emitted from the OLED. If necessary, the dynamics of the photoinduced conductivity can then be found by numerically differentiating the signal.

We apply this technique to characterize OLEDs grown in our laboratory by molecular beam deposition in ultra-high vacuum. They consist of a semitransparent indium-tin oxide (ITO) layer, an organic layer (Alq₃) and a top metal cathode (Mg). We chose simple single-layer Alq₃ devices in order to test the viability of this characterization method in a sample where the charge generation and transport occur in one material only. To avoid field distortions by the mobile space charge, a laser pulse of low intensity is used (30 μ J).

Fig.1 shows the evolution of the total charge which comes out of the device as a function of time in an used OLED. The signal consists of three regions. Initially, and

Poster Session III

until below $1 \mu\text{s}$ after the generation of the charge carriers, charge is being emitted at its maximum speed (line with slope 1 in the figure). Then there is an intermediate part (between $1 \mu\text{s}$ and $5 \mu\text{s}$) where there is a decay in the speed of charge accumulation (corresponding to a decay in the photoinduced conductivity). This is characterized by a slope of the order of ~ 0.2 in the log-log plot of Fig. 1. Finally there is a third part, which lasts for about three decades, where the photocurrent slowly decreases until there is no change anymore in the amount of charge accumulated on the device.

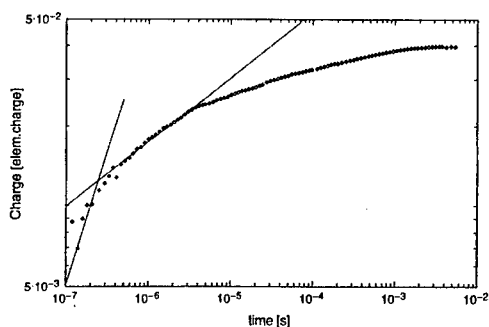


Figure 1: Log-log plot of the total charge emitted from an ITO/Alq (300nm)/Mg structure at an electric field of $2 \times 10^5 \text{ Vcm}^{-1}$ after illumination with a short laser pulse. The two solid lines have slopes of 1 and 0.2, respectively.

One of the conclusions we can draw from the above measurement is that even after 10 ms after the laser pulse left the sample, a finite amount of charges are still in the device. This tail is probably due to trapping, reflecting a dispersive transport which often occurs in disordered solids.

This method can be a valuable tool to study the dynamics of charge carriers in the same OLED structure that is used in a real device, and for the characterization of impurity states.

References

- [1] R. G. Kepler, P. M. Beeson, S. J. Jacobs, R. A. Anderson, M. B. Sinclair, V. S. Valencia and P. A. Cahill, "Electron and hole mobility in tris(8-hydroxyquinolinolato-N1,O8) aluminium", *Appl. Phys. Lett.* **66**, 3618-3620 (1995).
- [2] J. Kalinowski, N. Camaioni, P. Di Marco, V. Fattori and A. Martelli, "Kinetics of charge carrier recombination in organic light-emitting diodes", *Appl. Phys. Lett.* **72**, 513-515 (1998).

Injection and Charge Transport Phenomena in Polymer Multilayer Systems for Electronic Applications

A. Wedel, S. Janietz
 Fraunhofer-Institute of Applied Polymer Research
 Kantstrasse 55, D-14513 Teltow, Germany

The aim of our work was to investigate the injection and charge transport phenomena in polymer multilayer systems. The understanding of these processes are necessary to built up polymer light emitting devices (LED's), polymer diodes and transistors.

Introduction

The polymers we are used was a hole transport material (thianthrene containing polyimide) and an electron transport material (aromatic polyoxadiazole). The demands on such polymers were that they have to be soluble in common organic solvents for the spin-coating procedure. The layers must be insoluble for the following spin-coating processes. From the electrochemical measurements we estimated the homo and lumo energy levels.

Experimental

Materials

The hole transport material (PTPA) was synthesised from a soluble precursor polyamide, which spin-coated on the substrate and then thermally converted at 200 °C under vacuum condition to an insoluble polyimide. The electron transport material (PODH) we used was a soluble thermostable 2,5-dialkoxy substituted poly(phenyl-1,3,4-oxadiazole) [1].

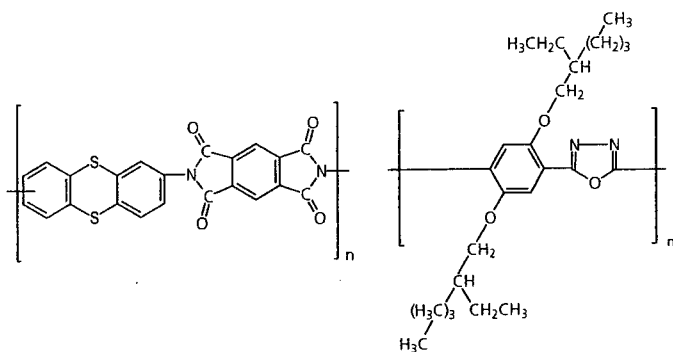


Figure 1: Structure of the thianthrene containing polyimide (PTPA) and of the soluble 2,5-dialkoxy substituted poly(phenyl-1,3,4-oxadiazole) (PODH).

Devices

The typical structure of an electroluminescence device and of a polymer transistor can be described as an metal-polymer/(polymer)-semiconductor interface. We investigated the current-voltage (I-V) characteristics for testing the diode character and capacitance-voltage (C-V) behaviour of different single and multilayer structures to describe the function of such devices. The efficiency of the injection of electrons and holes plays an important role

Poster Session III

for the electroluminescence of LED's. The electronic nature of the organic materials determined the parameters for good electron and hole injection and transport capability.

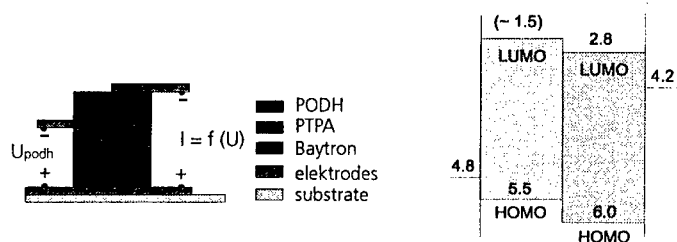


Figure 2: Typical transistor structure with a bilayer system. Energy level scheme for an ITO / PTPA / PODH / Al bilayer structure. Values are calculated in eV vs. vacuum level.

Results

The obtained reduction and oxidation peakpotentials by cyclovoltammetric measurements of thin layers allows to estimate the lumo and homo energy levels of the PTPA and PODH. The current-voltage curves of the bilayer systems are shown in Fig. 3. The onset voltage of the device can be controlled via a bias voltage between the hole transport layer and the ground electrode.

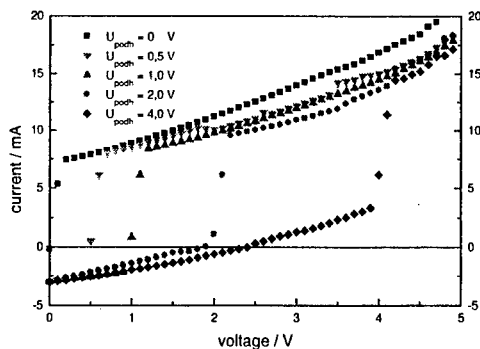


Figure 3: Current-voltage behaviour of a bilayer system of a polymer transistor.

Conclusions

We have prepared multilayer devices sandwiched between different electrodes to built up polymer LED's and polymer transistors. We found that, in general, bilayer devices incorporating an electron transport layer apart from the hole transport layer show drastically better electroluminescent behaviour than the corresponding single layer devices.

References

- [1] S. Janietz, A. Wedel, R. Friedrich, S. Anlauf „Synthesis of new thianthrene containing polymers and aromatic poly(oxadiazoles) and their application in OLEDs“, Pol. Prepr. **40**, 1219 (1999).

Authors Index

Author name	Contribution number	Author name	Contribution number
Abbate, G	A1	Bösch, M	C2, C3
Abdreimova, R	E21	Bosshard, C	A11, A18, B4, C2, C3, C9, D6, H4, H6, H9
Ågren, H	A12, E15	Bourgogne, C	H5
Agulló-López, F	C12, E20	Boyd, C	INV8
Akutagawa, T	H12	Bozec, H. Le	H16
Alain, V	H4, INV18	Brasselet, S	A16, A3, E12, H7
Albrecht, M	F1	Brédas, J-L	E28, INV19
Ananthavel, S	INV18	Broeck, K Van Den	B10, C13
Andraud, C	A2, A3, A4, E14, F9	Brotin, T	F9
Anémian, R	A2, A3, A4	Brun, A	C6
Aoyama, T	INV21	Bubeck, C	INV20
Arbez-Gindre, C	A15	Bulavin, L. A	E1
Asai, K	H23	Bussi, S	I8
Atamas, N.A	E1	Busson, B	INV25
Attias, A.-J	C8, H2, H1	Bykowski, D	H11
Audebert, P	H7, H8	Cai, C	C3, H6
Ayadi, M	F6	Cammack, J. K	INV18
Bader, M. A	G2	Campo, J. A	E20
Baldeck, P	INV26	Canfield, B. K	E3
Baldeck, P. L	A2, D8, A4, E14	Cano, M	E20
Balevicius, M. L	E21	Canva, M	INV15, C10, C11, C6
Bandrovskaja, I. K	E2	Carriedo, G. A	C12
Banfi, G. P	INV29, D 9	Casperson, J. D	B2
Bao, Z	I8	Casu, M. B	I3
Barisien, T	F1	Cavalli, C	H2
Barmenkov, Yu	B7	Cazenobe, I	E12
Barrientos, A	A6	Cha, M	I10, I11
Bartkiewicz, S	B9	Chan, K. P	INV15, C10
Barzoukas, M	H4	Chang, H.J	F2
Batlogg, B	INV23	Chaput, F	C4, C6
Batori-Tartzi, Z. I	E2	Che, C-M	I5
Belfield, K D	F3	Chérioux, F	F6, H1, H7, H8
Beljonne, D	INV19, E28	Chien, L.C	INV31
Ben-Asuly, A	A17, E13, H3, H21	Cho, W-R	C11
Berkovic, G	E13, H17	Choi, H	I10, I11
Berski, S	E1	Chollet, P-A	INV26, A2
Bertolotti, M	I8	Chubakov, P.A	F5
Biaggio, I	B4, H6, I4, I9, I14, E27	Chun, H	INV16
Bianco, A	INV26	Claesson, Å	G4
Bigot, J.-Y	F1	Clays, K	E28
Bittner, R	INV10	Clouqueur, A	G1
Blanchard-Desce, M	A13, C4, H26, H4	Cole, J. M	D1
Bloch, B	H2	Collet, A	A2, A3, A4, F9
Bloor, D	H22	Collomb, V	I12
Blum, R	C1	Comoretto, D	F10
Boilot, J.-P	C4, C6	Concilio, S	H30
Bondar, M. V	E19	Copic, M	E4
		Cravino, A	F10

Author Index**ii**

Author name	Contribution number	Author name	Contribution number
Cronstrand, P	E15	Fortusini, D	INV29
Cross, Graham H	H22	Fraser, S. E	INV18
Culjkovic, D	INV27	Freo, L Del	E6, E22
Cumpston, B	INV18	Frey, R	INV28
Cuniberti, C	F10	Friedrich, L	D3
Curtis, K	INV8	Frolova, N. P	E2
D'lorio, M	I13, I2	Fujihara, T	B5, B13
Dalton, Larry	INV4	Fur, Y Le	H5
Damman, P	E26	Gallego, F	INV10
Darracq, B	C4	Galvan-Gonzales, A	INV15
Datta, P. K	INV29	Gamboni, I	I4, I9
Davy, J	E5	García-Alonso, F. J	C12
Decher, G	C15	Gelli, F	F10
Degiorgio, V	INV29, D 9	Gerasimova, T.N	F5
Dell'Erba, C	F10	Gerritsma G.J	C16
Dellepiane, G	F10	Gindre, D	INV17
Deng, H. -H	G7	Giorgetti, E	F10
Denis, C	INV17	Giribabu, L	F8
Derrien, F	A1	Girlando, A	E6
Dhar, L	INV8	Glazer, E	B2
Díaz-García, M. A	B2	Gobbi, L	A11
Dickinson, M	INV18	Grabar, A. A	E2
Diederich, F	A11, H9	Grahn, W	H18
Dietzel, B	C15	Graja, A	E21
Donat-Bouillud, A	I13	Grishina, A.D	C14
Donval, A	C5	Gu, S	INV27
Dörfler, R	H18	Gubler, U	A11, A18, H4, H9
Dosière, M	E26	Guidoni, L	F1
Driessen, A	C16	Gulyi, I. S	E11
Duan, X-M	E28	Gunji, A	H10, INV21
Duff, A.-C Le	C6, C10, C11	Günter, P	A11, B4, B11, C2, C3, C9, D6, E27, H4, H6, H9, I4, I9, I14
Dumarcher, V	INV17		I5
Dumont, M	B3, H16	Guo, W	I10
Eckau, A	C10	Ha, C	INV7
Ehrensperger, M	D6	Haarer, D	A5
Eich, M	C1	Hache, F	H22
Eichner, H	INV20	Hackman, N.-A	INV28
Eilern, A	H3, H17	Haddad, M	B11
Elshocht, S. Van	INV25	Haertle, D	E19, F3
Eriksson, A	E5	Hagan, D. J	INV8
Fan, R	INV27	Hale, A	INV18
Fehn, T	D2	Halik, M	INV32
Feldner, A	D2, D3, H18	Han, P. Y	F2
Fidalgo, J. I	C12	Han, S.H	INV8
Fiorini, C	A15, INV17	Harris, A	H12
Fischer C	C3	Hasegawa, T	INV6
Fitrilawati, F	INV20	Hattori, T	INV27
Flueraru, C	C15	He, M	INV18
Flytzanis, C	INV28	Heikal, A	E7, B10
Follonier, S	B4	Hendrickx, E	
Fort, A	B8		

Author name	Contribution number	Author name	Contribution number
Henninot, J.F	A1	Kim, H	I10, I11
Heras, J. V	E20	Kim, K-S	H14
Hierle, R	C5, G1	Kim, N	E9, INV16
Hill, A	INV8	Kim, O-K	H14
Hörhold, H. H	INV10, INV20	Kim, T-D	INV5
Hong, H.-ki	D4	Kimoto, M	H19
Horinouchi, S	C7	Kimura-Suda, H	H10, INV21
Houbrechts, S	E8	Kippelen, B	E7, INV9
Howard, J. A. K	D1	Kir'yanov, A	B7
Hulliger, J	D7	Kiy, M	H6, I4, I9
Hully, V	INV26	Kiyohara, K	E16
Hult, A	G4	Kloc, Ch	INV23
Ibanez, A	A2, D8	Klunder D.J.W	C16
Imase, Y	INV21	Knoester, J	F5
Imperia, P	I3	Kobayashi, H	D5
Inoue, K	H12, H13	Kobayashi, T	INV11
Ishigure, K	H23	Kodzasa, T	E29
Isoshima, T	F4	Komatsu, K	G7
Ito, H	INV33	Korposh, O. I	E2
Ivanova, Z.M	F5	Kotani, M	D5
Iwai, T	INV13	Kotler, Z	A17, E13, H17
Jabbour, G. E	INV9	Kowalczyk, T. C	INV15
Jäger, M	A11, C2, C9	Koynov, K	INV20
Jahng, W. S	INV16	Kozhevnikov, N	B7
Jandke, M	I3	Kranzelbinder, G	I6
Janietz, S	I15	Krivenko, T.V	C14
Januszko, A	B9	Kroupa, J	A9
Jen, A. K.-Y	INV15	Kruhlik, R. J	E10, E3
Johannes, H.-H	H18	Kubo, Yuji	E8
Jonsson, F	INV28	Kudryavtsev, V. Y	E11
Joo, M	INV16, E9	Kuebler, S	INV18
Josse, D	A16, I6	Kumar, G. R	F8
Juen, P	H5	Kuzel, P	A9
Kaino, T	C9, G7, INV6	Kuzyk, M. G	E3, E10, INV30
Kajzar, F	B9, C10, C11, INV26	Labbé, P	G1
Kamada, K	E16,	Lackritz, H. S	INV15
Kamata, T	E29	Lagali N.S	C16
Kamanina, N. V	A6, A7, B6	Lahlil, K	C4
Kano, S	H24, H25	Lalayan, A	A10
Kaporskii, Lev N	A6, A7	Lam, J	I13
Karl, Nt	INV12	Lang, X. L	A3
Kasai, H	F7	Latajka, Zd	E1
Kato, N	A8, E24	Lavigne, J	I2
Katz, T. J	INV25	Lawrentz, U	H18
Kauranen, M	INV25	Lebus, S	H4
Kawahara, M	H24	Lecomte, S	A11
Kawamata, J	H12, H13	Ledoux, I	C8, E12, H16, H28
Kerkoc, P	C7	Ledoux-Rak, I	A3
Khodorkovsky, V	A17, E13, H3, H17, H21	Lee, J-H	C7
		Lee, J. H	H14
		Lee, K	I10

Author Index
iv

Author name	Contribution number	Author name	Contribution number
Lee, K.-S	C7, H14, INV5	Mertz, J	A13, H26
Lee, K	I11	Méry, S	B8
Lee, S	I10	Meshulam, G	E13, H17
Lemaitre, N	C8	Mesnil, H	A5
Lemmetyinen, H	B7	Michelotti, F	I8
Leszczynski, J	E1	Min, Yu H	INV5
Levy, Y	C4, C6	Miniewicz, A	B9
Leyderman, A	A6	Mladenova, M	C4
Li, E.H.	I5	Moerner, W. E	B2, INV27
Li, Z. H	I13	Moggio, I	F10
Liakatas, I	C2, C3, C9	Montemezzani, G	B11
Likhtorovich, S. P	E11	Moreaux, L	A13, H26
Lim, JinHong	E19	Morel, Y	A2, A4, E14, INV26
Lindgren, M	E5, G4		INV26
Lipson, M	INV18	Mori, Y	INV13
Liu, M	D3	Motschmann, H	C15
Liu, S.Y.	I5	Mountasser, R	F6
Liu, Z	I7	Mourad, W	F3
Lopes, C	E5	Nakahama, T	H27
Losio, P	I9	Nakahama, T	H12
Lukaszuk, K	H4	Nakanishi, H	E28, F7, INV14
Luo, Y	A12, E15	Nakao, S	H19
Luther-Davies, B	F9	Negres, R	E19, F3
Macak, P	A12, E15	Nicoud, J.-F	A2, B8, H5
Mager, L	B8	Nishchenko, M. M	E11
Maggini, M	INV26	Nogi, K	E28
Mailhotte, H	F6, H1, H8	Noh, J	I10
Maiya, B. G	F8	Norman, P	A12, E15
Malliaras, G.G	INV27	Nuckolls, C	INV25
Manetta, S	D6	Nunzi, J.M	A2, A4, A15, E21, INV17, INV26
Marder, S. R	E7, INV9, INV15, INV18, INV19	Ogata, Y	H13
Margheri, G	F10	Ohta, K	E16, H11
Markov, R.V	F5	Oikawa, H	E28
Marowsky, G	G2	Okada, S	E28
Martin, R	H9	Okada-Shudo, Y	E17
Martín, G	C12	Okuyama, H	D5
Mashiko, S	A14, H27	Olbrechts, G	E28
Masse, R	H5	Olenik, I. D	E4
Masson, P	H5	Ono, R	H6, I9
Mathevet, R	I6	Orlova, N.A	F5
Matsuda, H	F7	Ostroverkhov, V	B12, INV27, INV31
Matsuoka, M	H20	Ostroverkhova, O	INV27, INV31
Mauray, O	H16	Otomo, A	A14, H27
Mazor, R	E13, H17	Ozawa, K	B5, B13
McKay, T	E5	Paci, B	A2, A4, A15, INV26
Mecher, E	INV10		INV26
Meerholz, K	INV10	Painelli, A	E6, E22
Meier, J	C10, C11	Pan, F	INV32
Mel'nikov, M. Ya	H29	Park, J	D4
Melchior, H	INV1	Park, S-H	D3

V

Author Index

Author name	Contribution number	Author name	Contribution number
Parka, J	B9	Saito, K	A8, E24
Pashkin, A. V	A9	Sakurai, Y	H19
Peireira, E	I7	Samoc, A	F9
Pereshivko, L.Y	C14	Samoc, M	F9
Perry, J. W	INV18, INV19	Samyn, C	B10, C13
Persoons, A	B10, C13, E7, E28, INV25	Sandre, O	A13
Peruzzini, M	E21	Sanui, K	H23, H24, H25
Petschek, R. G	INV27, INV31	Sanz, N	A2, D8
Peyghambarian, N	E7, INV9	Sasabe, H	B5, B13, E8, F4, H10, INV21
Pfeifer, K	C1	Sasaki, K	C7
Pfister, P	H30	Sasaki, T	INV13
Pham, T.-A	F1	Sassa, T	B5, B13, H10
Philip, R	F8	Schadt, M	INV2
Phillips, K. E. S	INV25	Schafer, K. J	F3
Phu, X. N	H29	Schanne-Klein, M.C	A5
Pietrzyk, M. E	G3	Scherer, D	H18
Pinchuk, A. O	E18	Schilling, M	INV8
Piron, R	A16	Schmidt, C	A15
Pitois, C	G4	Schoer, G	C1
Plekhanov, A.I	F5	Schön, J. H	INV23
Pliska, T	C6, C10, C11, D3	Schrader, S	C15, I3
Pogorelov, V. E	E1	Schultz, B	C15
Prato, M	INV26	Schwoerer, M	D2, D3, H18, INV22
Przhonska, Olga V	E19	Scorrano, G	INV26
Raimond, P	INV17	Screttas, C. G	A15
Rangel-Rojo, R	F7	Segal, J	A17
Rao, D. N	F8	Semyonov, A	INV27
Rao, S. V	F8	Shapiro, L	E13, H3, H17, H21
Rashevskaya, T. A	E11	Sharkany, J	E23
Ratajczak, H	E1	Sharkany, J. P	E2
Ravi, M	H22	Shelkovnikov, V. V	F5
Raymond, Paul	C10, C11	Shen, Y.-R	INV3
Rechsteiner, P	D7	Shepherd, E. E. A	INV29
Rédoglia, S	H4	Sherwood, J. N	D 9, INV29
Reshetnyak, V	B12	Shibata, T	INV6
Reyes, J	C4	Shikata, R	E16
Reznikov, Yu	B12	Shin, D.-H	INV16
Ribierre, J.-C	B8	Shin, J	I10, I11
Ricci, V	C10, C11	Shin, S	I11
Richardson, T	INV8	Shiozaki, H	H19
Rikukawa, M	H23, H24, H25	Shirai, K	H20
Rini, M	D 9	Sigalov, M	A17, H21
Ro, J. H	I10, I11	Sikorski, P	B9
Rocha, L	INV17	Singer, K. D	B12, INV27, INV31
Rojo, G	C12, E20	Slominsky, Y. L	E19
Rodriguez, V	C17	Smith, B	B2
Ros, T. Da	INV26	Soares, J	I7
Rumi, M	INV18	Sobel, F	INV17
Rychwalski, R. W	C14	Song, S	INV16
Sahraoui, B	H29, INV17	Soos, Z. G	E6

Author Index

Vi

Author name	Contribution number	Author name	Contribution number
Sornin, A	INV26	Vogel, H	E28, INV19
Sottini, S	F10	Vogtmann, T	D2, D3, H18
Sourisseau C	C17	Wada, T	B5, B13, E8, F4, H10, INV21
Srinivas, N.K.M. N	F8		
Starodumov, A. N	B7	Wang, I	D8
Steenwinckel, D Van	B10	Wang, S	I2
Stegeman, G. I	C6, C10, C11, D3, INV15	Wang, X.-Y	INV31
	E14, I12	Warenghem, M	A1
Stephan, O	I3	Watanabe, A	E28
Strohriegl, P	E19, F3	Wedel, A	I15
Stryland, E W. Van	I10	Weinstein, J. A	H29
Suh, H	INV27, INV31	Welscher, M	H18
Sukhomlinova, L	B2	Wenselers, W	INV18
Sukhomlinova, L. I	G6	Wiesmann, D	G4
Sullivan, D. M	H30	Wilson, C. C	D1
Suter, U. W	E5	Wilson, W. L	INV8
Svensson, S	H22	Wintermantel, M	E27
Szablewski, M	H23	Wong, M. S	I13
Tabuchi, Y	INV8	Woo, H. Y	H14
Tackitt, M	INV13	Wortmann, R	H4
Takahishi, Y	G7	Wostyn, K	E28
Takayama, K	E21	Wright, D	B2, INV27
Tamuliene, J	E21	Wu, J.W	F2
Tamulis, A	INV32	Wu, Q	I2
Tani, M	E29	Wu, X	INV15
Tano, T	I2, I13	Yablochkov, S. M	E11
Tao, Y	H6, I9, I14	Yamagishi, A	H13
Tapponnier, A	E16	Yang, X. L	A3
Tawa, K	E22	Yap, Y. K	INV13
Terenziani, F	H24, H25	Yaremko, A.M	E1
Teshima, K	INV15, INV18	Yokoyama, M	B5, B13
Thayumanavan, S	H30	Yokoyama, S	A14, H27
Tirelli, N	E23	Yoon, C. S	D4, INV5
Todoran, D	E23	Yoshida, J	C7
Todoran, R	A16, C5, E12, E26, G1, I6	Yoshida, M	G7
Toussaere, E	B2, INV15, INV27, NV31	Yoshimura, M	INV13
	H9, H11	You, F	INV27
	A8, E24	Zabulon, T	A3
	B5, B13	Zauls, V	C15
	E29	Zgonik, M	E4
	E25	Zhang, G	B11
	E26	Zhang, J	B12
	C14	Zhang, X. Q	INV15
	B6	Zhang, X. C	INV32
	C4, H26	Zhao, Yi	I5
	C13, INV25	Zheligovskaya, N. N	H29
	C14	Ziegler, J	INV20
	I12	Zyss, J	A3, A16, C5, C8, E12, E26, G1, H7, H8, H16, H28, I6, INV24

Notes

Notes

Notes

Notes

Notes

Notes

Notes

Notes

Sponsors

We wish to thank the following for their contribution to the success of this Conference:

- European Office of Aerospace Research and Development
- U.S. Air Force Office of Scientific Research
- United States Air Force Research Laboratory
- U.S. Office of Naval Research - European Office



Swiss National Science Foundation
Wildhainweg 20, P.O. Box, CH-3001 Berne, Switzerland
<http://www.snf.ch/>



Swiss Federal Institute of Technology (ETH)
<http://www.ethz.ch/>



Nonlinear Optics Laboratory
ETH Zürich, Switzerland
<http://nlo-serv.ethz.ch/>



Bayer AG
Werk Leverkusen, 51368 Leverkusen, Germany
<http://www.bayer.com/>



Gordon and Breach Science Publishers
<http://www.gbhap.com/>



GMP SA
19, av. de Baumettes/CP, CH-1020 Renens 1, Switzerland
<http://www.gmp.ch/>



Rainbow Photonics AG
Einsteinstrasse HPF E7, CH-8093 Zürich, Switzerland
<http://www.rainbowphotonics.ethz.ch/>

Exhibitors

The following companies have agreed to take part in the exhibition:



Gordon and Breach Science Publishers
<http://www.gbhap.com/>



Sopra SA (Non-Linear Optical Spectrometer)
26 rue Pierre Joigneaux, F-92170 Bois Colombe, France
<http://www.sopra-sa.com/>



Springer

Springer-Verlag
Tiergartenstrasse 17, D-69121 Heidelberg, Germany
<http://www.springer.de/>

Sunday, March 12	Monday, March 13	Tuesday, March 14	Wednesday, March 15	Thursday, March 16
	<p>8.30-9.00 Opening Future Photonic Appl.</p> <p>9.00-10.30 Melchior Schadt Shen</p> <p>10.30-11.00 Coffee/Tee</p> <p>EO Polymers</p> <p>11.00-12.30 Dalton Lee Kaino</p> <p>12.30-14.30 Lunch</p> <p>Optical Memories</p> <p>14.30-16.30 Haarer Wilson Peyghamb. Meerholz</p>	<p>High NL Org. Crystals</p> <p>8.30-10.30 Kobayashi Karl Nakanishi Mori</p> <p>10.30-11.00 Coffee/Tee</p> <p>NLO Polymers</p> <p>11.00-12.30 Stegeman Kim Nunzi</p> <p>12.30-16.30</p> <p>Free time</p> <p>16.30-19.00</p> <p>Poster II</p> <p>19.00-20.00 Round Table Discussion</p>	<p>Third-order NLO</p> <p>8.30-10.30 Marder Brédas Bubeck Wada</p> <p>10.30-11.00 Coffee/Tee</p> <p>OLED's</p> <p>11.00-12.00 Schwoerer Batlogg</p> <p>12.00-14.30 Lunch</p> <p>Novel Molecules</p> <p>14.30-16.30 Zyss Persoons Kajzar Twieg</p> <p>16.30-19.00</p> <p>Poster III</p> <p>20.00 Conference Dinner (Hotel Belvedere)</p>	<p>Fund. Investigations</p> <p>8.30-10.30 Flytzanis Banfi Kuzyk Singer</p> <p>10.30-11.00 Coffee/Tee</p> <p>New Phenomena</p> <p>11.00-12.00 Zhang Ito</p> <p>12.00-12.30 Closing</p>
<p>16.00-18.00 Registration (House B, Congress Center)</p> <p>18.00-20.00 Welcome Reception (House B, Congress Center)</p>	<p>16.30-19.00</p> <p>Poster I</p> <p>19.30-21.30 Kirchner Museum (Conference Reception)</p>			